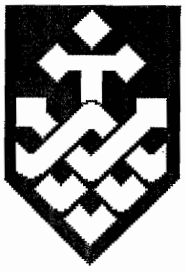
Assessment of the Structural Integrity of Timber Bridges Using Dynamic Approach

by

Fook Choon Choi

A thesis submitted to fulfilment
of the requirements for the degree of
Doctor of Philosophy



University of Technology, Sydney
Faculty of Engineering

March 2007

CERTIFICATE OF AUTHORSHIP/ORIGINALITY

I certify that the work in this thesis has not previously been submitted for a degree not has it been submitted as part of requirement for a degree except a fully acknowledged within the text.

I also certify that the thesis has been written by me. Any help that I have received in my research work and preparation of the thesis itself has been acknowledged. In addition, I certify that all information sources and literature used are indicated in the thesis.

Signature of Candidate

Production Note:
Signature removed prior to publication.

(Fook Choon Choi)

Sydney, March 2007

ABSTRACT

In this study, a systematic approach was adopted to investigate, numerically and experimentally, localised defects and/or damage in timber bridges, such as rot, using modal based damage detection techniques. An existing damage detection method namely damage index (DI) method that utilises modal strain energy before and after damaged state was adopted. One contribution of this study was to modify the DI method by an additional step of normalising the modal curvature, which would minimise the dominance of higher modes.

In the numerical models, a comparative study of the effects of numerical integration techniques used in a damage detection process was carried out. The results show that when mode shape curvature integrations use the rectangular rule for the numerical integration, it yields better results than the trapezoidal rule.

In the numerical examples using a finite element model of timber beam, the modified DI (MDI) methods were found to perform better than its original form for locating single and multiple damage scenarios. For the DI methods, two types of formulations were adopted and modified, and they are denoted as modified damage index I (MDI-I) and modified damage index II (MDI-II). Another modal based damage detection method, namely changes in flexibility (CIF), was adopted for locating damage. It was found that the CIF method performed reasonably well for single damage but not multiple damage scenarios.

As part of the study, the modified damage index methods were utilised for evaluating severity of damage. For the MDI-I method, the formulation was not derived to evaluate damage severity directly. Instead, a hybrid of the MDI-I and CIF methods (HMC), was proposed for evaluating severity of damage in terms of loss of 'I' (moment of inertia). Using three levels of damage, i.e. light (L), medium (M) and severe (S), the HMC method is able to predict the medium and severe damage quite well, but it is less efficient for light damage scenarios. For the MDI-II method, further manipulation of the algorithm can predict the severity of damage in terms of loss of 'I'. This method is able to predict the medium and severe damage quite well but is not as good for the light damage. Both methods, HMC and MDI-II, for predicting severity of damage, required some adjustment using a weighting factor in order to obtain reasonable results.

An experimental modal analysis (EMA) test program of timber beams was undertaken. This was done to verify the robustness of the modified damage index methods for detecting location and estimating severity of damage. The laboratory investigation was conducted on the corresponding changes of modal parameters due to loss of section. The MDI methods were used to detect location of damage and to evaluate the severity of damage in the test beams. A mode shape reconstruction technique was utilised to enhance the capability of the damage detection algorithms with limited number of sensors. The test results and analysis show that location of damage is quite accurately estimated with the available sensors. The methods demonstrate that they are less mode dependant and can detect damage with a higher degree of confidence. The MDI methods also show that they are able to predict the severe damage well, but it is less accurate for the medium damage and not as good for light damage.

The damage index II (DI-II) method extended to plate-like structures (DI-II-P) was adopted and evaluated for detecting damage. Based on finite element analysis (FEA) results of a laboratory timber bridge, the DI-II-P method which utilises two-dimensional (2-D) mode shape curvature was employed to detect location of damage. The results show that the method based on 2-D mode shape curvature is able to locate damage quite well, numerically. A supplementary work using the DI-II-P method in a timber plate model was carried out. The results also show that the method was able to predict the damage location well.

A process of updating a laboratory timber bridge, analytically, is presented. A finite element model was developed and updated with experimental modal data. Material properties of timber beam (girders) and plywood (deck) as well as the screw connection between deck and girder were experimentally investigated. These test results were then used for the finite element modelling. The model has been developed sequentially starting with a preliminary model having very simple features. It followed by the advanced model calibrated with the experimental modal data employing a global objective function, consisting of errors of natural frequencies and modal assurance criterion. The calibrated finite element model shows a good correlation to the experimental model with minor adjustments to the real material properties and boundary conditions. The calibrated model can reasonably be used to study the damaged behaviour of the laboratory timber bridge.

The bridge model was then used to verify the numerical results for detecting damage. The bridge was inflicted with various damage scenarios with loss of section similar to the timber beam models. The limited number of data was expanded using the 2-D cubic spline. Using the reconstructed data for detecting damage yields better results than just using 'as is' data. Using the undamaged and damaged modal data, the DI-II-P method was employed to detect the location of damage. The results of using the first nine modes showed that generally the severe damage is able to be located by the method. It performs reasonably well for the medium damage but does not perform as good in the light damage scenarios. However, in some cases the method can present some problems in identifying severe damage, which may be due to lack of normalisation of mode shape curvature. Complementary work was undertaken using the method on a timber plate, experimentally. The results showed that the damage detection process in the timber plate is less efficient compared to the laboratory timber bridge.

A comprehensive comparative study was carried out based on the results of the numerical and experimental investigation of damage detection on timber beam, laboratory timber bridge and timber plate. For the timber beam, both damage detection methods, MDI-I and MDI-II, were capable of detecting medium and severe damage in the numerical and experimental studies. However, the light damage was not identified well using the experimental data in the presence of noise. To estimate damage severity in the timber beam, the HMC method performed well for the medium and severe damage. The method did not work well in estimating severity of light damage. Similar conclusions can be drawn in using the MDI-II method to estimate the damage severity. The results of applying the DI-II-P method (using 9 modes) to locate damage in the laboratory timber bridge showed that numerical and experimental data are capable of detecting all severe damage for damage cases with less than three damage locations. While for light and medium damage, the experimental data did not work well as compared to the numerical one. For the timber plate (a complementary work), the numerical and experimental results also showed that they are able to detect the severe damage well. However, there were serious false positives appearing in the light damage cases in the experimental results.

Acknowledgement

This PhD project could not have been possible without the unfailing assistance, understanding and guidance rendered by numerous people throughout the project. The author would very much like to record his deepest appreciation to his principal supervisor, Professor Bijan Samali, who had given the author invaluable advice, encouragement, understanding and assistance throughout the course of this study and in preparation of this thesis. Utmost gratitude is also forwarded to Dr. Jianchun Li, Professor Keith Crews and Dr. Ali Saleh, who had lent their helping hand for various aspects and at different stages of this project. In particular, Dr. Jianchun Li, who had been a mentor and sparing partner to the author in his search for 'light at the end of a tunnel'. The author also gratefully acknowledges the financial assistance provided by the University of Technology Sydney (International Research Scholarship) and Centre for Built Infrastructure Research (CBIR) of the Faculty of Engineering, UTS.

Furthermore, the author would like to thank the Structures Laboratory staff for their help in the experimental work and they have been fantastic. Special thanks must also go to David Hooper, David Dicker, Warwick, Ian, Mario, Scott, Harold, Bill, Gregory and Marika as well as the young blood in the laboratory such as Zeid and Nima. I wish to sincerely thank Peter, Setu, Imelda, Ulrike and Dr. Mohammed for helping the author in setting up the acquisition system for the experimental tests and for responding quickly and positively unforeseen problems and breakdowns. The author also feels a deep sense of gratitude to all the academic and non-academic staff in the Faculty of Engineering for the help rendered. Last, but surely not least, and certainly not short of contribution and support, the author wish to forward very special thanks to Rami, Laurence and Wolf, whom have been unselfishly sharing their expertise with the author, gave a helping hand whenever needed and were a dear friend in many ways. The author is certain that the list is not exhaustive and so may the ones that I may have forgotten accept my sincerest apologies.

To friends and/or colleagues at UTS and elsewhere, the author wishes to express his gratitude. Special thanks must go to Asela, Damith and Tonmoy, whom had shared with the author his new journey in Australia. Sincere thanks must also go to Janitha (machang), Peter Brady, Alison, Dom, Nassif, Reza, Fabio, Rong, Yujue,

Nikhil, and others who shared their time and friendship with the author and rendered invaluable help. The author would also like to acknowledge Joko for sharing his expertise and time, which helped the author in many ways in his journey of striving towards permanent head damage (PhD). Very warm and special thanks must go to two special friends, Chris and Debbie. The journey in this course of study would be dull without them sharing with the authors their sincere and genuine thoughts and ideas in the research areas as well as in daily life matters. It is through them that the author learned to appreciate and respect cultural differences, especially the European way of life, which was new to the author. With compassion and love, the author wishes them all the best and happiness.

The author's abundant love must go to the person who has scarified her career and left behind the family in Malaysia accompanying the author to venture his new journey in Australia. On top of that, she has been the spiritual friend, financial sponsor and cook to the author. This must be the only one for the author, the beloved wife, Pui Yeng. The author thanks her for the support and love. (I love you too). In addition, the author is grateful to his family for their moral support throughout this journey. To all others who have helped in one way or another, the author would like to say a big thank you.

Lastly, the author would like to dedicate this thesis to his beloved wife and family for their continuous support.

Sadhu! Sadhu! Sadhu!

Fook Choon Choi

List of Publications Based on This Research

Refereed Journal Articles

1. **Choi, F.C.**, Li, J, Samali, B. & Crews, K. 2007, 'Application of modal-based damage detection method to locate and evaluate damage in timber beams', *Journal of Wood Science*, DOI 10.1007/s10086-006-0881-5 (Awarded Emachu Research Fund for publication of the paper).

2. **Choi, F.C.**, Li, J, Samali, B & Crews, K. 2007, 'Application of the Modified Damage Index method to timber beams', *Engineering Structures*, (accepted for publication on 16 July 2007).

3. Li, J, **Choi, F.C.**, Samali, B. & Crews, K. 2007 'Damage localisation and severity evaluation of a beam-like timber structures based on modal strain energy and flexibility approaches', *Journal of Building Appraisal*, Vol. 2, No. 4, pp. 323-334.

4. **Choi, F.C.**, Li, J., Samali, B. & Crews, K. 2007, 'An Experimental Study on Damage Detection of Structures using a Timber Beam', *Journal of Mechanical Science and Technology - MOVIC Special Edition*, Vol. 21, pp. 903-907.

Refereed Conference Papers

5. **Choi, F.C.**, Samali B. & Crews, K. 2004, 'Pilot investigation of continuity effect of corbel in timber bridges", *18th Australasian Conference on the Mechanics of Structures and Materials*, 1-3 December 2004, Perth, Australia, pp. 505-510.

6. **Choi, F.C.**, Samali, B., Crews, K., & Li, J. 2005, 'Static and dynamic evaluation of continuity effect of corbels in timber bridges', *4th Australasian Congress on Applied Mechanics*, 16th -18th February 2005, Melbourne, Australia, pp. 285-292.

7. Li, J., Samali, B., Crews, K., **Choi, F.** & Shestha, R. 2005, 'Theoretical and experimental studies on assessment of bridges using simple dynamic procedures', *Australian Structural Engineering Conference 2005: Structural Engineering - Preserving and Building into the Future*, 11-14 September, Newcastle City Hall, Australia: Structural College of EA, (published on CDROM).

8. **Choi, F.C.**, Samali, B., Li, J., Brown, P. & Dackermann, U. 2005, 'Investigation on the dynamic response of a damaged timber bridge', *Proceedings of the 11th Asia–Pacific Vibration Conference*, 23-25 November, Langkawi, Malaysia: Institute of Noise & Vibration, University of Technology Malaysia, pp. 274-280.

9. Li, J., Samali, B., **Choi, F.C.** & Dackermann, U. 2005, 'Damage identification of timber bridges using vibration based methods', *Proceedings of the 11th Asia–Pacific Vibration Conference*, 23-25 November, Langkawi, Malaysia: Institute of Noise & Vibration, University of Technology Malaysia, pp. 662-668.

10. **Choi, F.C.**, Li, J., Samali, B. & Crews, K. 2006, 'Damage evaluation of a timber beam using modal-based method', *19th Australasian Biennial Conference on the Mechanics of Structures and Materials*, July 11, 2006, University of Canterbury, Christchurch, New Zealand, pp. 1005-1010.

11. Li, J., **Choi, F.C.** & Samali, B. 2006, 'Modal-based damage identification methods for plate-like structures', *19th Australasian Biennial Conference on the Mechanics of Structures and Materials*, July 11, 2006, University of Canterbury, Christchurch, New Zealand, pp. 909-914.

12. **Choi, F.C.,** Li, J., Samali, B. & Crews, K. 2006, 'Impact of Different Numerical Techniques on Damage Identification in Structures', *Tenth East Asia-Pacific Conference on Structural Engineering and Construction*, August 3-5, 2006, Bangkok, Thailand, pp. 111-116.

13. **Choi, F.C.**, Li, J., Samali, B. & Crews, K. 2006, 'An Experimental Study on Damage Detection of Structures using a Timber Beam', *The 8th International Conference on Motion and Vibration Control*, August 27 – 30, 2006, Daejeon, Korea, pp. 226-231.

Other Conference Papers

14. Li, J., **Choi, F.C.**, Samali, B. & Crews, K. 2006, 'Damage detection in a timber beam', *Structural Faults + Repair*, June 13 - 15, 2006, Edinburgh, United Kingdom, (published on CDROM).

15. Li, J., **Choi, F.C.**, Samali, B. & Crews, K. 2006, 'Damage localisation and severity evaluation of a beam-Like timber structure based on modal strain energy and flexibility approaches', *Structural Faults + Repair*, June 13 - 15, 2006, Edinburgh, United Kingdom, (published on CDROM).

16. **Choi, F.C.**, Samali, B., Crews, K. & Li, J. 2006, 'Calibration of a laboratory timber bridge finite element model using the experimental modal data', *9th World Conference on Timber Engineering*, August 6-10, 2006, Portland, Oregon, United States of America, (published on CDROM).

LIST OF CONTENTS

DECLARATION.....i

ABSTRACT.....ii

ACKNOWLEDGEMENT.....v

LIST OF PUBLICATIONS.....vii

LIST OF CONTENTS.....x

LIST OF FIGURES.....xviii

LIST OF TABLES.....xxv

LIST OF NOTATIONS.....xxvii

CHAPTER 1 INTRODUCTION **1**

1.1 General 1

1.2 Objectives of the Study 5

1.3 Scope of the Work 6

1.4 Contribution to Knowledge 8

1.5 Organisation of the Thesis 10

CHAPTER 2 LITERATURE REVIEW **12**

2.1 Introduction 12

2.2 Timber Bridges in Australia 12

2.2.1 Background 12

2.2.2 Problems Faced 14

2.2.2.1 Biotic Degradation of Wood 15

2.2.2.2 Physical Degradation of Wood 16

2.2.3 Methods to Overcome Problems 17

2.2.4 Condition Assessment for Timber Bridges 19

2.2.4.1 Visual Inspection 19
2.2.4.2 Resistance Drilling 20
2.2.4.3 Sounding 20
2.2.4.4 Stress Wave or Ultrasound Techniques 20
2.2.4.5 Proof Load Test 21
2.2.4.6 Vibration Techniques 21
2.2.5 Finite Element Modelling for Timber Bridges 24
2.3 Damage Detection 25
2.3.1 Previous Literature Reviews and Surveys 26
2.3.2 Natural Frequency Based Methods 28
2.3.3 Mode Shape Based Methods 33
2.3.4 Mode Shape Curvature Based Methods 34
2.3.5 Strain Mode Shape Based Methods 36
2.3.6 Modal Strain Energy Based Methods 36
2.3.7 Flexibility Based Methods 42
2.3.8 FRF Based Methods 44
2.3.9 Model Updating Based Methods 45
2.3.10 Artificial Intelligence Based Methods 46
2.3.11 Time Domain Based Methods 48
2.4 Research and Development Needs 49

CHAPTER 3 MATERIAL PROPERTIES AND MATERIAL TESTING PROCEDURES 50

3.1 Introduction 50
3.2 Material Properties of Timber/Wood 50
3.2.1 Structure of Wood 52
3.2.2 Physical Properties 54
3.2.3 Mechanical Properties 56

3.3 Determination of Characteristic Properties 57
3.3.1 Flexural Properties for Timber Beams 57
3.3.2 Flexural Properties for Plywood 59
3.4 Pullout Tests for Screw Connections 60
3.5 Summary 64

CHAPTER 4 FINITE ELEMENT MODELLING 65

4.1 Introduction 65
4.2 Modelling of Beam-like Structures 66
4.2.1 Finite Element Model for Undamaged Timber Beam 66
4.2.2 Mesh Density 70
4.2.3 Simulation of Damage in Beam Model 72
4.2.4 Correlation Analysis 74
4.2.4.1 Natural frequencies 74
4.2.4.2 Mode shapes 76
4.3 Modelling of Plate-like Structures 77
4.3.1 Isotropic Plate 78
4.3.2 Orthotropic Plate 80
4.3.3 Damaged Plate 80
4.4 General Modelling Considerations for Timber Bridge Structures 82
4.4.1 Grillage Model for Comparison 82
4.4.2 Different Elements Used in Modelling 84
4.4.3 Comparison of FE Models Using Normalised Stiffness Matrix 85
4.4.3.1 Shell-Shell Model 85
4.4.3.2 Shell-Beam Model 86
4.4.3.3 Shell-Solid Model 87
4.4.4 Comparison of FE Models Using Natural Frequency 89
4.4.5 Mode Shape 90

4.4.6 Preliminary Parametric Studies for the Shell-Solid Model 91
4.4.6.1 Properties of Wood 91
4.4.6.2 Rigid Link 93
4.4.6.3 Orthotropic Material 95
4.4.6.4 Boundary Conditions 97
4.5 Finite Element Model Updating 99
4.5.1 Material Properties 99
4.5.2 Preliminary Finite Element Model 101
4.5.3 Development of an Advanced Model 102
4.6 Considerations of Sensitivity Analysis in Modelling 103
4.6.1 Correlation Analysis 106
4.6.2 Damage Scenarios for the Bridge Model 109
4.7 Summary of Modelling Approaches 111

CHAPTER 5 DAMAGE DETECTION CRITERIA 112

5.1 Introduction 112
5.2 Natural Frequency and Damping Ratio 112
5.3 Changes in Flexibility (CIF) 114
5.4 Damage Indices I and II (DI-I and DI-II) 115
5.5 Modified Damage Indices I and II (MDI-I and MDI-II) 121
5.6 Hybrid of MDI-I and CIF 122
5.7 Damage Severity Estimation using MDI-II 124
5.8 Utilising Plate Theory in DI-II 124
5.9 Summary 128

CHAPTER 6 DAMAGE DETECTION - NUMERICAL STUDIES 129

6.1 Introduction 129
6.2 Impact of Numerical Integration Methods 129

6.2.1 Comparison of Numerical Integration Techniques 131

6.3 Damage Detection for Timber Beam 133

6.3.1 Damage Localisation 136

6.3.1.1 Discussion on Damage Index I Method 137

6.3.1.2 Application of Changes in Flexibility on Timber Beam 144

6.3.1.3 Modification Made to DI-I Method to Improve Damage Detection 148

6.3.1.4 Discussions on Damage Index II Method 155

6.3.1.5 Modification Made to DI-II method to Improve Damage Detection 162

6.3.2 Estimation of Severity of Damage 169

6.3.2.1 Evaluation of Severity of Damage using Hybrid of MDI-I and CIF 170

6.3.2.2 Estimation of severity of damage using Modified Damage Index II 174

6.4 Damage Detection - Timber Plate 179

6.5 Damage Detection - Laboratory Timber Bridge 188

6.5.1 Damage Localisation 193

6.5.1.1 Discussions on Damage Index II Method for Plate-like Structures 194

6.6 Summary 203

CHAPTER 7 MODAL TESTING AND EXPERIMENTAL MODAL ANALYSIS FOR TIMBER BEAMS 205

7.1 Introduction 205

7.2 Fundamentals of Modal Testing and Experimental Modal Analysis 206

7.2.1 Signal Processing 206

7.2.2 Frequency Response Function 210

7.2.3 Modal Parameter Estimation 212

7.3 Experimental Set Up and Testing 217

7.3.1 Test Beams 217

7.3.2 Inflicted Damage in Test Beams 219
7.3.3 Modal Test Set Up 221
7.3.4 Modal Analysis 227
7.4 Results and Discussions for Beams 230
7.4.1 Natural Frequency 230
7.4.2 Damping Ratio 233
7.4.3 Effects of Sensor Density 234
7.4.4 Mode Shape Reconstruction Techniques 239
7.4.5 Damage Localisation 242
7.4.5.1 Damage Index I 242
7.4.5.2 Modified Damage Index I 250
7.4.5.3 Damage Index II 258
7.4.5.4 Modified Damage Index II 261
7.4.6 Estimation of Severity of Damage 265
7.4.6.1 Hybrid of MDI-I and CIF 266
7.4.6.2 Modified Damage Index II 271
7.5 Summary 275

CHAPTER 8 MODAL TESTING AND EXPERIMENTAL MODAL ANALYSIS FOR PLATE-LIKE TIMBER STRUCTURES 276

8.1 Introduction 276
8.2 Experimental Set Up and Testing 276
8.2.1 A Laboratory Timber Bridge 276
8.2.2 Inflicted Damage in Laboratory Timber Bridge 279
8.2.3 Modal Test Set Up 282
8.2.4 The Laboratory Timber Plate 286
8.3 Results and Discussions - the Laboratory Timber Bridge 291
8.3.1 Natural Frequency 291

8.3.2 Damping Ratio 293

8.3.3 Effects of Sensor Density 294

8.3.4 Damage Localisation 299

8.3.4.1 Damage Index II for Plate-like Structures 300

8.4 Results and Discussions for Laboratory Timber Plate 311

8.5 Summary 316

CHAPTER 9 COMPARISON OF NUMERICAL AND EXPERIMENTAL STUDIES 317

9.1 Introduction 317

9.2 Inflicted Damage in Timber Beam 318

9.3 Results and Discussions for Timber Beams 320

9.3.1 Damage Localisation 320

9.3.1.1 Discussions on Modified Damage Index I Method 320

9.3.1.2 Discussions on Modified Damage Index II Method 328

9.3.2 Estimation of Severity of Damage 331

9.3.2.1 Discussions on HMC Method 332

9.3.2.2 Discussions on Modified Damage Index II Method 335

9.4 Inflicted Damage in Laboratory Timber Bridge 339

9.5 Results and Discussions for Laboratory Timber Bridge 340

9.5.1 Damage Localisation 340

9.5.2 Damage Index II for Plate-like Structures 341

9.6 Results and Discussions for Laboratory Timber Plate 349

9.7 Summary 353

CHAPTER 10 CONCLUSIONS AND RECOMMENDATIONS 355

10.1 Conclusions 355

10.2 Recommendations and Future Work 360

REFERENCES.....**362**

APPENDICES.....**382**

LIST OF FIGURES

Figure 1.1 Typical timber girder bridge in Australia. 2
Figure 2.1 Structural details of typical timber beam bridges in NSW. 13
Figure 3.1 Wood microstructure (Miller 2005) 52
Figure 3.2 Simplified depiction of the structure of wood (Ritter 1990). 53
Figure 3.3 Cross section of a tree trunk (Ritter 1990). 54
Figure 3.4 The three principal axes of wood with respect to grain direction and growth rings (Ritter 1990). 55
Figure 3.5 Experimental set up for four point being test for timber beams and plywood. 57
Figure 3.6 A typical load-displacement curve for timber beams. 58
Figure 3.7 Plan views of face grain orientations for plywood test panels. 59
Figure 3.8 A typical load-displacement curve for plywood. 60
Figure 3.9 Test samples for pullout test in all directions. 61
Figure 3.10 Pullout test set up. 62
Figure 3.11 Typical pullout test set up in all directions. 62
Figure 3.12 Typical pullout test results in all directions. 63
Figure 4.1 Nodes and elements for FE model of the timber beam. 66
Figure 4.2 Cross section of the FE model. 67
Figure 4.3 The geometric properties of SOLID45 (ANSYS Inc. 2005b). 67
Figure 4.4 "Pinned" connections between the girder, deck and abutment 68
Figure 4.5 First five flexural mode shapes for the FE beam model. 69
Figure 4.6 Damage location detection using fine mesh density with 201 nodes in the FE model. 71
Figure 4.7 Damage location detection using coarse mesh density with 41 nodes in the FE model. 71
Figure 4.8 Configurations of a typical damage case. 73
Figure 4.9 Frequency pair between FE model and modal tests for the Beam. 75
Figure 4.10 The geometric properties of SHELL63 element (ANSYS Inc. 2005b). 78
Figure 4.11 Geometric configuration of the isotropic plate. 79
Figure 4.12 Boundary conditions of the isotropic plate. 79

Figure 4.13 A close-up plan view of a typical damage on the plate model. 81
Figure 4.14 Layout of the grillage model..... 83
Figure 4.15 Normalised stiffness matrix of the analytical model. 83
Figure 4.16 Plan view of the laboratory timber bridge. 85
Figure 4.17 Normalised stiffness matrix of the shell-shell model. 86
Figure 4.18 Normalised stiffness matrix of the shell-beam model. 87
Figure 4.19 Cross sectional view of a shell-solid element with rigid link. 88
Figure 4.20 Normalised stiffness matrix of the shell-solid model Case B..... 88
Figure 4.21 Normalised stiffness matrix of the shell-solid model Case BM. 89
Figure 4.22 Mode shapes of the shell-solid model. 90
Figure 4.23 Three principlal axes of wood with respect to grain direction and growth rings (General Technical Report FPL-GTR-113 1999). 92
Figure 4.24 The effect of changes in EX and EY on natural frequency. 96
Figure 4.25 Original pin-roller boundary condition..... 97
Figure 4.26 Boundary condition BC1. 97
Figure 4.27 Boundary condition BC2. 97
Figure 4.28 Finite element modelling strategy for the composite section. 102
Figure 4.29 Modelling of bridge supports..... 103
Figure 4.30 Fabricated pin support. 104
Figure 4.31 Nine vibration mode shapes of the laboratory timber bridge FE model.... 107
Figure 4.32 Frequency pair between FE model and modal tests for Bridge..... 108
Figure 4.33 Plan view of damage locations on the bridge model. 110
Figure 5.1 Schematic diagram of a simply supported beam. 116
Figure 5.2 Schematic drawing of subdivisions of a beam (Cornwell, Doebling & Farrar 1999). 117
Figure 5.3 Mode shape curvature for flexural modes one to five. 121
Figure 5.4 Schematic diagram of the process for HMC..... 123
Figure 5.5 Schematic diagram showing subregions of a plate (Cornwell, Doebling & Farrar 1999)..... 125
Figure 6.1 Numerical integration techniques (NSF Dynamic Systems 2006). 130
Figure 6.2 Comparison of numerical integration methods for 4S..... 132
Figure 6.3 Comparison of numerical integration methods for 4S6L. 132
Figure 6.4 Comparison of numerical integration methods for 4S5M6S. 133
Figure 6.5 Comparison of numerical integration methods for 2S4S5S6M..... 133

Figure 6.6 Configuration of elements and nodes for the timber beam FE model. 134
Figure 6.7 Comparison of percentage of drop in natural frequencies for various damage cases for finite element model of a timber beam. 136
Figure 6.8 Single damage cases using DI-I method. 138
Figure 6.9 Two damage cases using DI-I method 140
Figure 6.10 Three damage cases using DI-I method 142
Figure 6.11 Four damage cases using DI-I method. 143
Figure 6.12 Single damage cases using CIF method. 146
Figure 6.13 Two damage cases using CIF method. 147
Figure 6.14 Three damage cases using CIF method. 147
Figure 6.15 Four damage cases using CIF method. 147
Figure 6.16 Single damage cases using MDI-I method. 149
Figure 6.17 Two damage cases using MDI-I method. 151
Figure 6.18 Three damage cases using MDI-I method. 153
Figure 6.19 Four damage cases using MDI-I method. 154
Figure 6.20 Single damage cases using DI-II method. 156
Figure 6.21 Two damage cases using DI-II method. 158
Figure 6.22 Three damage cases using DI-II method. 160
Figure 6.23 Four damage cases using DI-II method. 161
Figure 6.24 Single damage cases using MDI-II method. 163
Figure 6.25 Two damage cases using MDI-II method 165
Figure 6.26 Three damage cases using MDI-II method 167
Figure 6.27 Four damage cases using MDI-II method. 168
Figure 6.28 Single damage severity estimation using HMC method 171
Figure 6.29 Two damage severity estimation using HMC method. 172
Figure 6.30 Three damage severity estimation using HMC method. 173
Figure 6.31 Four damage severity estimation using HMC method. 174
Figure 6.32 Single damage severity estimation using MDI-II method. 176
Figure 6.33 Two damage severity estimation using MDI-II method. 177
Figure 6.34 Three damage severity estimation using MDI-II method. 178
Figure 6.35 Four damage severity estimation using MDI-II method 179
Figure 6.36 Plan view of damage locations for a timber plate 181
Figure 6.37 Six vibration mode shapes of the timber plate FE model. 182

Figure 6.38 Comparison of natural frequencies for finite element model of a timber plate. 183
Figure 6.39 Single damage cases using DI-II-P method for plate. 185
Figure 6.40 Two damage cases using DI-II-P method for plate. 186
Figure 6.41 Three damage cases using DI-II-P method for plate. 187
Figure 6.42 Plan view of damage locations on the bridge model. 190
Figure 6.43 Nine vibration mode shape of the laboratory timber bridge FE model. 191
Figure 6.44 Comparison of natural frequencies for the finite element model of the laboratory timber bridge..... 192
Figure 6.45 Single damage cases using DI-II-P method for bridge. 195
Figure 6.46 Two damage cases using DI-II-P method for bridge. 198
Figure 6.47 Three damage cases using DI-II-P method for bridge. 200
Figure 6.48 Four damage cases using DI-II-P method for bridge..... 202
Figure 7.1 Digital signal processing (Abdul Rahman 1999). 207
Figure 7.2 Basic sensor build-up (Zwonlinski 1998)..... 207
Figure 7.3 Aliasing phenomenon (Maia & Silva 1997). 208
Figure 7.4 Transfer function method (Agilent Technologies 2000). 211
Figure 7.5 Classification of modal analysis identification methods (Maia & Silva 1997). 213
Figure 7.6 Curve-fitting different bands using different methods (Avitabile 2001)..... 214
Figure 7.7 Experimental modal analysis example (Agilent Technologies 2000). 216
Figure 7.8 Half-power points definition. 216
Figure 7.9 Geometric configurations and measurement locations of the test beams. ... 218
Figure 7.10 Wood moisture detector..... 218
Figure 7.11 Specially designed pin support. 218
Figure 7.12 Side view of a typical damage inflicted in beams. 219
Figure 7.13 Schematic diagram of modal tests. 221
Figure 7.14 Calibration of accelerometers using a three-degree-of-freedom steel structure..... 222
Figure 7.15 Modal hammer. 223
Figure 7.16 Battery powered signal conditioner. 223
Figure 7.17 Piezoelectric accelerometers..... 224
Figure 7.18 Multi-channel signal conditioner. 224
Figure 7.19 HP E1432A Vxi system. 225

Figure 7.20 A typical frequency response function spectrum.....226
Figure 7.21 Window functions.....226
Figure 7.22 FRF graphs in rectangular and polar coordinates for a single degree of freedom system (Agilent Technologies 2000).....228
Figure 7.23 Mode shapes obtained from experiment (9 points).....229
Figure 7.24 Reconstructed mode shapes (41 points).....229
Figure 7.25 Comparison of percentage of drop in natural frequencies for Beam1 for various damage cases.....232
Figure 7.26 Comparison of percentage of drop in natural frequencies for Beam2 for various damage cases.....232
Figure 7.27 Single damage scenario 4L inflicted at midspan (5 modes used).....236
Figure 7.28 Three damage scenario 2L4L6L inflicted at ¼, mid and ¾ span (2 modes used).....236
Figure 7.29 Three damage scenario 2M4M6S inflicted at ¼, mid and ¾ span (2 modes used).....237
Figure 7.30 Three damage scenario 2S4M6S inflicted at ¼, mid and ¾ span (5 modes used).....237
Figure 7.31 Single damage scenario 4M inflicted at midspan (5 modes used).....238
Figure 7.32 Three damage scenario 2S4S6S inflicted at ¼, mid and ¾ span (5 modes used).....238
Figure 7.33 Single damage scenario 4L inflicted at midspan (5 modes used).....240
Figure 7.34 Three damage scenario 2M4M6S inflicted at ¼, mid and ¾ span (5 modes used).....241
Figure 7.35 Two damage scenario 4S6L inflicted at mid and ¾ span (2 modes used).241
Figure 7.36 Three damage scenario 2S4M6S inflicted at ¼, mid and ¾ span (5 modes used).....241
Figure 7.37 Four damage scenario 2S4S65SS inflicted at ¼, mid, 5/8 and ¾ span (5 modes used).....242
Figure 7.38 Single damage cases using DI-I method.....244
Figure 7.39 Two damage cases using DI-I method.....246
Figure 7.40 Three damage cases using DI-I method.....248
Figure 7.41 Four damage cases using DI-I method.....250
Figure 7.42 Single damage cases using MDI-I method.....252
Figure 7.43 Two damage cases using MDI-I method.....254

Figure 7.44 Three damage cases using MDI-I method. 256
Figure 7.45 Four damage cases using MDI-I method. 257
Figure 7.46 Single damage cases using DI-II method. 258
Figure 7.47 Two damage cases using DI-II method. 259
Figure 7.48 Three damage cases using DI-II method. 260
Figure 7.49 Four damage cases using DI-II method. 261
Figure 7.50 Single damage cases using MDI-II method. 262
Figure 7.51 Two damage cases using MDI-II method. 263
Figure 7.52 Three damage cases using MDI-II method. 264
Figure 7.53 Four damage cases using MDI-II method. 265
Figure 7.54 Estimation of damage severity using HMC method. 268
Figure 7.55 Comparison of simulated and predicted damage severity using HMC method. 270
Figure 7.56 Estimation of damage severity using MDI-II method. 272
Figure 7.57 Comparison of simulated and predicted damage severity using MDI-II method. 274
Figure 8.1 Geometric configurations of the laboratory timber bridge. 277
Figure 8.2 Specially designed pin support. 278
Figure 8.3 The laboratory timber bridge. 278
Figure 8.4 Plan view of damage locations and measurement locations for the bridge. 280
Figure 8.5 Side view of various inflicted damage. 281
Figure 8.6 Schematic diagram of modal tests on the laboratory timber bridge. 282
Figure 8.7 A typical FRF spectrum for the laboratory timber bridge. 284
Figure 8.8 Experimental 81-point mode shapes for the laboratory timber bridge. 285
Figure 8.9 Plan view of damage and measurement locations for a timber plate. 287
Figure 8.10 Support system used for the timber plate. 287
Figure 8.11 The laboratory timber plate. 288
Figure 8.12 Plan view of inflicted damage. 289
Figure 8.13 Experimental 45-point mode shapes for the plywood. 290
Figure 8.14 Change of frequency for the laboratory timber bridge. 292
Figure 8.15 Changes in damping ratios for the laboratory timber bridge. 294
Figure 8.16 A three damage scenario case for the bridge (g2Sg4Sg3S). 296
Figure 8.17 Single damage scenario case for the bridge (g2S). 297
Figure 8.18 Two damage scenario case for the bridge (g2Sg4S). 298

Figure 8.19 Single damage cases using DI-II-P method for bridge. 302
Figure 8.20 Two damage cases using DI-II-P method for bridge. 305
Figure 8.21 Three damage cases using DI-II-P method for bridge. 307
Figure 8.22 Four damage cases using DI-II-P method for bridge 310
Figure 8.23 Three damage case (L2(II)B-L3(IV)B-L3(VI)B) using DI-II-P method for plate. 313
Figure 8.24 Damage cases using DI-II-P method for plate 315
Figure 9.1 Single damage cases using MDI-I method (5 modes). 322
Figure 9.2 Two damage cases using MDI-I method (5 modes). 324
Figure 9.3 Three damage cases using MDI-I method (5 modes). 326
Figure 9.4 Four damage cases using MDI-I method (5 modes) 327
Figure 9.5 Single damage cases using MDI-II method (5 modes) 328
Figure 9.6 Two damage cases using MDI-II method (5 modes) 329
Figure 9.7 Three damage cases using MDI-II method. 330
Figure 9.8 Four damage cases using MDI-II method. 331
Figure 9.9 Estimation of damage severity using HMC method. 335
Figure 9.10 Estimation of damage severity using MDI-II method. 337
Figure 9.11 Single damage cases using DI-II-P method for bridge (9 modes) 343
Figure 9.12 Two damage cases using DI-II-P method for bridge (9 modes) 345
Figure 9.13 Three damage cases using DI-II-P method for bridge (9 modes) 347
Figure 9.14 Four damage cases using DI-II-P method for bridge 349
Figure 9.15 Damage cases using DI-II-P method for plate (6 modes) 353

LIST OF TABLES

Table 2.1 Problems faced by timber bridges due to degradation of wood..... 15
Table 3.1 Modulus of Elasticity for timber beams and plywood..... 58
Table 3.2 Details of screw connection test samples in all directions..... 61
Table 3.3 Pullout test results..... 64
Table 4.1 Description of mode shape..... 69
Table 4.2 Dimensions of inflicted damage..... 73
Table 4.3 Comparison of natural frequencies for FE model and modal tests for the Beam..... 75
Table 4.4 Mode shapes correlation between FE model and modal tests for the Beam... 76
Table 4.5 Dimensions of inflicted damage in plate..... 81
Table 4.6 Preliminary input values for element MATRIX27..... 88
Table 4.7 Natural frequency of different models..... 89
Table 4.8 Preliminary material properties for the shell-solid model..... 93
Table 4.9 Parametric study of element MATRIX27..... 94
Table 4.10 Natural frequencies corresponding to cases B1 to B8..... 94
Table 4.11 Parametric studies of orthotropic material of plywood..... 95
Table 4.12 Dynamic results of the parametric studies on orthotropic material for plywood..... 96
Table 4.13 Dynamic results of different boundary conditions..... 98
Table 4.14 MOE test results and other material properties for beams and plywood... 100
Table 4.15 Pullout test results and other physical property values..... 101
Table 4.16 Summary of the effects of key parameters on the advanced model..... 105
Table 4.17 Description of mode shapes extracted from the advanced FE model..... 106
Table 4.18 Comparison of natural frequencies: FE model vs experimental model..... 108
Table 4.19 Mode shapes correlation between FE and experimental models..... 109
Table 6.1 Damage scenarios for the finite element model of a timber beam..... 135
Table 6.2 Natural frequencies for finite element model of a timber beam..... 135
Table 6.3 Estimation of severity of damage using HMC method..... 170
Table 6.4 Estimation of severity of damage using MDI-II method..... 175
Table 6.5 Damage scenarios for the analytical model of a timber plate..... 180

Table 6.6 Natural frequencies for analytical model of a timber plate..... 183
Table 6.7 Damage scenarios for the analytical model of a laboratory timber bridge... 189
Table 6.8 Natural frequencies for the analytical model of a laboratory timber bridge. 192
Table 7.1 Dimensions of damage inflicted in timber beams..... 220
Table 7.2 Comparison of natural frequencies for Beam1. 231
Table 7.3 Comparison of natural frequencies for Beam2. 231
Table 7.4 Comparison of damping ratios for Beam1. 234
Table 7.5 Comparison of damping ratios for Beam2. 234
Table 7.6 Estimation of damage severity using HMC method. 269
Table 7.7 Estimation of damage severity using MDI-II method. 273
Table 8.1 Dimensions of inflicted damage in the bridge. 281
Table 8.2 Description of mode shapes for the laboratory timber bridge. 286
Table 8.3 Dimensions of inflicted damage in the plate..... 289
Table 8.4 Natural frequencies of the laboratory timber bridge. 292
Table 8.5 Damping ratios for the laboratory timber bridge. 293
Table 8.6 Natural frequencies for the plate. 311
Table 8.7 Damping ratios for the plate..... 312
Table 9.1 Dimensions of inflicted damage in timber beams..... 319
Table 9.2 Estimation of damage severity using HMC method. 333
Table 9.3 Estimation of damage severity using MDI-II method. 338
Table 9.4 Dimensions of inflicted damage in the bridge. 340
Table 9.5 Dimensions of inflicted damage in the plate..... 350

List of Notations

$\overline{\beta}_{ij}$	damage indicator for the modified DI methods
$\overline{\alpha}_j$	severity estimator of modified DI-II method for all j-th element
$\overline{\phi}_i''$	normalised curvature vector for undamaged state for modified DI methods
$\overline{Z}_j$	normalised $\overline{\beta}_{ij}$ into the standard normal space
ν	Poisson's ratio (Chapters 2 to 4)
$v(x)$	deflected shape (Chapter 5)
Φ	eigenvector matrix
Ω	eigenvalue matrix
Δ	Difference of S_u and S_d
ζ	damping ratio
υ (for DI-II-P)	Poisson's ratio of an isotropic plate (for Chapter 5)
ρ, DENS	density
$\mu_{\beta j}$	mean of β_j values for all j-th element
$\sigma_{\beta j}$	standard deviation of β_j values for all j-th element
$(\delta_j)_{max}$	maximum absolute value of elements δ_{ij}
(3.375m, 0.9m)	convention for damage at position of 3.375m along the span length and 0.9m across the width for laboratory timber bridge and timber plate
ω_{dk}	damped natural frequency of mode k
$(EI)_j$	Stiffness of j-th element
λ_i	square of ω_i or pole value for mode i
ω_i	circular frequency of mode i
ϕ_i	mode shape or eigenvector of mode i
(i modes)	i modes used in the damage detection algorithms
δ_{ij}	i-th column of Δ
β_{ij}	damage indicator for the DI methods

β_{ijk}	damage indicator for the DI-II-P method
α_j	severity estimator of DI-II method for all j-th element
δ_k	damping factor of mode k
ν_{LR}	Poisson's ratio of applied stress in longitudinal direction and accompanying lateral strain in radial direction
ν_{LT}	Poisson's ratio of applied stress in longitudinal direction and accompanying lateral strain in tangential direction
ν_{RL}	Poisson's ratio of applied stress in radial direction and accompanying lateral strain in longitudinal direction
ν_{RT}	Poisson's ratio of applied stress in radial direction and accompanying lateral strain in tangential direction
ν_{TL}	Poisson's ratio of applied stress in tangential direction and accompanying lateral strain in longitudinal direction
ν_{TR}	Poisson's ratio of applied stress in tangential direction and accompanying lateral strain in radial direction
σ_x	stress in x direction
ε_x	strain in x direction
*	denoting damaged case
1-D	one-dimensional
2-D	two-dimensional
2M4S5S6S	cumulative damage scenario of medium damage at 2/8 span, severe damage at 4/8, 5/8 and 6/8 span
3-D	three-dimensional
A (for damage)	small damage inflicted in timber plate
A (for DI-II-P)	area of the plate surface (for Chapter 5)
ADC	analogue-to-digital converter
B (for damage)	large damage inflicted in timber plate
c	damping coefficient
c_{cr}	critical damping coefficient
CIF	changes in flexibility
COMAC	coordinate modal assurance criterion
D (for DI-II-P)	flexural rigidity of a plate (for Chapter 5)
DD	damage detection

$Denom_{ij}$	denominator of β_{ij}
DFA	dynamic frequency analysis
DI	damage index
DI-I	damage index I
DI-I	damage index II
DI-II-P	damage index II method for plate-like structures
DOF	degree of freedom
DSP	digital signal processing
E, MOE	modulus of elasticity
EI	stiffness
E_L, E_R, E_T	MOE in directions of longitudinal, radial and tangential, respectively
EX, EY, EZ	MOE in global directions of X, Y and Z, respectively, for FE models
$f(\omega)$	input signal with respect to frequency ω
FE	finite element
FEA	finite element analysis
FEM	finite element model
FFT	fast Fourier transform
FIFO	file-input-file-output
F_{ij}	fractional modal strain energy for undamaged beam
f_{ij}	$\int_j \left(\frac{\partial^2 \phi_i}{\partial x^2}\right)^2 dx \Big/ \int_0^L \left(\frac{\partial^2 \phi_i}{\partial x^2}\right)^2 dx$, ratio of integrations for square second derivative of ϕ_i for j-th element of mode i and the overall structure
F_{ijk}	fractional modal strain energy of subregion jk for undamaged beam
f_{ijk}	$\frac{\int_{b_k}^{b_{k+1}} \int_{a_j}^{a_{j+1}} \left(\frac{\partial^2 \phi_i}{\partial x^2}\right)^2 + \left(\frac{\partial^2 \phi_i}{\partial y^2}\right)^2 + 2\upsilon \left(\frac{\partial^2 \phi_i}{\partial x^2}\right)\left(\frac{\partial^2 \phi_i}{\partial y^2}\right) + 2(1-\upsilon)\left(\frac{\partial^2 \phi_i}{\partial x \partial y}\right)^2 dxdy}{\int_0^b \int_0^a \left(\frac{\partial^2 \phi_i}{\partial x^2}\right)^2 + \left(\frac{\partial^2 \phi_i}{\partial y^2}\right)^2 + 2\upsilon \left(\frac{\partial^2 \phi_i}{\partial x^2}\right)\left(\frac{\partial^2 \phi_i}{\partial y^2}\right) + 2(1-\upsilon)\left(\frac{\partial^2 \phi_i}{\partial x \partial y}\right)^2 dxdy}$, ratio of integrations for second derivatives of ϕ_i for subregion jk of mode i and the overall structure

f_n	cyclic natural frequency
FRF	frequency response function
G	modulus of rigidity
$g(\omega)$	output signal with respect to frequency ω
g2Sg4Sg3Sg1M	cumulative damage scenario of medium damage at 1/8 span of girder 1, severe damage at 6/8 span of girder 2, 4/8 span of girder 4 and 2/8 span of girder 3
$G_{ff}(\omega)$	output auto-spectrum with respect to frequency ω
$G_{fg}(\omega)$	cross input-output spectrum with respect to frequency ω
gi	girder no. i
G_{LR}	G in longitudinal-radial plane
G_{LT}	G in longitudinal-tangential plane
G_{RT}	G in radial-tangential plane
GXY	shear modulus in XY plane for FE models
GXZ	shear modulus in XZ plane for FE models
GYZ	shear modulus in YZ plane for FE models
h	height
H_{ij}	FRF between the response of DOF i and reference DOF j
HMC	hybrid of MDI-I and CIF
HOT	higher order terms
I	moment of inertia
i, n	mode number
K	stiffness matrix
KX, kx	Stiffness of rigid link simulating screw connections in local x direction for laboratory timber bridge FE models
KY, ky	Stiffness of rigid link simulating screw connections in local y direction for laboratory timber bridge FE models
KZ, kz	Stiffness of rigid link simulating screw connections in local z direction for laboratory timber bridge FE models
L (for damage)	light damage for timber beam and laboratory timber bridge
L (for wood)	longitudinal direction
L, l, L (for measurement)	span length

L2(II)B-L3(IV)B-L3(V)A	cumulative damage scenario of small damage at location V of Line 3, large damage at location II of Line 2 and location IV of Line 3
L_b	length of timber beam
Li	Line no. i
L_p	length of plywood
LSCE	least square complex exponential
LVDT	displacement transducer
M	mass matrix
m	mass per unit length
M (for damage)	medium damage for timber beam and laboratory timber bridge
MAC	modal assurance criterion
MACerror	MAC error between FE and experimental models
MDI-I	modified damage index I
MDI-II	modified damage index II
MDOF	multiple degree of freedom
mi	mode no. i
MIMO	multiple-input-multiple-output
MSE	modal strain energy
NDE	nondestructive evaluation
NDE	nondestructive testing
NFerror	natural frequency difference between FE and experimental models
NM, N	number of modes
Num_{ij}	numerator of β_{ij}
NUXY, NUXZ, NUYZ	Poisson's ratio in planes of XY, XZ and YZ, respectively, for FE models
N_x, N_y	subdivision in the directions of x and y
OF	objective function
P (for damage)	light damage for FE models of isotropic and orthotropic plates
q	an arbitrary distributed load

Q (for damage)	medium damage for FE models of isotropic and orthotropic plates
R (for damage)	severe damage for FE models of isotropic and orthotropic plates
R (for wood)	radial direction
r_{ijk}	residual value for mode k
S	stiffness matrix (Chapters 2 to 4) flexibility matrix (Chapter 5)
S (for damage)	severe damage for timber beam and laboratory timber bridge
S_d	damaged flexibility (for Chapter 5)
SDOF	single degree of freedom
SIMO	single-input-multiple-output
S_u	undamaged flexibility (for Chapter 5)
SX	Stiffness of rigid link simulating supports in global X direction for laboratory timber bridge FE models
SY	Stiffness of rigid link simulating supports in global Y direction for laboratory timber bridge FE models
SZ	Stiffness of rigid link simulating supports in global Z direction for laboratory timber bridge FE models
t (for DI-II-P)	thickness of a plate (for Chapter 5)
T (for wood)	tangential direction
T_b	thickness of timber beam
T_p	thickness of plywood
U	strain energy
U_i	modal strain energy of mode i
U_{ij}	modal strain energy of j-th element for mode i
W_b	width of timber beam
W_p	width of plywood
X	direction along the width of laboratory timber bridge
X_{Mr}	peak amplitude for half-power bandwidth method
Y	direction along the length of laboratory timber bridge
Z	out-of-plane direction of laboratory timber bridge

Z_j	normalised β_{ij} into the standard normal space

Chapter 1

Introduction

1.1 General

Timber bridges have been widely built and used in Australia since 1788 (Walter 1996). The importance of timber bridges has been cited in the local government NOLG 2002-2003 publication (Department of Transport and Regional Services 2003), stating that Australian local governments have about 29,000 timber bridges still in service. However, many of these bridges are old, some with functional deficiency. About half of these bridges are subject to increasing traffic loads and intensity. Risk management techniques consider these bridges to be unsafe if their structural "health" and load carrying capacity is unknown. The partial collapse of a timber bridge in Singleton Shire, New South Wales, resulting in injury to the driver and damage to the heavy vehicles is a vivid example of failure to detect degraded girders. Such an incident is avoidable if the condition of the bridge is properly inspected and monitored. Therefore, assessing the condition and safety of timber bridges has now become essential for asset managers in order to protect human life and maintain community assets.

Since assessment and evaluation of timber bridges are crucial, it is important, first of all, to understand the structural mechanics of a timber bridge system and how it behaves under different load events. As mentioned by Benitez and Li (2002) timber bridges in Australia are constructed mainly as girder-deck systems (see Figure 1.1). Round timber logs of local hardwood species act as girders with one or two layers of timber decking; with the primary decking laid transversely to the girders and where used, running boards running parallel to the girders. Lag bolts are normally used to connect the deck to the girders, which are responsible for the load transfer between the deck and girders. It is also important to understand the effects of changes in material or member properties that occur as a consequence of degradation due to both biological and mechanical means.



Figure 1.1 Typical timber girder bridge in Australia.

This is normally achieved by using conventional visual inspection, but where more detailed condition assessment is required, load testing of some sort is usually undertaken. This can be supplemented by "desk top" analysis, including three dimensional (3-D) finite element (FE) modelling as an effective way to model the behaviour of timber bridges statically and dynamically (Li et al. 2005; Wang et al. 2005). The current "state of the art" load assessment technology for bridges in Australia utilises what is known as dynamic frequency analysis (DFA), developed by Samali et al. (2000). This technique determines the global stiffness using a modal analysis method and converts this to girder strength utilising a probabilistic strength model that has been derived from an extensive program of experimental work (Crews et al. 2004). The next generation of this technology focuses on using modal based damage identification techniques to detect damage in timber structures at an early stage in their development. This study is part of the development looking into using global nondestructive evaluation (NDE) to identify localised damage and/or defects with single and multiple damage scenarios for timber structures in particular timber bridges.

As mentioned earlier, many of timber bridges in Australia are often exposed to various forms of damage, which included those caused by traffic overloads and harsh environmental conditions. This damage, in turn, may lead to a compromise on structural integrity that is detrimental to the structures and safety of the users. It is therefore appropriate to use the science and art of determining the state of health of the structures without impairing them. Nondestructive evaluation (NDE) is one of the tools

that are useful for this purpose. A variety of inspection techniques have been used in the field of NDE for timber, such as visual inspection, stress wave, ultrasonic, drill resistance, radiography, microwave/ground penetrating radar and vibration analysis (Emerson et al. 1998). Most of these methods work well in small areas to identify localised damage and the evaluation of the entire structure using these methods can be very time consuming, costly and inefficient. Thus, in this study, it is desirable to explore method(s) of nondestructive testing (NDT) for timber structures that can identify damage or decay from a global perspective.

In the light of current developments in bridge structures, damage detection using dynamic approach has gained much attention (Farrar et al. 1994). This has created opportunities for global NDE of timber structures using a dynamic approach (Morison et al. 2002, 2003). Among various methods, modal based methods developed by Stubbs, Kim and associates (Jeong-Tae Kim & Stubbs 1995; Stubbs, Kim & Farrar 1995) based on changes in modal strain energy as an indicator of localised damage or stiffness loss in a structure has shown great potential. In the literatures, the method developed by Stubbs, Kim and associates (Jeong-Tae Kim & Stubbs 1995; Stubbs, Kim & Farrar 1995) is often referred to as the damage index (DI) method. The method was developed for application to a wide range of structural systems. An improved version of the DI method was published by Kim & Stubbs (2002), which was shown to be better than the previous methods for single damage location. Many applications of damage detection methods including the DI methods were used in steel and concrete structures. Few studies have been carried out on timber beams and timber bridges (Peterson, McLean & Pollock 2003; Peterson et al. 2001a, 2001b) in which the method of damage localisation using the DI methods was applied. The studies showed that the DI method successfully detected and located the inflicted damage for single damage location cases.

In this study, numerical and experimental investigation for timber beams were employed to study the capabilities and limitations of using two DI methods based one-dimensional (1-D) beam theory (Jeong-Tae Kim & Stubbs 1995; Stubbs, Kim & Farrar 1995) and their modified DI methods proposed by the author as well as changes in flexibility (CIF) method (Pandey & Biswas 1994) for locating damage in timber, especially multiple damage scenarios. The first two methods are named "DI-I" and "DI-II", while "MDI-I" and "MDI-II" denote the following two methods, throughout this study. It should be noted that the CIF method was used in the numerical study but not in the experimental study for beam-like structures. The numerical model of a timber beam

has been developed using finite element analysis (FEA). Corresponding to the numerical model, two timber beams have been used and tested in the laboratory to provide data for verification of the methods in real structures. The MDI methods were found to perform better than their original formulae as well as the CIF method in detecting damage especially for multiple damage scenarios.

Further to the damage localisation using the one-dimensional damage index (DI), modified damage index (MDI) methods and changes in flexibility (CIF) method, work was extended to quantify the severity of inflicted damage using the MDI methods. Due to the formulation of the MDI-I method that forbids a meaningful quantification of severity of damage, a hybrid method between MDI-I and CIF methods, designated as HMC, was proposed. With a few simple calibration steps, the HMC method was shown to be able to provide some meaningful results for severity of damage in terms of loss of 'I' (moment of inertia). Nevertheless, a weighting factor was required to enhance the accuracy of the HMC method to quantify the damage. The MDI-II method was further manipulated in its formulae, which also provides some meaningful results for severity of damage in terms of loss of 'I' (moment of inertia) using a weighting factor as well. These two methods for quantifying severity of damage were comparable.

The full experimental damage detection tests on a laboratory timber bridge employing experimental modal analysis have been carried out as the subsequent stage of work after the beam. Accompanying with the experimental work, the laboratory timber bridge was studied numerically using FEA. For the bridge, only the DI-II method for plate-like structures, which adopts two-dimensional (2-D) plate theory for detecting location of single and multiple damage scenarios was used. The DI-II method for plate-like structures, denoted DI-II-P method, was able to detect quite well single and multiple damage scenarios, especially for severe damage.

The process of establishing a reasonable and reliable finite element (FE) model of a laboratory timber bridge was carried out systematically. A preliminary FE model was first established based on dynamic similitude of typical short-span timber bridges. Experimental tests to quantify timber material and geometrical properties were undertaken. An advanced FE model was then evolved from the nominal model with more comprehensive features, such as simulating the outcomes of the test results. A pin-pin supported one-span laboratory timber bridge was fabricated to simulate real timber bridges in terms of their fundamental frequency and experimental modal tests were performed in a laboratory environment to study the bridge's dynamic behaviour. The

advanced FE model was then calibrated with the experimental modal data to produce an FE model for the study of damage detection in this thesis with potential application in actual load rating.

As a complimentary work on the laboratory timber bridge, a timber plate was studied numerically and experimentally. Even though it is rare to have plate-type timber bridges, it is worth checking the DI-II-P method with inflicted damage on a timber plate.

1.2 Objectives of the Study

The principal objective of the study described in this thesis is to investigate the application of modal based damage detection methods, particularly the damage index methods, to detect damage in timber bridges. The details of the work are:

1. To adopt and utilise existing damage index (DI) methods for detecting location of damage in timber beams, numerically, using a finite element model with single and multiple damage scenarios.
2. To adopt and utilise an existing flexibility method for detecting location of damage in timber beams, numerically, using a finite element model only with single and multiple damage scenarios.
3. To modify the damage index methods in order to detect location of damage better than their original formulae, numerically, particularly for multiple damage scenarios in timber beams (i.e. developing the MDI methods).
4. To utilise and extend the modified damage index (MDI) methods to quantify severity of damage in terms of loss of 'I' (moment of inertia).
5. To study the capabilities and limitations of different numerical integration techniques and mode shape reconstruction techniques.
6. To validate the damage detection results for the finite element of a timber beam using experimental modal analysis with two pin-pin supported timber beams inflicted with single and multiple damage scenarios.
7. To adopt and utilise existing damage index II (DI-II) method for plate-like structures (DI-II-P) for detecting location of damage in a laboratory timber bridge, numerically, using a finite element model with single and multiple damage scenarios.

8. To verify the applicability of the analytical model of the laboratory timber bridge by updating the finite element model using modal parameters (natural frequencies and mode shapes).
9. To validate the damage detection results for the finite element model using experimental modal analysis with a pin-pin supported laboratory timber bridge inflicted with single and multiple damage scenarios using the DI-II-P method.
10. To compliment damage detection work on the laboratory timber bridge with a timber plate model, numerically and experimentally, with single and multiple damage scenarios.

1.3 Scope of the Work

This study is concerned with the damage detection in timber bridges, typically short span timber girder/beam bridges in Australia. The damage considered here is of localised defects such as rot in timber bridges. Global damage in timber bridges is not included in the scope of this study. In the light of complexity of a bridge structural system, the work started with a simpler structural system, that is, a timber beam, which is representative of girders in a bridge. An analytical model was developed using finite element analysis (FEA) for a timber beam adopting material properties of radiata pine sawn timber. Localised damage was inflicted by removing sections of the beam starting from the soffit at single and multiple locations. Employing modal parameters (natural frequency and mode shape) obtained from the finite element (FE) model, modal based damage detection methods such as damage index (DI) methods and changes in flexibility (CIF) method were adopted to detect damage location for single and multiple damage scenarios. The DI methods were modified to improve the capability to locate damage compared to its original formulae and they are named modified damage index (MDI) methods. Extending algorithms of the MDI methods, determining the severity of damage in terms of loss of 'I' (moment of inertia) was enabled. Comparison between the DI, CIF and MDI methods was made using various single and multiple damage scenarios.

Experimental modal analysis was conducted on two radiata pine timber beams before and after the beam was inflicted with various damage scenarios. The data acquisition technique implemented in this study was transfer function method (TFF).

This technique is adopted to obtain modal data from the undamaged and damaged beams. By comparing the data obtained, the effect of inflicted damage such as rot on the modal parameters (natural frequencies, damping ratio, mode shapes and their derivatives) can be studied and investigated. The modal data was compared by employing the DI and MDI methods.

Subsequent to the timber beam, the study investigated, numerically and experimentally, damage localisation for a laboratory timber bridge. An analytical model of a laboratory timber bridge was developed using FEA. Since a bridge system is complex, various elements were used to model the girders, deck and connections between them. The laboratory timber bridge FE model was updated with the experimental modal data such as natural frequency and mode shape as well as the actual material properties of the structural elements. Using the updated bridge model, modal data for the undamaged and damaged state of the laboratory timber bridge was acquired to perform damage localisation using an existing damage index method for plate-like structures (DI-II-P). Various single and multiple damage scenarios were inflicted on the model by removing sections from the girders starting from the soffit. Experimental modal analysis was utilised to obtain modal data before and after damage for the laboratory timber bridge. Employing the modal data in the DI-II-P method, damage localisation was carried out to investigate capabilities and limitations of the method. Evaluation of severity of damage for the laboratory timber bridge is not included in the scope of work of this study.

As a complimentary work, the work on the laboratory timber bridge was applied to a timber plate. Numerical and experimental investigation on the timber plate was carried out for locating damage with single and multiple damage scenarios.

1.4 Contribution to Knowledge

The principal contribution of this study was to develop and apply modal based damage detection methods to detect damage in timber bridges. The original contributions of the thesis include:

1. From literature review (Chapter 2), it is clear that there are very few works reported on using modal based damage detection methods to detect and evaluate damage in timber structures, especially timber bridges in Australia. Therefore, in this study, existing damage index (DI) methods based on modal strain energy were adopted for damage detection in a timber beam (representing a single girder of a timber bridge), a laboratory timber bridge (representing a real timber bridge) and a timber plate (a complementary work). In addition, changes in flexibility (CIF) method was also adopted for damage detection in timber beam only.
2. A modified version of the DI methods was developed in order to detect location of damage better than its original formulae. The modification of the algorithm involved normalising mode shape curvature of each considered mode with respect to the maximum curvature value of the corresponding mode for one-dimensional (1-D) beam structures. The advantage of normalising the mode shape curvature is that non-normalised curvature would underestimate the contribution of lower modes in the algorithm when only a few modes are considered. In other words, the summation of non-normalised mode shape curvature will distort the damage index in favour of higher modes, which may result in false damage detection. To the best knowledge of the author, normalisation of mode shape curvature used in the modified damage index (MDI) methods based on modal strain energy has not been reported earlier.
3. The modified damage index (MDI) methods were further extended for evaluating severity of damage. Based on the modified damage index I (DI-I) and changes of flexibility (CIF) methods, a hybrid method, denoted HMC, was developed for estimating damage severity in terms of loss of 'I' (moment of inertia). In addition, further manipulation of the MDI-II algorithm also provides estimation of severity of damage in terms of loss of 'I'.
4. The effectiveness of the damage detection methods, introduced above, is closely related to the number of elements of the structure or components. The number of

elements to be used for damage detection is dictated by the number of sensors used for measurement. In order to produce reliable and accurate results, a relatively large number of sensors are required to produce the fine coordinates of the mode shapes. In the numerical simulation, the coordinates can be controlled by mesh density. However, in the experimental testing, the evaluation of the coordinates of the mode shape vectors is limited by the number of sensors used in the testing which is often far less than what is desired. To overcome this limitation, some techniques for reconstructing mode shapes, to increase the number of coordinates, are proposed. In this study, cubic spline was used for reconstruction of the mode shapes. The measured mode shape coordinates can be interpolated using this technique to generate mode shape vectors of greater length. A discussion on the advantage of using cubic spline compared to Shannon Sampling Theorem, which is more popular in use, is also presented.

5. An investigation was also carried out to study the capabilities and limitations of using different numerical integration techniques in the damage detection methods. To perform the integration, two commonly used methods were adopted, namely the rectangular rule and the trapezoidal rule. It is important to note that the outcomes of damage detection using any numerical integration technique will heavily rely on the ability of the technique to reveal the damage location and not the accuracy of the value produced.
6. The study was intended to locate and evaluate damage in multiple damage locations on the timber beam, laboratory timber bridge and timber plate. The damage cases began with single damage location up to maximum of four damage locations, which also consist of three different levels of damage. The coverage of the inflicted damage scenarios is considered quite thorough to examine the robustness of the damage detection methods.
7. A more refined finite element model was developed to represent the laboratory timber bridge, which may find application in modelling a real timber bridge in the future. This has been enabled by utilising different elements such as solid, shell and link to simulate different parts of the laboratory timber bridge such as girders, deck and screw connections, respectively. In addition, the support condition was also modelled using link elements to simulate the actual support. The material properties of the girders (timber beam), deck (structural plywood) and screw connection were obtained from material testing of small test samples.

8. The FE model of the laboratory timber bridge was updated using modal data (natural frequency and mode shape) obtained from experimental modal analysis. Correlation analysis was employed to examine quantitatively and qualitatively the differences between the FE and experimental models using a global objective function.
9. To validate the methods developed and adopted for damage detection, an extensive experimental program was undertaken on two timber beams, a laboratory timber bridge and a timber plate. Experimental modal analysis was carried out on the test samples to obtain modal parameters (natural frequency, damping ratio and mode shape) to be used in the damage detection methods.
10. For the laboratory timber bridge, the damage index (DI) method for plate-like structures using two-dimensional (2-D) plate theory was adopted for damage localisation and designated as DI-II-P in this study. Higher modes were utilised in the DI-II-P method to locate single and multiple damage scenarios. To the best knowledge of the author, there is no previous work done to adopt and apply the two-dimensional damage index method to timber bridges.
11. A complimentary work to the laboratory timber bridge was extended to a timber plate, numerically and experimentally.

1.5 Organisation of the Thesis

In Chapter 1, an introduction to the work and an overview of the objectives of the study, scope of the work and contribution to knowledge is given.

In Chapter 2, a literature review is undertaken on a brief history of timber bridges in Australia and application of different damage detection methods used in timber bridges. It also covers a general review of damage detection methods, mainly focusing on modal based damage detection methods.

In Chapter 3, a general description of the material properties of wood/timber is presented. It also covers some aspects pertaining to variability in wood that makes it a unique construction material, unlike others, whereby its structural performance is not easily defined. Material testing pertaining to timber beams, structural plywood and screw connections are documented in this chapter.

In Chapter 4, the process of developing finite element models that can represent well the real structures, such as timber beam, laboratory timber bridge and timber plate, is shown.

In Chapter 5, a detailed derivation of the damage detection methods adopted and modified in this study is presented.

In Chapter 6, damage detection results from the finite element model of a timber beam using different damage detection methods are presented. This chapter also shows the comparison of using different numerical integration techniques for damage detection purposes. Also, damage detection results from the finite element model of a laboratory timber bridge using different damage detection methods are presented. This chapter also shows the supplementary work on detecting damage in a timber plate numerically.

In Chapter 7, an overview of the tests utilising experimental modal analysis on timber beams is given. Different damage scenarios are discussed and the proposed damage detection methods are used to identify and evaluate damage. The comparison of using different mode shape reconstruction techniques for damage detection purposes is included in this chapter.

In Chapter 8, brief discussions on experimental modal analysis of the laboratory timber bridge and timber plate are provided. Different damage scenarios are discussed and proposed damage detection methods are used to identify and evaluate damage. The comparison of data reconstructed using two-dimensional cubic spline and 'as is' data for damage detection purposes is included in this chapter.

In Chapter 9, validations between the numerical and experimental damage detection results are presented for the timber beam, laboratory timber bridge and timber plate.

In Chapter 10, conclusions and recommendations for future research are presented.

Chapter 2

Literature Review

2.1 Introduction

This chapter introduces background of timber bridges in Australia, followed by problems faced and ways that are available to overcome them. It continues with some general aspects of condition assessment of timber bridges including assessment of timber bridges using dynamic approach. Dynamic methods for damage detection are becoming more popular with new applications to timber bridges. As such, an overview of damage detection is introduced. To sum up this chapter, the emerging needs for research are also included.

2.2 Timber Bridges in Australia

2.2.1 Background

Historically, timber was the primary material for bridges, in the form of fallen tree trunks across streams. These structures, namely timber bridges, were the principal structures of the road and railway network of land transport in the late 18^{th} to early 20^{th} centuries in New South Wales, Australia. The earliest recorded timber bridge built in Australia was the Bridge Street bridge over the Tank Stream in Sydney constructed in 1788 (Walter 1996). Since then, timber bridges have contributed significantly to the development of the country until they were slowly replaced by iron, steel and concrete in early 20^{th} century. Besides serving as means for transportation, timber bridges, nowadays also have significant heritage values. According to the Department of Transport and Regional Services Australia (DOTARS) (2003), there are approximately 29,000 timber bridges in Australia, many are still in service. The enormous number of timber bridges, which form a significant portion of bridge assets, reflects the importance of these structures to the country's economic growth and the daily life of Australians.

There are two main categories of older timber bridges in Australia: that is, timber beam bridges and timber truss bridges. Timber beam bridges are deck-girder

systems commonly used in older timber bridges that were nail-laminated or bolt-laminated using lag bolts to assemble nominal size planks placed transversely to the supporting stringers or girders (square or round logs). In many instances, a second layer of longitudinal running planks was found atop the laminated deck to add strength and serve as a wearing surface. These bridges were the most common type of road bridges before World War II and before prestressed concrete was introduced as reported by the Roads and Traffic Authority of New South Wales (RTA 2006). Figure 2.1 shows photographs of typical timber beam bridges and their structural details. Indeed, short span timber beam bridges are the main focus of this study since they are found extensively in the rural areas throughout Australia.



(a) A typical timber bridge.



(b) Corbel at top of trestle.



(c) First layer of cross planks on the girders.



(d) Second layer of longitudinal planks.

Figure 2.1 Structural details of typical timber beam bridges in NSW.

Timber truss bridges are generally considered as an American innovation. This type of bridges was used in early to mid 19th century to overcome the span requirements (RTA 2006; Walter 1996). As recorded by the RTA of NSW (2006), the slower and

lighter road traffic could do with timber bridges (mostly 10 m (30-foot) span timber beam bridges and timber truss spans up to 27 m (90 feet)). The focus of this study is not on timber truss bridges, thus it is not discussed further. The interested reader is referred to (RTA 2006) for more information.

For modern timber bridges, many advances in technologies have contributed to their evolution. Most notable have been the development and refinement of wood preservatives and the use of structural glue-laminated timber (glulam), stress-laminating and structural composite lumber. Since the focus of this study is not on new technologies of timber bridges, it is not discussed further. The interested reader is referred to (Duwadi & Ritter 1997) for more information.

2.2.2 Problems Faced

In light of the long history of timber bridges in Australia, DOTARS (2003) has estimated that a third of them are in excess of 50 years old and some of these bridges are functionally obsolete and are structurally deficient. Due to their age and ill 'health' condition, it is necessary to perform periodic inspections on them to ensure the safety of people using these structures as well as to preserve these heritage-valued structures of the country (McInnes 2005).

Timber bridges are naturally made of timber/wood. Wood is a combination of polymers that are formed in the tree and subjected to deterioration by a variety of agents. In general, wood deterioration is a process that adversely alters wood properties. Degradation of wood can become detrimental to a timber bridge and other timber structures. In broad terms, wood deterioration can be attributed to two primary causes that are biotic (living) and physical (nonliving) agents (Ritter 1990). According to Duwadi, Ritter and Cesa (2000), the problem of wood or timber deterioration is mainly due to biotic agents. Nevertheless, Benitez and Li (2002) highlighted that timber bridges in Australia, besides biotic degradation, are also subjected to continually increasing traffic loads (physical degrading agent for wood) and intensities often far exceeding their design limits, which may impart damage to the structure. In Australia, the degradation of wood in timber bridges has resulted in several problems as listed in Table 2.1 (Murray 2002).

Table 2.1 Problems faced by timber bridges due to degradation of wood.

No	Problem
1	Locally damaged running boards
2	Globally damaged running boards
3	Rotted corbels
4	Deteriorated girders
5	Rotted or split pier piles
6	Rotted guardrail
7	Rotted or missing abutment retaining wall boards

2.2.2.1 Biotic Degradation of Wood

There are two primary biotic degradation of wood namely decay (or rot) and insect attack (Bootle 1985). Decay or rot is usually caused by organisms that attack wood including bacteria and fungi. These organisms live on wood. Under favourable conditions of moisture and temperature, and in the presence of oxygen, they attack wood. They use wood as their food source where the sugar and starches are being digested. It is well understood that wood will decay above 30% moisture content (Morris & Winandy 2002) and will not decay below 20% or when saturated with water (Bootle 1985). Moisture content between 20% and 30% is a grey area. At 20% moisture content, majority of wood will be air-dried and this may well have become infected with fungi during the drying process. Meanwhile, decay produces water, so it is more difficult to stop than it is to prevent it from starting. Decay will cause rapid loss in strength of wood ((Curling, Clausen & Winandy 2000) and (Winandy & Morrel 1993) in (Morris & Winandy 2002)).

Insect attack happens in wood because many insects use the foliage of trees as a source of food or shelter. Insect attack is generally obvious from tunnels and cavities in the wood whereby wood powders and frass (insect feces) are visible. Among them, the two major destroyers of wood are termites and borers (Bootle 1985). Termites are of common occurrence as scavengers of wood in all parts of Australia. There are many different types of termite. Some attack only the living trees and others exist in timber structures such as timber bridges and buildings. Termite attack is basically a series of excavated galleries with connecting wood tissues to maintain the general shape of the wood member and having external entry points. Detection of this damage is often not easy because the shell of untouched wood remains until considerable damage is caused.

While for borers attack, the first essential identification is holes left by the borer. There are many types of beetle (borer) that are likely to lay their eggs in the bark or wood. Once the eggs are laid, the subsequent life cycles are larva or grub, pupa and adult beetle. It is the larva stage which does most of the boring and eating of wood but the exit holes are usually made by the escaping adult beetle. The presence of borer holes does not necessarily mean that active destruction is occurring. It should be noted that there are marine borers that attack timber structures located in salt or brackish water. The marine borer attack may cause severe damage.

2.2.2.2 Physical Degradation of Wood

As the needs for transportation systems change, the loading requirements and demands on the transportation infrastructure also change. According to DOTARS (2003), about half of the timber bridge stocks in Australia (14,152) are in use on heavy vehicles routes. This has resulted in increased number of timber bridges that are labelled structurally deficient or functionally obsolete since many of the bridges were built prior to present loading requirements. Many of these bridges are open to vehicular and railroad traffic but only at posted loading or reduced speed limits. In order to best use the existing bridge resource and/or schedule repair or replacement strategies, methods need to be developed to assess the actual condition of these structures. In United States of America, the railroad industry has been dealing with an increase in the number of bridges that do not fulfil present loading requirements (M.L. Peterson & Gutkowski 1999; Ritter, Wipf & Wood 1998) in contrast to the highway infrastructure where the vast majority of bridges are constructed of steel and concrete. The railroads possess a huge inventory of timber bridges. These railroad bridges are located on all types of routes; from highly travelled main transcontinental routes to seldom used short spur lines. In all these cases the timber bridges are aging and posing more demand on limited maintenance and repair budgets. The heavy traffic and competitive nature of railroads place further pressure on the timber railroad bridges. On the main lines, the cost of closing bridges for inspection is very high and should be avoided. In contrast, spur lines may not generate sufficient revenue to justify extensive inspection and evaluation expenditures.

Apart from the usual wear and tear due to frequent usage, the other physical factors that are likely to limit the life of wood are weathering and fire (Bootle 1985).

Weathering of wood is due to the affinity of wood for water. The surface layers readily absorb rain and dew, and expand in hot sun. A lowered humidity then forces this moisture out so the surface of unprotected wood is in a continual state of stress. Slow erosion of the surface is also promoted by oxidative degradation caused by the ultra-violet radiation in sunlight and by the softening caused by "soft rot" fungi which can attack an uncoated surface. With respect to fire, wood is usually ignited at 350°C to 450°C and its strength properties will be degraded slowly and not as abrupt as metal and concrete even though they have higher ignition temperatures.

2.2.3 Methods to Overcome Problems

Often the problems in wood/timber structures lie not in the effectiveness of preserving systems of the material itself but in not having the correct tools necessary to locate deterioration (Duwadi, Ritter & Cesa 2000). Thereby, it delays application of remedial treatments to prevent further degradation in the structures. The current-state-of-the-practice for condition assessment of timber bridges is through destructive and semidestructive means. A wide variety of techniques are being used to verify deterioration or rot in timber members (Ross, Brashaw & Wang 2006). Resistance drilling, probing and coring are all destructive or semidestructive methods that are utilised to assess deterioration or rot in in-service wood members.

On the other hand, nondestructive evaluation (NDE) is defined as the science of identifying physical and mechanical properties of a piece of material without altering its end-use capabilities (Ross & Pellerin 1994). Such evaluations need nondestructive testing (NDT) techniques to provide accurate information pertaining to the properties, performance or condition of the materials being tested. NDE for wood is slightly different from other homogeneous and isotropic materials such as plastics and ceramics. It requires measurements of how natural and environmentally induced irregularities interacting in a wood member to determine its mechanical properties. Visual inspection, sounding and stress wave or ultrasonic based techniques are common NDTs used either individually or in combination to non-destructively evaluate wood-based materials. However, these methods are mostly used on small and accessible areas, and they are time consuming to perform on large timber structures like timber bridges, thereby, it is costly. This led to the need for global methods that would be able to reduce testing time and hence reduce the cost involved and disruption to traffic flow. The

global methods, if necessary, can then combine with other more localised NDE methods for detailed evaluation if possible damage sites are identified.

Over the last few decades, many methods of structural integrity assessment for timber bridges (entire structural wood/timber system) have been developed. The development in research for in-situ NDE and NDT for decay detection and subsequent strength assessment are highlighted as one of the needs and goals for research in a workshop published by ASCE (Fridley 1998). Preceding to the ASCE workshop Ou and Weller (Ou & Weller 1986) also reported concerns on overlooked studies in inspection of timber bridges in early eighties. Proof load testing is one of the commonly used methods, but it has a number of deficiencies, including endangering the remaining strength of a tested bridge. Therefore, recently more work has been carried out to assess the in-service stiffness of timber structures like short-span timber bridges and floor systems within buildings using vibration techniques. A simple dynamic testing has been developed by Samali et al. (2000) to evaluate the stiffness and strength of in-service timber bridges. This dynamic method is generally tailored to be both easily performed and cost effective. In addition, the operators are not required to have high skills and can be easily trained on job to perform the dynamic timber testing. Application of vibration techniques for condition assessments in timber bridges were also found in works by Peterson et al. (2001a; 2001b), Peterson, McLean and Pollock (2003), Yang et al. (2002a), Morison et al. (2002; 2003), Hu at al. (2005a; 2005b), Hu and Afzal (2006a; 2006b), and Ross, Brashaw and Wang (2006).

In Australia, development of nondestructive evaluation (NDE) or nondestructive techniques (NDT) are generally divided into two major groups, that is, localised methods and global methods. For localised methods, nuclear densometer method and resistograph method have been used. The nuclear densometer is a real time density measuring system that produces a graph showing the net thickness of the timber section (Bale & Browne 2004). The work shows that change in thickness due to deterioration can be measured within the tested sections. Resistograph or resistance drilling method is a quasi static method that measures the resistance of the timber to the penetration of a small 1.4mm diameter drill bit. The method shows that with deterioration, the drill will penetrate deeper into the girder. The quantification of the damage is possible (Bale & Browne 2004; Wilkinson, Thambiratnam & Ferreira 2005). For the global methods group, as mentioned above, Samali et al. (2000) have developed a dynamic testing method to detect the global structural stiffness and strength of timber

bridges. The authors are progressively expanding the research work to detect the location of damage and evaluate damage severity.

2.2.4 Condition Assessment for Timber Bridges

Periodic condition assessment is important for assessing the condition of wood used in structures to determine the extent of deterioration so that degraded members may be replaced or repaired to avoid structural failure. An assessment is very important for structures in regions affected by catastrophic events like earthquake and cyclone. As suggested by Ross, Brashaw and Wang (2006), a structural condition assessment consists of the followings:

1) Storing data systematically and performing detailed analysis of the physical and mechanical properties of material in use;
2) assessing and evaluating the data collected; and
3) suggesting actions to be taken, based on evaluation of the collected data.

A wide variety of techniques are used to assess the condition of wood in timber bridges and some of them are discussed briefly below. The interested reader is referred to (Duwadi & Ritter 1997; Fu 1999; Ou & Weller 1986; Ross, Brashaw & Wang 2006; Ross & Pellerin 1994) for more information.

2.2.4.1 Visual Inspection

Visual inspection is one of the most widely used NDE methods for assessing timber bridges. The advantage of this method is its simplicity and speed in locating visible deterioration. The inspector is required to observe the structure for two groups of signs of actual and potential deterioration (Ou & Weller 1986). The first group includes signs of presence of decay such as fruiting bodies, abnormal surface shrinkage or sunken faces, and insect activity. The second group is to identify six conditions conducive to decay such as excessive wetting, rust strain, plant and moss growth, accumulation of soil, joint interface and water-catching seasoning checks. Visual inspection requires strong light and access to the deterioration prone sites. It is suitable for detecting intermediate or advanced surface decay, water damage, mechanical damage or failed members (Ross, Brashaw & Wang 2006). It cannot detect early decay,

when remedial treatment is most effective. In addition, visual inspection is less accurate for inspecting internal decay and areas that are not accessible.

2.2.4.2 Resistance Drilling

Resistance drilling is a semidestructive method that is used increasingly for assessing timber structures (Ross, Brashaw & Wang 2006). This method is an automated system using a mechanical drill system to measure the relative resistance (drilling torque) of the material as a rotating drill bit is driven into the wood at a constant speed. It produces a chart showing the relative resistance for each drill path. The resistance of each drill path can be correlated to the internal condition of structural members.

2.2.4.3 Sounding

Sounding is one of the most common nondestructive means to verify deterioration or rot in timber members (Duwadi, Ritter & Cesa 2000). A hammer is utilised to impact on a wood member and the sound produced is used to quantify the extent of deterioration. This technique requires expertise in differentiating the sound and it is always subjected to individual interpretation depending on the experience of the inspector. The test is more suitable for small areas of suspected distress determined from other techniques, such as visual inspection or vibration techniques.

2.2.4.4 Stress Wave or Ultrasound Techniques

The one NDE technique that has been used more widely for inspecting wood members is stress-wave or ultrasound technology (Ou & Weller 1986). The stress wave transmission techniques are mostly used in decay detection of wood members. In principle, a stress wave travels faster through sound wood than it does through wood that is deteriorated. The transmission time is the parameter used to predict physical conditions inside the wood. It is useful for large timbers or glulam timbers larger than and same as 89 mm in thickness for which traditional hammer sounding is not effective. However, this method is limited by access to the structural members under consideration. Stress wave propagation method works well to detect localised decay in

timbers for a smaller region and the measurements should be made in-transverse paths (perpendicular to the grain). Parallel-to-grain travel paths (longitudinal direction) have also been proposed (M.L. Peterson & Gutkowski 1999). However, longitudinal wave can bypass regions of decay and therefore are not very effective. Furthermore, use of this technology remains limited because of a need for qualified personnel for equipment use and better data interpretation.

2.2.4.5 Proof Load Test

According to Fu (1999), proof load testing refers to a full scale examination for determining safe load carrying capacity of a structure. This method utilises a predetermined load being applied on a structure with the intention to envelope (with certain level of confidence) possible loads over the expected service life of the structure. In principle, if the structure responds elastically under the proof load, the structure is deemed to have passed the test and possess the required strength. In brief, a proof load test for a structure is usually a quasi static load applied with heavy trucks and placed in various positions to provide the best representation of the design loading. The advantage of this method is that it provides a direct measurement of the load carrying capacity of the tested bridge. However, its disadvantages are that proof load tests may overload the structure causing overstress and distress in the structure. This may be detrimental to the tested structures and endanger the safety of the users.

2.2.4.6 Vibration Techniques

Vibration techniques have received considerable attention as NDT techniques (Ross & Pellerin 1994). For timber structures, the focus of developments on vibration techniques has been on assessing the condition of wood in service based on techniques that evaluate individual members and small area defects within a wood member. For the past decades, work has been carried out using different vibration-based methods to evaluate deterioration in wood. The basis of vibration-based methods is that any changes in the physical properties of wood such as mass, damping and stiffness, will in turn alter its dynamic characteristics, namely, natural frequency, damping ratio and mode shape.

Peterson et al. (2001a; 2001b) reported adopting damage index method for one-dimensional (1-D) system that utilises modal strain energy before and after damage for identifying local damage and decay in timber beams using the first two flexural modes. They also mentioned that the mode shapes to be used in the damage localisation algorithm should be selected according to the location of damage. The method is quite promising for single damage scenarios but it does not work well for two damage scenarios in a timber beam. Furthermore, the results showed that the method is quite mode dependant. Similar work was extended to a laboratory timber bridge by Peterson, McLean and Pollock (2003) using the same damage localisation algorithm. The test showed that the method can detect well single damage locations. However, the results showed that using modes 4 and 5 were the most sensitive detect decay at the end of a girder. When cumulative damage was inflicted on another girder, modes 1, 2 and 3 were the most sensitive to the effects of the damage. This again implies that the method is mode dependant. In addition, the 1-D damage index method showed additional false positive indications of damage at girders where no damage was inflicted.

Morison et al. (2002) reported the possibility of extending global testing methods, specifically, impact testing, for determining if damage in the form of decay is present in timber bridges. The project also intended to provide cost and time savings over existing methods of inspecting timber bridges. The method is to correlate the first natural frequency (fundamental frequency) with stiffness characteristics of timber bridge stringers (girders) using an algorithm derived from a partial differential equation governing the transverse vibration of a simple flexural beam. However, the largest obstacles encountered in this study were the actual boundary conditions of a bridge in the field, which are difficult to determine. Similar effort was extended by Morison et al. (2003) investigating dynamic characteristics of timber bridges using several existing methods such as damage index derived from estimated and measured curvature and flexibility influence coefficient estimated by the direct current (DC) value of the frequency response function (FRF) matrix. The results showed that broadband curvature method was successful in showing a difference between the original state and the damaged state. However, it is far from a quantitative prediction of damage. While, the flexibility influence coefficient method is able to show a change in the system when a weaker stringer replaces an original stringer, it failed to identify which stringer was replaced. Similar work was reported by Wang et al. (2005)

Yang et al. (2002a; 2002b) reported the possibility of using the shapes of flexural vibration waves and curvature of the first mode to detect presence of defects and to determine their locations. However, the method required the study of damage pattern manually. It is essential for a damage detection algorithm to evaluate defects location and/or severity automatically using some form of damage detection algorithm. Furthermore, a damage detection algorithm must be suitable for multiple defects and/or forms of damage, and it should not be mode dependant.

A simple dynamic testing method, based on the Structural Frequency Shift (SFS), was developed by Samali et al. (2000; 2002; 2003; 2003) (also published in Benitez and Li (2002), Li et al. (2005)) to lower the cost and shorten the testing time. The method has been successfully used to undertake field-testing of more than 200 timber bridges across NSW. The testing procedure involves the attachment of accelerometers underneath the bridge girders and exciting the bridge with a modal hammer with and without extra mass blocks at mid-span of the bridge. In order to refine the method and to further reduce cost and testing time as well as evaluate some of the practical issues during the field testing, a project was initiated to investigate the effects of using alternative mass forms, such as use of a trailer to replace currently used mass blocks, and adding mass at locations other than mid-span, on the bridge vibrations and subsequent integrity assessment. The work required further investigation to be able to identify the location of damage.

Hu and Afzal (2006a) used a damage indicator for the detection of single and two damage cases of timber beams. The damage indicator is derived from the difference of the mode shapes before and after damage. The indicator is then expressed using discrete Laplace transform and finally normalised statistically in space. The method using either first or second modes, successfully identified single artificial defect at different locations and a two damage case with equal spacing and similar level of damage severity. However, the method is incapable of evaluating quantitatively the severity of damage. In addition, the method also found difficulty in generating higher mode shapes as well as the combination of first and second modes. The damage indicator was also sensitive to different damage locations and different modal orders. The results of this study were based on 43 impact points for each set of data from the modal tests and this may be too time consuming and hence not cost effective. Similar work by Hu and Afzal (2006b) was extended to using a wavelet transform to post-process the mode shape for damage pattern recognition. The results showed that using

the first or second modes, the wavelet coefficients are sufficiently sensitive for identifying single damage cases with different level of damage severity and a two damage case with equal spacing and similar level of damage severity. The wavelet coefficient method is less sensitive to modal orders. However, the capability to quantify the damage severity was not shown in the study.

2.2.5 Finite Element Modelling for Timber Bridges

For infrastructures, especially bridge structures, two-dimensional (2-D) grillage model is commonly used by engineers for design purposes. The grillage model is sufficient for sizing the structural members but insufficient to provide detailed modal information for vibration-based damage detection methods. As such, finite element (FE) modelling was adopted in this study to obtain relevant modal data for damage detection purposes.

FE modelling provides a complete set of analytical and theoretical modal parameters for a structure, which may have no closed-form solution. However, these parameters and outputs are not necessarily 100% accurate. The experimental data is also considered accurate to some extent, but usually incomplete and may have been affected by noise and interference. It is, therefore, relevant to validate the FE model with experimental data using any model updating methods. The updated FE model is considered "accurate" in representing a real test sample or structure. This model can subsequently be used as a test sample to demonstrate the performance of various damage detection algorithms with different damage scenarios.

There are quite a number of researchers that have used FE to model concrete and/or steel bridge structures. However, to the best knowledge of the author, there are few works found in the literature on modelling of timber bridges using finite element analysis (FEA) for the purpose of structural dynamic system identification and damage detection. Kurian (2000) has used FE model to study the static behaviour of timber bridge structures. The connection between the deck and joist/girder were of full-composite, where deck and joist/girder share the same connecting nodes. Duan (2003) utilised finite element analysis to characterise the dynamic behaviour of a laminated timber bridge. Several two-dimensional (2-D) and three-dimensional (3-D) models were developed using plastic analysis with different elements such as shell and beam as well as spring elements. The results showed that models with springs yield results closer to

the experimental data compared to the ones without spring. Since the work done on FE modelling of timber bridges is limited, the search extended to FE modelling of other timber structures such as work done by Gerber et al. (2005) (FE modelling of timber flooring). In the case of Gerber et al. (2005), they have utilised an arbitrarily element to model the connection between deck and joists, even then the connections were considered 100% composite. The results show that the FE model is capable to model, quite precisely, a timber structure validated with the static tests.

2.3 Damage Detection

The basic concept of damage detection can be defined as ways or methods that are able to capture the changes in structural characteristics due to damage or degradation. Many damage detection methods are categorised as global nondestructive evaluation (NDE) or nondestructive inspection (NDI) because they assess structures without removing any structural components and cause no harm to the integrity of the structures. The major scope of work for this study is to utilise and advance modal based damage detection methods. Modal based damage detection methods usually use changes in modal parameters, namely, natural frequency, modal damping, mode shape and their derivatives, for detecting and evaluating damage in a structural system. The changes are closely related to the changes in the corresponding physical properties such as mass, damping and stiffness. In broad terms, modal parameter changes occur due to damage in a structural system. In terms of physical properties, damage generally reduces mass and stiffness, and increases damping ratio.

As quoted in the review by Doebling at al. (1996), the report by Wang and Zong (2002) and the PhD thesis of Sánchez (2005), damage detection can be categorised into four levels as proposed by Rytter (1993) as follows:

Level 1: Determining the presence of damage.

Level 2: Finding the geometric location of the damage.

Level 3: Quantifying the severity of the damage.

Level 4: Predicting the remaining service life of the structure.

The damage detection at Levels 2 and 3 using modal based methods are the aim of this study.

2.3.1 Previous Literature Reviews and Surveys

For the past few decades, significant work has been done in the area of damage detection in structures using dynamic approaches. Many researches have been using the vibration of structures as means to highlight distress in structural systems. Many literature reviews and surveys on topics related to using vibration to detect damage have been conducted. As quoted by Farrar et al. (1994), Richardson (1980) has carried out a detailed survey of damage detection using modal changes. The survey has covered many literatures up to 1979, focusing on structural integrity monitoring of nuclear plants, large structures, rotating machinery and offshore platforms.

Since 1979, the later literature on damage detection especially application in bridges between 1980 and 1993 was reviewed by Farrar et al. (1994). The authors summarised that modal frequencies changes were primarily used for damage detection in some early works. However, frequency changes were found to be insufficient in some later research work. There was more attention paid to changes in mode shape, which is more sensitive to local changes. Damping changes have not been observed to be useful for damage detection in bridges. Some innovative ways to detect damage, such as pattern recognition and using frequency response function (FRF), were also mentioned in the review.

An extensive literature review covering the period 1968 to 1996 has been performed by Doebling et al. (1996). The review has covered a wide range of damage identification methods using different modal parameters and approaches. The focus of the review was on modal based damage detection methods. The modal based parameters included frequency changes, mode shape changes and its derivatives, flexibility changes and matrix updating. The authors also discussed some important areas such as nonlinear methods, intelligent system based methods and some comparative studies. Examples of the application of damage identification and health monitoring in structures were also given. In the review, the authors have highlighted major findings of the research work on damage detection using vibration measurements. The issues raised were many, e.g., identification methods dependence on prior or undamaged data, reliance on a linear structural model and required measurable excitation force. Few works attempted to address the significant of number and location of measured sensors.

Several other review papers that address damage identification and related issues have been published. Each one contains its own literature search and documentation of theory and their own scope of work. Farrar and Doebling (1997)

(1997) and Doebling at al. (1998) reported an overview of modal based damage identification methods. Salawu (1997) reviews the use of natural frequency to detect damages in a structure. This is because natural frequency can be easily acquired and it is considered by the author that natural frequencies are sensitive indicators of structural integrity. Bishop (1994) reviewed the types and the functions of neural networks. The author has demonstrated several usages of neural networks, one of them being to solve inverse problem for pattern recognition. This tool is powerful for damage identification in structures. A guide to the neural literature was also appended. Housener et al. (1997) have reported an extensive review of structural control from 80's to 90's. This review has included the state-of–the-art in structural health monitoring (SHM) indicating the importance of damage detection especially in civil structures. Zou, Tong and Steven (2000) reviewed online damage detection and health monitoring techniques for delamination damage on composite structures. Avitabile (2002) provided a summary of the developments on structural dynamic modification techniques for the past two decades, which is related to damage identification. The technique is useful for the study of structural changes of a system. A comprehensive review of new technical developments published between 1996 and 2001 in the discipline of structural health monitoring was done by Sohn et al. (2003). This review report summarised the state–of-the-art in SHM technologies and identified the need to advance the application of SHM. Carden and Fanning (2004) also presented a review on vibration based condition monitoring, emphasizing on articles published after 1996 till early 2002. This review can be considered an extension of the review done by Doebling et al. (1996).

There is also a rich source of damage identification methods coming from finite element model updating. Friswell and Mottershead (1995) reviewed extensively the articles and papers that fall into the category of finite element model updating such a matrix updating methods. Indeed, many methods that do not use matrix updating methods directly in damage identification, usually rely on a correlated or calibrated numerical model of the structure in its original state. An overview of fault detection using intelligent systems in systems and structures was presented by Worden and Dulieu-Barton (2004). The work encompasses taxonomy of the relevant concepts in damage detection, operational evaluation of a hierarchical damage identification scheme, sensor optimisation and data processing methodology based data fusion method.

In conducting the literature review for this study, the author decided to present the review in a few categories relevant to the focus of the research work or future developments of the work. The categories are similar to the ones proposed by Doeblings et al. (1996) and adopted by Carden and Fanning (2004), and are listed as follows:

Natural Frequency Based Methods

Mode Shape Based Methods

Mode Shape Curvature Based Methods

Strain Mode Shape Based Methods

Modal Strain Energy Based Methods

Flexibility Based Methods

Model Updating Methods

Frequency Response Function Based Methods

Artificial Intelligence Based Methods

Time Domain Methods

The review emphasized on papers and articles published after 2000. However, any articles and papers deemed relevant to the scope of this research prior to year 2000 were also included. Readers interested in the state-of–the-art in the damage detection area pre-2000 are referred to the reviews and surveys mentioned above.

2.3.2 Natural Frequency Based Methods

Natural frequency has been used in damage detection in the late 1970s and early 1980s particularly in aerospace and oil industries. Changes in natural frequencies, if any, were considered as classical damage indicators. This method, no doubt, has been the most widely used method and is still in use, particularly for structural health monitoring. The main reason for their great popularity is that natural frequencies are rather easy to determine with a relatively high level of confidence and only a single sensor is required in many applications. Furthermore, natural frequencies are sensitive to many kinds of damage, namely local and global. However, the drawback is that natural frequencies are easily affected by environmental changes such as fluctuations in temperature and humidity. This has created problems for detecting damage in real structures. Therefore, nowadays, natural frequencies are being coupled with other modal parameters in order to enhance their ability to detect damage. As mentioned earlier, Salawu (1997) has reviewed 65 articles on detecting damage using frequency changes.

Most of the early works using natural frequencies were based on simple structures and structural elements. One of the most popular papers quoted for using natural frequencies in damage detection is by Cawley and Adams (1979). This paper demonstrated analytically and experimentally that a single point in the structure can be used to detect, locate and quantify damage. The main idea behind the method is to use the ratio of frequencies in two modes as a function of the damage locations. Positions where this theoretically determined ratio equals the experimentally measured value are deemed possible damage sites. The loci for several pairs of modes may be superimposed and the actual damage site predicted by the intersection of the curves. This method was successfully applied to free-free carbon fibre reinforced polymer (CFRP) plates. The other objective of this study was to filter out the influence of temperature from the measured natural frequencies. However, Banks et al. (1996) presented a different opinion and stated that the prediction of damage, using natural frequencies, is dependent on geometry of the damage. For some types of damage, the method may be appropriate but for other configurations it may not be. A similar opinion was also expressed by Adam et al. (1978) (in Banks et al. (1996))

The popularity of using natural frequency changes for damage detection can be evidenced by the large number of publications in 1980s and 1990s, using small and simple structures with only single damage scenarios. Ju and Mimovich (1986; 1988) utilised the concept of frequency changes as a result of structural softening stemming from the presence of a set of cracks in a cantilever aluminium beam. A relative change of pre- and post-damage frequencies was utilised. The inverse problem can be used to diagnose the locations and intensity of cracks. The frequency variations of modes 2 and 3 were used in the diagnosis. Using the theoretical rigid end condition, the location of the crack damage or slit can be diagnosed with a small percentage of error (about 3 percent). However, comparing the experimentally determined intensities with the theoretical predictions, the error is significant. Ismail, Ibrahim and Martin (1990) investigated the effect of crack closure on the frequency changes of cracked cantilever beams numerically and experimentally. It was found that relying on the drop in the natural frequency alone, especially for the higher modes, may lead to serious underestimation of the crack severity. Nevertheless, the vibration testing method proved to be able to detect the presence and nature of the crack.

Hearn and Testa (1991) demonstrated dependence of natural frequencies and modal damping coefficient on deterioration in experiments conducted on a welded steel

frame exposed to fatigue loading and on wire ropes damaged by sawcuts. The magnitude of change in natural frequencies was utilised as an indication of the severity and of the location of deterioration in structures. In addition, ratios of changes in natural frequencies, normalised with respect to the largest frequency change, were used to indicate the location of deterioration. With single damage scenarios used in the experiments, frequencies dropped as the damage was induced. While using relative changes in frequencies, in conjunction with characteristic ratio ensembles, locating damage was successful. Hassiotis and Jeong (1995) presented an identification of localised reduction in stiffness of a structure using natural frequency measurements. A set of underdetermined equations, which minimise the element stiffness change, the norm of global stiffness change and eigenvalue residuals, were used to detect damage. Using a numerical ten-storey building, 10-90% stiffness reduction at a single location was detected. This was verified by an aluminium cantilever beam experimentally. Bicanic and Chen (1997) proposed a novel procedure utilising natural frequencies of original and damaged states of framed structures to generate a set of equations. The direct iteration techniques and Gauss-Newton least-square techniques were used to determine structural damage from the derived equations. With numerical examples of a grid, a plane frame and a composite structure, the procedure can be successful in predicting damage location as well as determining the extent of structural damage.

Vestroni and Capecchi (2000) formulated two methods for identifying concentrated damage in a vibrating beam or beam systems, using frequencies measured in the undamaged and damaged conditions. The models used were created by finite element analysis (FEA). The first method was modal equation procedure that employed an implicit expression in the eigenvalue using damage parameters of degree and location vectors of damage. The intersection of graphs produced with different natural frequency pairs indicated damage locations. It was found that the method can successfully identify single and dual damage scenarios. However, the discrepancies between experimental and identified frequencies from the FE model may not lead to satisfactory results. The second method, the response quantity procedure, is based on direct output comparison of natural frequencies between experimental and analytical values. A normalising term for the frequencies is introduced to produce a minimum function to identify damage locations. This method was found to identify well the single damage location by just using two modes rather than more modes. The reason is that with more modes, the measurement data may produce more experimental error. The

single damage detection was extended to a continuous three span beam system and results were satisfactory. However, this method did not demonstrate its applicability to multiple damage scenarios.

Friswell and Motterhead (2001) made some very useful observations on selecting appropriate range of natural frequencies to detect damage. The authors reported that the range of frequencies employed in locating damage location has a great influence on the resolution of the results as well as the range of applications. For low frequencies and their corresponding global modes, the vibration sensors may be mounted away from the damage site. And fewer sensors may be used to detect damage successfully. Nonetheless, the problem with low frequency modes is that the spatial wavelength of the modes is large and is typically larger than the extent of the damage. A significant change between two adjacent potential damage sites may be required in order to identify the damage. This means for low frequency modes the spatial wavelength of the mode plays an important role in damage detection.

Palacz and Krawczuk (2002) have examined the sensitivity of different damage indicators with two of them being methods based on changes in natural frequency proposed by Cawley and Adams (1979) (C-A) criterion as mentioned earlier and damage location assurance criterion (DLAC) by Messina, Jones and Williams (1996). The DLAC criterion uses the experimental frequency change vector and the theoretical frequency change for detecting damage. The formulation is similar to modal assurance criterion (MAC). DLAC values close to 0 indicate no correlation while 1 indicates an exact match between the patterns of frequency changes. The location giving the highest DLAC value determines the predicted damage site. From the results of applying the C-A criterion, measuring more frequencies would give a better damage location prediction. Nevertheless, with only two natural frequencies with no measurement errors, locating damage is possible. While for the DLAC criterion, similar findings were confirmed, that is, using more frequencies would yield a better damage location prediction. Comparatively, the DLAC method has a greater chance of overestimating the damage location in comparison with the C-A method. Both methods are very sensitive to even very small frequency measurement errors (0.1%).

Kim et al. (2003) utilised a frequency based damage detection (FBDD) method to locate damage and estimate the damage size. The FBDD method is based on the ratio of fractional change in eigenvalue due to damage and fractional of modal energy (sensitivity). The two fractional ratios were used to form a single damage indicator that

would predict location of damage using a localisation error norm. Damage is located when the single damage indicator approaches its peak. To determine size of damage, an algorithm based on Euler-Bernoulli beam theory was developed using the relationship between fractional changes in modal strain energy and fractional changes in frequency. Next, the change in the modal strain energy, due to crack, could be correlated with the energy loss rate. Eventually, this will lead to a relationship between crack depth and fractional change in eigenvalue. For single damage scenarios, the FBDD method is able to predict damage location close to the inflicted damage but not exactly. Furthermore, it displays a symmetrical false positive for damage inflicted at quarter span. In determining the size of damage, the method produced errors ranging from 2% to 57%. The FBDD method seems to work reasonably well for single damage but for the study did not address multiple damage scenarios. The attempt to quantify the damage size using changes in frequency is also encouraging.

Kim, Park and Lee (2006) performed experimental tests using natural frequency to predict severity of damage and filtered effects from environmental factors such as fluctuation of temperature. A statistically based control technique was implemented to monitor occurrence of damage in the test specimen exposed to various temperatures. When the structure experiences variations in temperature the mean and variances of the extracted natural frequencies are expected to change. A control chart is then obtained in terms of natural frequencies versus temperatures. The existence of a damage was predicted if anything fell outside the control limits. For locating damage, the FBDD method mentioned earlier was adopted. With varying temperatures, a statistical normalisation hypothesis was applied to the single damage indicator to form a new damage index. With this new damage index, any number larger or equal to 3 would indicate a 99.7% confidence level with respect to damage locations. Estimation of severity of damage using the FBDD method mentioned earlier was adopted. The results associated with a light saw cut on the flange was not detected for all 4 modes but the severe saw cut was detected except for mode 1 using the control chart. For damage localisation, the FBDD method, coupled with a statistical approach, is able to pin-point single damage location at room temperature but other temperatures would cause the predicted damage location to deviate from the actual location. The prediction of damage severity is similar to damage localisation, whereby it is only accurate at room temperatures, but suffers from errors for other temperatures. Again, the methods mentioned were performed only for single damage cases and on a simple beam.

2.3.3 Mode Shape Based Methods

The mode shape is a unique characteristic of a structural system and is known as the spatial description of the amplitude of each resonance frequency. It is commonly acknowledged that local damage will cause changes to the mode shapes in the vicinity of the damage. Damage detection methods have been developed for the identification of damage based on directly measured mode shapes or their derivatives.

The most widely used mode shape method to identify existence of damage is modal assurance criterion (MAC) (Allemang & Brown 1983), which is based on comparison between two sets of mode shape data. Further developed MAC method, the coordinate modal assurance criterion (COMAC) (Lieven & Ewins 1988) was used to detect location of damage. These two methods are still in use, mainly in the model updating process or calibration of finite element models with experimental modal data. The direct comparison of mode shapes, combined with other modal-based damage detection methods, are also used for structural health monitoring.

Shi, Law and Zhang (2000) presented a sensitivity- and statistically-based method to localise structural damage by direct use of incomplete mode shapes. The method utilises multiple damage location assurance criterion (MDLAC) (Messina, Williams & Contursi 1998) combining the incomplete mode shapes at the same measured degrees of freedom (DOFs) to localise damage site. A numerical simulation of a bar-truss structure was used to illustrate the performance and robustness of the proposed method. The damage sites were identified approximately using incomplete mode shapes first and the true damage sites and their extent were determined using the more accurate measured modal frequencies.

Abdul Razak et al. (2001) suggested a simplified version of Laplacian Operator (C P Ratcliffe 1997) to detect a sawcut damage for a reinforced concrete beam. The simplified Laplacian operator (SLO) utilises the difference of discrete functions of the mode shape displacements to detect single localised damage. This method proved to be more appropriate compared to its original formulae. The results showed that higher modes could detect and identify crack locations for less severe cases. The method does not require a comparative data set to determine the damage locations for single damage scenarios.

Abdo and Hori (2002) proposed a damage indicator using changes in the rotations or slope of mode shapes to identify presence of structural damage. A finite element model of a steel plate was utilised to demonstrate the robustness of the method.

It was found that rotational mode shapes are more sensitive than the changes in the displacement mode shapes. The numerical results showed that higher modes are not necessary for identifying small damage (5% reduction in the modulus of elasticity). The method requires a good choice of mode shapes in order to get good results and this can be done using sensitivity of natural frequency to damage.

Ismail, Abdul Razak and Abdul Rahman (2006; Z. Ismail et al. 2001) presented a method to determine, experimentally, damage location of a single crack and honeycombs in reinforced concrete beams using mode shape derivatives. An indicator, namely local stiffness indicator utilising $|\lambda^4|$ derived from the Euler beam equation is used to identify damage location with changes in natural frequencies or flexural stiffness for undamaged and damaged states. The results show that the values of the indicator increases closer to the crack and around the middle of the honeycombs. However, the results only pertain to single damage scenarios and they are mode dependant.

2.3.4 Mode Shape Curvature Based Methods

The modal curvatures are more sensitive to damage compared to the modal displacement which often hardly change when compared to the initial mode shapes of the undamaged structure. The use of mode shape curvatures in damage detection is usually based on the assumption that the changes in the curvatures of mode shapes are highly localised to the region of damage. The curvature is often calculated using the second derivatives of mode shape displacement and numerically obtained by a central difference approximation. Mode shape curvature is one of the most commonly used damage detection techniques and the use of mode shape curvature changes has been listed as one of the structural health monitoring techniques for civil engineering structures in 'Guidelines for Structural Health Monitoring' published by ISIS Canada (Mufti 2001).

The concept of mode shape curvature was introduced by Pandey, Biswas and Sammam (1991). Using finite element models of a cantilever beam and a simply supported beam, mode shape curvatures were obtained numerically by a central difference approximation for intact and damaged states. For the simply supported beam, the results showed that for a damaged case with 50% reduction in modulus of elasticity and pertaining to a single damage scenario, mode shape curvature is far more sensitive

than modal assurance criterion (MAC) and coordinate modal assurance criterion (COMAC) values.

Yoon et al. (2001) expanded a global fitting method, namely 'gapped smoothing method' (Colin P Ratcliffe 2000; C P Ratcliffe & Bagaria 1998), for locating structural damage in a beam using a 'global optimised smooth shape method' on mode shape functions. The difference in mode shape curvatures by subtracting the damaged state values from those of the undamaged one was adopted (Pandey, Biswas & Samman 1991; Wahab & De Roeck 1999). The mode shape of the damaged beam was differentiated twice to obtain mode shape curvature (step A). Meanwhile, the smoothing of mode shape by a global curve-fitting method (third order polynomial curve-fitting) was carried out. The smoothed mode shape is subsequently differentiated twice to obtain the mode shape curvature (step B). The curvature obtained from step A is subtracted from that of step B and forms a damage index. The damage index can be summed up by normalising the curvature change peak values to increase the damage detection capability. Using a finite element model and an experimental test, the method localised the single damage scenarios with the depth to thickness ratios less than 1% using the former and localised damage with at least 20% depth to thickness ratio using the latter. This method showed that input from undamaged state is not required to detect location of damage.

Maeck and De Roeck (2002), PhD thesis of Maeck (2003) and Unger, Teughels and De Roeck (2005) presented a technique making use of the calculated modal bending moments and curvatures to derive the bending stiffness at each location. The direct stiffness calculation (DSC) technique was developed to calculate the modal curvatures and torsion rates without direct numerical derivation using the modal displacements. Combined with modal internal forces, this leads to direct estimation of decrement in stiffness due to damages in a structure. The technique was validated on a reinforced concrete beam that was loaded in six steps by a four point bending static test. Bending as well as torsional stiffness decreased significantly as the damage became severe. Curvature provided good qualitative damage detection but to a lesser degree when quantifying the damage.

Hamey et al. (2004) utilised mode shape curvatures to identify damage in carbon/epoxy composite beams experimentally. Smart piezoelectric materials were used as sensors or actuators to acquire the curvature modes of structures. These materials were surface-bonded to the beams. Delamination damage was inflicted at a single

location on the cantilever test beams. From the experimental results, the curvature modes and piezoelectric materials can be effectively used in damage detection and health monitoring for composite structures.

2.3.5 Strain Mode Shape Based Methods

Since curvature is proportional to the bending strain, in experimental tests, mode shape curvatures can be obtained directly by measuring strain instead of displacement or acceleration. For the past decade, some researchers have demonstrated the feasibility of measuring strain mode shape with the help of strain gauges (Bernasconi & Ewins 1989; D.B. Li, Zhuge & Wang 1989; Tsang 1990; Yam et al. 1996). Kim and Kwak (2001) utilised absolute difference of strain mode shapes to identify cracks in plates. Li et al. (2002) presented two novel damage sensitive parameters to determine the damage locations for plate-like structures, based on the continuity and the residual strain mode shape technique.

2.3.6 Modal Strain Energy Based Methods

The strain energy in a Bernoulli-Euler Beam can be associated with a mode shape in the modal domain. The mode shape displacement requires to be differentiated twice to obtain mode shape curvature commonly using a central difference approximation. When a mode shape stores an enormous amount of modal strain energy in a structural load path, the frequency and shape of the mode are highly sensitive to changes in that load path. Therefore, the modal strain energy has been widely used as an indicator of localised damage. For further details refer to Chapter 5.

The literature has generally concentrated on one-dimensional (1-D) beam model, though application to two-dimensional (2-D) and three-dimensional (3-D) is made possible, commonly by decomposition into beam-like elements. Some work regarding modal stiffness (related to modal strain energy) was conducted by Stubbs (1990a; 1990b). Stubbs, Kim and Topole (1992) presented a method based on the fraction of modal energy before and after damage for a particular mode in a member to detect damage location. This damage indicator was evaluated by a numerical study of a framed structure. Eleven damage cases and the results showed that the method is robust in detecting the location of damage. Kim and Stubbs (1995) proposed a method that

normalised the damage indictor derived from modal strain energy with respect to the standard space. This is referred as 'damage index' in the literature. Using a two span plate girder model, a single damage can be confidently located with relatively small localisation error and a relatively small false negative (missing detection of true damage locations) error but a relatively large false positive (prediction of locations that are not damaged) error. It was reported that severity of damage can be estimated with relatively large error. In another paper, Stubbs, Kim and Farrar (1995) proposed a similar damage index method but the fractional modal energy is summed with a unity in the numerator and denominator. This step was used to derive a consistent indicator of damage localisation and to overcome division-by-zero simply by shifting the axis of reference. Employing the first three modes in the numerical and experimental models of a steel plate girder, damage localisation for single damage cases were accurate but with some false positives.

Further development of the damage index method was progressively carried out. Park and Stubbs (1995), and Stubbs and Park (1996) utilised the reconstruction of mode shape using Shannon's sampling theorem combining with the damage index method to locate damage with fewer sensor data points. Stubbs and Garcia (1996) applied the concept of pattern recognition in the damage index method to classify elements in the feature space into undamaged and damaged classes. The formulation was applied to a 3-D finite element (FE) model of a bridge girder using single and dual damage scenarios. The accuracy of the localisation is considered good utilising the arithmetic mean and a weighted mean of the components of the feature vector, which had no false negative but produced one false positive prediction. Stubbs and Kim (1996) attempted to apply the damage index method to predict damage location without baseline modal parameters. Using a continuous beam FE model, the baseline modal parameters were identified using a proposed system identification algorithm. The damage localisation and severity estimation was reasonably good for single damage scenarios.

The damage index method was used in many civil engineering applications by Stubbs and associate authors, such as Egger and Stubbs (1994), Abraham, Park and Stubbs (1995), Maduakolam and Stubbs (1995), Kim (1995), Garcia, Stubbs and Bütler (1996), Park and Stubbs (1996), Serna and Stubbs (1996), and Park, Kim and Stubbs (2002). Kim and Stubbs (2002) derived a new damage index, which improved accuracy of damage localisation in a simulated two span beam compared to Kim and Stubbs

(1995). The improved damage index method incorporates eigenvalue changes before and after damage as well as the mass changes. For single damage scenarios, the improved method performed better than the original formulae in locating damage and estimating severity of damage. The application of the improved damage index method is also published in Kim and Stubbs (2003a; 2003b) and Kim et al. (2003) In the Phd thesis of Sánchez (2005), it was mentioned that the improved damage index method did not provide the results expected numerically. Hence, an alternative damage localisation index was proposed with a format similar to the original one. Utilising single and two damage scenarios for a beam structure, the damage indicator accurately identified the damage location.

The modal strain energy based methods have been widely used by many researches in various fields and applications. Worden, Manson and Allamn (2001) applied the strain energy method for detecting and locating damage in an aluminium sheet experimentally. Damage was simulated by a sawcut on the stringer ranging from 10% to 90% depth of cut. The mode shape was normalised. Using the one-dimensional strain energy method, the damage index using nine measurement points was unable to localise the damage at a non-sensor location. A cubic convolution polynomial interpolation was used to estimate the mode shape at 19 equally spaced points between sensors. Utilising the reconstructed mode shape, the damage indices of modes 1 to 5 gave poor results, only highest level of damage was flagged for modes 1, 3 and 5. Furthermore, the results showed many excursions above threshold at no-damaged locations. When all the modes were used, the two highest damage levels were detected. However, there was a small indication of damage at a spurious location. The paper reported that, in general, damage location predictions were biased toward sensor locations and supported the importance of sampling of the mode shapes.

Duffey et al. (2001) derived a method using vibration strain energy stored in the axial or torsional modes for damage identification. It is different to the conventional strain energy based methods that utilise transverse modal displacement in the formulation. This newly derived method was verified by application to an analytical eight degree of freedom model. Experimental validation was also carried out using an experimental eight degree of freedom spring-mass structure. The method was successful in detecting damage for 10% reduction in elemental stiffness for single damage scenarios in the analytical simulation. For the experimental cases, the method performed well in locating damage at all three levels of damage investigated.

Shi et al. (1998; 2000) proposed using the ratio of changes in modal strain energy in each element as another damage indicator. The approach requires only the elemental stiffness matrix, the analytical mode shapes and incomplete measured mode shapes. The effect of analytical mode truncation, incomplete measured mode and measurement noise in the damage detection were discussed. Results from the modal simulation and experiment with a two-storey partial steel frame indicated that the presented method is effective in localizing damage, but it is noise sensitive in the damage quantification to some extent. Shi et al. (2002) improved the quantification of stiffness change by reducing the modal truncation error in the calculation of the damage indicator.

Moshley (2002) developed a method that considered changes in the strain energy of the structure when excited by external sources (mechanically or acoustically) as a means for detecting localised defects, namely the damage location indicator (DLI). Numerical analysis and experimental tests were performed on a cantilever aluminium beam. For a simulated single damage with 25% loss of flexural rigidity, it was noticed that the damage has a minor effect on mode shape. With the DLI, the peak of the graph correctly located the single damage. However, two small peaks adjacent to the actual damage site appeared due to errors introduced by slope computation of the modal displacement data using the spline fitting. For the experimental test, a process was introduced for selecting appropriate modes used in the DLI. The DLI managed to detect the single damage. However, this method is mode dependent with respect to the experimental test results.

Ndambi, Vantomme and Harri (2002) presented a framework for the development of a health monitoring system using experimental results for a 6 meter long reinforced concrete beam subjected to progressive cracking introduced at different steps. The health monitoring of the structure was carried out based on changes of dynamic characteristics, namely MAC, COMAC, strain energy and flexibility methods. Comparing the capability of damage localisation for the COMAC factors, the strain energy evolution and the changes in flexibility matrices, the strain energy method appeared to be more precise than others. This is also supported by the findings of Alvandi and Cremona (2006), where among few evaluated techniques, the strain energy method presented the best stability in damage detection with induced different levels of noise and damage.

Sazonov et al. (2002a; 2002b) proposed a new non-baseline method utilising modal strain energy for locating damage. Based on Fourier analysis of the modal strain energy, the method was developed and analytically verified for the cases of a pinned-pinned and a free-free beam. This method looks for characteristic changes in the power spectrum of the modal strain energy in order to locate and identify damage. The analytical results for both the finite element model and the impact tests on a free-free aluminium beam have been verified using single and multiple damage scenarios. Applying the method to Armoured Vehicle Launched Bridge (AVLB) with the first two modes, the non-baseline method has effectively yielded similar information compared to the traditional modal strain energy method. However, the method may not have the capability to distinguish between changes in cross section and damage. A possible solution may be found by matching the method to the geometric configuration of the structure, thus discarding the false peak due to geometric changes. Alqaradawi et al. (2002) presented an attempt to create baseline information for the pre-damaged one-dimensional beam structures analytically using stereolithography for detecting damage employing modal strain energy method.

The feasibility of extracting the information of an initial undamaged structure has also been successfully demonstrated using iterative methods by Stubbs and Kim (1996). Barroso and Rodriguez (2004) proposed a new method to estimate a baseline from damaged response data using a noniterative method for the first generation benchmark problem for structural health monitoring developed by the American Society of Civil Engineers (ASCE) Task Group on Structural Health Monitoring. The stiffness-mass ratio approach utilising the ratio of stiffness to mass is proportional to the square of the frequency with small variations between undamaged and damaged states. With certain steps including substituting eigenvalue and eigenvector of damaged structure into the matrices of eigenparameter, the baseline state of the structure can be created. Using the damage index method, the damage was accurately identified where the severity of damage was high. Nonetheless, for some damage cases, some false positive damage locations were also identified.

Choi and Stubbs (1997) developed a nondestructive damage detection algorithm for two-domensional plates using local modal strain energy. The method was developed from expressions for the elastic strain energy of a plate. The damage indices are obtained for each mode and are transformed to probability space and superimposed as weighted general means (WGM). In the WGM, a fraction of modal strain energy of

the element is used as the weighting for each mode. Using a numerical simply supported plate model with single and two damage scenarios, the method did not perform very well in locating the damage.

Pereyra et al. (1999) employed out-of-plane mode shape data before and after the inflicted damage to evaluate, experimentally, a global nondestructive evaluation damage localisation technique based on modal strain energy differences for plate-like structures. A bi-variate curve-fitting procedure was employed to estimate the curvatures obtained from finite differences of the mode shapes. Strain energy differences between pairs of matching modes of the damaged and undamaged states were used to indicate damage judging by the increment in the modal strain energy. The damage indications, provided by several modes, are normalised using a standard norm and fused using an average approach to create damage maps. Considering the bending curvature in the x-direction only, the actual locations of cuts on the stiffened plate were accurately detected. However, for smaller cuts, over 33% of the cuts were not detected. In general, the single damage with larger damage severity can be detected but not the lighter damage.

Conrwell, Doebling and Farrar (1997; 1999) extended the 1-D strain energy method to a 2-D strain energy method for application to plate-like structures. It should be noted that by decomposing the 2-D and 3-D structures into beam-like elements, the 1-D strain energy method has been successfully used for detecting damage. It is assumed that the decomposition technique using the 1-D algorithm will not outperform the 2-D algorithm as it does not preserve the torsional stiffness between slices. Both 1-D and 2-D methods were tested numerically and experimentally. In the numerical simulation, a pinned-pinned plate with several elements with reduced 10% stiffness, using the first four modes, the 2-D method identified the general location of damage but not the 1-D decomposition method. For the experimental test using an aluminium plate with two sawcuts, both methods performed comparably. At low levels of damage, both methods exhibited a tendency to produce spurious damage locations.

Gutschmidt and Cornwell (2001) presented, developed and established statistical bounds for damage indicators such as flexibility method and modal strain energy method for plate-like structures. Statistical bounds are important in order to estimate the limits of a change that is necessary to distinguish damage from natural variability associated with any measurement for structural health monitoring. A false positive damage indication method (FPDIM) was presented and applied experimentally

using a plate with progressive damage. Using the modal strain energy method combining with FPDIM, a clear boundary can be used to differentiate natural variability and damage. The FPDIM would help to eliminate false positives.

Lee and Yun (2006) presented an effective method for damage estimation of a steel girder bridge using ambient vibration data and the damage indicator method based on modal strain energy (DIM-MSE) for plate-like structures. The coarse mode shapes obtained from field testing were interpolated into finer grids using cubic polynomial function. Employing neural network techniques, the mode shape differences between before and after damage were used as the error-insensitive input data. Various damage scenarios were inflicted on the flange and web of the bridge. A success rate (SR) was employed for screening process out of 100 randomly perturbed cases for each damage case. In general, a SR of 43% was achieved in locating damage for single and two damage scenarios. It may seem to be quite low. However, it is deemed difficult to consistently recognise an actually damaged member, or members, using the DIM-MSE with the presence of a significant noise level.

2.3.7 Flexibility Based Methods

Dynamically measured flexibility matrix is used to estimate changes in the static behaviour of the structure. Because the flexibility matrix is defined as the inverse of the static stiffness, the flexibility matrix relates the applied static force to the resulting structural displacement. Thus, each column of the flexibility matrix represents the displacement pattern associated with a unit force applied at the associated degree of freedom (DOF). The dynamically measured flexibility matrix is generally estimated from the matrix of measured mode shapes and the diagonal matrix of associated measured natural frequencies squared. The details are found in Chapter 5.

One of the mostly cited articles on using flexibility to detect damage is by Pandey and Biswas (1994). The measured flexibility of the structure was tested with numerical examples and then with experimental data collected on a wide range of steel beams. The results of the single damage scenarios for both the numerical and experimental examples showed that the location of damage could be identified from just the first two measured modes of the structure.

Bernal and Gunes (2002) explored an approach that allows extension of flexibility based damage localisation method to cases where only output measurements

are available. The idea is that lack of deterministic information on the input can be partially compensated by knowledge of the structure of the mass matrix. A damage locating vector (DLV) (Bernal 2002; Bernal & Levy 2001) was proposed to locate the damage by inspecting stress fields created by vectors that are contained in the null space of the change in flexibility. Using a numerical example of a cantilevered spring-mass system, the flexibility matrices can be extracted from the data without knowledge of the input, while the single damage at the first spring was correctly located. Gao and Spencer (2002) proposed to utilise DLV method to handle the ambient vibration case. This method uses flexibility based damage localisation method combined with a modal expansion technique to eliminate the need to measure the input excitation. Besides locating the damage, the method is capable of estimating the extent of damage. A numerical example, analysing a truss structure with limited sensors and noisy measurement, was used to test the method. The results were quite reasonable and single damage as small as 15% stiffness loss on a local element was detected. Gao and Spencer (2006) extended the method for online damage diagnosis of civil structures.

Kim, Stubbs and Sikorsky (2002) introduced a new method based on modal flexibility to identify location and severity of damage in a structure using limited modal data. An assumption was made that a small damage event will have an insignificant effect on the internal forces in a structure under certain loading conditions. In the case of coarse sensor intervals, cubic spline interpolation technique was adopted to create a finer grid. Using the modal flexibility and its relationship with slope deflection formulae, the flexural damage index equation (FDIE) was formulated. The Z24 bridge was tested with the FDIE. The example of a single damage case showed that using the first three modes the damage was detected.

Patjawit and Kanok-Nukulchai (2005) presented a method for health monitoring of a highway bridge utilising a global flexibility index (GFI) based modal flexibility method. The method is based on the concept that the flexibility matrix reflects global structural damage and its norm can be used as a good overall indication of its flexibility condition. Experimental example of a steel beam, a concrete beam and field testing of an existing bridge were carried out to test the method. The results showed that the GFI decreases as the single cut size increases. This shows that the GFI is sufficiently sensitive to damage. The GFI value of the bridge was measured and this served as a datum for future determination of the state of health of the bridge.

2.3.8 FRF Based Methods

The frequency response function (FRF) is, in general, a complex valued function or waveform defined over a frequency range (Richardson & Formenti 1982). Some researches have used FRF measurement directly, instead of using modal data extracted from the FRF measurements. In some work, derivatives of FRF measurements are employed for damage detection or structural health monitoring. Sampaio, Maia and Silva (1999) proposed a frequency response function (FRF) curvature method that encompasses damage detection in terms of its presence, localisation and extent of damage based on only the measured data without the need for any modal identification. The method uses frequency response at different locations of the structure to formulate the curvature. The absolute difference between the FRF curvatures of the damaged and undamaged structure is then utilised. Numerical and experimental examples were used to test the method. A numerical 10 degree of freedom lumped mass system and the experimental data gathered from the I-40 bridge have shown the capability of the method in detecting, locating and quantifying damage for single damage scenarios. This method needs further development and better characterisation.

Kessler et al. (2002) presented an experimental and analytical application of FRF method to detect damage in graphite/epoxy specimens. The FRF method was found to be successfully detecting even small amounts of damage in a simple composite structure. However, the information about the damage type, size, location and orientation of damage was not obtained since combinations of the several variables can yield identical response signatures. Tung and Tran (2003) adopted a method, namely, damage location plot (DLP), to detect structural damage using FRF in a cantilever beam. The DLP method was developed by He and Fu (2001) and was derived from the relationship between dynamic stiffness matrix and FRF matrix at a particular frequency. The method was shown to be able to identify possible damage locations and relative severity of damage at various damage sites. Bayissa and Haritos (2005) performed damage identification and condition assessment of a reinforced concrete T-beam using changes in FRF. It was observed that the changes in FRF due to damage were greater than the changes due to noise and nonlinearities. However, there were some inconsistent variations in the FRF amplitudes, which seem to be contradicting the theoretical expectations, whereby damaged ones should have higher amplitude and undamaged ones lower.

2.3.9 Model Updating Based Methods

Model updating based methods basically utilise a well-correlated numerical model of the structure in its initial or undamaged state for many damage detection algorithms or structural health monitoring. One of the important issues for these methods is the accuracy of the initial model in representing real structures for damage detection using an updating algorithm. Generally, model updating utilises finite element models as a platform to perform a decision-based process for damage detection. A survey of model updating in structural dynamics was done by Mottershead and Friswell (1993) listing 243 papers and articles up to 1992. Carden and Fanning quoted about 20 papers and articles that utilises model updating methods for damage detection and structural health monitoring, mainly before 2000.

Teughels, Maeck and De Roeck (2002a; 2002b) presented a sensitivity-based finite element model (FEM) updating method using experimental modal data for damage localisation and quantification. The updating procedure is based on the structural damage being represented by a reduction factor on the elements' bending stiffness. An objective function (non-linear least squares) was applied on experimental modal data like frequency residuals and mode shape residuals. The updating parameters are the uncertain physical properties of the numerical model. Using some mathematical techniques, the modal sensitivities were established, correlating the element stiffness matrix with frequency and mode shape data. Optimisation of the updating parameters was carried out by the Trust Newton algorithm. This conventional FEM updating method was improved by the use of damage functions. For simplicity, the Young's modulus in the FEM was corrected. The damage functions are determined by means of one-dimensional shape functions (simple polynomial functions (Szabó & Babuška 1991)), known from finite element (FE) theory. For damage detection, the standard element was mapped as 'damage elements' during the updating process. The procedure was applied on a laboratory tested reinforced concrete beam on which a modal test has been carried out before and after damage was inflicted. The inflicted single damage can be identified successfully. This model updating method was applied to the highway bridge Z24 for structural damage identification (Teughels & De Roeck 2003, 2004). The damage in the bridge was identified by updating the Young's modulus and the shear modulus.

Teughels, De Roeck and Suykens (2002a; 2002b; 2002c; 2003a; 2003b) proposed a new FE model updating method to find the global minimum of a cost

function to establish a damage pattern. This new efficient global optimisation technique, namely, coupled local minimisers (CLM), is a cooperative search mechanism being set up to ensemble local optimiser, each starting from a different point in the search space. At each search point, the objective function and derivative values were calculated and used to direct the search process, employing minimisers, towards the global minimum. The CLM technique is implemented with the augmented Lagrangian method. The method was tested using a reinforced concrete beam on which a modal test had been carried out before and after infliction of damage. The correct single damage pattern in the beam was identified with the method.

2.3.10 Artificial Intelligence Based Methods

Neural networks provide a range of powerful new techniques for solving problems in pattern recognition, data analysis and control. It arose from the study of biological neurons and refers to a computational structure composed of processing units that represent neurons. A review article on neural network and its applications was published by Bishop (1994) and contained 88 articles and papers up to 1992. Neural networks have been applied successfully in many diverse applications including vibration based damage detection and structural health monitoring for the past decade (Gutierrez, Ferregut & Osegueda 1996; Kudva, Munir & Tan 1992; Loh & Yeh 2000).

Suresh et al. (2004) utilised modal frequencies of a cantilever beam having transverse surface crack to train a neural network to identify both crack location and depth. The structure was created analytically and various crack locations and depths were inflicted using a fracture mechanics based crack model with an effective spring at the crack location. A principal component analysis (PCA) (Oja 1989) based neural network was used to visualise the multi-dimensional modal frequency data. The multi-layer perceptron (MLP) and radial basis function (RBF) networks were utilised for damage detection. The MLP network was trained with a back-propagation algorithm (Haykins 1998), while the RBF (Ranaweera, Hubele & Papalexopoulus 1995) network was trained using a three-step scheme. The results showed that the RBF network performs better than the MLP network, however, the former needs longer training time.

Kao and Hung (2005) presented a novel neural network based approach for damage detection. The method is carried out in two steps, that is, system identification using neural system identification networks (NSINs) for the first step and it continues

with structural damage detection. The NSINs was used to identify the undamaged and damaged state of a structural system, while structural damage detection used the trained NSINs to generate free vibration responses with the same initial condition or impulsive force. Using comparison between the period and amplitude of the free vibration responses of the damaged and undamaged states, it allows the extent of changes in a structural system to be assessed. An experimental example of a five storey steel frame subjected to various intensities of the 1995 Kobe earthquake on shake table was used to test the method and notably the method is very promising for application to linear and nonlinear structures.

Xu and Humar (2005) utilised artificial neural networks to capture the changes in modal characteristic for damage detection, which can be treated as a pattern recognition problem. This would help to resolve problems in practical structures, such as the effect of measurement errors, uncertainties induced by environmental and boundary conditions, the need to use incomplete mode shapes, mode truncation and the non-unique nature of dynamic solutions. A new robust two step algorithm (perceptron and back-propagation) was presented for detecting the location and magnitude of damage. Damage index method that utilises modal strain energy was employed as the input to the network. Using a simple finite element model of a slab and girder bridge, the proposed method is quite effective in identifying the location and magnitude of single and two damage scenarios, although there were some measurement errors in the input data.

Genetic algorithm (GA) is an attractive class of computational models that mimic natural evolution to solve problems in wide variety of domains. A genetic algorithm emulates biological evolutionary theory to solve optimisation problems and has found applications in damage detection in civil engineering structures. For example, Hao and Xia (2002) utilised a GA with real number encoding for identifying damage in structures by minimising the objective function (frequency and mode shape changes), which directly compares the changes in the vibration measurements before and after damage. Numerical results showed that the damaged element can be detected using genetic algorithm. Ratnam and Parameswara Rao (2004) developed a technique for detecting damage (microscopic structural damage) in elastic structures using genetic algorithm for locating and quantifying the damage. Using finite element models, it is possible to identify the inflicted damage to a reasonable level of accuracy.

2.3.11 Time Domain Based Methods

In time domain based methods, the time history is used. The system parameters are determined from the observational data sampled in time. Damage is evaluated through the properties of structural system changes with time under the external loading. The methods could be independent of modal domain methods and the time data can be easily obtained using simple tools. In recent years, the time domain based methods have gained much attention for damage detection and structural health monitoring in civil engineering structures.

Yang, et al. (2004) have made use of damage events of a structure in time for structural damage detection. Two methods were employed: empirical mode decomposition (EMD) and EMD and Hilbert transform. The EMD method was intended to extract damage spikes of a sudden change in structural stiffness from the measured time history, thereby detecting the damage time instants and damage locations. While, the second method, based on EMD and Hilbert transform, is capable of detecting the damage time instants as well as determining the natural frequencies and damping ratios of the structure before and after damage. These methods were demonstrated on a benchmark problem established by the ASCE Task Group on Structural Health Monitoring. The first method was found to be able to detect the damage if the noise pollution level is very small and the changes in the structure are not abrupt. The second method showed that it is capable of accurately determining the time instant when damage occurs regardless of the noise level and also identified the natural frequencies and damping ratios quite accurately. Similar work was also performed by Xu and Chen (Y.L. Xu & Chen 2004) using EMD to detect sudden change of structural stiffness for a three-story shear building model, experimentally.

Zhu and Law (2006) have presented a new method for crack identification of beam bridge structures using wavelet analysis of the operational deflection time history with a moving load. Numerical and experimental examples were used to demonstrate the response at a single measuring point employing continuous wavelet transform to detect the location of damage. A damage index was proposed to estimate relative depth of cracks. The method showed that it is robust in determining the damage location for single and multiple cracks for the numerical cases, but it failed to determine crack locations for the experimental cases.

Omenzetter and Brownjohn (2006) presented an application of time series analysis to bridge structural health monitoring (SHM). The work was used to address

the problem of long term SHM through the analysis of time history of static strain data obtained for Singapore-Malaysia Second Link, also refereed to as the Tuas Link, and operating continuously over a long time. A vector seasonal autoregressive integrated moving average (ARIMA) mode was formulated for recording the strain signals. The coefficient of the ARIMA model varies with time and was identified using an adaptive extended Kalman filter (Harvey 1989). By observing various changes in the ARIMA model coefficients, unusual events as well as structural changes or damage sustained can be revealed.

2.4 Research and Development Needs

Based on the insights gained from this literature review, there is now a considerable body of knowledge based on research and development efforts in academia and industry regarding damage detection methods and techniques. However, there has been little work done on detecting damage in timber bridges using modal based damage detection methods. It is, therefore, necessary to fill this gap in order for the modal based damage detection methods to be adopted more widely for structural assessment of timber bridges. The following issues are therefore addressed in this study:

(1) To enhance existing damage detection methods using damage index for locating damage in timber structures. They should be less mode dependant and work for single and multiple damage scenarios.

(2) Estimation of severity of damage in timber structures.

(3) Simulation of timber bridges using finite element analysis.

(4) Expansion of limited number of sensors using appropriate mode shape reconstruction techniques to improve capability of the adopted and modified methods for detecting damage.

(5) Adopt suitable numerical differentiation methods for calculations as well as numerical integration in the damage detection algorithms.

(6) Utilise two-dimensional theory of the damage index method for plate-like structures such as timber bridge decks.

Chapter 3

Material Properties and Material Testing Procedures

3.1 Introduction

This chapter discusses, in broad terms, the structure of wood, its physical and mechanical properties, mainly for softwood species. Nevertheless, this information on the general characteristics of softwood is applicable to hardwoods. Additional information on wood properties and characteristics can be found in the references quoted here. This Chapter also presents details of the experimental procedures undertaken for characterising the behaviour of girders, deck and screw connections between deck and girders for a laboratory timber bridge. These procedures were defined as a series of testing programs for elements (timber beams and plywood) and components (screw connections). The program of material characterisation was undertaken to provide reliable data for finite element modelling of the laboratory timber bridge and timber beam. Photographs and sketches have been included in this chapter to illustrate the process of the testing especially for the screw connection pullout test, which is not commonly found in standard procedures.

3.2 Material Properties of Timber/Wood

Wood differs from other construction materials, such as steel and concrete, because it is biologically 'produced' in a growing tree to meet the needs of the tree itself. In this respect, it is a high quality fibre composite, naturally grows to resist loads acting on the tree, but also provides for transport of water and nutrients (Thelandersson 2003). Wood is unique, as it possesses material properties that may be significantly different from other materials normally encountered in structural design (Ritter 1990). It is important to have a general understanding of the properties and characteristics of wood. This includes the anatomical, physical and mechanical properties of wood as a material as well as its manufacturing process (not discussed in this study). Because of

the inherent variability and non-isotropic nature of wood its stiffness and strength characteristics are governed by its growth environment and conditions.

Variability, or variation in properties, is common to all materials. Nonetheless, it is more significant for wood/timber, because wood is a natural material and the tree is subject to many constantly changing influences, such as moisture, soil conditions and growing space. Its properties vary considerably even for materials from the same tree. As noticed by Crews (2002), the material properties of wood is not easily defined or well established. This is also confirmed by Thelandersson (2003) quoting a description of Borg Madsen (1992):

Mother nature spent millions of years devising an arrangement whereby the branches grew perpendicular to the stem of the tree without impairing the strength of the branch and retaining the full strength of the stem. ... It is well known that poles made from the stem are very strong but when we cut through the knots representing the intricate handiwork of mother nature, what was a proficient pattern to carry the branch becomes a severe weakness. The interlocking of the fibres is destroyed, leaving the unsupported fibres where tension perpendicular to grain stresses can initiate crack growth.

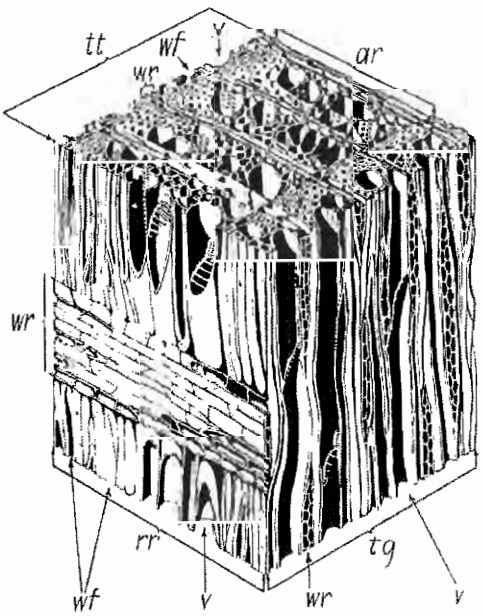
For sawn timber, it is a non-homogeneous material that contains growth defects in the form of knots, zones with compression wood, oblique fibre orientation and others. Therefore, the presence and character of knots and other defects vary from one timber board to another, which means the structural properties of sawn timber exhibit significant variabilities.

Furthermore, the changes in the environmental conditions such as humidity and temperature would affect the stiffness and strength characteristics of wood (US Forest Products Laboratory 2005). According to Cooperative Research Centre (CRC) Wood Innovations (2005), wood is a hydroscopic material. It will swell and shrink in response to changes in atmospheric humidity. It also changes after prolonged exposure to the ultraviolet (UV) component of the sunlight. Besides, the strength of timber also depends upon the rate of loading and duration of the load for all structural timber (Thelandersson 2003). This effect is less significant in other structural materials, but for timber the loss of strength under sustained load can be so large that it has to be considered in everyday engineering design.

3.2.1 Structure of Wood

In order to fully understand and appreciate wood as a structural material, it is very important to understand wood anatomy and structure. This can be considered at two levels, that is, microstructure and macrostructure.

First is a description of the microscopic properties that can only be examined using a microscope. Wood comprises of mainly hollow fibre cells or wood cells or tracheid (similar to short soda straws) made of lignin and cellulose as depicted in Figure 3.1 (Miller 2005). When closely packed, these wood cells form a strong composite system that is often analogised as a bundle of dinking straws. The lignin acts as an adhesive holding the cells together, while the cellulose, which is a fibrous material that is hygroscopic, attracts water like a sponge. The lignin is very strong producing typical failures in wood by crushing of the cellulose structure rather than the lignin. The direction of load is important for the wood to react. As illustrated in Figure 3.2, using the analogy of straws, compression parallel to their longitudinal axis would resist higher load (see A in Figure 3.2 (Ritter 1990)), while in the perpendicular direction would resist lighter loads (see B in Figure 3.2 (Ritter 1990)).



Notes:
tt = tg = transverse
rr = radial
wr = wood ray
v = void
wf = wood fibre

Figure 3.1 Wood microstructure (Miller 2005).

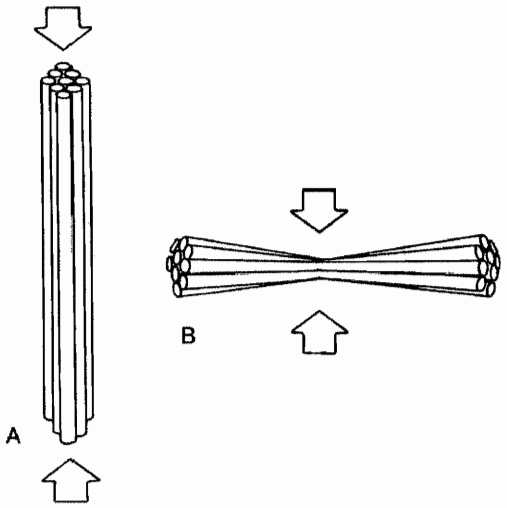


Figure 3.2 Simplified depiction of the structure of wood (Ritter 1990).

Secondly, the macro structure for wood is normally visible with naked eyes. It can be divided into three basic parts, namely bark, cambium and wood (Ritter 1990). A cross section of a tree as shown in Figure 3.3 depicts the components that form the three basic parts of a tree. For bark, it can be divided into an outer corky dead part (outer bark) and an inner living thin part (inner bark). The inner bark is the area that carries food from leaves to growing parts of a tree. Wood of most species is divided into sapwood, heartwood and pith. Sapwood consists of both active and inactive cells and carries sap from the roots to the leaves. Heartwood is composed mostly of inactive cell that formed by a gradual change in the sapwood. It is usually of much darker colour compared to sapwood. Pith is a small core of tissue located at the centre of tree stem, branches and twigs about which initial wood growth takes place.

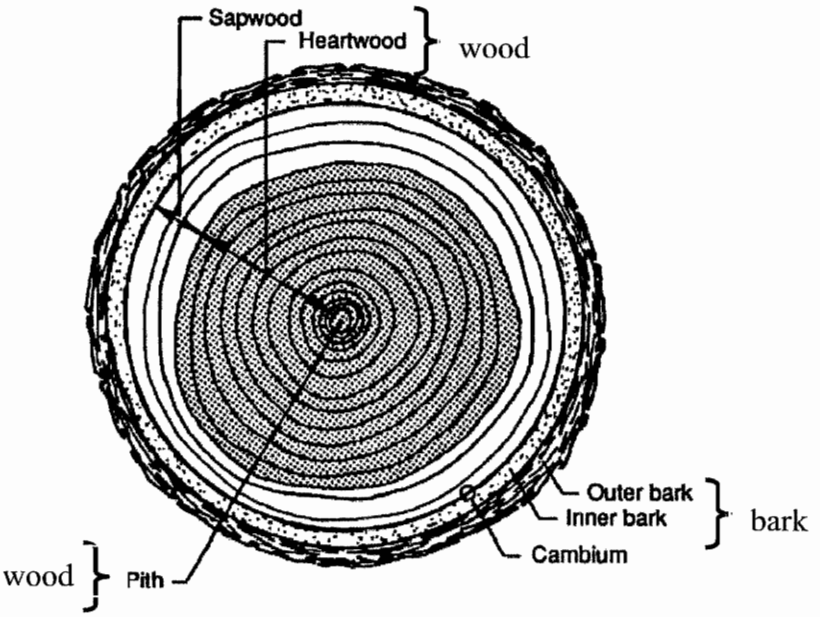


Figure 3.3 Cross section of a tree trunk (Ritter 1990).

3.2.2 Physical Properties

Physical properties of wood exhibit its quantitative characteristics and behaviour to external influences other than applied structural forces, such as directionality, moisture content, dimension stability, thermal and pyrolytic (fire) properties, natural durability and chemical resistance (Ritter 1990). Basic understanding of physical properties is essential because those properties can significantly influence the performance and strength of wood used in structural applications. The two major physical properties, namely, directional properties and moisture content will be briefly discussed here.

Wood may be described as an orthotropic material (General Technical Report FPL-GTR-113 1999). It has unique and independent properties in the directions of three mutually perpendicular axes, namely longitudinal (L), radial (R) and tangential (T). These axes are shown in Figure 3.4. The longitudinal axis L is parallel to the fibre (grain). The radial axis R is normal to the growth rings and it is perpendicular to the grain in the radial direction. The tangential axis T is perpendicular to the grain but tangent to the growth rings. Although wood properties differ in each of these three directions, differences between the radial and tangential directions are usually not significant compared to their differences with the longitudinal direction. Therefore,

most wood properties for structural applications are provided only for directions parallel to grain (longitudinal) and perpendicular to grain (either radial or tangential).

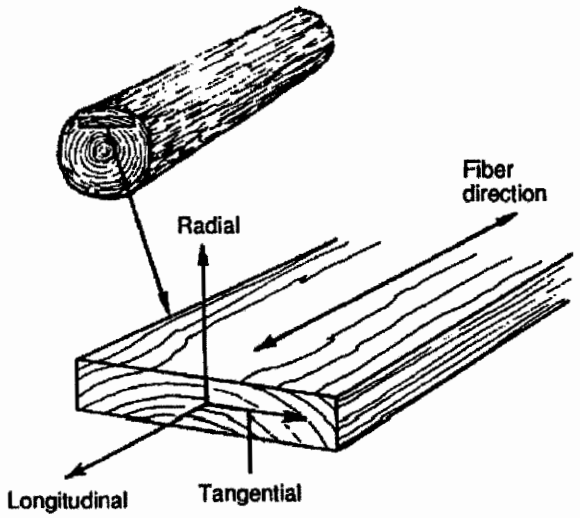


Figure 3.4 The three principal axes of wood with respect to grain direction and growth rings (Ritter 1990).

The moisture content (MC) of wood plays an important role in its physical properties as water constitutes a major portion of green wood. For a living tree, depending on the species and types of wood, the moisture content ranges from approximately 30 percent to more than 250 percent, which is two-and-a-half times the weight of the solid wood material (Ritter 1990). Wood is considered a hygroscopic material that absorbs moisture in humid environments and losses moisture in dry environments. Hence, a wood element will always strive for an equilibrium corresponding to the relative humidity of the surroundings to reach equilibrium moisture content (EMC). The effect of relative humidity and temperature of the surrounding air on wood is not rapid but it needs to be monitored to maintain its structural integrity.

3.2.3 Mechanical Properties

Mechanical properties describe the characteristics of a material with respect to externally applied forces (Ritter 1990). The major mechanical properties of wood are elastic properties that measures resistance to deformation and distortion caused by a predetermined range of externally applied loads, and strength properties that reflect ultimate resistance to applied loads. The basic mechanical properties of wood are obtained from laboratory tests of small pieces of wood termed "clear" and "straight grained" because they do not contain defects such as knots, cross grain, checks and split. Although they are not representative of the wood/timber typically used for construction, properties of these ideal samples are still useful for establishing a reference between different species and for deriving the allowable properties.

For elastic properties of wood, twelve constants (nine are independent) describe its elastic behaviour (General Technical Report FPL-GTR-113 1999). Three of them are moduli of elasticity (E), three moduli of rigidity (G) and six Poisson's ratios (ν). Modulus of elasticity relates the stress applied along one axis to the strain occurring on the same axis. The deformation generated by low stress should be completely recoverable after the loads are removed. The three moduli of elasticity for wood are denoted E_L, E_R and E_T reflecting the elastic moduli in the directions of longitudinal, radial and tangential, respectively. The modulus of rigidity, also called shear modulus, relates the resistance to deflection (shear strains) caused by shear stresses. The three shear moduli for wood are denoted G_{LR}, G_{LT} and G_{RT} for the longitudinal-radial, longitudinal-tangential and radial-tangential planes, respectively. Poisson's ratios relate the strain parallel to an applied stress to the accompanying strain occurring laterally. It is the ratio of the transverse to axial strain. The six Poisson's ratios for wood are denoted ν_{LR}, ν_{LT}, ν_{RL}, ν_{RT}, ν_{TL} and ν_{TR}. The first letter of the subscript refers to the direction of applied stress while the second letter refers to the direction of the accompanying lateral strain.

Strength properties are the ultimate resistance of a material to externally applied loads. They include material behaviour related to compression, tension, shear, bending, torsion and shock resistance. Similar to other wood properties, strength properties vary in the three primary directions, namely longitudinal, radial and tangential, but differences between the tangential and radial directions are relatively

minor and are randomised when a tree is cut into lumber. As a result, mechanical properties are described only for directions parallel to grain and perpendicular to grain.

3.3 Determination of Characteristic Properties

3.3.1 Flexural Properties for Timber Beams

Characteristic Modulus of Elasticity (MOE) properties were derived for girders of a laboratory timber bridge, using four point bending tests, in accordance with the testing requirements of AS/NZS 4063:1992 (Australian/New Zealand Standard™ 1992). Four timber beams were required for the girders in each laboratory timber bridge, with the minimum span length of 4,500mm. Samples were selected from the materials available (30 treated sawn radiata pine timber beams), to be used in the fabrication of the bridge samples. Some of the timber beams were used for the timber beam modal tests and corresponding material properties were used in the finite element (FE) modelling.

The experimental test set up for the four point bending test is illustrated in Figure 3.5. Two point loads were applied on the test sample (either timber beam or plywood) at the locations of 1/3 and 2/3 of the span length (1,620mm from either ends). Displacement transducers (LVDT) were positioned at the midspan, 1/3 and 2/3 of the span length of the test sample to register deflections. The test was carried out within the elastic range. From the test results, load-displacement curves were plotted. The gradients of the curves as shown in Figure 3.6 were used for the computation of the MOE for the test samples and the results are tabulated in Table 3.1.

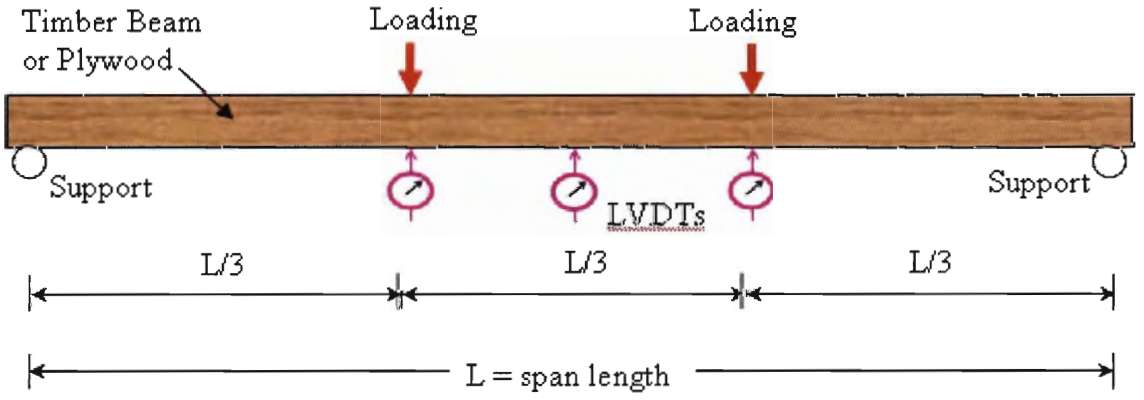


Figure 3.5 Experimental set up for four point being test for timber beams and plywood.

Table 3.1 Modulus of Elasticity for timber beams and plywood.

Item	Modulus of Elasticity (MPa)
Beam	Laboratory Timber Bridge 12,687 (Girder 1) 13,776 (Girder 2) 13,386 (Girder 3) 13,353 (Girder 4) Timber Beams 12,063 (Beam 1) 12,196 (Beam 2)
Plywood	Laboratory Timber Bridge 3,000 (Face grain $\perp$ to span) 6,730 (Face grain // to span)

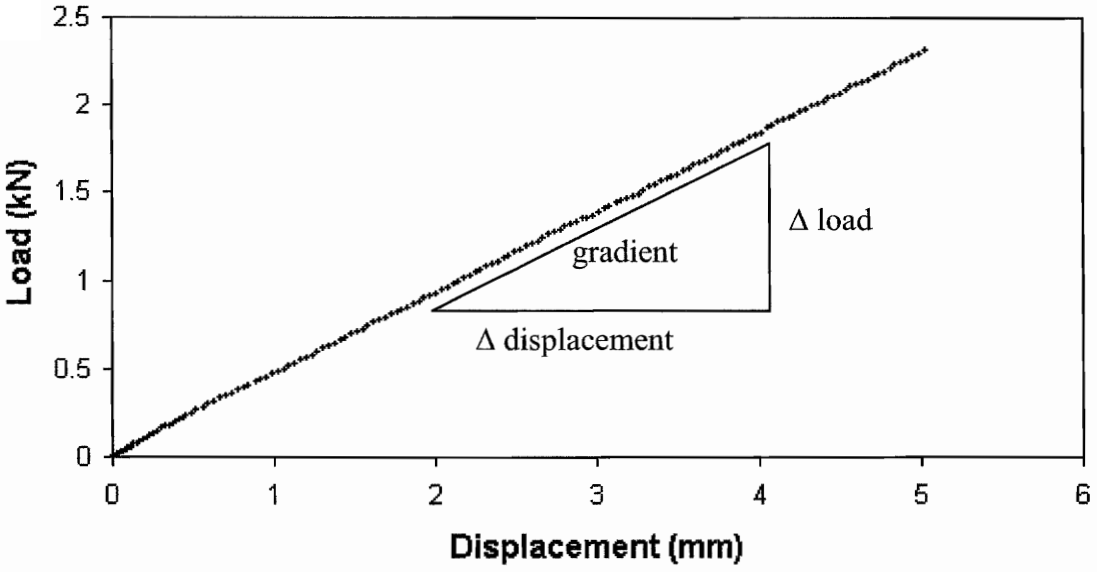
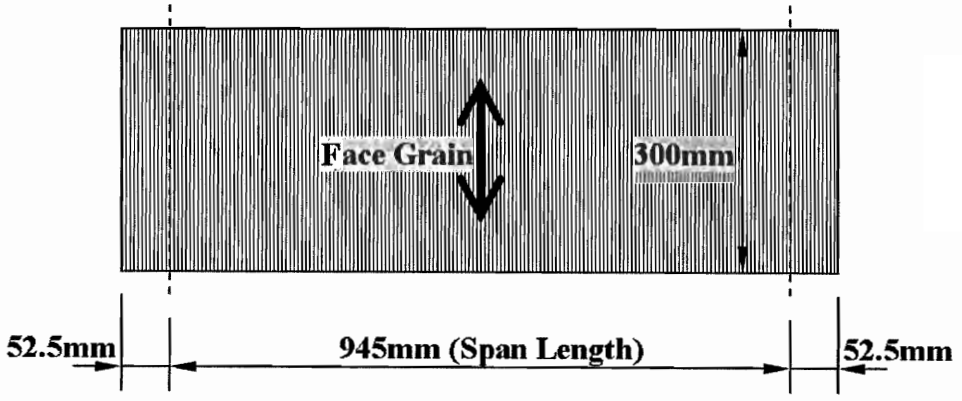


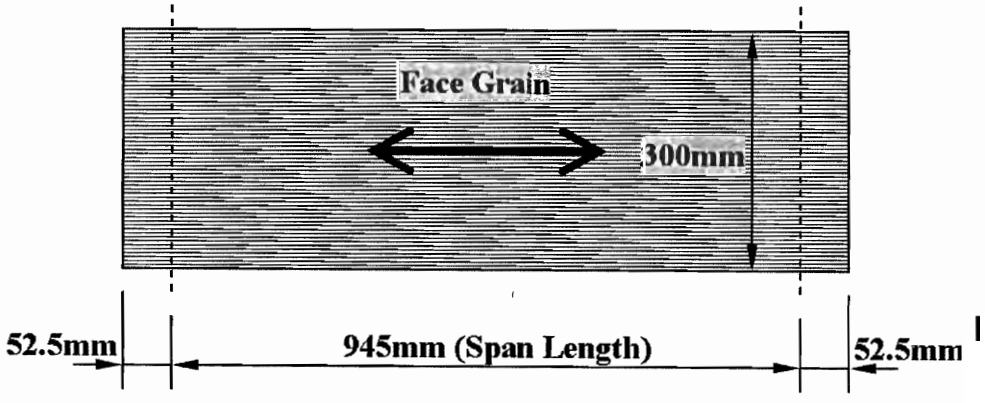
Figure 3.6 A typical load-displacement curve for timber beams.

3.3.2 Flexural Properties for Plywood

Characteristic Modulus of Elasticity (MOE) properties for plywood were derived using four point bending tests in accordance with the testing requirement of AS/NZS 2098:1995 (Australian/New Zealand Standard™ 1995). Test samples were taken from the batch of grade F11 structural plywood used to build the deck of the laboratory timber bridge. Specimens which were perpendicular and parallel to the face grain of plywood as shown in Figure 3.7 were used. Three pieces of each (1050mm x 300mm) with the span length of 945mm were used for the four point bending test. The test set up and test procedures are similar to the timber beams as discussed in section 3.3.1. The average modulus of elasticity of plywood is given in Table 3.1. A typical load-displacement curve is depicted in Figure 3.8.



(a) Bending test piece perpendicular to face grain.



(b) Bending test piece parallel to face grain.

Figure 3.7 Plan views of face grain orientations for plywood test panels.

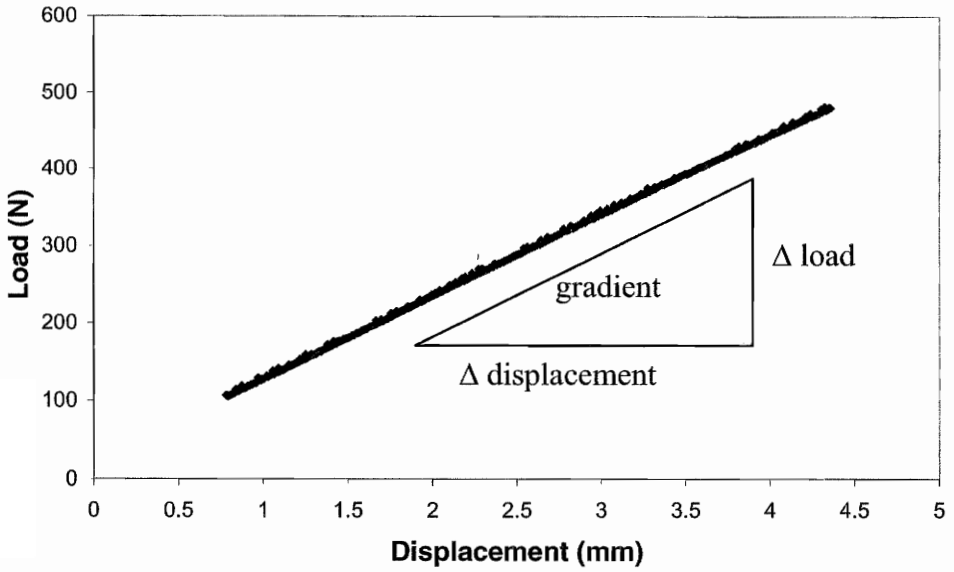
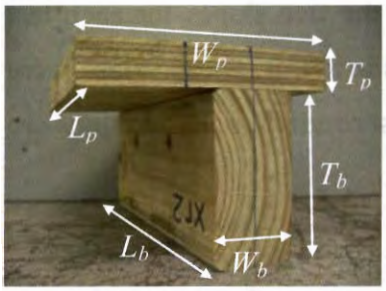


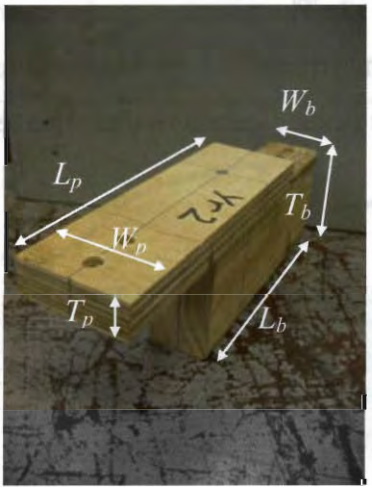
Figure 3.8 A typical load-displacement curve for plywood.

3.4 Pullout Tests for Screw Connections

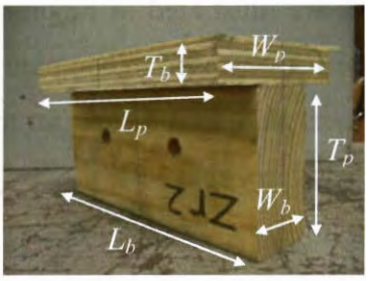
A pullout test was undertaken to determine the screw connection properties between deck (plywood) and girders (beams). It is referred here as screw connection strength. Basically, testing procedures and test sample configurations for the screw connections were designed referring to AS 1720.1:1997 Section 4 (Australian Standard™ 1997) and taking into consideration characteristic property requirements in the directions of X, Y and Z for finite element modelling. Specimens containing single self-tapping screw (countersunk head, 50.8mm (2"), 8g, Phillips) with continuous threads in each interface between plywood and timber beam as shown in Figure 3.5 were used. The screw diameter was 4mm and its length 50.8mm. The details of plywood and timber beam dimensions for all directions are provided in Figure 3.9 and Table 3.2.



(a) X direction.



(b) Y direction.



(c) Z direction.

Figure 3.9 Test samples for pullout test in all directions.

Table 3.2 Details of screw connection test samples in all directions.

Direction	Plywood			Timber Beam		
	Width W_p (mm)	Length L_p (mm)	Thickness T_p (mm)	Width W_b (mm)	Length L_b (mm)	Thickness T_b (mm)
X[1]	135	200	21	45	200	90
Y[2]	65	200	21	45	200	90
Z[3]	100	200	21	45	200	90

[1] *Centre of timber beam is 17.5mm offset from centre of plywood in width direction.*

[2] *Centre of timber beam is 50mm offset from centre of plywood in length direction.*

[3] *Centre of timber beam is centre of plywood in both directions.*

The general test set up for the screw connections in all directions (X, Y and Z) is depicted in Figure 3.10. A test frame was used to assemble the test samples, loading actuator and displacement transducers (LVDTs). The plywood and beam were secured by top and bottom clamps. A load was applied to separate plywood and beam fastened with a screw to obtain the corresponding pullout strength as illustrated in Figure 3.11. This system was connected to a data acquisition system logging the test data. The applied load to the screw connection was measured by a load cell and a LVDT was used to capture the displacement between the plywood and beam specimens. For each series of tests in the direction of X, Y and Z, five test specimens were used. Load-displacement values were continuously recorded until failure occurred. A straight line drawn tangent to the initial portion of the load-displacement curve estimated the initial slope. Typical load-displacement results for screw connection in directions of X, Y and

Z are illustrated in Figure 3.12. The average gradient of the five slopes for each test series was used to compute the strength of the connections in kN/m. These values were then taken as the input for the finite element model. The test results for all directions are listed in Table 3.3.

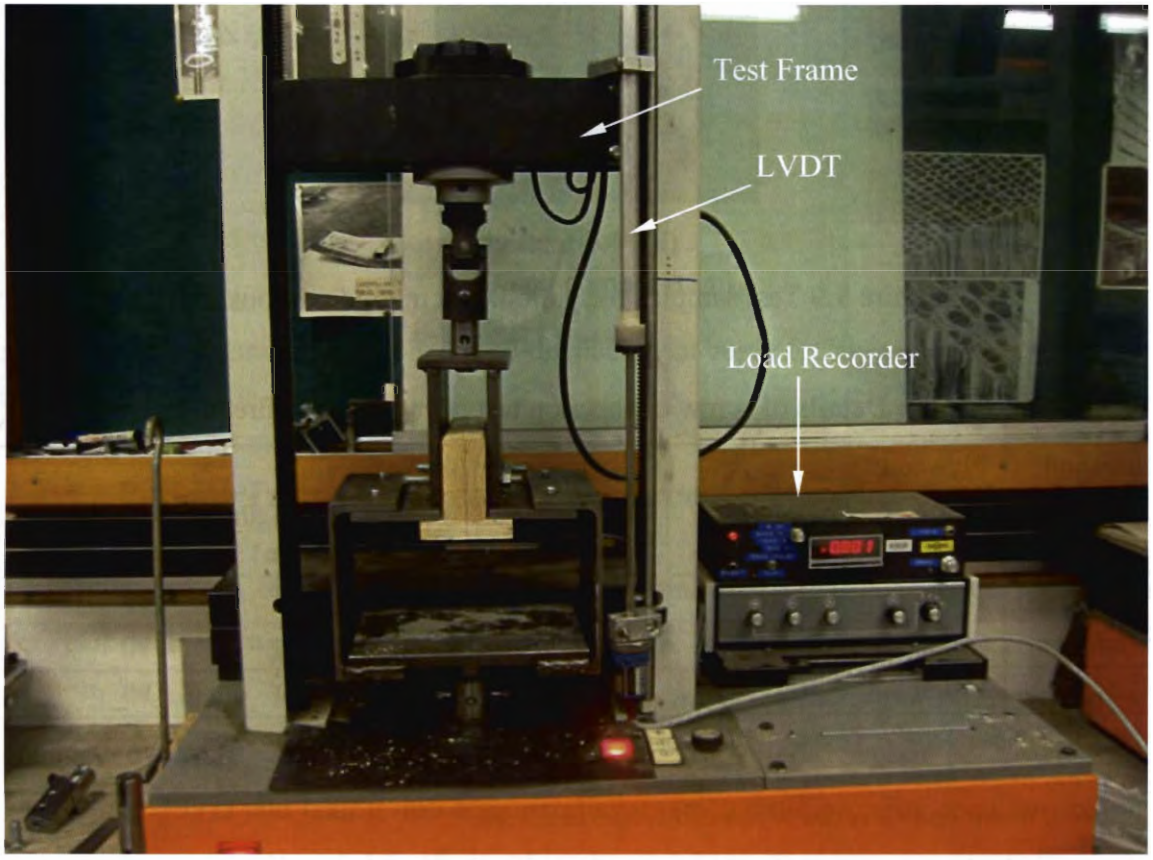
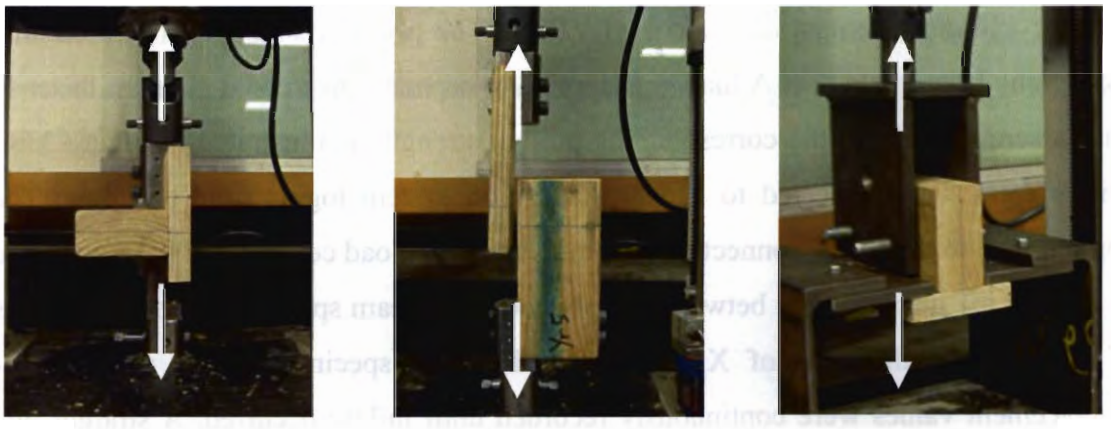
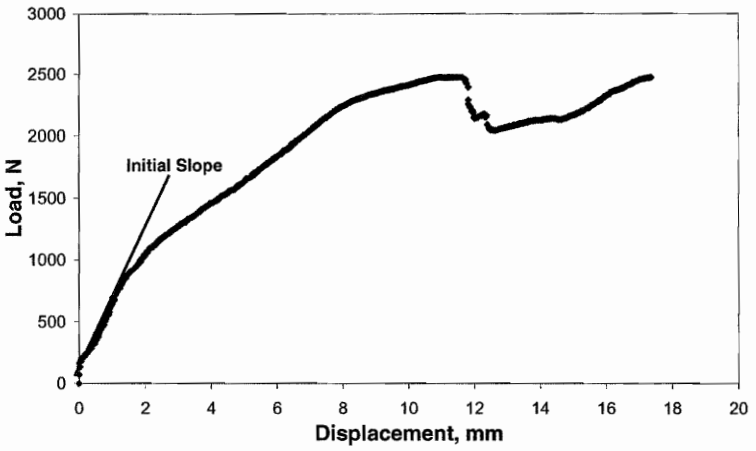


Figure 3.10 Pullout test set up.

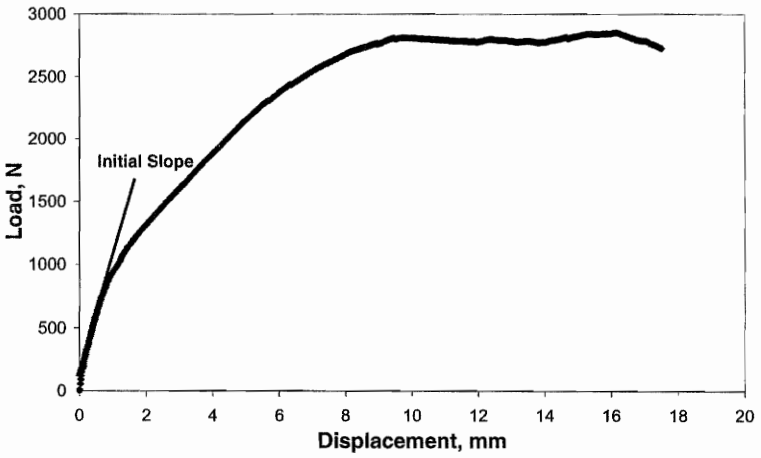


(a) X direction. (b) Y direction. (c) Z direction.

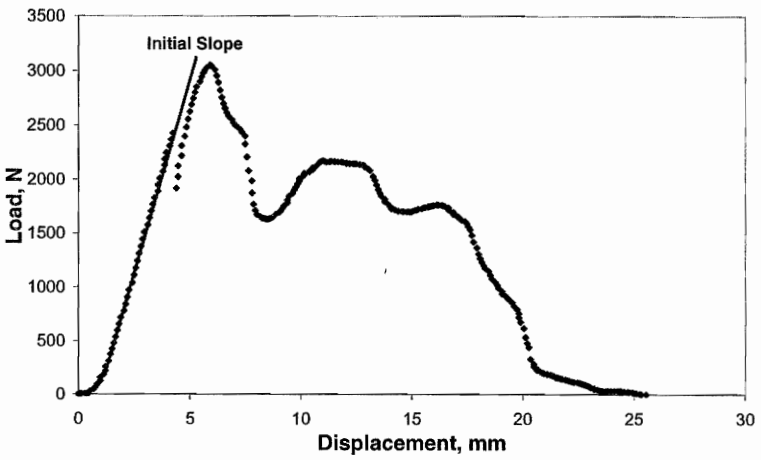
Figure 3.11 Typical pullout test set up in all directions.



(a) X direction.



(b) Y direction.



(c) Z direction.

Figure 3.12 Typical pullout test results in all directions.

Table 3.3 Pullout test results

Direction	Test Sample (kN/m)					Average Pullout Strength (kN/m)	Standard Deviation (kN/m)
	1	2	3	4	5		
X	599.04	777.29	569.88	733.40	437.24	623	136
Y	892.10	789.28	936.84	753.75	950.93	865	89
Z	742.19	877.87	852.93	791.99	777.68	809	56

3.5 Summary

A basic knowledge of material properties of wood confirms that wood/timber is a construction material with inherent natural variability which behaves differently along its principal directions. These make damage detection for wood/timber structures not as straight forward when compared to other construction materials. The material testing procedures were performed as a series of testing programs to characterise material properties of the elements for the laboratory timber bridge (timber beams and plywood), and to quantify the screw connection behaviour of a laboratory timber bridge. Testing specifications were defined with due regard to all aspects required for finite element modelling by documenting the outcomes as well as displaying typical results. This program of material characterisation was undertaken to provide reliable data for modelling and interpretation of the behaviour of the laboratory bridge.

Chapter 4

Finite Element Modelling

4.1 Introduction

In this chapter, the processes of establishing reasonable and reliable Finite Element (FE) models of a laboratory timber beam and a laboratory timber bridge are presented. The modelling for the timber beam FE model is quite straight forward while that for the laboratory timber bridge FE model is more complicated and more steps are required to achieve a reasonably good model. A series of FE models were generated using different elements (available in ANSYS (2005b)) aiming to search for an appropriate model that behaves like a grillage bridge model (benchmark case). The selected model type (shell-solid) was used to carry out parametric studies to understand the effects of different components in the model. Subsequently, a preliminary laboratory timber bridge FE model was established based on dynamic similitude of typical short-span timber bridges in Australia. It was followed by adopting experimental tests data for timber material and geometrical properties in the model. An advanced FE model was then developed from the preliminary model with more comprehensive features by incorporating the outcomes of the test results. The advanced FE model was updated with the experimental modal data based on a global objective function producing a FE model for detailed study of damage detection. The procedures of updating the bridge FE model may have application in actual load rating, which is not included in the scope of this investigation.

4.2 Modelling of Beam-like Structures

Using a finite element (FE) model, modal analysis was performed numerically on a sawn timber beam (a beam-like structure) widely available in Australia. All the FE analyses were carried out using a commercial finite element analysis (FEA) package, namely, ANSYS (2005a). The modelling of a beam-like structure is straight forward.

4.2.1 Finite Element Model for Undamaged Timber Beam

A schematic diagram of the finite element (FE) model of a timber beam without any damage is shown in Figure 4.1. The FE model of timber beam was used to simulate girders of timber bridges that contribute most to the structure flexural stiffness. The specimen's breath and depth were 45mm and 90mm (see Figure 4.2), respectively, with a span length of 4,500mm. The material properties were assumed isotropic because it was deemed sufficient to represent the flexural stiffness in longitudinal direction along the span length as this is the major contribution to the overall stiffness of a girder-deck system. The beam model is of radiata pine timber with modulus of elasticity of 12,196N/mm^2, obtained from a four point bending test (for details refer to Chapter 3). The solid elements (SOLID45) were utilised to model the beam, to which different damage scenarios can easily be introduced. The SOLID45 element was selected as recommended for the 3-D modelling of solid structures in ANSYS documentation (ANSYS Inc. 2005b). The element is defined by eight nodes having three degrees of freedom at each node, i.e., translations in the nodal x, y, and z directions. The geometry, node locations, and the coordinate system for this element are shown in Figure 4.3. The element is equipped with orthotropic material properties.

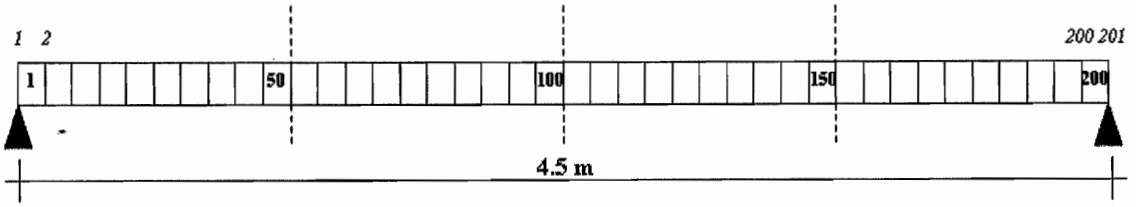


Figure 4.1 Nodes and elements for FE model of the timber beam.

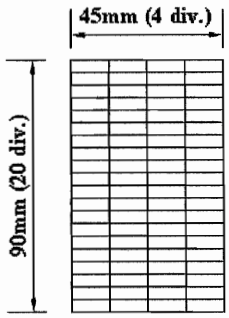


Figure 4.2 Cross section of the FE model.

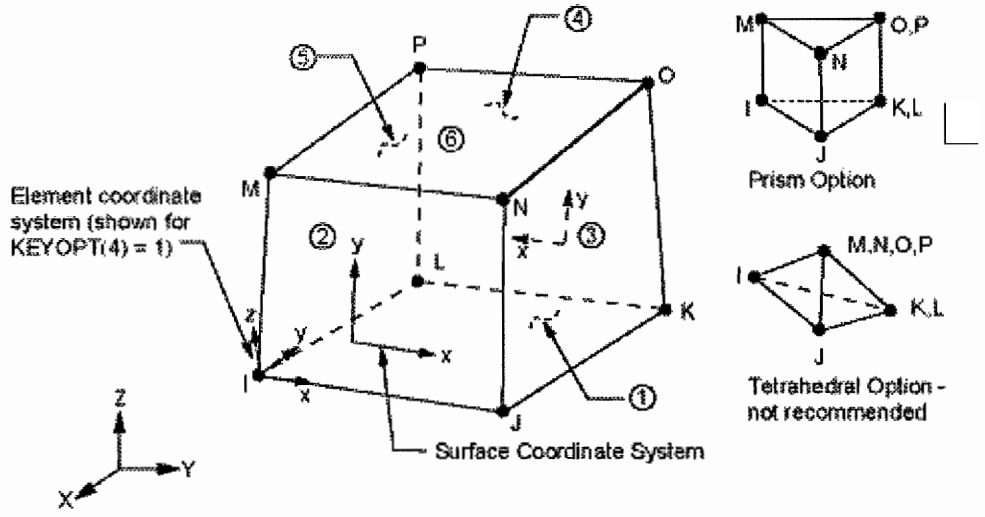


Figure 4.3 The geometric properties of SOLID45 (ANSYS Inc. 2005b).

There are 201 nodes and 200 elements used in the longitudinal directions of the model, denoted by numbers with and without italic, respectively, as shown in Figure 4.1. At the cross sectional area, there are 20 elements across the height and 4 elements along the width as shown in Figure 4.2. The FE model, in total, consists of 21,105 nodes and 16,000 elements. With this mesh configuration, the beam model had 63,315 degrees of freedom (DOF). The boundary conditions for the model were set as pin-pin, which is close to the real boundary condition of girder-deck timber bridge system as shown in Figure 4.4. It is quite obvious from the figure that lag bolts were used to connect the girder and deck as well as the abutment on the river bank, which behave like a pin support. Solving the eigenvalue problem using the modal analysis module in ANSYS, the first five flexural mode shapes were extracted from the FE model as shown in Figure 4.5 and described in Table 4.1. These mode shape data were mass normalised (Farrar & Juaragui 1996), such that the modal vector satisfies the following condition.

$$\{\phi_n\}^T [m]\{\phi_n\} = 1 \qquad \text{Equation 4.1}$$

where $\{\phi_n\}$ is the normalised modal vector and $[m]$ the mass matrix. Letting Ψ_n represent the original modal amplitudes obtained numerically or experimentally before the mass normalisation process, the normalised modal amplitude ϕ_n is formulated using Equation 4.2.

$$\{\phi_n\} = \frac{1}{\sqrt{M_n}} \{\Psi_n\}, \qquad \text{Equation 4.2}$$

where

$$M_n = \sum_{i=1}^{p} \Psi_{in}^2 m_i \quad . \qquad \text{Equation 4.3}$$

In Equation 4.3, p represents the number of measured points and n is the mode shape number.



Figure 4.4 "Pinned" connections between the girder, deck and abutment.

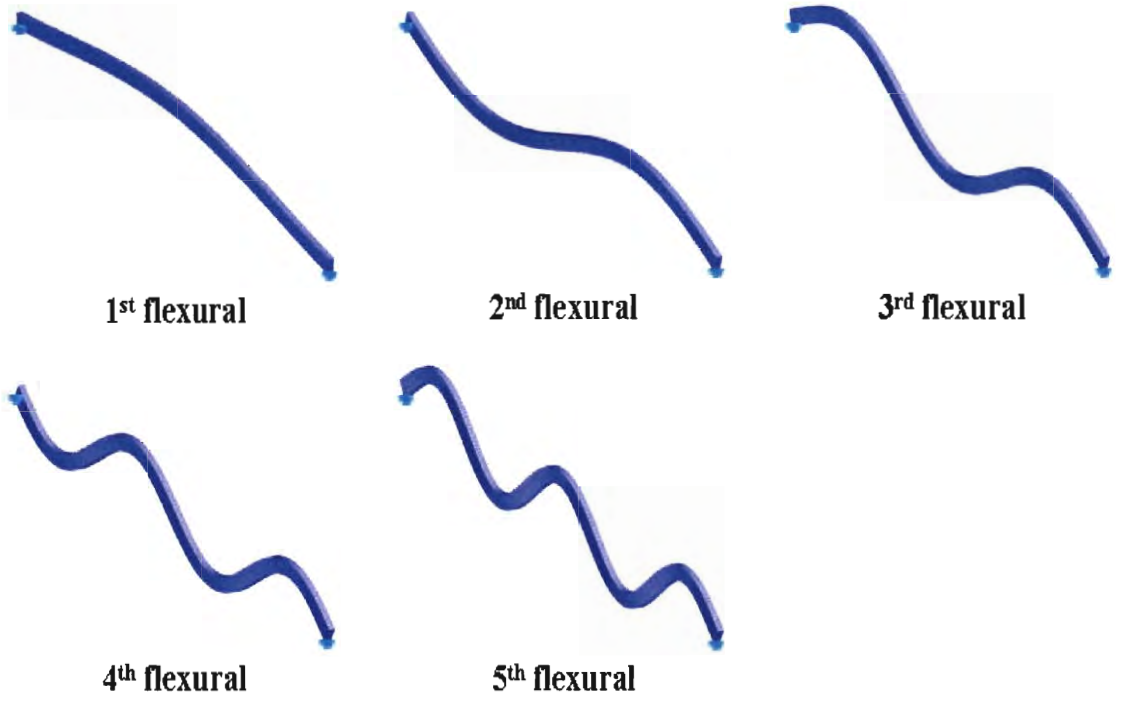


Figure 4.5 First five flexural mode shapes for the FE beam model.

Table 4.1 Description of mode shape.

No	Mode	Mode Shape
1	1	First flexural mode
2	2	Second flexural mode
3	3	Third flexural mode
4	4	Fourth flexural mode
5	5	Fifth flexural mode

The input material properties for the timber beam in the FE model were:

E (modulus of elasticity) = 12,196 N/mm^2,

ν (Poisson's ratio) = 0.3, and

ρ (density) = 500 kg/m^3.

The shear modulus (GXY) defaults by ANSYS to $EX/(2(1+\nu))$. Also, Poisson's ratio can not be equal or greater than 0.5. The modulus of elasticity was obtained from a four point bending test for a timber beam as detailed in Chapter 3. The density was estimated from the same test sample using the ratio of self weight over the volume. The value of Poisson's ratio was approximated using Wood Handbook (General Technical Report FPL-GTR-113 1999) for species of Pine.

4.2.2 Mesh Density

As mentioned earlier, the updating of the FE model using the modal parameters aims to study, analytically, damage detection in timber structures. Hence, the effectiveness of damage detection methods to be introduced is closely related to the number of elements of the structure or components. The number of elements to be used for damage detection is dictated by the number of sensors used in the measurement. In order to produce reliable and accurate results, a relatively large number of sensors are required to produce the fine coordinates of the mode shapes. In the analytical simulation, the coordinates can be controlled by mesh density. Referring to Figure 4.1, the FE model has 201 nodes with intervals of 22.5mm along the span for all longitudinal grids. The coordinates are considered very fine for damage detection as shown in Figure 4.6, where modified damage index I (MDI-I) algorithm was utilised to detect damage using the first five flexural modes for cases 6S and 4S6S. With higher number of degrees of freedom in the vertical direction used for extracting the mode shape data, more computing resources are required to analyse a damage case which may not be necessary for the purpose of this investigation. For instance, case 6L (see Figure 4.6a) using 201 nodes in the damage localisation algorithm is capable of detecting a range of damage index (Z_j) values larger than zero, indicating the presence of damage at that region (from 3.3075m to 3.4425m). From this group of damage index values, the peak amongst them represents the predicted damage location which is at ¾ span (3.375m from left support). Comparing to the actual inflicted damage length in longitudinal direction of 45mm or 1% of the span length, the predicted damage length is 157.5mm using 201 nodes to identify the damage location, for instance case 6L (see Figure 4.6a). While for a less dense mesh comprising 41 nodes with intervals of 112.5mm, (suggested based on the requirement to have equal spacing between all nodes as well as the predicted damage region) for instance case 6L (see Figure 4.7a) is 112.5mm which is similar to the same case using 201 nodes in the algorithm. From Figures 4.6 and 4.7, the damage detection results using 41 nodes in the damage localisation algorithm are comparable to the 201 node results as depicted. Although the damage index values are generally smaller using the 41 nodes, they are high enough and able to locate the inflicted damage location very precisely. It is deduced that 41 nodes used in the analytical investigation for damage detection is deemed sufficient and all following discussions will be based on using 41 nodes.

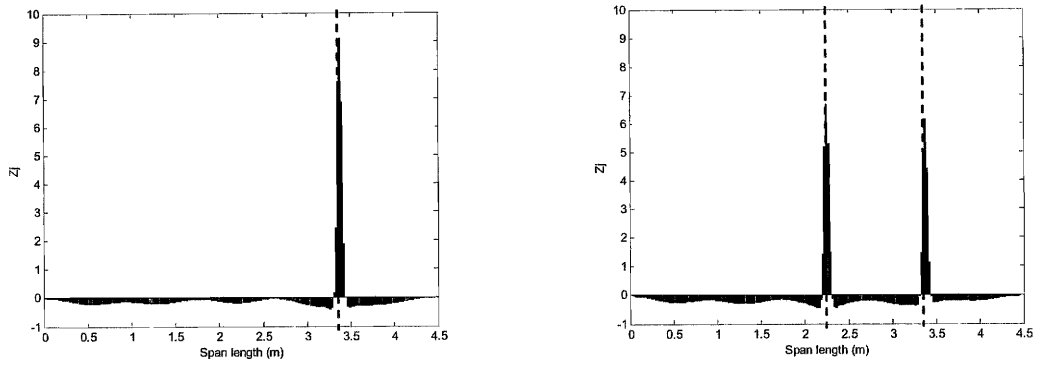


Figure 4.6 Damage location detection using fine mesh density with 201 nodes in the FE model.

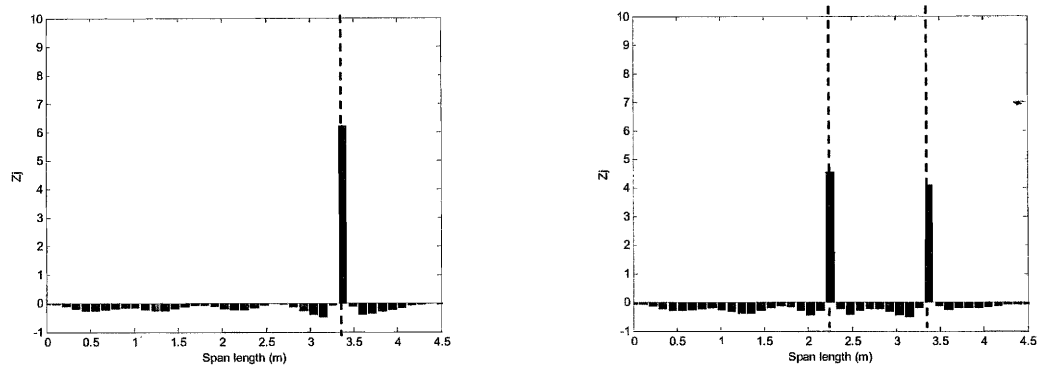


Figure 4.7 Damage location detection using coarse mesh density with 41 nodes in the FE model.

In the latter part of this study, the numerical investigation will be validated with the experimental results. It is commonly known that in the field applications or experimental testing, the evaluation of the coordinates of the mode shape vectors is limited by the number of sensors used in the testing, which is often far less than what is desired. In order to obtain comparable number of FE data with the experimental tests in terms of measurement locations, 9 data points with spacings of 1/8 of the span length on the top chord of the beam, including the supports, were required. To overcome this limitation, the techniques for reconstructing mode shapes, to increase the number of coordinates, are proposed. In this study, two available interpolation techniques namely, Shannon sampling theory and cubic spline, were adopted and compared, for reconstruction of the mode shapes. The measured mode shape coordinates can be interpolated using either technique to generate mode shape vectors of greater length.

The cubic spline interpolation technique is preferred to the Shannon's sampling theorem. The details of the comparison will be discussed in Chapter 6. Referring to Figures 4.6 and 4.7, the results of reconstructed 201 and 41 nodes are similar. This again reaffirms the rational for using 41 nodes.

4.2.3 Simulation of Damage in Beam Model

The damage to be simulated in this investigation is pockets from rotten wood or termite attack, typically found in the girders of timber bridges. Single and multiple damage scenarios were introduced on a timber beam representing a typical girder found in timber bridges. The damage cases as described in Table 4.2 consist of a rectangular opening from the soffit of the beam along the span length. These damages are inflicted at 2/8, midspan, 5/8 and 6/8 of the span length to simulate rot or damage by termite attack, which usually starts from the top surface in timber girders. They are represented by numbers 2, 4, 5 and 6, respectively. The damage models were intended to study the changes in modal parameters numerically due to different location and severity of damage. In this investigation and the discussions that follow, L, M and S denote light, medium and severe damage, respectively. All the inflicted damage are 1% of the total span length (45mm) in length and consist of cuts of 10%, 30% and 50% of the beam depth, designating damage cases L, M and S, respectively, as shown in Table 4.2. The 10%, 30% and 50% of the beam depth cut in cross section correspond to 27.1%, 65.7% and 87.5% of loss of the second moment of area, respectively. The configuration of the damage cases is shown in Figure 4.8. The method of modelling the damage involves changing the geometry only, and does not introduce nonlinearities into the model. It is therefore sufficient to perform a linear analysis to ascertain the effects of the damage on the dynamic properties of the structure.

Table 4.2 Dimensions of inflicted damage.

Damage Case	Damage Scenario	Location per 8th of span length	Length *l* (mm)	Depth *h* (mm)	% loss of 'I'
0	Undamaged	0	0	0	0
1	4L	4	45	9	27.1
2	4M	4	45	27	65.7
3	4S	4	45	45	87.5
4	4S6L	4, 6	45	45, 9	87.5, 27.1
5	4S6M	4, 6	45	45, 27	87.5, 65.7
6	4S6S	4, 6	45	All 45	All 87.5
7	4S5L6S	4, 5, 6	45	45, 9, 45	87.5, 27.1, 87.5
8	4S5M6S	4, 5, 6	45	45, 27, 45	87.5, 65.7, 87.5
9	4S5S6S	4, 5, 6	45	All 45	All 87.5
10	2L4S5S6S	2, 4, 5, 6	45	9, 45, 45, 45	27.1, 87.5, 87.5, 87.5
11	2M4S5S6S	2, 4, 5, 6	45	27, 45, 45, 45	65.7, 87.5, 87.5, 87.5
12	2S4S5S6S	2, 4, 5, 6	45	All 45	All 87.5
13	6L	6	45	9	27.1
14	2L6L	2, 6	45	All 9	All 27.1
15	2L4L6L	2, 4, 6	45	All 9	All 27.1
16	2L4L6M	2, 4, 6	45	9, 9, 27	27.1, 27.1, 65.7
17	2M4L6M	2, 4, 6	45	27, 9, 27	65.7, 27.1, 65.7
18	2M4M6M	2, 4, 6	45	All 27	All 65.7
19	2M4M6S	2, 4, 6	45	27, 27, 45	65.7, 65.7, 87.5
20	2S4M6S	2, 4, 6	45	45, 27, 45	87.5, 65.7, 87.5
21	2S4S6S	2, 4, 6	45	All 45	All 87.5
22	2S4S5L6S	2, 4, 5, 6	45	45, 45, 9, 45	87.5, 87.5, 27.1, 87.5
23	2S4S5M6S	2, 4, 5, 6	45	45, 45, 27, 45	87.5, 87.5, 65.7, 87.5
24	2S4S5S6S	2, 4, 5, 6	45	All 45	All 87.5

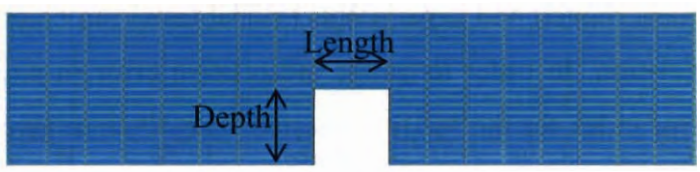


Figure 4.8 Configurations of a typical damage case.

4.2.4 Correlation Analysis

Correlation analysis is a technique to examine quantitatively and qualitatively the correspondence and difference between analytically and experimentally obtained modal parameters (Brownjohn & Xia 1999). This comparison forms a basis for selection of modal parameters pertaining to dynamic responses for model updating. In the beam analysis, dynamic responses, namely natural frequencies and mode shapes, were used as the indices for the objective function (*OF*) for the correlation analysis. The goal of updating or calibration process of the finite element (FE) model was to minimise the objective function. The global objective function used is shown in Equation 4.4.

$$OF = f(NFerror, MACerror) \qquad \text{Equation 4.4}$$

Besides matching the FE and experimental models using the *OF* by manual adjustment, another aspect, seldom considered by many researches, is the order of mode shapes. The author has found that boundary conditions play an important role in producing an identical sequence of mode shapes between FE and experimental models. Basically this means that if the order of mode shapes is not matched, there is likely to be an error in defining the boundary conditions.

For mode shapes, two criteria were adopted for comparison between all possible mode shape pairs, that is, the order of mode shape and compatibility between modes. Numerical mode shape correlation techniques such as the Modal Assurance Criterion (*MAC*) can be used to check all possible mode shape pairs and calculate a quantity that expresses the level of compatibility.

4.2.4.1 Natural frequencies

For Natural Frequencies (*NF*), the relative error or difference between the analysis (finite element model) and experiments (modal tests) can be computed in order to check their correlation. In order to gauge the relative error in natural frequencies more clearly, an error index for the *NF* is suggested. The *NFerror* given in the *OF* is a function of natural frequency difference between FE and experimental models and is given as follows:

$$NFerror = \frac{\left|\omega_{Exp} - \omega_{FE}\right|}{\omega_{Exp}} 100 \qquad \text{Equation 4.5}$$

where ω is the natural frequency and its subscripts *Exp* and *FE* denote experimental and finite element results, respectively. The values of the natural frequency and *NFerror* are displayed in Table 4.3. The *NFerror* in general is less than 7%, except for mode 4. The reason for slightly larger *NFerror* value for mode 4 may be due to the fact that impact location falls on the anti-node point of this mode. From Figure 4.9, the dotted linear line, representing the correlation between the FE and experimental models, is close to the 45 degree line. It means they match very well and the FE model is able to represent the experimental model well.

Table 4.3 Comparison of natural frequencies for FE model and modal tests for the Beam.

Mode	FE (Hz)	Experimental (Hz)	Difference (Hz)	*NFerror* (%)
1	14.59	13.67	0.92	6.29
2	37.50	37.23	0.27	0.73
3	91.89	91.47	0.42	0.46
4	146.73	132.08	14.65	9.98
5	239.48	227.87	11.61	4.85

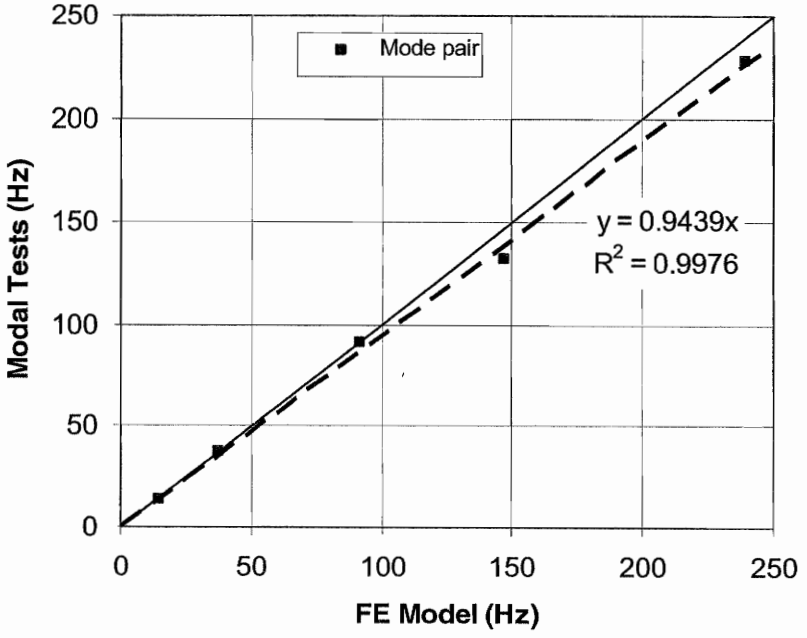


Figure 4.9 Frequency pair between FE model and modal tests for the Beam.

4.2.4.2 Mode shapes

Modal Assurance Criterion (*MAC*) (Allemang & Brown 1983) is one of the most popular measures of correlating two sets of mode shapes. This parameter provides a measure of the least-squares deviation of the points from the straight-line correlation. The *MACerror* utilises *MAC* for indicating the correlation between finite element (*FE*) and experimental (*Exp*) model results.

$$MACerror\left(\varphi_{Exp},\varphi_{FE}\right)=1-\frac{\left|\{\varphi_{Exp}\}^{T}\{\varphi_{FE}\}\right|^{2}}{\left(\{\varphi_{Exp}\}^{T}\{\varphi_{Exp}\}\right)\left(\{\varphi_{FE}\}^{T}\{\varphi_{FE}\}\right)} \qquad \text{Equation 4.6}$$

where φ is the mode shape vector. A value close to 1 indicates poor correlation between the mode shapes, whilst a value close to 0 indicates good correlation. The extent of calibration can be determined through the evaluation of change in the correlation between the mode shapes. The *MACerror* results are tabulated in Table 4.4. The *MACerror* values are generally lower than 0.05. This means that both sets of mode shapes match very well as the *MACerror* values are less than 0.1 (or 90% for MAC), which are considered acceptable (Brownjohn & Xia 1999; Maia & Silva 1997). It is important that the order of mode shapes matches well between both models (Živanovć, Pavic & Reynolds 2006). This is very important for determining whether the geometrical properties of a FE model are close to the real situation, especially the boundary conditions. The order of mode shapes for both FE and experimental models match well. This implies that the physical properties of the analytical model are close to the experimental ones.

Table 4.4 Mode shapes correlation between FE model and modal tests for the Beam.

Mode	*MAC*	% *MAC*	*MACerror*	% *MACerror*
1	1.00	100	0	0
2	1.00	100	0	0
3	0.99	99	0.01	1
4	0.96	96	0.04	4
5	0.97	97	0.03	3

From the results of the *NFerror* and *MACerror* as well as the correctness of the order for the mode shapes between the FE and experimental models, it is inferred that

the finite element (FE) model is simulating very well the experimental model. Therefore, the FE model does not require any updating or tuning and it can be used for all damage cases proposed for the beam in this investigation.

4.3 Modelling of Plate-like Structures

The detailed discussion on the modelling of a timber beam, analytically, is followed by the investigation of the modelling of a timber bridge. A timber bridge is a complex structural system consisting of beam (girders) and plate (deck) systems. In many circumstances, it can be compared to an orthotropic plate-membrane reinforced by a set of equidistant ribs. Some literatures (Lee & Yun 2006; Polensek 1973) utilise orthotropic plate in simulating the dynamic behaviour of a bridge. As suggested by Bodig and Jayne (1993), most wood composites are orthotropic (three mutually perpendicular planes of symmetry). Analysing a bridge using an isotropic plate is also possible and proposed by some researchers (Bodig & Jayne 1993; Yagiz & Skaman 2006). It is therefore advisable to at least briefly look into the impact of the proposed Damage Detection (DD) algorithms utilising the data from undamaged and damaged plate systems at first. This would help to better understand the effects and limitations of applying the proposed DD algorithms to the undamaged and damaged complex girder-deck systems (a timber bridge). In this investigation, a plate with isotropic material properties was first adopted. This was followed by considering an orthotropic system and finally the complex system of a laboratory timber bridge in section 4.4. The modelling of isotropic and orthotropic plates would provide some useful information on the differences of plates (isotropic and orthotropic) and stiffened plate (beam and orthotropic plate system) results when applying the proposed damage detection algorithms.

4.3.1 Isotropic Plate

For the isotropic plate model, the deck was simulated using the SHELL63 element in ANSYS. This element has both bending and membrane capabilities. Both in- and out of plane loads are permitted. The element has six degrees of freedom at each node, that is, translations in the nodal x, y, and z directions and rotations about the nodal x, y, and z-axes as shown in Figure 4.10. Since the plate is modelled as an isotropic one, it should exhibit no internal symmetry and hence no directional properties. The material properties of the isotropic deck are listed below:

EX (modulus of elasticity) = 8,112 N/mm^2

v (Poisson's ratio) = 0.3

ρ (density) = 510 kg/m^3

Since the plate is isotropic, the shear modulus (GXY) defaults by ANSYS to *EX*/(2(1+ v)). The Poisson's ratio should also be equal to less than 0.5. The modulus of elasticity was obtained from a four point bending test for plywood as detailed in Chapter 3. The density was estimated from the same test samples using the ratio of self weight over the volume. The value of Poisson's ratio was adopted from the timber beam since it has little effect on the response (Crews 2002).

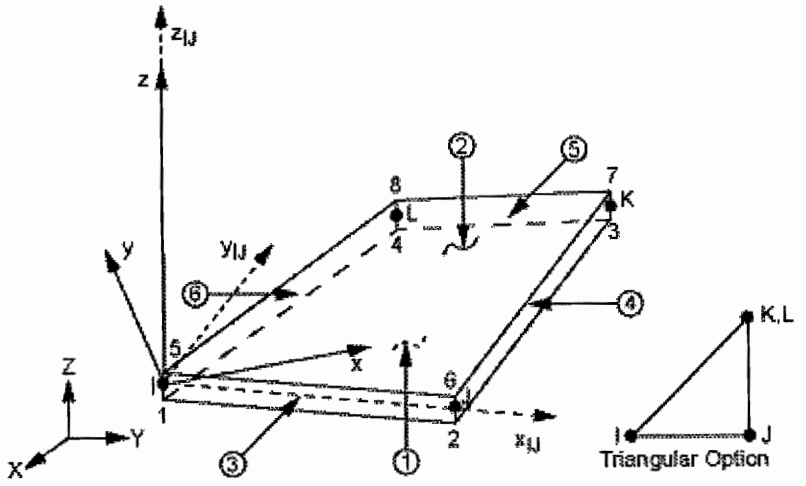


Figure 4.10 The geometric properties of SHELL63 element (ANSYS Inc. 2005b).

The geometric configuration of the deck simulated by isotropic plate elements is shown in Figure 4.11. The deck is 4.5m long and 2.4m wide with a thickness of

21mm. These configurations are the same as those for the laboratory timber beam model to be discussed later. Pin supports were applied to the positions where the girders are placed as shown in Figure 4.12. The modal parameters (natural frequencies and mode shapes) were extracted using the eigenvalue solution through modal analysis in ANSYS. These modal parameters were later applied in the proposed damage detection algorithm to detect damage.

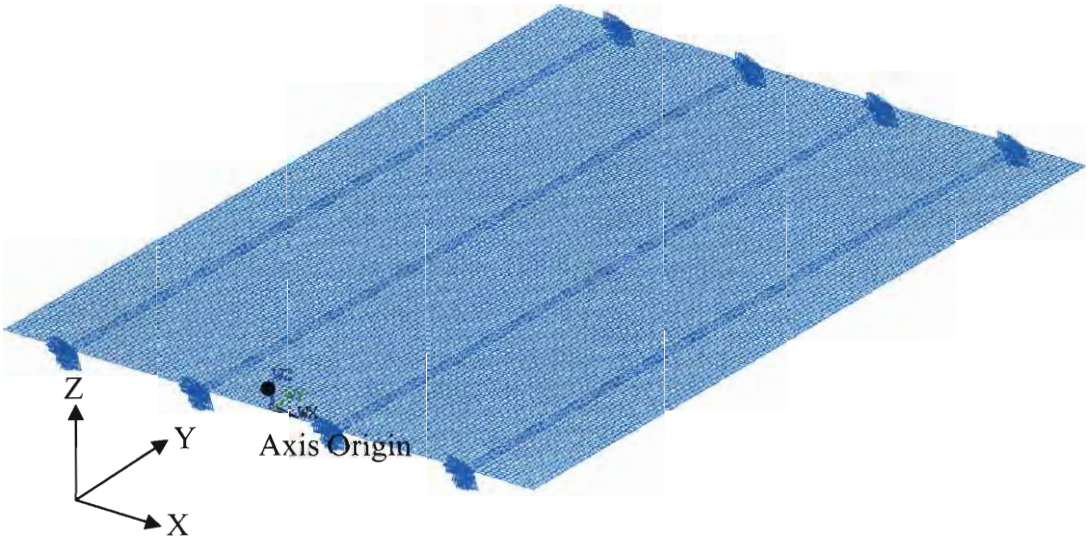


Figure 4.11 Geometric configuration of the isotropic plate.

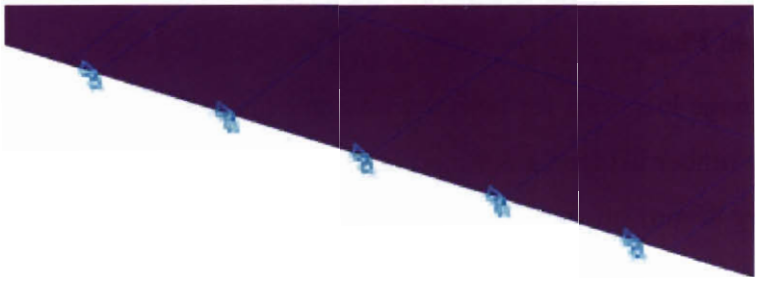


Figure 4.12 Boundary conditions of the isotropic plate.

4.3.2 Orthotropic Plate

The geometric configuration and boundary conditions of the orthotropic plate model is exactly the same as the isotropic plate model. The only difference is their material properties. Orthotropic plates exhibit different material properties in the two orthogonal directions (strong and weak directions) and symmetric about three mutually perpendicular planes. The material properties of the orthotropic deck are listed below:

EX (modulus of elasticity) = 3,600 N/mm^2
EY (modulus of elasticity) = 8,112 N/mm^2
EZ (modulus of elasticity) = 3,600 N/mm^2
NUXY (Poisson's ratio) = 0.04
NUYZ (Poisson's ratio) = 0.04
NUXZ (Poisson's ratio) = 0.04
GXY (shear modulus) = 595 N/mm^2
GXY (shear modulus) = 198 N/mm^2
GXY (shear modulus) = 179 N/mm^2
ρ (density) = 510 kg/m^3

The moduli of elasticity along the three major axes were obtained from a four point bending test for plywood as detailed in Chapter 3 and various engineering standards such as Finnish Wood Handbook (Finnish Forest Industries Federation 2002). The density was estimated from the same test samples using the ratio of self weight over the volume. The value of Poisson's ratio was adopted from Kollmann, Keunzi and Stamm (1975). More details of the material properties of the orthotropic plate model will be discussed in section 4.4.1.

4.3.3 Damaged Plate

The damage locations for both the isotropic and orthotropic plates are the same as the laboratory timber bridge as outlined in Table 4.5. One simulated damage with the area of 45mm by 45mm on the FE plate model is illustrated in Figure 4.13. With the plate idealised as a laboratory timber bridge, and in the absence of girders (beam), the damage was simulated on the deck (plate). It was intended to gain a full understanding of the complex nature and behaviour of a damaged timber bridge (deck-girder system). The damage induced is divided into three categories, that is, light (P), medium (Q) and severe (R), corresponding to a reduction of the modulus of elasticity of 10%, 25% and

50%, respectively. It should be noted that the damage severity here is different from the timber beam and laboratory timber bridge. The dynamic responses of the plates were used in the proposed damage algorithms for comparison with the laboratory bridge.

Table 4.5 Dimensions of inflicted damage in plate.

Damage Scenario	Damage girder/Location	% reduction of modulus of elasticity
UP	-	-
g2P	G2/¾ span	10
g2Q	G2/¾ span	25
g2R	G2/¾ span	50
g2Rg4P	G2/¾ span, G4/midspan	50,10
g2Rg4Q	G2/¾ span, G4/midspan	50,25
g2Rg4R	G2/¾ span, G4/midspan	50,50
g2Rg4Rg3P	G2/¾ span, G4/midspan, G3/¼ span	50,50,10
g2Rg4Rg3Q	G2/¾ span, G4/midspan, G3/¼ span	50,50,25
g2Rg4Rg3R	G2/¾ span, G4/midspan, G3/¼ span	50,50,50
g2Rg4Rg3Rg1P	G2/¾ span, G4/midspan, G3/¼ span, G1/1/8 span	50,50,50,10
g2Rg4Rg3Rg1Q	G2/¾ span, G4/midspan, G3/¼ span, G1/1/8 span	50,50,50,25
g2Rg4Rg3Rg1R	G2/¾ span, G4/midspan, G3/¼ span, G1/1/8 span	50,50,50,50

Notes:

UP = Undamaged Plate

gi = girder No. i

P, Q, R representing light (P), medium (Q) and severe (R) damage, correspond to 10%, 25% and 50% reduction of modulus of elasticity (E)

(e.g., g2Rg4Rg3Rg1Q denotes a cumulative damage scenario of medium damage on 1/8 span of girder 1, severe damage on ¼ span of girder 3, ¾ span of girder 2 and ½ span of girder 4)

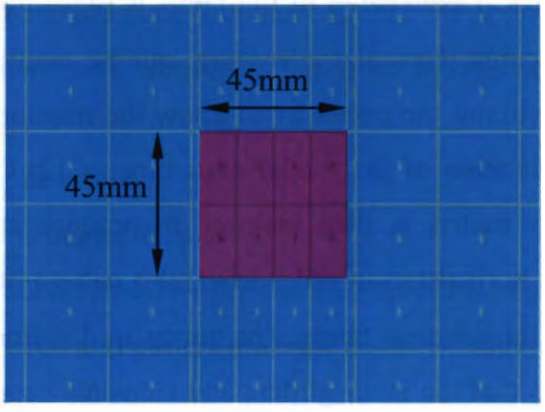


Figure 4.13 A close-up plan view of a typical damage on the plate model.

4.4 General Modelling Considerations for Timber Bridge Structures

One of the problems confronting any Finite Element (FE) model approach to timber structures such as a timber bridge is determination and/or selection of appropriate values for the elastic properties required for accurate modelling (Crews 2002). As mentioned by Crews (2002), very little work has been done in this area and the inherent variability of timber must always be remembered as a "reality check" when applying characteristic values of material properties for any analytical model. Therefore, one of the important outcomes of this investigation has been the updating of the FE model of a laboratory timber bridge using the experimental modal data utilising correlation and sensitivity analysis of key modal parameters.

4.4.1 Grillage Model for Comparison

Initially, a hand-calculated grillage analytical model was established using beam theory with simply supported boundary conditions. The torsional rigidity and the effect of deformation caused by the shearing forces were neglected. As suggested by Ghali, Neville and Cheung (1978), to generate the stiffness matrix requires the analysis of a statically indeterminate structure for each column of a stiffness matrix [*S*]. The stiffness matrix [*S*] is obtained by inversion of the flexibility matrix. The layout of the grillage model using the concept suggested by Ghali, Neville and Cheung (1978) is illustrated in Figure 4.14. There are three degrees of freedom at any joint of the grid, that is, vertical translation and rotation about two perpendicular axes in the plane of the grid. However, if the vertical translation of the joints is prevented, the grid becomes a system of continuous beams. Hence, the system can be analysed for the effect of movement of one joint without the necessity to know the rotations. By applying a unit load at one designated location of the model each time, a 12x12 flexibility matrix is produced. The flexibility matrix is then inverted to produce stiffness matrix of the system. This matrix was normalised in order to exhibit pattern of stiffness distribution in the system, especially the diagonal terms. The normalised stiffness matrix is shown in Figure 4.15. It is obvious that the inner girders and elements near the mid-span exhibit higher stiffness.

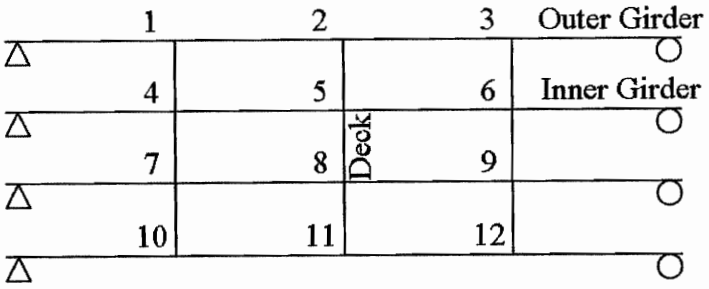


Figure 4.14 Layout of the grillage model.

$$\begin{bmatrix}
0.59 & -0.52 & 0.21 & & & & & & & & & \\
-0.52 & 0.80 & -0.52 & & & & & & & & & \\
0.21 & -0.52 & 0.59 & & & & & & & & & \\
 & & & 0.79 & -0.52 & 0.21 & & & & & & \\
 & & & -0.52 & 1.00 & -0.52 & & & & & & \\
 & & & 0.21 & -0.52 & 0.79 & & & & & & \\
 & & & & & & 0.79 & -0.52 & 0.21 & & & \\
 & & & & & & -0.52 & 1.00 & -0.52 & & & \\
 & & & & & & 0.21 & -0.52 & 0.79 & & & \\
 & & & & & & & & & 0.59 & -0.52 & 0.21 \\
 & & & & & & & & & -0.52 & 0.80 & -0.52 \\
 & & & & & & & & & 0.21 & -0.52 & 0.59
\end{bmatrix}$$

Figure 4.15 Normalised stiffness matrix of the analytical model.

This grillage model and its static (normalised stiffness matrix) as well as dynamic (natural frequencies and mode shapes) responses serve as a benchmark to validate FE models composed of different elements. The materials and geometric properties assumptions for the grillage model are listed below:

1. Isotropic material input,
2. The girder and deck have the same E value = 12,222 MPa,
3. The girders' second moment of area is based on a T-section, while the deck is a rectangular section,
4. Boundary conditions: pin-roller,
5. The torsional rigidity is neglected and
6. The effect of deformation caused by the shearing forces is neglected.
7. Connection between deck and girders are rigid or fully composite.

4.4.2 Different Elements Used in Modelling

A laboratory timber bridge consists of a timber deck of structural plywood grade F11 and girders that are of radiata pine sawn timber grade MGP12. The geometry configuration of the bridge is shown in Figure 4.16. Finite element models developed in this investigation were adopted to describe the dynamic behaviour of the laboratory timber bridge, assembled using different elements provided by ANSYS (ANSYS Inc. 2005b) element library. The "ideal" model was then utilised for the damage detection in the latter part of this investigation. Three dimensional FE models are preferred as they can account for distribution of mass and stiffness much closer to the real structures. Unlike in the plate models, some structural components were ignored, which may be the major reason for the significant discrepancy between the results of the analytical model and the real response of the bridge. Precise geometry of the bridge deck and girders has played an important role on the overall dynamic response of the bridge.

In general, the deck was modelled by a plate/shell element, whereas girders by plate/shell, beam or solid elements. Kurian (2000) suggested that deck can be modelled using a four-noded shell element, namely, SHELL63 and girders with either a three dimensional (3-D) two-noded beam element BEAM4 or a shell element. In the Kurian's work, the two models compared very well with each other. However, there is more composite action for a model using both shell elements for the deck and girders. The author also mentioned that a model with beam elements for the girders exhibited problem at the location of supports. Hence, it is recommended by the author to use shell elements for deck and girders and the other model can be used as a good approximation. Based on this, three initial combinations of elements for deck/girder are proposed, that is, shell/shell, shell/beam and shell/solid (not used by Kurian). These finite element models were compared based on two criteria, namely, normalised stiffness matrix and natural frequency.

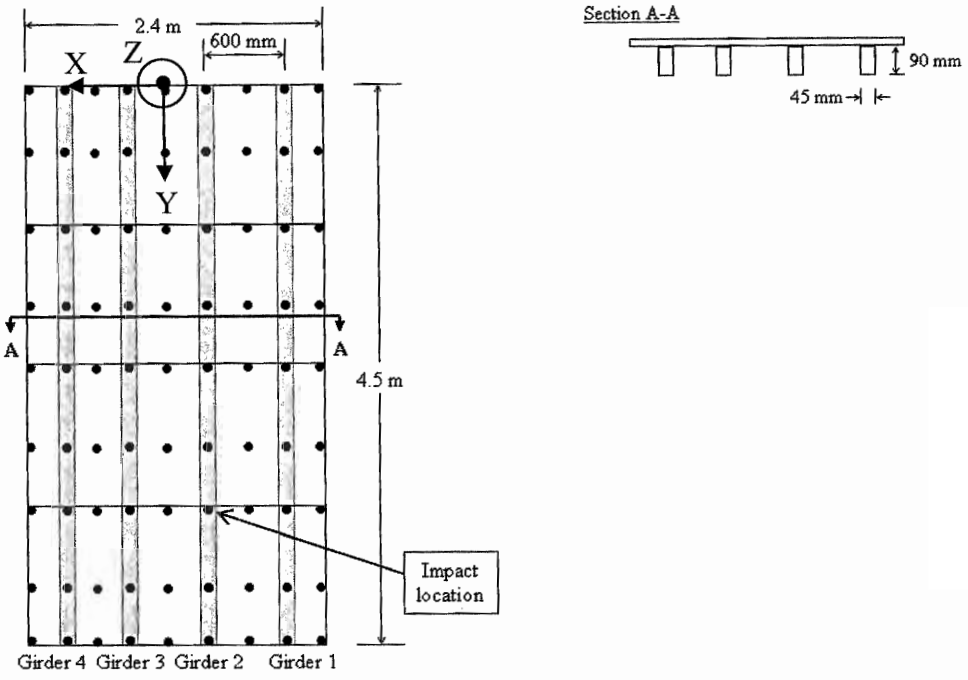


Figure 4.16 Plan view of the laboratory timber bridge.

4.4.3 Comparison of FE Models Using Normalised Stiffness Matrix

4.4.3.1 Shell-Shell Model

Based on the model used by Kurian (2000), the first Finite Element (FE) model simulating the laboratory timber bridge was developed using shell elements for both deck and girders. A coarser mesh was used to simulate the deck and girder bridge system. The materials and geometric input as well as boundary conditions were the same as the analytical grillage model (benchmark for comparison). The normalised stiffness matrix obtained from the shell-shell model is illustrated in Figure 4.17. The sub-matrix is obviously not symmetric although the entire matrix is symmetric. In this discussion, the 3x3 submatrices are considered symmetric, if (1,1) and (3,3) elements on the diagonal are equal, in addition to (i,j) elements being equal to (j,i) elements. The elements for the inner girders showed an inverse trend compared to the benchmark, whereby the elements near the pin support has higher stiffness than the mid-span for the inner girders. This trend is not in accordance with the general principles of structural mechanics. The unsymmetrical sub-matrix may be due to the membrane stiffness effect of the shell element. A shell element is basically designed for in-plane axial force and

out-of-plane bending. Therefore, the in-plane bending for the girders may not be simulated very well by the shell element.

$$\begin{bmatrix}
0.67 & -0.45 & 0.15 & & & & & & & & & \\
-0.45 & 0.70 & -0.42 & & & & & & & & & \\
0.15 & -0.42 & 0.54 & & & & & & & & & \\
 & & & 1.00 & -0.47 & 0.13 & & & & & & \\
 & & & -0.47 & 0.98 & -0.44 & & & & & & \\
 & & & 0.13 & -0.44 & 0.84 & & & & & & \\
 & & & & & & 1.00 & -0.47 & 0.13 & & & \\
 & & & & & & -0.47 & 0.98 & -0.44 & & & \\
 & & & & & & 0.13 & -0.44 & 0.84 & & & \\
 & & & & & & & & & 0.67 & -0.45 & 0.15 \\
 & & & & & & & & & -0.45 & 0.70 & -0.42 \\
 & & & & & & & & & 0.15 & -0.42 & 0.54
\end{bmatrix}$$

Figure 4.17 Normalised stiffness matrix of the shell-shell model.

4.4.3.2 Shell-Beam Model

Since the shell-shell model did not produce a desirable trend for stiffness matrix, a hybrid model was introduced using shell elements for deck and beam elements for girders. A coarser mesh was used in this case. The materials and geometric input as well as boundary conditions were the same as the benchmark model. However, in this case, the centre of gravity of the beam element was not offset. This may produce a weaker system. Nonetheless, this may have no significant effect on the trend of the normalised stiffness matrix. The normalised stiffness matrix is illustrated in Figure 4.18. It is apparent that this matrix is symmetrical. The model shows a comparable trend to that of the benchmark. Although it depicts higher stiffness distribution for the inner girders, the normalised stiffness trend is acceptable.

$$\begin{bmatrix}
0.36 & -0.18 & 0.03 & & & & & & & & & \\
-0.18 & 0.42 & -0.18 & & & & & & & & & \\
0.03 & -0.18 & 0.36 & & & & & & & & & \\
 & & & 0.94 & -0.23 & 0.03 & & & & & & \\
 & & & -0.23 & 1.00 & -0.23 & & & & & & \\
 & & & 0.03 & -0.23 & 0.94 & & & & & & \\
 & & & & & & 0.94 & -0.23 & 0.03 & & & \\
 & & & & & & -0.23 & 1.00 & -0.23 & & & \\
 & & & & & & 0.03 & -0.23 & 0.94 & & & \\
 & & & & & & & & & 0.36 & -0.18 & 0.03 \\
 & & & & & & & & & -0.18 & 0.42 & -0.18 \\
 & & & & & & & & & 0.03 & -0.18 & 0.36
\end{bmatrix}$$

Figure 4.18 Normalised stiffness matrix of the shell-beam model.

4.4.3.3 Shell-Solid Model

The shell-beam model has provided a "correct" trend for the stiffness matrix. However, the model is considered not very suitable for inflicting damage in terms of removing elements from the girders to simulate a real situation. Therefore, a new hybrid model was introduced using shell element SHELL63 for deck and solid element SOLID45 for girders, which was not mentioned in Kurian's work. Due to the geometric set up of the model, a slightly finer mesh was used for this model to avoid violation of element shape aspect ratio. The materials and boundary conditions were the same as the benchmark. SHELL63 and SOLID45 elements have six and three Degrees of Freedoms (DOFs), respectively. An additional arbitrary element MATRIX27 was also used to connect the shell and solid elements, with different numbers of DOFs. The MATRIX27 is capable of representing properties such as stiffness, damping and mass matrix. It is used as a rigid link between the two elements to simulate screw connections. The stiffness of the rigid link was arbitrarily chosen and is listed in Table 4.6. The close-up view of the geometric set up of the model is shown in Figure 4.19.

In this model, two types of shell element behaviour were introduced, that is, 'with bending stiffness only' (Case B) and 'with bending and membrane stiffness' (Case BM). The Cases B and BM normalised stiffness matrices are illustrated in Figures 4.20 and 4.21. It is apparent that the matrix for Case B is symmetrical and while for Case BM is not at the sub-matrix level. From these two matrices, it is clear that the membrane stiffness contributes to the lack of symmetry at the sub-matrix level. This may be due to pin support attracting larger forces compared to roller support. If a pin-pin boundary

condition is introduced, the matrix for Case BM should be symmetric. Nevertheless, the two cases show quite similar stiffness distribution trends compared to the benchmark. Although they depict higher stiffness distribution for the inner girders, the normalised stiffness trend is still considered acceptable.

Table 4.6 Preliminary input values for element MATRIX27.

Translational	N/m
kx	10^4
ky	$7x10^5$
kz	10^{14}
Rotational	Nm/rad
krotx	1*kx
kroty	1*ky
krotz	1*kz

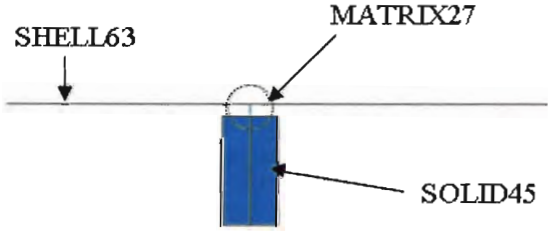


Figure 4.19 Cross sectional view of a shell-solid element with rigid link.

$$\begin{bmatrix}
0.42 & -0.30 & 0.10 & & & & & & & & & \\
-0.30 & 0.54 & -0.30 & & & & & & & & & \\
0.10 & -0.30 & 0.42 & & & & & & & & & \\
 & & & 0.90 & -0.31 & 0.08 & & & & & & \\
 & & & -0.31 & 1.00 & -0.31 & & & & & & \\
 & & & 0.08 & -0.31 & 0.90 & & & & & & \\
 & & & & & & 0.90 & -0.31 & 0.08 & & & \\
 & & & & & & -0.31 & 1.00 & -0.31 & & & \\
 & & & & & & 0.08 & -0.31 & 0.90 & & & \\
 & & & & & & & & & 0.42 & -0.30 & 0.10 \\
 & & & & & & & & & -0.30 & 0.54 & -0.30 \\
 & & & & & & & & & 0.10 & -0.30 & 0.42
\end{bmatrix}$$

Figure 4.20 Normalised stiffness matrix of the shell-solid model Case B.

$$\begin{bmatrix}
0.71 & -0.51 & 0.19 & & & & & & & & & \\
-0.51 & 0.77 & -0.49 & & & & & & & & & \\
0.19 & -0.49 & 0.58 & & & & & & & & & \\
 & & & 0.99 & -0.50 & 0.17 & & & & & & \\
 & & & -0.50 & 1.00 & -0.47 & & & & & & \\
 & & & 0.17 & -0.47 & 0.83 & & & & & & \\
 & & & & & & 0.99 & -0.50 & 0.17 & & & \\
 & & & & & & -0.50 & 1.00 & -0.47 & & & \\
 & & & & & & 0.17 & -0.47 & 0.83 & & & \\
 & & & & & & & & & 0.71 & -0.51 & 0.19 \\
 & & & & & & & & & -0.51 & 0.77 & -0.49 \\
 & & & & & & & & & 0.19 & -0.49 & 0.58
\end{bmatrix}$$

Figure 4.21 Normalised stiffness matrix of the shell-solid model Case BM.

4.4.4 Comparison of FE Models Using Natural Frequency

Besides considering the normalised stiffness matrix, which is an important characteristic of the system, the dynamic response of the Finite Element (FE) models was also being considered in terms of their natural frequencies. The three models discussed above were used again for comparison with the benchmark. They are shell-shell, shell-beam and shell-solid FE models. In this case, the first five sets of natural frequencies are compared as tabulated in Table 4.7.

Table 4.7 Natural frequency of different models

Set	Shell-Shell, Hz	Shell-Beam, Hz	Shell-Solid#, Hz
1	9.78*	3.27*	7.45*
2	18.13**	7.18	10.34**
3	37.01	10.16**	12.39
4	42.36***	13.22***	24.86***
5	54.35	13.96	28.72

 # SHELL63 with bending and membrane stiffness

** 1st flexural mode (fundamental frequency)*

*** 1st transversal mode*

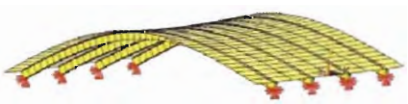
**** 2nd flexural mode*

From Table 4.7, the shell-shell and shell-solid models showed a reasonably close fundamental frequency compared to the preliminary modal test and experimental modal analysis (EMA) results of 7.10Hz for the fundamental frequency. However, the

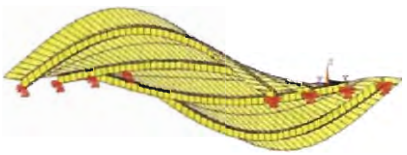
shell-beam model fundamental frequency is about 50% less than the experimental value. For the shell-shell model, the normalised stiffness had shortcoming and hence the shell-solid model was finally chosen to perform further parametric studies based on a reasonably accurate model to represent the laboratory timber bridge.

4.4.5 Mode Shape

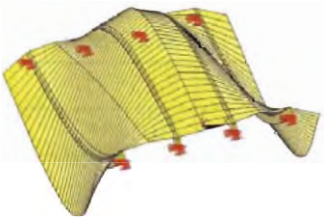
Mode shapes are inherent properties of a structure. They do not depend on the forces acting on the structures. Mode shapes will change if the material properties, such as mass, stiffness and damping or boundary conditions of the structure change. They are a convenient way of describing resonant vibration or natural frequency of a system (Richardson 1997). The first five modes of the shell-solid model are illustrated in Figure 4.22. These modes serve as a basis for comparison between different FE models.



(a) First flexural mode



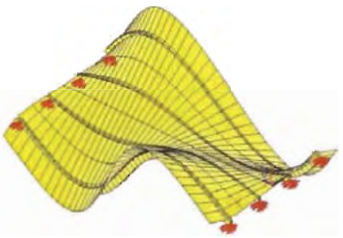
(b) First torsional mode



(c) First transversal mode



(d) Second flexural mode



(e) Second torsional mode

Figure 4.22 Mode shapes of the shell-solid model.

4.4.6 Preliminary Parametric Studies for the Shell-Solid Model

The purpose of these preliminary parametric studies is to understand the contribution and effects of material and physical properties of the shell-solid model on the dynamic response. Even though the values used in these preliminary parametric studies were arbitrary (before material tests were performed), some insights were gained in producing an "accurate" finite element model to represent the laboratory timber bridge.

4.4.6.1 Properties of Wood

Understanding of the characteristics of wood is an important factor when inputting relevant material properties in the finite element model. Most wood composites are orthotropic, i.e., symmetrical about three mutually perpendicular planes. Orthotropic materials are also characterised by directional properties. Wood properties with distinctively different characteristics are defined in the longitudinal (L), rotational (R) and tangential (T) directions as illustrated in Figure 4.23. However, some woods can be regarded as approximately isotropic (Bodig & Jayne 1993). Generally, the difference in wood properties between the radial and tangential directions is minor compared to differences in the longitudinal direction. Hence, most wood properties for structural applications are given only for direction parallel to the grain, that is, longitudinal.

The ANSYS (ANSYS Inc. 2005a) finite element software package defines the orthotropic materials according to the specification of the element type. In general, the properties associate with the corresponding material axes as shown in Figure 4.23. There are no defaults in orthotropic material input in ANSYS and all values must be given.

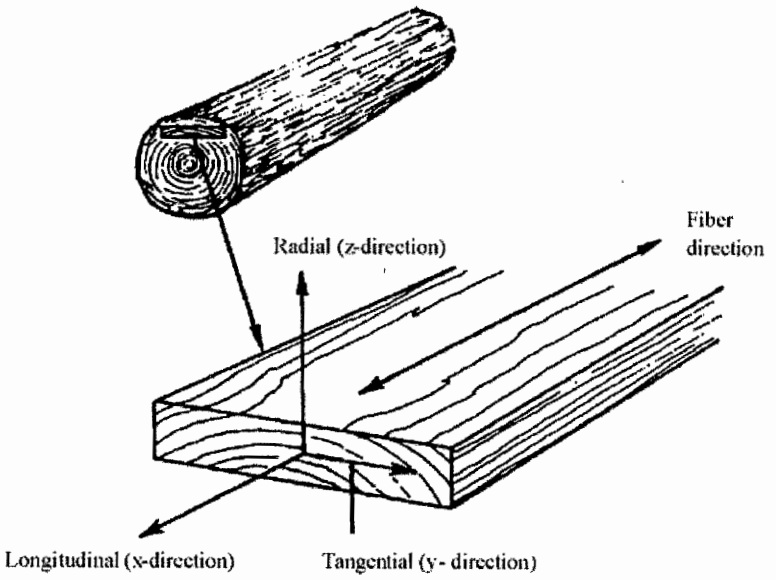


Figure 4.23 Three principlal axes of wood with respect to grain direction and growth rings (General Technical Report FPL-GTR-113 1999).

From the preliminary models mentioned above, the shell-solid model of Case BM, that is, SHELL63 with bending and membrane stiffness, was chosen to perform further investigation. The girder SOLID45 is characterised with isotropic material properties as listed in Table 4.8. The reason is that for radiata pine sawn timber, the L direction is easy and obvious to determine but not the R and T directions. Furthermore, the lateral loading is not playing an important role in the analysis. The deck (SHELL63), being made up of structural plywood, was manufactured from veneer sheets with alternate grain directions. As such, it possesses different second moment of area (I) for along and perpendicular to face grain directions using the method of transformed section as stated in Appendix B-Table B1 AS/NZS 2269:2004 (Australian/New Zealand Standard™ 2004). The initial material properties for both girder and deck are tabulated in Table 4.8. With these values, they serve as a preliminary benchmark to perform further parametric studies. The following parametric studies were to characterise the model in terms of its dynamic behaviour in terms of their natural frequencies. The parameters used to study the behaviour of the shell-solid model are listed below:

1. Stiffness of MATRIX27 in terms of its translational and rotational stiffness,
2. Orthotropic materials input of plywood for the deck and
3. Boundary conditions.

Table 4.8 Preliminary material properties for the shell-solid model

Isotropic	MPa
EX	12,700*
Orthotropic	MPa
EX[1]	10,500*
EY[2]	10,500*
EZ[3]	10,500*
GXY[4]	525*
GYZ[5]	525
GXZ[6]	52.5
NUXY[7]	0.04 (dimensionless)**
NUYZ[8]	0.04 (dimensionless)
NUXZ[9]	0.04 (dimensionless)

* *These values were obtained from AS 1720.1-1997 (Australian Standard™ 1997), MGP12 and F11 for radiata pine and structural plywood, respectively.*

[1] *This element local x-direction corresponds to the global Y-direction.*

[2] *This element local y-direction corresponds to the global X-direction.*

[3] *This element local z-direction corresponds to the global Z-direction.*

[4, 5] *Strong direction.*

[6] *Weak direction, assumed 10% of the value of the strong direction.*

** *This value was obtained from a book by Kollmann, Kuenzi and Stamm (1975).*

[7,8,9] *These were assumed the same as they have no significant effect on the model.*

E=modulus of elasticity

G=modulus of rigidity

NU=minor axis Poisson's ratio

4.4.6.2 Rigid Link

The parametric studies for the rigid link MATRIX27 were performed using isotropic materials for both deck and girders. The preliminary EX values used for both deck and girders are 12,222 MPa and boundary condition is pin-roller. The rigid link material properties for these parametric studies are listed in Table 4.9. From Table 4.9, the reference case is B1, whereby the translational and rotational stiffness of the rigid link in the three major axes are the same, 1E15N/m and 1E15Nm/rad, respectively. For cases B2 to B8, different parameters were changed to study their effects on the model. The dynamic results of the first five modes for theses eight cases are tabulated in Table 4.10. The parameter kz was not changed since it represents the screw connection between deck and girder, which is assumed very rigid in the vertical direction.

Comparing the natural frequencies of the first five modes for B1 and B2, confirms that changing rotational stiffness has no effect on the model. Whereas in B3 and B4, the change of stiffness for kx and ky from 1E15 to 1 has reduced by 40% the natural frequencies, regardless of changes in krot stiffness. As the stiffness values for kx and ky increase, the natural frequencies also increase. A very low kx and ky has created more local modes in the lower frequency region, which are not listed in Table 4.10.

Table 4.9 Parametric study of element MATRIX27.

Translational, N/m	B1*	B2	B3	B4	B5	B6	B7	B8
kx	1E15	1E15	1	1	1E1	1E2	1E3	1E4
ky	1E15	1E15	1	1	1E1	1E2	1E3	1E4
kz	1E15	1E15	1E15	1E15	1E15	1E15	1E15	1E15
Rotational, Nm/rad								
krotx	1E15	1	1E15	1	1E15	1E15	1E15	1E15
kroty	1E15	1	1E15	1	1E15	1E15	1E15	1E15
krotz	1E15	1	1E15	1	1E15	1E15	1E15	1E15

* *Reference*

Table 4.10 Natural frequencies corresponding to cases B1 to B8.

Case	Mode, Hz				
	1	2	3	4	5
B1	8.70	13.31	23.85	33.91	40.32
B2	8.70	13.31	23.85	33.91	40.32
B3	5.11	6.99	20.10	20.39	22.27
B4	5.11	6.99	20.10	20.39	22.27
B5	5.11	6.99	20.10	20.39	22.27
B6	5.11	6.99	20.10	20.39	22.27
B7	5.09	7.00	20.10	20.40	22.28
B8	5.13	7.03	20.12	20.65	22.35

4.4.6.3 Orthotropic Material

As mentioned above, wood is considered an orthotropic material. This feature is anticipated to play an important role on the behaviour of the model. In this study, the preliminary orthotropic values of modulus of elasticity of plywood for the deck as tabulated in Table 4.8 are varied to study their effect on the model. These changing parameters are shown in Table 4.11. The rigid link stiffness for both translation and rotation are arbitrarily set as 1E15. The moduli of elasticity for the three major axes are reduced from 100% to 70%, 50% and 10%.

Table 4.11 Parametric studies of orthotropic material of plywood.

Case	EX , MPa	EY, MPa	EZ, MPa
Preliminary, T1*	10,500 (100%)	10,500 (100%)	10,500 (100%)
T2	7,350 (70%)	10,500	10,500
T3	5,250 (50%)	10,500	10,500
T4	1,050 (10%)	10,500	10,500
T5	10,500	7,350 (70%)	10,500
T6	10,500	5,250 (50%)	10,500
T7	10,500	1,050 (10%)	10,500
T8	10,500	10,500	7,350 (70%)
T9	10,500	10,500	5,250 (50%)
T10	10,500	10,500	1,050 (10%)

** Reference*

As can be seen from Table 4.12, in general, the changes of modulus of elasticity values have caused some reduction of natural frequencies for certain modes. Case T1 is taken as a reference for comparison with other cases. In cases T2, T3 and T4, the reduction of EX value has caused the frequency of longitudinal flexural and torsional modes to drop more than the transverse modes. This is due to the EX value, being perpendicular to the plywood grain face and along the span, has been weakened. By comparing T1 to T5, T6 and T7 where the EY has been reduced, the frequency for transverse modes drop more than the longitudinal flexural and torsional modes. This indicates a less stiff transverse system. The role of EX and EY in the behaviour of the FE model is also depicted in Figure 4.24. As for T8 to T10, there are no changes in the dynamic results as EZ is reduced. This trend has been anticipated since the vertical direction stiffness does not play an important role in the system behaviour.

Table 4.12 Dynamic results of the parametric studies on orthotropic material for plywood.

Case	Mode, Hz				
	1[1]	2[2]	3[3]	4[4]	5[5]
T1	8.54	11.11	19.04	32.21	34.87
T2	8.21	10.63	18.85	31.04	33.54
T3	7.86	10.13	18.70	29.87	32.24
T4	6.11	7.80	18.26	24.00	32.40
T5	8.54	11.10	17.23	32.10	34.56
T6	8.54	11.09	15.90	31.95	34.11
T7	8.51	10.90	12.58	-	-
T8	8.54	11.11	19.04	32.21	34.87
T9	8.54	11.11	19.04	32.21	34.87
T10	8.54	11.11	19.04	32.21	34.87

[1] 1st flexural mode; [2] 1st torsional mode; [3] 1st transversal mode; [4] 2nd flexural mode; [5] 2nd torsional mode

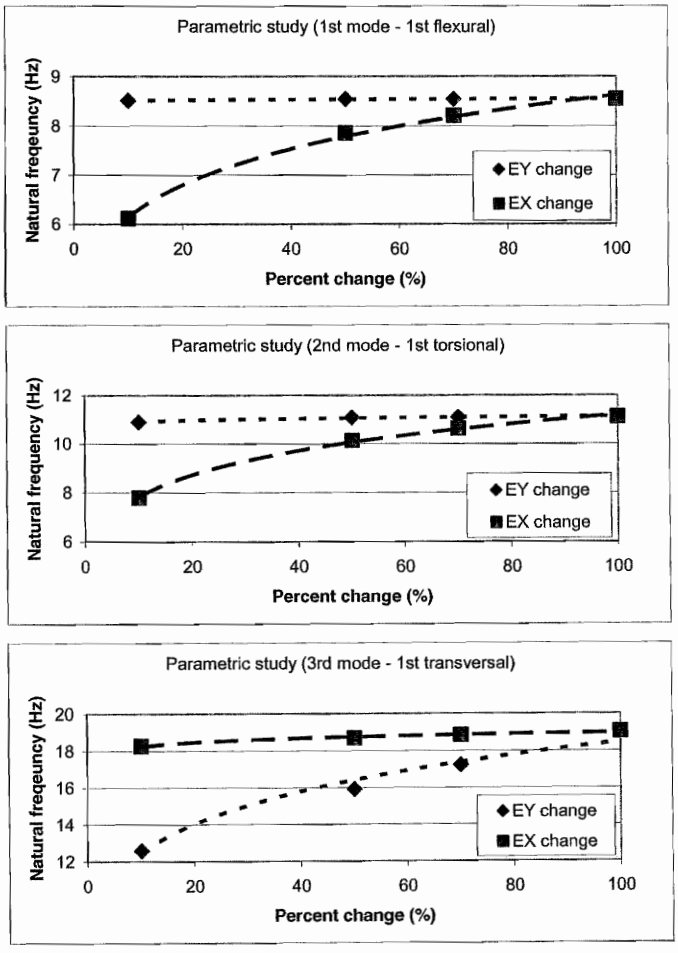


Figure 4.24 The effect of changes in EX and EY on natural frequency.

4.4.6.4 Boundary Conditions

Boundary condition is an important issue in determining behaviour of a system. Thus, by changing the configuration of a boundary condition, the system behaviour is altered. The original pin-roller and the other two types of altered boundary conditions are shown in Figures 4.25 to 4.27, respectively. Boundary condition BC1 has two complete pin-roller supports at the inner girders and only vertical restraint at the two outer girders. While for boundary condition BC2, the horizontal restraints were introduced at the transverse edge-centre of the deck with all girders having restraint only in the vertical direction. The dynamic results of these two latter models were then compared to the standard pin-roller and are shown in Table 4.13.

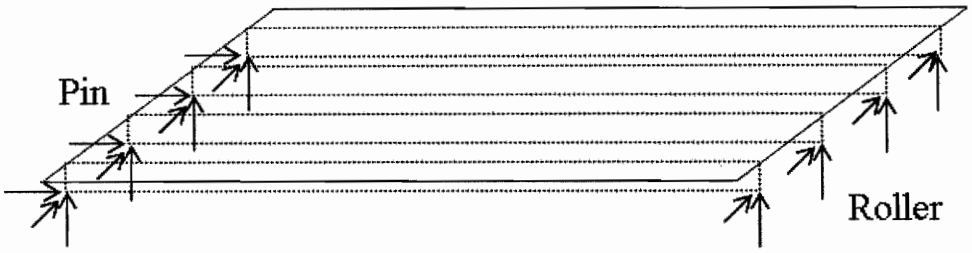


Figure 4.25 Original pin-roller boundary condition.

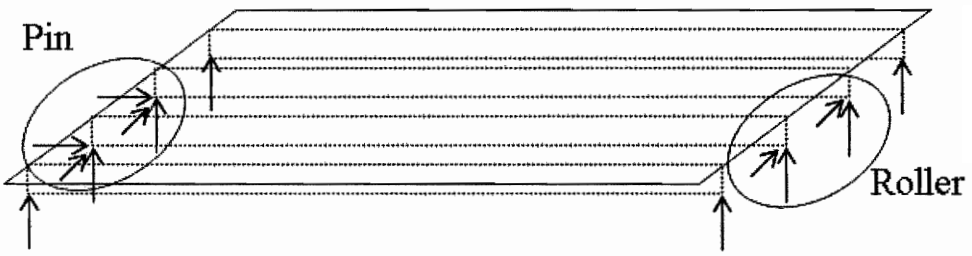


Figure 4.26 Boundary condition BC1.

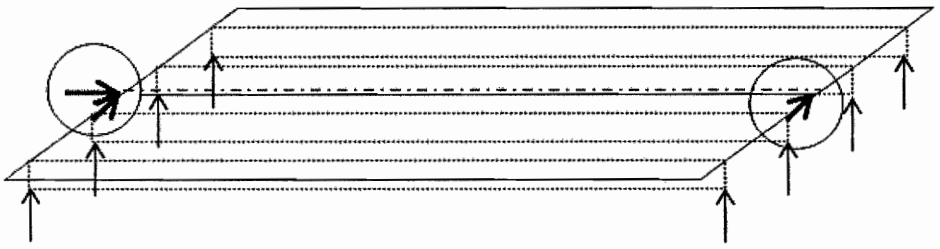


Figure 4.27 Boundary condition BC2.

From Table 4.13, the change of boundary did not change the natural frequencies much from the original pin-roller support except for mode 2 (torsional mode). BC1 and BC2 have provided less horizontal restraint and caused a reduction in frequency for the torsional modes.

Table 4.13 Dynamic results of different boundary conditions.

Mode	"Ideal", Hz	Exp., Hz	BC1, Hz	BC2, Hz
1	7.28	7.10	7.28	7.30
2	9.34	7.80	7.72	7.37
3	16.64	16.90	14.87	14.90
4	27.92	25.00	27.89	28.00
5	29.97	26.00	27.77	27.57

These preliminary parametric studies were aimed at establishing some understanding of the behaviour of the finite element (FE) model of the laboratory timber bridge using arbitrary values of material and physical properties. Different FE models were created and compared in terms of normalised stiffness matrix and dynamic response (natural frequency). The outcomes of the parametric studies are highlighted below:

1. Normalised stiffness matrix: Shell-solid model is more comparable to the hand-calculated grillage beam model than the Shell-shell and Shell-beam models.
2. Shell-solid model: SHELL63 'with bending stiffness only' has the closest trend to the grillage model with a symmetrical matrix. While, SHELL63 'with bending and membrane stiffness' showed also a comparable trend but with a non-symmetrical sub-matrix. Nevertheless, the latter is postulated to represent the laboratory timber bridge system better and was hence chosen for further parametric studies.
3. Mode shape: a simple and useful tool to compare different FE models.
4. Rigid link (MATRIX27): reduction of kx and ky (horizontal translational) caused drop in natural frequencies. While, varying kz (vertical translational) and krot (all rotational) did not affect the system.
5. Orthotropic material (plywood): reduction of EX and EY caused drop in natural frequencies for certain affected modes. The EX has more effects on the flexural and torsional modes, whereas the EY affected more the transverse torsional modes. However, changes in EZ did not affect the system.

6. Boundary conditions: Introducing fewer restraints on certain supports in the horizontal direction caused significant drop in natural frequencies for torsional modes.

4.5 Finite Element Model Updating

Based on the insight gained from the preliminary parametric studies conducted on the material and physical properties of the Finite Element (FE) model (shell-solid) using arbitrary values, it is important to establish a rigorous process applying the measured material tests values (from Chapter 3) to enhance the proposed FE model and establish a reasonable and reliable model representing the laboratory timber bridge. A preliminary 'real' FE model (adopted from shell-solid model in section 4.4) was established based on dynamic similitude of typical short-span timber bridges. Experimental tests to quantify timber material and geometric properties were undertaken (Chapter 3). An advanced FE model was then evolved from the preliminary model with more comprehensive features, and by incorporating the outcomes of the test results. A pin-pin supported (close to actual boundary condition) one-span laboratory timber bridge was fabricated to simulate real timber bridges in terms of their fundamental frequency, and experimental modal tests were performed in a laboratory environment to study the bridge's dynamic behaviour. The advanced FE model was then calibrated with the experimental modal data to produce an FE model for further study of damage detection in the following chapters that may also have application in actual load rating (not in the scope of this investigation) of bridges.

4.5.1 Material Properties

The Modulus of Elasticity (MOE) of the girders (timber beams) and deck (plywood) of the bridge was determined using a four point bending test, in accordance with AS/NZS 4063:1992 (Australian/New Zealand Standard™ 1992). Displacement transducers (LVDT) were positioned at the midspan, 1/3 and 2/3 of the span length of the test sample to register deflections. The test was carried out within the elastic range. From the test results, load-displacement curves were plotted the gradients of the initial portion of the curves were used for the computation of the MOE for all test samples. The results are tabulated in Table 4.14. The details of the tests can be found in Chapter 3. The density of the beams and plywood can be obtained by using the ratio of self

weight over the volume of the small test samples. The density of the test beams (550 kg/m^3) are close to the value given by Kollmann, Kuenzi and Stamm (1975) that is 540 kg/m^3, while the density of plywood (510 kg/m^3) falls in the range of values given by Austral Plywood (2005) for pine plywood of 500-650 kg/m^3. The shear modulus of the plywood was adopted from Handbook of Finnish Plywood (Finnish Forest Industries Federation 2002) with some adjustments based on the difference in the modulus of elasticity given in the handbook and the results of material tests. The Poisson's ratio was assumed based on the values given by Kollmann, Kuenzi and Stamm (1975). The Poisson's values are not very critical in the FE modelling as it has no significant effect on the responses (Crews 2002).

Table 4.14 MOE test results and other material properties for beams and plywood.

Item	Material Properties	Input in ANSYS
Beams*	Modulus of Elasticity (MPa) (Test)	
(Girders)	12,687 (Girder 1)	EX
	13,776 (Girder 2)	EX
	13,386 (Girder 3)	EX
	13,353 (Girder 4)	EX
	Density (kg/m^3)	
	550	DENS
Plywood**	Modulus of Elasticity (MPa) (Test)	
(Deck)	3,000 (Face grain $\perp$ to span)	EX, EZ
	6,760 (Face grain // to span)	EY
	Shear Modulus# (MPa)	
	496	GXY
	165	GYZ
	149	GXZ
	Poisson's ratio##	
	0.04	NUXY, NUYZ, NUXZ
	Density (kg/m^3)	
	510	DENS

* *In ANSYS, for isotropic material input, EX is adopted to represent the modulus of elasticity.*

** *In ANSYS, for orthotropic material input, all material properties are to be input.*

\# *These values were obtained from Handbook of Finnish Plywood (Finnish Forest Industries Federation 2002) using the ratio of 0.8 based on the comparison of mean modulus of elasticity to the MOE test results.*

\#\# *This average value was obtained from a book by Kollmann, Kuenzi and Stamm (1975).*

A series of pullout tests for the screw connection between the timber and plywood was also undertaken to estimate the connection strength in the X-, Y- and Z-directions. Five test samples were used in each series. The average gradient of five sets for each test series was used to compute the strength of the connections in terms of N/m. These values were then input to the preliminary FE model. The test results for all directions are listed in Table 4.15. The details are given in Chapter 3. The support stiffness values in X- Y- and Z-directions designated SX, SY and SZ, respectively, are also tabulated in Table 4.15. These values were considered optimum obtained from a series of parametric studies. The SX and SZ were set to an arbitrary large number as they have no significant effects on the model, while SY was purposely set larger than 1.85E5 N/m (the global stiffness of the bridge) to avoid a "soft" support.

Table 4.15 Pullout test results and other physical property values.

Direction	Physical Properties	Input in ANSYS
	Average Pullout Strength (N/m) (Test)	
X	623E3	KX
Y	865E3	KY
Z	809E3	KZ
	Support Stiffness (N/m) (Arbitrary)	
X	1E15	SX
Y	4E6	SY
Z	1E15	SZ

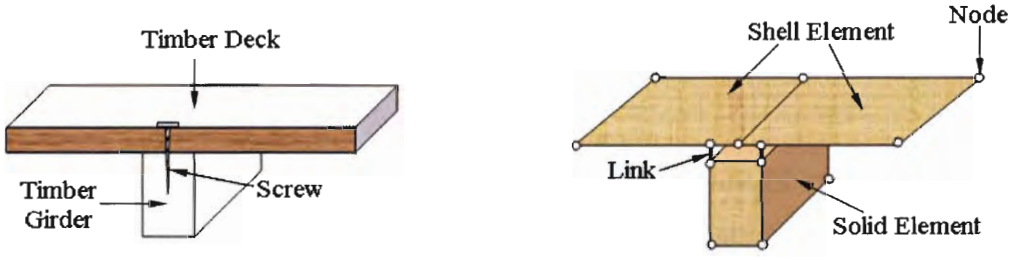
4.5.2 Preliminary Finite Element Model

A preliminary 'real' analytical model was developed using the Finite Element (FE) analysis package ANSYS (ANSYS Inc. 2005a). The FE model was constructed based on commercially available timbers in Australia and based on the set up of the bridge model as illustrated in Figure 4.16. All the material properties are given in the previous section (4.5.1). This preliminary FE model was built with very simple features such as fully composite sections between deck and girder, and idealised pin-pin supports. This model was utilised for sizing of structural members used for the test specimens. The criterion was that the fundamental frequency of the model should fall

between 5 to 20 Hertz. The three dimensional (3-D) preliminary model also served as a tool to help planning a comprehensive modal test by estimating strategic impact locations and optimal placement of sensors.

4.5.3 Development of an Advanced Model

A more sophisticated model was subsequently developed from the preliminary FE model by incorporating more complex features such as the boundary conditions, continuity conditions, material properties and geometry - to simulate the behaviour of a real structure as close as possible. Some of the strategies used in the modelling are discussed as follows. The solid elements (SOLID45) were utilised to model the girders, while shell elements (SHELL63) were used for the deck as shown in Figure 4.28. The shell element has six degrees of freedom (DOF) per node, while the solid element has three DOF per node. It is, therefore, necessarily to use two rigid links (MATRIX27, hereafter referred as screw-link) to represent a real screw connection in order to transfer the rotational DOFs from shell to solid elements as illustrated in Figure 4.28. The stiffness of the screw-link elements controls the level of composite action between the deck and girders. All the test results for timber beams and plywood, as well as the strength of the screw connections, were inputted in the model. The material properties for the deck were considered orthotropic, whilst those of the girders were isotropic.



(a) Cross section

(b) Finite element

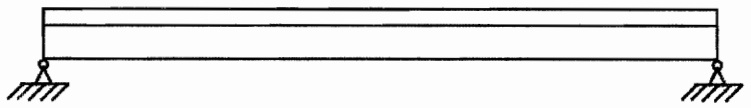
Figure 4.28 Finite element modelling strategy for the composite section.

In the preliminary model, "ideal" pinned supports were defined to simulate the boundary condition of the laboratory timber bridge (Figure 4.29a). For the experimental tests, special pins were fabricated for the supports (Figure 4.30). Whilst these pins do

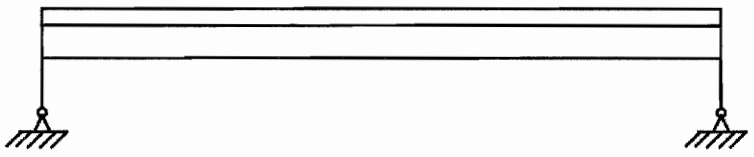
not perfectly reflect the idealised case, they are considered to be sufficiently accurate for the purposes of this investigation. After investigating a number of different modelling options, the option selected was that indicated in Figure 4.29b.

4.6 Considerations of Sensitivity Analysis in Modelling

After the advanced model was generated, some or all of the key parameters of the model needed to be updated to better replicate the actual condition of the bridge. The updating process is an iterative process, which can be performed manually (as in this study) or with an automated routine (not in the scope of this investigation). Adjustments were made to improve the simulations of boundary conditions and material properties using differences between the analytical and experimental frequencies and mode shape indices as measures of accuracy. This is a form of sensitivity analysis that can determine how the structural responses of a model are influenced by modifying properties like boundary conditions, material constants and geometric parameters etc. A sensitivity coefficient can be defined as mentioned by Brownjohn and Xia (1999) but is not adopted in this investigation.



(a) Preliminary model



(b) Advanced model

Figure 4.29 Modelling of bridge supports.



Figure 4.30 Fabricated pin support.

In the advanced model, additional link elements (MATRIX27, referred as support-links) were used to support the bridge on top of the pin supports. These were considered appropriate since the girders were actually 100mm above the pivot point of the fabricated pins as depicted in Figure 4.30. All degrees of freedom (DOFs) were restrained at the contact points between support-links and girders, whilst translational DOFs were restrained and rotational DOFs were released in the three directions corresponding to X, Y and Z for the contact points between support-links and rigid frame. In the bridge model, the stiffness of the support-links was adjusted manually during the calibration using natural frequencies as the response feedback.

One of the most critical parameters that was adjusted in the calibration process is the level of composite action between deck and girder. As mentioned earlier, the pullout test results were utilised for the input of the screw-links representing the composite action in the FE model. Due to variability and complex features of timber, minor adjustments of the pullout test results were required. Sensitivity adjustments of up to (+/- 20%) were also made to the MOE material properties to reflect the variability and non homogeneity of the timber.

From the features mentioned above, one of the important outcomes of the modelling performed in this investigation has been the completion of a sensitivity analysis of key parameters used in the advanced model. By maintaining the girders as isotropic and not altering their modulus of elasticity, the sensitivity analysis results of other key parameters is summarised in Table 4.16. From this it is concluded that inevitably the longitudinal stiffness of the girders affects the predicted response (natural frequencies) of the advance model significantly. While the support stiffness in Y-direction (SY) between deck and girders also affects the system ina major way. The

effects of shear modulus and screw connection stiffness were less pronounced. It is also worth noting that the Poisson's ratio values were not changed as they are deemed insignificant as shown in the studies carried out by Crews (2002).

Table 4.16 Summary of the effects of key parameters on the advanced model.

No	Key Component	Direction	General Effects on Natural Frequency	Effects %
1	Modulus of elasticity for deck	EX	Affects flexural and torsional modes more than transverse modes	0.1-0.9
		EY	Affects transverse modes more than flexural and torsional modes	0.1-6.2
		EZ	No significant effect	-
2	Shear modulus for deck	GXY	Affects torsional and transverse, and their hybrid modes more than transverse modes, except for 2nd transverse mode	0.1-0.8
		GYZ		
		GXZ		
3	Poisson's ratio for deck	NUXY	No significant effect (Crews 2002)	-
		NUYZ		
		NUXZ		
4	Supports stiffness between girders and pin	SX	No significant effect	-
		SY	Affects flexural and torsional modes If SY<1.85E5 N/m (estimated bridge global stiffness), the support is too soft and the model is not representing the system well	1-25
		SZ	No significant effect If SZ<1.85E5 N/m (estimated bridge global stiffness), the support is too soft and the model is not representing the system well	-
5	Screw connections between deck and girders	KX	No significant effect	-
		KY	Affects flexural and torsional, and their hybrid modes more than transverse modes	0.1-2
		KZ	Affects torsional and transverse, and their hybrid modes more than flexural modes	0.4-1

4.6.1 Correlation Analysis

As mentioned in section 4.2.4, correlation analysis was utilised to evaluate the correspondence and difference between the analytical and experimental results using modal parameters. The global objective function (*OF*) shown in Equation 4.4 is again used here. The goal of the *OF* was to update the advanced finite element (FE) laboratory bridge model matching the experimental model by manual adjustments using the key parameters mentioned above. Both the natural frequencies and the mode shapes were adopted in the *OF* to perform the correlation analysis. The correlation analysis of the deemed as optimum updated FE model is based on the nine mode shapes extracted from the FE model as documented in Table 4.17 and as shown in Figure 4.31.

Table 4.17 Description of mode shapes extracted from the advanced FE model.

No	Mode	Description of mode shapes
1	1	First flexural
2	2	First torsional
3	3	First transversal
4	4	Second flexural
5	5	Second torsional
6	6	Mix of first transversal and second flexural
7	7	Second transversal
8	8	Mix of second transversal and second flexural
9	9	Third flexural

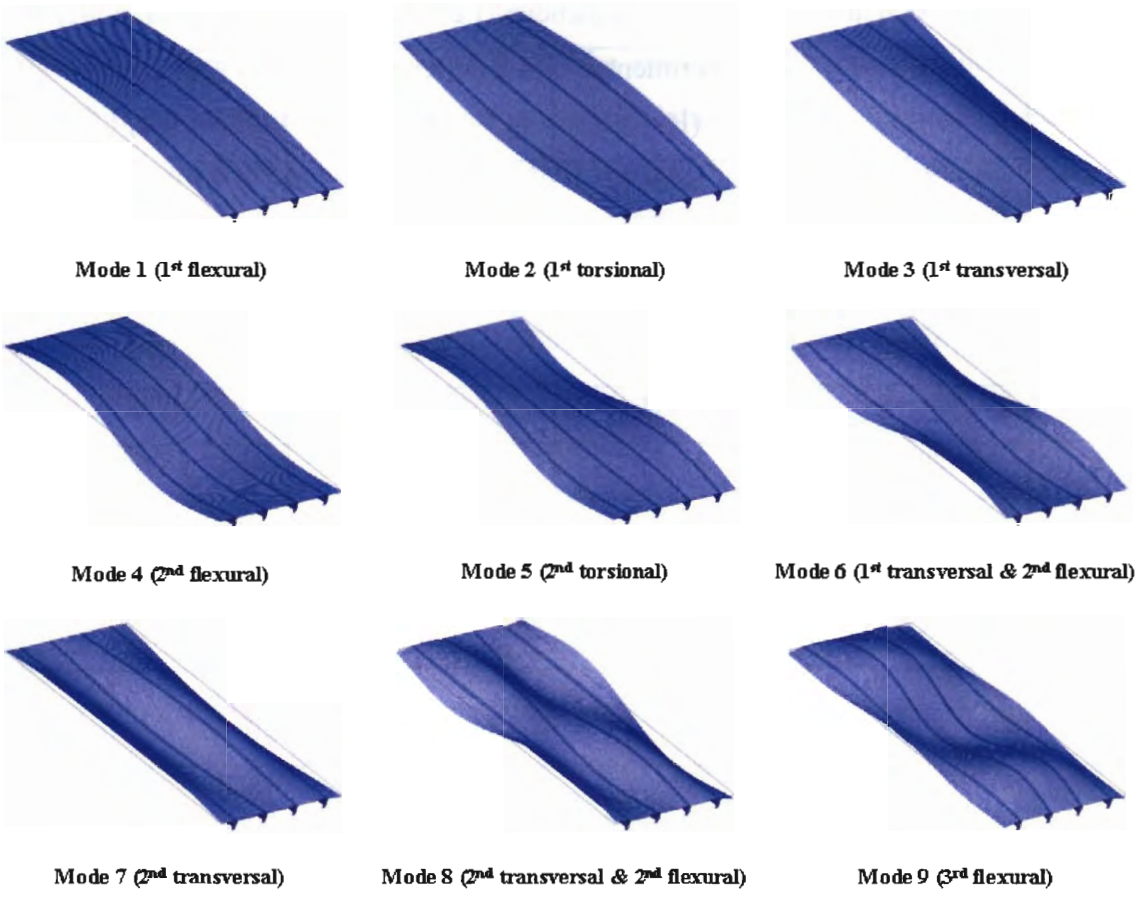


Figure 4.31 Nine vibration mode shapes of the laboratory timber bridge FE model.

For the comparison, using natural frequencies, the *NFerror* values (as given in Equation 4.5) shown in Table 4.18 are generally less than 10%, except for mode 6 and it is very low for lower modes (≤5). The reason for larger NFerror in higher modes may be due to the complexity of the modes, which the simple array of screw-links failed to properly represent their complex nature. From Figure 4.32, the dotted line representing the correlation between the FE and experimental models is close to the 45 degree line. It means that they match very well and the FE model is able to represent the experimental laboratory timber bridge globally. The slight inadequacy of the screw-links may not affect the overall performance of the FE model much judging from Figure 4.32.

Table 4.18 Comparison of natural frequencies: FE model vs experimental model.

Mode	FE (Hz)	Experimental (Hz)	|Difference| (Hz)	*NFerror* (%)
1	8.94	8.99	0.05	0.56
2	9.64	9.46	0.18	1.87
3	17.87	18.11	0.24	1.34
4	23.90	24.18	0.28	1.17
5	24.88	25.31	0.43	1.73
6	29.89	35.45	5.56	18.60
7	40.04	37.06	2.98	7.44
8	47.14	49.71	2.57	5.45
9	53.72	59.24	5.52	10.28

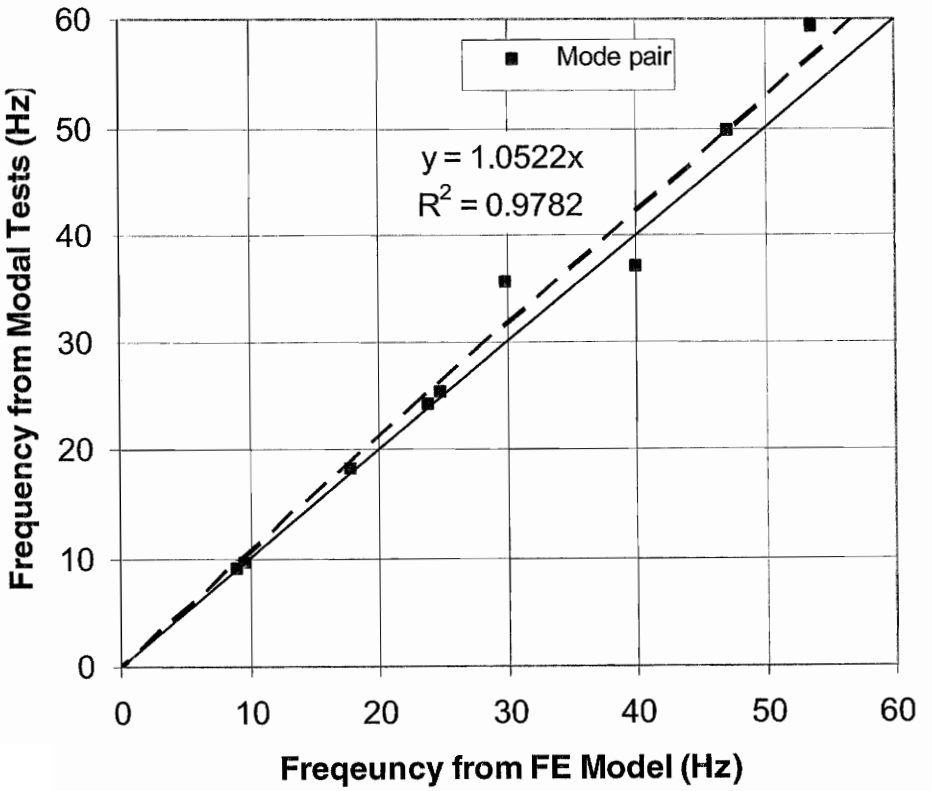


Figure 4.32 Frequency pair between FE model and modal tests for Bridge.

For the comparison, using mode shapes, the *MACerror* values (as given in Equation 4.6) are presented in Table 4.19. The extent of calibration can be determined through the evaluation of the changes in the correlation between the mode shapes. The *MACerror* values are generally lower than 0.1, except for mode 2, where the frequency response function was not well defined in the experimental work. It is also important to note that the order of mode shapes matches well between both the FE and experimental models. This indicates that the FE model, in general, replicates well the laboratory timber bridge, especially the boundary conditions that highly influence the order of mode shapes.

Table 4.19 Mode shapes correlation between FE and experimental models.

Mode	*MAC*	% *MAC*	*MACerror*	% *MACerror*
1	0.88	88	0.12	12
2	0.70	70	0.30	30
3	1.00	100	0	0
4	0.89	89	0.11	11
5	0.88	88	0.12	12
6	0.95	95	0.05	5
7	0.97	97	0.03	3
8	0.94	94	0.06	6
9	0.91	91	0.09	9

4.6.2 Damage Scenarios for the Bridge Model

Common damages found in timber bridges are rot (decay of timber surface due to moisture) and termite attacks. In this investigation, the damage due to rot is simulated in the FE model by an opening on the web of the girders from the soffit simulating rot. The damage is denoted by its length and depth forming a rectangular opening on the web similar to Figure 4.8 (for Beam in section 4.2.3). The damage cases were similar to the plate damage as documented in Table 4.5 (section 4.3.3). The inflicted damage was initially introduced at the ¾ span of an inner girder designated Girder 2 or in short g2 as shown in Figure 4.33. This was followed by additional damage (cumulative) at midspan of Girder 4 (g4). The loss of section (cumulative) continued at ¼ span of another inner

girder, namely, Girder 3 (g3). The final damaged state was reached by introducing cumulative damage near the 1/8 span of Girder 1 (g1). There were three levels of damage severity for each damage location, that is, 'light', 'medium' and 'severe' corresponding to 27.1%, 65.7% and 87.5% loss in sectional moment of inertia ('I'), respectively. The FE models were intended to study the changes in modal parameters due to different levels of damage severity and damage location.

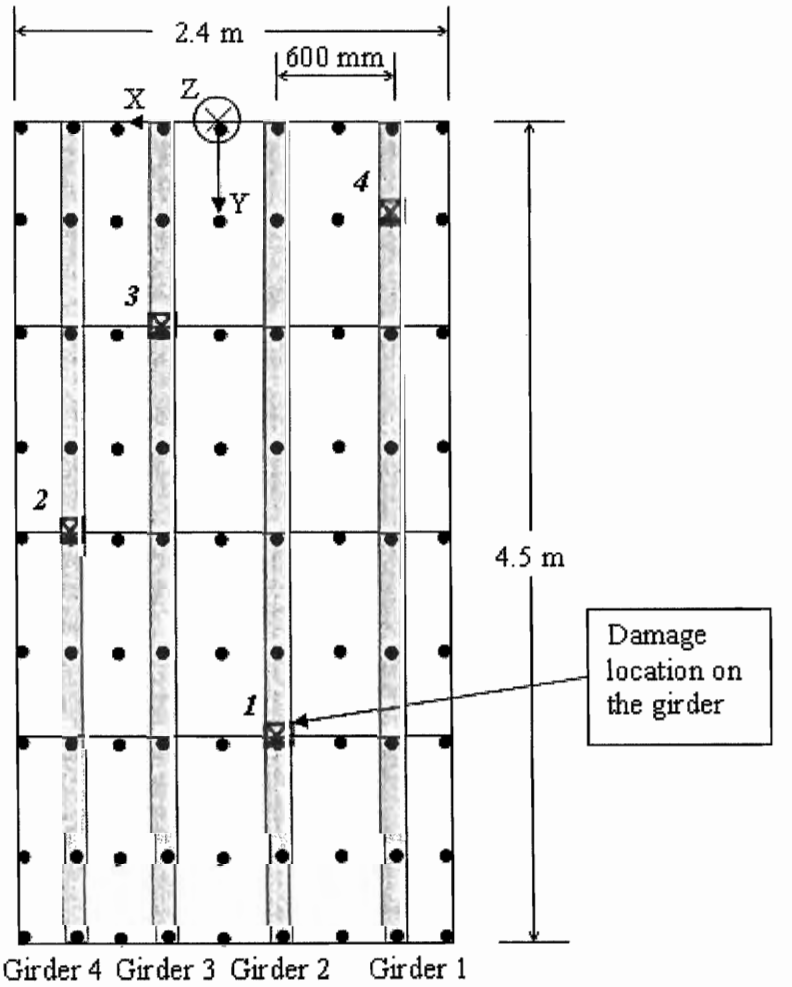


Figure 4.33 Plan view of damage locations on the bridge model.

4.7 Summary of Modelling Approaches

The Finite Element (FE) modelling of the timber beam (replicating girders in timber bridges) is quite straight forward and simple. Solid element was utilised in the FE model simulating well the actual timber beam. While for the laboratory timber bridge, more steps and care were required in order to obtain an accurate and reliable FE model. Three models with different combination of elements were validated against the grillage model. It was found that the shell-solid model stood out to be quite reasonably representing a deck-girder structural system. Using the shell-solid model, parametric studies were performed to study the capabilities and limitations of different parts of the model. With the knowledge accumulated from the shell-solid model, a systematic process of updating an 'Ideal' FE model with experimental modal data was carried out. The procedures were developed sequentially - starting with a preliminary model, incorporating more complex features to form the advanced model and finally adjustment of physical and material properties of the FE model to match the experimental ones. The fine tuning of the model with respect to the experimental data was performed based on the information gathered from the sensitivity analysis and comparisons using correlation analysis. The updating process using modal data is accurate and safer compared to using proof load test results, which may endanger the structural integrity of the tested structure.

Chapter 5

Damage Detection Criteria

5.1 Introduction

This Chapter presents details of damage detection criteria and algorithms used in this investigation to identify damage locations and to estimate its severity. The main contribution of this work is enlisted in sections 5.5 and 5.6, where modification of adopted algorithms (damage index methods) have performed better than its original forms based on the findings in the following chapters. Extension of the damage index method, based on modal strain energy for beam-like structures to include damage detection in plate-like structures, is also presented.

5.2 Natural Frequency and Damping Ratio

Natural frequency is an important dynamic property of any structure, often referred to as the eigenvalue. It is easy to extract from a structural system and hence popular in system identification. Natural frequency and mode shapes are sensitive to changes in system parameters such as mass, stiffness and were used to monitor the overall condition of structures (Hassiotis & Jeong 1995). These modal characteristics of structures can also be used to help find the location and severity of damage. Cawley and Adam (1979) utilised an incomplete set of measured natural frequencies to identify the location of damage and also provided a rough quantitative estimation of structural damage. Among the investigators, the basic eigenvalue equation (Equation 5.1) is usually used to perform the eigenvalue sensitivity analysis. By this method, the sensitivities of the natural frequencies of a system to small changes in the stiffness are calculated.

$$(K - \lambda_i M)\phi_i = 0 \qquad \text{Equation 5.1}$$

where M = mass matrix; K = stiffness matrix; λ_i = square of the circular natural frequency ω_i; and the eigenvector ϕ_i = corresponding natural mode shape of the system.

In a simpler form, the natural frequency of a linear vibratory system in the form of a simply supported beam is given as follows (Demeter 1973):

$$f_n = \frac{n^2 \pi}{2} \sqrt{\frac{EI}{mL^4}} \qquad \text{Equation 5.2}$$

where f_n = cyclic natural frequency; n = mode number; E = modulus of elasticity; I = moment of inertia; m = mass per unit length; and L = span length. From Equation 5.2, a reduction in stiffness (EI) leads to a reduction in the natural frequencies. Likewise, a reduction in natural frequencies indicates that some form of deterioration has occurred in the system.

Besides the sensitivity of natural frequencies, the frequency range also plays an important role in damage detection. When employed in damage localisation, it has a great impact on the resolution of the results as well as physical range of applications (Friswell & Mottershead 2001). For bridge structures, a lower frequency range is usually used to capture the first few modes of vibration. These low frequency vibration measurements are generally global and hence fewer vibration sensors may be used and they may be mounted away from the damage. However, the low frequency modes may have large spatial wavelength that are, in many occasions, far larger than the extent of damage.

Besides natural frequency, damping is another feature of all vibratory systems whenever there is energy dissipation. This occurs in mechanical structures, such as timber bridges, even though most of them are inherently lightly damped. In situations where there is free vibration, the loss of energy from damping in the system results in the decay of the amplitude of motion. Where forced vibration occurs, the loss of energy is balanced by the energy supplied by excitation. In either situation, the effect of damping is to remove energy from the system. Damping mechanism can be modelled by an equivalent viscous damping component which actually only accounts for energy loss from the system and the remaining portion of damping due to non-linearity that does not cause energy dissipation. It was found by Adam et al. (1975) that, with fibre reinforced plastics, a damaged state could be detected by an increase in damping. Hence, increased measurements of structural damping could reflect existence of damage. However, the disadvantage of using damping in system identification is that, in experimental work, it is not easy to obtain consistent results and the variations are high. As stated by Unger,

Teughels and De Roeck (2005) quoting Ndambi (2002), damping value does not monotonously increase as a function of damage.

In short, natural frequencies and damping ratios can be used in system identification, but the indication of changes in frequencies and damping before and after damage, reflecting some changes in structural state, may not be conclusive (Aktan et al. 1994).

5.3 Changes in Flexibility (CIF)

Flexibility matrix is basically the inverse of stiffness matrix of a structure. The flexibility matrix converges rapidly with increasing frequency and hence a good estimation of flexibility matrix can be obtained from only a few of the lower frequency modes (Pandey & Biswas 1994). This was also proven by Guo and Spencer (2002). This unique characteristic enables a small number of truncated modes to be used to assemble a reasonably accurate representation of the flexibility matrix.

Theoretically, an estimation of the flexibility matrix is obtained from the eigensolution of a structural dynamic system using inverse vibration (Doebling 1995). Suppose that an undamped free vibration of a system consists of N by N second order differential equation as shown in Equation 5.3.

$$M\ddot{x} + Kx = 0 \qquad \text{Equation 5.3}$$

The eigensolution of this system comprises eigenvalue matrix $\boldsymbol{\Omega}$ and eigenvector matrix Φ, which are scaled as given in Equations 5.4 and 5.5.

$$\Phi^T K \Phi = \Omega \qquad \text{Equation 5.4}$$

$$\Phi^T M \Phi = I \qquad \text{Equation 5.5}$$

where K and M are stiffness and mass matrices, respectively, and I is the identity matrix. Solving for the stiffness matrix K from Equation 5.4 yields

$$K = \Phi^{-T} \Omega \Phi^{-1} = \left(\Phi \Omega^{-1} \Phi^T\right)^{-1} \qquad \text{Equation 5.6}$$

The flexibility matrix is defined as the inverse of the stiffness matrix

$$S = K^{-1}$$ Equation 5.7

Substituting Equation 5.6 into Equation 5.7 yields the inverse representation of the flexibility matrix *S*. Hence, the flexibility matrix in the form of modal parameters is presented in Equation 5.8, adopted from the work of Pandey and Biswas (1994). It should be noted that the mode shapes are mass normalised.

$$S = \Phi\Omega^{-1}\Phi^T = \sum_{i=1}^{n} \frac{1}{\omega_i^2} \phi_i \phi_i^T$$ Equation 5.8

where ω_i is the *i*-th modal frequency, *n* is the number of degrees of freedom, Ω is ω_i^2 and *S* is the flexibility matrix. In practice, it is relatively more difficult to obtain higher modes, thus resulting in an approximate flexibility matrix with only a few lower modes. The change in flexibility Δ is defined as the difference of flexibility between the undamaged (S_u) and damaged (S_d) structure as given by

$$\Delta = S_u - S_d$$ Equation 5.9

For each degree of freedom *j*, let $(\delta_j)_{max}$ be the maximum absolute value of the elements (δ_{ij}) in the corresponding *i*-th column of Δ as shown in Equation 5.10.

$$\left(\delta_j\right)_{\max} = \max_i \left|\delta_{ij}\right|$$ Equation 5.10

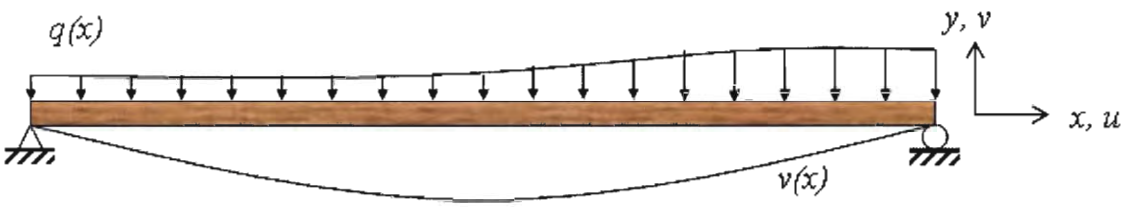
The magnitude of $(\delta_j)_{\max}$ is the measure of changes in flexibility (CIF) for each measurement location which is used to detect and locate damage in a structure.

5.4 Damage Indices I and II (DI-I and DI-II)

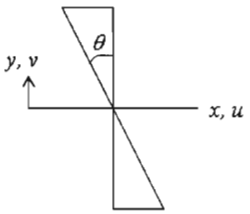
The damage index method developed by Stubbs, Kim and Farrar (1995) and adopted by Peterson et al. (2001a) was the first algorithm selected to locate the inflicted damage in this investigation. This damage detection algorithm is designated damage index I (DI-I). This method utilises characteristics of mode shape curvature for a beam-like structure as the main variable in the derived damage localisation algorithm based on the relative differences in modal strain energy before and after damage.

The damage index algorithms are derived below for a simply supported timber beam. The derivation is developed for beam-like structures. For a clearer demonstration,

an expression of the strain energy for a beam associated with normal stresses is considered. The deflected shape, v, of a simply supported beam under an arbitrary distributed load, q, are shown in Figure 5.1a.



(a) Beam subjected to an arbitrary loading.



(b) Idealisation of deflection curve

Figure 5.1 Schematic diagram of a simply supported beam.

Assuming small deformations and rotations, for linear elastic materials plane sections always remain plane after deflection, and the relationship between stress and strain of the system are given by Equations 5.11 and 5.12.

$$\sigma_x = E\varepsilon_x \qquad \text{Equation 5.11}$$

$$\varepsilon_x = \frac{du}{dx} \qquad \text{Equation 5.12}$$

where E is the longitudinal modulus of elasticity and, σ_x and ε_x are stress and strain in the x-direction, respectively. From Figure 5.1b, it can be seen that,

$$u = -y\theta = -y\frac{dv}{dx} \qquad \text{Equation 5.13}$$

$$\varepsilon_x = \frac{du}{dx} = -y\frac{d^2v}{dx^2} = -yv'' \qquad \text{Equation 5.14}$$

Considering a general Euler-Bernoulli beam, the strain energy (U) stored in a prismatic member is given by

$$U = \frac{1}{2}\int_V \sigma_x \varepsilon_x dV = \frac{1}{2}\int_0^L E(v'')^2 dx \int_A y^2 dA \qquad \text{Equation 5.15}$$

or

$$U = \frac{1}{2}\int_0^L EI\left(\frac{\partial^2 v}{\partial x^2}\right)^2 dx \qquad \text{Equation 5.16}$$

where EI is the flexural rigidity of the beam. An analogy of the energy in modal space associated with $\partial^2\phi_i/\partial x^2$ or $\phi_i''(x)$ (the second derivative of the ith mode shape (ϕ_i)) is

$$U_i = \frac{1}{2}\int_0^L EI\left(\frac{\partial^2 \phi_i}{\partial x^2}\right)^2 dx \qquad \text{Equation 5.17}$$

If the beam is subdivided into N elements as shown in Figure 5.2, then the modal strain energy associated with the jth element for the ith mode is given by

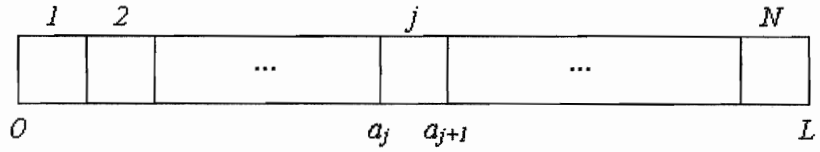


Figure 5.2 Schematic drawing of subdivisions of a beam (Cornwell, Doebling & Farrar 1999).

$$U_{ij} = \frac{1}{2}\int_j (EI)_j\left(\frac{\partial^2 \phi_i}{\partial x^2}\right)^2 dx \qquad \text{Equation 5.18}$$

The fractional energy, denoted by F_{ij}, is, therefore, expressed as

$$F_{ij} = \frac{U_{ij}}{U_i} \text{ and} \qquad \text{Equation 5.19}$$

$$\sum_{j=1}^{N} F_{ij} = \sum_{j=1}^{N} \frac{U_{ij}}{U_i} = 1 \qquad \text{Equation 5.20}$$

where $F_{ij} << 1$.

By choosing the sub-regions to be relatively small, the flexural rigidity for the jth element, $(EI)_j$ is roughly constant within the element. Hence, F_{ij} becomes

$$F_{ij} = \frac{\frac{1}{2}(EI)_j \int_j \left(\frac{\partial^2 \phi_i}{\partial x^2}\right)^2 dx}{U_i} \qquad \text{Equation 5.21}$$

Similarly, one can obtain the expression for the fractional energy for the damaged beam, in which a superscript asterisk is used to denote the damaged state. If the damage is principally assumed to be located at a single subdivision, thus the fractional strain energy remains relatively constant in the undamaged subdivision resulting in $F_{ij} \approx F_{ij}^*$. Assuming a single damaged location at subdivision j, it is found that;

$$\frac{\frac{1}{2}(EI)_j \int_j \left(\frac{\partial^2 \phi_i}{\partial x^2}\right)^2 dx}{U_i} = \frac{\frac{1}{2}(EI)_j^* \int_j \left(\frac{\partial^2 \phi_i^*}{\partial x^2}\right)^2 dx}{U_i^*} \qquad \text{Equation 5.22}$$

If the flexural rigidity is essentially constant over the entire length of the beam for both the damaged and undamaged modes, thus (EI) and $(EI)^*$ for U_i and U_i^*, respectively, are assumed similar. Thus, Equation 5.22 can be rearranged to provide an indication of the change in the flexural rigidity of the subdivision as given in Equation 5.23.

$$\frac{(EI)_j}{(EI)_j^*} = \frac{\int_j \left(\frac{\partial^2 \phi_i^*}{\partial x^2}\right)^2 dx \Big/ \int_0^L \left(\frac{\partial^2 \phi_i^*}{\partial x^2}\right)^2 dx}{\int_j \left(\frac{\partial^2 \phi_i}{\partial x^2}\right)^2 dx \Big/ \int_0^L \left(\frac{\partial^2 \phi_i}{\partial x^2}\right)^2 dx} \equiv \frac{f_{ij}^*}{f_{ij}} \qquad \text{Equation 5.23}$$

In order to avoid possible singularity problems with the quotient f_{ij}^*/f_{ij}, shifting of the axis of reference to avoid numerical sensitivities is recommended by Stubbs and Garcia (1996). Thus, the following approximate expression is used, where the origin is

shifted from f_{ij}=0 to f_{ij}=-1 for the undamaged state which also applies to the damaged state:

$$f_{ij} \rightarrow 1 + f_{ij} \qquad \text{Equation 5.24}$$

$$f_{ij}^{*} \rightarrow 1 + f_{ij}^{*} \qquad \text{Equation 5.25}$$

The damage indicator, β_{ij}, for the ith mode may then be defined as

$$\beta_{ij} = \frac{1+f_{ij}^{*}}{1+f_{ij}} = \frac{\left[\int_{j}\left\{\phi_i''^{*}(x)\right\}^2 dx + \int_{0}^{L}\left\{\phi_i''^{*}(x)\right\}^2 dx\right]\int_{0}^{L}\left\{\phi_i''(x)\right\}^2 dx}{\left[\int_{j}\left\{\phi_i''(x)\right\}^2 dx + \int_{0}^{L}\left\{\phi_i''(x)\right\}^2 dx\right]\int_{0}^{L}\left\{\phi_i''^{*}(x)\right\}^2 dx} \qquad \text{Equation 5.26}$$

It was suggested that each mode shape coordinate in the mode shape matrix be divided by the Euclidean norm of the matrix to obtain a normalised mode shape matrix (Peterson et al. 2001a). The damage index method was then used to compare the normalised mode shape vector for each girder for each of the damage cases versus the corresponding normalised undamaged mode shape vector. To account for all available modes, NM, the damage indicator value for a single element j is given as:

$$\beta_j = \frac{\sum_{i=1}^{NM} Num_{ij}}{\sum_{i=1}^{NM} Denom_{ij}} \qquad \text{Equation 5.27}$$

where Num_{ij} = numerator of β_{ij} and $Denom_{ij}$ = denominator of β_{ij} in Equation 5.26, respectively. Assuming that the collection of the damage indicators, β_j, represent a sample population of a normally distributed random variable, thus, transforming the damage indicator values into the standard normal space, the normalised damage index Z_j is obtained:

$$Z_j = \frac{\beta_j - \mu_{\beta j}}{\sigma_{\beta j}} \qquad \text{Equation 5.28}$$

where $\mu_{\beta j}$ = mean of β_j values for all j elements and $\sigma_{\beta j}$ = standard deviation of βj for all j elements. A judgment-based threshold value is selected and used to determine which of the j elements are possibly damaged which in real applications is left to the user to define based on what level of confidence is required for localisation of damage within the structure. For more details, the reader is referred to Stubbs and Garcia (1996) or to the cited references for a more thorough derivation of the above equations.

In this investigation, another form of damage index developed by Kim and Stubbs (1995a) was also selected to detect the inflicted damage. This damage detection algorithm is denoted damage index II (DI-II). This algorithm is similar to DI-I but it did not consider the feature of shifting the axis of reference. Basically, the DI-II algorithm maintains the original form of ratio of the undamaged and damaged elemental flexural rigidities. Hence, the algorithm used to calculate the damage index for the jth element and the ith mode, β_{ij}, is given as

$$\beta_{ij} = \frac{f_{ij}^*}{f_{ij}} = \frac{\int_j \left\{\phi_i''^*(x)\right\}^2 dx \int_0^L \left\{\phi_i''(x)\right\}^2 dx}{\int_j \left\{\phi_i''(x)\right\}^2 dx \int_0^L \left\{\phi_i''^*(x)\right\}^2 dx} \qquad \text{Equation 5.29}$$

The derivation of Equation 5.29 is discussed in Kim and Stubbs (1995b). It should be noted that the statistical approach given in Equations 5.27 and 5.28 used in DI-I is also applicable to DI-II. In addition, the DI-II method can be formulated to estimate severity of damage in the jth member using the following expression,

$$\alpha_j = 1 - \frac{1}{\beta_j} \qquad \text{Equation 5.30}$$

where α_j = severity estimator.

5.5 Modified Damage Indices I and II (MDI-I and MDI-II)

The damage index methods (DI-I and DI-II) introduced above have been successful in single damage localisation but problems have been encountered during the identification of multiple damage cases (Peterson, McLean & Pollock 2003; Peterson et al. 2001a, 2001b). One of the reasons is the fact that Equation 5.27 accounts for all available mode shapes through the summation and combination of mode shape curvatures. Although mode shape vectors have been normalised to the Euclidean norm of the matrix, the mode shape curvatures used for the damage index calculation are not normalised. Values of mode shape curvature are dependant on the shapes of each individual mode shape. The amplitude difference between mode shape curvatures for flexural modes one to five is illustrated in Figure 5.3. Instead of reflecting the changes in the curvature due to damage, the summation of non-normalised mode shape curvatures will distort the damage index in favour of higher modes, which results in false damage identifications. To solve this problem, the following algorithm is proposed in this investigation:

(1) the mode shape vector is normalised with respect to mass;

(2) mode shape curvatures for the *i*th mode of a given beam are normalised with respect to the maximum value of the corresponding mode.

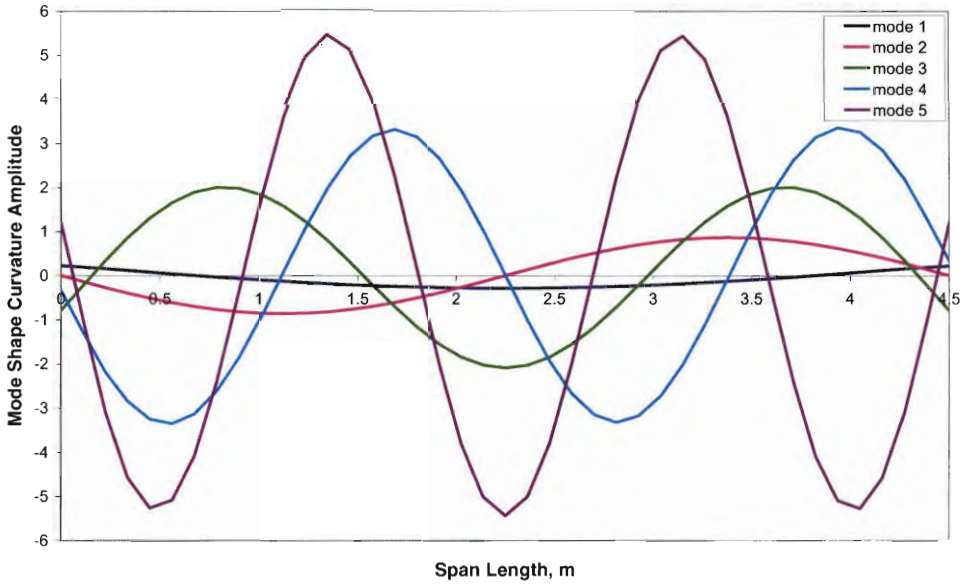


Figure 5.3 Mode shape curvature for flexural modes one to five.

After implementing these modifications, Equations 5.31 and 5.32 are obtained as follows for DI-I and DI-II, respectively. Equations 5.31 and 5.32 are denoted modified damage index I (MDI-I) and modified damage index II (MDI-II), respectively.

$$\overline{\beta_{ij}} = \frac{\left[\int_j \left\{\bar{\phi}_i^{//*}(x)\right\}^2 dx + \int_0^L \left\{\bar{\phi}_i^{//*}(x)\right\}^2 dx\right]\int_0^L \left\{\bar{\phi}_i^{//}(x)\right\}^2 dx}{\left[\int_j \left\{\bar{\phi}_i^{//}(x)\right\}^2 dx + \int_0^L \left\{\bar{\phi}_i^{//}(x)\right\}^2 dx\right]\int_0^L \left\{\bar{\phi}_i^{//*}(x)\right\}^2 dx} \qquad \text{Equation 5.31}$$

$$\overline{\beta_{ij}} = \frac{\int_j \left\{\bar{\phi}_i^{//*}(x)\right\}^2 dx \int_0^L \left\{\bar{\phi}_i^{//}(x)\right\}^2 dx}{\int_j \left\{\bar{\phi}_i^{//}(x)\right\}^2 dx \int_0^L \left\{\bar{\phi}_i^{//*}(x)\right\}^2 dx} \qquad \text{Equation 5.32}$$

where $\bar{\phi}_i^{"*}$ and $\bar{\phi}_i^{"}$ are normalised curvature vectors for damaged and undamaged state, respectively. Once again a statistically normalised damage index can be obtained by using Equation 5.28.

5.6 Hybrid of MDI-I and CIF

A hybrid of modified damage index I (MDI-I) and changes in flexibility (CIF) (referred as HMC in the following discussions) is proposed to estimate the severity of damage. The formulation for the HMC is given in Equation 5.33 and the schematic diagram of the process of obtaining the estimated severity of damage is depicted in Figure 5.4. This combination is proposed based on the findings that the MDI-I algorithm was capable of locating the damage but not evaluating its severity, while the magnitude of the CIF algorithm was able to show progressive severity of damage but not performing well in locating the damage. Hence, combining the two algorithms by multiplying the normalised damage indicator of MDI algorithm $\overline{Z_j}$ and the CIF algorithm $(\delta_j)_{max}$, a new indicator is obtained. In order to estimate the severity of

damage using the HMC algorithm, a weighting (calibration) process is employed to calibrate the values against single damage scenarios of severe damage condition (87.5% loss of 'I' (moment of inertia) at selected locations of 1/8 to 7/8 of the span length at intervals of 1/8). The selected 7 damage locations are deemed sufficient to represent the damage behaviour of a one-dimensional beam system. The HMC values of the selected single damage scenarios were then curve-fitted using a 3-dimensional Gaussian nonlinear regression. The initial outputs of the curve-fitted values were used to estimate the severity of damage in terms of percentage of cut depth from the soffit of the beam. Using the relationship between cut depth and loss of 'I', the initial values were subsequently converted to final output values that can be used to estimate the severity of damage in terms of percentage of loss of 'I'.

$$HMC = \overline{Z_j}\left(\delta_j\right)_{\max} \qquad \text{Equation 5.33}$$

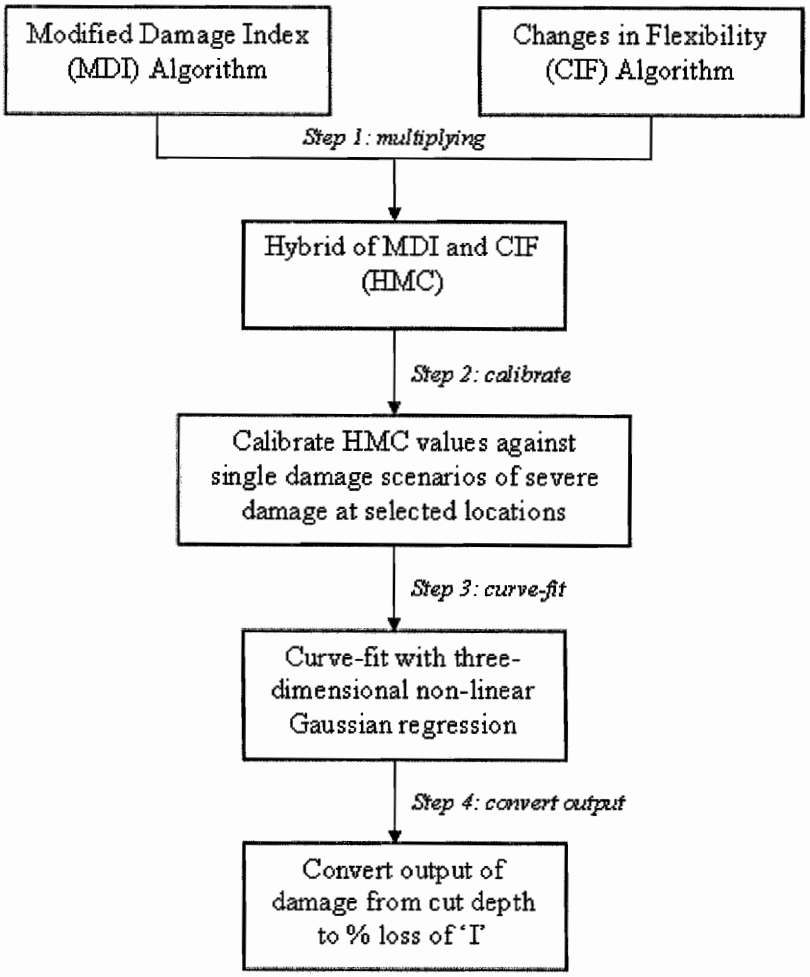


Figure 5.4 Schematic diagram of the process for HMC.

5.7 Damage Severity Estimation using MDI-II

The modified damage index II method is capable of locating damage locations well and estimating the severity of damage qualitatively with reasonable confidence. However, the method has not been intended to estimate the actual quantity of damage. It requires further development of Equation 5.32 to obtain the actual damage severity in the *j*th member as shown in Equation 5.34.

$$\bar{\alpha}_j = \left(1 - \frac{1}{\bar{\beta}_j}\right) \times 100(\%) \qquad \text{Equation 5.34}$$

where $\bar{\alpha}_j$ = severity estimator for the MDI-II method.

The severity of damage can be used to estimate the severity of damage in terms of percentage of loss of 'I' (moment of inertia).

5.8 Utilising Plate Theory in DI-II

The damage index methods characterised by one dimensional beam theory are presented in sections 5.4 and 5.5. It is of great interest to apply the concept of mode shape curvature to detect damage in complex structural system, such as plate-like structures, investigating issues such as capabilities and limitations of such a method applied to a laboratory timber bridge (a stiffened-plate-like structure). Cornwell, Doebling and Farrar (1997; 1999) extended the damage index method for beam-like structures to include the detection of damage for plate-like structures characterising by a two dimensional mode shape slope and curvature. Choi and Stubbs (1997) also utilised plate theory in strain energy method to detect damage.

Theoretically, for a thin plate of uniform thickness, the strain energy may be written in terms of deflection, *v*, as shown in Equation 5.35.

$$U = \frac{D}{2}\int\int_A \left(\frac{\partial^2 v}{\partial x^2}\right)^2 + \left(\frac{\partial^2 v}{\partial y^2}\right)^2 + 2\upsilon\left(\frac{\partial^2 v}{\partial x^2}\right)\left(\frac{\partial^2 v}{\partial y^2}\right) + 2(1-\upsilon)\left(\frac{\partial^2 v}{\partial x \partial y}\right)^2 dxdy \qquad \text{Equation 5.35}$$

where A is the area of the plate surface, $D\ (=Et^3/12(1-\upsilon^2))$ and υ are the flexural rigidity of a plate and the Poisson's ratio for isotropic material, respectively. For a particular

mode shape, $\phi_i(x,y)$, the strain energy associated with that mode shape of undamaged state and derivatives is

$$U_i = \frac{D}{2}\iint_A \left(\frac{\partial^2\phi_i}{\partial x^2}\right)^2 + \left(\frac{\partial^2\phi_i}{\partial y^2}\right)^2 + 2\upsilon\left(\frac{\partial^2\phi_i}{\partial x^2}\right)\left(\frac{\partial^2\phi_i}{\partial y^2}\right) + 2(1-\upsilon)\left(\frac{\partial^2\phi_i}{\partial x\partial y}\right)^2 dxdy$$

Equation 5.36

If the plate is subdivided into *Nx* subdivisions in the *x* direction and *Ny* subdivisions in the *y* direction, as shown in Figure 5.5, the strain energy associated with the subregion *jk* for the *i*th mode is given as follows:

$$U_{ijk} = \frac{D_{jk}}{2}\int_{b_k}^{b_{k+1}}\int_{a_j}^{a_{j+1}} \left(\frac{\partial^2\phi_i}{\partial x^2}\right)^2 + \left(\frac{\partial^2\phi_i}{\partial y^2}\right)^2 + 2\upsilon\left(\frac{\partial^2\phi_i}{\partial x^2}\right)\left(\frac{\partial^2\phi_i}{\partial y^2}\right) + 2(1-\upsilon)\left(\frac{\partial^2\phi_i}{\partial x\partial y}\right)^2 dxdy$$

Equation 5.37

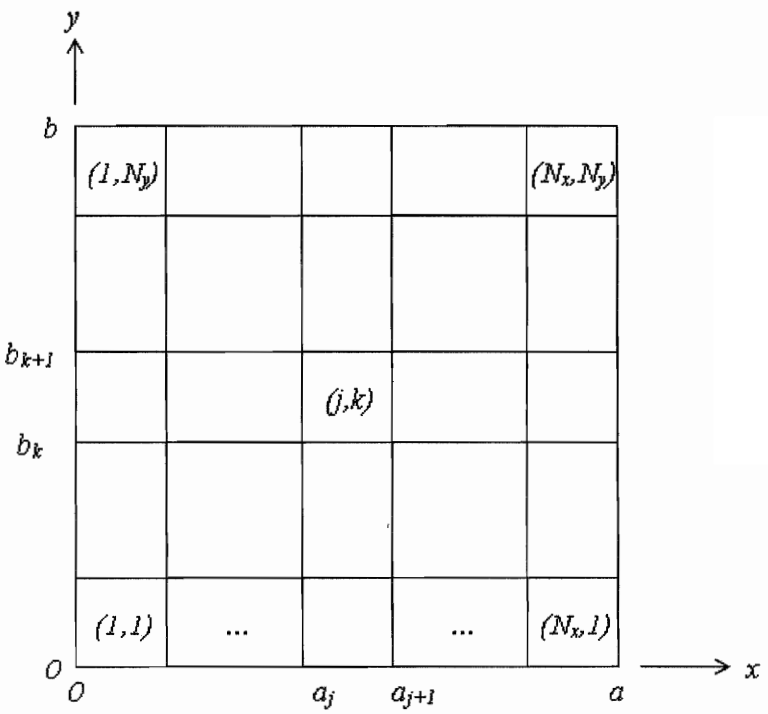


Figure 5.5 Schematic diagram showing subregions of a plate (Cornwell, Doebling & Farrar 1999).

The summation of modal strain energy for subregion *jk* can be expressed as

$$U_i = \sum_{k=1}^{N_y} \sum_{j=1}^{N_x} U_{ijk} \qquad \text{Equation 5.38}$$

The fractional of modal strain energy at subregion *jk* is defined as

$$F_{ijk} = \frac{U_{ijk}}{U_i} \qquad \text{Equation 5.39}$$

and

$$\sum_{k=1}^{N_y} \sum_{j=1}^{N_x} F_{ijk} = 1 \qquad \text{Equation 5.40}$$

Similar expressions, as shown above, can be written for the damaged state of a structure with addition of an asterisk, e.g., ϕ_i^* denoting the *i*th mode shape of a damaged structure. Analogous arguments used for beam-like structures (Equation 5.23) in terms of the ratio of elemental flexural rigidity that can be used to indicate the change of stiffness in a structure, are utilised for the plate-like structure as shown in Equations 5.41 and 5.42.

$$\frac{D_{jk}}{D^*_{jk}} = \frac{f^*_{ijk}}{f_{ijk}} \qquad \text{Equation 5.41}$$

where

$$f_{ijk} = \frac{\int_{b_k}^{b_{k+1}} \int_{a_j}^{a_{j+1}} \left(\frac{\partial^2 \phi_i}{\partial x^2}\right)^2 + \left(\frac{\partial^2 \phi_i}{\partial y^2}\right)^2 + 2\upsilon \left(\frac{\partial^2 \phi_i}{\partial x^2}\right)\left(\frac{\partial^2 \phi_i}{\partial y^2}\right) + 2(1-\upsilon)\left(\frac{\partial^2 \phi_i}{\partial x \partial y}\right)^2 dxdy}{\int_0^b \int_0^a \left(\frac{\partial^2 \phi_i}{\partial x^2}\right)^2 + \left(\frac{\partial^2 \phi_i}{\partial y^2}\right)^2 + 2\upsilon \left(\frac{\partial^2 \phi_i}{\partial x^2}\right)\left(\frac{\partial^2 \phi_i}{\partial y^2}\right) + 2(1-\upsilon)\left(\frac{\partial^2 \phi_i}{\partial x \partial y}\right)^2 dxdy}$$

Equation 5.42

and an analogous term f_{ijk}^{*} can be defined using the damaged mode shape, $\phi_i^{*}(x,y)$. Hence, the algorithm used to calculate the damage index for the subregion jk and the ith mode, β_{ijk}, is given as

$$\beta_{ijk} = \frac{f_{ijk}^{*}}{f_{ijk}} \qquad \text{Equation 5.43}$$

$$\beta_{ijk} = \frac{\left\{\int_{b_k}^{b_{k+1}}\int_{a_j}^{a_{j+1}}\left(\frac{\partial^2\phi_i^{*}}{\partial x^2}\right)^2+\left(\frac{\partial^2\phi_i^{*}}{\partial y^2}\right)^2+2\upsilon\left(\frac{\partial^2\phi_i^{*}}{\partial x^2}\right)\left(\frac{\partial^2\phi_i^{*}}{\partial y^2}\right)+2(1-\upsilon)\left(\frac{\partial^2\phi_i^{*}}{\partial x\partial y}\right)^2 dxdy\right\}\left\{\int_0^b\int_0^a\left(\frac{\partial^2\phi_i}{\partial x^2}\right)^2+\left(\frac{\partial^2\phi_i}{\partial y^2}\right)^2+2\upsilon\left(\frac{\partial^2\phi_i}{\partial x^2}\right)\left(\frac{\partial^2\phi_i}{\partial y^2}\right)+2(1-\upsilon)\left(\frac{\partial^2\phi_i}{\partial x\partial y}\right)^2 dxdy\right\}}{\left\{\int_{b_k}^{b_{k+1}}\int_{a_j}^{a_{j+1}}\left(\frac{\partial^2\phi_i}{\partial x^2}\right)^2+\left(\frac{\partial^2\phi_i}{\partial y^2}\right)^2+2\upsilon\left(\frac{\partial^2\phi_i}{\partial x^2}\right)\left(\frac{\partial^2\phi_i}{\partial y^2}\right)+2(1-\upsilon)\left(\frac{\partial^2\phi_i}{\partial x\partial y}\right)^2 dxdy\right\}\left\{\int_0^b\int_0^a\left(\frac{\partial^2\phi_i^{*}}{\partial x^2}\right)^2+\left(\frac{\partial^2\phi_i^{*}}{\partial y^2}\right)^2+2\upsilon\left(\frac{\partial^2\phi_i^{*}}{\partial x^2}\right)\left(\frac{\partial^2\phi_i^{*}}{\partial y^2}\right)+2(1-\upsilon)\left(\frac{\partial^2\phi_i^{*}}{\partial x\partial y}\right)^2 dxdy\right\}}$$

Equation 5.44

To account for all available modes, NM, the damage indicator value for a single subregion jk is given as:

$$\beta_{jk} = \frac{\sum_{i=1}^{NM} f_{ijk}^{*}}{\sum_{i=1}^{NM} f_{ijk}} \qquad \text{Equation 5.45}$$

Once again the damage indicator values for plate-like structures can be transformed into the standard normal space and normalised damage index Z_j is obtained using Equation 5.28.

5.9 Summary

The adopted algorithms in this investigation to detect damage are derived in this chapter. The modifications done on the adopted methods of damage index I (DI-I) and damage index II (DI-II) are discussed. A combined algorithm of modified damage index I (MDI-I) and changes in flexibility (CIF) has also been presented, enabling estimation of damage severity that is not possible by the MDI-I method alone. Adaptation to plate theory of damage index method presented in this chapter.

Chapter 6

Damage Detection - Numerical Studies

6.1 Introduction

This Chapter presents details of damage detection utilising damage index methods using numerical simulation results (finite element results) for a timber beam, a timber plate and a laboratory timber bridge. Previously, the impacts of utilising two different numerical integration methods on a damage detection algorithm (modified damage index I method) were discussed. The numerical integration method that was found to perform better (i.e. rectangular rule) will be adopted for all damage detection cases in this study.

6.2 Impact of Numerical Integration Methods

Numerical integration is a common and useful technique for performing integration on discrete data. Hence, in this study, numerical integration methods were utilised to perform integration in damage detection algorithms, specifically on the calculation of modal strain energy to be used in damage index methods. For example, to calculate modified damage index I (MDI-I) (β_{ij}) in Equation 6.1 (also in Chapter 5 Equation (5.31)) the mode shape and its derivatives are required.

$$\beta_{ij} = \frac{\left[\int_j \left\{\phi_i''^{*}(x)\right\}^2 dx + \int_0^L \left\{\phi_i''^{*}(x)\right\}^2 dx\right] \int_0^L \left\{\phi_i''(x)\right\}^2 dx}{\left[\int_j \left\{\phi_i''(x)\right\}^2 dx + \int_0^L \left\{\phi_i''(x)\right\}^2 dx\right] \int_0^L \left\{\phi_i''^{*}(x)\right\}^2 dx} \qquad \text{Equation 6.1}$$

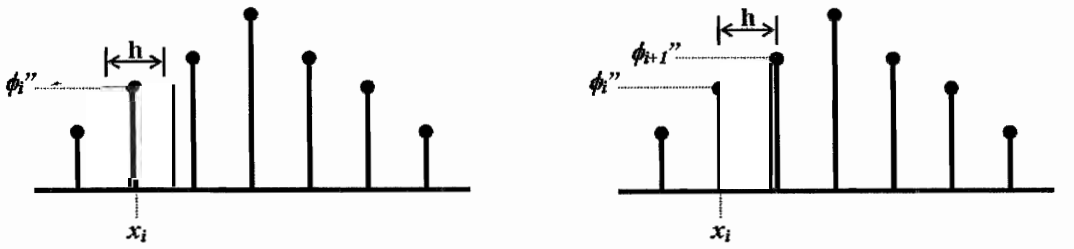
where $\phi_i''^{*}$ and ϕ_i'' are normalised mode shape curvature vectors for damaged and undamaged state, respectively. The central difference scheme for the second derivative as shown in Equation 6.2, based on three data points, is adopted for computing the mode shape curvature.

$$f''(x)=\frac{f(x-h)-2f(x)+f(x+h)}{h^2}+HOT \qquad \text{Equation 6.2}$$

where *HOT* is the higher order terms which will not be considered here.

To perform integration required by Equation 6.1, two commonly used methods are adopted, namely the rectangular rule and the trapezoidal rule. Figures 6.1a and 6.1b illustrate application of the two methods in performing the numerical integration of Equation (6.1.) The rectangular rule is producing '*n*' output data and the trapezoidal rule with only '*n-1*' from an *n*-point data set. It is important to note that the outcomes of damage detection using Equation 6.1 are sensitive to the numerical integration scheme.

It is commonly acknowledged that to obtain an accurate estimation of integration of a given discrete function, the trapezoidal rule is a preferred option over the rectangular rule (NSF Dynamic Systems 2005). However, for damage detection, this common belief may not be true. It is because, for damage detection, the main objective is to reveal the damage and not just the accuracy of the numerical integrations. Despite the importance of numerical integration techniques in damage detection, there are not many publications addressing this issue (to the best knowledge of the author). Therefore, a section of this chapter is devoted to comparing the damage detection results for the two common numerical integration techniques, namely the rectangular rule and trapezoidal rule.



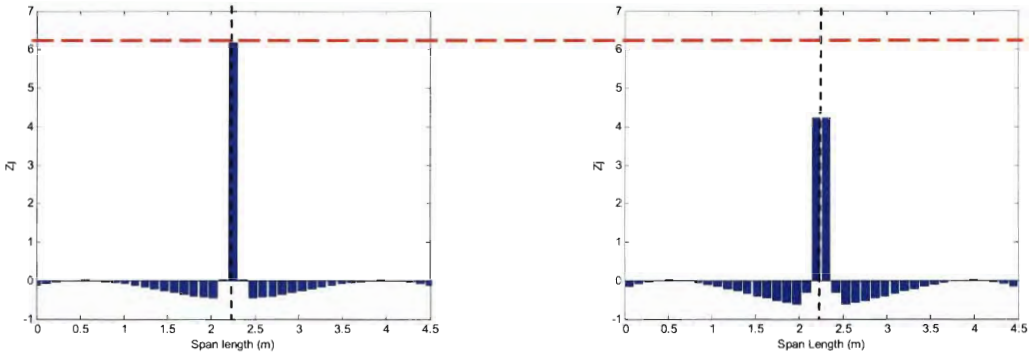
(a) Rectangular rule. (b) Trapezoidal rule.

Figure 6.1 Numerical integration techniques (NSF Dynamic Systems 2006).

6.2.1 Comparison of Numerical Integration Techniques

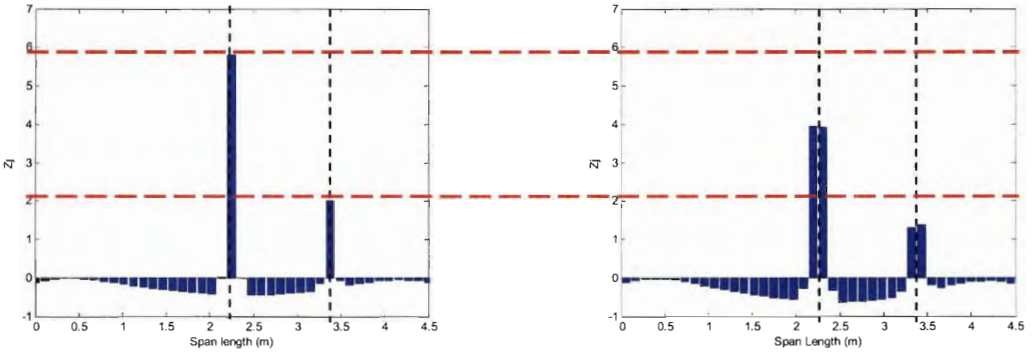
A finite element model of a timber beam was developed for comparing the adopted numerical integration techniques by applying them to the modified index I (MDI-I) method as presented in Equation 6.1. In order to compare different numerical techniques and other results pertaining to the timber beam, the statistically normalised damage indicator values (Zj), for each of the damage cases, are plotted against the beam span length (4.5 m). The damage indicator values (Zj) that are larger than zero (the probability-based criterion for damage) are considered as damage occurred at that location. Damage indices less than zero ($Zj<0$) have no physical meaning. In all the figures involving the timber beam, the damage locations are shown with dashed lines.

The comparison between the rectangular and the trapezoidal rules for single damage (4S) and two damage (4S6L) cases are illustrated in Figures 6.2 and 6.3, respectively. For the single damage case, '4' denotes damage location at 4/8 of the span length (1/2 span, midspan or 2.25m), while 'S' represents severe damage (87.5% loss of 'I'). Likewise, 4S6L corresponds to damage locations at 4/8 and 6/8 of the span length (2.25m and 3.375m) with severe (S) (87.5% loss of 'I') and light (L) (27.1% loss of 'I') damage, respectively. The medium (M) damage corresponds to 65.7% loss of 'I". The details of damage cases for the timber beam finite element model can be found in Chapter 4. From Figures 6.2 and 6.3, all damage locations were detected using both numerical integration techniques. Nevertheless, it is quite obvious that the rectangular rule is associated with a higher magnitude of damage indicator value at damage location, which in turns provides a higher confidence of existence of damage compared to the trapezoidal rule. In addition, the rectangular rule indicates the precise location of damage compared to the trapezoidal one.



(a) Rectangular rule. (b) Trapezoidal rule.

Figure 6.2 Comparison of numerical integration methods for 4S.

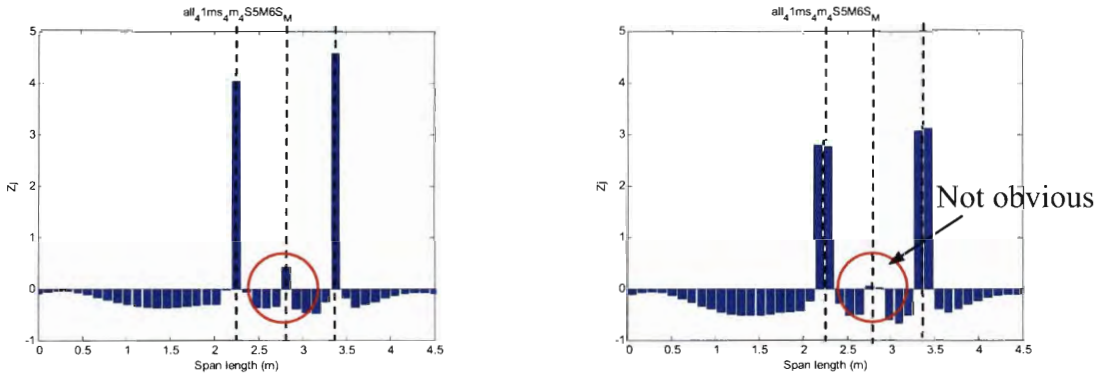


(a) Rectangular rule. (b) Trapezoidal rule.

Figure 6.3 Comparison of numerical integration methods for 4S6L.

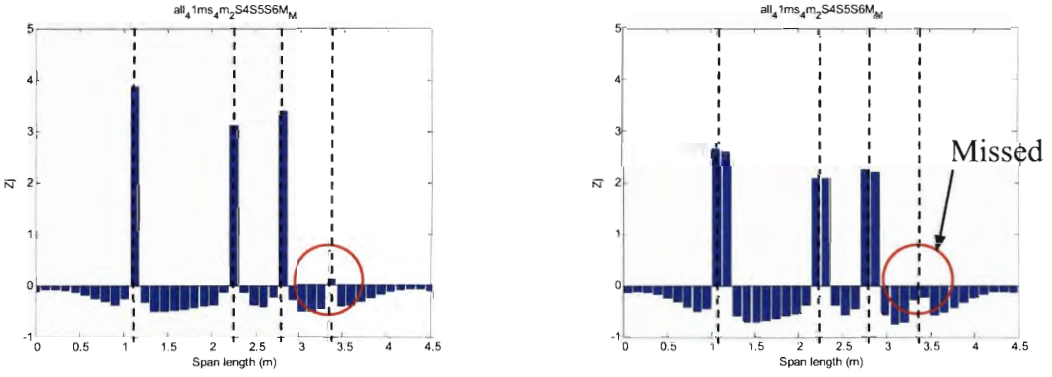
Figures 6.4 and 6.5 show the comparison between the rectangular rule and the trapezoidal rule, for damage cases 4S5M6S and 2S4S5S6M, respectively. It is apparent that the rectangular rule is superior to the trapezoidal rule in damage detection applications. In Figure 6.4, the medium damage at location 2.8125m can be detected when using the rectangular rule for integration, but failed to do so when the trapezoidal rule was applied. It is also observed that the probability of damage is more pronounced when rectangular rule is applied. This reinforces the previous findings. It should be noted that a larger damage indicator value is particularly important when the damage index is used for the experimental results, which are usually contaminated with noise. The rectangular rule performs better because it takes advantage of every mode shape curvature at each mode shape coordinate, instead of taking into account the average

between two as in the trapezoidal rule. Hence, the rectangular rule was chosen for all subsequent analyses, results and discussions in the current study.



(a) Rectangular rule. (b) Trapezoidal rule.

Figure 6.4 Comparison of numerical integration methods for 4S5M6S.



(a) Rectangular rule. (b) Trapezoidal rule.

Figure 6.5 Comparison of numerical integration methods for 2S4S5S6M.

6.3 Damage Detection for Timber Beam

The modal analysis of a pin-pin supported timber beam with and without damage was performed using the finite element (FE) software package ANSYS (2005b). Modal responses of the beam are generated using finite element models before and after damage. The details of the FE models are presented in Chapter 4. For damage detection purposes in the analytical investigation, a fine mesh is adopted with the beam divided into 40 elements and 41 nodes denoted by normal and italic numbers, respectively, as shown in Figure 6.6.

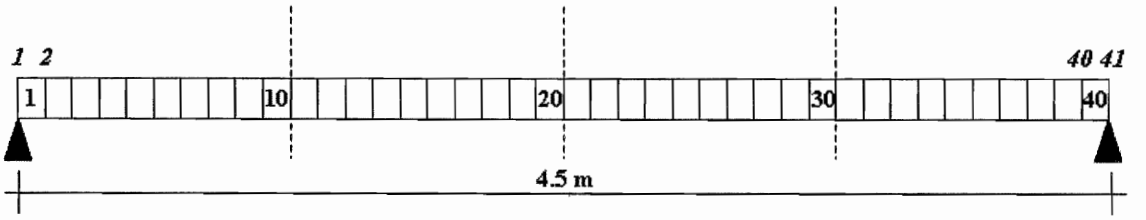


Figure 6.6 Configuration of elements and nodes for the timber beam FE model.

In numerical studies, as many damage cases as possible can be generated. Nonetheless, for the purpose of comparison, all the damage cases used in the experimental work were reproduced using finite element models (as listed in Table 4.2 Chapter 4), while extra damage cases were also produced to take advantage of numerical studies. The damage cases for the finite element model of timber beam discussed in this chapter are documented in Table 6.1. For each damage scenario, the modal parameters (natural frequencies and mode shapes) before and after damage were numerically generated using the ANSYS program (ANSYS Inc. 2005a). It should be noted that damping is not included in the finite element modelling thus it is not discussed further in this chapter. The first five natural frequencies are listed in Table 6.2. The results in Table 6.2 and Figure 6.7 show that there is a general trend of decreasing frequency as damage becomes more severe. According to the simulated damage scenarios in the table and figure, the fundamental frequency (first natural frequency) has shifted down by about 2% compared to the undamaged (Un) cases. There is a decrease in natural frequencies for the higher modes ranging from -0.2% to 20% for the second mode, 0.3% to 19% for the third mode, 0% to 9% for the fourth mode and 0.3% to 15% for the last mode for timber beam in this study. The downward trend in natural frequency due to damage can be seen clearly, but many of these changes are less than 5%. Also, it can be noted that the shift of frequency for the cases 4L (single damage), 2L6L (two damage) and 2L4L6L (three damage) is practically the same. In practice, the influence of noise in the signal and the impact of environmental factors (temperature and humidity) would contribute at least 5% change to the natural frequencies and this would most probably overshadow the effect of damage (Kim, Park & Lee 2006). Also, the changes in natural frequencies cannot provide information about the location and severity of damage directly. This conclusion tallies with the work done by Sánchez (2005).

Table 6.1 Damage scenarios for the finite element model of a timber beam.

Damage Case	Location(s) per $1/8^{th}$ of span length	Length *l* (mm)	Height *h* (mm)	% loss of 'I' (%)
4L*	4	45	9	27.1
5M	5	45	27	65.7
6S	6	45	45	87.5
2L6L*	2, 6	45	9, 9	All 27.1
4L6L	4, 6	45	9, 9	All 27.1
4S6L*	4, 6	45	45, 9	87.5, 27.1
2L4L6L*	2, 4, 6	45	9, 9, 9	All 27.1
2S4S6S*	2, 4, 6	45	All 45	All 87.5
4S5L6S	4, 5, 6	45	45, 9, 45	87.5, 27.1, 87.5
2M4S5S6S*	2, 4, 5, 6	45	27, 45, 45, 45	65.7, 87.5, 87.5, 87.5
2S4S5L6S*	2, 4, 5, 6	45	45, 45, 9, 45	87.5, 87.5, 27.1, 87.5
2S4S5S6S*	2, 4, 5, 6	45	45, 45, 45, 45	All 87.5

* *denotes damage cases that were replicated in the experimental tests.*

Notes:

2i = damage at 2/8 span with damage severity i

L, M, S representing light, medium and severe damage, correspond to 27.1, 65.7 and 87.5% loss of 'I'

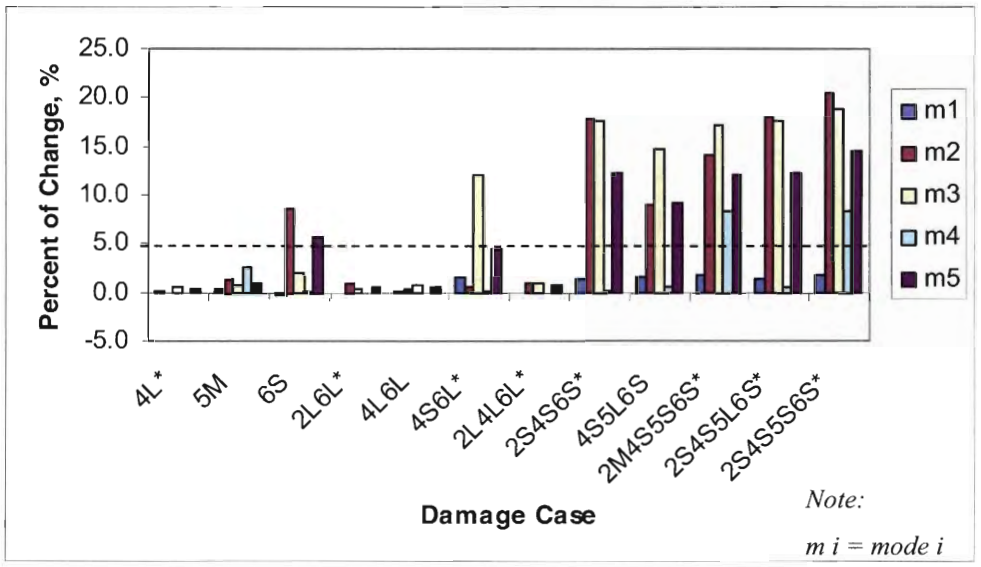
(e.g. 2M4S5S6S denotes a cumulative damage scenario of medium damage on 2/8 span (1.125m), severe damage on 4/8 span (midspan or 2.25m), 5/8 span (2.8125m) and 6/8 span (3.375m))

Table 6.2 Natural frequencies for finite element model of a timber beam.

Mode	Natural frequencies (Hz)						
	Un	4L*	5M	6S	2L6L*	4L6L	4S6L*
1	14.59	14.58	14.54	14.61	14.60	14.58	14.36
2	37.50	37.50	36.95	34.26	37.17	37.34	37.33
3	91.89	91.34	91.11	90.11	91.65	91.22	80.89
4	146.73	146.73	143.02	146.68	146.75	146.74	146.66
5	239.48	238.77	237.43	225.66	238.21	238.13	228.72

Mode	Natural frequencies (Hz)						
	Un	2L4L6L*	2S4S6S*	4S5L6S	2M4S5S6S*	2S4S5L6S*	2S4S5S6S*
1	14.59	14.59	14.38	14.36	14.33	14.38	14.32
2	37.50	37.17	30.81	34.10	32.20	30.77	29.81
3	91.89	91.10	75.72	78.45	76.06	75.69	74.52
4	146.73	146.75	146.54	145.99	134.49	145.94	134.33
5	239.48	237.51	210.15	217.61	210.66	209.91	204.91

* *denotes damage cases that were replicated in the experimental tests.*



* *denotes damage cases that were replicated in the experimental tests.*

Figure 6.7 Comparison of percentage of drop in natural frequencies for various damage cases for finite element model of a timber beam.

6.3.1 Damage Localisation

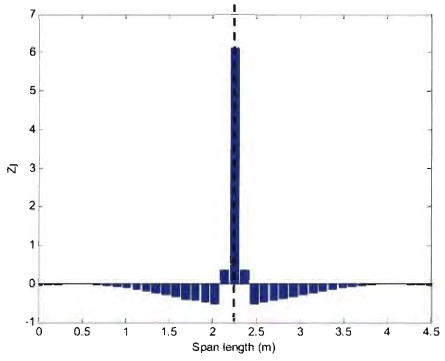
For damage localisation, the damage detection (DD) algorithms used either the first two or first five flexural modes. All mode shapes considered in the finite element models in this study have been normalised with respect to the mass matrix (details can be found in Chapter 4). The formulations of the DD algorithms used in the following discussions were presented in details in Chapter 5. The first two flexural modes were chosen to apply in the DD algorithms because they are commonly used (Peterson et al. 2001b) and they are easily acquired. However, the first two modes may not be capable to identify closely spaced damage scenarios. It is, therefore, proposed in this study to adopt the first five flexural modes in the DD algorithms (Garcia, Osegueda & Meza 1998; Sánchez 2005). Furthermore, the first five flexural modes were able to be captured in the experimental work (Chapter 7). With the development of the latest technologies in the sensors, it is possible nowadays to obtain higher modes for a large-scale structural system. This would definitely help in damage detection. It should be noted that a few representative damage detection results are shown in this chapter and the remaining are appended at Appendix A.

In the analytical investigation presented in the following, the statistically normalised damage indicator values Z_j for damage indices I and II and modified damage

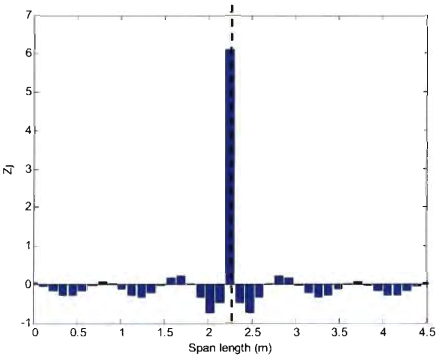
indices I and II, changes in flexibility index and hybrid index for each of the damage cases are plotted against the beam span length. In principle, when the index value Z_j is larger than zero (probability-based criterion for damage), it is considered as damage occurred at that location. The actual damage locations are indicated with vertical dashed lines in all the figures for timber beam.

6.3.1.1 Discussion on Damage Index I Method

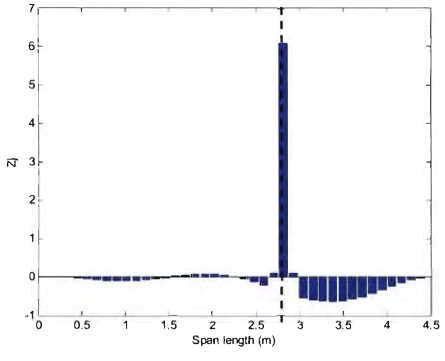
Figures 6.8a, 6.8c and 6.8e show the results of applying damage index I (DI-I) algorithm to detect single damage cases with light, medium and severe damage, inflicted at location 4/8 (2.25 m), 5/8 (2.8125 m) and 6/8 (3.375 m) of the span length, respectively. The first two flexural modes (2 modes) were used in the computation, which is common for this damage localisation method. The method shows clear indications of damage locations for damage cases 4L, 5M and 6S. Similar single damage cases but using the first five flexural modes (5 modes) in the DI-I algorithm are illustrated in Figures 6.8b, 6.8d and 6.8f. Such combination of modes used in damage localisation is not commonly found in the literature. The damage, in these cases is being located but some false detection did appear although the magnitudes of these false positives are small, indicated by positive Z_j values at locations other than the actual damage. The magnitude of Z_j for the spurious damage locations are very small compared to the actual damage, for example in Figure 6.8d, they are 0.5 and 6, respectively. Therefore, they can be easily distinguished. However, in the analytical investigation, noise and environmental factors are not present. As a result, slight contamination in the data may be amplified many fold in the damage indices when used for real test data that is quite noisy in nature.



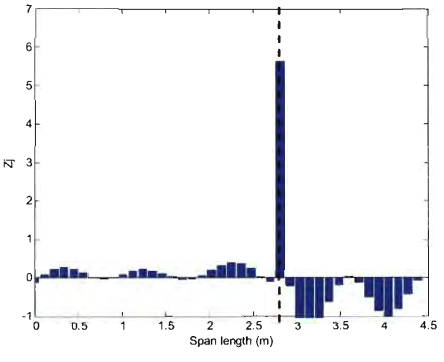
(a) 4L (2 modes)*.



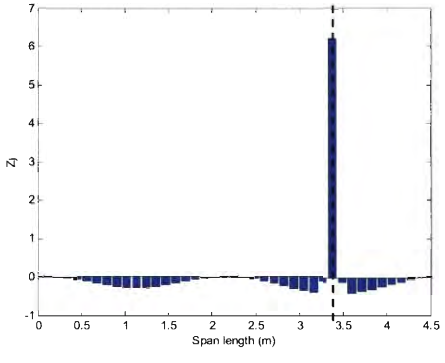
(b) 4L (5 modes)*.



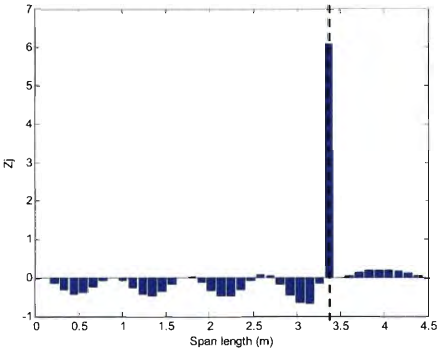
(c) 5M (2 modes).



(d) 5M (5 modes).



(e) 6S (2 modes).

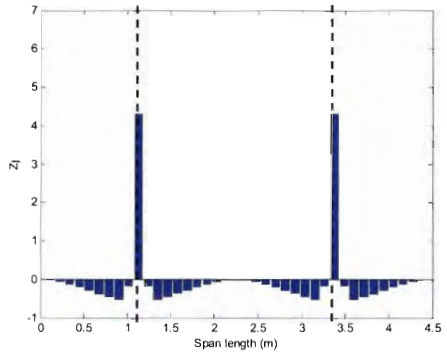


(f) 6S (5 modes).

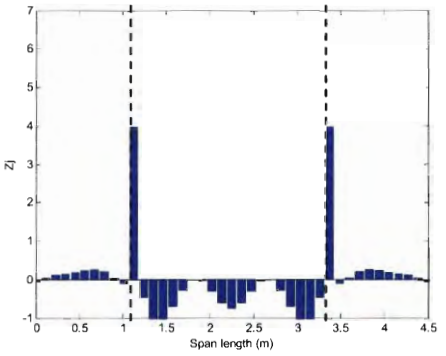
* *denotes damage cases that were replicated in the experimental tests.*

Figure 6.8 Single damage cases using DI-I method.

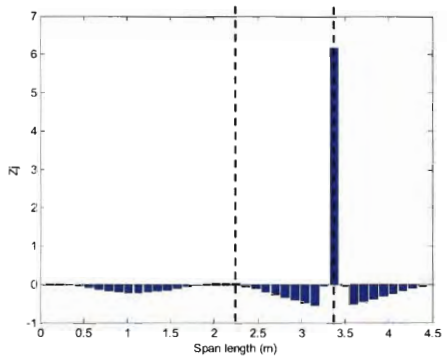
Figures 6.9a, 6.9c and 6.9e and Figures 6.9b, 6.9d and 6.9f show the results of two damage cases using the first two and first five flexural modes in the damage localisation algorithm, respectively. From Figures 6.9a (2 modes) and 6.9b (5 modes), both light damage at locations 1.125m and 3.375m for case 2L6L were located, but the latter one indicates the appearance of few false positives (indication of spurious damage locations) towards both supports. From Figure 6.9c, the light damage at location 2.25m for case 4L6L (2 modes) was not identified, while using 5 modes (see Figure 6.9d), both light damage locations (2.25m and 3.375m) were clearly located in spite of some appearances of false positives. This may imply that the higher modes are more sensitive to the existence of damage. However, exception is found in case 4S6L as depicted in Figures 6.9e and 6.9f for 2 modes and 5 modes, respectively. Referring to Figure 6.9f, using higher modes failed to locate the light damage at 3.375m. While both damage locations were detected by using 2 modes as illustrated in Figure 6.9e, but the magnitude of Z_j for severe damage (2.25m) is far too small compared to the light damage at 3.375m, which is opposite to the reality. From these three cases, one observation is that if the damage locations are well separated, the DI-I method is capable to locate the damage well. On the other hand, if the damage locations are close to each other, higher modes should be used which provide a better indication of the real damage severity for the severe damage, even if the light damage location may not be identified.



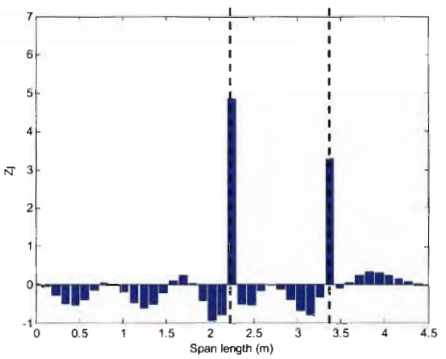
(a) 2L6L (2 modes)*.



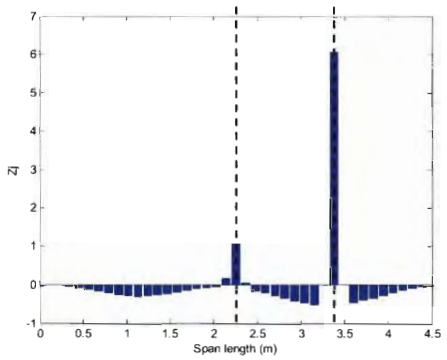
(b) 2L6L (5 modes)*.



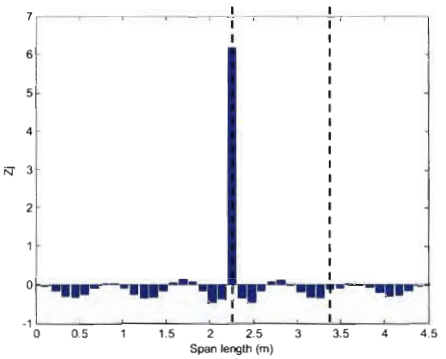
(c) 4L6L (2 modes).



(d) 4L6L (5 modes).



(e) 4S6L (2 modes)*.



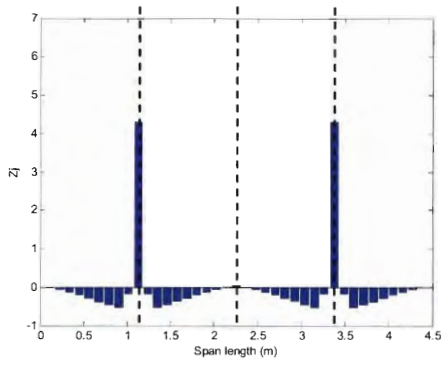
(f) 4S6L (5 modes)*.

* *denotes damage cases that were replicated in the experimental tests.*

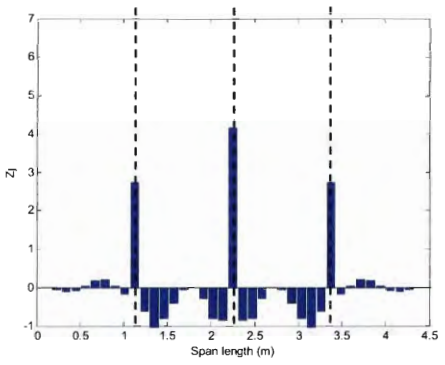
Figure 6.9 Two damage cases using DI-I method.

Figures 6.10 and 6.11 illustrate the results of cases with three damage (2L4L6L, 2S4S6S and 4S5L6S) and with four damage (2M4S5S6S, 2S4S5L6S and 2S4S5S6S) scenarios, respectively. It is apparent, from Figures 6.10a, 6.10c and 6.10e, and Figures 6.11a, 6.11c and 6.11e, that using the first 2 modes in the DI-I algorithm either failed to locate damage locations or provided a misleading Z_j amplitude of damage (one example is shown in Figure 6.11a) as more damage appeared. The shortcomings of using only the first two modes have partly been overcome by using the first five modes in the damage localisation algorithm as shown in Figures 6.10b, 6.10d and 6.10f, and Figures 6.11b, 6.11d and 6.11f for three and four damage scenarios, respectively. The improvement is that all severe damage locations have been able to be identified even though using higher modes produced more false positives of small Z_j amplitude. This indicates that incorporating higher modes in the DI-I method contribute to identifying damage at locations which is otherwise not possible when using just the first two flexural modes.

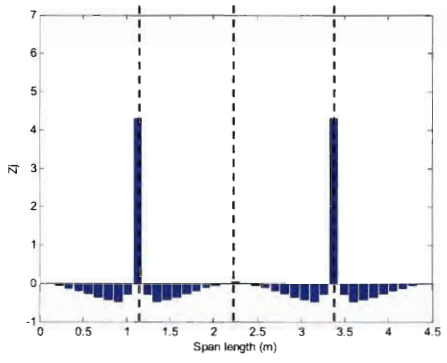
It is concluded that the DI-I method is capable of locating severe damage for single and multiple damage locations using the first five flexural modes. However, for example case 4S6L (see Figures 6.9e and 6.9f), using higher modes may miss the light damage, which was located by using the first two modes. In addition, using higher modes in the DI-I method produces some spurious damage locations that may affect damage detection when applying with real data, which is usually polluted by noise. The effect of incorporating higher modes in the DI-I method although not common, it nevertheless, improves damage detection in certain ways. It is, therefore, useful to fill the knowledge gap by modifying the DI-I method. The results are shown in section 6.3.1.3.



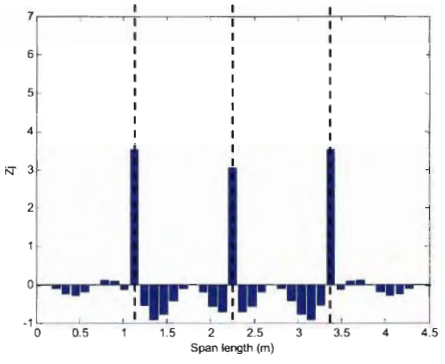
(a) 2L4L6L (2 modes)*.



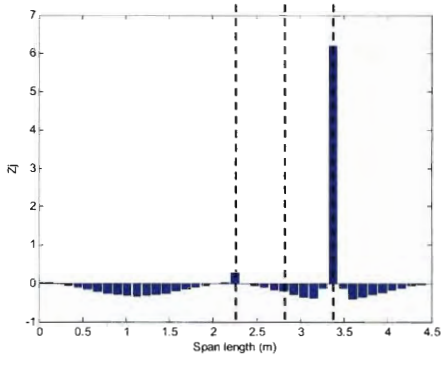
(b) 2L4L6L (5 modes)*.



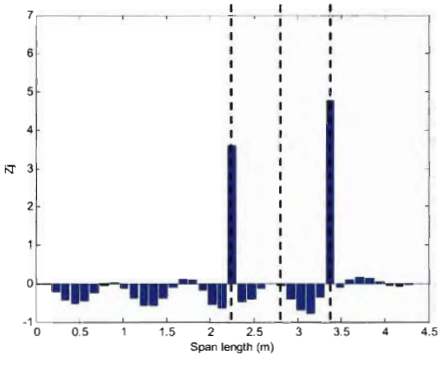
(c) 2S4S6S (2 modes)*.



(d) 2S4S6S (5 modes)*.



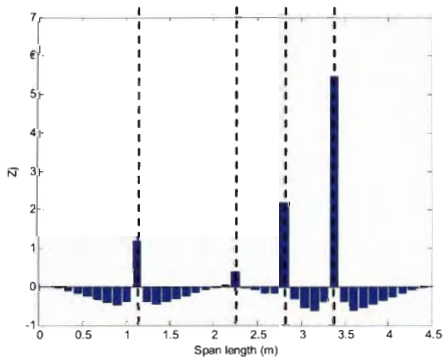
(e) 4S5L6S (2 modes)*.



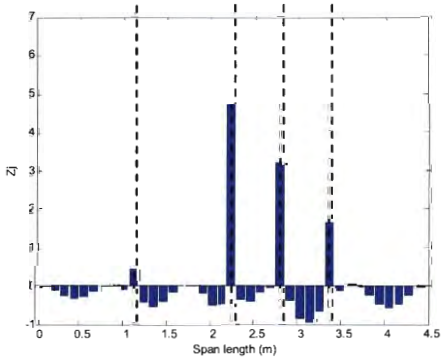
(f) 4S5L6S (5 modes)*.

* *denotes damage cases that were replicated in the experimental tests.*

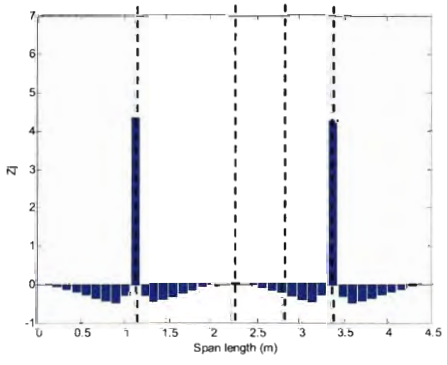
Figure 6.10 Three damage cases using DI-I method.



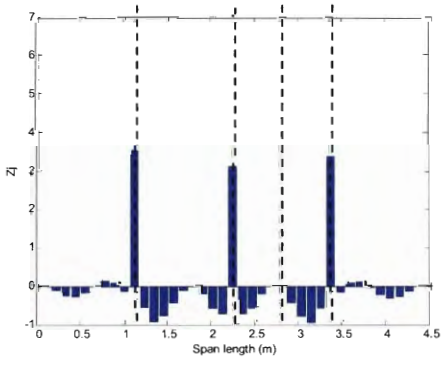
(a) 2M4S5S6S (2 modes)*.



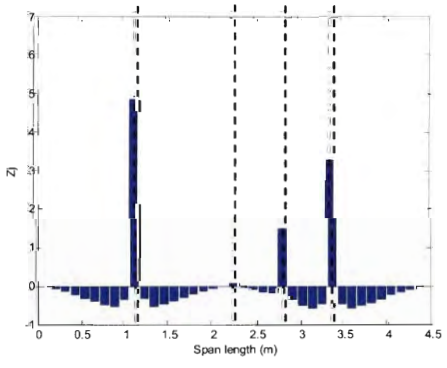
(b) 2M4S5S6S (5 modes)*.



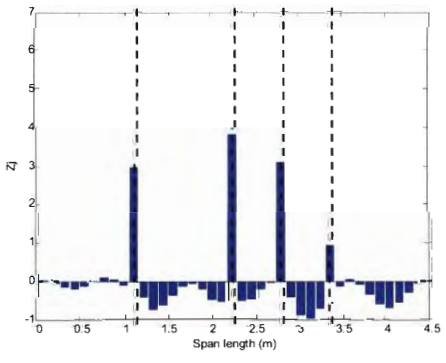
(c) 2S4S5L6S (2 modes)*.



(d) 2S4S5L6S (5 modes)*.



(e) 2S4S5S6S (2 modes)*.



(f) 2S4S5S6S (5 modes)*.

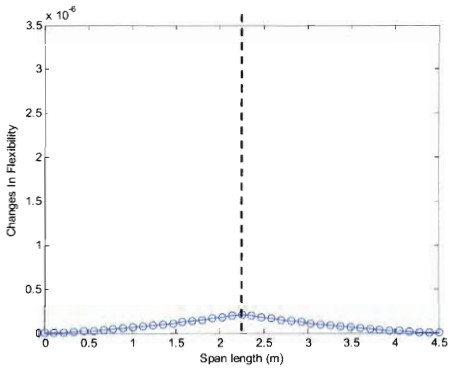
* *denotes damage cases that were replicated in the experimental tests.*

Figure 6.11 Four damage cases using DI-I method.

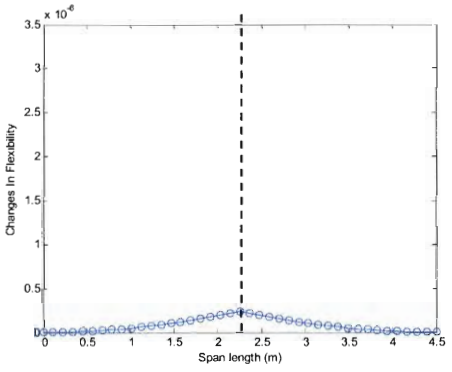
6.3.1.2 Application of Changes in Flexibility on Timber Beam

In this study, an attempt has been made to apply changes in flexibility (CIF) in a timber beam numerically to detect location of single and multiple damage, for which not much work has been published, especially in the application of CIF with boundary conditions of pin-pin. It should be noted that values of flexibility matrix has been used for determining structural integrity of girders in a timber bridge, but the results are not satisfactory (Morison et al. 2003).

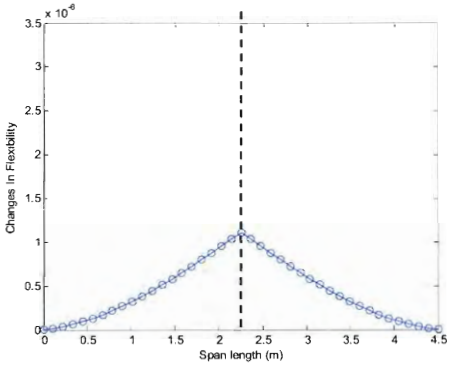
The single damage cases 4L, 4M, 4S, 5M and 6S are shown in Figures 6.12a, 6.12c, 6.12e, 6.12g and 6.12i, and Figures 6.12b, 6.12d, 6.12f, 6.12h and 6.12j, using the changes in the flexibility matrix and including the first two and first five flexural modes, respectively. Referring to Figures 6.12a to 6.12f, the CIF index starts with zero at the supports and increases nonlinearly (usually linear in a simply supported case) as it moves towards the midspan of the beam. The method identifies the single damage location at 2.25m (midspan) for damage cases 4L, 4M and 4S where the changes in the flexibility index reaches its maximum as suggested by Pandey and Biswas (1994). The CIF indices increase from 0.25×10^{-6} to 1.25×10^{-6} and then 3.0×10^{-6} as the severity of damage increases from light, medium to severe, respectively. This indicates that the method is capable of estimating the severity of damage for single damage scenarios. The behaviour of CIF in the 4L, 4M and 4S cases is similar to the cases 5M and 6S as shown in Figure 6.12. The shift of damage location, however, has created another "hump" (local maximum) next to the damage site. This phenomenon was not reported in previous studies on simply supported beam model (Pandey & Biswas 1994). The "hump" may be attributed to the pin-ended support, which has restricted translational movement resulting in additional forces. It is also important to note that the number of modes used in the algorithm has not affected the results much.



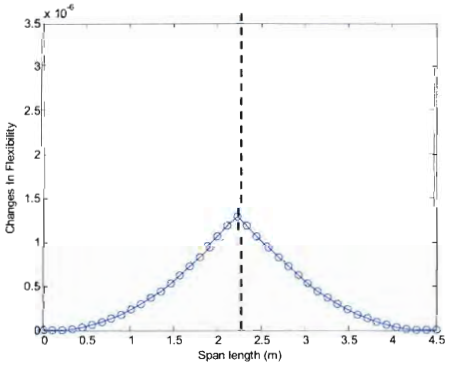
(a) CIF- 4L (2 modes)*.



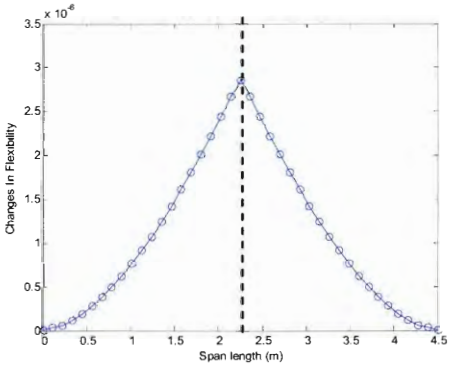
(b) CIF- 4L (5 modes)*.



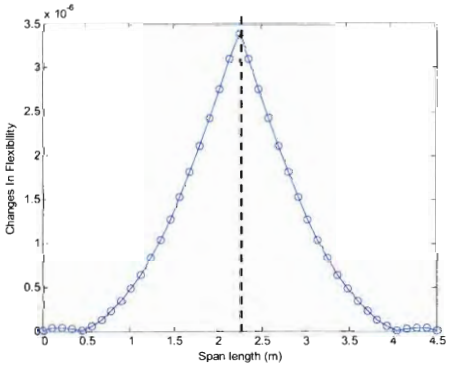
(c) CIF- 4M (2 modes)*.



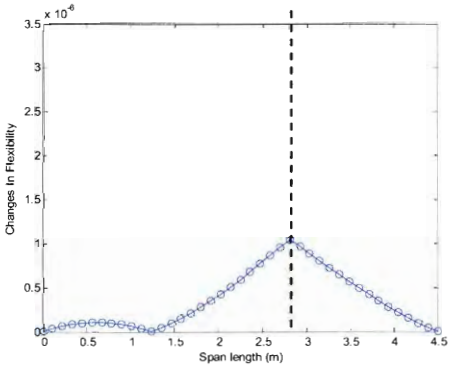
(d) CIF- 4M (5 modes)*.



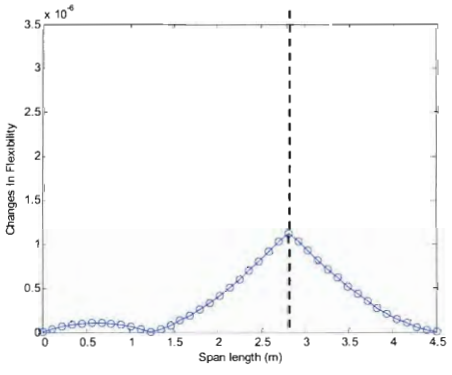
(e) CIF- 4S (2 modes)*.



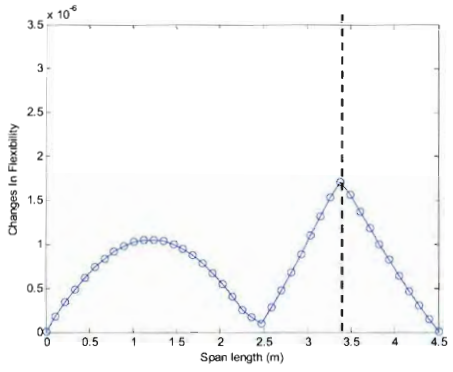
(f) CIF- 4S (5 modes)*.



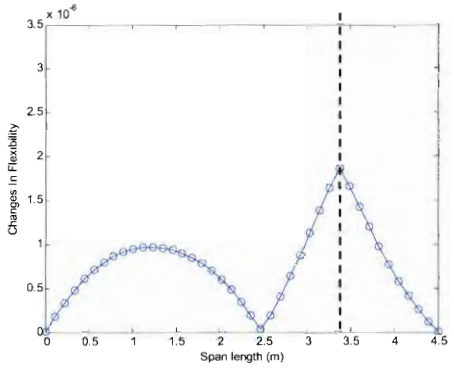
(g) CIF- 5M (2 modes).



(h) CIF- 5M (5 modes).



(i) CIF- 6S (2 modes).

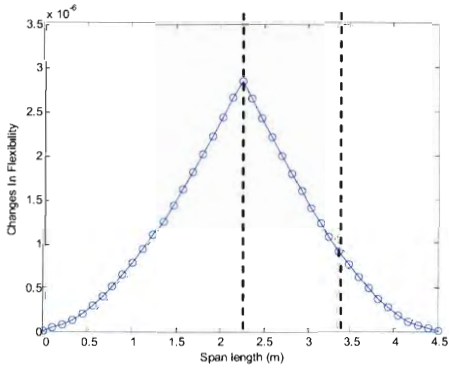


(j) CIF- 6S (5 modes).

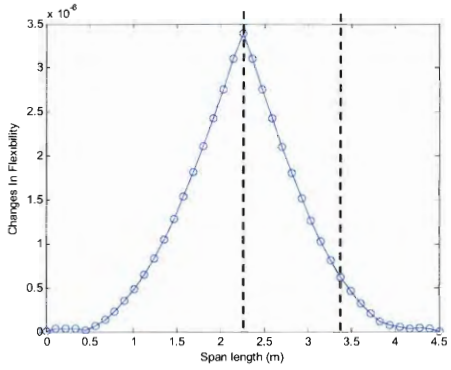
* *denotes damage cases that were replicated in the experimental tests.*

Figure 6.12 Single damage cases using CIF method.

To identify multiple damage locations using the changes in flexibility (CIF) method (not reported by (Pandey & Biswas 1994)), it is proposed in this study that any distinguishable peak appearing in the results would be considered as a damage site. The multiple damage scenarios involving cases with two damage (4S6L), three damage (4S5L6S) and four damage (2M4S5S6S) were considered utilising CIF algorithm and using the first two and first five flexural modes for calculation and they are displayed in Figures 6.13 to 6.15, respectively. The severe damage, at 2.25m (midspan) for case 4S6L as shown in Figure 6.13 and, likewise at locations 2.25m and 3.375m for case 4S5L6S as illustrated in Figure 6.14, were identified by the method, but it failed to locate the light damage location. For four damage location case (2M4S5S6S) using the first two flexural modes in Figure 6.15a, the method missed the medium and severe damage at locations 1.125m and 3.375m, respectively. While using the five modes (Figure 6.15b), it missed the medium damage (1.125m) and did not indicate clearly the severe damage at location 3.375m. It is deduced that the CIF method is capable of locating single damage location but does not provide any information about damage regions. Furthermore, it did not perform well in identifying all damage locations for multiple damage scenarios. These findings are in agreement with the work done by Sánchez (2005).



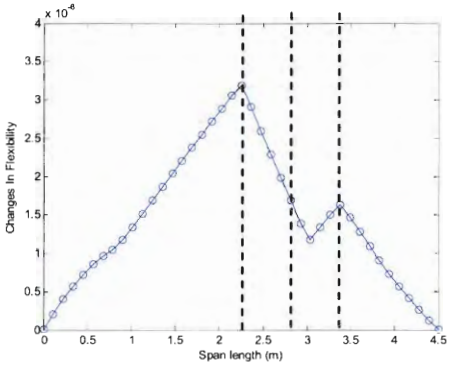
CIF- 4S6L (2 modes)*.



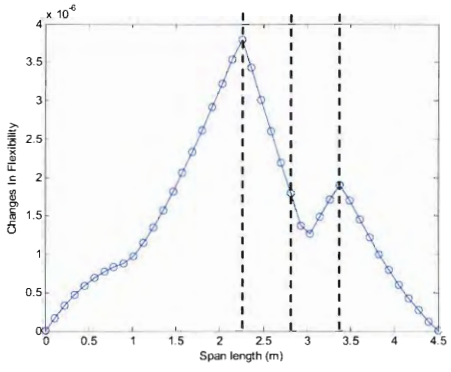
CIF- 4S6L (5 modes)*.

* *denotes damage cases that are replicated in the experimental tests.*

Figure 6.13 Two damage cases using CIF method.



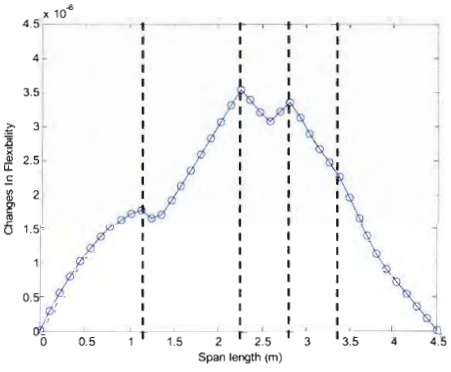
CIF- 4S5L6S (2 modes)*.



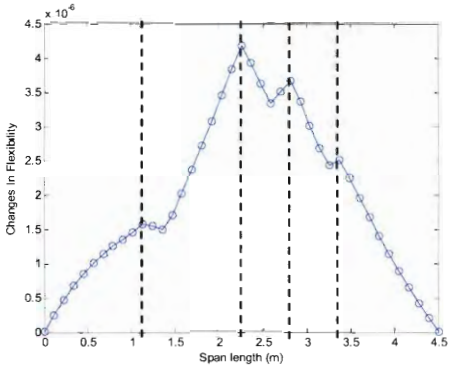
CIF- 4S5L6S (5 modes)*.

* *denotes damage cases that are replicated in the experimental tests.*

Figure 6.14 Three damage cases using CIF method.



CIF- 2M4S5S6S (2 modes)*.



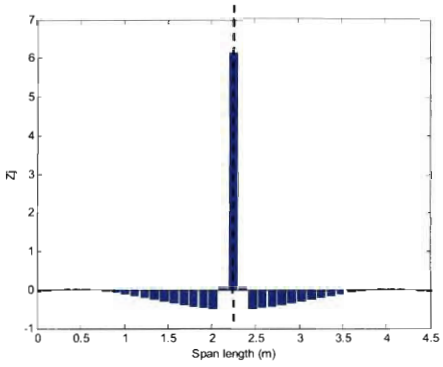
CIF- 2M4S5S6S (5 modes)*.

* *denotes damage cases that are replicated in the experimental tests.*

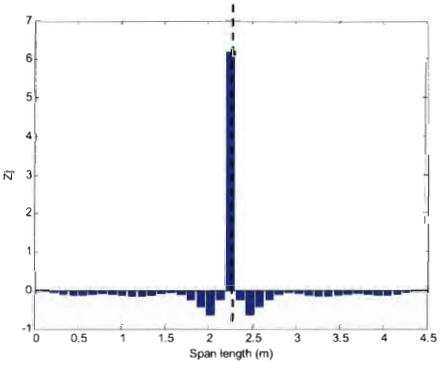
Figure 6.15 Four damage cases using CIF method.

6.3.1.3 Modification Made to DI-I Method to Improve Damage Detection

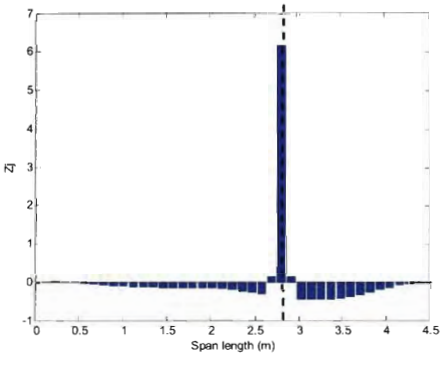
From the preceding two sections on damage index I (DI-I) and changes in flexibility (CIF) methods, it is apparent that damage detection results for multiple damage scenarios were not satisfactory. It is, therefore, proposed in this study to modify the DI-I method by normalising the mode shape curvature before the calculation, referred to herein as modified damage index I (MDI-I) method. In Figure 6.16, the MDI-I results are plotted for single damage cases 4L, 5M and 6S using the first two modes and the first five modes (flexural modes) for computation. It is clearly evident that the method is capable of detecting all damage locations without much contamination of spurious damage locations regardless of the number of modes used. It should be noted that the magnitude of the damage indicator did not change much (approximately equals to 6) for various levels of damage severity in single damage scenarios. This implies that the method is not capable of quantifying damage severity.



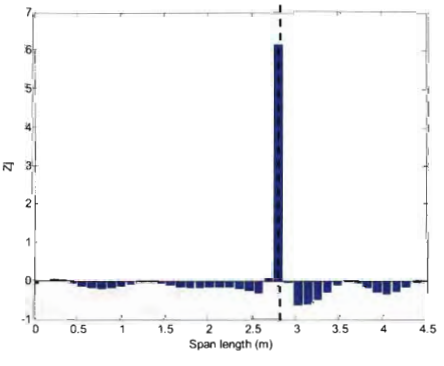
(a) 4L (2 modes)*.



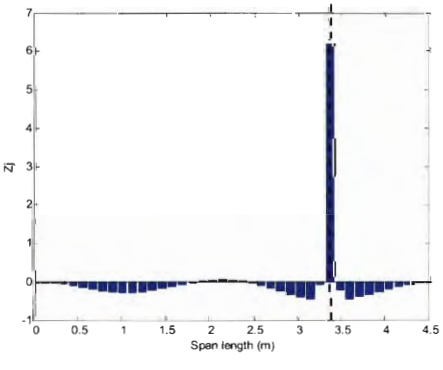
(b) 4L (5 modes)*.



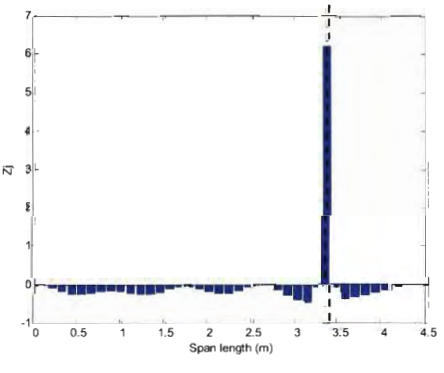
(c) 5M (2 modes).



(d) 5M (5 modes).



(e) 6S (2 modes).

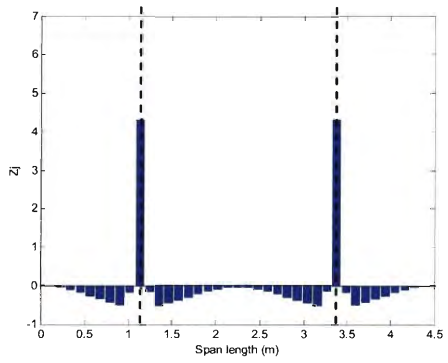


(f) 6S (5 modes).

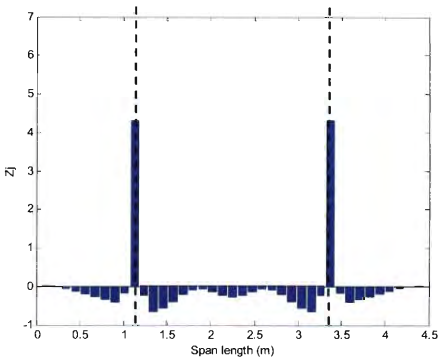
* *denotes damage cases that were replicated in the experimental tests.*

Figure 6.16 Single damage cases using MDI-I method.

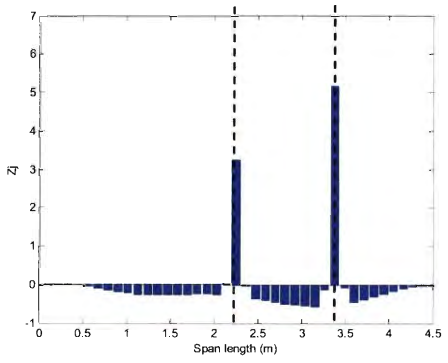
Damage localisations for the cases of two damage (2L6L, 4L6L and 4S6L) using either 2 modes or 5 modes in the MDI-I algorithm are shown in Figure 6.17. It can be seen that the MDI-I method is able to capture all localised damage at locations 1.125m and 3.375m for case 2L6L and, 2.25m and 3.375m for both cases 4L6L and 4S6L. In these figures, the magnitude of the damage index at the damage location changes with the number of modes selected for computation. The results using 5 modes show a more reasonable trend in terms of representing the probability of damage for the simulated damage cases. To illustrate this, using case 4L6L as an example (see Figures 6.17c and 6.17d) for similar damage levels, the case using 2 modes depicts more difference in the Z_j values compared to the one using 5 modes. It is shown here that the MDI-I method is capable of detecting all damage locations and performs better than the DI-I and CIF method. It is also less dependent on the number of mode shapes selected for locating the damage. It confirms that inclusion of higher modes in the MDI-I algorithm can produce better or equally good results than those of using only the first two modes. It is also observed that (referring to Figure 6.17f) using the MDI-I method for multiple damage scenarios can indicate damage severity level but not with great accuracy.



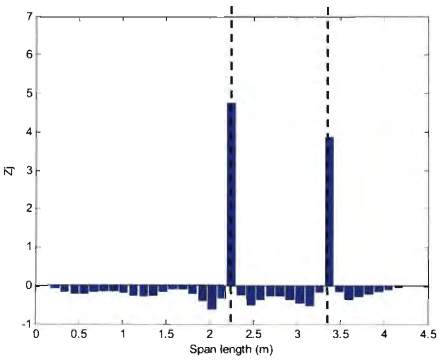
(a) 2L6L (2 modes)*.



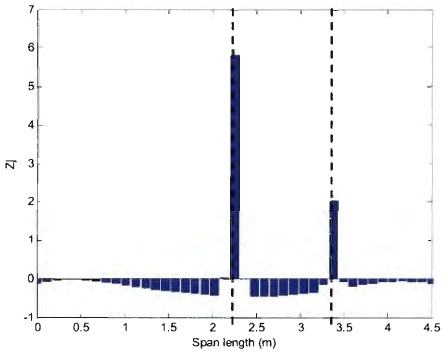
(b) 2L6L (5 modes)*.



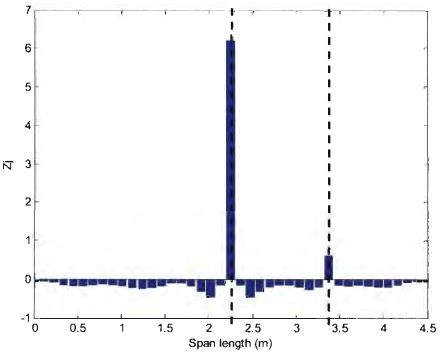
(c) 4L6L (2 modes).



(d) 4L6L (5 modes).



(e) 4S6L (2 modes)*.

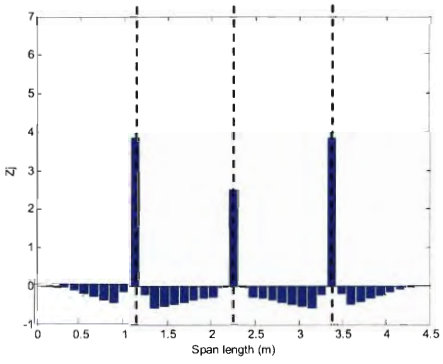


(f) 4S6L (5 modes)*.

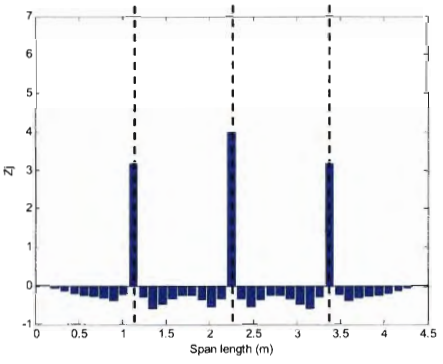
* *denotes damage cases that were replicated in the experimental tests.*

Figure 6.17 Two damage cases using MDI-I method.

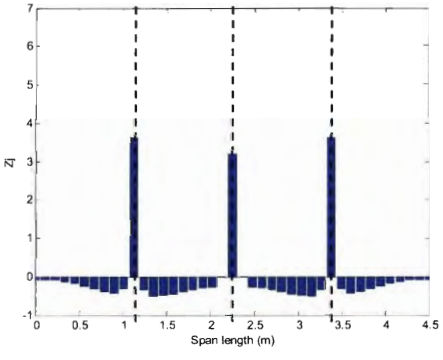
Cases of three (2L4L6L, 2S4S6S and 4S5L6S) and four (2M4S5S6S, 2S4S5L6S and 2S4S5S6S) damage locations are illustrated in Figures 6.18 and 6.19. From these cases, when 2 modes are used in the computation, it identifies all the damage locations except the light damage that lies between two severe damage locations with close spacings as illustrated in Figures 6.18e and 6.19c. Whereas when 5 modes are used, all damage locations were identified as shown in Figures 6.18f and 6.19d. It is, therefore, concluded that for multiple damage scenarios with different levels of severity of damage, employing higher modes in damage localisation with MDI-I method produces better results.



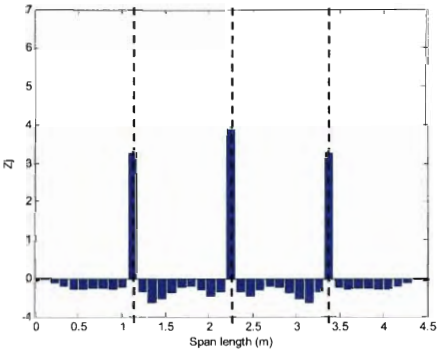
(a) 2L4L6L (2 modes)*.



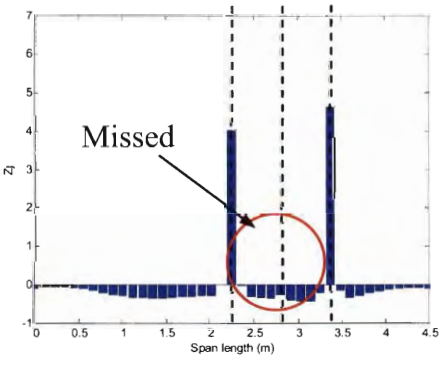
(b) 2L4L6L (5 modes)*.



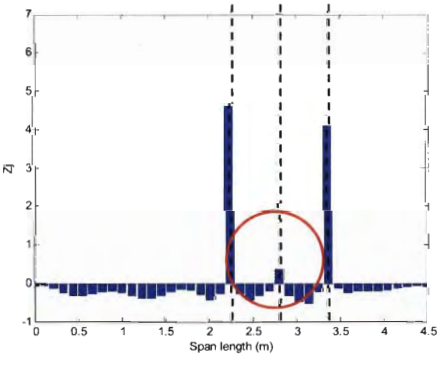
(c) 2S4S6S (2 modes)*.



(d) 2S4S6S (5 modes)*.



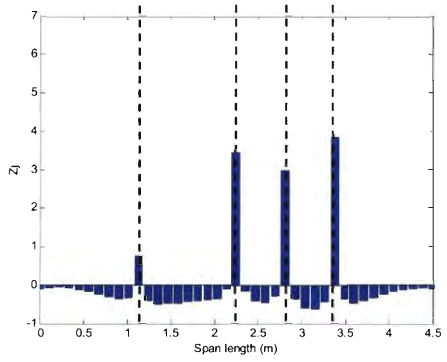
(e) 4S5L6S (2 modes)*.



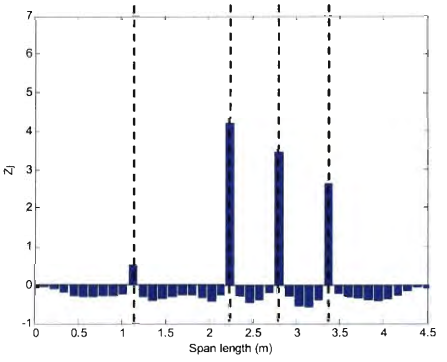
(f) 4S5L6S (5 modes)*.

* *denotes damage cases that are replicated in the experimental tests.*

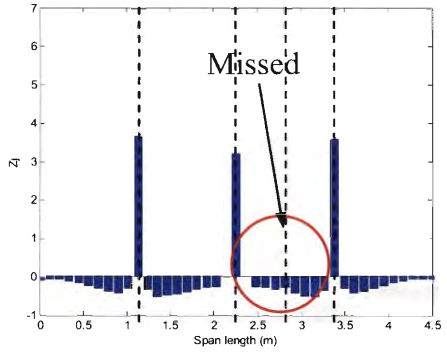
Figure 6.18 Three damage cases using MDI-I method.



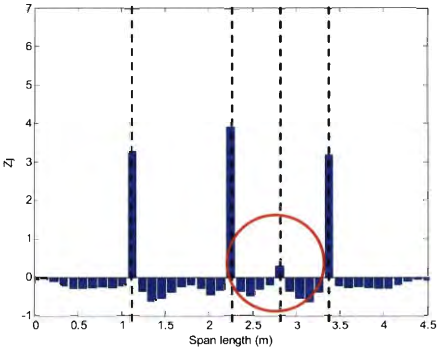
(a) 2M4S5S6S (2 modes)*.



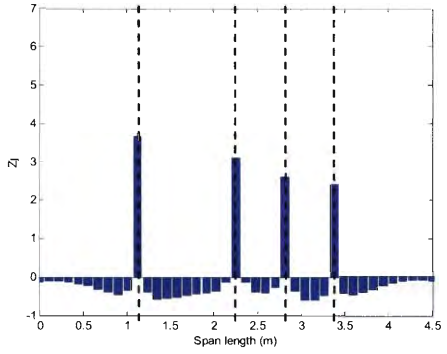
(b) 2M4S5S6S (5 modes)*.



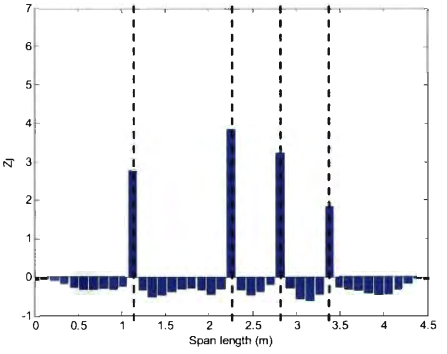
(c) 2S4S5L6S (2 modes)*.



(d) 2S4S5L6S (5 modes)*.



(e) 2S4S5S6S (2 modes)*.



(f) 2S4S5S6S (5 modes)*.

* *denotes damage cases that were replicated in the experimental tests.*

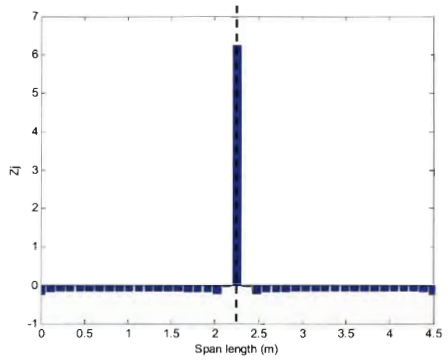
Figure 6.19 Four damage cases using MDI-I method.

6.3.1.4 Discussions on Damage Index II Method

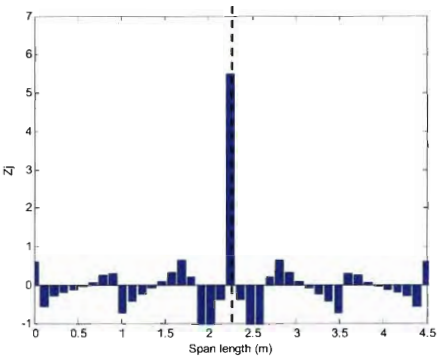
Further to the discussions on application of damage index I (DI-I) method and its modified version, namely modified damage index I (MDI-I) method, to detect damage, it is of interest to explore application of the original form of damage index I (DI-I) method (Kim & Stubbs 1995), denoted as damage index II (DI-II) in this study whereby the axis of reference for the modal sensitivities is not shifted by a value of one (Refer to Chapter 5). To the best knowledge of the author, the damage index II (DI-II) method has not been applied to timber structures to detect damage and this study may be the first of its kind.

Employing a finite element (FE) model of a timber beam, an analytical investigation was carried out using the DI-II method for detecting damage for single and multiple damage scenarios. The damage cases used for the investigation in this section correspond to damage cases using DI-I in Section 6.3.1.1. In the following results, the statistically normalised damage indicator values Z_j for each of the damage cases, are plotted against the beam span length (4.5m). In principle, the index value Z_j larger than zero (probability-based criterion for damage) is considered as possible damage existing at that location. As before, the actual damage locations are indicated with vertical dashed lines in all figures for timber beam.

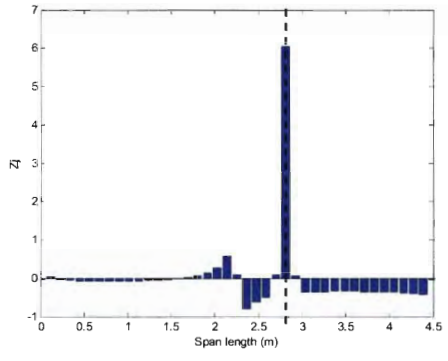
Figures 6.20a, 6.20c and 6.20e show the results of applying damage index II (DI-II) algorithm to detect single damage cases with light (L), medium (M) and severe (S) damage at location 4/8 (2.25 m), 5/8 (2.8125 m) or 6/8 (3.375 m) of the span length (4.5 m) using the first two flexural modes (2 modes) for computation. The damage in the single damage cases 4L, 5M and 6S, corresponded to loss of 'I' (moment of inertia) of 27.1%, 65.7% and 87.5%, respectively. It is clear that the damage index II method has located the damage for all single damage cases discussed here, but this method has also produced false positives (indications of spurious damage locations) of damage as seen in Figures 6.20c and 6.20e. Similar single damage cases using the first five flexural modes in the DI-II algorithm are illustrated in Figures 6.20b, 6.20d and 6.20f. The damage, in these cases is located but a few false detections did also appear, indicated by positives Z_j values at locations other than the actual damage.



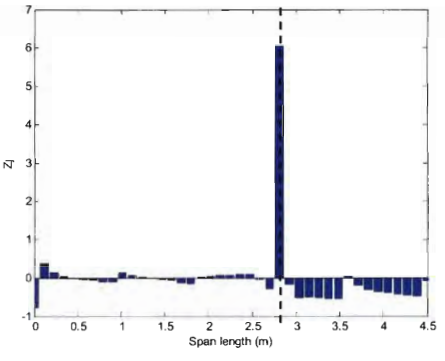
(a) 4L (2 modes)*.



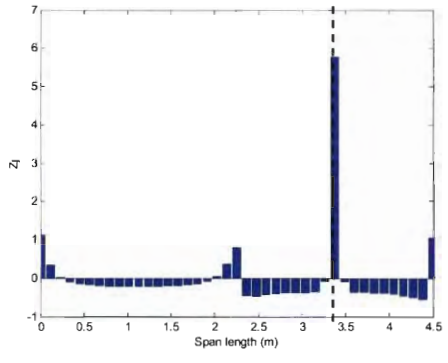
(b) 4L (5 modes)*.



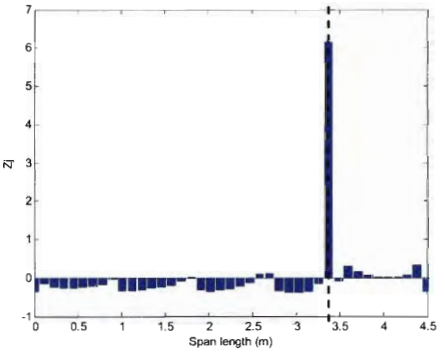
(c) 5M (2 modes).



(d) 5M (5 modes).



(e) 6S (2 modes).

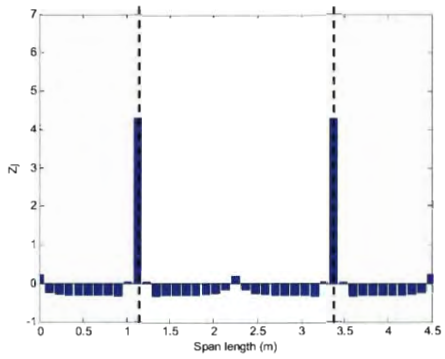


(f) 6S (5 modes).

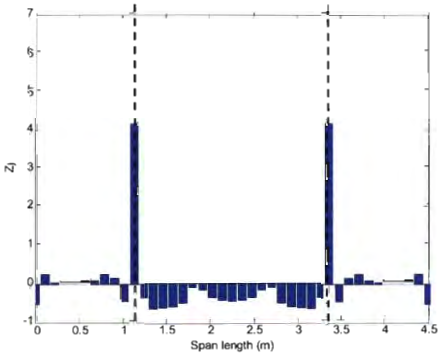
* *denotes damage cases that were replicated in the experimental tests.*

Figure 6.20 Single damage cases using DI-II method.

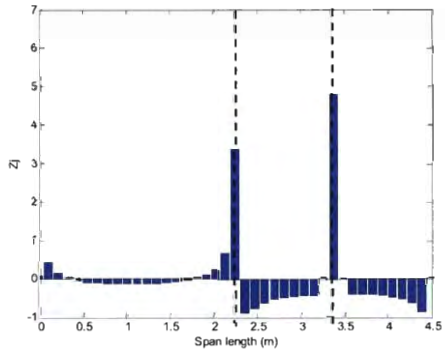
Figure 6.21 shows the results of applying the DI-II method using the first two and the first five flexural modes in damage cases 2L6L, 4L6L and 4S6L, where two damage locations were inflicted in the numerical model. The actual inflicted damage locations for case 2L6L are 1.125m and 3.375m, while for cases 4L6L and 4S6L are 2.25m and 3.375m. The damage localisation algorithm identifies all damage locations, except light damage at 3.375m for case 4S6L (using 5 modes) as shown in Figure 6.21f. Despite its ability to detect damage, the damage index II method yields some spurious damage locations even with a dense meshed numerical model. The use of five modes was not anticipated to be less efficient than using two modes as it is commonly acknowledged that using higher modes usually performs better in system identification for a dynamic system. This discrepancy suggests the need for an additional procedure to enhance the efficiency of damage localisation when incorporating higher modes in the damage index II method. It is important to note here that the method is also able to provide some indication of different levels of severity, as exampled in case 4S6L using 2 modes (refer to Figure 6.21e). The severe damage at location 2.25m has much higher probability of damage existing at that locations compared to the light damage at 3.375m.



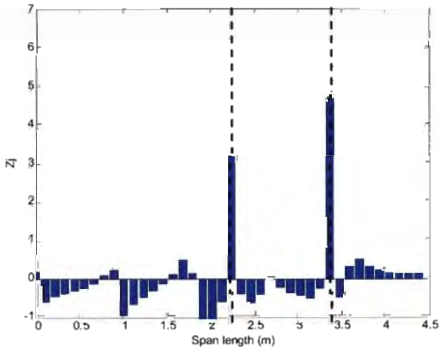
(a) 2L6L (2 modes)*.



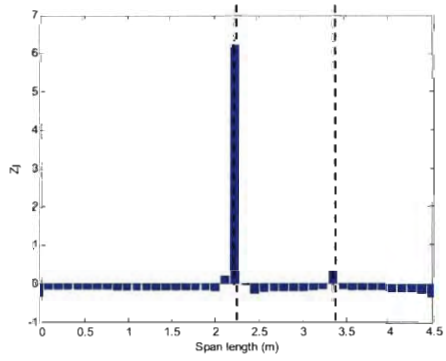
(b) 2L6L (5 modes)*.



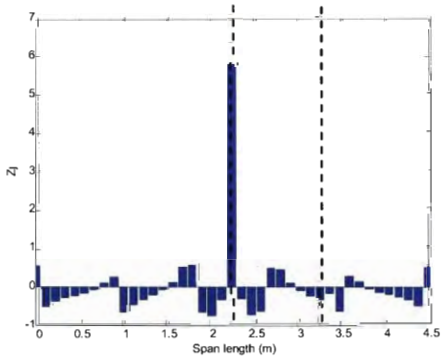
(c) 4L6L (2 modes).



(d) 4L6L (5 modes).



(e) 4S6L (2 modes)*.

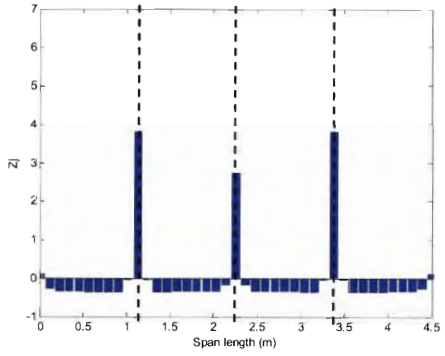


(f) 4S6L (5 modes)*.

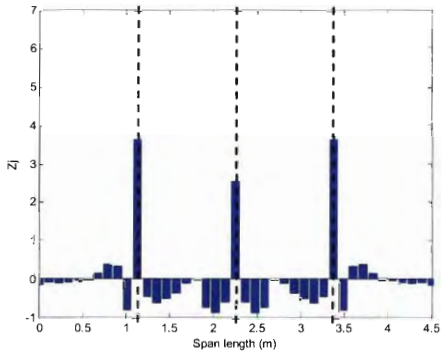
* *denotes damage cases that were replicated in the experimental tests.*

Figure 6.21 Two damage cases using DI-II method.

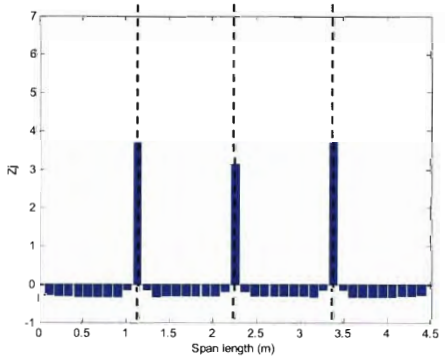
Figure 6.22 shows the results of three damage scenarios, namely 2L4L6L, 2S4S6S and 4S5L6S. It is apparent that the damage localisation algorithm is able to identify all damage locations when similar levels of damage severity is inflicted in the analytical model as depicted in Figures 6.22a to 6.22d for both 2 modes and 5 modes. However, they failed to locate the light damage where there are different levels of damage and closer spacing of damage locations as seen in Figures 6.22e and 6.22f. Another observation that should be made here is that in contrast to the two damage cases, the estimation of damage severity is unreliable even for similar level of damage severity as exampled in the severe damage of case 4S5L6S (see Figures 6.22e and 6.22f). Similar pattern is also observed in Figures 6.23a to 6.23f, where four damage scenario cases 2M4S5S6S, 2S4S5L6S and 2S4S5S6S, respectively, were applied using the damage index II method. A conclusion can be drawn here and that the damage index II (DI-II) method is capable of identifying single damage locations quite well with some false positives, but it did not work too well for the multiple damage cases.



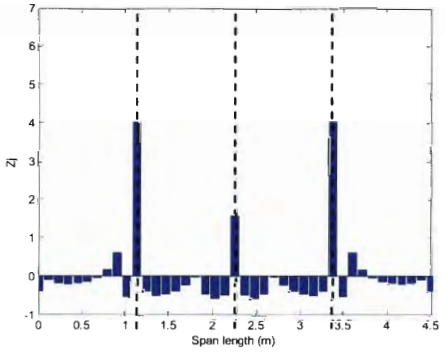
(a) 2L4L6L (2 modes)*.



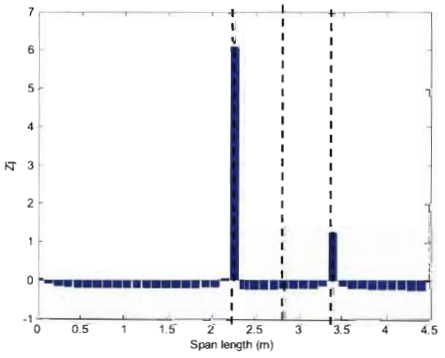
(b) 2L4L6L (5 modes)*.



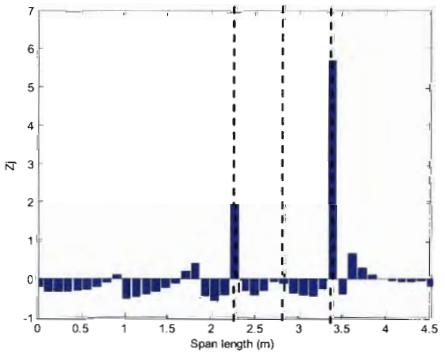
(c) 2S4S6S (2 modes)*.



(d) 2S4S6S (5 modes)*.



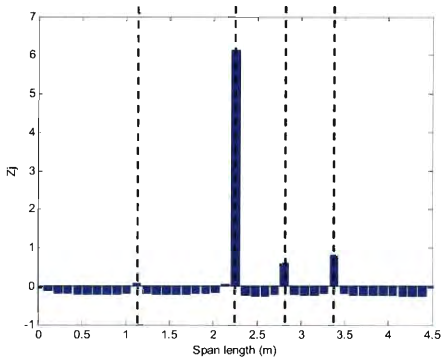
(e) 4S5L6S (2 modes)*.



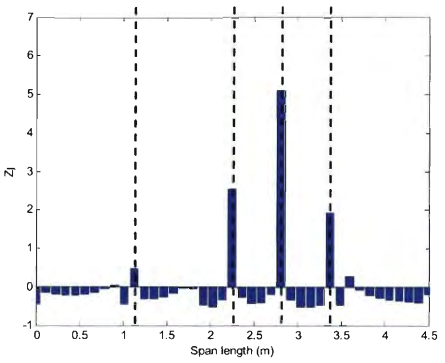
(f) 4S5L6S (5 modes)*.

* *denotes damage cases that were replicated in the experimental tests.*

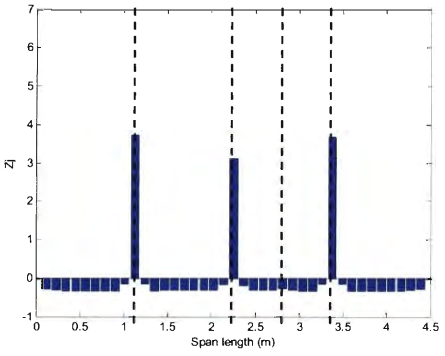
Figure 6.22 Three damage cases using DI-II method.



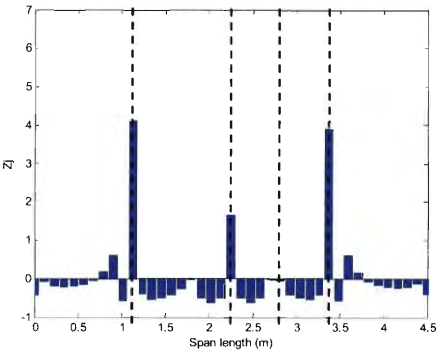
(a) 2M4S5S6S (2 modes)*.



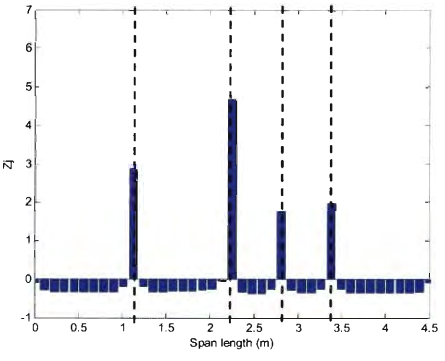
(b) 2M4S5S6S (5 modes)*.



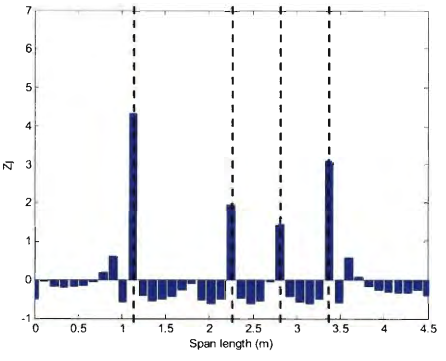
(c) 2S4S5L6S (2 modes)*.



(e) 2S4S5L6S (5 modes)*.



(f) 2S4S5S6S (2 modes)*.



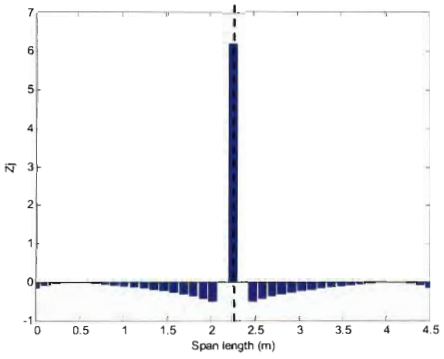
(g) 2S4S5M6S (5 modes)*.

* *denotes damage cases that were replicated in the experimental tests.*

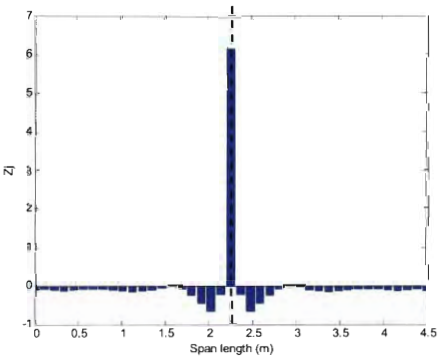
Figure 6.23 Four damage cases using DI-II method.

6.3.1.5 Modification Made to DI-II method to Improve Damage Detection

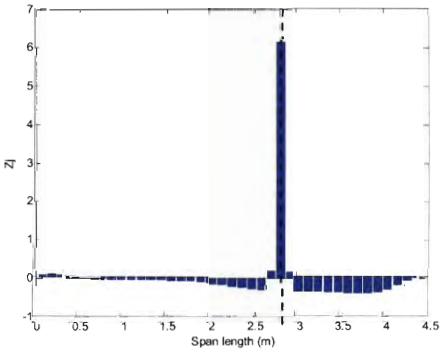
Based on the findings in the preceding section, the damage index II method failed to locate multiple damage scenarios in a timber beam. It was proposed in this study to modify the DI-II method by normalising the mode shape curvature, which will enhance its capabilities to detect damage (details of the modification can be found in the section 5.5 of Chapter 5). This modified algorithm is named modified damage index II (MDI-II). In Figure 6.24, the MDI-II is used to plot single damage cases of 4L, 5M and 6S using the first two (2 modes) and first five (5 modes) flexural modes to compute. Referring to Figure 6.24, it is evident that all damage is precisely located. While for 5 modes, as shown in Figures 6.24b, 6.24d and 6.24f, similar results were achieved. It is possible to infer that, for single damage cases, the modified damage index II (MDI-II) method has improved results of damage localisation with less false positives compared to its original form.



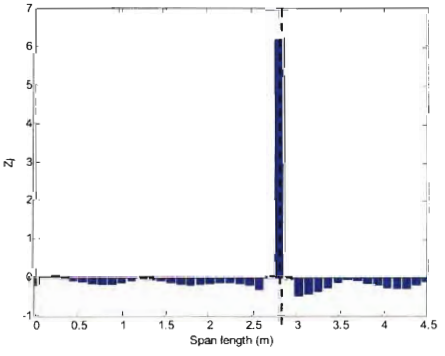
(a) 4L (2 modes)*.



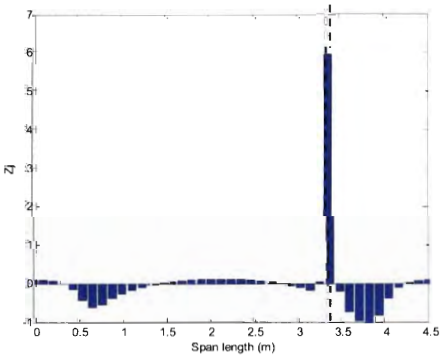
(b) 4L (5 modes)*.



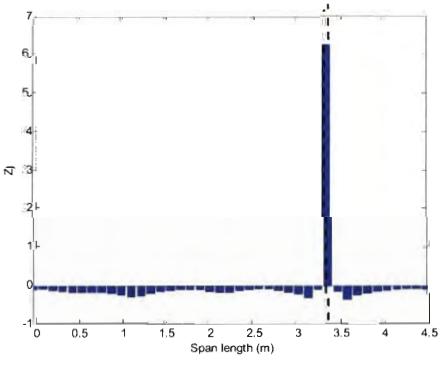
(c) 5M (2 modes).



(d) 5M (5 modes).



(e) 6S (2 modes).

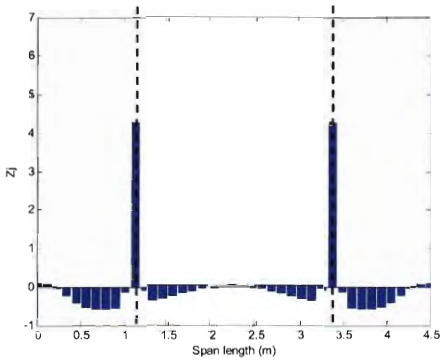


(f) 6S (5 modes).

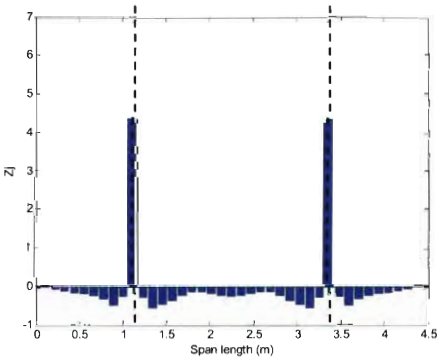
* *denotes damage cases that were replicated in the experimental tests.*

Figure 6.24 Single damage cases using MDI-II method.

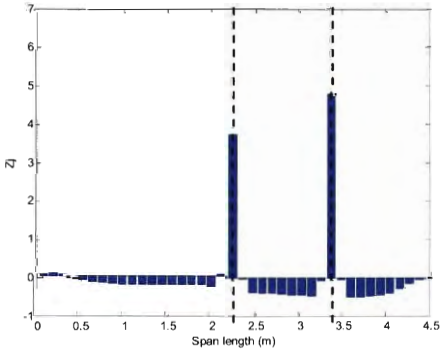
Damage localisations for the cases of two damage scenarios 2L6L, 4L6L and 4S6L, using either the first two or the first five modes, are shown in Figures 6.25a, 6.25c and 6.25e, and Figures 6.25b, 6.25d and 6.25f, respectively. It can be seen that the MDI-II method is able to capture all localised damage at locations 1.125m and 3.37m for case 2L6L, as well as at 2.25m and 3.375m for cases 4L6L and 4S6L. The results indicated that the method is effective in identifying two damage locations regardless of the number of modes used, in contrast to the original damage index I (DI-I) shown in section 6.3.1.4. In other words, the MDI-II method is less dependent of the number of modes selected. In addition, the magnitude of the damage index corresponds very closely to the level of damage severity inflicted in the analytical model. It should also be noted that using the first five modes provides better indication of damage severity. With the same level of damage severity, it produces a smaller Z_j difference than that of the two modes one as seen in Figures 6.25c and 6.25d. This reinforces the findings mentioned previously in which the higher modes would probably provide better damage detection.



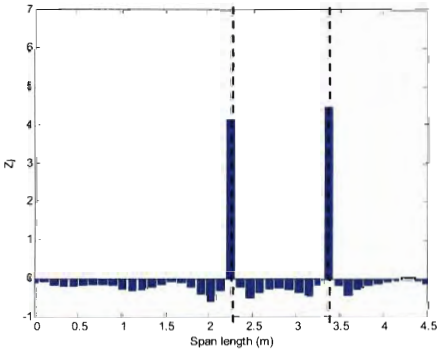
(a) 2L6L (2 modes)*.



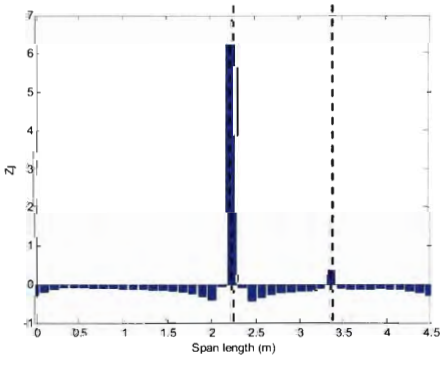
(b) 2L6L (5 modes)*.



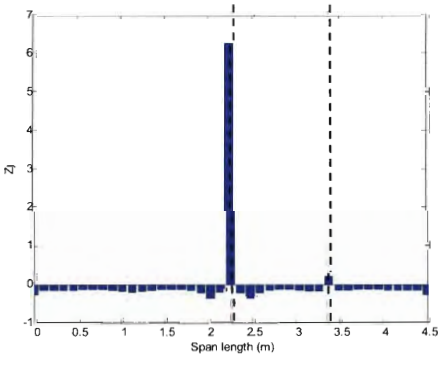
(c) 4L6L (2 modes).



(d) 4L6L (5 modes).



(e) 4S6L (2 modes)*.

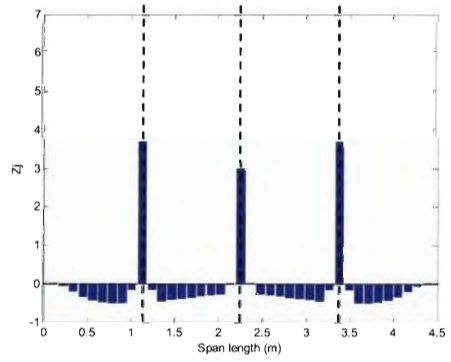


(f) 4S6L (5 modes)*.

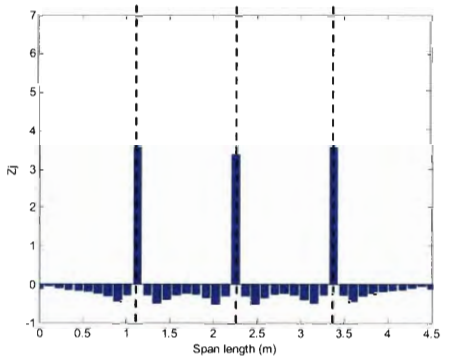
* *denotes damage cases that were replicated in the experimental tests.*

Figure 6.25 Two damage cases using MDI-II method.

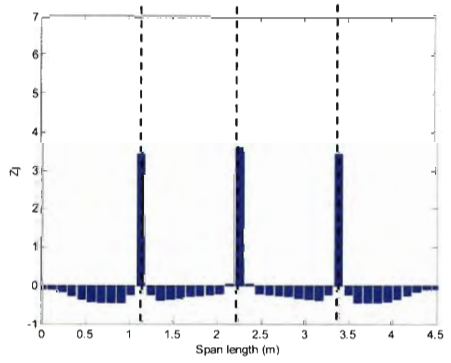
Cases of three (2L4L6L, 2S4S6S and 4S5L6S) and four damage (2M4S5S6S, 2S4S5L6S and 2S4S5S6S) locations are illustrated in Figures 6.26 and 6.27, respectively. For all these cases, when 2 modes are used in the computations, it located all the medium and severe damage locations, but failed to identify the light damage locations as shown in Figures 6.26e and 6.27c. Whereas, when 5 modes are used, all damage locations were identified although with less distinction for the light damage. Therefore, it can be concluded that for multiple damage scenarios employing higher modes in damage localisation with MDI-II algorithm produces better results. The MDI-II method was found to be superior to its original formulae (DI-II). Comparing MDI-I and MDI-II methods, the former performs slightly better in identifying light damage using the first five modes as exampled in case 4S5L6S and shown in Figures 6.18f and 6.26f, respectively. Based on the results above, it is possible to deduce that the MDI-I and MDI-II are capable of providing an indication of damage severity but not accurately.



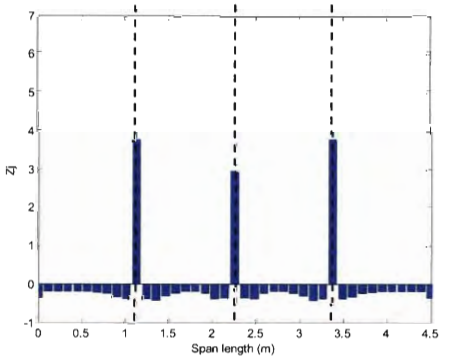
(a) 2L4L6L (2 modes)*.



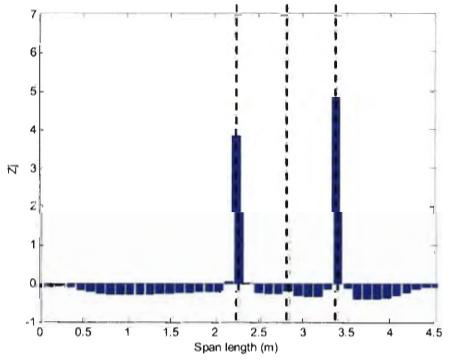
(b) 2L4L6L (5 modes)*.



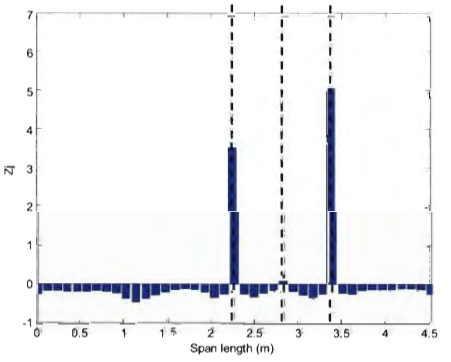
(c) 2S4S6S (2 modes)*.



(d) 2S4S6S (5 modes)*.



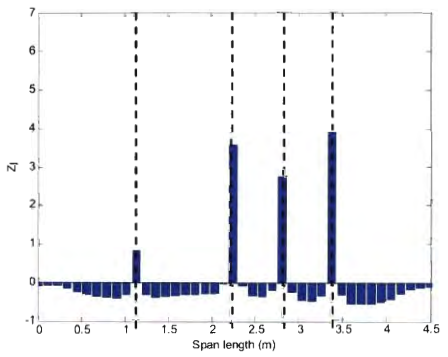
(e) 4S5L6S (2 modes)*.



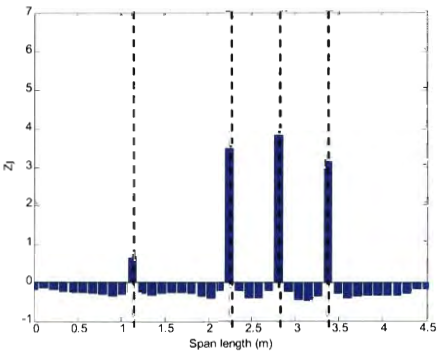
(f) 4S5L6S (5 modes)*.

* *denotes damage cases that were replicated in the experimental tests.*

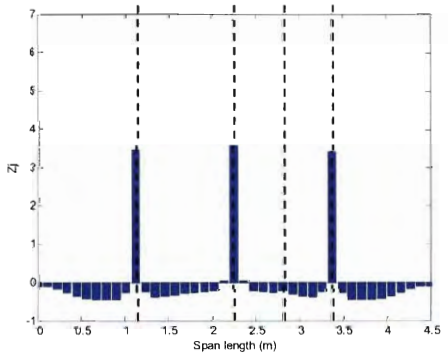
Figure 6.26 Three damage cases using MDI-II method.



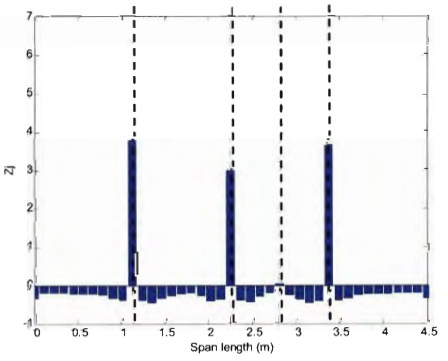
(a) 2M4S5S6S (2 modes)*.



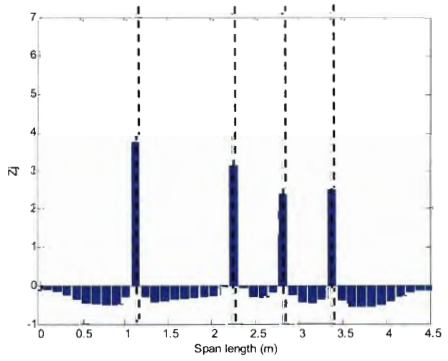
(b) 2M4S5S6S (5 modes)*.



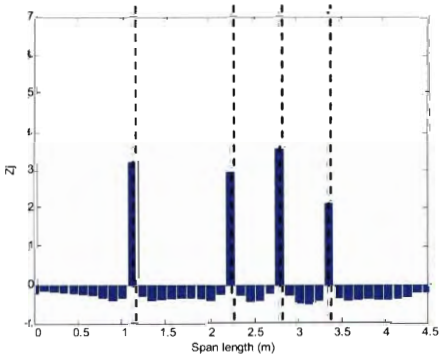
(c) 2S4S5L6S (2 modes)*.



(d) 2S4S5L6S (5 modes)*.



(e) 2S4S5S6S (2 modes)*.



(f) 2S4S5S6S (5 modes)*.

* *denotes damage cases that were replicated in the experimental tests.*

Figure 6.27 Four damage cases using MDI-II method.

6.3.2 Estimation of Severity of Damage

The two proposed modified damage localisation algorithms used in the preceding sections 6.3.1.3 and 6.3.1.5, namely MDI-I and MDI-II, have proven to be able to detect damage location well for single and multiple damage scenarios compared to their original formulae (DI-I and DI-II). These modified algorithms have also shown that, in general, using more modes (5 modes) in the algorithm would perform better in locating multiple damage scenarios than just using the first two modes (2 modes). This phenomenon is consistent with the general principle in structural dynamics that higher modes would help to detect damage better. The modified algorithms are also capable of estimating the severity of damage qualitatively with reasonable confidence. However, the MDI-I has not been formulated to estimate the actual quantity of damage severity. This also applies to the MDI-II algorithm. The two algorithms need further development to allow the estimation of actual magnitude of damage severity. In the light of these shortcomings, it is an important contribution to this study to propose a method to evaluate severity of damage in wood as presented in the following section.

As mention earlier, the modified damage index I (MDI-I) has not been formulated to estimate the magnitude of damage severity. Hence, a hybrid of modified damage index I (MDI-I) and changes in flexibility (CIF- mentioned earlier in the section 5.3 of Chapter 5) algorithms, abbreviated as HMC, is proposed for estimating the location and severity of damage. The details of HMC can be found in the section 5.6 of Chapter 5. For modified damage index II (MDI-II), the formula was further manipulated in order to enable it to be used for estimating the damage severity (can be found in the section 5.7 of Chapter 5). The estimation of damage severity for both methods (HMC and MDI-II) is presented in terms of percentage of loss of "I" (moment of inertia). In all figures, a horizontal red dash-dotted line was used to indicate actual severity of damage for timber beam. Based on the findings of the damage localisation investigations, the first five flexural modes were used in the damage severity estimation in the following discussions.

6.3.2.1 Evaluation of Severity of Damage using Hybrid of MDI-I and CIF

As mentioned earlier, the modified damage index I (MDI-I) algorithm is capable to detect locations of damage, but not capable of evaluating its severity. It was found that combining the MDI-I and changes in flexibility (CIF) and benchmarking against single damage scenarios from the analytical model using the first five flexural modes (can be found in the section 5.6 Chapter 5) provides a means that could estimate the severity of damage. This hybrid algorithm is named hybrid of MDI-I and CIF and is abbreviated as HMC. The inflicted and predicted severity of damage is tabulated in Table 6.3. For the results shown in the following graphs, the severity of damage below zero percent has no physical meaning, thus they are not shown.

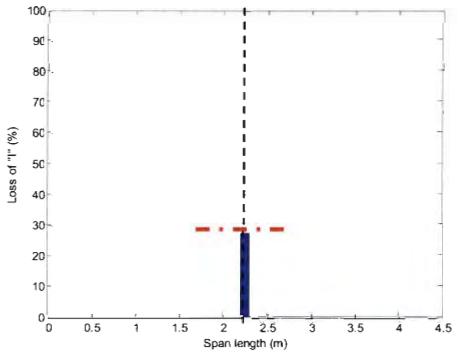
Table 6.3 Estimation of severity of damage using HMC method.

Damage Case	Location(s) per $1/8^{th}$ of span length	Simulated Damage (loss of 'I') (%)	Predicted Damage using HMC method (%)
4L*	4	27.1	26.7
5M	5	65.7	69.1
6S	6	87.5	87.5
2L6L*	2, 6	All 27.1	14.6, 14.6
4L6L	4, 6	All 27.1	19.1, 11.8
4S6L*	4, 6	87.5, 27.1	90.4, 0.6
2L4L6L*	2, 4, 6	All 27.1	8.9, 14.1, 8.9
2S4S6S*	2, 4, 6	All 87.5	83.3, 84.4, 83.3
4S5L6S	4, 5, 6	87.5, 27.1, 87.5	86.6, 7.7, 79.1
2M4S5S6S*	2, 4, 5, 6	65.7, 87.5, 87.5, 87.5	21.3, 86.8, 82.3, 75.4
2S4S5L6S*	2, 4, 5, 6	87.5, 87.5, 27.1, 87.5	83.3, 84.8, 8.3, 83.1
2S4S5S6S*	2, 4, 5, 6	All 87.5	80.6, 86.4, 85.6, 74.6

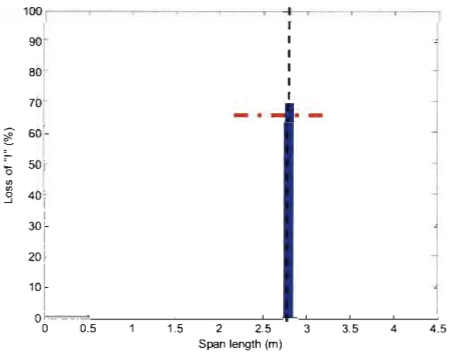
* *denotes damage cases that were replicated in the experimental tests.*

The results of single damage scenarios with ascending damage severity are illustrated in Figures 6.28a to 6.28c, for cases 4L, 5M and 6S, respectively. From these graphs, it is obvious that the method is correctly pin-pointing the damage at locations 2.25 m, 2.8125 m and 3.375 m for cases 4L, 5M and 6S, respectively. It should be noted that there is no appearances of false positives (indication of spurious damage locations). From Table 6.3, the estimation of severity for both damage cases of 4L and 5M, that is 26.7 and 69.1% loss of 'I', respectively, is very close to the simulated value (27.1% and 65.7% loss of 'I') with percentage differences of no more than 5%. For the severe

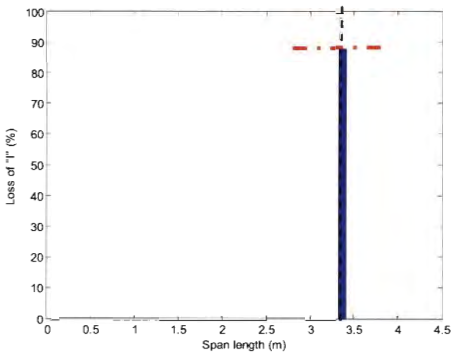
damage, at a single location, the difference between the inflicted and predicted severity of damage is very small, practically no difference. It is obvious that the HMC algorithm is very effective in evaluating the severity of single damage scenarios of different levels of damage severity, especially severe damage. The remarkable results in estimating the severe damage at single location may be attributable to the nature of the HMC method derived from various single location severe damage cases.



(a) 4L (5 modes)*.



(b) 5M (5 modes).



(c) 6S (5 modes).

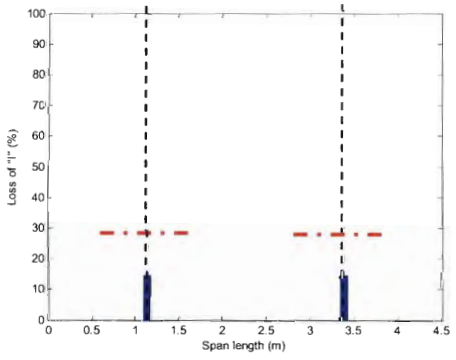
* *denotes damage cases that were replicated in the experimental tests.*

Figure 6.28 Single damage severity estimation using HMC method.

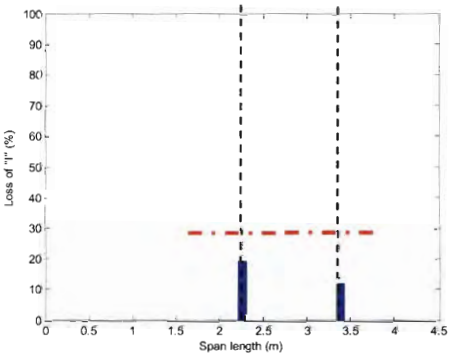
Figures 6.29 to 6.31 illustrate the HMC algorithm being applied to multiple damage cases. The algorithm has demonstrated again its capability to identify all multiple damage locations for the damage cases discussed here with no appearances of spurious damage locations. The feature of no contamination from spurious damage locations are very significant for damage detection when it is applied in field testing that is usually polluted with noise. The HMC method also predicted damage severity well for the damage cases of two (2L6L, 4L6L and 4S6L), three (2L4L6L, 2S4S6S and

4S5L6S) and four (2M4S5S6S, 2S4S5L6S and 2S4S5S6S) damage locations with percentage of difference between inflicted and estimated severity being less than 15% (2S4S5S6S) for severe damage as documented in Table 6.3. However, in all multiple damage scenarios discussed in this section, the algorithm has relatively high prediction error of as high as 68% (2M4S5S6S) and 98% (4S6L) for all medium and light damage, respectively.

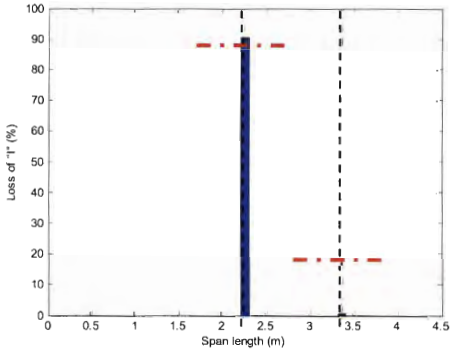
In summary, the newly proposed hybrid of modified damage index I method and changes in flexibility method, HMC, is found to be capable of detecting damage locations and estimating damage severity with high level of accuracy for single damage and at a reasonable level of confidence for multiple damage scenarios.



(a) 2L6L (5 modes)*.



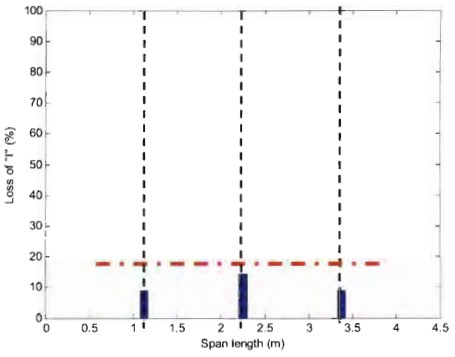
(b) 4L6L (5 modes).



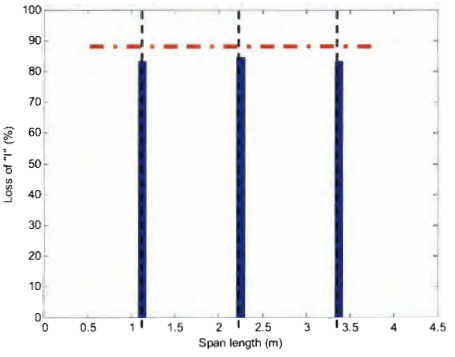
(c) 4S6L (5 modes)*.

* *denotes damage cases that were replicated in the experimental tests.*

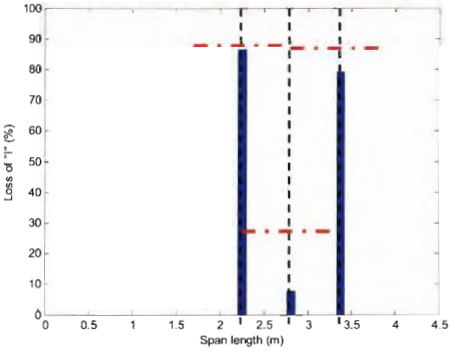
Figure 6.29 Two damage severity estimation using HMC method.



(a) 2L4L6L (5 modes)*.



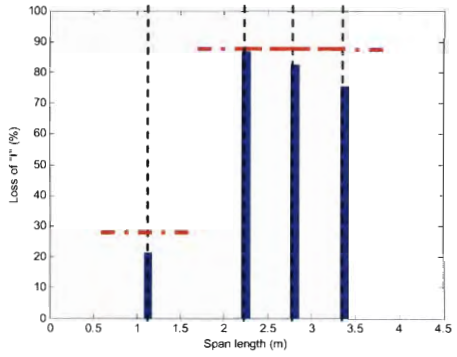
(b) 2S4S6S (5 modes)*.



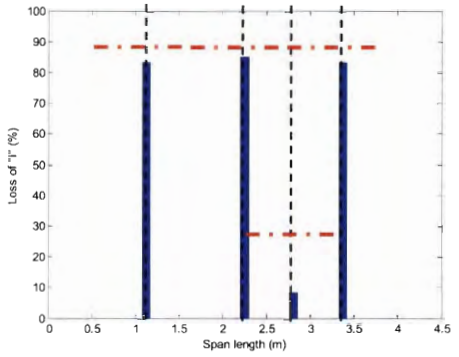
(c) 4S5L6S (5 modes)*.

* *denotes damage cases that were replicated in the experimental tests.*

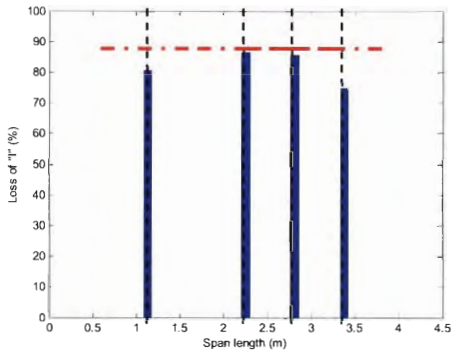
Figure 6.30 Three damage severity estimation using HMC method.



(a) 2M4S5S6S (5 modes)*.



(b) 2S4S5L6S (5 modes)*.



(c) 2S4S5S6S (5 modes)*.

* *denotes damage cases that were replicated in the experimental tests.*

Figure 6.31 Four damage severity estimation using HMC method.

6.3.2.2 Estimation of severity of damage using Modified Damage Index II

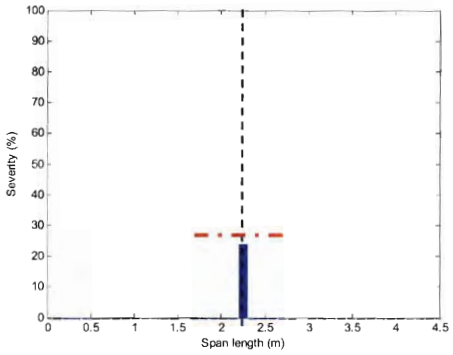
Damage cases that were used for estimating damage severity in the HMC method were adopted for estimating damage severity in the MDI-II algorithm (section 5.7 of Chapter 5). Based on the findings in sections 6.3.1.4 and 6.3.1.5, it is proposed here to use the first five flexural modes in the MDI-II method. For the results shown in the following graphs, the severity of damage below zero percent has no physical meaning, thus they were not shown. The results of the severity evaluation using the MDI-II algorithm for the four types of damage scenarios are shown in Figures 6.32 to 6.35 and the magnitude of simulated and predicted severity of damage is tabulated in Table 6.4.

Table 6.4 Estimation of severity of damage using MDI-II method.

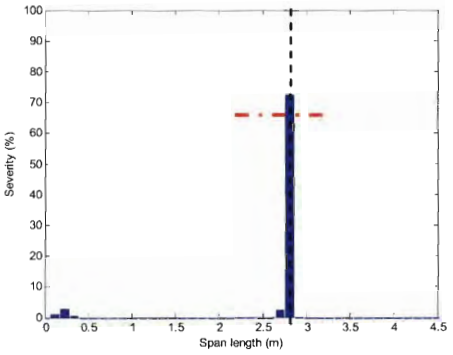
Damage Case	Location(s) per 1/8th of span length	Simulated Damage (loss of 'I') (%)	Predicted Damage using HMC method (%)
4L*	4	27.1	23.7
5M	5	65.7	72.3
6S	6	87.5	83.5
2L6L*	2, 6	All 27.1	24.0, 24.0
4L6L	4, 6	All 27.1	23.1, 24.4
4S6L*	4, 6	87.5, 27.1	84.9, 20.7
2L4L6L*	2, 4, 6	All 27.1	23.5, 22.6, 23.5
2S4S6S*	2, 4, 6	All 87.5	83.3, 79.7, 83.3
4S5L6S	4, 5, 6	87.5, 27.1, 87.5	82.5, 16.3, 87.1
2M4S5S6S*	2, 4, 5, 6	65.7, 87.5, 87.5, 87.5	45.3, 83.0, 84.3, 81.5
2S4S5L6S*	2, 4, 5, 6	87.5, 87.5, 27.1, 87.5	83.4, 80.0, 15.2, 83.0
2S4S5S6S*	2, 4, 5, 6	All 87.5	82.7, 81.5, 84.2, 76.0

* *denotes damage cases that were replicated in the experimental tests.*

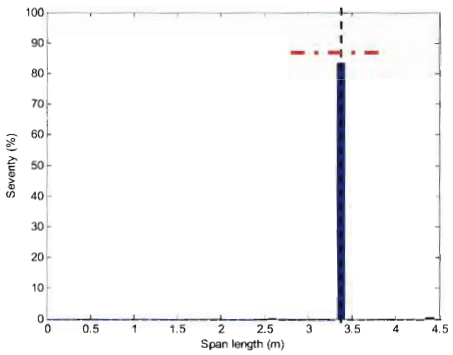
The estimation of damage severity for single damage location cases 4L, 5M and 6S are illustrated in Figures 6.32a to 6.32c, respectively. The method is capable of capturing accurately the location of damage at locations 2.25 m, 2.8125 m and 3.375 m, respectively, with some minor false positives especially near the support for case 5M (see Figure 6.32b). The predicted damage severity for the light, medium and severe damage is 23.7%, 72.3% and 83.5% loss of 'I'. Comparing to the actual inflicted damage of 27.1%, 65.7% and 87.5% loss of 'I', the error is less than 13% as presented in Table 6.4. It is possible to draw a conclusion that the HMC method performs slightly better than the MDI-II method for single damage cases because the former did not produce any false positive and the percentage of error was also lower.



(a) 4L (5 modes)*.



(b) 5M (5 modes).



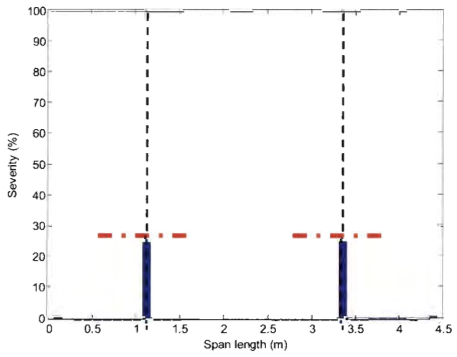
(c) 6S (5 modes).

* *denotes damage cases that were replicated in the experimental tests.*

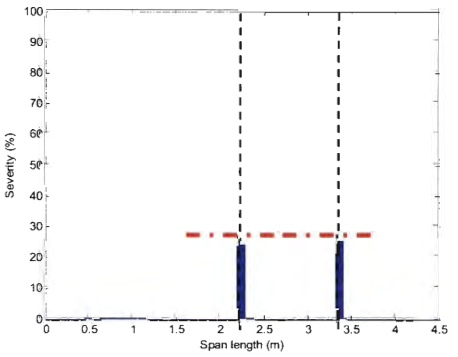
Figure 6.32 Single damage severity estimation using MDI-II method.

The two (2L6L, 4L6L and 4S6L), three (2L4L6L, 2S4S6S, 4S5L6S) and four (2M4S5S6S, 2S4S5L6S and 2S4S5S6S) damage location cases are depicted in Figures 6.33 to 6.35, respectively. Referring to these figures, all damage locations are neatly identified with no appearances of false positives (indication of spurious damage locations). For all multiple damage scenario cases discussed here, the predicted damage severity for severe damage cases is quite close to the simulated value with a maximum percentage error of not more than 13% (case 2S4S5S6S). For medium damage, the highest percentage of error is 31% (2M4S5S6S), while for the light damage the percentage of error range from 10 to 44%. For severe damage in the multiple damage scenarios, the MDI-II method performs equally well compared to the HMC method. Nevertheless, the former achieves better results in medium and light damage. It is, therefore, concluded that both HMC and MDI-II method are comparatively good to

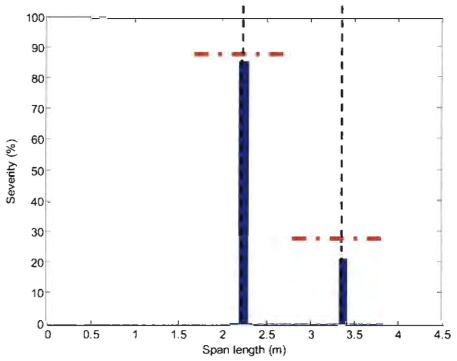
estimate severity of damage especially the severe damage, which are most important for avoidance of any catastrophic failure.



(a) 2L6L (5 modes)*.



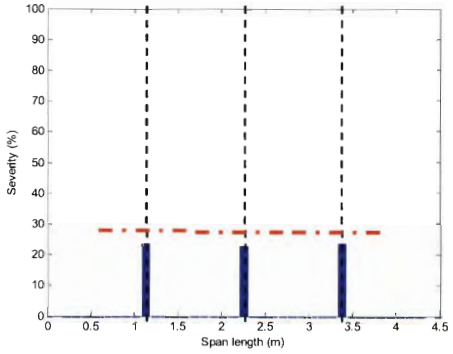
(b) 4L6L (5 modes).



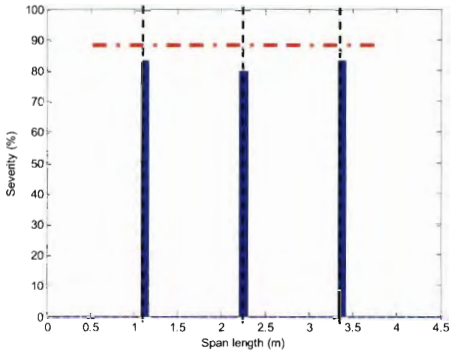
(c) 4S6L (5 modes)*.

* *denotes damage cases that were replicated in the experimental tests.*

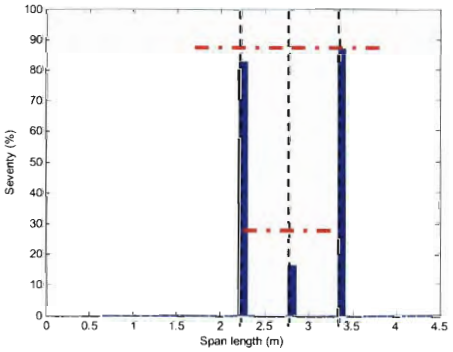
Figure 6.33 Two damage severity estimation using MDI-II method.



(a) 2L4L6L (5 modes)*.



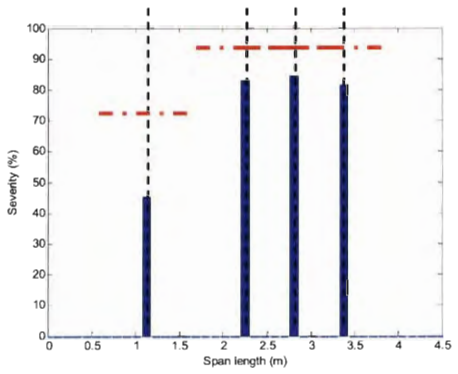
(b) 2S4S6S (5 modes)*.



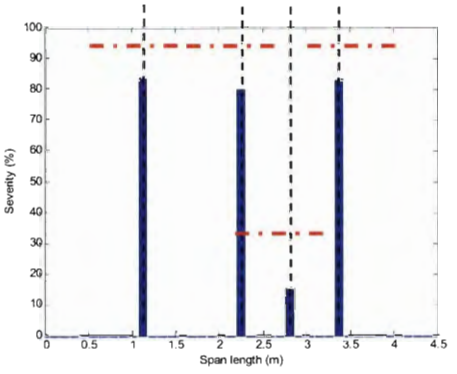
(c) 4S5L6S (5 modes)*.

* *denotes damage cases that were replicated in the experimental tests.*

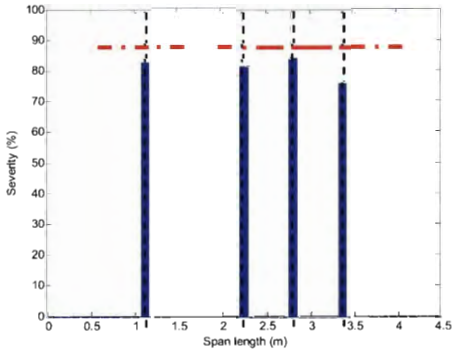
Figure 6.34 Three damage severity estimation using MDI-II method.



(a) 2M4S5S6S (5 modes)*.



(b) 2S4S5L6S (5 modes)*.



(c) 2S4S5S6S (5 modes)*.

* *denotes damage cases that were replicated in the experimental tests.*

Figure 6.35 Four damage severity estimation using MDI-II method.

6.4 Damage Detection - Timber Plate

The results and discussions of damage detection using different damage detection methods for a timber beam analytically, is followed by the investigation of damage detection for a timber bridge. A timber bridge is a complex structural system consisting of beam (girders) and plate (deck) systems. It is, therefore, advisable to at least look into a supplementary work to the scope of this study to apply the damage localisation algorithm on a timber plate-like structure analytically. Although it is rare to have plate-type timber bridges, it is of interest to explore the application of damage detection methods on a timber plate structure (orthotropic plate) developed from a finite element model. All the damage scenarios simulated in this section are similar to the experimental tests as tabulated in Table 6.5 and the details are shown in Figure 6.36. In all damage scenarios, the damage consists of square openings on the timber plate. In this

study and the subsequent discussions that follows, 'A' and 'B' denote small and large damage area, respectively. The inflicted damage for small and large damage area consist of 2% (37.5mmx37.5mm) and 6% (75mmx75mm) loss of area. The percent loss of area is calculated based on a damaged area divided by an area of 300mmx300mm (a bay of measurement grids in the experimental work). (e.g. L2(II)-BL3(IV)B-L3(V)A denotes a cumulative damage scenario of small damage at location V (1143.75mm) of Line 3, large damage at locations II (675mm) of Line 2 and IV (1725mm) of Line 3). The six mode shapes extracted from the finite element is shown in Figure 6.37.

Table 6.5 Damage scenarios for the analytical model of a timber plate.

Damage Case	Damage Scenario	Location (mm) /Line number	Length *l* (mm)	Breath *b* (mm)	% loss of Area*
Plate1	P1	Undamaged	-	-	-
1	L2(I)A	I (656.25)/L2	37.5	37.5	2
2	L2(II)B	II (675)/L2	75	75	6
3	L2(II)B-L3(III)A	II (675)/L2, III (1743.75)/L3	75, 37.5	75, 37.5	6, 2
4	L2(II)B-L3(IV)B	II (675)/L2, IV (1725)/L3	75, 75	75, 75	6, 6
5	L2(II)B-L3(IV)B-L3(V)A	II (675)/L2, IV (1725)/L3, V (1143.75)/L3	75, 75, 37.5	75, 75, 37.5	6, 6, 2
6	L2(II)B-L3(IV)B-L3(VI)B	II (675)/L2, IV (1725)/L3, VI (1125)/L3	75, 75, 75	75, 75, 75	6, 6, 6

** % loss of Area is calculated based on damaged area divided by 300mmx300mm (a bay of the measurement grids).*

Notes:

Li = Line no. i

A,B = representing small and large damage, correspond to 2% and 6% loss of area, respectively

(e.g. L2(II)B-L3(IV)B-L3(V)A denotes a cumulative damage scenario of small damage at location V (1143.75mm) of Line 3, large damage at locations II (675mm) of Line 2 and IV (1725mm) of Line 3)

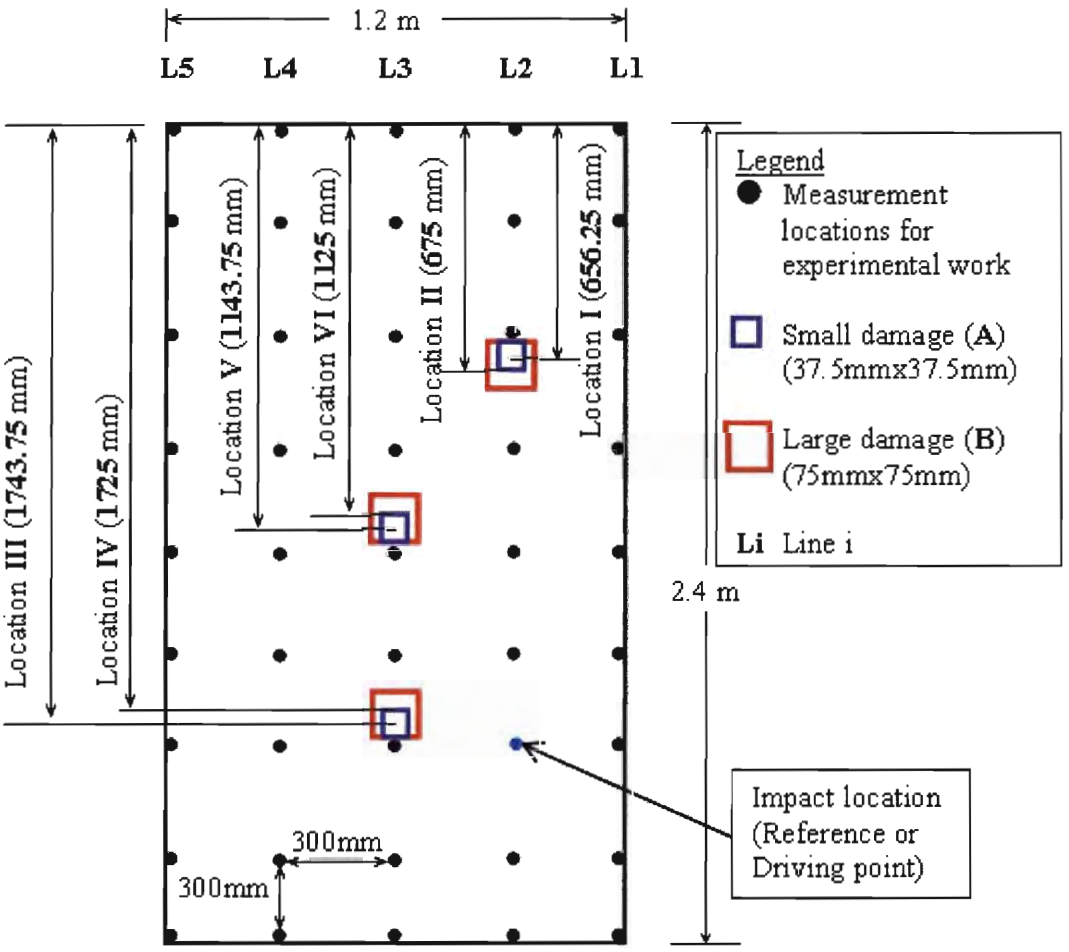


Figure 6.36 Plan view of damage locations for a timber plate.

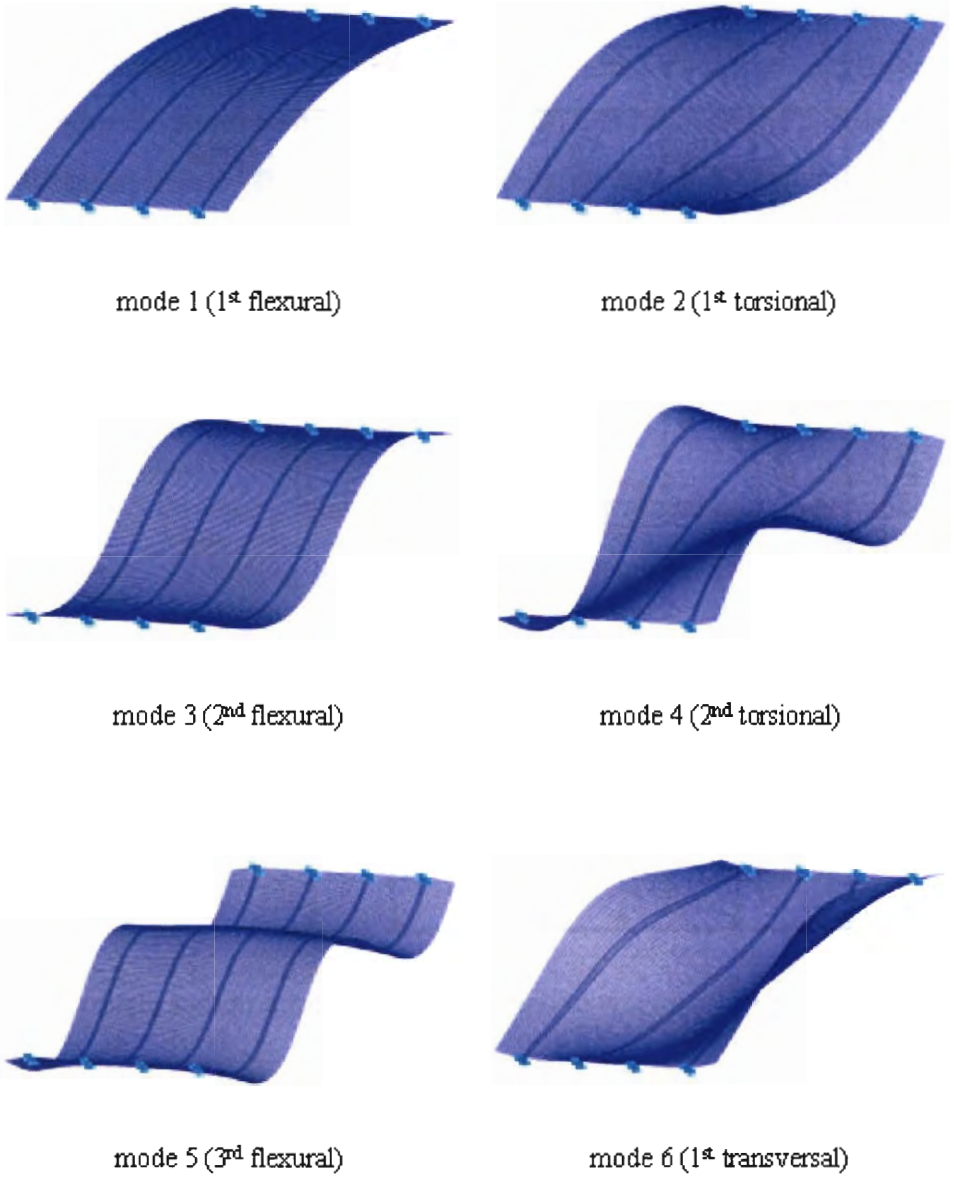


Figure 6.37 Six vibration mode shapes of the timber plate FE model.

In the analytical model of a timber plate (plywood), the natural frequencies for undamaged and damaged cases are presented in Table 6.6. From Table 6.6 and Figure 6.38, the changes of frequencies are minimal for the damaged cases compared to the undamaged case with the highest difference of less than 1.5% for mode 5 of the most serious damage case L2(II)B-L3(IV)B-L3(VI)B. The results show that the inflicted damage, even for the most serious case assigned to the plate, constituting 0.6% of area loss compared to the overall area (1.2m x 2.4m), may not be substantial enough to cause much change to the natural frequency. It is, therefore, concluded that natural frequencies may not be a good damage detection tool for small damage.

Table 6.6 Natural frequencies for analytical model of a timber plate.

Mode	Natural frequencies (Hz)						
	P1	L2(I)A	L2(II)B	L2(II)B-L3(III)A	L2(II)B-L3(IV)B	L2(II)B-L3(IV)B-L3(V)A	L2(II)B-L3(IV)B-L3(VI)B
1	5.62	5.62	5.61	5.60	5.59	5.59	5.57
2	8.78	8.77	8.76	8.76	8.76	8.76	8.76
3	22.14	22.12	22.05	22.03	21.96	21.96	21.96
4	25.89	25.88	25.83	25.83	25.83	25.82	25.81
5	37.26	37.25	37.20	37.16	37.00	36.93	36.69
6	48.39	48.38	48.36	48.35	48.32	48.27	48.11

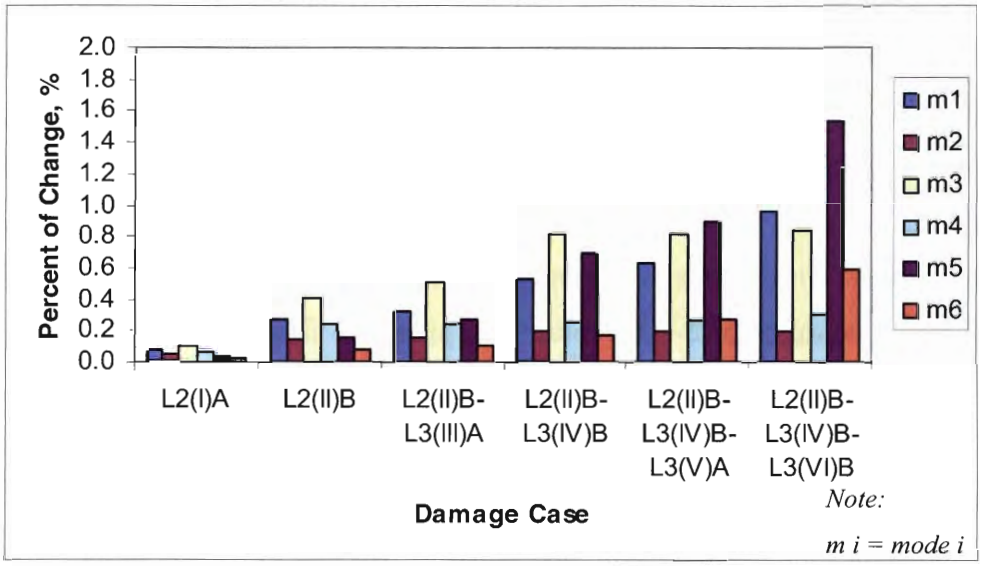


Figure 6.38 Comparison of natural frequencies for finite element model of a timber plate.

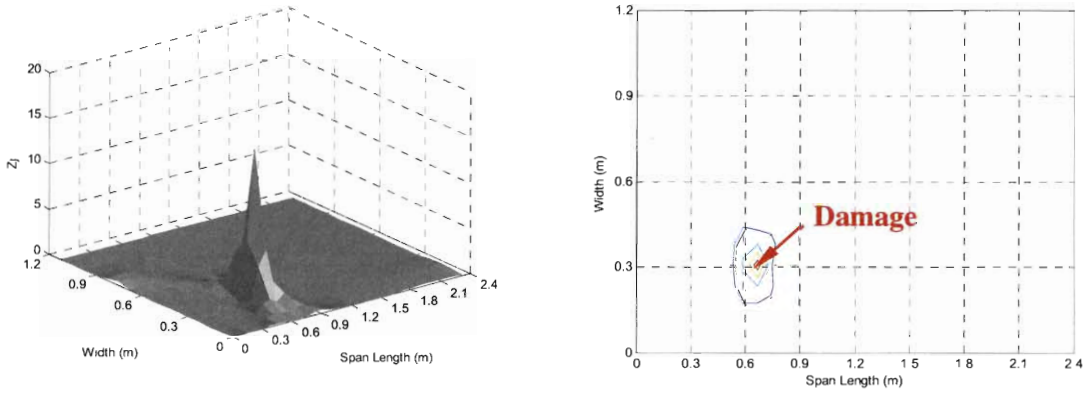
For damage localisation in plate-like timber structures, an extension of the damage index II (DI-II) method proposed by Stubbs et al. (1995), and used by Cornwell, Doebling and Farrar (1999), is adopted to detect damage locations. This extended method is named damage index II for plate-like structures in this study and can be abbreviated as DI-II-P (details can be found in Chapter 5). The original formulation by Stubbs et al. (1995) is intrinsically limited to one-dimensional structures, characterised by one-dimensional (1-D) mode shape and curvatures. Due to the nature of the DI-II method that utilises one-dimensional modal strain energy derived from a beam-like structure, it can be applied to structures that behave globally in a beam-like manner or can be decomposed into beam elements. As mentioned by Cornwell, Doebling and Farrar (1999), the 1-D strain energy method has been successfully applied

to two-dimensional (2-D) and three-dimensional (3-D) structures, but only by decomposing them into beam-like elements. However, the authors did not expect the beam-like algorithm, with slicing mode, applied to plate-like structures to perform well in detecting damage as it does not preserve the torsional stiffness between slices. Based on this observation, in this study the damage index II for plate-like structures (DI-II-P) method was adopted to locate damage for analytical models of a timber plate and a laboratory timber bridge discussed in this chapter. To the best knowledge of the author, the DI-II-P method has not been used for damage localisation for plate-like timber structures. It should be noted that slicing mode of DI-I method (using one-dimensional mode shape curvatures) has been applied to a laboratory timber bridge (Peterson, McLean & Pollock 2003). The author would like to highlight here that normalisation of mode shape curvatures (working well for damage index methods for beam-like structures in this study) was not incorporated in the DI-II-P method as it encounters some difficulties with respect to normalising two-dimensional (2-D) curvatures and slope. The normalisation of 2-D curvatures for plate-like structures is planned as part of the future work.

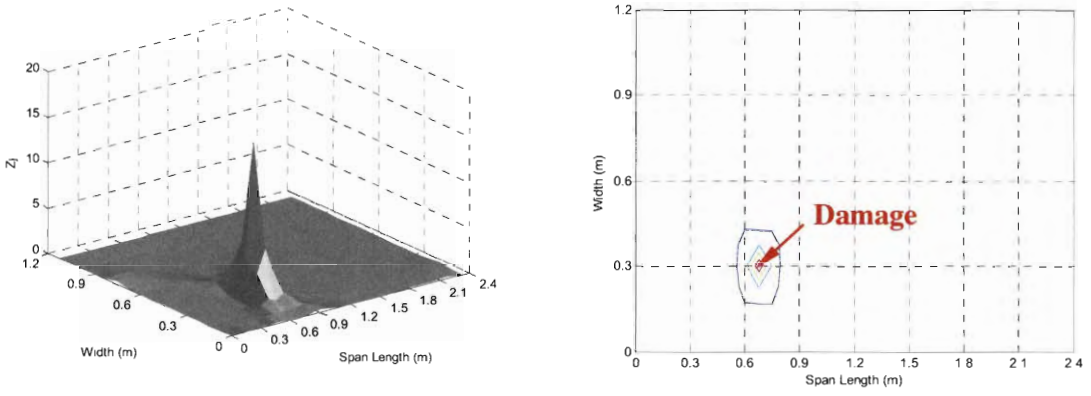
In the following results, all damage indicator indices, Zj, for each of the damage cases are plotted against the plate span length (2.4 m) and width (1.2 m). The damage indicator indices larger than and equal to two ($Zj \geq 2$) for the timber plate was adopted providing an approximately 95% level of confidence in indicating the actual damage locations (Park & Stubbs 1995; Peterson et al. 2001a). To indicate the damage site in the graphs, the actual damage locations are marked with a red colour arrow sign and the word 'Damage' in all the following figures. For damage localisation of the timber plate, two types of graphs were used in this investigation, that is, surface and contour plots. The surface plot provides an overview of the distribution of the damage indicators above zero ($Zj > 0$), while the contour plots give information on predicted damage locations with $Zj \geq 2$. Damage localisation for the analytical model of a timber plate was demonstrated using the damage index II for plate-like structures (DI-II-P) using the first six vibration modes that were able to be captured in the experimental tests.

Single damage cases L2(I)A (small damage area of 37.5 mm x 37.5 mm) and L2(II)B (large damage area of 75 mm x 75 mm) where one of the damage area edges is offset by 37.5 mm from 0.6 m mark along the span length, are depicted in Figure 6.39. For case L2(I)A as shown in the contour plots of Figure 6.39 a, the damage location at

position (0.656m, 0.3m) (use as a convention in discussions that follows representing 0.656m along the span length and 0.3m across the width) was identified. Likewise, the damage at position (0.675m, 0.3m) for case L2(II)B as shown in Figure 6.39 b is also located. In general, the DI-II-P method used for the timber plate is able to identify all damage (2% and 6% loss of area for small and large damage, respectively, of a bay area of 300mm x 300mm).



(a) L2(I)A (6 modes).

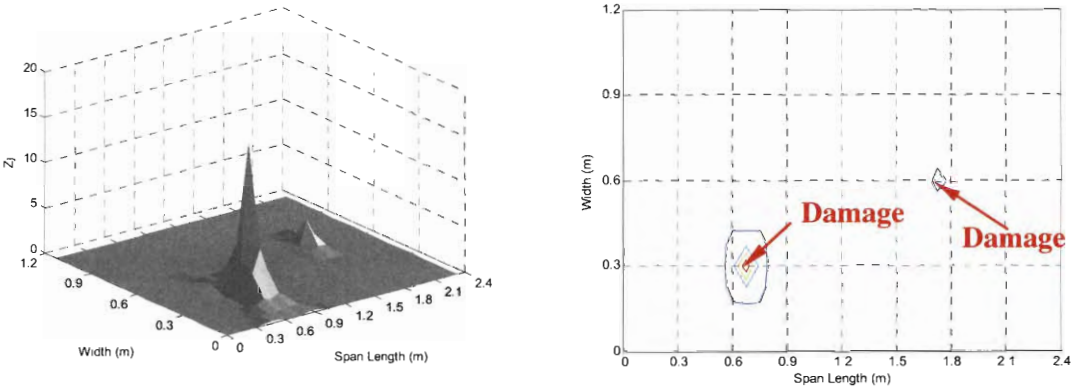


(b) L2(II)B (6 modes).

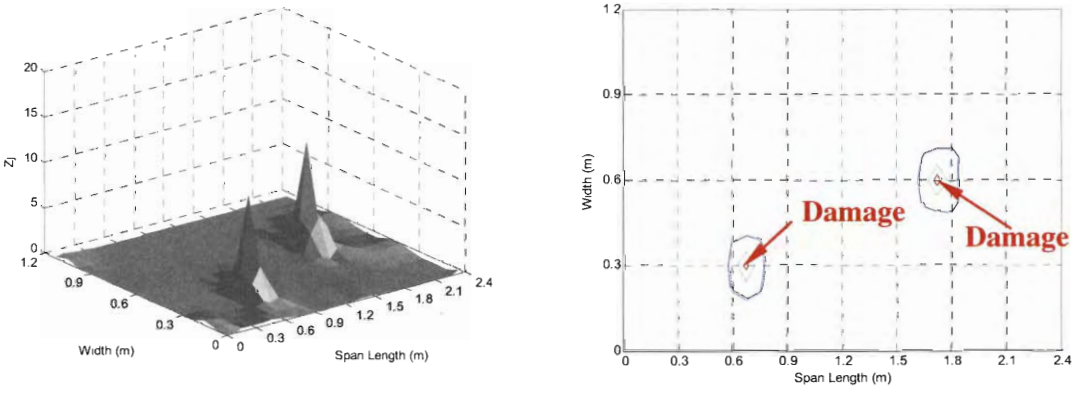
Figure 6.39 Single damage cases using DI-II-P method for plate.

For two damage case L2(II)B-L3(III)A as shown in the contour plots of Figure 6.40a, the large damage at position (0.675m, 0.3m) was identified but the small damage at position (1.743m, 0.6m) was not clearly indicated. While for case L2(II)B-L3(IV)B (see Figure 6.40b), both large damage scenarios at positions (0.675m, 0.3m) and (1.725m, 0.6m) are clearly located. The three damage cases are illustrated in Figures

6.41a and 6.41b, for cases L2(II)B-L3(IV)B-L3(V)A and L2(II)B-L3(IV)B-L3(VI)B, respectively. All damage locations are identified except the small damage (2% loss of area with respect to a bay area of 300mm x 300mm) at position (1.143m, 0.6m) as shown in the contour plot of Figure 6.41a. The DI-II-P method works well for the analytical model of a timber plate using higher modes (six modes).

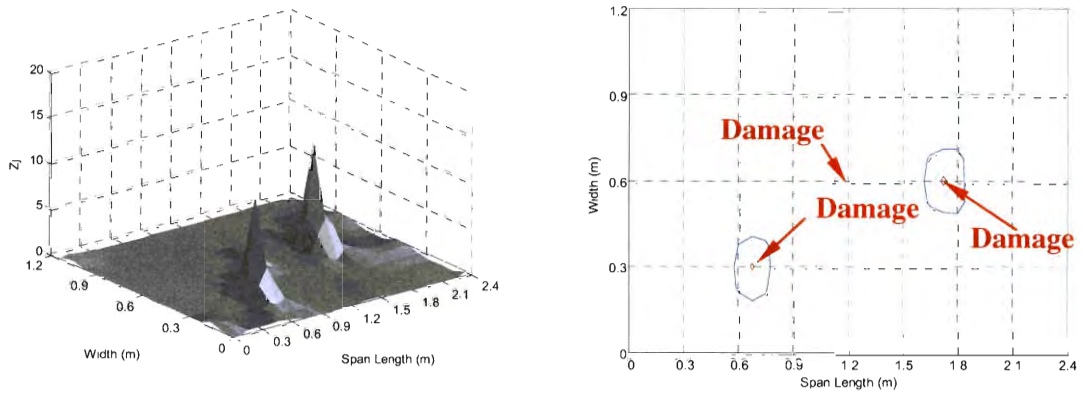


(a) L2(II)B-L3(III)A (6 modes).

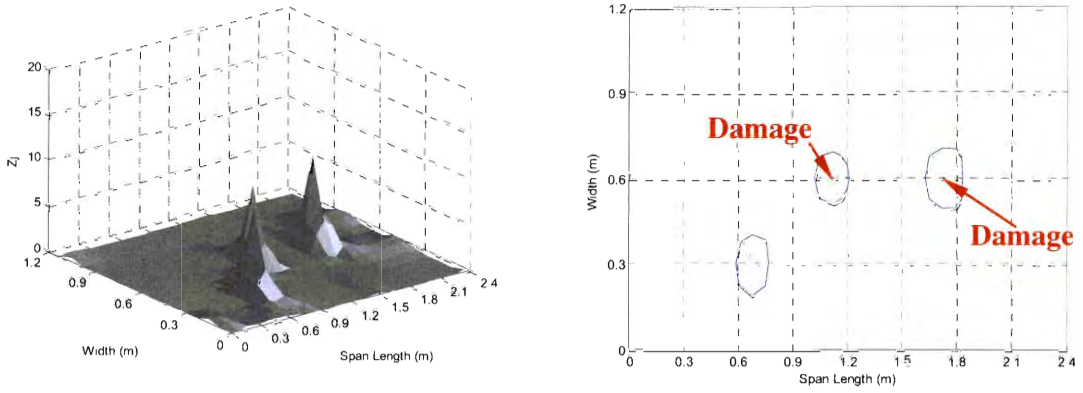


(b) L2(II)B-L3(IV)B (6 modes).

Figure 6.40 Two damage cases using DI-II-P method for plate.



(a) L2(II)B-L3(IV)B-L3(V)A (6 modes).



(b) L2(II)B-L3(IV)B-L3(VI)B (6 modes).

Figure 6.41 Three damage cases using DI-II-P method for plate.

6.5 Damage Detection - Laboratory Timber Bridge

The analytical model for a laboratory timber bridge was developed using a finite element analysis program. In this study, the model was updated with measured modal data. This model updating work was done only to verify that the model was accurate enough to predict the dynamic response of the structure. Model updating damage identification methods, which required correlated finite element models, were not included in the scope of this study. The details of the model updating can be found in Chapter 4.

For damage detection, natural frequency can be used as a tool to indicate changes in a dynamic system before and after modifications occurring in the system. This means if a shift in natural frequency occurs in a system, it can be inferred that the system has undergone changes. From the bridge analytical model, the changes are related to inflicted loss of section in timber girders that represent rot in wood. The damage inflicted in the model is that of single and multiple damage scenarios, which correspond to the damage scenarios in experimental tests (Chapter 8). The damage scenarios are featured in Table 6.7 and Figure 6.42, and its details can also be found in section 4.6.2 of Chapter 4. The 'L', 'M' and 'S' damage denote levels of damage severity for each damage location, that is, 'light', 'medium' and 'severe' corresponding to 27.1%, 65.7% and 87.5% loss of 'I' (moment of inertia) (e.g. g2Sg4Sg3M denotes a cumulative damage scenario of medium (M) damage on ¼ span (1.125m) of girder 3, severe damage (S) on ¾ span (3.375m) of girder 2 and ½ span (2.25m) of girder 4). The nine mode shapes extracted from the FE model is shown in Figure 6.43.

Table 6.7 Damage scenarios for the analytical model of a laboratory timber bridge.

Damage Case	Damage Scenario	Location per 8th of span length/Girder number	Length *l* (mm)	Depth *h* (mm)	% loss of 'I'
Deck 2	D2	Undamaged	-	-	-
1	g2L	6/g2 (3.375m)	45	9	27.1
2	g2M	6/g2	45	27	65.7
3	g2S	6/g2	45	45	87.5
4	g2Sg4L	6/g2, 4/g4 (3.375, 2.25m)	45	45, 9	87.5, 27.1
5	g2Sg4M	6/g2, 4/g4	45	45, 27	87.5, 65.7
6	g2Sg4S	6/g2, 4/g4	45	All 45	All 87.5
7	g2Sg4Sg3L	6/g2, 4/g4,2/g3 (3.375, 2.25, 1.125m)	45	45, 45, 9	87.5, 87.5, 27.1
8	g2Sg4Sg3M	6/g2, 4/g4, 2/g3	45	45, 45, 27	87.5, 87.5, 65.7
9	g2Sg4Sg3S	6/g2, 4/g4, 2/g3	45	All 45	All 87.5
10	g2Sg4Sg3Sg1L	6/g2, 4/g4, 2/g3, 1/g1 (3.375, 2.25, 1.125, 0.625m)	45	45, 45, 45, 9	87.5, 87.5, 87.5, 27.1
11	g2Sg4Sg3Sg1M	6/g2, 4/g4, 2/g3, 1/g1	45	45, 45, 45, 27	87.5, 87.5, 87.5, 65.7
12	g2Sg4Sg3Sg1S	6/g2, 4/g4, 2/g3, 1/g1	45	All 45	All 87.5

Notes:

gi = girder No. i

L, M, S representing light, medium and severe damage, correspond to 27.1, 65.7 and 87.5% loss of 'I'

(e.g. g2Sg4Sg3M denotes a cumulative damage scenario of medium damage on ¼ span (1.125m) of girder 3, severe damage on ¾ span (3.375m) of girder 2 and ½ span (2.25m) of girder 4)

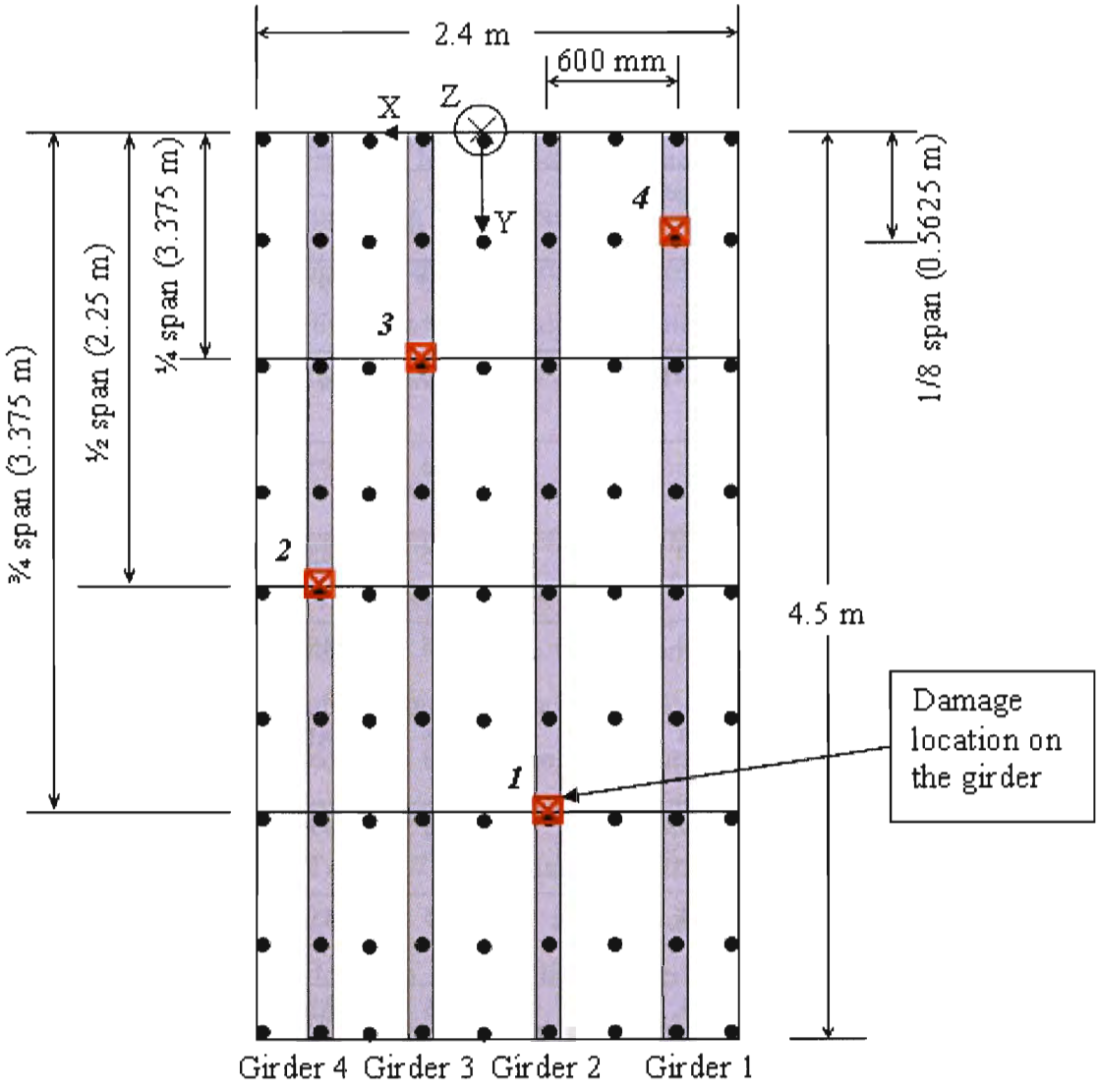


Figure 6.42 Plan view of damage locations on the bridge model.

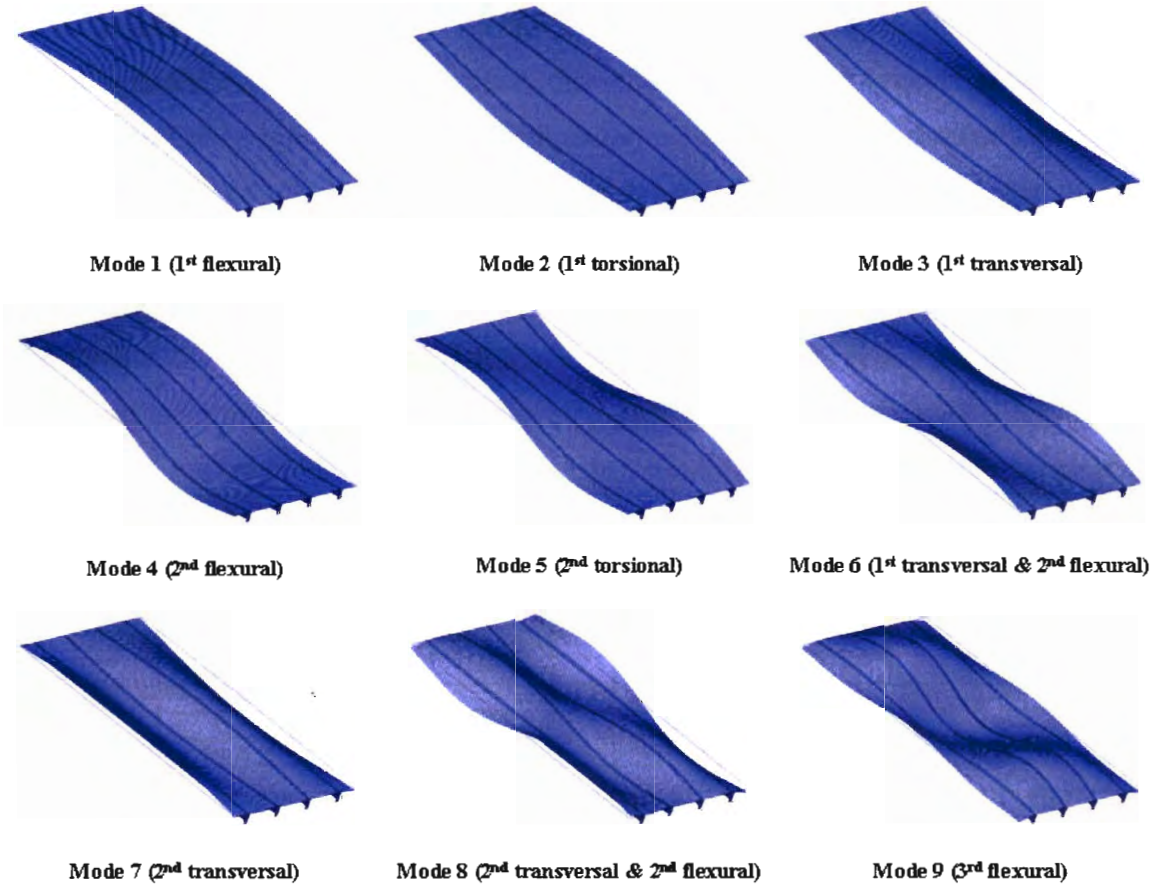


Figure 6.43 Nine vibration mode shape of the laboratory timber bridge FE model.

The values of natural frequencies for the first nine modes obtained from modal analysis of the undamaged and damaged state of the laboratory timber bridge are listed in Table 6.8. According to Table 6.8 and Figure 6.44, there is a general change of natural frequencies for the bridge analytical model as the severity of damage increases. The change in natural frequency for the bridge analytical model is obviously higher for more severe damage cases such as case g1S (the most severe damage case) with 5% changes compared to the undamaged state for mode 4 (the second flexural mode). It is noticed that mode 7 (the second transversal mode) practically did not exhibit any change in the natural frequency for all damage cases. This may be attributed to the nature of second transversal mode (mode 7), which is governed mainly by the deck stiffness rather than the girders (in which all damage was inflicted). Thus the damage did not affect mode 7 much.

In general, it is apparent that as more damage is inflicted in the girders of the bridge, it reduces the flexural capacity and causing higher reduction in natural frequencies. It should also be noted that for some severe damage the changes in

frequencies are minimal as exampled by case g2S. It is inferred that natural frequency can be used to identify the existence and assess qualitatively the extent of damage in the laboratory timber bridge. However, more care is required when change of frequency is used to detect damage in real structures because it was found that changes of 5% in frequency may be caused by changes in environmental conditions and not from the damage (Aktan et al. 1994; Creed 1987).

Table 6.8 Natural frequencies for the analytical model of a laboratory timber bridge.

Mode	Natural frequencies (Hz)						
	Un	g2L	g2M	g2S	g2Sg4L	g2Sg4M	g2Sg4S
1	8.94	8.94	8.93	8.92	8.92	8.89	8.80
2	9.64	9.64	9.64	9.64	9.63	9.58	9.48
3	17.88	17.87	17.87	17.86	17.86	17.85	17.83
4	23.90	23.87	23.73	23.39	23.39	23.39	23.39
5	24.87	24.87	24.86	24.85	24.85	24.85	24.85
6	29.89	29.87	29.74	29.48	29.48	29.48	29.47
7	40.04	40.04	40.04	40.04	40.04	40.04	40.04
8	47.13	47.12	47.01	46.77	46.77	46.77	46.62
9	53.72	53.68	53.47	53.09	53.08	53.05	53.01

Mode	Natural frequencies (Hz)						
	Un	g2Sg4Sg3L	g2Sg4Sg3M	g2Sg4Sg3S	g2Sg4Sg3Sg1L	g2Sg4Sg3Sg1M	g2Sg4Sg3Sg1S
1	8.94	8.80	8.79	8.78	8.78	8.78	8.78
2	9.64	9.48	9.48	9.48	9.48	9.48	9.47
3	17.88	17.83	17.82	17.82	17.82	17.81	17.80
4	23.90	23.37	23.26	22.97	22.95	22.86	22.60
5	24.87	24.84	24.79	24.69	24.68	24.59	24.43
6	29.89	29.45	29.36	29.16	29.15	29.12	29.06
7	40.04	40.04	40.04	40.04	40.04	40.03	40.02
8	47.13	46.62	46.60	46.33	46.33	46.33	46.32
9	53.72	52.97	52.78	52.44	52.44	52.43	52.40

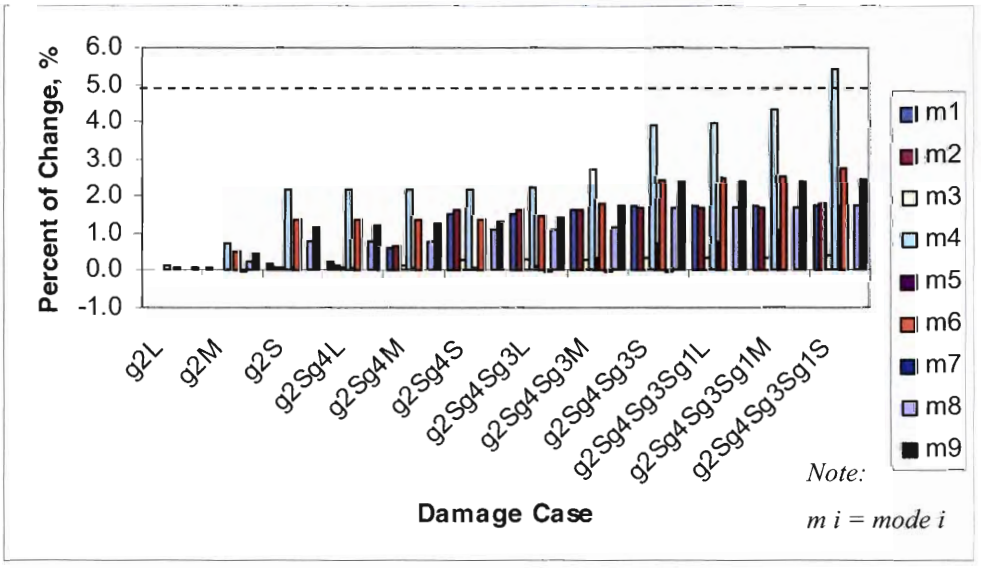


Figure 6.44 Comparison of natural frequencies for the finite element model of the laboratory timber bridge.

6.5.1 Damage Localisation

For damage localisation using the DI-II-P method, an analytical model of a laboratory timber bridge was developed using a finite element model (details can be found in Chapter 4). As the number of modes, to be experimentally, captured are limited to nine, hence the first three and first nine modes were used for comparison in the damage index algorithm for plate-like structures (DI-II-P). The formulation details for the DI-II-P algorithm used in the following discussions were presented in Chapter 5. The first three modes are used as these modes are easily acquired for a real timber bridge and the combination of modes is also commonly used (Peterson, McLean & Pollock 2003). However, the first three modes may not be sufficient to identify all damage locations. Hence it is suggested to adopt all the acquired modes (9 modes) in the damage localisation algorithm (Cornwell, Doebling & Farrar 1999). In addition, with the latest developments in sensor technologies, it is possible nowadays to obtain higher modes of a structural system. This would definitely help to promote the use of higher modes in damage detection. The analytical model is subjected to single and multiple damage scenarios, which correspond to the damage scenarios in experimental tests, simulating rot, a common defect for timber. The damage scenarios are listed in Table 6.7 and are shown in Figure 6.42.

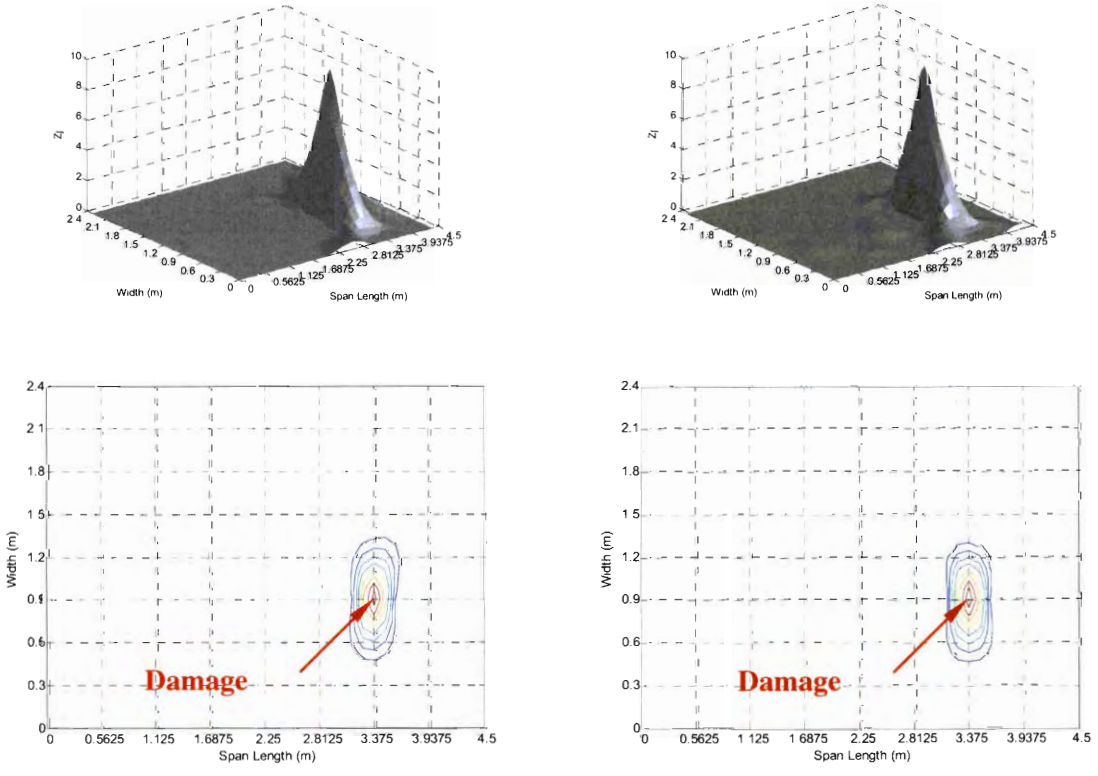
In all following figures, the damage index Zj for each of the damage cases is plotted against the laboratory timber bridge span length (4.5m) and width (2.4m). In principle, the statistical normalised damage index value greater than or equal to two represents the likely location of damage (the probability-based criterion for damage). The localisation of damage using the criterion of $Zj \geq 2$ was adopted as it would provide an approximately 95% level of confidence indicating the actual damage locations (Park & Stubbs 1995; Peterson et al. 2001a). The level of Zj for plate-like timber structures is set slightly higher than the timber beams because plate-like structures such as a deck-girder timber bridge is a far more complicated system compared to a simple beam system, and more likely to produce errors in the damage detection process.

To show the damage site in the graphs (contour plots), the actual damage locations are marked with a red colour arrow sign and the word 'Damage' in all the following figures. For damage localisation of the laboratory timber bridge, two types of graphs were used in this study, that is, surface and contour plots. The surface plot provides an overview of the distribution of the damage indicator above zero ($Zj>0$),

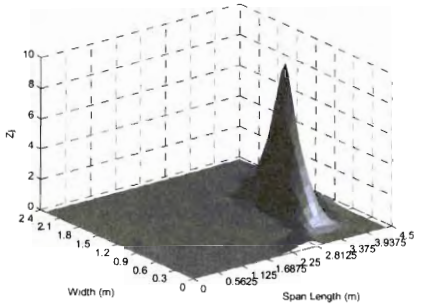
while the contour plot gives information on predicted damage locations with $Zj \geq 2$. The damage index value Zj lower than zero has no physical meaning and hence not plotted.

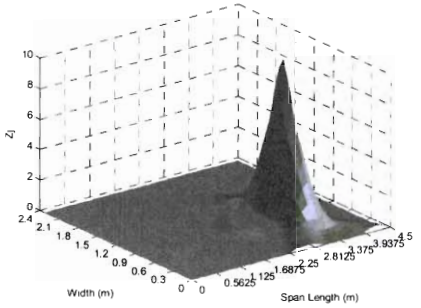
6.5.1.1 Discussions on Damage Index II Method for Plate-like Structures

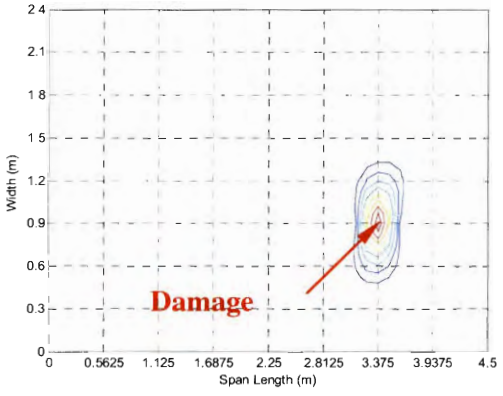
The single damage cases applied in the damage index II algorithm for plate-like structures (DI-II-P) computed using the first three and first nine modes are illustrated in Figure 6.45. It is clear from the surface plots of Figure 6.45 that the DI-II-P algorithm using either the first three or the first nine modes successfully locates the single damage at position (3.375m, 0.9m) (use as a convention for location of damage in all discussions that follows, representing 3.375m along the span length and 0.9m across the width) for damage cases g2L, g2M and g2S corresponding to light (27.1% loss of 'I' in the girders), medium (65.7% loss of 'I') and severe (87.5% loss of 'I') damage, respectively.



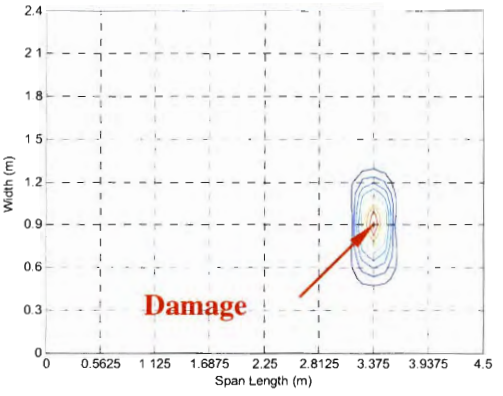
(a) g2L (3 modes). (b) g2L (9 modes).



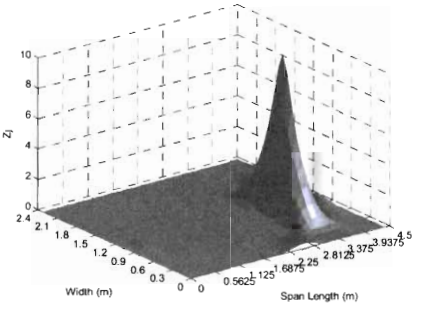


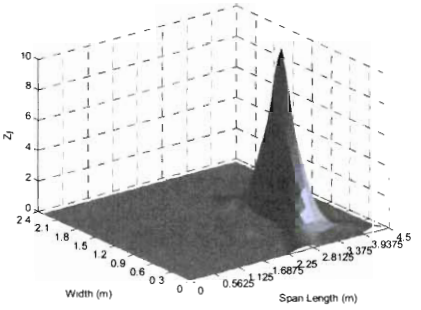


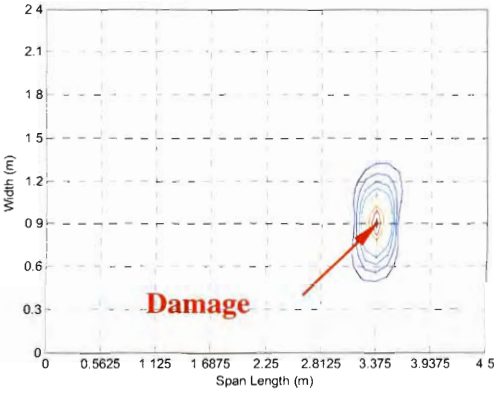
(c) g2M (3 modes).



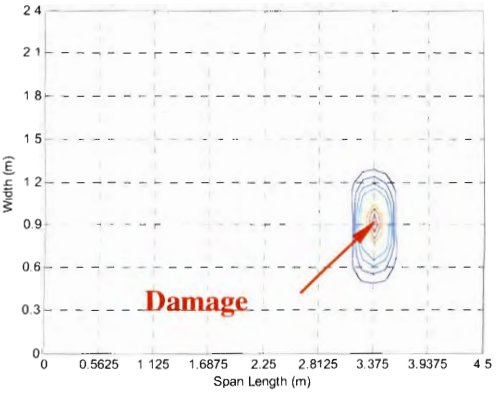
(d) g2M (9 modes).







(e) g2S (3 modes).

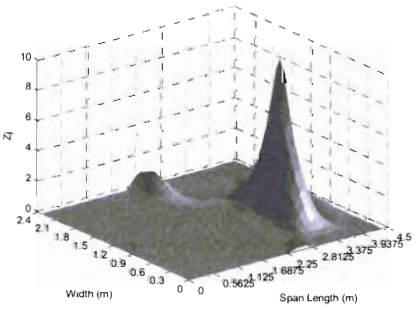


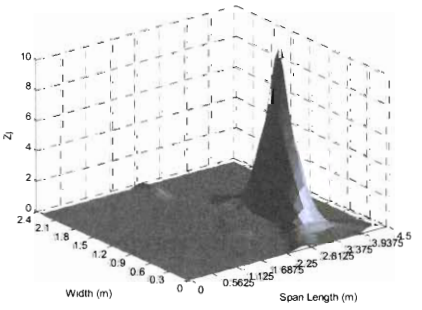
(f) g2S (9 modes).

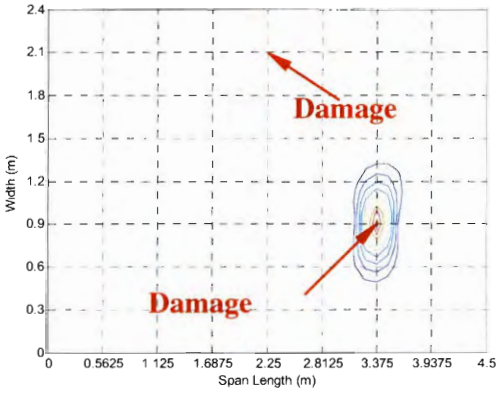
Figure 6.45 Single damage cases using DI-II-P method for bridge.

In Figure 6.46, the two damage cases applied to the DI-II-P algorithm are shown. From the contour plot results when using the first three modes (see Figures 6.46a, 6.46c and 6.46e) and the first nine modes (see Figures 6.46b, 6.46d and 6.46f), all severe damage locations at position (3.375m, 0.9m) were identified for damage cases g2Sg4L and g2Sg4M, except case g2Sg4S. While for case g2Sg4S, the severe damage at position (2.25m, 2.1m) was captured using both combinations of modes. However, the light damage at position (2.25m, 2.1m) were not identified for case g2Sg4L as depicted in the contour plots of Figures 6.46a (3 modes) and 6.46b (9 modes). This may be due to the change in mode shape curvature caused by the severe damage overwhelmingly dominating the calculation of Z_j. It should be noted that the second damage was prevailed for medium damage because this damage was approaching comparable severity to the first severe damage, which would provide sufficient changes in mode shape curvature.

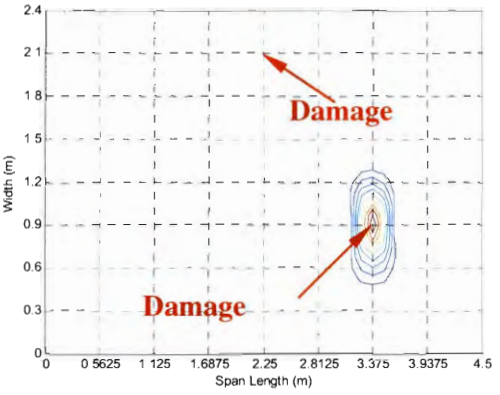
Comparing the surface plots of Figures 6.46e and 6.46f for damage case g2Sg4M with 3 and 9 modes, respectively, it was found that the damage indicator in the former plot (3 modes) has provided a misleading representation of the probability of existence of medium damage at position (2.25m, 2.1m) and has a large index value (higher probability to be identified as a damage location) that is comparable to the severe damage. On the other hand, the latter figure shows that both medium and severe damage locations pose a relatively different damage index value, which reflects better the simulated damage scenarios. For the two damage cases, using the first nine modes in the damage localisation algorithm for plate-like structures offers a better damage indication compared to just using the first three modes. This may indicate that the method could have some problems identifying two damage locations, if using only the lower modes (3 modes).



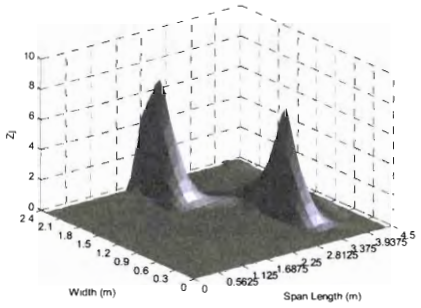


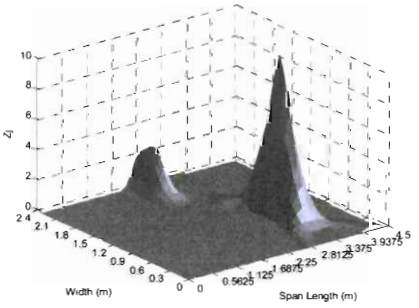


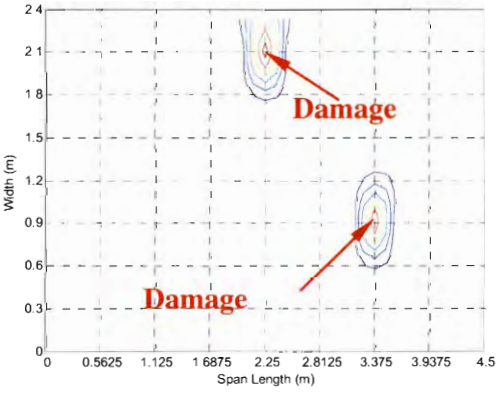
(a) g2Sg4L (3 modes).



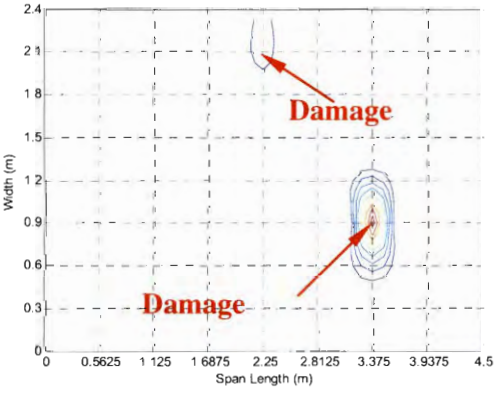
(b) g2Sg4L (9 modes).



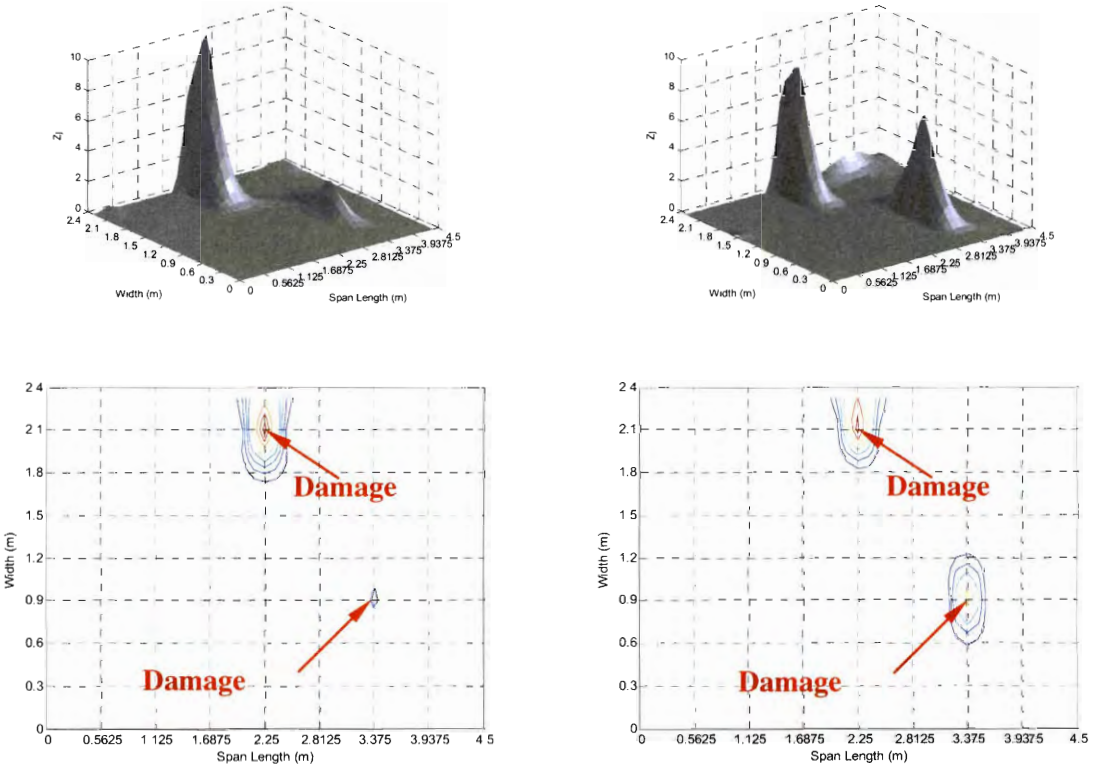




(c) g2Sg4M (3 modes).



(d) g2Sg4M (9 modes).

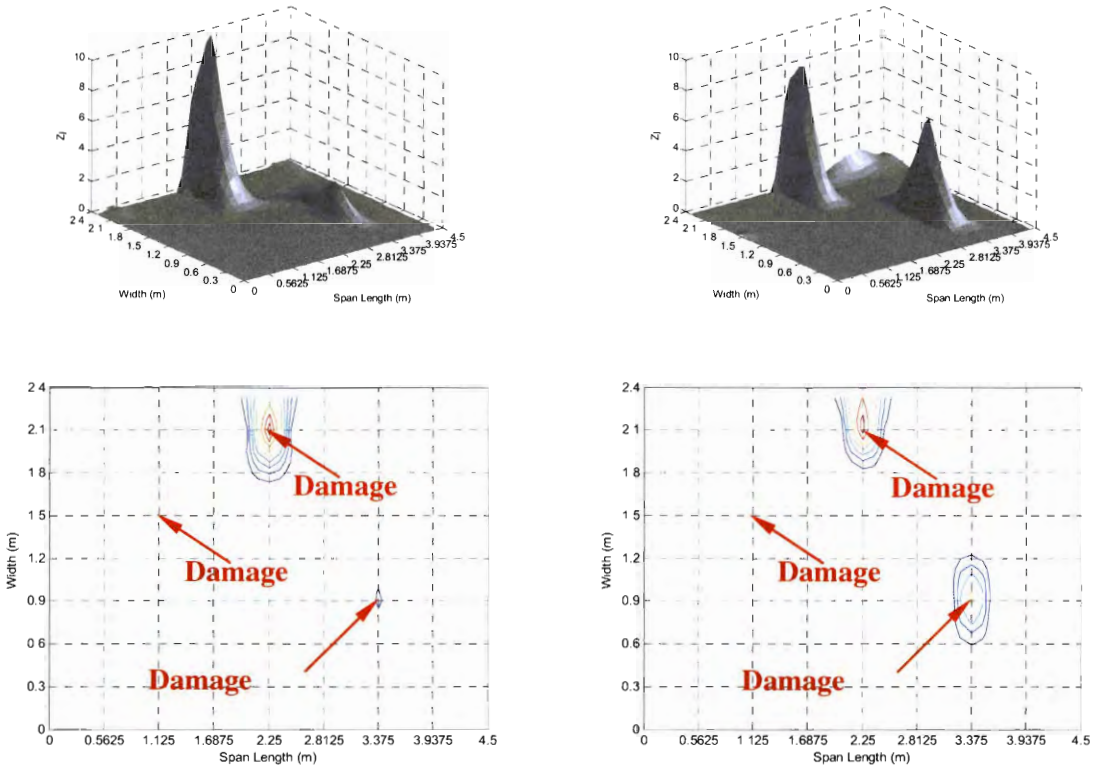


(e) g2Sg4S (3 modes). (f) g2Sg4S (9 modes).

Figure 6.46 Two damage cases using DI-II-P method for bridge.

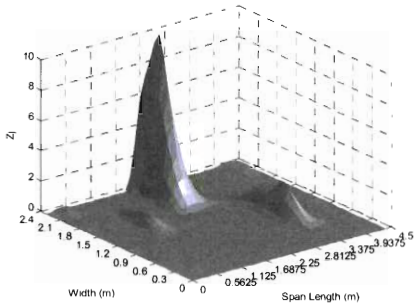
For three damage location cases, the results of the damage indicator using the DI-II-P algorithm are shown in Figure 6.47. By using either the first three or the first nine modes in the damage index method for damage cases g2Sg4Sg3L (Figures 6.47a (3 modes) and 6.47b (9 modes)) and g2Sg4Sg3M (Figures 6.47c (3 modes) and 6.47d (9 modes)), the contour plots show that the light and medium damage at position (1.125m, 1.5m) were not identified. In addition, using the first three modes in the localisation algorithm failed to capture the severe damage at position (3.375m, 0.9m) for similar damage cases. Referring to damage case g2Sg4Sg3S, as illustrated in Figure 6.47e, using the first three modes in the DI-II-P algorithm could not detect the severe damage at positions (3.375m, 0.9m) and (1.125m, 1.5m). While for the same case using nine modes, as illustrated in the contour plot of Figure 6.47f, all severe damage locations were identified. It should be noted also that for case g2Sg4Sg3S, the damage index values for the three severe damage locations, calculated with nine modes (see surface plot of Figure 6.47f), are quite similar and agreed well with the actual damage condition. This reinforces the findings in the cases of two damage locations where the

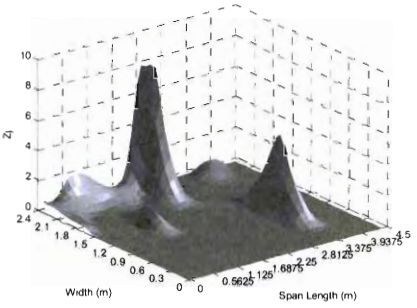
higher modes contribute more significantly to damage detection using the DI-II-P method.

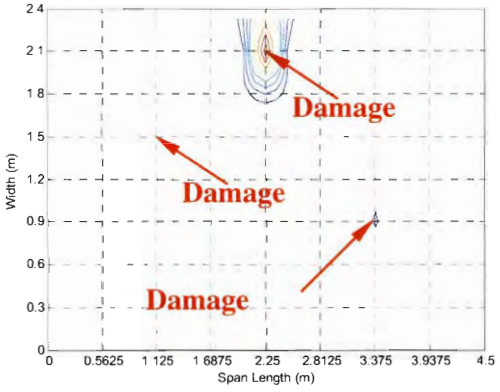


(a) g2Sg4Sg3L (3 modes).

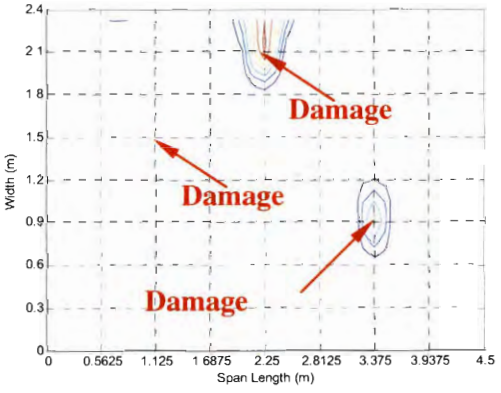
(b) g2Sg4Sg3L (9 modes).



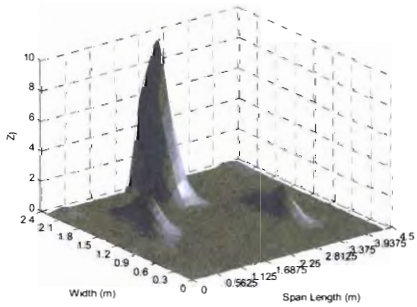


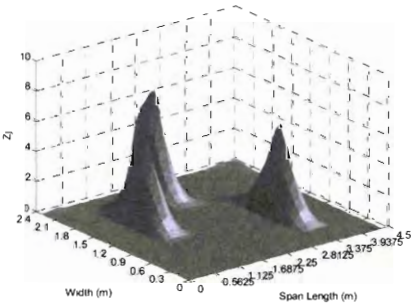


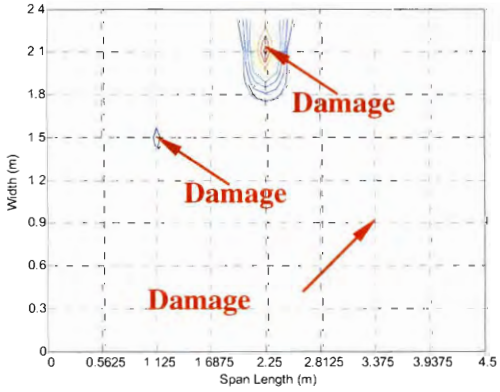
(c) g2Sg4Sg3M (3 modes).



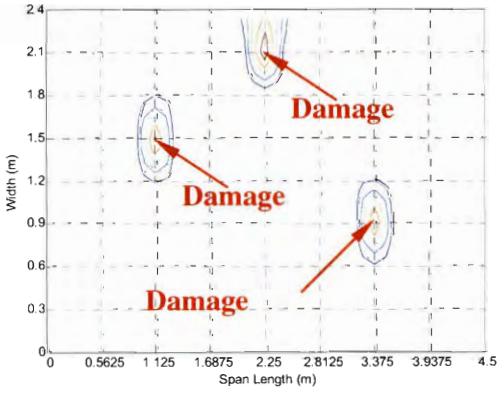
(d) g2Sg4Sg3M (9 modes).







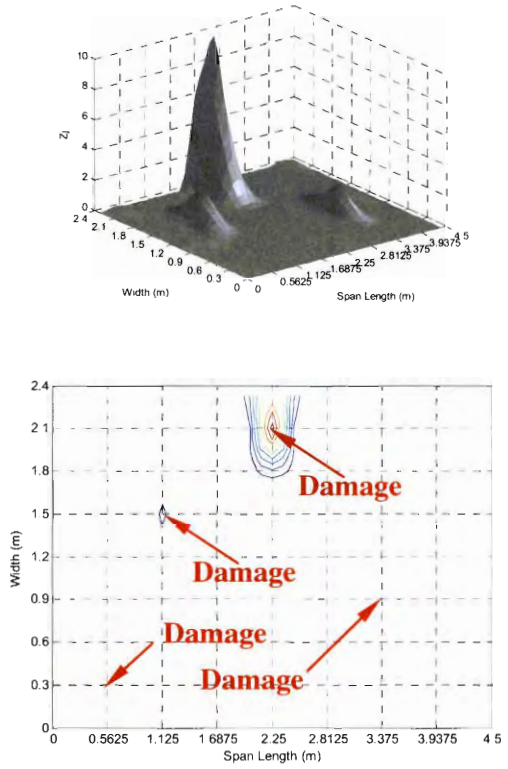
(e) g2Sg4Sg3S (3 modes).



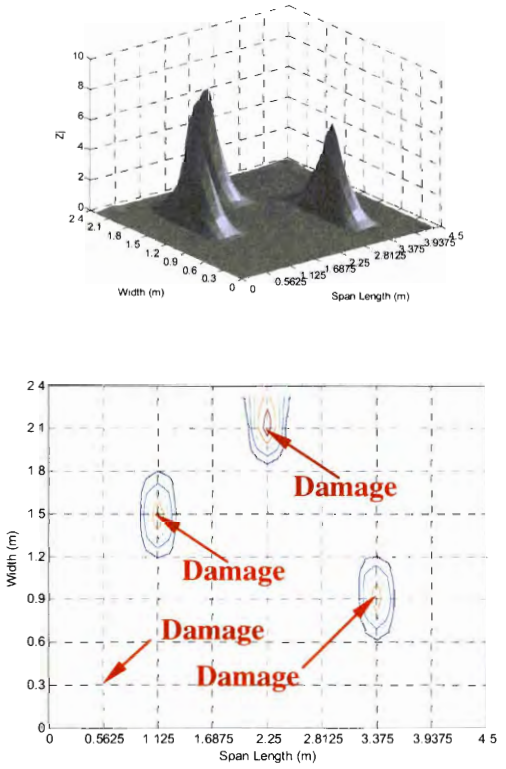
(f) g2Sg4Sg3S (9 modes).

Figure 6.47 Three damage cases using DI-II-P method for bridge.

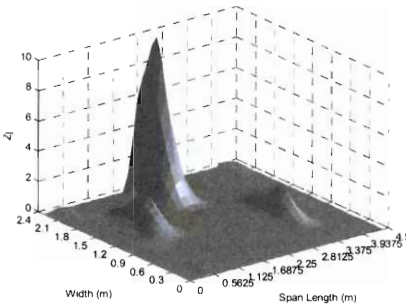
The results of four damage location scenarios applying the first three and the first nine modes in the DI-II-P algorithm are illustrated in Figure 6.48. For cases g2Sg4Sg3Sg1L, g2Sg4Sg3Sg1M and g2Sg4Sg3Sg1S, the damage locations were not all captured by the damage indicator using the first three modes as shown in Figures 6.48a 6.48c and 6.48e. Instead only the severe damage at position (2.25 m, 2.1 m) was located. When calculated with the nine modes, all severe damage locations were identified but the light and medium damage locations were missed (as illustrated in Figures 6.48b and 6.48d). This reaffirms the findings above that the DI-II-P algorithm using the first nine modes provides a better damage indicator than using the first three modes and it also gives a more realistic reflection of the damage situation particularly for the severe damage.

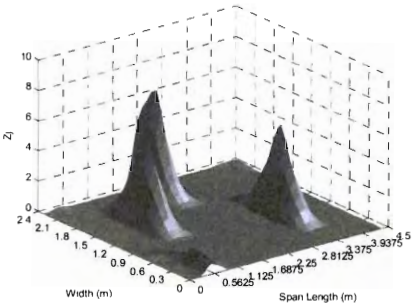


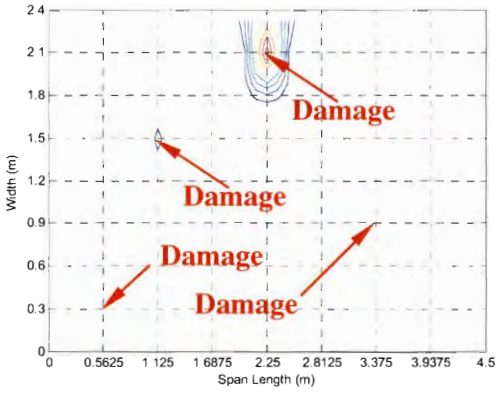
(a) g2Sg4Sg3Sg1L (3 modes).



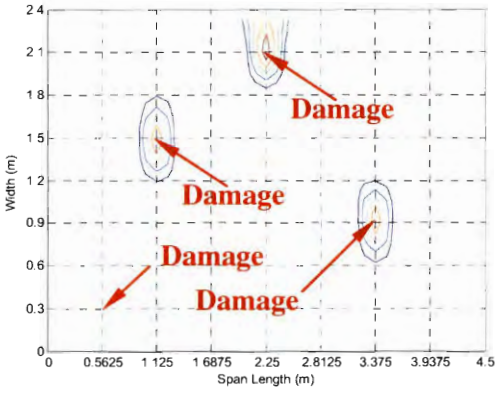
(b) g2Sg4Sg3Sg1L (9 modes).



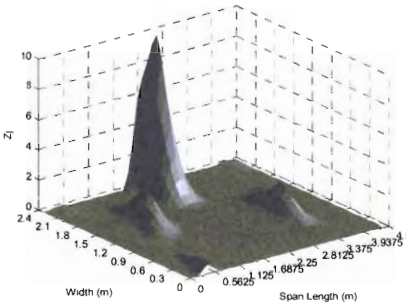


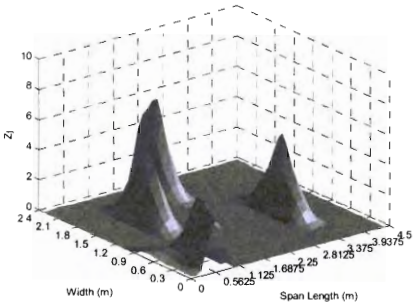


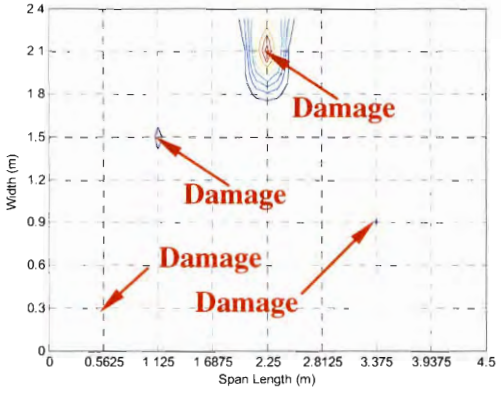
(c) g2Sg4Sg3Sg1M (3 modes).



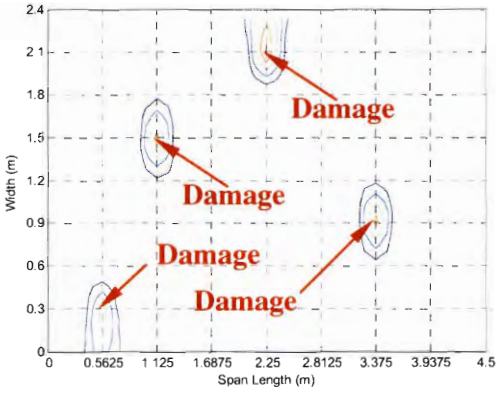
(d) g2Sg4Sg3Sg1M (9 modes).







(e) g2Sg4Sg3Sg1S (3 modes).



(f) g2Sg4Sg3Sg1S (9 modes).

Figure 6.48 Four damage cases using DI-II-P method for bridge.

6.6 Summary

In this chapter, finite element (FE) models of a timber beam, a timber plate and a laboratory timber bridge were utilised to investigate, analytically, the robustness of damage detection using various damage index methods. Damage detection methods used for damage localisation in the timber beam model were index I and II (DI-I and DI-II), change in flexibility (CIF) and modified damage index I and II (MDI-I and MDI-II). For damage severity estimation, the hybrid of MDI-I and CIF methods, abbreviated as HMC, and further development of MDI-II method were utilised. Prior to studies on damage detection of a timber beam model, a comparative study was conducted on two numerical integration methods, namely, trapezoidal rule and rectangular rule. The comparison was done using the MDI-I method to determine which method performs better in detecting damage.

Subsequent to the timber beam FE model damage detection studies, a timber plate FE model was used (as a supplementary work) to investigate damage localisation utilising damage index II method for plate-like structures (DI-II-P). With the understanding gained from the timber plate, the DI-II-P method was applied to a laboratory timber bridge FE model (a complex structural system).

From the numerical integration comparisons, it is clear that numerical techniques used in a damage detection process can significantly affect the outcomes of the detection results. For example when mode shape curvature integrations use the rectangular rule for the numerical integration, it yields better results than the trapezoidal rule. With this finding, the rectangular rule was used for all damage detection using different damage index algorithms in this study.

For damage localisation of timber beam employing damage index methods, namely, damage index I (DI-I) and II (DI-II) as well as changes in flexibility (CIF), it was found that these methods are capable of detecting single damage quite well but encountered difficulties for multiple damage scenarios even when higher modes were employed. Hence, modifications were proposed for the damage index algorithms by normalising the mode shape curvature. Employing normalisation of mode shape curvature to its maximum value reduced dominance of higher modes and more even contribution from each mode shape curvature used in the algorithms for one-dimensional beam structures. The modified versions of damage index I and II methods, are denoted modified damage index I (MDI-I) and II (MDI-II). The modified algorithms

performed well in locating single and multiple damage scenarios for the analytical model of a timber beam. It is also concluded that using higher modes can detect multiple damage better because higher modes have smaller spatial wavelength, and can highlight the damage better.

For estimation of severity of damage for the timber beam, hybrid of modified damage index I (MDI-I) and changes in flexibility (CIF) designated as HMC, as well as manipulation of modified damage index II (MDI-II) were used. Both methods were found capable of identifying location of damage well. They also estimated the severity of damage for severe damage for single and multiple damage scenarios well. While for medium damage, the methods provide reasonable damage severity estimates. However, estimation of light damage did not work well using these methods.

The damage index II method was extended to plate-like structures incorporating plate theory. The damage index method for plate-like structures, denoted as DI-II-P, was adopted to detect damage in plate-like structures, such as the analytical model of a laboratory timber bridge. A timber bridge is a complex system. It is, therefore, advisable to at least look into a supplementary work to apply the DI-II-P method on a timber plate. The results show that by using the first six modes (higher modes) damage localisation is good.

From the laboratory timber bridge analytical results, it was found that using the first nine modes in the proposed algorithm, all severe damage could be located whether in single or multiple damage scenarios. While using just the first three modes, some severe damage was not detected. This reinforces the finding that higher modes would perform better in detecting damage. It should be noted that normalisation of mode shape curvature for DI-II-P is not straightforward and this is intended to be part of the future work.

Chapter 7

Modal Testing and Experimental Modal Analysis for Timber Beams

7.1 Introduction

Modal testing and experimental modal analysis (MT&EMA) is a process of characterising the dynamic properties of a test structure by exciting the structure artificially and identifying its modes of vibration (Ramsey 1983). The dynamic properties of the test structure provide an insight into the behaviour of the structure. Any change in the structural behaviour of a system would also alter the corresponding dynamics properties. This has provided a rationale for damage detection using vibration characteristics in a structural system for which MT&EMA serves as a mean to extract dynamic properties for the given structures. This chapter describes briefly the theory, procedure and results of modal testing and experimental modal analysis (MT&EMA) of two timber beams inflicted with various damage scenarios. The output of MT&EMA such as natural frequencies, damping ratios and mode shapes together with their derivatives were employed in various damage detection algorithms to detect damage. The damage algorithms adopted for damage localisation are the damage index I (DI-I) and damage index II (DI-II). The modified versions of these two damage localisation algorithms were also proposed and denoted as the modified damage index I (MDI-I) and modified damage index II (MDI-II), respectively. In addition, a hybrid algorithm of MDI-I and changes in flexibility (CIF) was proposed to estimate the severity of damage. The re-developed MDI-II algorithm was also extended to evaluate the severity of damage.

7.2 Fundamentals of Modal Testing and Experimental Modal Analysis

Vibration or dynamic motion is an essential component in modal testing and experimental modal analysis. Reliable vibration and dynamic analysis tools are needed in order to analyse the response of machines and structures when subjected to external and internal forces, which may cause deformations and overall motions. Experimental modal analysis is one of these tools, which provides an understanding of structural characteristics, operating conditions and performance criteria (National Instruments 2006). In many practices of structural dynamics, modal testing is regarded as an extensive subject of vibration testing for modal analysis (Maia & Silva 1997). Modal analysis theory basically refers to the portion of classical vibrations that explain, theoretically, the existence of natural frequencies, damping ratios and mode shapes for a linear system. While, experimental modal analysis is defined as the process of determining the modal parameters (frequencies, damping ratios, modal vector and modal scaling) of a linear, time invariant system by way of an experimental approach (Structural Dynamic Research Laboratory 1999).

Nowadays, experimental modal analysis (EMA) consists of a vast range of different areas, like modal correlation and updating, modal testing methods, nonlinear modal analysis, substructuring and structural modification (Maia & Silva 1997). Generally, the understanding of modal testing and experimental modal analysis can be divided into three major categories i.e. signal processing, frequency response function (FRF) and modal parameter estimation.

7.2.1 Signal Processing

Basically, signal processing is analysis processes for electrical signals. Such signals are transformed from physical quantities and can be processed and analysed in time and frequency domains. The process of acquiring and converting physical quantities from analogue to digital electrical signals is shown in Figure 7.1 (Abdul Rahman 1999). In the process, the interference or noise is removed as much as possible in order to obtain a better spectrum of the results.

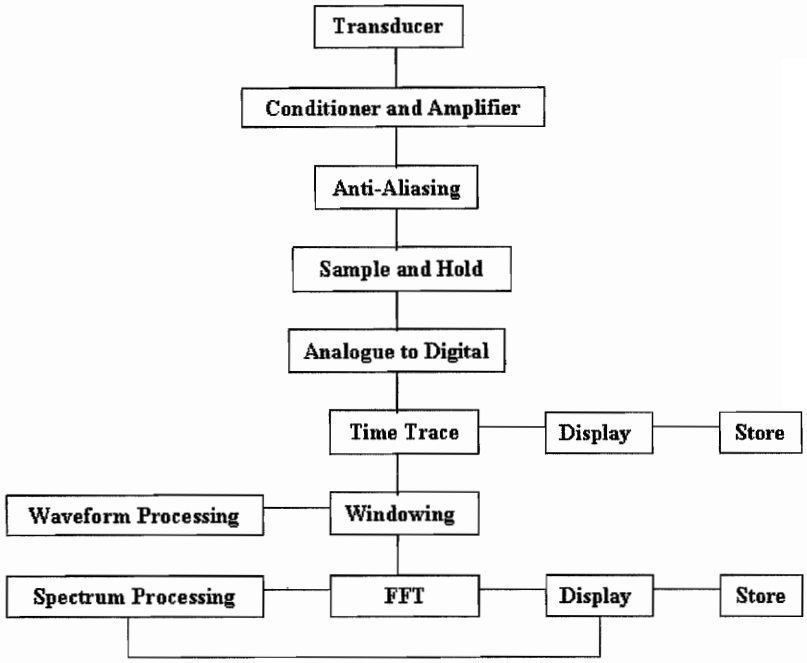


Figure 7.1 Digital signal processing (Abdul Rahman 1999).

When a structure is excited, its physical motion is captured by transducers. Transducers convert the physical signals to electrical signals. Common transducers for vibration measurement include piezoelectric accelerometers and force transducers in mechanical and structural applications. The basic build-up of a transducer is shown in Figure 7.2 (Zwonlinski 1998). The piezoelectric sensors are commonly constituted of materials such as quartz or ceramic. When the piezoelectric sensor experience a change in load such as compressive force, an electrical charge is generated, this is usually a function of frequency. The piezoelectric sensor can measure the generated charge by preloading the internal frictional forces. These types of sensors usually manage to operate within a wide range of frequency.

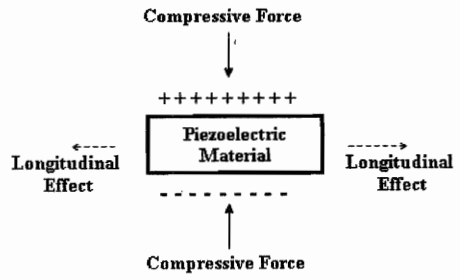


Figure 7.2 Basic sensor build-up (Zwonlinski 1998)

The electrical signals acquired by a transducer are analogue signals, which require conditioning and amplifying. A signal conditioner is used to condition these signals from the transducer into voltage proportional to the measured physical quantities.

In the signal processing, there are some pitfalls that might result in the loss of fidelity of the signal during the process, for example, aliasing, spectral leakage, etc. Aliasing is a phenomenon that occurs when the sampling rate is less than twice the highest frequency in the data. It produces a distorted representation of data. It also occurs when converting analogue (continuous) data to digital (discrete) data. This could result in erroneous frequency interpretation in vibration analysis. Figure 7.3 gives an illustration of this phenomenon.

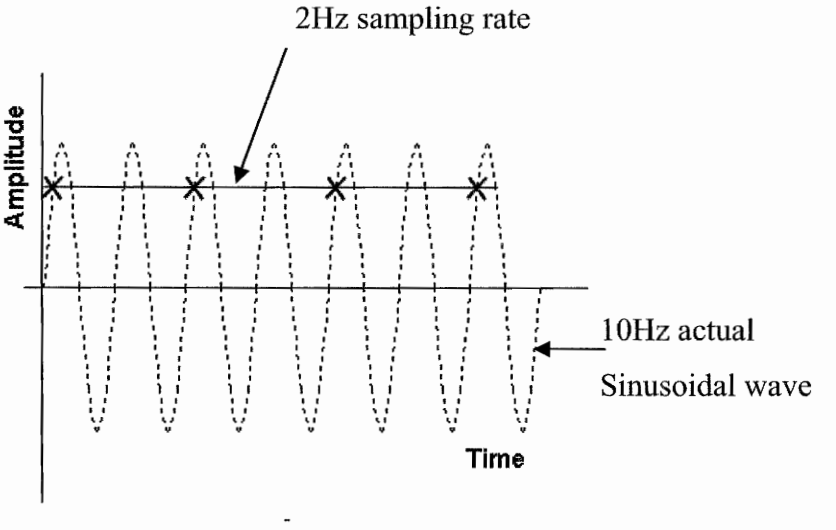


Figure 7.3 Aliasing phenomenon (Maia & Silva 1997).

The above problem can be minimised by setting the sampling rate at least twice the highest frequency present in the data. This is known as the Nyquist-Shannon sampling theorem. For example, a signal that contains data up to a maximum of 500Hz needs to be sampled at least 1000 samples per second or 1000Hz. An alternative solution is to use anti-aliasing filter. It is a low-pass filter which automatically cuts-off frequencies set at or below half of the sampling frequency.

An analogue-to-digital converter (ADC) converts the analogue input signal into a digital form. The acquired continuous signal is first sampled and then converted into a discrete-time series digital signal. The time interval between two sampling frequencies is the inverse of sampling period. The amplitude of each signal sample is quantified into

one of 2^B level, where B is the number of bits used to represent a sample in the ADC. For example, a 16-bit ADC will discretise the amplitude range of the signal to a resolution of 65536 grids.

After the digitising process, the continuous time signals are discretised into a sequence of values commonly known as discrete time series. A discrete time signal has values which are defined only at discrete values of time or some other appropriate variables, for example space. The signal can then be displayed on a digital screen. It can also be stored on a disk or further processed digitally.

In general, a discrete time signal is also known as a signal in the time domain. It can be described, in general terms, as any parameter expressed as a function of time. A discrete time signal or time domain signal usually consists of many frequency components that are superimposed. The frequency presentation of the signal is also known as the signal in the frequency domain, which is associated with the description of any functions in terms of frequency. Hence, in many cases, especially complex waveforms, signals cannot be easily visualised or interpreted effectively in the time domain. Raw time domain data is preferably converted to frequency domain via a transformation process called Fast Fourier Transform (FFT). During this process, some problems such as leakage, associated with the transformation, may occur. Leakage is referred to as the unwanted distortion caused by artificial truncation of a sampled data (Maia & Silva 1997).

The common tool used to overcome leakage problem is windowing. Windowing is a function which minimises leakage in the process of transforming time domain signal to frequency domain signal. This function consists of a process of 'weighting' the original time history data to reduce the noise distortion and the effect of leakage. There are a few developed window functions. The common ones are hanning, flattop, exponential and force windows.

As mentioned earlier, a time domain signal is required to be transformed to its various frequency components. One of the common ways is to use Fast Fourier transform (FFT) to perform this task. FFT is an algorithm given as

$$x(k) = \sum_{j=0}^{N-1} X(j) W_N^{-jk} \qquad \text{Equation 7.1}$$

Equation 7.1 represents the discrete series $x(k)$ at the time instant k of a sampled data N, k=0, 1, 2, ….., N-1 and j=0, 1, 2, ….., N-1 where W_N expresses $e^{-i2\pi/N}$. The spectrum of frequency domain signals can now be displayed or stored on a disk.

7.2.2 Frequency Response Function

Frequency response function (FRF) method (also known as transfer function method) has been widely used for dynamic system identification in the industries, including the automotive, machine tool and structural engineering industries for the past few decades. The method is fast and easy to perform. The general procedure using the FRF method is shown in Figure 7.4. In general, frequency response function (FRF) is a form of transfer function with frequency as its variable. To produce FRF requires transducers to be attached to the test structure to record output electric signal, while the input signal is obtained from the source of excitation. For example, the input signal $f(\omega)$ with respect to frequency ω basically is the force applied to the structure with a modal hammer and the output signal $g(\omega)$ is the response motion signal obtained from the accelerometers attached to the system. The conventional FRF ($H_1(\omega)$) for each point on a system is determined by dividing the output by the input after Fourier transformation as shown in Equation 7.2.

$$H_1(\omega) = \frac{output}{input} = \frac{g(\omega)}{f(\omega)} \qquad \text{Equation 7.2}$$

There is another form of FRF, which is obtained by normalising the cross input-output spectrum $G_{fg}(\omega)$ by the output auto-spectrum $G_{ff}(\omega)$ as written in the following equation:

$$H_2(\omega) = \frac{G_{fg}(\omega)}{G_{ff}(\omega)} \qquad \text{Equation 7.3}$$

where $G_{fg}(\omega)=f(\omega)*g(\omega)$ is the cross spectrum, while $G_{ff}(\omega)=f(\omega)*f(\omega)$ is the auto-spectrum of a sampled data. In short, FRF is a function based upon the use of digital signal processing techniques and the fast Fourier transform (FFT) algorithm to measure transfer functions between different points on the test structure. The relationship between the FRF and the modal parameters is given in Equation 7.4 (Craig & Kurdila 2006).

$$H_{ij}(j\omega) = \sum_{k=1}^{N} \left(\frac{r_{ijk}}{(j\omega - \lambda_k)} + \frac{r_{ijk}^{*}}{(j\omega - \lambda_k^{*})} \right) \qquad \text{Equation 7.4}$$

Where:

$H_{ij}(j\omega)$ = FRF between the response DOF i and reference DOF j

ω = frequency (rad/sec)

N = number of modes of vibration that contribute to the structure's dynamic response within the frequency range under consideration

r_{ijk} = residue value for mode k

λ_k = pole value for mode k

* designates complex conjugate

The pole value λ_k can be expressed as shown in Equation 7.5.

$$\lambda_k = \delta_k + j\omega_{dk} \qquad \text{Equation 7.5}$$

Where:

ω_{dk} = the damped natural frequency of mode k

δ_k = the damping factor of mode k

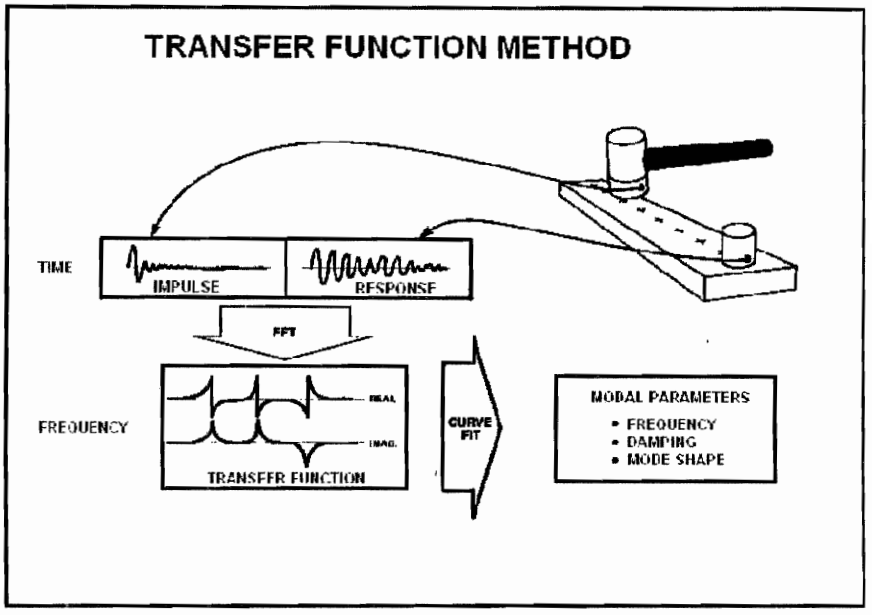


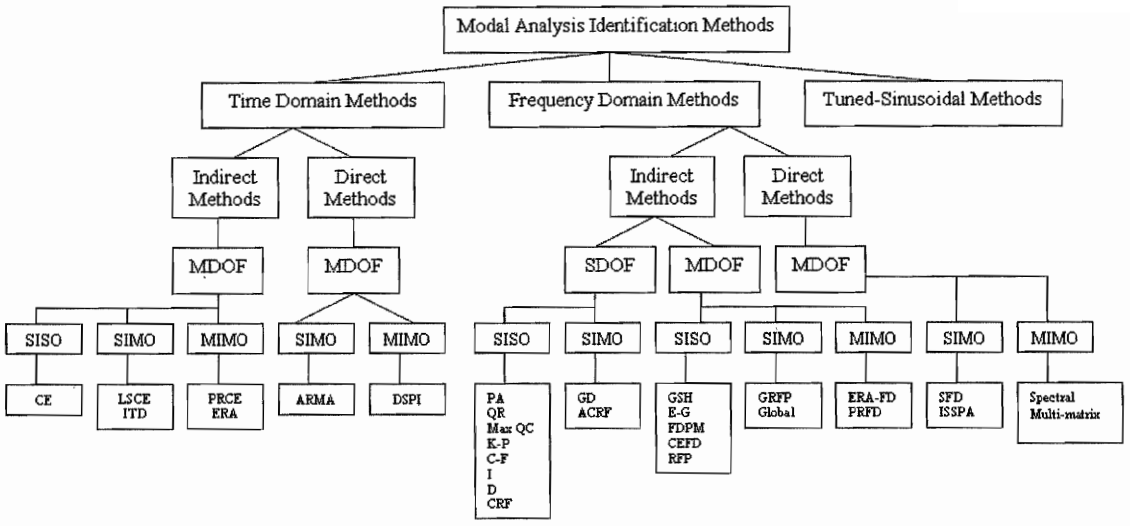
Figure 7.4 Transfer function method (Agilent Technologies 2000).

7.2.3 Modal Parameter Estimation

Modal parameter estimation is concerned with the practical problem of estimating the modal parameters, based upon a choice of mathematical model as justified by the experimental modal analysis method, from the measured data (Structural Dynamic Research Laboratory 1999). This is the identification of the dynamic properties of a structure from the measured data based on curve-fitting techniques. For the modal analysis identification methods (curve-fitting methods), the major grouping concerns the domain in which the data are treated numerically. There are three major categories, namely, time domain, frequency domain and tuned-sinusoidal methods. The first two methods will be discussed briefly below as they are widely used in EMA, while the third method is not discussed in this thesis. The interested readers looking for more details pertaining to these methods are referred to (Maia & Silva 1997).

In broad terms, time domain methods tend to provide the best results when a large frequency range or large number of modes exists in the data, while frequency domain methods tend to provide the best results when the frequency range of interest is limited and the number of modes is relatively small. It should be noted that the time domain methods have a major disadvantage, that is, they can only estimate modes inside the frequency range of analysis and take no account of the residual effects of modes that lie outside that range. A general classification of modal analysis identification methods is shown in Figure 7.5.

From Figure 7.5, time domain and frequency domain methods can be subdivided into two categories which are indirect and direct methods. The indirect method is also referred to as modal method and the identification of the FRF(s) is based on the modal model, i.e. on the modal parameters (natural frequencies, damping ratios, modal constants and their phase). The direct method means that the identification is directly based on the spatial model, i.e. on the general matrix equation of dynamic equilibrium.



Time Domain Methods:

CE = Complex Exponential
LSCE = Least Squares Complex Exponential
ITD = Ibrahim Time Domain
PRCE = Polyreference Complex Exponential
ERA = Eigensystem Realisation Algorithm
ARMA = Autoregressive Moving Average
DSPI = Direct System Parameter Identification

Frequency Domain Methods:

PA = Peak Amplitude
QR = Quadrate Response
Max QC = Maximum Quadrate Component
K-P = Kennedy-Pancu (or Maximum Frequency Spacing)
C-F = Circle Fitting
I = Inverse
D = Dobson
CRF = Characteristic Response Function
GD = Global Dobson
ACRF = Advanced Characteristic Response Function
GSH = Gaukroger-Skingle-Heron
E-G = Ewin-Gleeson
FDPM = Frequency Domain Prony Method
CEFD = Complex Exponential Frequency Domain
RFP = Rational Fraction Polynomial
GRFP = Global Rational Fraction Polynomial
ERA-FD = Eigensystem Realisation Algorithm in Frequency Domain
PRFD = Polyreference Frequency Domain
SFD = Simultaneous Frequency Domain
ISSPA = Identification of Structural System Parameters

Figure 7.5 Classification of modal analysis identification methods (Maia & Silva 1997).

A further division of the indirect and direct methods is the number of modes that can be analysed. In this respect, there are single degree of freedom (SDOF) and multiple degree of freedom (MDOF) analyses. For time domain, the analysis is available only for MDOF for both indirect and direct methods. While, in the frequency domain, the SDOF and MDOF are applicable to indirect methods but direct methods only apply to MDOF analysis. In real applications, a system is usually MDOF, thus the most common methods employ multiple mode analytical models (see Figure 7.6). However, in many circumstances, the FRF of a MDOF system is separated into many SDOF systems for the analysis when the modes are relatively isolated from each other. At times, the very simple single mode methods will produce reasonably good results for most engineering analyses.

Some identification methods can be applied only to a single frequency response function (FRF) at a time and are called single FRF or single-input-single-output (SISO) methods. Some other methods permit several FRFs to be analysed simultaneously, with response taken at various points on the structure using just one excitation point. These methods are named global or single-input-multi-output (SIMO) methods. The global methods estimate the global dynamic properties (natural frequencies and damping ratios) of a structure. Hence, the dynamic properties do not vary (theoretically) from one FRF to another FRF. These methods would automatically average out small variations in those analyses using single FRF at a time. Finally, there are methods that can process all available FRFs simultaneously, from various excitation and response locations. These methods are called polyreference or multi-input-multi-output (MIMO) methods.

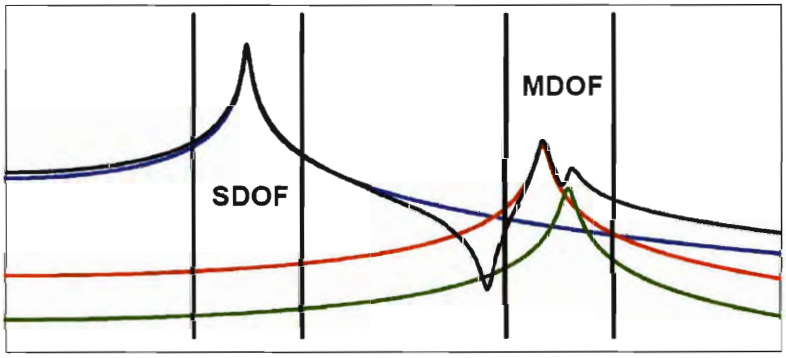


Figure 7.6 Curve-fitting different bands using different methods (Avitabile 2001).

Performing further analysis, such as experimental modal analysis, helps to identify modal parameters based on obtained FRF measurements. The standard procedure to obtain modal parameters from FRF measurements is shown in Figure 7.7. As mentioned earlier, curve-fitting techniques (modal analysis identification method) is an analytical process to determine the mathematical parameters yielding the closest possible fit to the measured data. For example, the method of least squares complex exponential (LSCE) can be used for curve fitting (see Figure 7.5). However, other curve-fitting algorithms can also be used to identify modal parameters.

As shown in Figure 7.7, modal parameters can be obtained from FRF measurements. Modal frequencies correspond to the peaks in the imaginary part of the frequency response functions (FRFs). A peak should exist at the same frequency in all

measurements in FRFs, except those measured at the node points. The node point is where the modal amplitude is zero. The frequency corresponding to the peak amplitude is denoted as ω_n. The peak amplitude (X_{Mr}) is given by

$$X_{Mr} = \frac{1}{2\zeta}\frac{F_0}{k} \qquad \text{Equation 7.6}$$

For a SDOF system or at least the case where modes are well separated in a MDOF system, the width of the modal peak is related to the damping of the mode. The wider the peak, the higher the modal damping becomes. The damping ratio ζ can be determined by using half-power band points R_1 and R_2, which correspond to the frequencies ω_1 and ω_2 at the response amplitude of $\frac{X_{Mr}}{\sqrt{2}}$ as illusatred in Figure 7.8. The equation is as below:

$$\zeta = \frac{\omega_2 - \omega_1}{2\omega_n} \qquad \text{Equation 7.7}$$

The bandwidth method is suitable for low damping and is not recommended for non-linear systems. An alternative way to define damping properties of a system is measuring the decay in the time domain. However, the method is not discussed here as it is not adopted in this study and further details can be found in Bachmann et al (1995).

The mode shapes can be obtained by assembling the peak values at the same frequency from all the measurements (see Figure 7.5 for PA or Peak Amplitude method). As shown in Figure 7.7, as modal frequency increases, the complexity of the mode shape also increases. For further details of modal analysis and modal testing refer to Ewins (2000), Maia and Silva (1997) and Agilent Technologies Application Note 243-3 (2000).

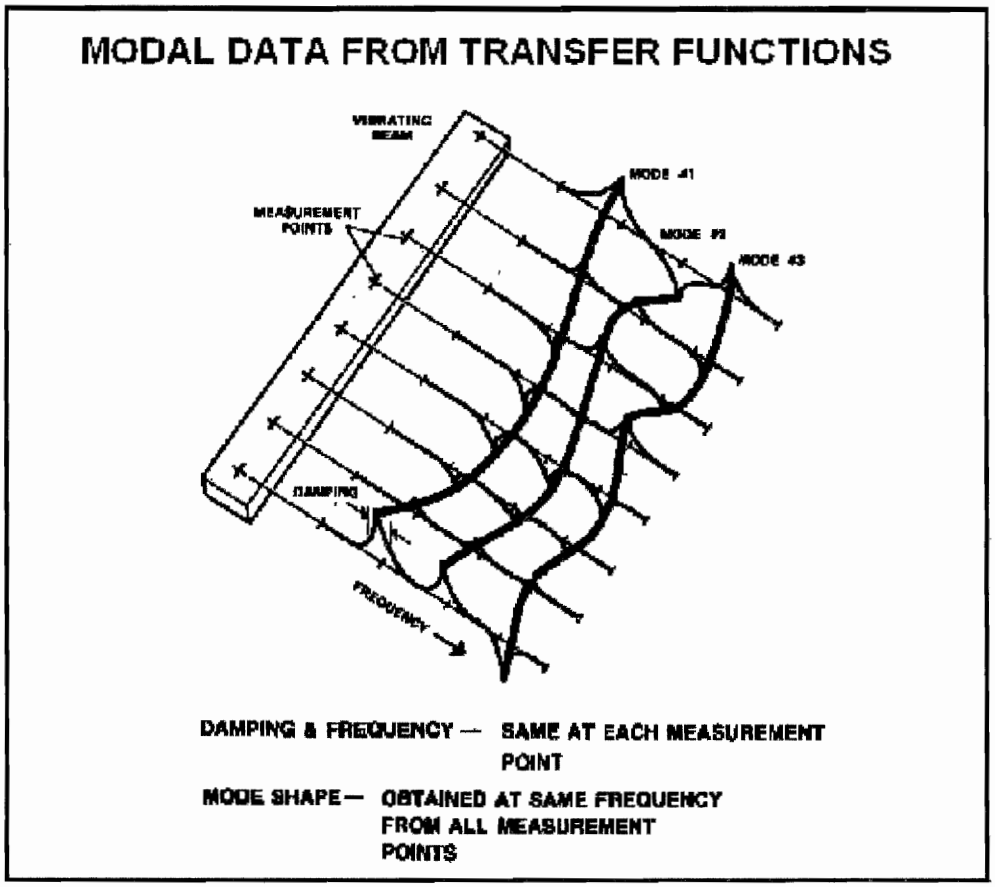


Figure 7.7 Experimental modal analysis example (Agilent Technologies 2000).

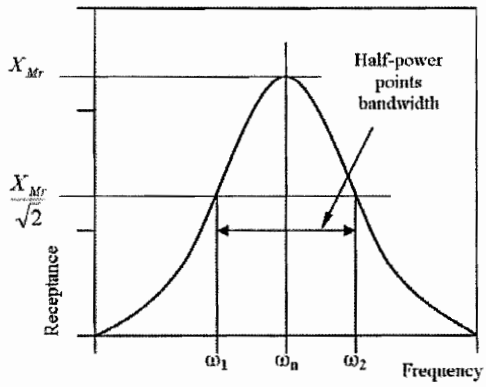


Figure 7.8 Half-power points definition.

7.3 Experimental Set Up and Testing

7.3.1 Test Beams

Timber beams were used in the experimental work, which intended to represent the scaled girders of typical timber bridges in Australia. The scaling for the beams was based on dynamic similitude of the girders in terms of their first natural frequencies, which usually range from 5 to 20Hz. The basic dimensions of the beams are shown in Figure 7.9. The beams are of treated radiata pine sawn timber measuring nominal dimensions of 45mm by 90mm in cross section with a span length of 4,500mm. The modulus of elasticity (MOE) of the beams is about 12GPa obtained from four point bending tests. The details of the four point bending test and MOE results are found in Chapter 3. The moisture content of the beams was estimated to be around 7-8% using Protimeter, a wood moisture detector (see Figure 7.10). A specially designed support system was used between the beam and the concrete supports to provide a well-defined boundary condition that is very close to a pin-pin condition as depicted in Figure 7.11. Two timber beams, namely Beam1 and Beam2, were used to designate the undamaged state as denoted by Un1 and Un2, respectively. The results form the basis of comparison for various damage cases utilising the extracted modal parameters and their derivatives.

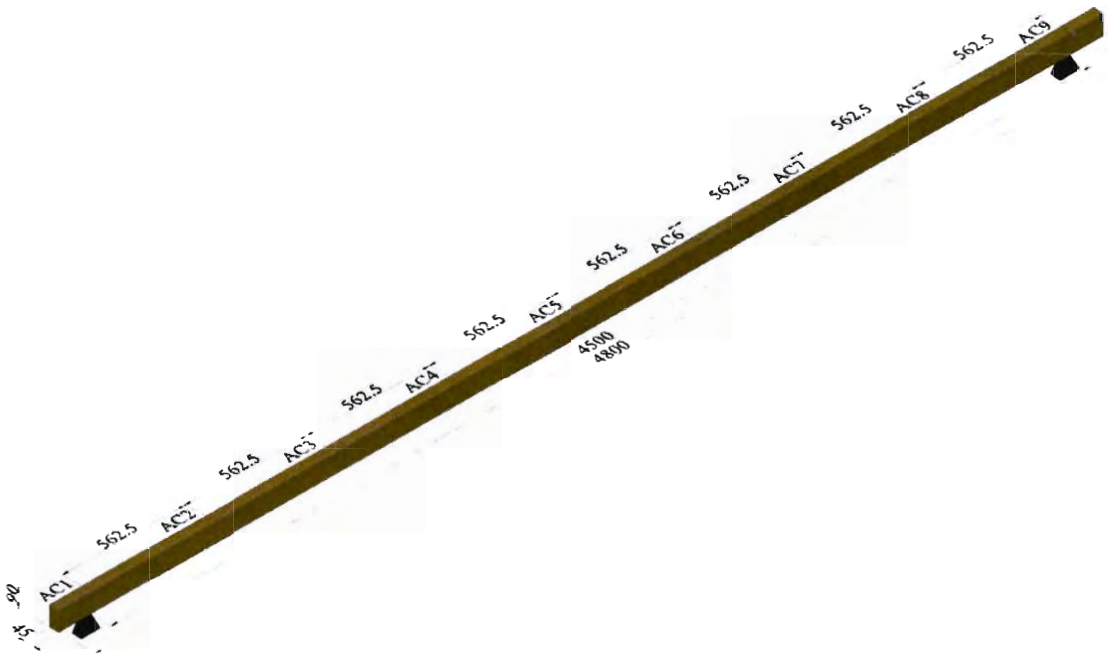


Figure 7.9 Geometric configurations and measurement locations of the test beams.



Figure 7.10 Wood moisture detector.

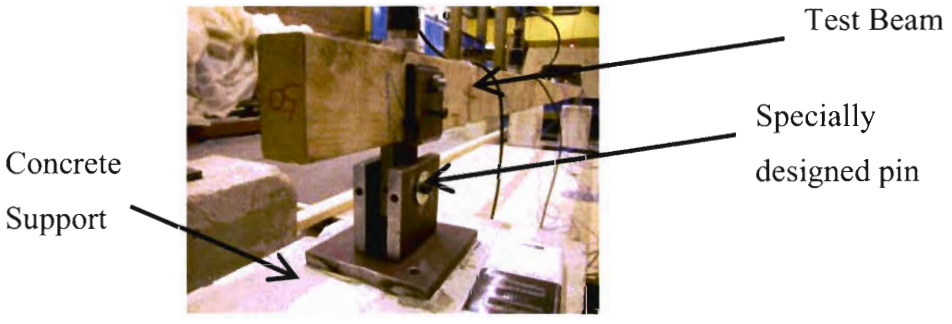


Figure 7.11 Specially designed pin support.

7.3.2 Inflicted Damage in Test Beams

The goal of this study was to detect damage typically found in timber bridges. It is intended to detect damage in multiple locations on a timber beam. The damage cases considered are described in Table 7.1. In all damage scenarios, the damage consists of a rectangular opening along the span starting from the soffit of the beam, located at 2/8, midspan, 5/8 and 6/8 of the span length to simulate pockets of rot that usually starts from the top surface in timber girders. In this study and the subsequent discussions that follows, 'L', 'M' and 'S' denote light, medium and severe damage, respectively. All inflicted damage are 1% of the total span length (45mm) and consist of 10%, 30% and 50% of the beam depth, designated as damage cases 'L', 'M' and 'S' as shown in Table 7.1. The severity of the inflicted damage can also be interpreted as loss in 'I' (sectional moment of inertia) from the depth of cut. The loss in section of 10% (L), 30% (M) and 50% (S) of beam depth, correspond to 27.1%, 65.7% and 87.5% loss in 'I', respectively. A typical damage inflicted is shown in Figure 7.12.

From Table 7.1, there are twenty-four damage scenarios designed to be performed on the two test beams, each with 12 damage cases. For each test beam, the damage scenarios are divided into two main categories that are number of damage locations and severity of damage. Four types of locations of damage were selected to represent single and multiple damage scenarios i.e. 1, 2, 3 and 4 locations of damage. Within each type of damage locations, three damaged severity levels were nominated to represent light, medium and severe damage that may find in timber structures. Similar damage scenarios listed in Table 7.1 can be found in Chapter 6 that was used in the analytical investigation.

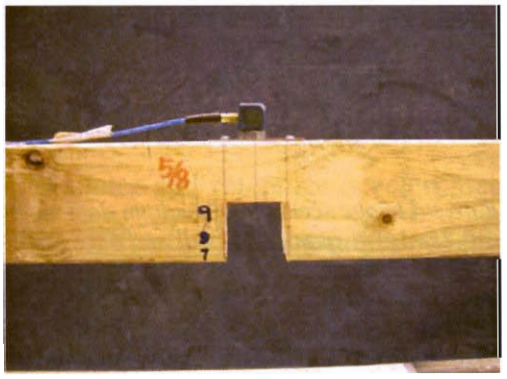


Figure 7.12 Side view of a typical damage inflicted in beams.

Table 7.1 Dimensions of damage inflicted in timber beams.

Damage Case	Damage Scenario	Location per 8th of span length	Length l (mm)	Depth h (mm)	% reduction of 'I'
Beam 1	Un1				
1	4L	4	45	9	27.1
2	4M	4	45	27	65.7
3	4S	4	45	45	87.5
4	4S6L	4, 6	45	45, 9	87.5, 27.1
5	4S6M	4, 6	45	45, 27	87.5, 65.7
6	4S6S	4, 6	45	All 45	All 87.5
7	4S5L6S	4, 5, 6	45	45, 9, 45	87.5, 27.1, 87.5
8	4S5M6S	4, 5, 6	45	45, 27, 45	87.5, 65.7, 87.5
9	4S5S6S	4, 5, 6	45	All 45	All 87.5
10	2L4S5S6S	2, 4, 5, 6	45	9, 45, 45, 45	27.1, 87.5, 87.5, 87.5
11	2M4S5S6S	2, 4, 5, 6	45	27, 45, 45, 45	65.7, 87.5, 87.5, 87.5
12	2S4S5S6S	2, 4, 5, 6	45	All 45	All 87.5
Beam 2	Un2				
13	6L	6	45	9	27.1
14	2L6L	2, 6	45	All 9	All 27.1
15	2L4L6L	2, 4, 6	45	All 9	All 27.1
16	2L4L6M	2, 4, 6	45	9, 9, 27	27.1, 27.1, 65.7
17	2M4L6M	2, 4, 6	45	27, 9, 27	65.7, 27.1, 65.7
18	2M4M6M	2, 4, 6	45	All 27	All 65.7
19	2M4M6S	2, 4, 6	45	27, 27, 45	65.7, 65.7, 87.5
20	2S4M6S	2, 4, 6	45	45, 27, 45	87.5, 65.7, 87.5
21	2S4S6S	2, 4, 6	45	All 45	All 87.5
22	2S4S5L6S	2, 4, 5, 6	45	45, 45, 9, 45	87.5, 87.5, 27.1, 87.5
23	2S4S5M6S	2, 4, 5, 6	45	45, 45, 27, 45	87.5, 87.5, 65.7, 87.5
24	2S4S5S6S	2, 4, 5, 6	45	All 45	All 87.5

Notes:

2i = damage at 2/8 span with damage severity i

L, M, S representing light (L), medium (M) and severe damage (S), correspond to 27.1, 65.7 and 87.5% loss of 'I'

(e.g. 2M4S5S6S denotes a cumulative damage scenario of medium damage on 2/8 span (1.125m), severe damage on 4/8 span (midspan or 2.25m), 5/8 span (2.8125m) and 6/8 span (3.375m))

7.3.3 Modal Test Set Up

The modal test set up and instrumentation arrangement during the modal tests is shown in Figure 7.13. Based on digital signal processing techniques and the Fast Fourier transform (FFT) algorithm, the time domain data were acquired and processed, which subsequently produced frequency domain data in terms of frequency response function (FRF) among different points on the test structure. In this study, the MT&EMA is a means to obtain natural frequency, damping ratio and their corresponding mode shapes from test structures. The tests were intentionally conducted under similar environmental conditions, that is, temperature of 22°C±2° and ambient humidity of 60%±5% to minimise environmental factors on the modal parameters.

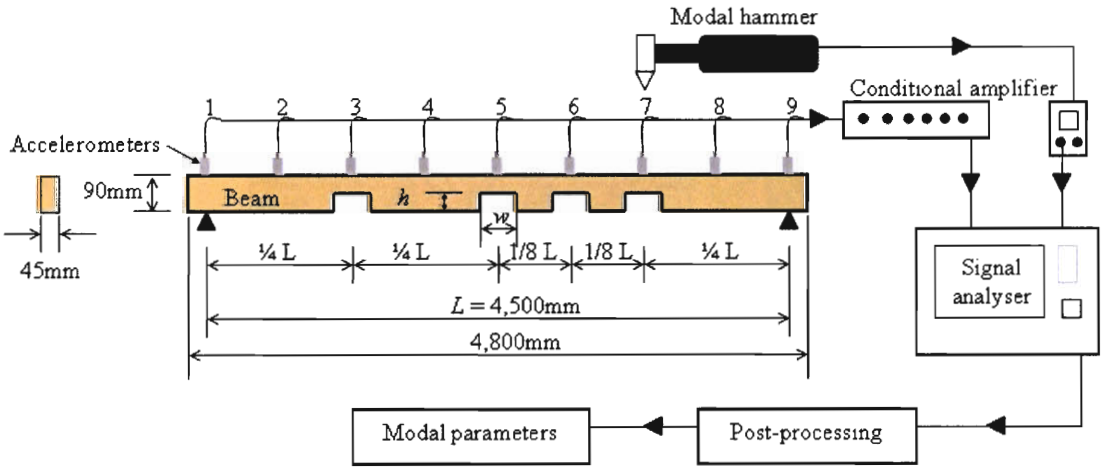


Figure 7.13 Schematic diagram of modal tests.

Piezoelectric accelerometers were used in the modal tests to measure the acceleration responses due to an impact action. All accelerometers used in the modal test were calibrated against one reference accelerometer selected amongst them in order to obtain a relatively synchronised mode shape data. The calibration process was done by attaching the test accelerometer and reference accelerometer adjacent to each other onto a miniature three-degree-of-freedom steel structure at the same level as illustrated in Figure 7.14. The test structure was then excited using a modal hammer. The test was repeated three times and the mode shape amplitudes was averaged and used to calibrate the sensitivity of the test accelerometers. The purpose of the calibration test was to ensure that the experimental mode shape was not skewed due to different sensitivities

among the accelerometers. This is particularly important since mode shape based algorithms were used for damage detection, and the presence of damage also causes changes to the mode shape.

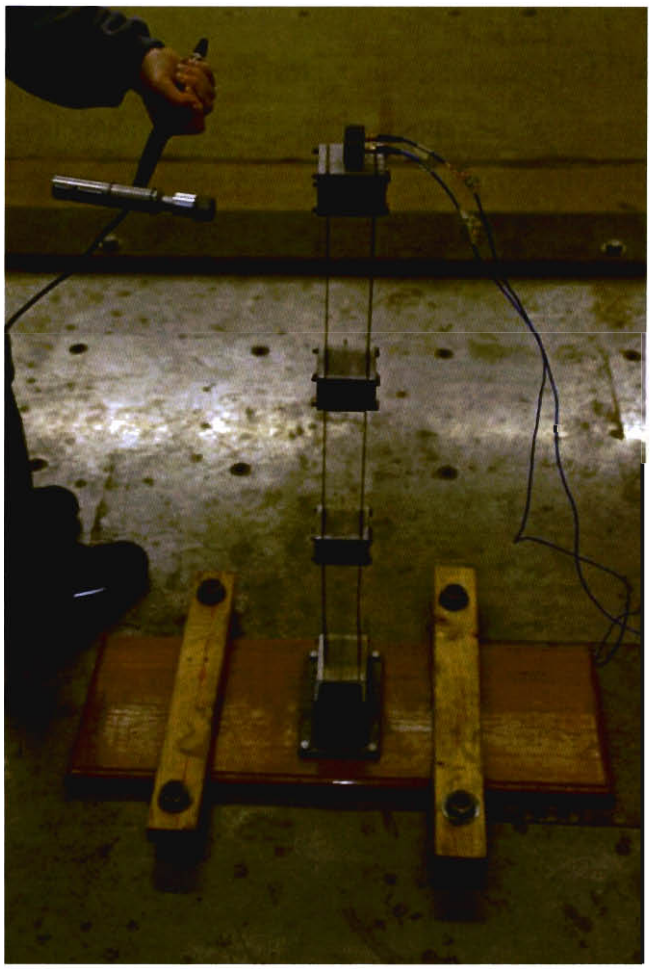


Figure 7.14 Calibration of accelerometers using a three-degree-of-freedom steel structure

To conduct structure identification, impulse excitation was used in this study. An impact hammer (model HP 086C05) (see Figure 7.15) was used to excite the test sample at the reference or driving point, i.e. point number 7 (see Figure 7.13). The impact location was set at 3/4 of the span length so that it could excite more lower modes simultaneously. The input force generated by the impact hammer was measured by means of a force transducer in the hammer with a sensitivity of 0.24mV/N. The input signal was amplified and conditioned using a battery powered signal conditioner (model PCB 480E06) as depicted in Figure 7.16. The response signals were measured using nine low impedance piezoelectric accelerometers as shown in Figure 7.17 (model PCB

356A08 and PCB 337A26) with a sensitivity ranging from 94mV/g to 100mV/g, respectively. The response signals were also amplified and conditioned using a multi-channel signal conditioner (model PCB 483B03) as shown in Figure 7.18. The accelerometers were used to measure the acceleration responses at the top surface of the beam as illustrated in Figure 7.13. Nine measuring points were set and the sensor density was deemed sufficient for reconstructing mode shapes with the required accuracy using interpolation techniques. One of the accelerometers was used as the driving point measurement (point 7) enabling the experimental mode shape to be mass normalised. Each accelerometer was attached onto a small steel plate with approximate dimensions of 40x90x1mm using a magnetic base and secured onto the top of the beams. The distance between each accelerometer was 1/8 of the span length starting from one end support of the beam to the other end as shown in Figure 7.13.



Figure 7.15 Modal hammer.

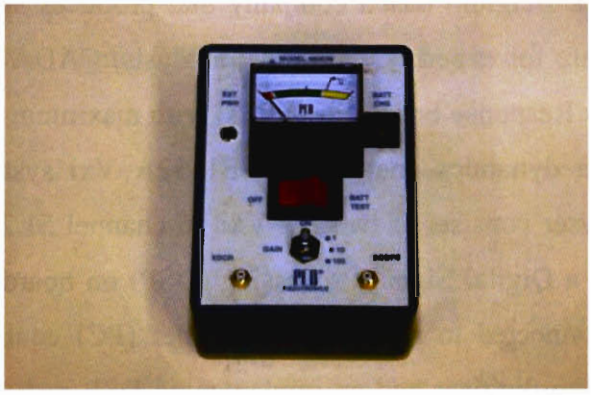


Figure 7.16 Battery powered signal conditioner.



(a) Model PCB 356A08.



(a) Model PCB 337A26.

Figure 7.17 Piezoelectric accelerometers.



Figure 7.18 Multi-channel signal conditioner.

In the LMS (a Belgium based company that produces signal acquisition and post-processing software for experimental modal analysis) CADA-X signal acquisition module, the Frequency Response Functions (FRFs) with maximum bandwidth of 500Hz were acquired using a dynamics analyser HP E1432A Vxi system as illustrated in Figure 7.19. The analyser consists of two HP Vxi 16 channel 51.2 kHz digitisers with anti-aliasing filter and a Digital Signal Processing (DSP) on board in a C-sized frame. The Vxi module is connected to a personal computer (PC) equipped with the LMS CADA-X software. The digitiser had an implemented DSP and a 4-32MB File Input File Output (FIFO) digital anti-aliasing filter. A typical FRF spectrum acquired using the system is shown in Figure 7.20. The measurements were recorded using 10,000 Hz sampling rate for a frequency span of 500Hz and 8,192 data points, thus giving a

frequency resolution of 0.061Hz per data point. A pre-trigger delay, plus force and exponential windowing were applied to increase accuracy. A pre-trigger was employed as the impulse signal usually exists for a very short period of time, it is therefore important for the analyser to begin acquiring data prior to the impact excitation (Schwarz & Richardson 1999). The force and exponential windowing functions were used for the excitation and response signals, respectively, to minimise the spectral leakage. For the excitation channel (impact hammer), the force window was applied to remove noise from the impulse signal. Ideally, the impulse signal is non-zero for the small time period of the excitation (hammer hit) and zero for the remaining time. Therefore, any non-zero data following the impulse signal is assumed to be noise and thus, is considered to be zero as shown in Figure 7.21a. For the response channels (accelerometers), the exponential window was selected to ensure that the transient signal decays sufficiently at the end of the sampling period as illustrated in Figure 7.21b. This is done by introducing artificial damping into the measurement data (Schwarz & Richardson 1999).

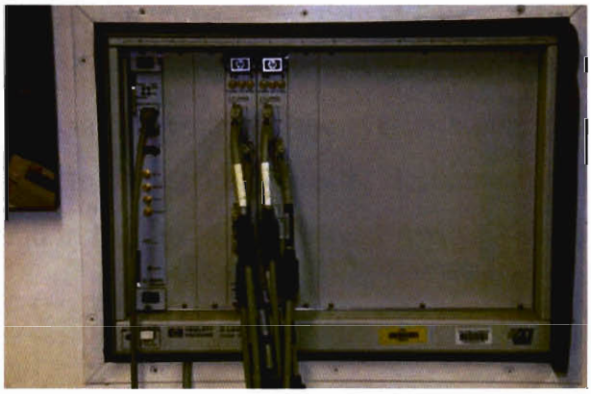


Figure 7.19 HP E1432A Vxi system.

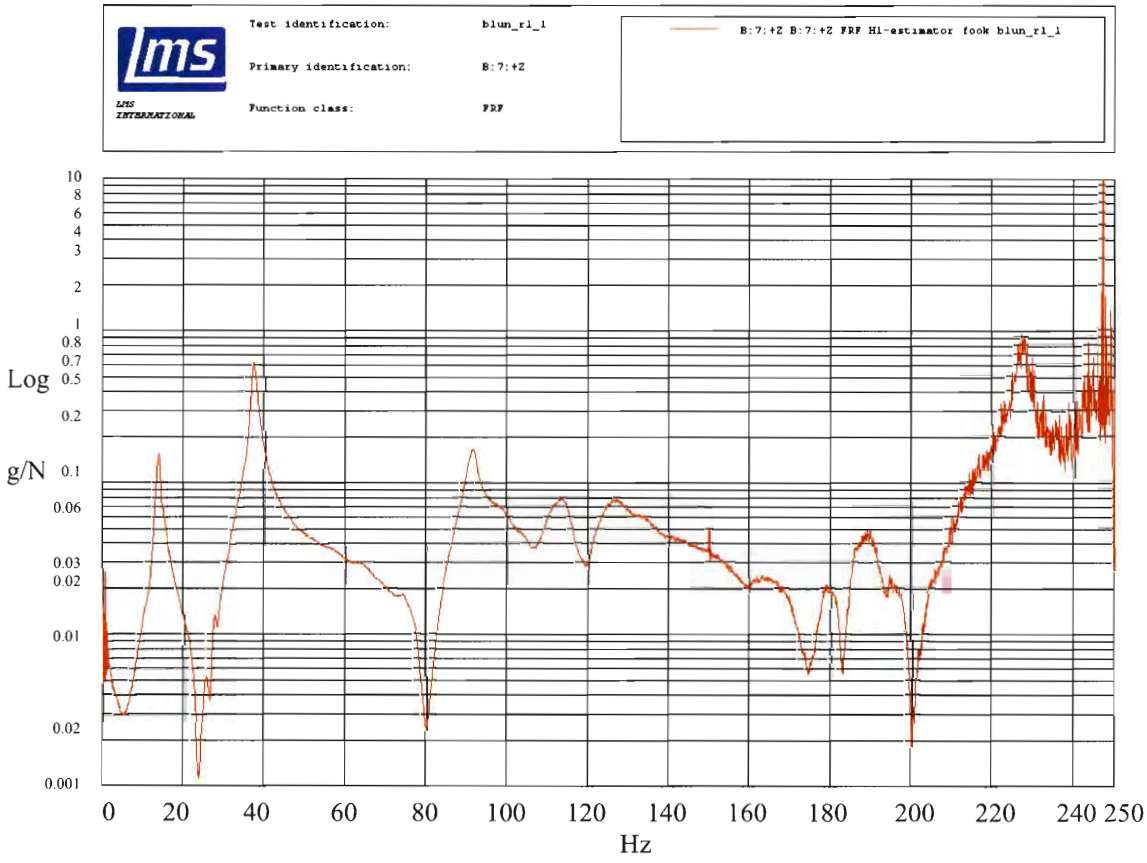


Figure 7.20 A typical frequency response function spectrum.



(a) Force window. (b) Exponential window.

Figure 7.21 Window functions.

7.3.4 Modal Analysis

Modal analysis is a subsequent step after modal tests to estimate modal parameters from the measured data such as FRFs spectrum. The modal parameter estimation is often referred to as curve-fitting. This is implemented using computer software that utilises mathematical algorithms to estimate the modal characteristics from the measured data. The basic parameters extracted are frequency, damping and mode shape. To enable curve-fitting, the measured FRFs are usually broken into many single degree of freedom (DOF) systems. There are varieties of curve-fitting techniques, i.e. some techniques employ time domain data while others use frequency domain data. In this experimental modal analysis, the Frequency Direct Parameter Identification (FDPI) technique was employed to estimate the natural frequencies, damping values and mode shapes of several modes simultaneously (LMS International 1992). This technique operates directly on frequency domain data. Hence, it is capable of taking into account the effects of modes outside the frequency band of analysis, which improves the analysis results. The basis of FDPI method is the second order differential equation for mechanical structures. When transformed into frequency domain, the differential equation can be reformulated in terms of measured FRFs as shown in Equation 7.8. The measurement data can be described by a second order linear model with constant matrix coefficients. From the identified matrices, the system's pole and mode shapes can be estimated through an eigenvalue and eigenvector decomposition of the system matrix. The details can be found in LMS CADA-X Modal Analysis manual (LMS International 1992).

$$[-\omega^2 + j\omega A_1 + A_0][H(\omega)] = j\omega B_1 + B_0 \qquad \text{Equation 7.8}$$

Where:

ω = frequency variable

$A_1 = M^{-1}C$, mass modified damping matrix (N_0 by N_0)

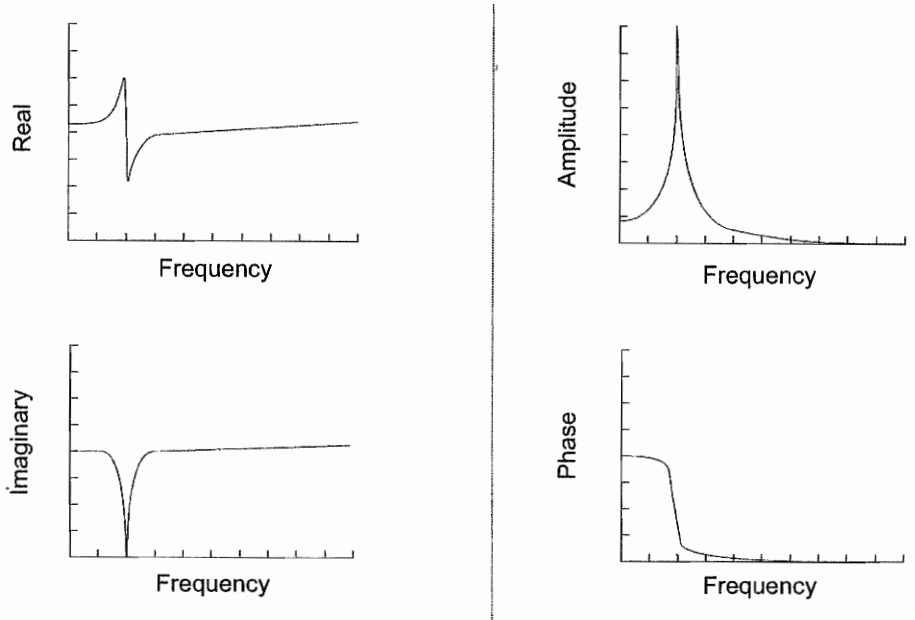
$A_0 = M^{-1}K$, mass modified stiffness matrix (N_0 by N_0)

$H(\omega)$ = matrix of FRF's (N_0 by N_i)

B_0, B_1 = the force distribution matrices (N_0 by N_i)

The output of the curve-fitting can be presented in rectangular coordinates (real and imaginary) or in polar coordinates (amplitude and phase) for a single-degree-of-freedom system as illustrated in Figure 7.22(a) and (b), respectively. At resonance, in the rectangular coordinate system, the imaginary part reaches maximum and the real

part becomes zero, while for the polar coordinate system, the magnitude reaches a maximum and the phase lags by 90°. These characteristics enable the identification of the modal parameters of a structure from the FRF.



(a) Rectangular coordinate system. (b) Polar coordinate system.

Figure 7.22 FRF graphs in rectangular and polar coordinates for a single degree of freedom system (Agilent Technologies 2000).

As mentioned earlier, using the modal analysis module in the LMS CADA-X software, a frequency domain direct measurement curve-fitting technique was used to extract the natural frequencies, damping ratios and mode shapes from the measured FRF data. From the modal testing and experimental modal analysis, five vibration modes and a frequency range spanning from 10Hz to 200 Hz, were captured as shown in Figure 7.23. The nine-point measured mode shapes can be reconstructed using cubic spline interpolation technique, generating mode shape vectors with 41 points as shown in Figure 7.24. The mode shapes with finer coordinates have shown better chance of locating damage compared to using coarse coordinates. The reconstructed mode shapes were then used in the damage detection algorithms for locating and evaluating the inflicted damage. It should be noted that the fourth flexural mode (mode 4) was not as good as others because the impact location was close to its node point. Nevertheless, this mode was still used in the subsequent discussions.

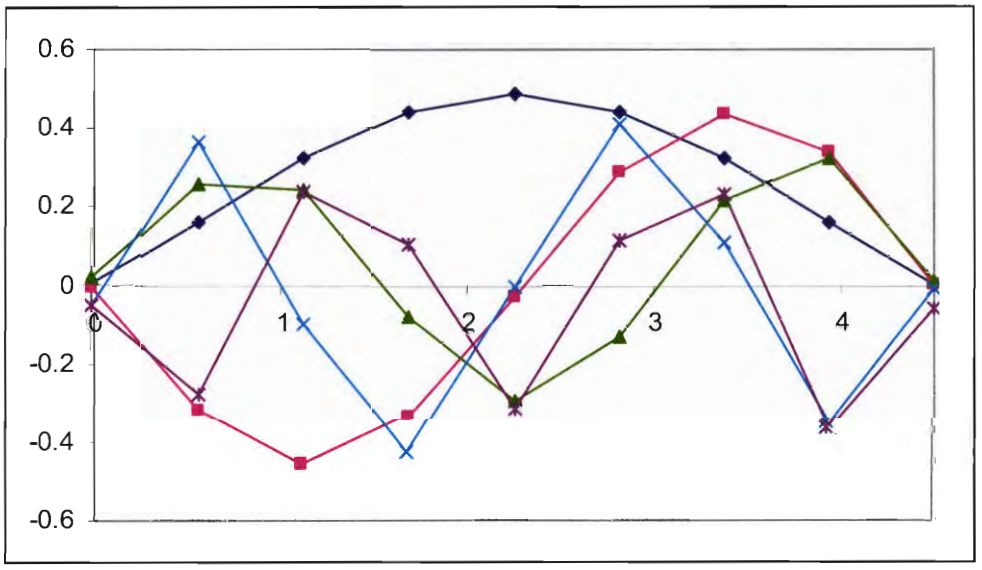


Figure 7.23 Mode shapes obtained from experiment (9 points).

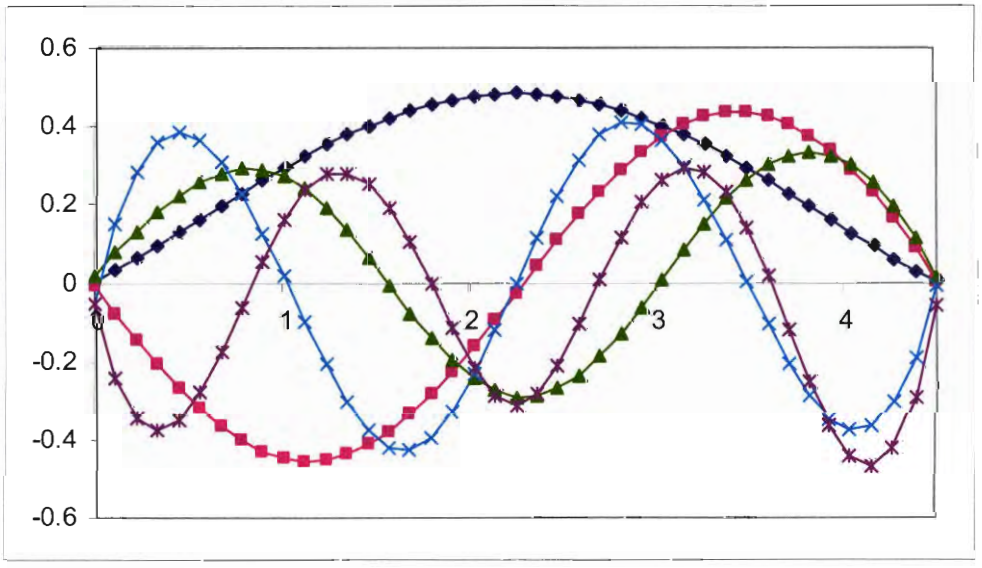


Figure 7.24 Reconstructed mode shapes (41 points).

7.4 Results and Discussions for Beams

7.4.1 Natural Frequency

Natural frequencies are an important dynamic property of any structure. The analytical solution for natural frequency of a linear vibratory system, in the form of a bi-pinned system, is given as follows (Geradin & Rixen 1997):

$$\omega_n^2 = (n\pi)^4 \frac{EI}{\overline{m}L^4} \qquad \text{Equation 7.9}$$

where ω_n is the circular natural frequency of the nth mode of the system with modulus of elasticity E, moment of inertia I, mass per unit length $\overline{m}$ and span length L. The circular natural frequency ω_n can be converted to cyclic natural frequency f_n by dividing it by 2π. From Equation 7.9, a reduction in stiffness (EI) leads to a reduction in the natural frequencies. Likewise, a reduction in natural frequencies can indicate that some form of deterioration has occurred in the system if the system mass remains the same.

If natural frequency decreases in a system, it can be inferred that the system has undergone a state of damage. In this investigation damage was induced by removing sections along span length of the test sample. This resulted in changes in the values of frequencies for the first five modes obtained from modal testing of the undamaged and damaged beams, as shown in Tables 7.2 and 7.3 as well as in Figures 7.25 and 7.26. In the figures, the percentage of reduction in natural frequency is defined as the percentage difference between natural frequencies of undamaged and damaged beams.

As can be seen from Figures 7.25 and 7.26, there is a general increase in the percentage of reduction in natural frequencies for Beam1 and Beam2 as the severity of damage increases, although there are small fluctuations. The percent of change for Beam1 ranges from 0% to about 30% while for Beam2 ranges from -2% to 32%. As more damage is inflicted at different locations of the beams, the flexural capacity is also reduced, causing greater reduction in natural frequencies. The fluctuation in the reduction percentage may be due to the measurement noise that affects the quality of spectra. The trend reinforces the earlier findings for the finite element model in Chapter 6, that is, natural frequency can be used to identify the existence and assess, qualitatively, the extent of damage in timber beams. Other studies conducted by Salawu and Williams (Salawu & Williams 1995) also came to similar conclusions. It is apparent that under the same scenario, last damage cases for Beam 1 and Beam 2, both produce

similarly high reductions in all modes e.g. about 30% for mode 2. This can be seen as a proof for test repeatability. The increase in natural frequencies for mode 4 of damage case 13 to 16 as depicted in Figure 7.26 should not be interpreted as the system is getting stronger, because damage is being induced. This false indication is due to the poor quality of frequency response function as the impact location was very close to the node point of mode 4. As such, it is recommended to carefully scrutinise the modes where node points are close to impact point. It is also observed that in general, the trend associated with the percentage of reduction in natural frequencies is increasing for modes 2 and 3, where the damage effect is more pronounced as the location of damage situated at or close to its anti-node points.

Table 7.2 Comparison of natural frequencies for Beam1.

Mode	Natural frequencies (Hz)						
	Un1	4L	4M	4S	4S6L	4S6M	4S6S
1	13.67	13.34	13.03	11.94	11.86	11.80	11.13
2	37.23	37.21	37.21	37.15	36.98	35.19	31.72
3	91.47	90.72	86.69	77.65	76.93	75.09	72.40
4	132.08	131.53	128.46	124.47	124.26	125.04	122.97
5	227.87	224.82	219.04	209.69	209.75	204.20	196.13

Mode	Natural frequencies (Hz)						
	Un	4S5L6S	4S5M6S	4S5S6S	2L4S5S6S	2M4S5S6S	2S4S5S6S
1	13.67	11.13	11.40	10.86	11.17	11.41	11.77
2	37.23	31.68	31.42	30.68	30.52	29.29	26.05
3	91.47	72.34	72.46	71.66	71.84	69.79	66.46
4	132.08	126.08	122.56	115.52	115.89	113.43	115.33
5	227.87	196.49	196.16	195.24	194.76	192.68	188.79

Table 7.3 Comparison of natural frequencies for Beam2.

Mode	Natural frequencies (Hz)						
	Un2	6L	2L6L	2L4L6L	2L4L6M	2M4L6M	2M4M6M
1	13.19	12.81	12.96	12.84	12.92	12.73	11.85
2	38.21	38.31	37.91	37.79	36.21	34.71	34.70
3	93.70	93.04	92.62	92.02	91.30	89.50	85.24
4	130.06	131.86	130.45	130.58	132.55	129.86	129.35
5	232.96	230.40	229.88	231.34	225.46	217.05	215.39

Mode	Natural frequencies (Hz)						
	Un	2M4M6S	2S4M6S	2S4S6S	2S4S5L6S	2S4S5M6S	2S4S5S6S
1	13.19	12.71	12.72	12.29	11.78	12.64	10.92
2	38.21	31.23	27.96	27.95	28.08	27.67	26.56
3	93.70	82.76	79.96	70.51	75.74	73.30	63.51
4	130.06	129.78	128.65	127.58	124.18	122.87	115.55
5	232.96	206.44	199.53	195.74	196.01	194.85	193.84

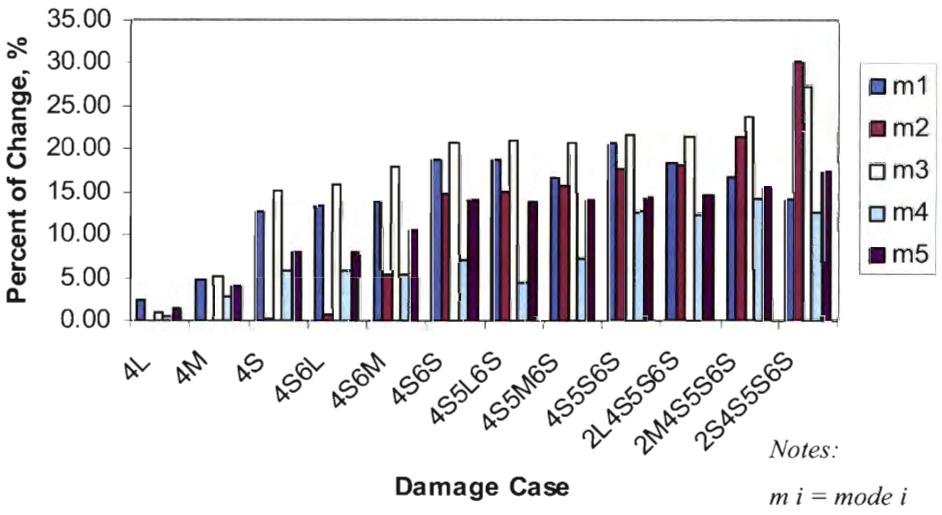


Figure 7.25 Comparison of percentage of drop in natural frequencies for Beam1 for various damage cases.

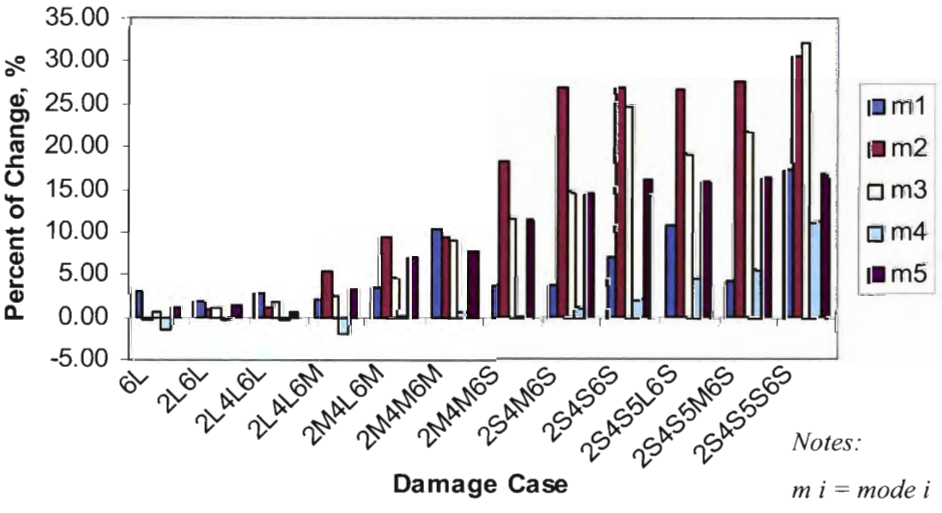


Figure 7.26 Comparison of percentage of drop in natural frequencies for Beam2 for various damage cases.

7.4.2 Damping Ratio

Damping exists in all vibratory systems and responsible for energy dissipation. This is also true for structures even though most exhibit inherently light damping. For free vibration, the loss of energy due to damping in the system results in the decay of the amplitude of motion. The effect of damping is to dissipate energy from the system through the work done by the damping force. The damping is usually quite small and only affects the vibration behaviour significantly near resonance (Bachmann et al. 1995). In this study, damping ratio is used, which represents the ratio of damping coefficient c and critical damping coefficient c_{cr}.

$$\zeta = \frac{c}{c_{cr}} \qquad \text{Equation 7.10}$$

From Tables 7.4 and 7.5, generally, an inconsistent trend for damping ratio is observed in all five modes for Beam1 and Beam2. These damping values cover a wide range from 0.1% to 9.5% for Beam1 and from 0.2% to 15% for Beam2. For example, for mode 2 of Beam1, the damping ratios of all damage cases fluctuate but they are all lower than 1.39% of the Un1. This observation is in contradiction with the general principles in structural dynamics whereby damping ratio increases as damage increases. Another observation is that for both Beam1 and Beam2 and for both damaged and undamaged case the damping ratio associated with mode 1 was the highest and for mode 5, the lowest with a couple of exceptions. Studies conducted by Kato and Shimada (1986) and Salawu and William (1995) came to the same conclusions that a reasonable consistent trend could not be established for damping ratios unlike natural frequencies before and after damage. The reason for such inconsistency is that damping is difficult to evaluate accurately due to the measurement errors introduced by background noise as well as by the interference of the measuring equipment. The damping ratio is estimated from the half-power bandwidth of the FRFs after undergoing the curve fitting process. Thus, the original signal is manipulated and, coupled with the curve-fitting process, produced a less accurate estimation of the damping ratios. In this study, due to the inconsistency of damping ratios, no further investigation is recommended on correlating damping to systems damage.

Table 7.4 Comparison of damping ratios for Beam1.

Mode	Damping ratio (%)						
	Un1	4L	4M	4S	4S6L	4S6M	4S6S
1	3.10	3.66	4.51	3.09	4.34	3.69	3.80
2	1.39	1.10	1.14	1.37	1.36	1.20	1.01
3	1.23	0.12	1.70	3.77	3.55	2.05	2.29
4	2.77	0.63	1.62	3.54	1.59	2.96	2.71
5	0.39	0.75	0.94	1.29	1.31	1.12	1.08

Mode	Damping ratio (%)						
	Un1	4S5L6S	4S5M6S	4S5S6S	2L4S5S6S	2M4S5S6S	2S4S5S6S
1	3.10	4.03	9.47	3.11	5.56	5.92	5.89
2	1.39	0.99	1.17	0.98	1.01	0.88	1.07
3	1.23	2.59	1.70	1.91	2.03	1.71	2.82
4	2.77	0.60	2.09	1.78	1.75	2.59	2.21
5	0.39	0.93	0.60	0.77	0.13	0.78	0.74

Table 7.5 Comparison of damping ratios for Beam2.

Mode	Damping ratio (%)						
	Un2	6L	2L6L	2L4L6L	2L4L6M	2M4L6M	2M4M6M
1	1.97	3.37	4.58	6.42	3.98	8.26	5.93
2	0.76	1.01	0.94	1.18	0.89	0.82	0.73
3	0.96	1.24	1.12	1.57	1.18	1.38	1.20
4	2.70	2.52	3.43	2.81	1.40	3.11	3.09
5	0.39	0.19	1.44	0.19	0.38	0.88	0.77

Mode	Damping ratio (%)						
	Un2	2M4M6S	2S4M6S	2S4S6S	2S4S5L6S	2S4S5M6S	2S4S5S6S
1	1.97	2.98	3.34	4.44	11.47	15.12	5.64
2	0.76	0.77	0.92	0.91	0.8	0.94	1.27
3	0.96	0.71	0.49	1.2	2.38	3.48	4.56
4	2.7	2.98	2.59	0.81	2.19	1.8	1.2
5	0.39	0.88	0.82	0.45	0.54	0.4	0.86

7.4.3 Effects of Sensor Density

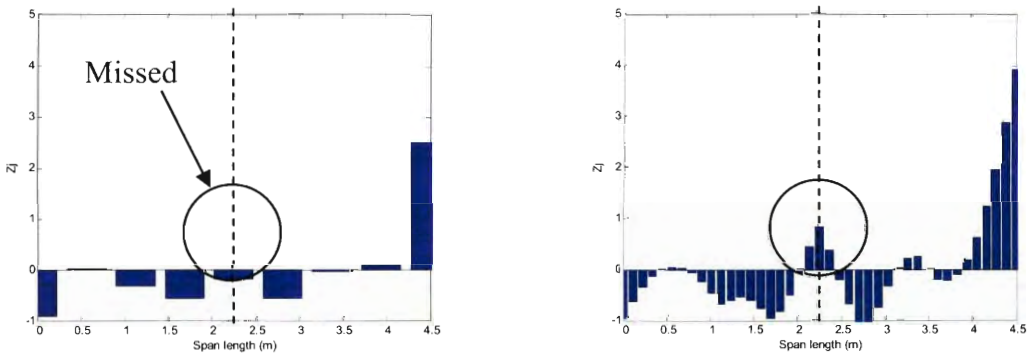
The density of sensors (accelerometers) is an important factor in reliable damage detection using vibration based methods. The selection of number and location of sensors in a structure have a major influence on the quality of the damage detection (Stubbs & Park 1996; Wang & Zong 2002). It is commonly acknowledged that as more information is obtained, the damage detection will be more accurate. When the collected data is below a certain level, the results of damage detection inevitably become unreliable. This implies that a large number of sensors are preferred in a modal test to produce accurate damage detection results. However, it is often found that it is impractical and very costly to have a dense sensor array. This is unlike the finite element model, where the density of the sensors is linked to the mesh size and can be easily changed. In the experimental work, a reasonable number of sensors are essential

to balance the pros and cons of an optimal damage detection process. In this investigation, nine equally spaced sensors were used to acquire the accelerations of the test samples in the modal tests. With the cubic spline interpolation technique, the limited experimental data was expanded to forty one data points, which would enhance the effectiveness of the damage detection.

The comparison between the 'as is' data and the reconstructed data using cubic spline and its effect of damage detection can be demonstrated using the modified damage index I (MDI-I) damage localisation algorithm with either the first two or first five flexural modes on various damage scenarios. In the following results, all damage indicator indices, *Zj*, for each damage case are plotted against the beam span length. In principle, the statistically normalised damage indicator values *Zj* larger than zero (the probability-based criterion for damage), indicates that damage has occurred at that location. The actual damage locations are indicated with vertical dashed lines in all figures. For cubic spline, Matlab (The Mathwork Inc. 2005) provides an easy access to the data interpolation using Spline function. A tri-diagonal linear system is being solved for the information needed to describe the coefficients of the various cubic polynomials which make up the interpolating spline.

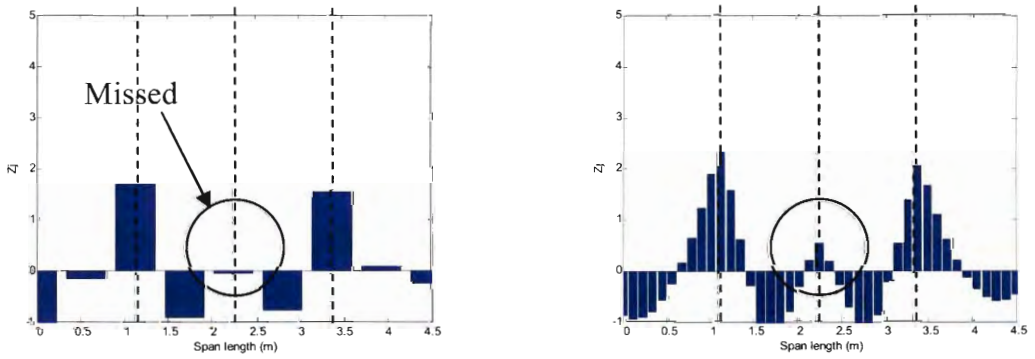
From Figure 7.27a, the 'as is' data used in the damage detection with the first five flexural modes is unable to identify the location of damage at midspan (2.25m) for case 4L. While in Figure 7.27b, the damage localisation algorithm using the data after the reconstruction has clearly detected the location of damage although there are also a few spurious damage locations. In the multiple damage location scenarios using 'as is' data in the algorithm, often tends to 'miss' some damage locations, while, using the reconstructed data will prevent this. In Figures 7.28a and 7.30a, the damage location at midspan was not identified but was detected in Figures 7.28b and 7.30b for damage case 2L4l6L and 2S4M6S, respectively. The actual damage at midspan was completely missed by just using the 'as is' data in the damage localisation algorithm computation. This may be due to the curvature estimation at the midspan being overshadowed by the existence of the two adjacent equal or higher severity of damage. With more data point interpolated in between them, the actual difference of curvature between two adjacent actual damage locations can be better defined. Hence, from the reconstructed data, the actual damage at midspan is not subsided. This explanation is also applicable to the damage cases in Figure 7.29 whereby the more severe damage has overwhelmed the two less severe damage locations in the 'as is' situation causing the submergence of the

two actual damage locations. Employing the cubic spline interpolation for data reconstruction, the missing damage locations resurfaced as shown in Figure 7.29b. In summary, it is clear that without sufficient number of sensors (either measured or reconstructed), the damage localisation method, MDI-I, in many circumstances cannot detect the actual damage location.



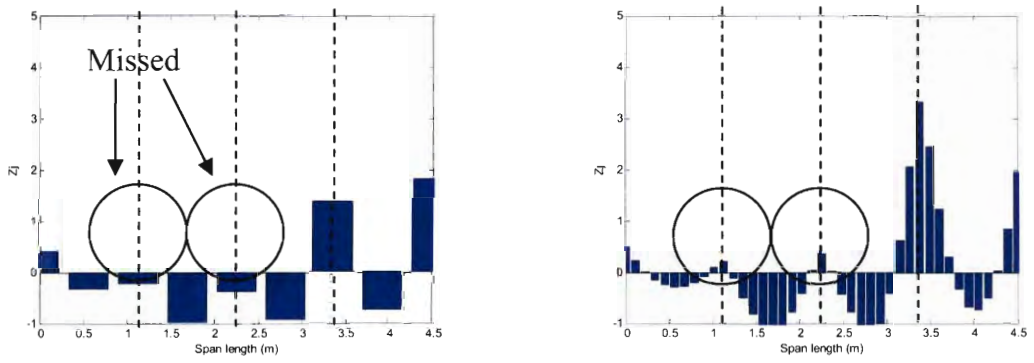
(a) As is (b) Cubic spline

Figure 7.27 Single damage scenario 4L inflicted at midspan (5 modes used).



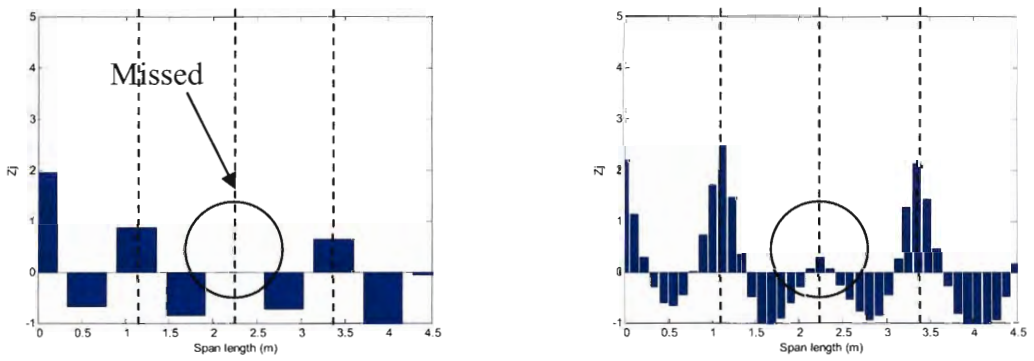
(a) As is (b) Cubic spline

Figure 7.28 Three damage scenario 2L4L6L inflicted at ¼, mid and ¾ span (2 modes used).



(a) As is (b) Cubic spline

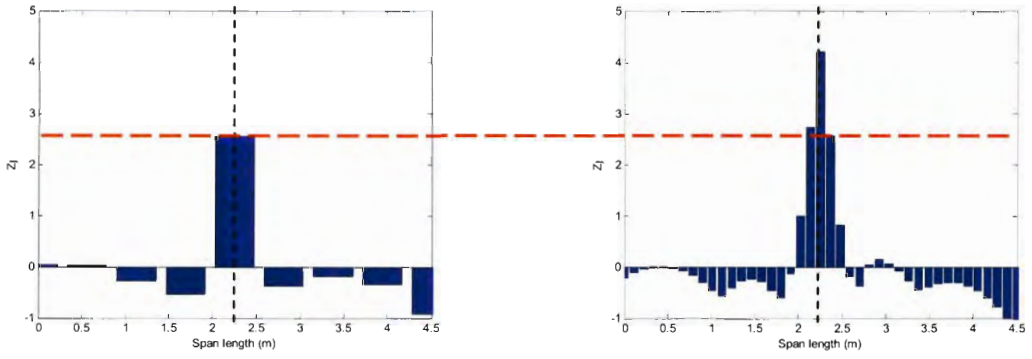
Figure 7.29 Three damage scenario 2M4M6S inflicted at ¼, mid and ¾ span (2 modes used).



(a) As is (b) Cubic spline

Figure 7.30 Three damage scenario 2S4M6S inflicted at ¼, mid and ¾ span (5 modes used).

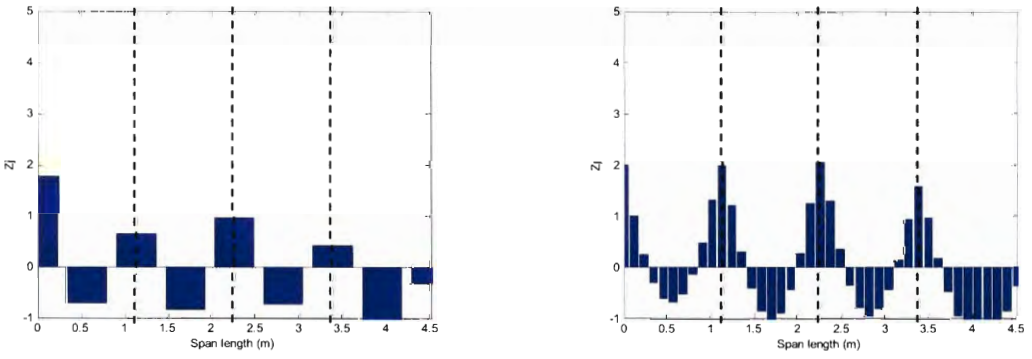
Besides pin pointing actual damage locations, the reconstruction of mode shape, using the cubic spline interpolation technique in the reconstructed result, has helped to increase the damage index value from 2.5 in the 'as is' results to 4.0 for the case 4M as depicted in Figures 7.31a and 7.31b, respectively. The enhancement of the damage index values is important to establish the existence of damage at a location, with higher confidence in deciding a damage site. This promising trend was observed in all damage cases conducted in this investigation.



(a) As is (b) Cubic spline

Figure 7.31 Single damage scenario 4M inflicted at midspan (5 modes used).

The reconstruction technique, if not working better, it at least performs equally good compared to merely using the 'as is' data to calculate the damage indices. This is illustrated in Figure 7.32, whereby both 'as is' data and the results from cubic spline technique used in damage localisation method were able to identify all damage locations. Considering the practicality of field testing, to reconstruct mode shapes in order to produce sufficiently fine coordinates is an essential part of the damage localisation process. From the damage cases discussed above, it can be concluded that data reconstructed with the cubic spline interpolation technique has improved detection of damage. Therefore, in the following discussions, the cubic spline interpolation technique is used for the reconstruction of mode shapes (41 data points) from the given 'as is' data (9 data points) for each beam in this investigation.



(a) As is (b) Cubic spline

Figure 7.32 Three damage scenario 2S4S6S inflicted at ¼, mid and ¾ span (5 modes used).

7.4.4 Mode Shape Reconstruction Techniques

Many researchers considered that Shannon's sampling theory provided good results in reconstruction of the mode shape vector (Peterson, McLean & Pollock 2003; Peterson et al. 2001a, 2001b; Stubbs & Park 1996). Therefore, subsequent to the comparison between 'as is' and cubic spline, a comparative study on the effect of reconstructing mode shapes with limited number of sensors using Shannon's sampling theorem and cubic spline was carried out. In order to make comparison, the modified damage index I (MDI-I) method with multiple damage scenarios simulated using a finite element (FE) model of a timber beam was employed. Both the Shannon's sampling theorem and cubic spline were applied to reconstruct mode shapes (41 points) from a coarser mesh (9 points) FE model. The reconstructed mode shapes from both techniques were then applied to the MDI-I method for comparison.

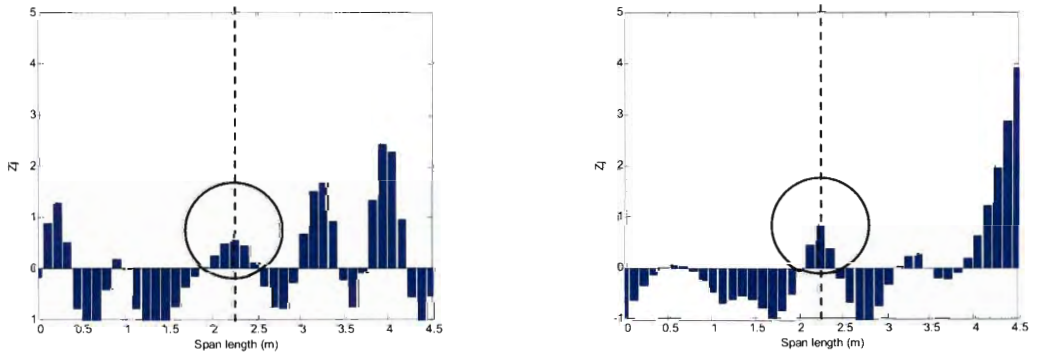
Shannon's sampling theorem defines correct interpolated signal values at points equally spaced between the samples. In here, the variables of interest are the position of the sensors on the beam. The interpolated mode shape should represent the exact reconstruction of the mode shape of interest when the summation is for all 'n' data points between minus and plus infinity, i.e., for an infinite number of spatially repeated experimental mode shape vectors. Acceptable results can be obtained using several repeats of the experimental mode shape coordinates, i.e., for a finite range of values of 'n'. The governing equation is shown in Equation 7.11. A more detailed explanation of how to apply Shannon's sampling theorem to reconstruct mode shapes can be found in (Park & Stubbs 1995).

$$S(x) = \sum_{n=-\infty}^{\infty} S(nT) \frac{\sin \pi(\frac{x}{T} - n)}{\pi(\frac{x}{T} - n)} \qquad \text{Equation 7.11}$$

where $S(x)$ and $S(nT)$ represent the values which are interpolated along x (the span length) and the sampling points from sensors, respectively. T is the spacing between the sensors.

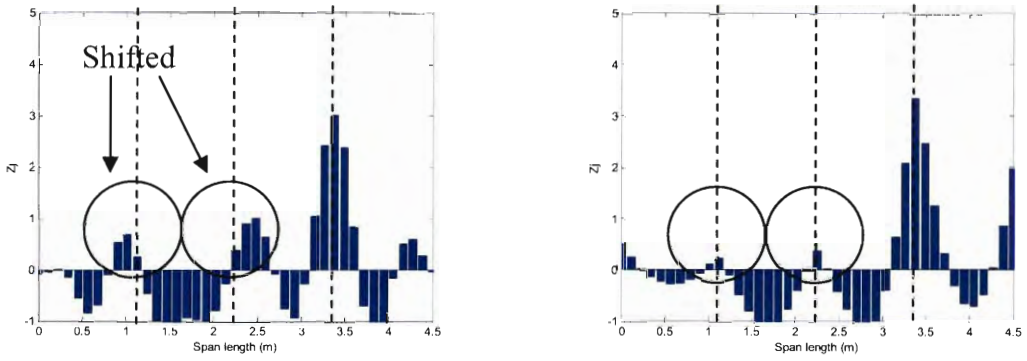
For the case 4L as shown in Figure 7.33, the light damage was detected using both Shannon's sampling theorem and cubic spline mode shape reconstruction techniques. However, the former presented more spurious damage locations than the latter one. Furthermore, Shannon's sampling theorem used in the damage detection algorithm may shift the actual damage location as shown in Figure 7.34a for damage

position ¼ and midspan, while the cubic spline technique successfully identified the actual damage locations (see Figure 7.34b). Using the Shannon's sampling theorem to reconstruct the mode shape, the light damage at ¾ of the span length was not detected as shown in Figure 7.35a for case 4S6L. In Figure 7.35b, when cubic spline was used, all damage regions were detected. Similar phenomenon is observed for case 2S4M6S as shown in Figure 7.36, whereby the medium damage at midspan was not identified using Shannon's sampling theorem (see Figure 7.36a) but was identified using the cubic spline (see Figure 7.36b). For case 2S4S5S6S, as illustrated in Figure 7.37, the severe damage at location 1/8 of the span length (1.125m) was not identified using Shannon's sampling theorem (see Figure 7.37a) but was detected by the cubic spline (see Figure 7.37b). The advantage of cubic spline is again confirmed with respect to the damage cases presented here. It reinforces that, in the following discussion, the cubic spline interpolation technique should be used for the reconstruction of mode shapes (41 data points) from the given 'as is' data (9 data points) for each beam in this investigation.



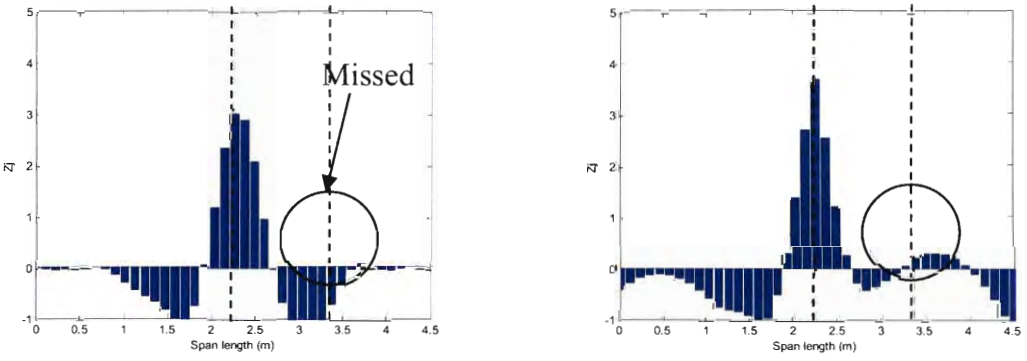
(a) Shannon's sampling theorem. (b) Cubic spline.

Figure 7.33 Single damage scenario 4L inflicted at midspan (5 modes used).



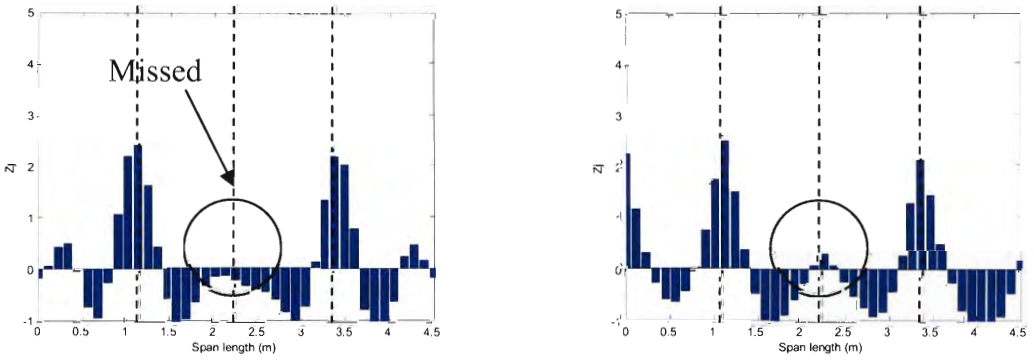
(a) Shannon's sampling theorem. (b) Cubic spline.

Figure 7.34 Three damage scenario 2M4M6S inflicted at ¼, mid and ¾ span (5 modes used).



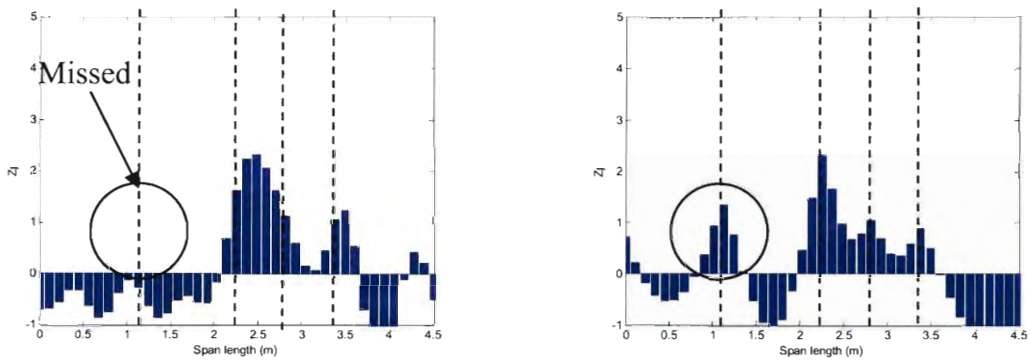
(a) Shannon's sampling theorem. (b) Cubic spline.

Figure 7.35 Two damage scenario 4S6L inflicted at mid and ¾ span (2 modes used).



(a) Shannon's sampling theorem. (b) Cubic spline.

Figure 7.36 Three damage scenario 2S4M6S inflicted at ¼, mid and ¾ span (5 modes used).



(a) Shannon's sampling theorem. (b) Cubic spline.

Figure 7.37 Four damage scenario 2S4S65SS inflicted at ¼, mid, 5/8 and ¾ span (5 modes used).

7.4.5 Damage Localisation

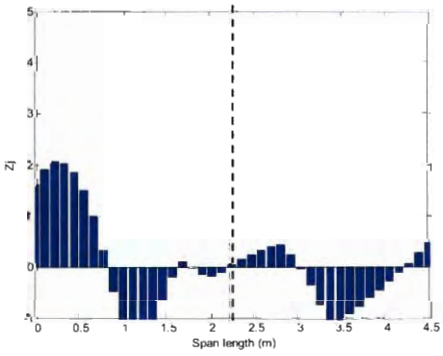
For damage localisation, the first two and first five flexural modes were used in the damage detection (DD) algorithms. The formulations of the DD algorithms used in the following discussions were presented in details in Chapter 5. Changes in flexibility algorithm are not used in the experimental results as it was found not effective in damage detection compared to the damage index methods in the analytical investigation in Chapter 6. As mentioned earlier, the first two flexural modes are commonly used (Peterson et al. 2001b) as these modes are easily acquired. However, the first two modes may not be sufficient to identify closely spaced damage scenarios, hence, it is suggested to adopt the first five flexural modes in the DD algorithms (Garcia, Osegueda & Meza 1998). In addition, with the development of the latest technologies in sensors, it is possible nowadays to obtain higher modes of a structural system. This would definitely help to promote the use of higher modes in damage detection.

7.4.5.1 Damage Index I

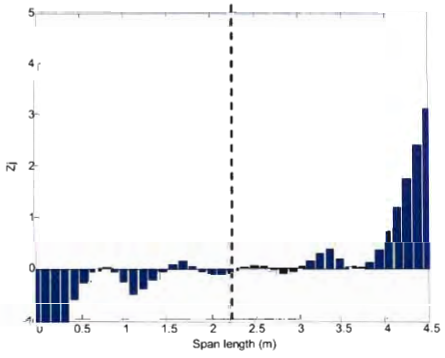
The single damage predictions using the damage index I (DI-I) method and adopting the first two and first five flexural modes are illustrated in Figure 7.38. In Figure 7.38, the statistically normalised damage indicators (*Zj*) are plotted against the span length of the beam. For single damage cases using the first two modes, the damage indicator is able to locate the damage location at midspan (2.25m) for the cases 4M and

4S, and at ¾ span (3.375m) for case 6L as shown in Figures 7.38e, 7.38g and 7.38c, respectively. From Figure 7.38a, the damage location at midspan is not distinctly indicated for the case 4L. In general, the DI-I algorithm is able to capture single damage scenarios but the results are contaminated with spurious damage locations or false positives (indication of false damage locations).

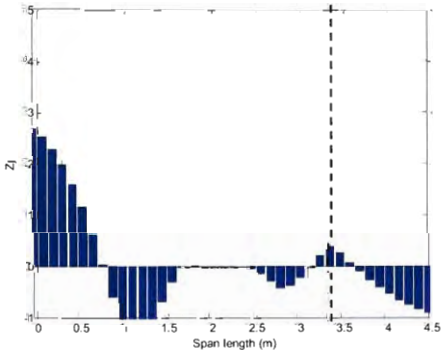
As a comparison, the DI-I method was applied for similar single damage cases using the first five flexural modes. For the light damage cases 4L and 6L as depicted in Figures 7.38b and 7.38d, the damage indicator fails to locate the damage at mid and ¾ span, respectively. For the medium and severe damage cases 4M and 4S as illustrated in Figures 7.38f and 7.38h, respectively, the damage locations are detected quite pronouncedly at the midspan even though there are still many appearances of false positives. For single damage cases, comparing the results of the DI-I method using the first two and first five flexural modes, shows that incorporating higher modes in the damage localisation method may produce better results for cases of medium or severe damage than just using the two lower modes, if one can overcome the false positive problem.



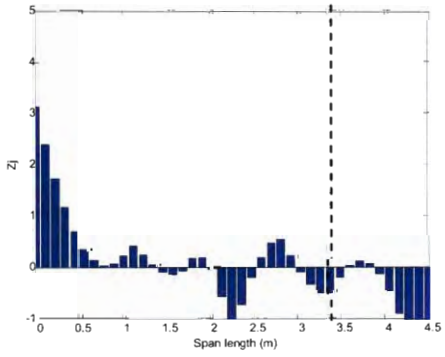
(a) 4L (2 modes).



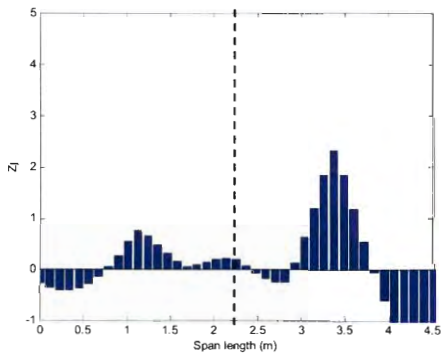
(b) 4L (5 modes).



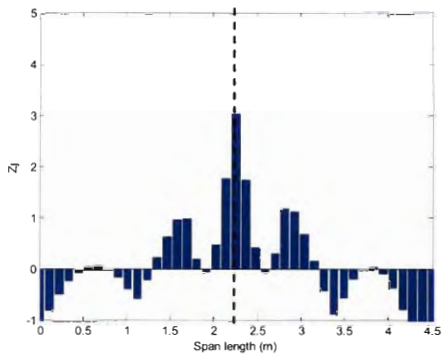
(c) 6L (2 modes).



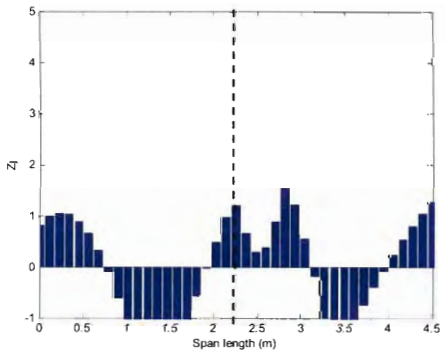
(d) 6L (5 modes).



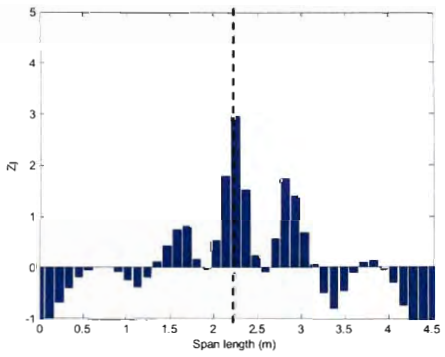
(e) 4M (2 modes).



(f) 4M (5 modes).



(g) 4S (2 modes).

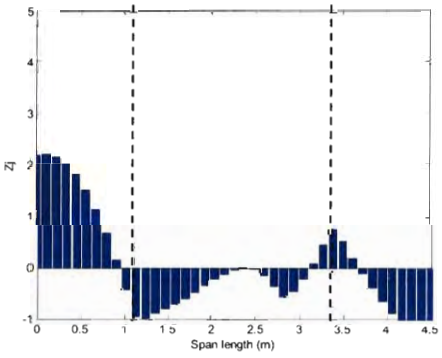


(h) 4S (5 modes).

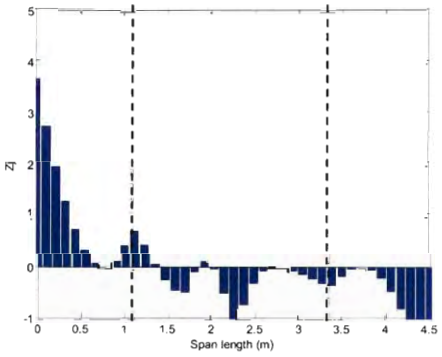
Figure 7.38 Single damage cases using DI-I method.

Shown in Figure 7.39 is the DI-I method applied to the double damage locations. Using the first two flexural modes in the method (see Figures 7.39a, 7.39c, 7.39e and 7.39g), basically all damage locations were identified, except for case 2L6L where the ¼ span (1.125m) damage was missed as depicted in Figure 7.39a. However, the damage indicator has provided a misleading representation of the probability of existence of damage as shown in Figures 7.39c, 7.39e and 7.39g. They show that less severe damage at ¾ span (3.375m) has a higher index value compared to the severe damage at midspan (2.25m). It is also worth noting here that the peak of a group of damage indicator elements (like a hump) at the midspan region (see Figures 7.39c, 7.39e and 7.39g) is not actually at the actual damage location at position 2.25m, instead is shifted by one element to the left. From the results of using the first five flexural modes in the method for two damage cases (see Figures 7.39b, 7.39d, 7.39f and 7.39h), the damage indicator identified only one damage location either at midspan or at ¾ span. In addition, the results were filled with many false positives, hence considerably

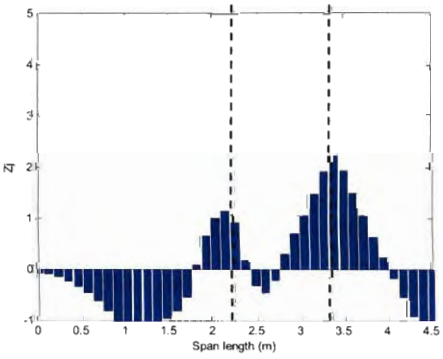
reducing the effectiveness of the localisation algorithm. For the two damage location cases, using the first two flexural modes in the DI-I method offers a better damage indication compared to using the first five flexural modes.



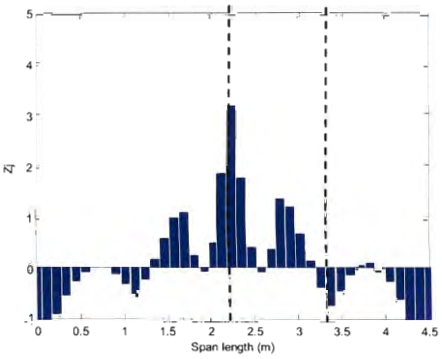
(a) 2L6L (2 modes).



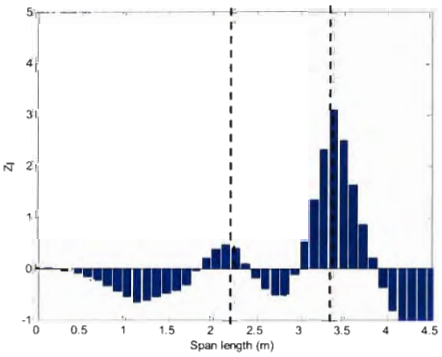
(b) 2L6L (5 modes).



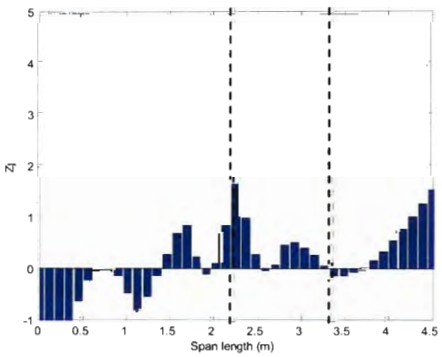
(c) 4S6L (2 modes).



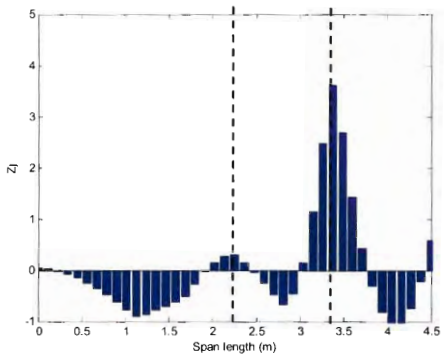
(d) 4S6L (5 modes).



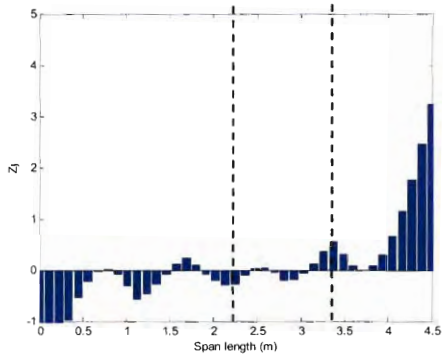
(e) 4S6M (2 modes).



(f) 4S6M (5 modes).



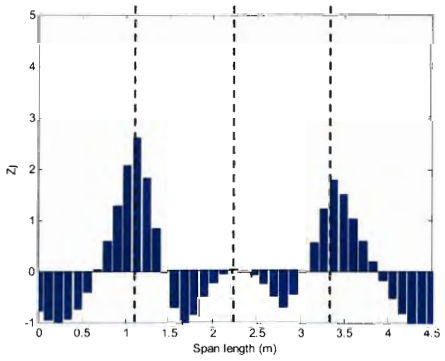
(g) 4S6S (2 modes).



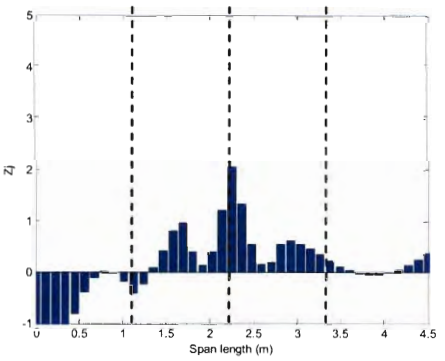
(h) 4S6S (5 modes).

Figure 7.39 Two damage cases using DI-I method.

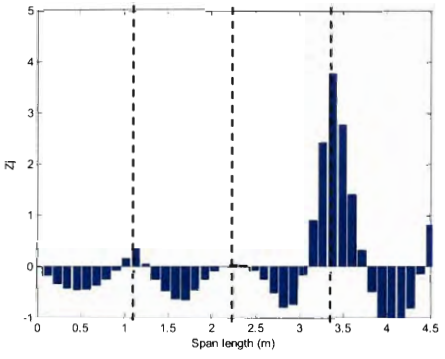
For three damage location cases, the results of the damage detection using the DI-I method are shown in Figure 7.40. By using the first two flexural modes in the damage index method (see Figures 7.40a, 7.40c, 7.40e and 7.40g) two out of three actual damage locations were clearly detected except for case 2M4M6S in Figure 7.40c, where the two medium damage locations at ¼ (1.125m) and midspan (2.25m) were not clearly detected. The low probability of damage (*Zj*) for the middle damage location for cases 2L4L6L, 2S4S6S and 4S5S6S may be due to the dominating contribution of second mode shape curvature in the DI-I algorithm, thus causing the suppression of damage index at the region of contra flexure at midspan for this mode. It is possible to infer that using the first two flexural modes in the DI-I algorithm computation for three damage location scenarios produces some misleading information about the damage situation. By using the first five flexural modes in the algorithm for the three damage scenarios as illustrated in Figures 7.40b, 7.40d, 7.40f and 7.40h, the damage indicator did not find the damage properly. However, for the case of 4S5S6S in Figure 7.40h, the damage was identified at location 2.8125m (5/8 span), which was missed when using the first two flexural modes in the algorithm. This has shed some light on the contribution of higher modes to detect certain damage sites that may not be possible by using just the first two lower modes in the DI-I method.



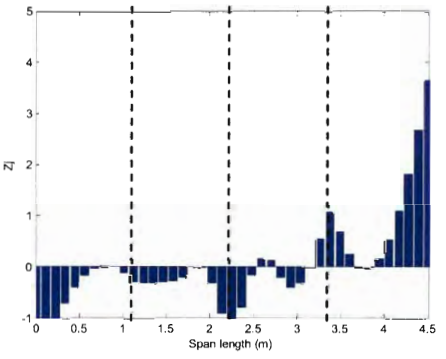
(a) 2L4L6L (2 modes).



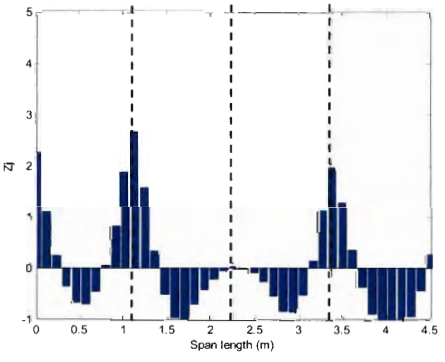
(b) 2L4L6L (5 modes).



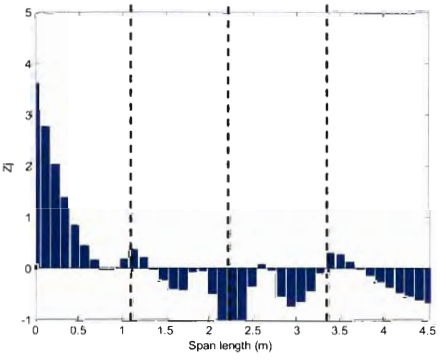
(c) 2M4M6S (2 modes).



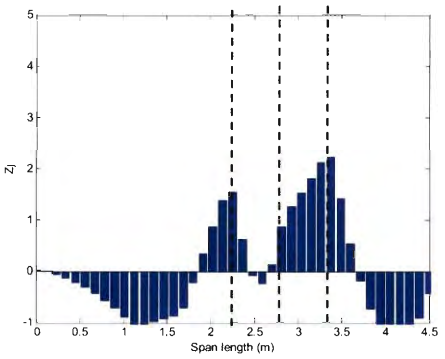
(d) 2M4M6S (5 modes).



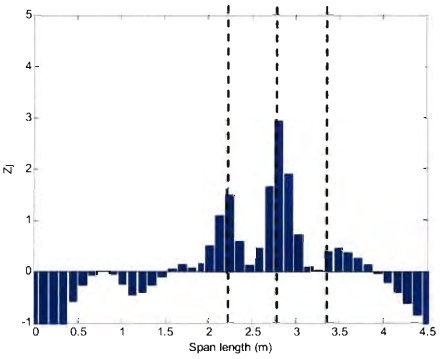
(e) 2S4S6S (2 modes).



(f) 2S4S6S (5 modes).



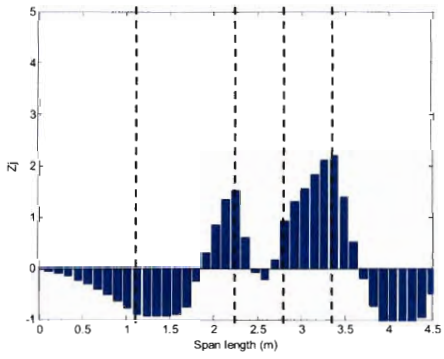
(g) 4S5S6S (2 modes).



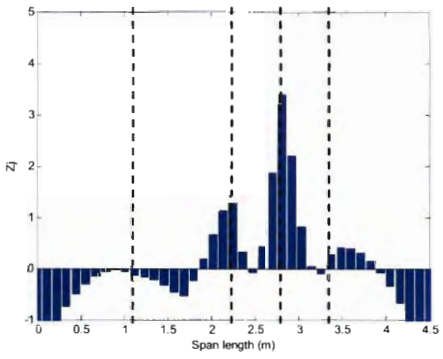
(h) 4S5S6S (5 modes).

Figure 7.40 Three damage cases using DI-I method.

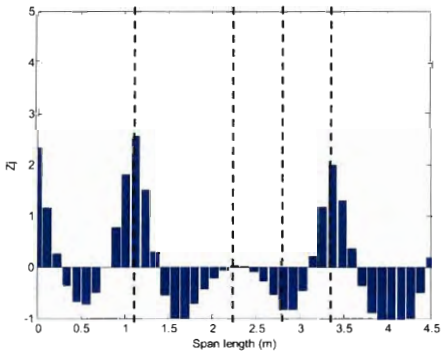
The results of applying the DI-I method for damage detection in four damage location scenarios are illustrated in Figure 7.41. The damage locations were not all accurately captured by the damage indicator. The performance using the first two modes was better than using the first five modes in the damage localisation but the latter may identify certain damage not detected by the former. This observation is clear in Figures 7.41e and 7.41f, where the damage indicator applied with the first two modes identified two damage locations at positions 1.125m and 3.375m out of the four inflicted damage. But using the first five modes, the damage at position 2.8125m was also identified, which was not captured by using the first two modes. This confirms the findings in the three damage scenarios earlier. In general, considering all damage cases discussed in this section, the DI-I method using the first two flexural modes has provided a better damage indicator than using the first five modes. However, using the first two modes in the algorithm has not performed well enough to comfortably detect damage, especially for multiple damage scenarios as it presented certain misleading information on the actual damage. Hence, it is important to overcome these shortcomings in order to offer a more reliable damage detection procedure.



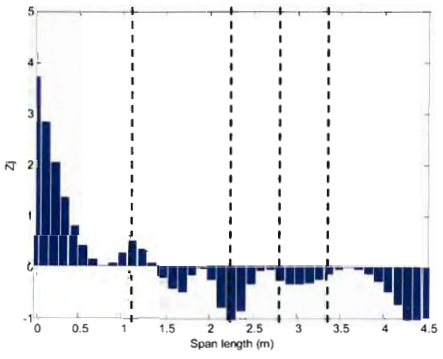
(a) 2L4S5S6S (2 modes).



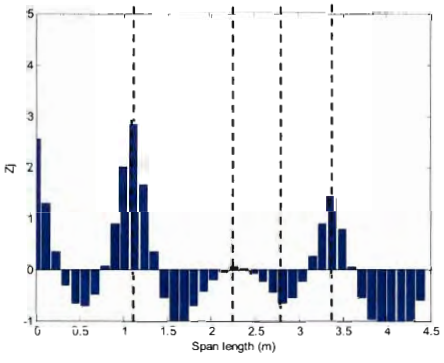
(b) 2L4S5S6S (5 modes).



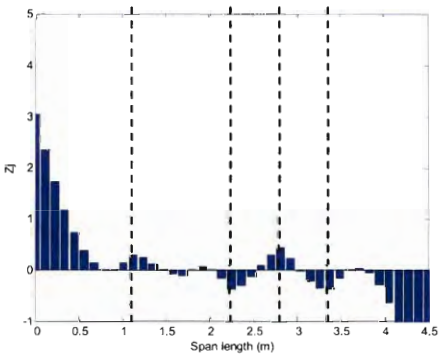
(c) 2S4S5L6S (2 modes).



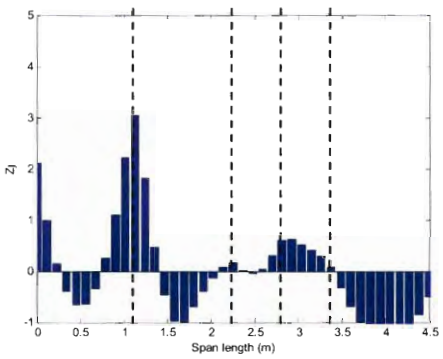
(d) 2S4S5L6S (5 modes).



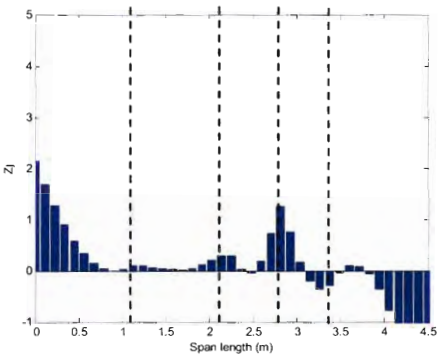
(e) 2S4S5M6S (2 modes).



(f) 2S4S5M6S (5 modes).



(g) 2S4S5S6S (2 modes).

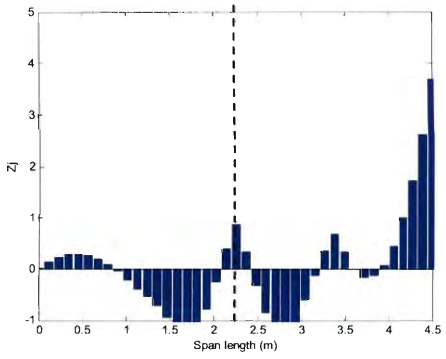


(h) 2S4S5S6S (5 modes).

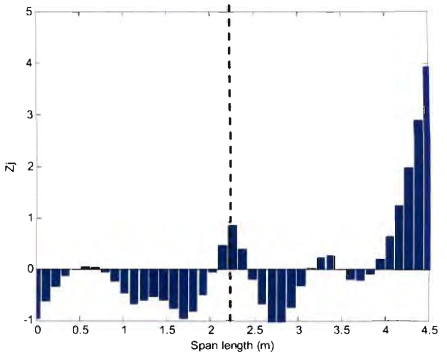
Figure 7.41 Four damage cases using DI-I method.

7.4.5.2 Modified Damage Index I

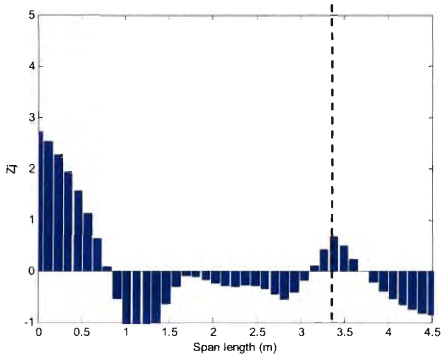
The investigation in previous section clearly shows that the contribution of higher modes can help in detecting damage but somehow it also distorted the results. Based on the results of the investigation in the preceding section, the modified damage index I (MDI-I) algorithm is proposed. In the modified DI-I, mode shape curvatures are normalised which prevents higher modes to distort the damage index. The damage indicator (Z_j) for single damage scenarios computed using the first two and first five flexural modes in the proposed MDI-I method are shown in Figure 7.42. From Figures 7.42a, 7.42e and 7.42g, the midspan (2.25m) damage is clearly pinpointed for cases 4L, 4M and 4S, respectively, as well as the damage at ¾ span (3.375m) for case 6L of Figure 7.42c for damage localisation using the first two flexural modes. However, there are some false positives also present. For the damage indicator produced by the first five modes, the damage detection results are equally good compared to the two mode ones. It is quite clear that comparing the MDI-I method with its original formula DI-I in the single damage cases, the modified method performs better in capturing the actual damage location with a more distinct peak at the actual damage locations. In addition, unlike its original form, the modified method is also able to incorporate higher modes in the algorithm without losing its capability. This has made the MDI-I method less dependant on selection of modes and can significantly improve the reliability of damage detection using modal strain energy.



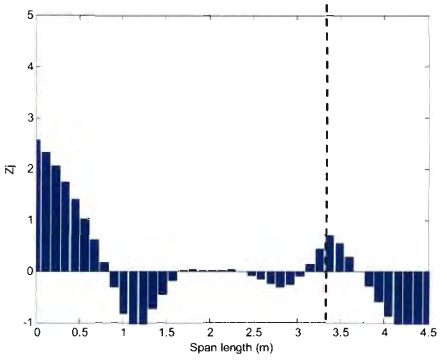
(a) 4L (2 modes).



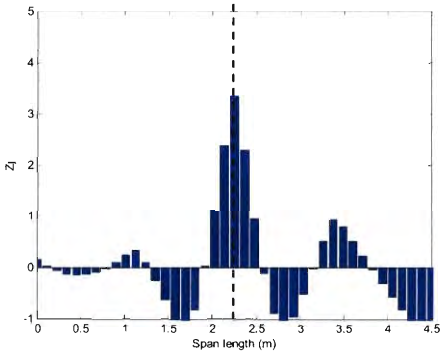
(b) 4L (5 modes).



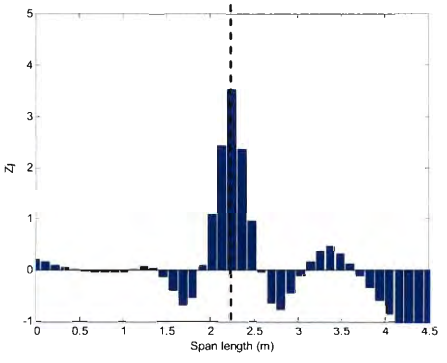
(c) 6L (2 modes).



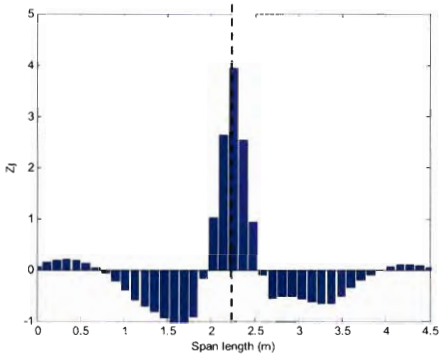
(d) 6L (5 modes).



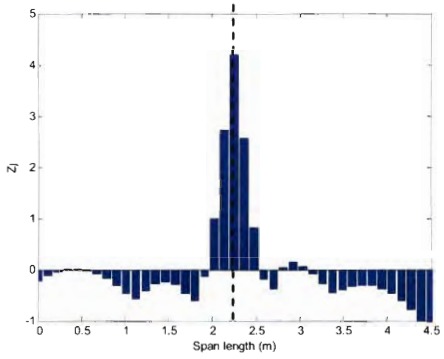
(e) 4M (2 modes).



(f) 4M (5 modes).



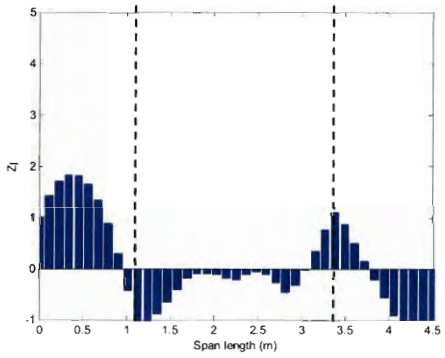
(g) 4S (2 modes).



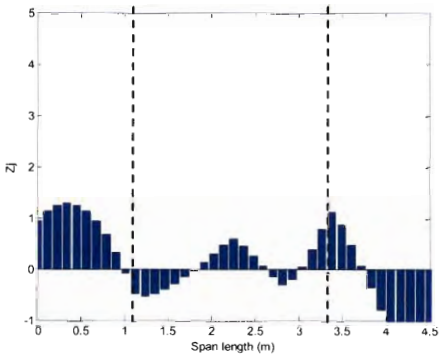
(h) 4S (5 modes).

Figure 7.42 Single damage cases using MDI-I method.

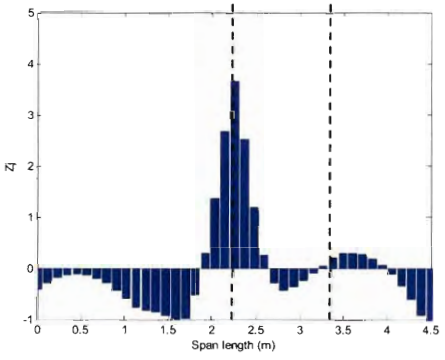
The results for two damage cases using the MDI-I method are presented in Figure 7.43. Basically, using the modified method, all the damage locations are identified except for one light damage location, namely, cases 2L6L and 4S6L at ¼ span (1.125m) and ¾ span (3.375m), respectively. For the cases 4S6M and 4S6S in Figures 7.43e to 7.43h, using the first five modes in the calculations yields a better representation of the damage than using two modes. For instance in the case 4S6M (see Figure 7.43e), the index value of the medium damage at ¾ span is quite similar to the severe damage at the midspan, which does not truly reflect the actual damage scenario. While using five modes in the MDI-I method (see Figure 7.43f), a more reasonable trend in damage level between medium and severe damage (damage index values of 1.5 and 3.5, respectively) is observed. In general, for two damage location cases, the MDI-I method is able to indicate the damage location better than the DI-I method. Between using two and five modes in the MDI-I method, the latter is more superior in addressing the damage severity qualitatively, even though both methods are locating well the damage sites.



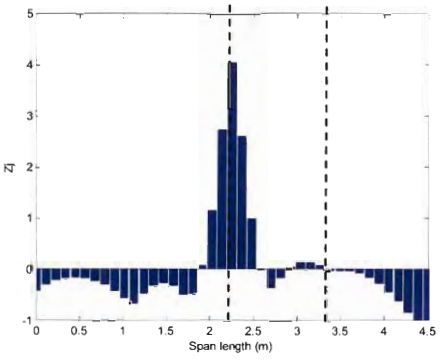
(a) 2L6L (2 modes).



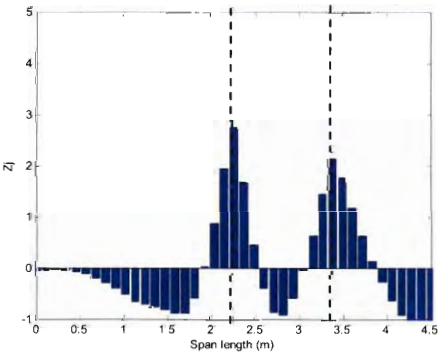
(b) 2L6L (5 modes).



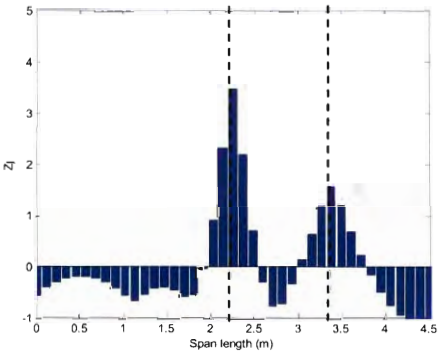
(c) 4S6L (2 modes).



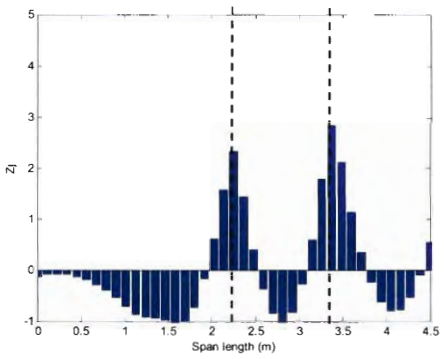
(d) 4S6L (5 modes).



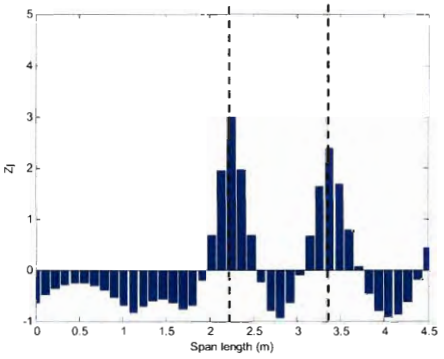
(e) 4S6M (2 modes).



(f) 4S6M (5 modes).



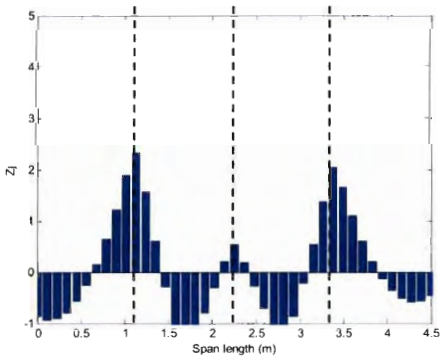
(g) 4S6S (2 modes).



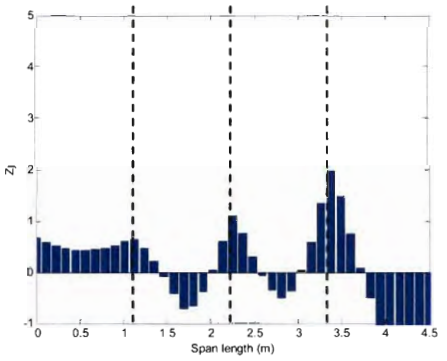
(h) 4S6S (5 modes).

Figure 7.43 Two damage cases using MDI-I method.

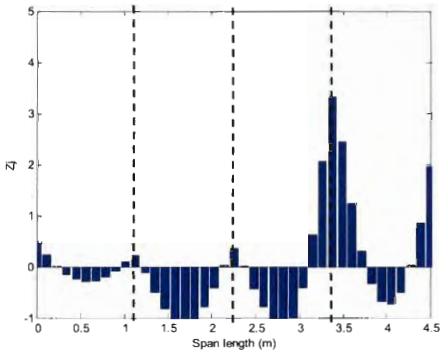
The damage detection using the MDI-I method for three damage location cases are shown in Figure 7.44. The algorithm is able to identify all three damage locations except for case 45S6S (2 modes) in Figure 7.44g which has not distinctly spotted the damage locations by a peak among the lump of damage index values at position 2.8125m. By adopting higher modes (5 modes) in the method, the damage indicator is capable of boosting the damage identification for more damage location scenarios. For example, referring to Figures 7.44c and 7.44d of case 2M4M6S, the damage indices in the vicinity of ¼ span (1.125m) has exhibited a small peak to indicate a damage when using the first two modes in the method, but when using the first five modes, the advent of a higher peak is a more distinct sign of damage site. This phenomenon is also shown in case 4S5S6S (see Figures 7.44g and 7.44h). Furthermore, espousing higher modes evens up the contribution of selected modes. This is quite apparent in case 2L4L6L, whereby Figure 7.44b (5 modes) has a more evenly distributed damage index values compared to Figure 7.44a (2 modes) for damage with similar severity level. It is therefore inferred that for the three damage location scenarios the MDI-I method achieves better damage localisation compared to the DI-I method. It confirms that applying the MDI-I method and including the higher modes offer more advantages in detecting damage compared to just using the two lower modes.



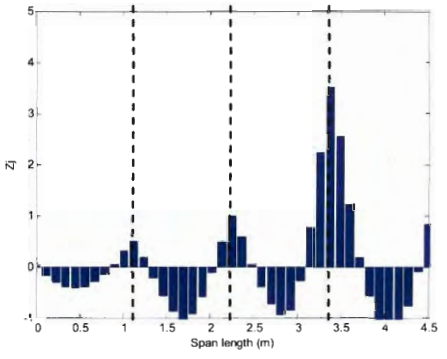
(a) 2L4L6L (2 modes).



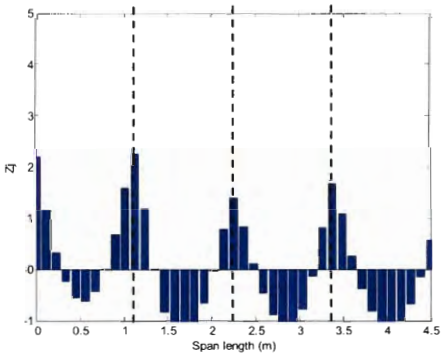
(b) 2L4L6L (5 modes).



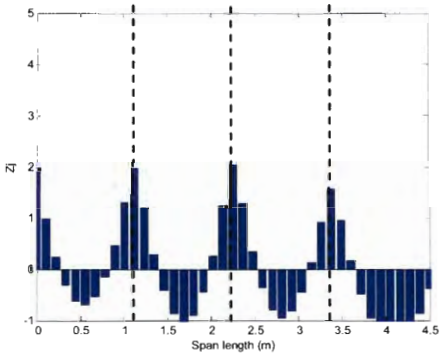
(c) 2M4M6S (2 modes).



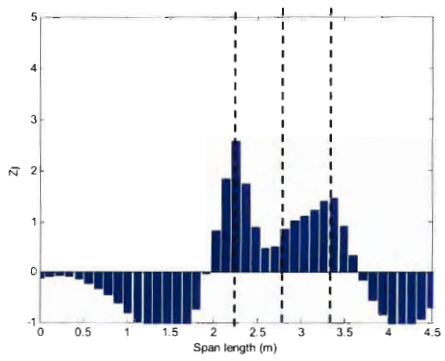
(d) 2M4M6S (5 modes).



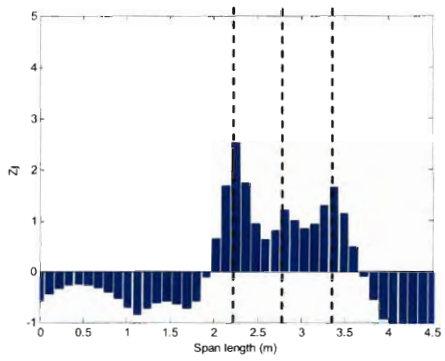
(e) 2S4S6S (2 modes).



(f) 2S4S6S (5 modes).



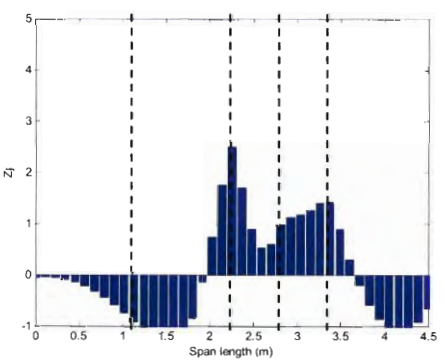
(g) 4S5S6S (2 modes).



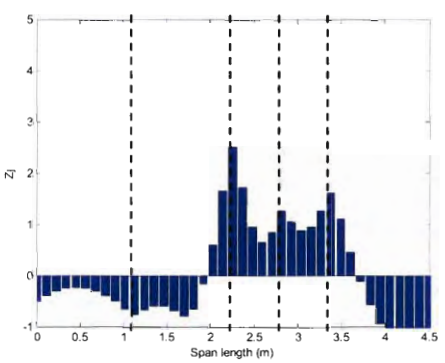
(h) 4S5S6S (5 modes).

Figure 7.44 Three damage cases using MDI-I method.

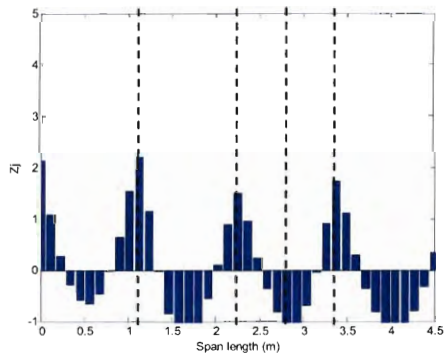
Figure 7.45 illustrates the damage detection results for the four damage location scenarios using the first two and first five flexural modes with the MDI-I method. Using the first two modes, the method is able to identify all severe damage locations except for damage at position 2.8125m for cases 2L4S5S6S (see Figure 7.45a) and 2S4S5S6S (see Figure 7.45g) as well as all light and medium damage. The light and medium damage were eclipsed amongst the severe damage locations, which may be due to the fact that the changes in curvature for the light and medium damage are not significant enough for the damage detection algorithm to pickup. The severe damage at position 2.8125m was not identified using the first two modes because the curvatures for first and second modes are not sensitive enough to such closely spaced damage. Higher modes have shorter wavelength and hence more likely to detect closely spaced damage locations as shown in Figures 7.45b and 7.45h. As a result, the contribution of the proposed modified damage index I (MDI-I) method is significant in integrating more modes and meanwhile not sacrificing its effectiveness to detect damage.



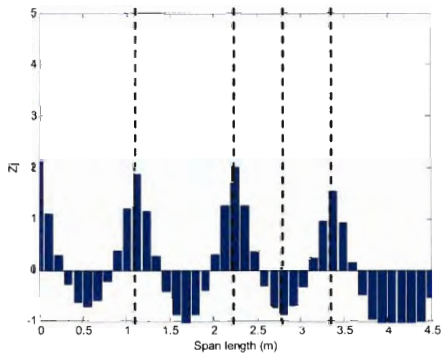
(a) 2L4S5S6S (2 modes).



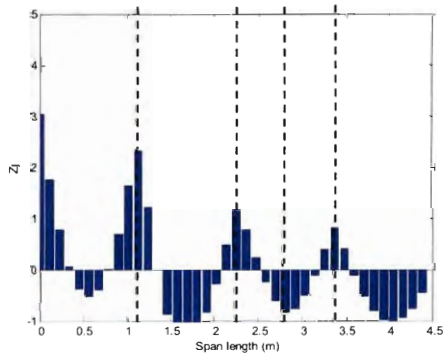
(b) 2L4S5S6S (5 modes).



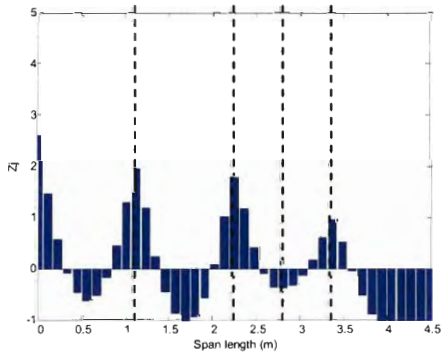
(c) 2S4S5L6S (2 modes).



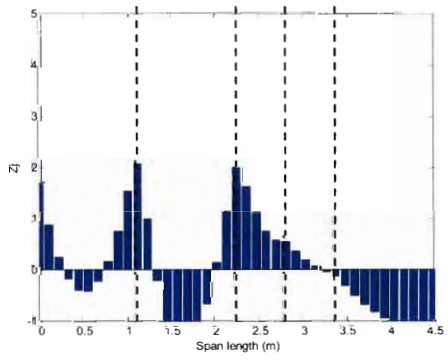
(d) 2S4S5L6S (5 modes).



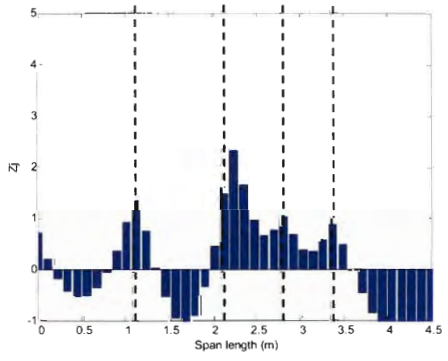
(e) 2S4S5M6S (2 modes).



(f) 2S4S5M6S (5 modes).



(g) 2S4S5S6S (2 modes).

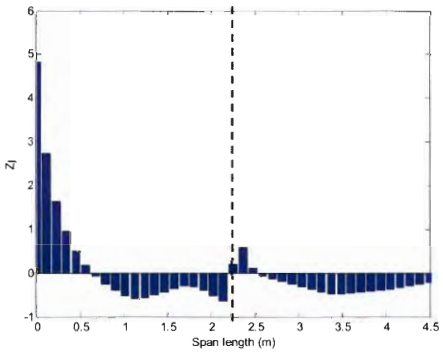


(h) 2S4S5S6S (5 modes).

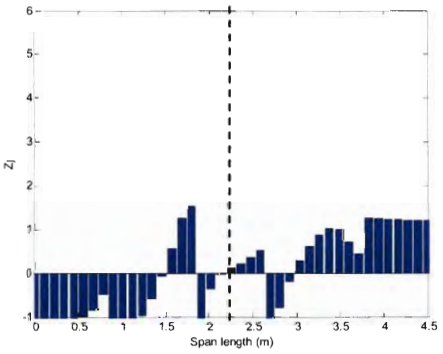
Figure 7.45 Four damage cases using MDI-I method.

7.4.5.3 Damage Index II

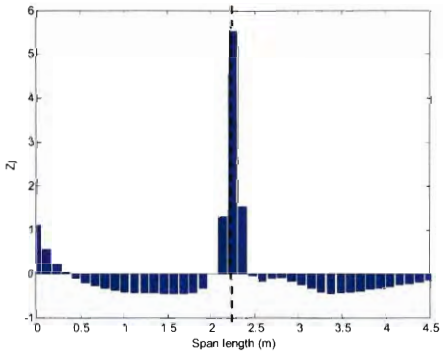
In Figure 7.46, the statistically normalised damage indicator (Z_j) for single damage cases 4L and 4S are plotted against the span length. In the figure, the first two and first five flexural modes were utilised to demonstrate the capability of the damage index II (DI-II) method adopted from Kim and Stubbs (1995) in locating damage. Figures 7.46a and 7.46c show that the DI-II method, computing (Z_j) using the first two modes is able to pinpoint clearly the severe damage but not the light damage for which the peak shifted to the right of the actual damage location for case 4L. It also produced a false positive near one support. Using the first five modes in the method, for some damage cases (shown in Figures 7.46b and 7.46d), the damage indicator did not convincingly identify the severe damage located at midspan (2.25m) and it is even worse for the light damage. It is observed that the DI-II method proposed by Kim and Stubbs (1995) is able to identify single damage well when using the first two modes but is not successful when the higher modes are used in the method.



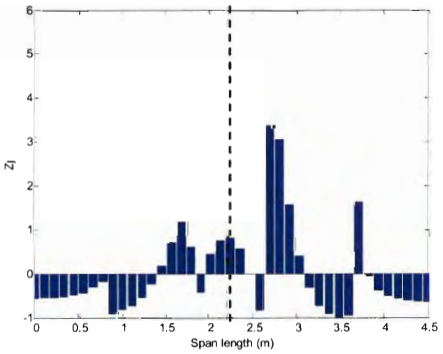
(a) 4L (2 modes).



(b) 4L (5 modes).



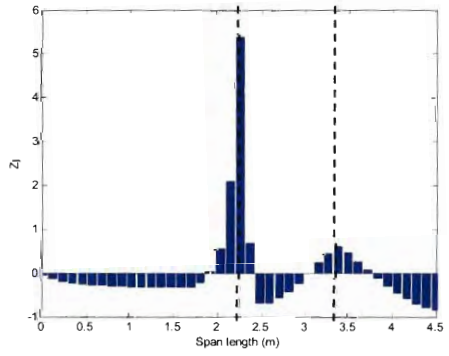
(c) 4S (2 modes).



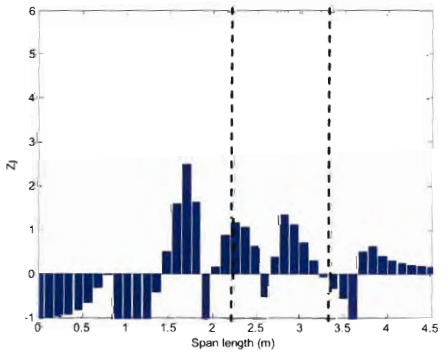
(d) 4S (5 modes).

Figure 7.46 Single damage cases using DI-II method.

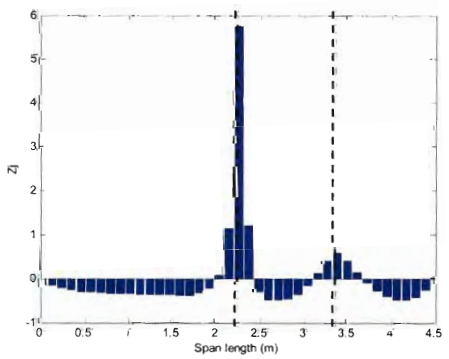
The damage localisation results for the two damage location scenarios (using 2 and 5 modes) applying the DI-II method are presented in Figure 7.47. Utilising the first two flexural modes, as shown in Figures 7.47a and 7.47c, both damage locations are well located. While using the first five modes, the damage locations are hardly identified as shown in Figures 7.47b and 7.47d. It is quite noticeable that the DI-II method is effective in spotting two damage location scenarios when the two lower modes were applied but not so when the higher modes were used. However, the shortcoming of the algorithm with two modes is that it does not show any obvious difference in the damage indicator values at position 3.375m for the medium and severe damage.



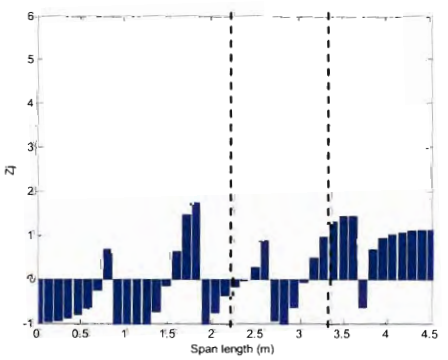
(a) 4S6M (2 modes).



(b) 4S6M (5 modes).



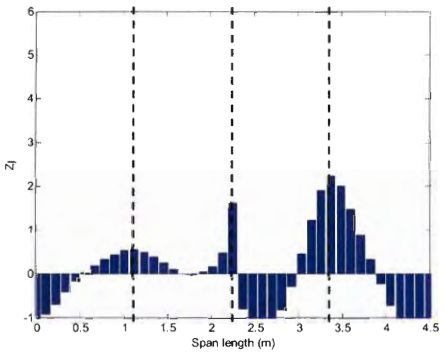
(c) 4S6S (2 modes).



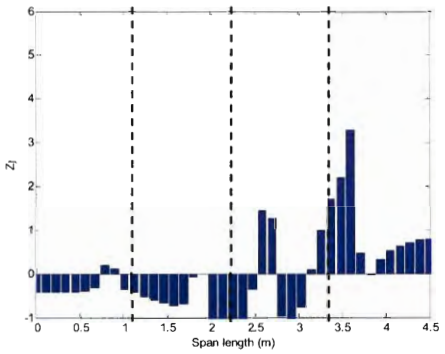
(d) 4S6S (5 modes).

Figure 7.47 Two damage cases using DI-II method.

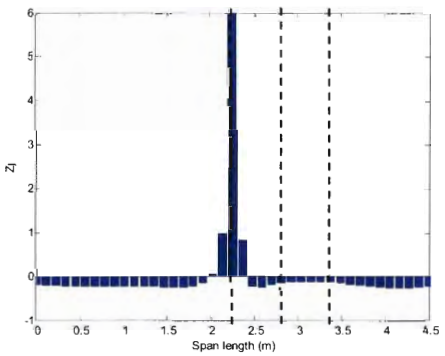
The three and four damage location scenarios are depicted in Figures 7.48 and 7.49, respectively. For these two scenarios, the results are rather similar. For both cases (using the first two and first five flexural modes), not all damage could be detected with the DI-II method. In addition, even some severe damage locations were not identified such as in the cases 4S5S6S and 2S4S5S6S as shown in Figures 7.48c and 7.49d. These results indicate that the DI-II method is not able to detect damage well for more than two damage locations, but it is reasonable for one or two damage location scenarios. Hence, the DI-II algorithm is not recommended for damage localisation as it may miss the severe damage that could cause catastrophic failure of a structural system. In addition, the results of damage detection using the DI-II method are heavily dependent upon the number of modes selected, which makes the method less reliable for applications.



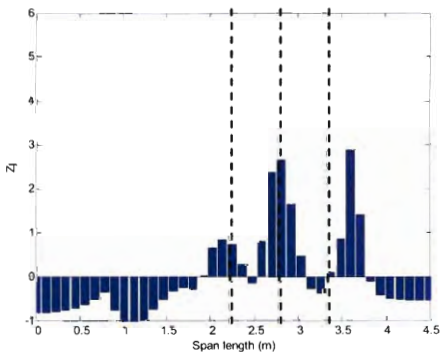
(a) 2L4L6M (2 modes).



(b) 2L4L6M (5 modes).

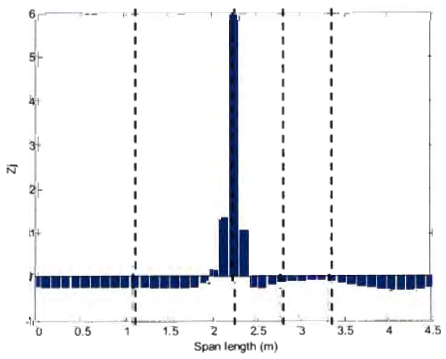


(c) 4S5S6S (2 modes).

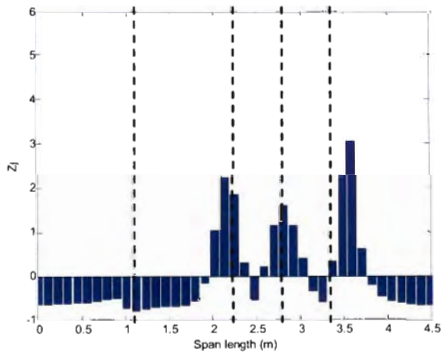


(d) 4S5S6S (5 modes).

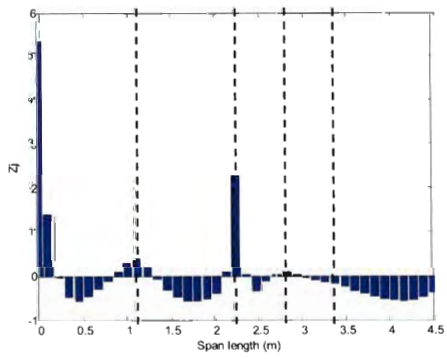
Figure 7.48 Three damage cases using DI-II method.



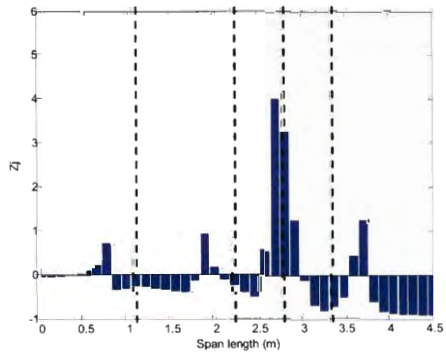
(a) 2L4S5S6S (2 modes).



(b) 2L4S5S6S (5 modes).



(c) 2S4S5S6S (2 modes).



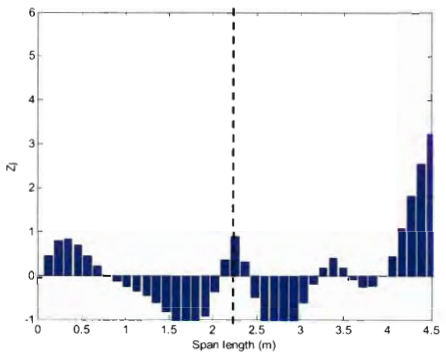
(d) 2S4S5S6S (5 modes).

Figure 7.49 Four damage cases using DI-II method.

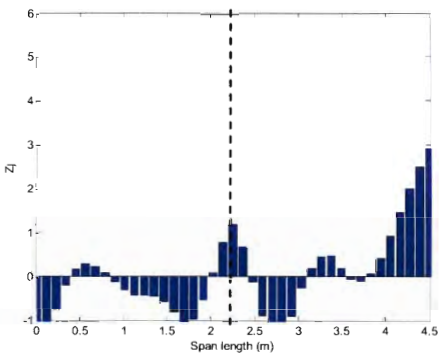
7.4.5.4 Modified Damage Index II

In the preceding section, the DI-II method was not suggested for damage localisation due to its incapability in detecting all severe damage locations for multiple damage scenarios. Therefore, a modified version of the DI-II method, namely, modified damage index II (MDI-II) is proposed. The results for single damage cases using the modified damage index II (MDI-II) method and employing the first two and first five flexural modes are illustrated in Figure 7.50. For single damage cases 4L and 4S, the damage indicator is able to show accurately the location of damage at position 2.25m with a few false positives (indication of false damage locations) at position 3.375m as well as near the supports. It is quite clear that as the severity of damage increases the damage index value gets larger, that is 1 and 4, for light and severe damage, respectively. The damage index is able to qualitatively estimate the severity of damage judging from the probability of existence of damage. However, the damage localisation

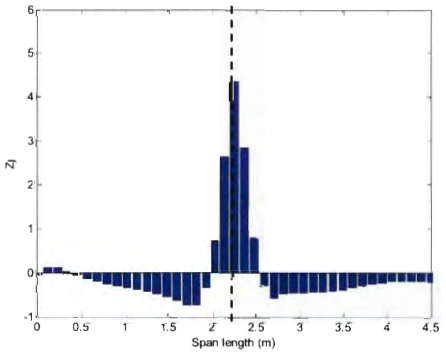
method is not suitable for estimating the extent of damage quantitatively. Using the first two and first five flexural modes in the algorithm, the damage index results are quite similar.



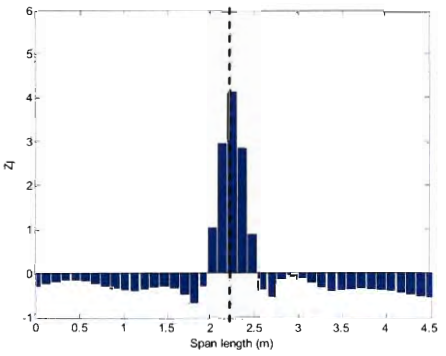
(a) 4L (2 modes).



(b) 4L (5 modes).



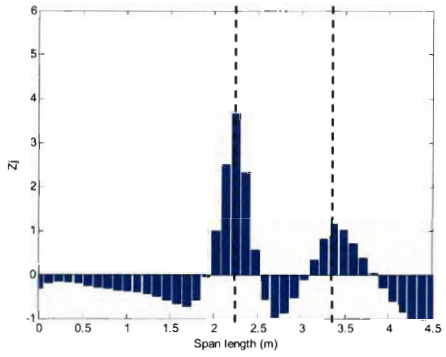
(c) 4S (2 modes).



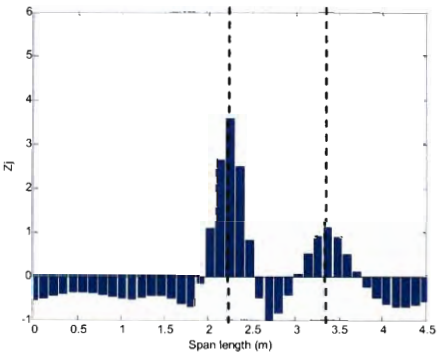
(d) 4S (5 modes).

Figure 7.50 Single damage cases using MDI-II method.

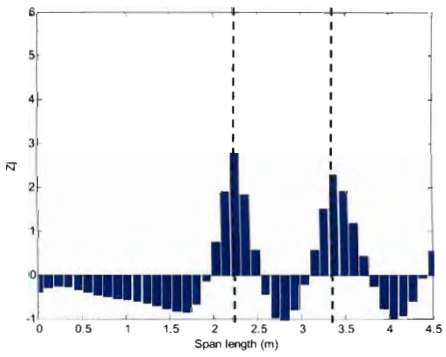
Figure 7.51 depicts the damage scenarios involving two damage locations positioned at 2.25m and 3.375m. The severe damage for damage cases 4S6M and 4S6S was precisely identified by the damage indicator at the midspan (2.25m). This is also true for the damage at position 3.375m. It is observed that the MDI-II method is capable of detecting damage in dual damage locations. By employing the first two or first five flexural modes in the algorithm, there is not much difference in the damage localisation results.



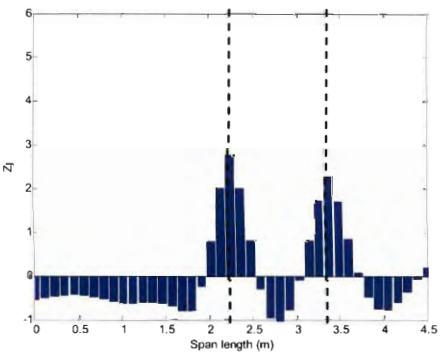
(a) 4S6M (2 modes).



(b) 4S6M (5 modes).



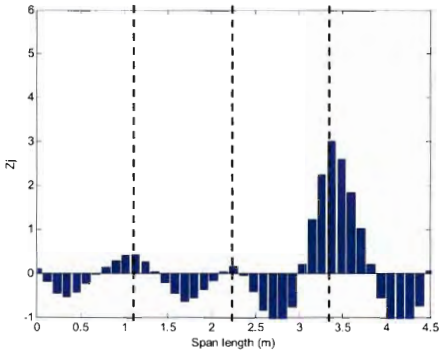
(c) 4S6S (2 modes).



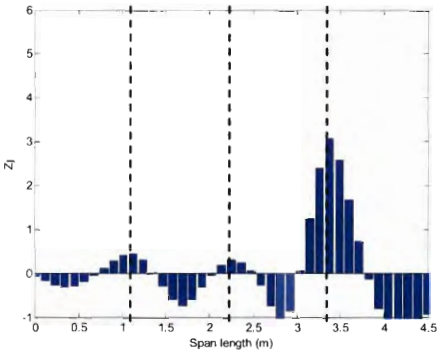
(d) 4S6S (5 modes).

Figure 7.51 Two damage cases using MDI-II method.

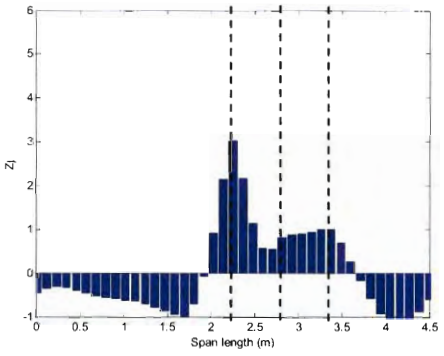
For three damage location scenarios in damage cases 2L4L6M and 4S5S6S, the damage localisation results, for both two and five modes utilised in the method, are illustrated in Figure 7.52. Again, the MDI-II algorithm quite clearly located all damage except one severe damage that was vaguely (not shown as a peak at the actual damage location) located by the damage index at position 2.8125m for case 4S5S6S (2 modes) as shown in Figure 7.52c. This shows that the algorithm is reliable in detecting localised damage accurately for up to three damage locations with the first two flexural modes, but performs even better when adopting higher modes in the method which provides more effective damage localisation. From case 2L4L6M, the relative probability of existence of damage for light and medium damage are clear. For the case 4S5S6S (see Figure 7.52d), using the first five modes in the method yields more evenly distributed damage index values, reflecting the actual damage severity level for all damage. While for the same case, using the first two modes as illustrated in Figure 7.52c, the damage index value is not reflecting the actual damage severity level.



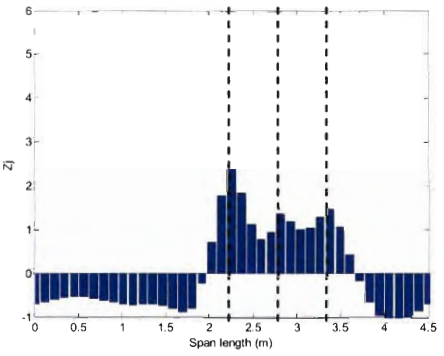
(a) 2L4L6M (2 modes).



(b) 2L4L6M (5 modes).



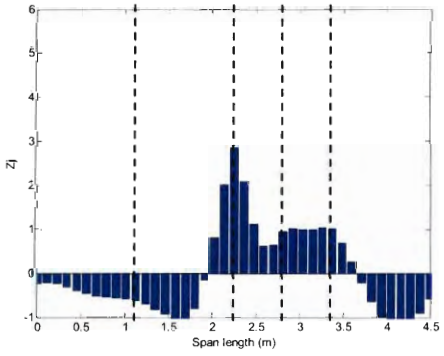
(c) 4S5S6S (2 modes).



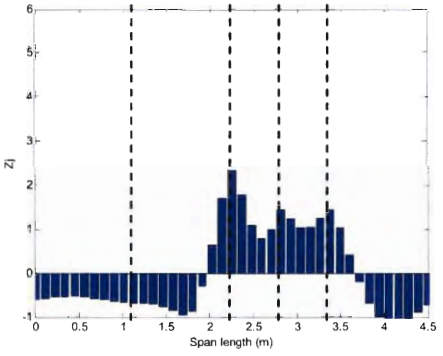
(d) 4S5S6S (5 modes).

Figure 7.52 Three damage cases using MDI-II method.

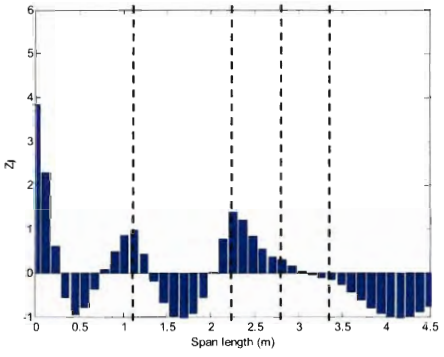
The cases involving four damage locations are illustrated in Figure 7.53. From these figures, it is noticed that most damage locations are identified except the light damage at position 1.125m for case 2L4S5S6S (using both 2 and 5 modes) as illustrated in Figures 7.53a and 7.53b and two severe damage locations at 2.815m and 3.375m for case 2S4S5S6S using 2 modes only in the MDI-II method as depicted in Figure 7.53c. From the damage cases discussed above, it is obvious that the MDI-II method is basically preferred to the DI-II method in identifying the damage location. This is even more noticeable when the first five modes were used in the DI-II and MDI-II methods, whereby the latter is superior in locating damage in single and multiple damage scenarios.



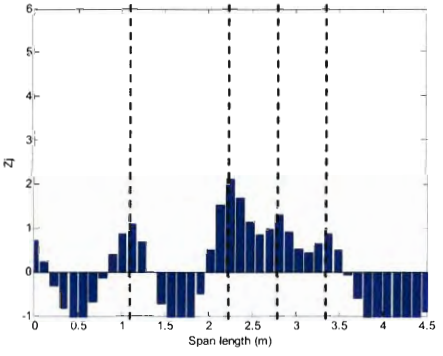
(a) 2L4S5S6S (2 modes).



(b) 2L4S5S6S (5 modes).



(c) 2S4S5S6S (2 modes).



(d) 2S4S5S6S (5 modes).

Figure 7.53 Four damage cases using MDI-II method.

7.4.6 Estimation of Severity of Damage

The two proposed modified damage localisation methods proposed in the preceding sections 7.4.5.2 and 7.4.5.4, namely, MDI-I and MDI-II methods, have been able to detect damage location well for single and multiple damage scenarios compared to their original formulae. These modified algorithms have also shown that, in general, using higher modes (5 modes) in the algorithm would yield better results in locating multiple damage compared to just using the two lower modes (2 modes). This observation is in accordance with the general principles of structural dynamics that higher modes are more sensitive to local damage. The current investigation on using higher modes in damage detection and its performance in multiple damage scenarios has filled the knowledge gap in this area of study. The modified algorithms also have the capacity to be extended to estimating the severity of damage, qualitatively, with reasonable confidence. However, the MDI-I has not been formulated to estimate the

absolute value of the severity of detected damage. In addition, the MDI-II algorithm also needs some further development to numerically correlate to a meaningful physical damage condition. With these shortcomings, it is, therefore, an important contribution to this study to propose a method to evaluate the severity of damage, as presented in the following section.

As mention earlier, the modified damage index I (MDI-I) is not formulated to estimate the damage severity. Hence, a hybrid of modified damage index I (MDI-I) and changes in flexibility (CIF- mentioned earlier in Chapter 6) methods, abbreviated as HMC, is proposed to estimate the severity of damage. For modified damage index II (MDI-II), the formula was further manipulated and then used in estimating the damage severity. The estimation of damage severity using both methods (HMC and MDI-II) is presented in terms of percentage of loss of "I" (moment of inertia). The horizontal dash-dotted line is used to illustrate the inflicted severity of damage in all figures. Based on the findings of the damage localisation, the first five modes were chosen for the calculation of the damage severity estimation in the following discussions.

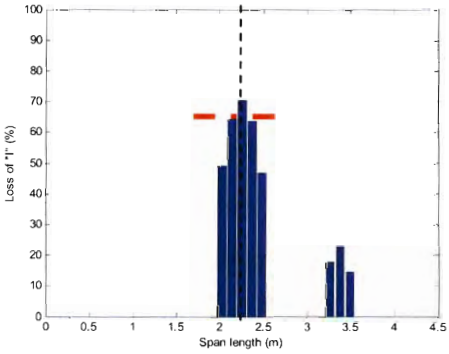
7.4.6.1 Hybrid of MDI-I and CIF

In the previous investigation, the modified damage index I (MDI-I) method was shown to be able to detect locations of damage. Hence, combining the MDI-I and changes in flexibility (CIF) method, incorporating curve-fitting for various single damage scenarios from the analytical model (refer to Chapter 5), provides an effective means of estimating the severity of damage. This hybrid algorithm is named 'hybrid of MDI-I and CIF methods' and is abbreviated as HMC. However, using any experimental data containing noise, the method requires some minor adjustment. For example, the noise polluting the data at 20% of threshold results in a weighting factor of 0.8. The severity of damage below zero percent is not meaningful, thus, they are not shown.

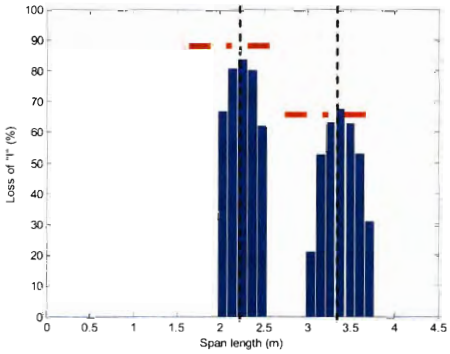
After the adjustment, four damage cases were selected to demonstrate the effectiveness of HMC algorithm in estimating the damage severity. The chosen damage scenarios are 4M, 4S6M, 2M4M6S and 2S4S5S6S as presented in Figures 7.54a, 7.54b, 7.54c and 7.54d, respectively. The predicted damage severity is given in Table 7.6. From Figure 7.54a, the simulated medium damage (65.7% loss of 'I') for the single damage scenario at location 2.25m is predicted quite accurately as 70.5% loss of 'I" (see Table 7.6), with less than 10% error as shown in Figure 7.55a. Besides evaluating the

damage severity, the HMC algorithm is also capable of identifying the location of damage precisely in spite of a false positive (indication of location of damage that was not inflicted). Figures 7.54b to 7.54d show the evaluation of damage severity using the HMC method for damage cases of two (4S6M), three (2M4M6S) and four (2S4S5S6S) damage locations, respectively, and the magnitude of severity of damage is presented in Table 7.6. These figures show that all damage locations for the multiple damage scenarios are identified using the HMC method computed with the first five flexural modes. For these three multiple damage cases, the algorithm is capable of evaluating severity of damage for severe damage (87.5% loss of 'I') with errors of less than 10%. While for the medium damage (65.7% loss of 'I'), it produced higher errors of about 25%.

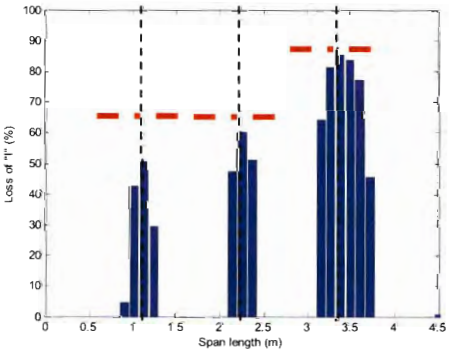
In Figure 7.55, the percentage of error, comparing the simulated and predicted severity of damage, using the HMC algorithm is presented. The positive percentage signifies that the actual damage is higher than the predicted using the HMC method, while a negative percentage means an over predicted damage severity. Referring to Figure 7.55, it is obvious that the light damage was not accurately predicted and even some of them were not detected at all. The prediction errors for light damage scenarios range from 100 to -220%. Despite high errors, most of the light damage was over predicted, which is considered conservative in the assessment procedure of any structure. For the medium damage, the HMC method predicted the damage severity better than the light damage scenario. The predicted errors for medium damage range from 50 to -30% and a few of them were not detected. For severe damage scenarios, the HMC algorithm is able to predict the severity of damage quite accurately with errors ranging from 20 to -5% and it detected all damage locations. This implies that the HMC algorithm is capable of estimating severity of damage well together with the location of damage for medium or severe damage but it requires more caution when applied to light damage scenarios. The shortcomings of the method can be compensated for by other NDE techniques, if necessary.



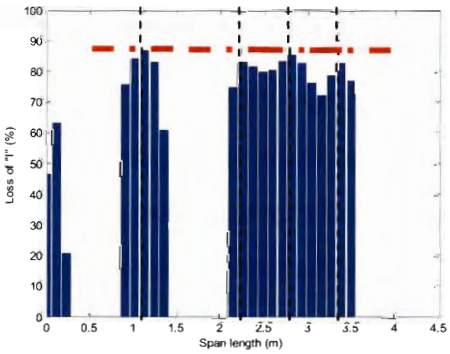
(a) 4M.



(b) 4S6M.



(c) 2M4M6S.

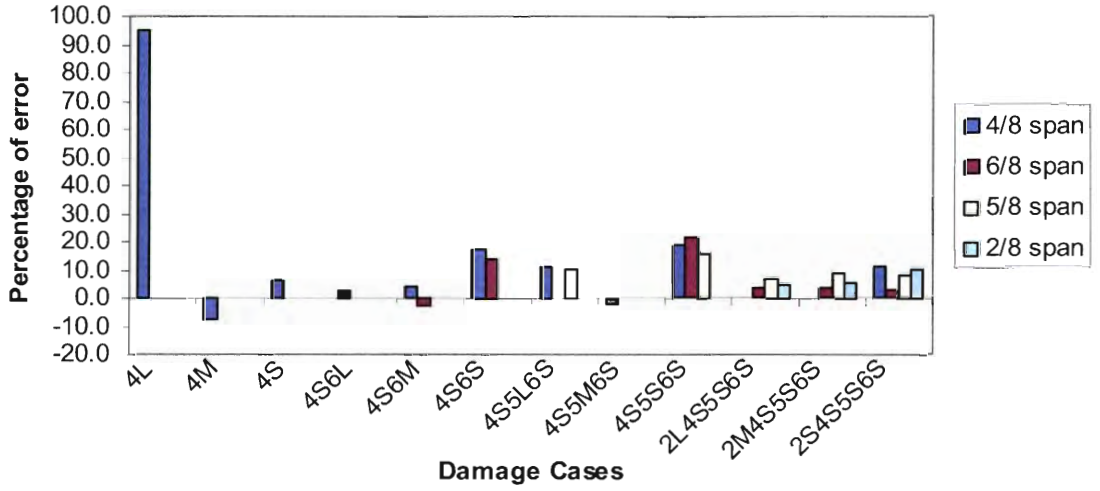


(d) 2S4S5S6S.

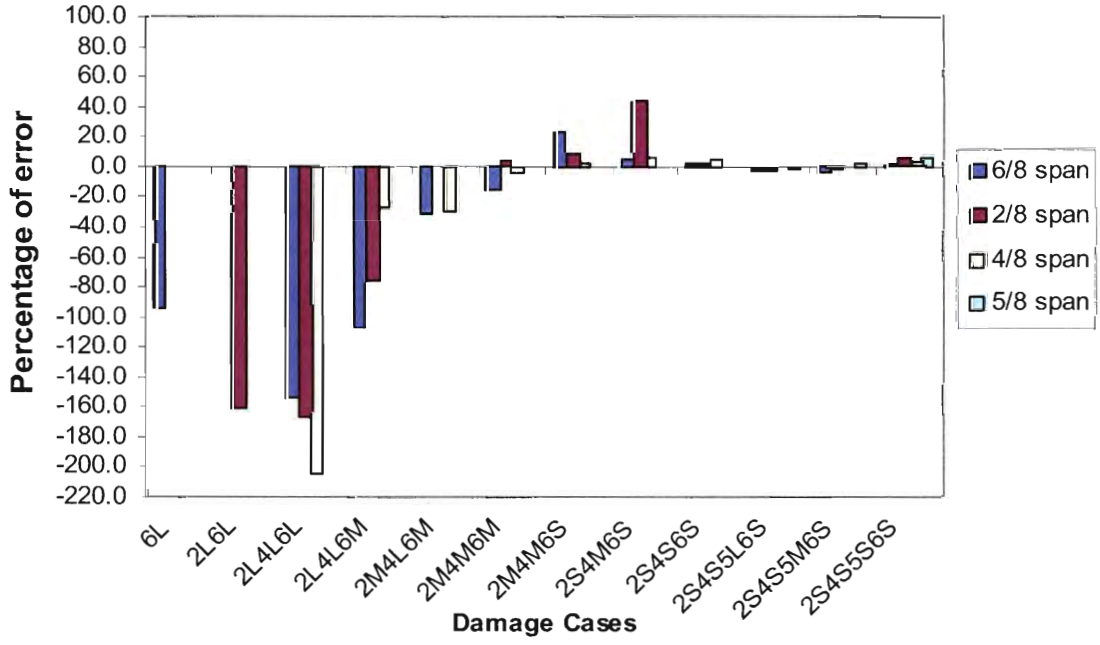
Figure 7.54 Estimation of damage severity using HMC method.

Table 7.6 Estimation of damage severity using HMC method.

Damage Case	Damage Scenario	Location per 8th of span length	Simulated Damage Severity (%)	Predicted Damage Severity (%)
Beam 1	Un1			
1	4L	4	27.1	1.3
2	**4M**	**4**	**65.7**	**70.5**
3	4S	4	87.5	82.2
4	4S6L	4, 6	87.5, 27.1	85.3, 0
5	**4S6M**	**4, 6**	**87.5, 65.7**	**83.6, 67.4**
6	4S6S	4, 6	ALL 87.5	72.6, 75.5
7	4S5L6S	4, 5, 6	87.5, 27.1, 87.5	78.0, 0, 78.6
8	4S5M6S	4, 5, 6	87.5, 65.7, 87.5	89.6, 0, 87.5
9	4S5S6S	4, 5, 6	ALL 87.5	71.3, 69.0, 73.8
10	2L4S5S6S	2, 4, 5, 6	27.1, 87.5, 87.5, 87.5	0, 84.6, 81.7, 83.1
11	2M4S5S6S	2, 4, 5, 6	65.7, 87.5, 87.5, 87.5	0, 84.5, 79.8, 82.4
12	2S4S5S6S	2, 4, 5, 6	ALL 87.5	77.8, 84.8, 80.0, 78.3
Beam 2	Un2			
13	6L	6	27.1	52.5
14	2L6L	2, 6	27.1, 27.1	0, 70.6
15	2L4L6L	2, 4, 6	27.1, 27.1, 27.1	68.9, 72.6, 82.4
16	2L4L6M	2, 4, 6	27.1, 27.1, 65.7	56.0, 47.6, 83.5
17	2M4L6M	2, 4, 6	65.7, 27.1, 65.7	86.0, 0, 85.7
18	2M4M6M	2, 4, 6	ALL 65.7	75.8, 63.6, 68.3
19	**2M4M6S**	**2, 4, 6**	**65.7, 65.7, 87.5**	**50.4, 60.2, 85.2**
20	2S4M6S	2, 4, 6	87.5, 65.7, 87.5	82.8, 37.3, 81.7
21	2S4S6S	2, 4, 6	ALL 87.5	85.4, 85.2, 83.7
22	2S4S5L6S	2, 4, 5, 6	87.5, 87.5, 27.1, 87.5	89.8, 89.5, 0, 88.5
23	2S4S5M6S	2, 4, 5, 6	87.5, 87.5, 65.7, 87.5	90.7, 89.2, 0, 85.2
24	**2S4S5S6S**	**2, 4, 5, 6**	**ALL 87.5**	**86.8, 82.8, 85.3, 85.5**



(a) Beam 1.



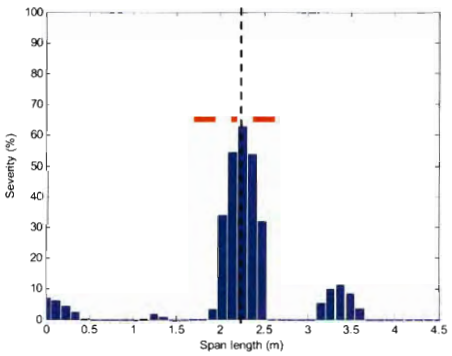
(b) Beam 2.

Figure 7.55 Comparison of simulated and predicted damage severity using HMC method.

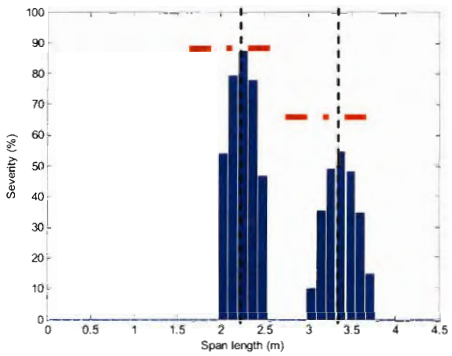
7.4.6.2 Modified Damage Index II

Similar damage cases were used in the estimation of severity of damage using the derived formulae from the MDI-II method. The severity of damage below zero percent is not meaningful, thus they are not shown. Employing the experimental data that contains noise, a weighting factor of 1.23 was adopted in the method based on calibration to the case 4S. The results of the severity evaluation using the MDI-II method for the four types of damage scenarios are shown Figure 7.56 and the magnitude of simulated and predicted damage is tabulated in Table 7.7. For the single damage location case 4M, as illustrated in Figure 7.56a, the MDI-II method captures the location of damage at position 2.25m very accurately, although there are a few false positives. The predicted damage severity for the medium damage is 62.7% loss of 'I'. Comparing to the actual inflicted damage of 65.7% loss of 'I', the error is about 5% as depicted in Figure 7.57. For the two (4S6M), three (2M4M6S) and four (2S4S5S6S) damage location cases, all damage locations are well spotted but the severity of damage were all under predicted. For these three damage scenarios, the medium damage errors ranged from 20 to 70%, while for the severe damage the errors were ranging from 20 to 60%.

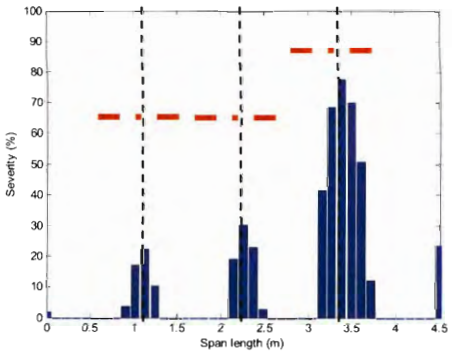
Referring to Figure 7.57, the percentage of error between the simulated and predicted severity of damage reveals that the MDI-II method generally underestimates the severity of inflicted damage for all scenarios. For the light damage scenarios, the errors of the estimated damage severity are ranging from 30 to 80%. The error range for the light damage is similar to the medium damage scenarios. While for the severe damage scenarios the damage severity prediction errors range from 20 to 60%. This confirms that the MDI-II algorithm produces better results for severe damage compared to the light and medium damage in damage severity estimation. Besides, the MDI-II method has performed well in pin-pointing the exact location of damage. The slight shortcomings of this method can be compensated by other NDT techniques which work well in a localised area and it is of utmost importance for a designer to detect the severe damage first in order to avoid catastrophic failures. This initial effort to estimate severity of damage in wood is believed to have advanced the knowledge of NDT for wood or timber structures significantly.



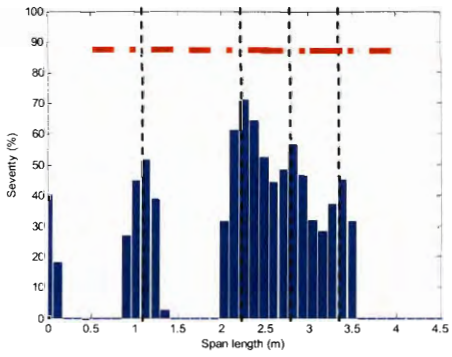
(a) 4M.



(b) 4S6M.



(c) 2M4M6S.

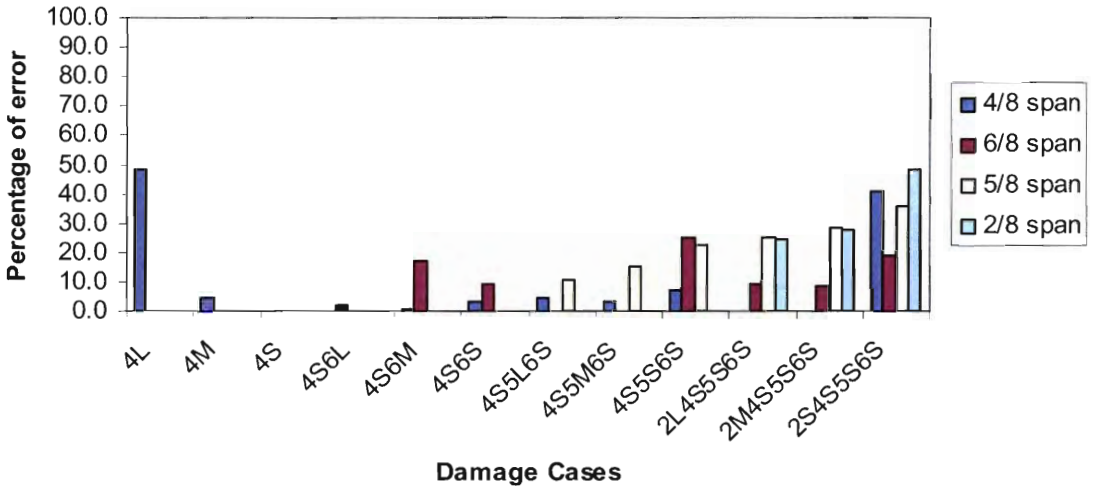


(d) 2S4S5S6S.

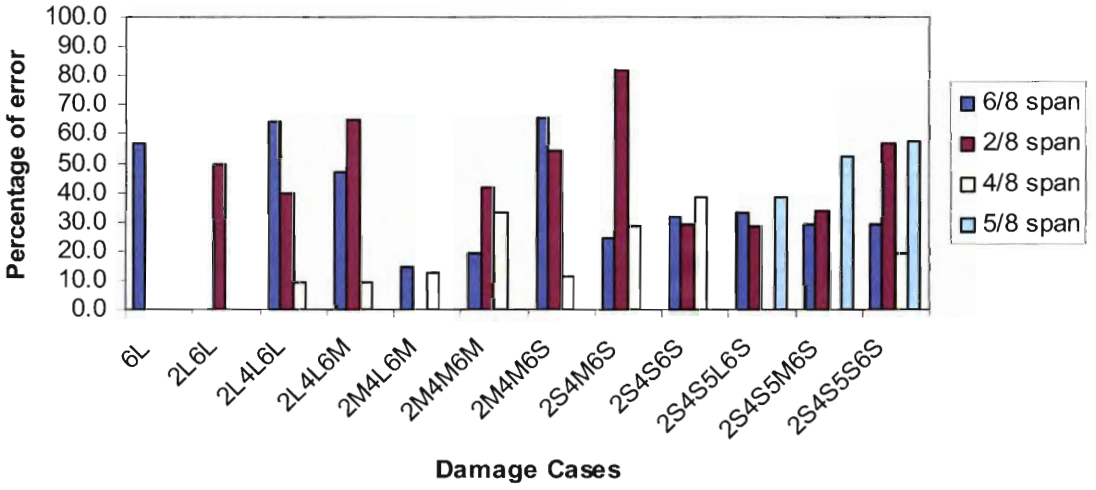
Figure 7.56 Estimation of damage severity using MDI-II method.

Table 7.7 Estimation of damage severity using MDI-II method.

Damage Case	Damage Scenario	Location per 8th of span length	Simulated Damage Severity (%)	Predicted Damage Severity (%)
Beam 1	Un1			
1	4L	4	27.1	14.0
2	**4M**	**4**	**65.7**	**62.7**
3	4S	4	87.5	87.5
4	4S6L	4, 6	87.5, 27.1	86.0, 0
5	**4S6M**	**4, 6**	**87.5, 65.7**	**87.0, 54.2**
6	4S6S	4, 6	ALL87.5	84.6, 79.2
7	4S5L6S	4, 5, 6	87.5, 27.1, 87.5	83.5, 0, 78.5
8	4S5M6S	4, 5, 6	87.5, 65.7, 87.5	84.8, 0, 74.3
9	4S5S6S	4, 5, 6	ALL 87.5	81.4, 65.4, 67.8
10	2L4S5S6S	2, 4, 5, 6	27.1, 87.5, 87.5, 87.5	0, 79.6, 65.7, 65.8
11	2M4S5S6S	2, 4, 5, 6	65.7, 87.5, 87.5, 87.5	0, 79.8, 62.5, 63.0
12	2S4S5S6S	2, 4, 5, 6	ALL 87.5	51.4, 70.8, 56.2, 45.0
Beam 2	Un2			
13	6L	6	27.1	11.6
14	2L6L	2, 6	27.1, 27.1	0, 13.6
15	2L4L6L	2, 4, 6	27.1, 27.1, 27.1	9.7, 16.4, 26.5
16	2L4L6M	2, 4, 6	27.1, 27.1, 65.7	14.4, 9.6, 59.6
17	2M4L6M	2, 4, 6	65.7, 27.1, 65.7	56.0, 0, 57.3
18	2M4M6M	2, 4, 6	ALL 65.7	53.2, 38.4, 44.0
19	**2M4M6S**	**2, 4, 6**	**65.7, 65.7, 87.5**	**22.5, 30.2, 77.6**
20	2S4M6S	2, 4, 6	87.5, 65.7, 87.5	66.0, 11.7, 62.8
21	2S4S6S	2, 4, 6	ALL 87.5	59.8, 62.1, 53.9
22	2S4S5L6S	2, 4, 5, 6	87.5, 87.5, 27.1, 87.5	58.5, 62.3, 0, 53.7
23	2S4S5M6S	2, 4, 5, 6	87.5, 87.5, 65.7, 87.5	61.8, 57.9, 0, 41.9
24	**2S4S5S6S**	**2, 4, 5, 6**	**ALL 87.5**	**61.9, 37.7, 70.7, 37.1**



(a) Beam 1.



(b) Beam 2.

Figure 7.57 Comparison of simulated and predicted damage severity using MDI-II method.

7.5 Summary

This chapter presents the verification of the damage index methods for timber beams using experimental work. Two timber beams were experimentally tested using experimental modal analysis. The theory and procedures of modal testing and experimental modal analysis is briefly described in this chapter.

It is clear that numerical techniques used in a damage detection process can significantly affect the outcomes of the detection. Using reconstructed data (expanded by the cubic spine interpolation technique) for detecting damage yields better results than just using 'as is' data. Despite its popularity, the Shannon's sampling theorem was observed to be not as effective as the cubic spline for mode shape reconstruction, especially for multiple damage cases.

Based on the results presented in this chapter, the damage index I (DI-I) method using the first two flexural modes performs better than using the first five flexural modes. This is not consistent with the principles of structural dynamics whereby higher modes would provide better system identification. Similar conclusions were drawn with respect to the adopted damage index II (DI-II) method. Due to the shortcomings in detecting multiple damage scenarios associated with the two adopted damage localisation methods, a modified version of the two methods were proposed. The two proposed modified methods are modified damage index I (MDI-I) and modified damage index II (MDI-II). The two proposed methods are superior compared to their original formulae in identifying damage locations, especially for multiple damage scenarios. Using the first five modes in the two modified algorithms provide a better damage detection in multiple damage scenarios compared to just using the first two modes. The importance of this development is that the modified methods are less dependent on the selected modes and much more reliable in the prediction outcomes.

Due to the fact that the formulation of MDI-I method does not provide a meaningful damage severity, it is proposed to use a hybrid of MDI-I and changes in flexibility (CIF) method (abbreviation as HMC) to evaluate damage severity. In general, the HMC algorithm predicts reasonably well the medium and severe damage, but it overestimates the light damage scenarios. Damage severity estimation using the MDI-II method can better predict the medium and severe damage but is less accurate for light damage scenarios. It generally underestimated severity of damage for all cases used in this investigation.

Chapter 8

Modal Testing and Experimental Modal Analysis for Plate-like Timber Structures

8.1 Introduction

This chapter aims to verify the damage index method using experimental work for plate-like timber structures. It is critically important to conduct experimental work to test the robustness of a proposed damage detection method. It is because experimental results, especially for timber structures, are subject to influence of noise, boundary conditions, material variances and environmental factors, which have huge impact on the damage detection results.

Modal testing and experimental modal analysis was conducted to obtain dynamic properties for detecting damage for timber structures, specifically a laboratory timber bridge. The modal parameters (natural frequency, damping ratio and mode shape) change as damages occur in a structure. The parameters and their derivatives were employed in damage index method for plate-like structures (abbreviated as DI-II-P) to detect damage for single and multiple damage scenarios. The DI-II-P method was utilised to detect location of damage in a laboratory timber bridge. The damage localisation using the DI-II-P method was extended to a timber plate, that of plywood (an orthotropic plate), as a supplementary work.

8.2 Experimental Set Up and Testing

8.2.1 A Laboratory Timber Bridge

A four-girder laboratory timber bridge was built in the laboratory to apply the damage detection method to timber structures. This laboratory bridge model was scaled to maintain dynamic similitude representing real timber bridges in terms of their fundamental frequencies, which usually range from 5Hz to 20Hz. The basic dimensions of the structure are shown in Figure 8.1. The bridge consisted of four girders of treated radiata pine sawn timber measuring 45mm x 90mm in cross section with a span length

of 4.5m. The deck consisted of four pieces of 21mm think x 2.4m wide and 1.2m long structural plywood of grade F11. The deck and girders were connected using 50mm self-tapping screws with 137.5 mm spacing. No gluing was applied in order to avoid fully-composite action, to simulate the interactions in a real timber bridge. The longitudinal modulus of elasticity (MOE) was determined using four-point bending test for each of the four girders and the deck (Refer to Chapter 3). This was done in order to select timbers that have similar material properties and used for material property input in the finite element models. The moisture content of the beams was estimated to be around 7-8% and for the plywood was around 11-12% using a Protimeter (a wood moisture detector). The ends of the bridge girders were supported on concrete blocks, and rigidly connected to the strong floor. A specially designed support system as shown in Figure 8.2 was used between girders and the concrete block to ensure a well-defined boundary condition that is very close to a pin-pin condition. The full bridge model is depicted in Figure 8.3. The laboratory timber bridge, namely Deck2, was used to designate the undamaged state as denoted by D2. The results form the basis of comparison for various damage cases utilising the extracted modal parameters and their derivatives.

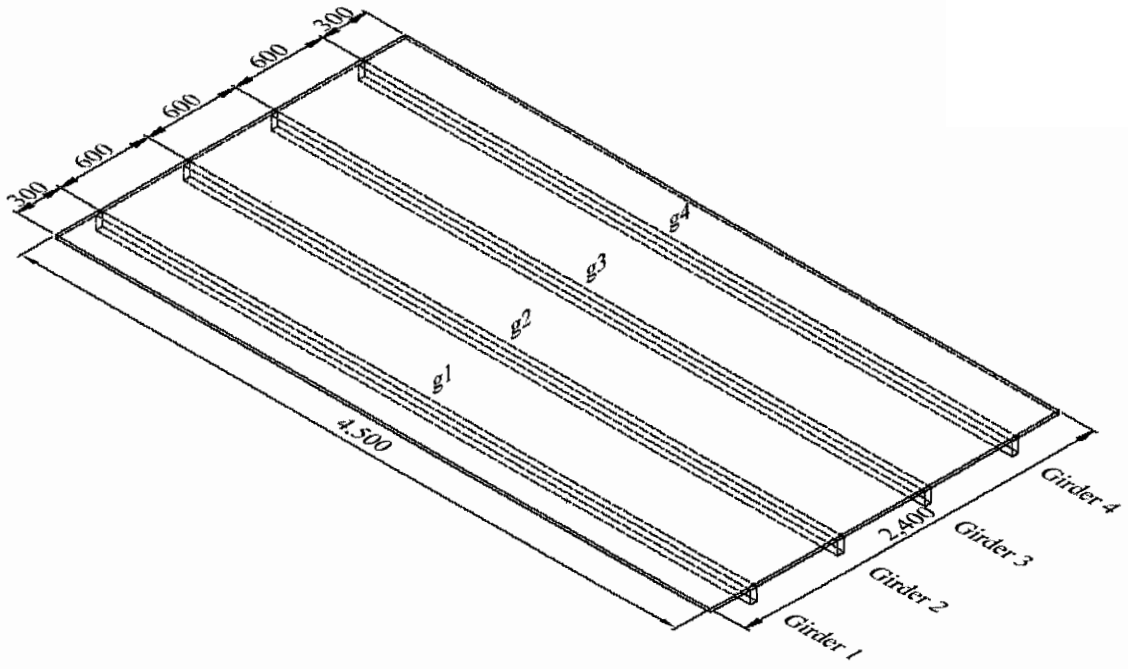


Figure 8.1 Geometric configurations of the laboratory timber bridge.



Figure 8.2 Specially designed pin support.



Figure 8.3 The laboratory timber bridge.

8.2.2 Inflicted Damage in Laboratory Timber Bridge

The goal of this study was to detect damage typically found in timber bridges, using the proposed modal-based damage detection methods to locate damage in single and multiple damage scenarios on a laboratory timber bridge. The inflicted damage cases considered are described in Table 8.1. In all damage scenarios, the damage consists of a rectangular opening along the span of a girder starting from the soffit, located either at 1/8, 2/8, 4/8 (midspan), or 6/8 of the span length to simulate pockets of rot that usually starts from the top surface in timber girders. The inflicted damage locations are illustrated in Figure 8.4. In this study and the discussions that follow, 'L', 'M' and 'S' denote light, medium and severe damage, respectively. All inflicted damage are 1% of the total span length (45mm) and consist of 10%, 30% and 50% of the beam depth, designated as damage cases 'L', 'M' and 'S' as shown in Table 8.1. The inflicted damage can also be interpreted as loss of 'I' (moment of inertia) from the depth of cut. The loss in section of 10% (L), 30% (M) and 50% (S) of beam depth, correspond to 27.1%, 65.7% and 87.5% loss of 'I', respectively. The three inflicted damage severities are shown in Figure 8.5.

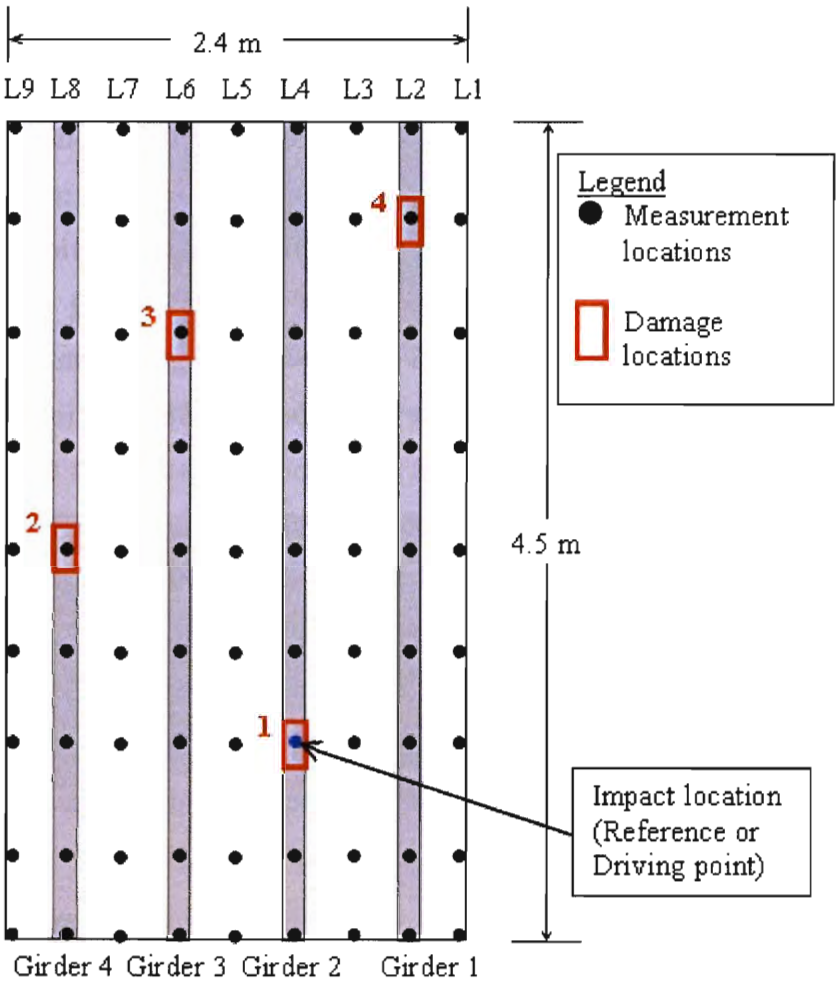
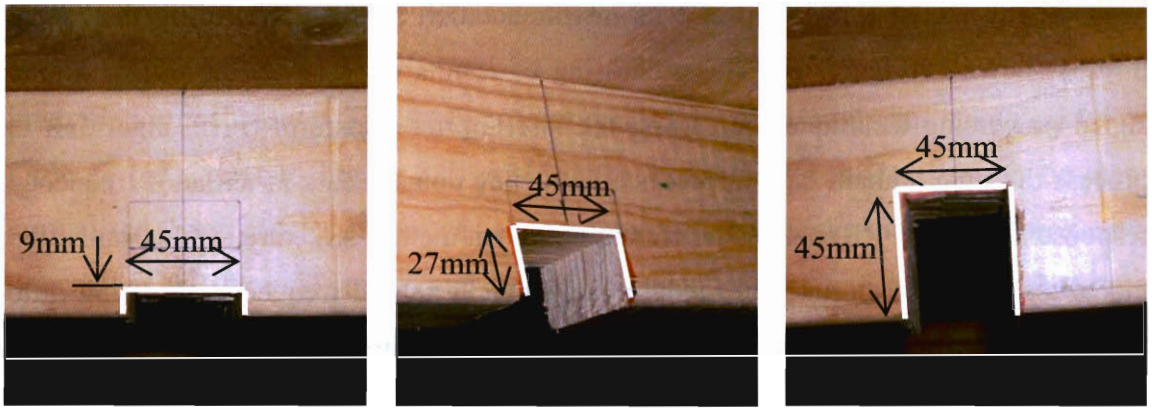


Figure 8.4 Plan view of damage locations and measurement locations for the bridge.

From Table 8.1, there are 12 damage scenarios. The damage scenarios are also illustrated in Figure 8.4. There are four damage locations representing single and multiple damage scenarios. They are locations 1, 2, 3 and 4 corresponding to sequence of damage 1 at girder 2 (g2), cumulative damage of damage 1 at girder 1 (g1) and damage 2 at girder 4 (g4), cumulative damage of damage 1 at girder 1 (g1), damage 2 at girder 4 (g4) and damage 3 at girder 3 (g3), and cumulative damage of damage 1 at girder 1 (g1), damage 2 at girder 4 (g4), damage 3 at girder 3 (g3), and damage 4 at girder 1 (g1), respectively. At each damage location, three damaged severity levels were nominated representing light, medium and severe damage found in timber structures. Similar damage scenarios to these listed in Table 8.1 can be found in Chapter 6 used in the analytical investigation. For example, g2Sg4Sg3M denotes a cumulative damage scenario of medium damage on ¾ span of girder 3, severe damage on ¾ span of girder 2 and ½ span of girder 4.



(a) Light damage (L). (b) Medium damage (M). (c) Severe damage (S).

Figure 8.5 Side view of various inflicted damage.

Table 8.1 Dimensions of inflicted damage in the bridge.

Damage Case	Damage Scenario	Location per 8th of span length/Girder number	Length *l* (mm)	Depth h (mm)	% loss of 'I'
Deck 2	D2	Undamaged	-	-	-
1	g2L	6/g2	45	9	27.1
2	g2M	6/g2	45	27	65.7
3	g2S	6/g2	45	45	87.5
4	g2Sg4L	6/g2, 4/g4	45	45, 9	87.5, 27.1
5	g2Sg4M	6/g2, 4/g4	45	45, 27	87.5, 65.7
6	g2Sg4S	6/g2, 4/g4	45	All 45	All 87.5
7	g2Sg4Sg3L	6/g2, 4/g4, 2/g3	45	45, 45, 9	87.5, 87.5, 27.1
8	g2Sg4Sg3M	6/g2, 4/g4, 2/g3	45	45, 45, 27	87.5, 87.5, 65.7
9	g2Sg4Sg3S	6/g2, 4/g4, 2/g3	45	All 45	All 87.5
10	g2Sg4Sg3Sg1L	6/g2, 4/g4, 2/g3, 1/g1	45	45, 45, 45, 9	87.5, 87.5, 87.5, 27.1
11	g2Sg4Sg3Sg1M	6/g2, 4/g4, 2/g3, 1/g1	45	45, 45, 45, 27	87.5, 87.5, 87.5, 65.7
12	g2Sg4Sg3Sg1S	6/g2, 4/g4, 2/g3, 1/g1	45	All 45	All 87.5

Notes:

gi = girder No. i

L, M, S = light, medium and severe damage, correspond to 27.1, 65.7 and 87.5% loss of 'I', respectively

(e.g. g2Sg4Sg3M denotes a cumulative damage scenario of medium damage on ¾ span of girder 3, severe damage on ¾ span of girder 2 and ½ span of girder 4)

8.2.3 Modal Test Set Up

The modal test set up and its instrumentation layout used during the modal tests is shown in Figure 8.6. The processing of results is based on the use of digital signal processing techniques and using the fast Fourier transform (FFT) algorithm to process the time domain data to produce frequency domain data in terms of frequency response function (FRF) between different points on the test structure. In this study, the modal testing and experimental modal analysis yield natural frequency, damping ratio and their corresponding mode shapes. The tests were mainly performed under similar environmental conditions, that is, temperature of 22°C±2° and ambient humidity of 60%±5% to minimise environmental factors on the modal parameters.

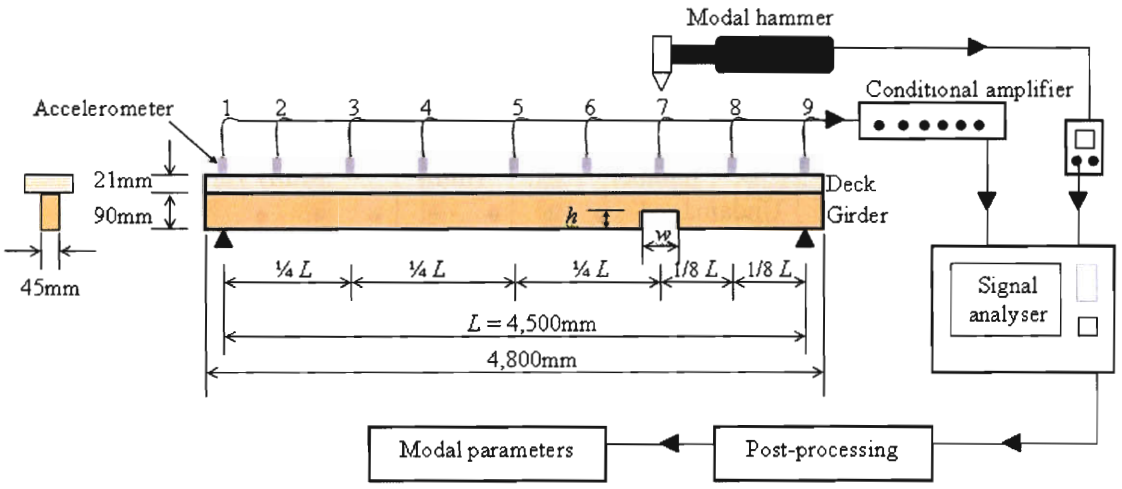


Figure 8.6 Schematic diagram of modal tests on the laboratory timber bridge.

The dynamic identification methods used in this study employ an impact hammer to excite the test sample at the reference or driving point as shown in Figure 8.4. The impact location (reference or driving point), at 3/4 of the span length of girder 2 (g2), is a strategic location and can excite more modes simultaneously. The response signal along the span was picked up using nine low impedance piezoelectric accelerometers and one stationary accelerometer was used at the driving point. For the laboratory timber bridge, there were 81 measuring points as depicted in Figure 8.4. Due to limited number of sensors available, the signal acquisition for the 81 points was repeated 9 times. The nine non-stationary accelerometers were moved from line-to-line, i.e., from line 1 (L1) to line 9 (L9) as illustrated in Figure 8.4, after every measurement on each line until all measurement locations were covered. These accelerometers were

used to measure the acceleration response on the top surface of the laboratory timber bridge as illustrated in Figure 8.6. The measurement points were set to nine as such sensor density was deemed sufficient for accurate reconstruction of mode shapes using interpolation techniques. The driving point measurement (3/4 of span length on L4 or girder 2 (g2), refer to Figure 8.4) enabled the experimental mode shape to be mass normalised. Each accelerometer was attached onto a small steel plate, with approximate dimensions of 40mmx90mmx1mm, using a magnetic base and the steel plate was secured on the top of the deck. The distance between each accelerometer was 1/8 of the span length (562.5mm) starting from one end support of the bridge to the other end as shown in Figures 8.4 and 8.6.

The frequency response functions (FRFs) were acquired using LMS CADA-X (1992) signal acquisition module and a dynamics analyser HP E1432A Vxi. A typical acquired FRF spectrum using the system for the laboratory timber bridge is shown in Figure 8.7. The measurements were recorded using the dynamic response at 10,000 Hz sampling rate for a frequency span of 500Hz and 8,192 data points, thus giving a resolution of 0.061Hz per data point. By employing an averaging of 5 ensembles, this reduces the interference of noise. The details of the acquisition system for the signal using the LMS CADA-X (1992) system was documented in Chapter 7.

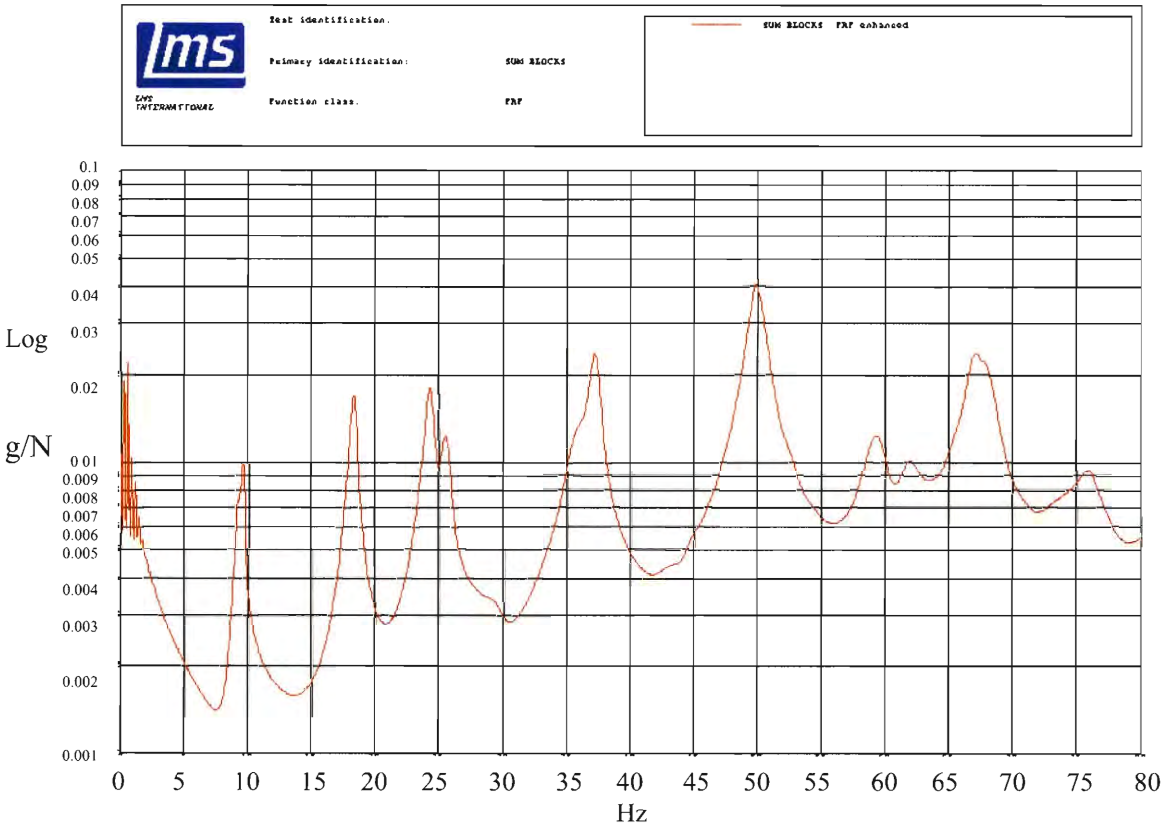


Figure 8.7 A typical FRF spectrum for the laboratory timber bridge.

Using the modal analysis module in the LMS CADA-X (1992) software, a frequency domain direct measurement curve-fitting technique was used to extract the natural frequencies, damping ratios and mode shapes from the measured FRF data. The post-processing procedures are detailed in Chapter 7. From the modal testing and experimental modal analysis, nine vibration modes and a frequency range spanning from 8Hz to 60 Hz, were captured. The captured mode shapes are shown in Figure 8.8 and their descriptions are listed in Table 8.2. Using the 81-point experimental mode shapes, they were reconstructed using two-dimensional (2-D) cubic spline interpolation technique, generating a mode shape vector having a length of 41 points in both longitudinal and transverse directions of the span. The reconstructed mode shapes with finer coordinates have better chance of locating damage compared to using coarse coordinates. The reconstructed mode shapes were then applied in the damage detection algorithms attempting to locate and evaluate the inflicted damage scenarios. It should be noted that the first and second torsional modes (modes 2 and 5) were not very good because the impact location was close to their node point. Nevertheless, these modes

were still used in the subsequent discussions. The details of experimental modal analysis can be found in Chapter 7. It should be noted that since the signal was acquired line-by-line covering all the measurement locations, the bridge data required post-processing with an additional step in the procedure of experimental modal analysis compared to the timber beam discussed in Chapter 7. The additional step was to combine all individual line (lines 1 to 9) measurements into a single Block Data Memory (BDM) before curve-fitting process was undertaken in order to obtain a complete modal parameters output for the system.

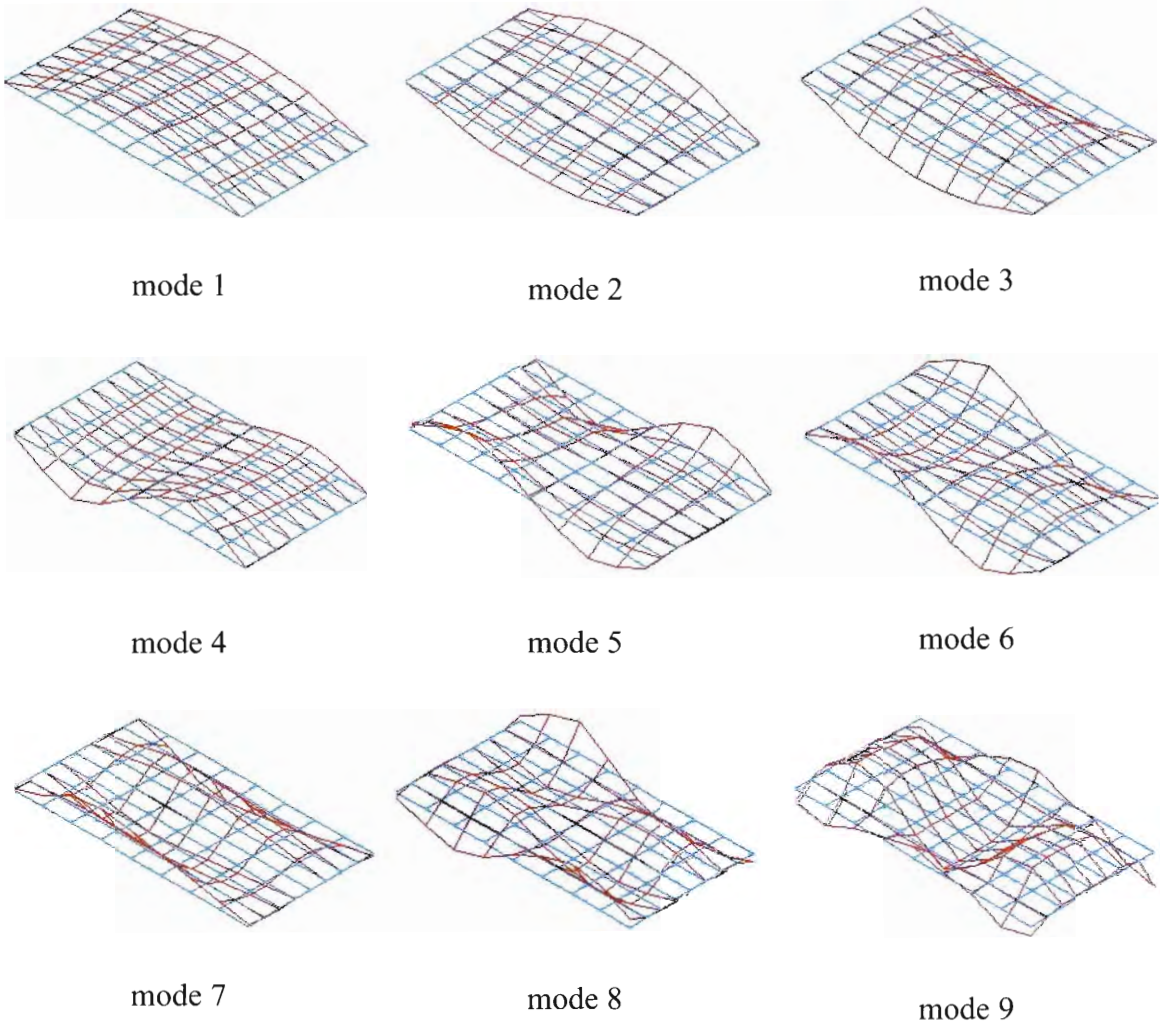


Figure 8.8 Experimental 81-point mode shapes for the laboratory timber bridge.

Table 8.2 Description of mode shapes for the laboratory timber bridge.

Mode	Description of mode shapes
1	First flexural mode
2	First torsional mode
3	First transversal mode
4	Second flexural mode
5	Second torsional mode
6	First transversal and second flexural
7	Second transversal mode
8	Second transversal and second flexural
9	Third flexural mode

8.2.4 The Laboratory Timber Plate

A piece of plywood was used in the laboratory to apply the damage detection method to timber plate-like structures. The plywood was used to simulate an orthotropic plate, which may be adopted to represent some slab-type bridges. Since plate-type or slab-type timber bridges are very rare, therefore, the purpose of this additional work was merely complementary and aimed to explore the capabilities and limitations of the damage detection algorithm in locating damage for a timber plate structure. Hence, the material properties of the plywood were not experimentally tested and were assumed to be the same as the plywood used in the laboratory timber bridge. Basic dimensions of the plywood plate are shown in Figure 8.9, i.e. 18mm thick x 2.4m wide and 1.2m long structural plywood of grade F11. The moisture content of the plywood was 11-12%. The support system used was similar to the laboratory timber bridge as shown in Figure 8.10. The full plate model is depicted in Figure 8.11. The timber plate system, namely Plate1, representing the undamaged state is denoted as P1, which forms the basis of comparison for various damaged stages utilising the extracted modal parameters and their derivatives.

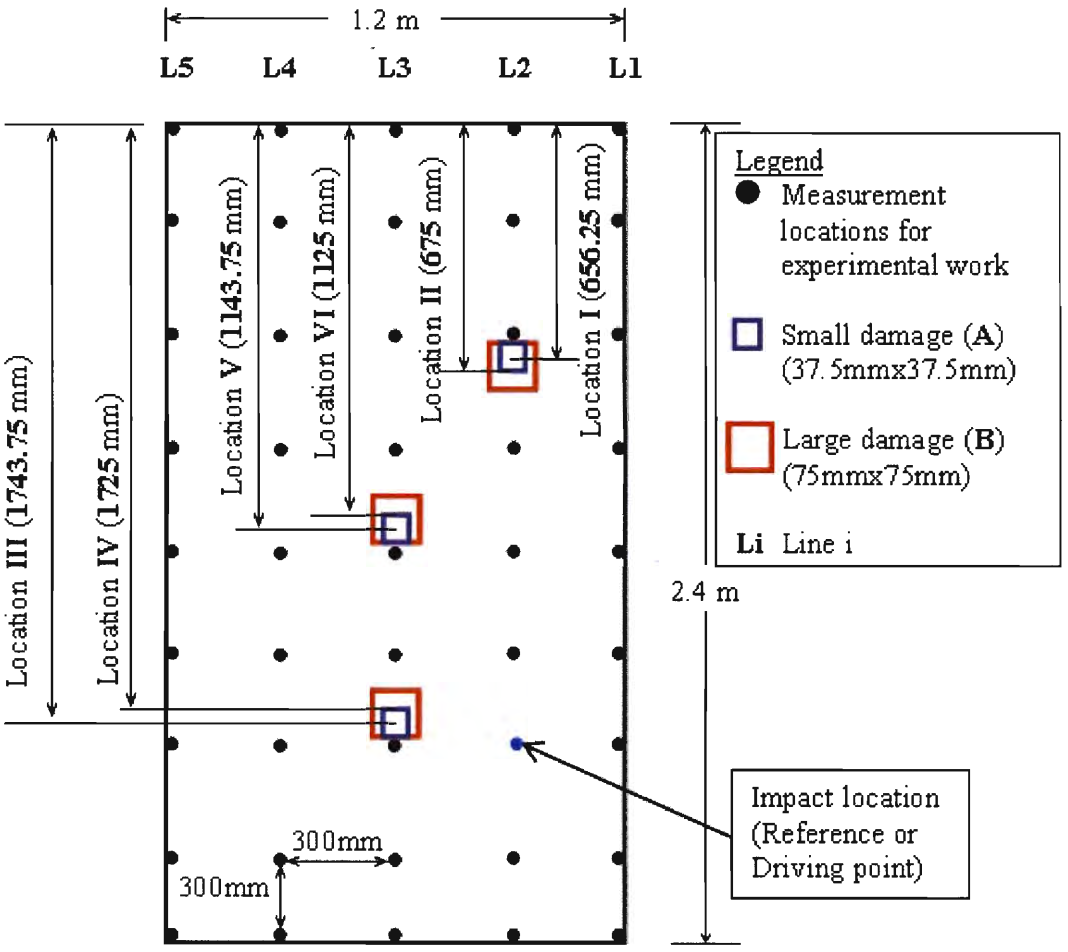


Figure 8.9 Plan view of damage and measurement locations for a timber plate.



Figure 8.10 Support system used for the timber plate.



Figure 8.11 The laboratory timber plate.

The plywood was inflicted with various damage scenarios as tabulated in Table 8.3 and shown in Figure 8.9. The damage was inflicted with a square opening with dimensions of either 37.5mm or 75mm, corresponding to small (A) and large (B) damage, respectively, as illustrated in Figure 8.12. The damage can also be represented by percentage of loss of area against a bay measuring 300mm by 300mm as shown in Figure 8.9. It works out to be 2% and 6% loss of area for small and large damage, respectively. For example, L2(II)B-L3(IV)B-L3(V)A denotes a cumulative damage scenario of small damage at location IV (1143.75mm) of Line 3, large damage at locations II (675mm) of Line 2 and IV (1725mm) of Line 3.

Table 8.3 Dimensions of inflicted damage in the plate.

Damage Case	Damage Scenario	Location (mm) /Line number	Length *l* (mm)	Breath *b* (mm)	% loss of Area*
Plate1	P1	Undamaged	-	-	-
1	L2(I)A	I (656.25)/L2	37.5	37.5	2
2	L2(II)B	II (675)/L2	75	75	6
3	L2(II)B-L3(III)A	II (675)/L2, III (1743.75)/L3	75, 37.5	75, 37.5	6, 2
4	L2(II)B-L3(IV)B	II (675)/L2, IV (1725)/L3	75, 75	75, 75	6, 6
5	L2(II)B-L3(IV)B-L3(V)A	II (675)/L2, IV (1725)/L3, V (1143.75)/L3	75, 75, 37.5	75, 75, 37.5	6, 6, 2
6	L2(II)B-L3(IV)B-L3(VI)B	II (675)/L2, IV (1725)/L3, VI (1125)/L3	75, 75, 75	75, 75, 75	6, 6, 6

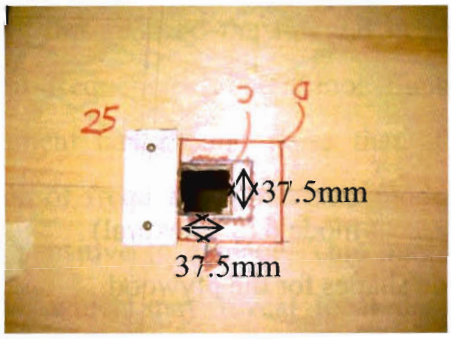
** % loss of Area is calculated based on damaged area divided by 300mmx300mm (a bay of the measurement grids).*

Notes:

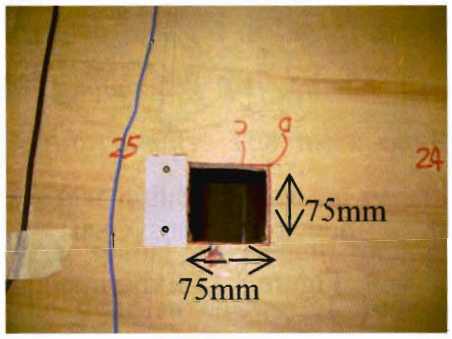
Li = Line no. i

A,B = small and large damage, correspond to 2% and 6% loss of area, respectively

(e.g. L2(II)B-L3(IV)B-L3(V)A denotes a cumulative damage scenario of small damage at location V (1143.75mm) of Line 3, large damage at locations II (675mm) of Line 2 and IV (1725mm) of Line 3)



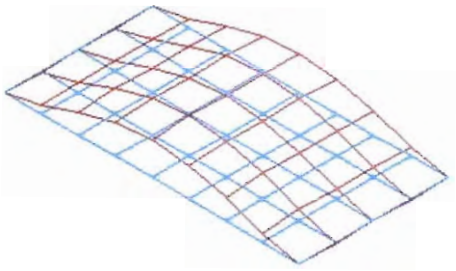
(a) Small damage (A).



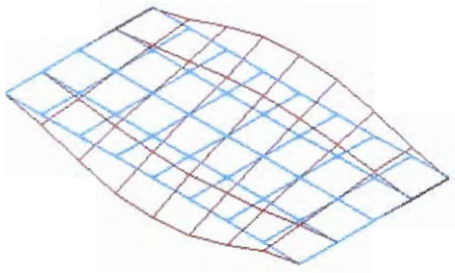
(b) Large damage (B).

Figure 8.12 Plan view of inflicted damage.

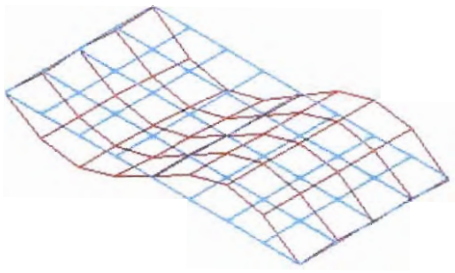
The modal testing and experimental modal analysis for plywood is similar to the laboratory timber bridge. The only difference is the number of measurement points for plywood which is 45 and requiring the signal acquisition to be repeated only 5 times (5 lines) for each set of measurements. For plywood, the first six modes were captured and are illustrated in Figure 8.13.



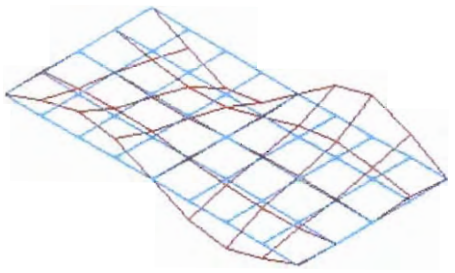
mode 1 (1st flexural)



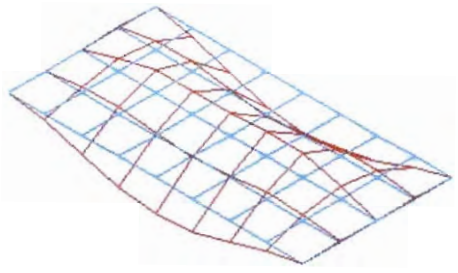
mode 2 (1st torsional)



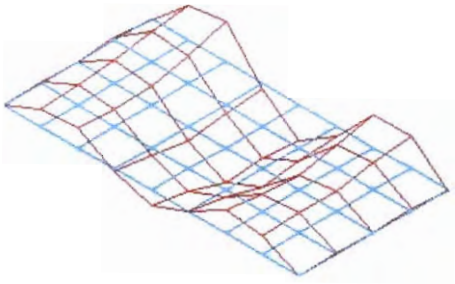
mode 3 (2nd flexural)



(e) mode 4 (2nd torsional)



mode 5 (1st transversal)



mode 6 (3rd flexural)

Figure 8.13 Experimental 45-point mode shapes for the plywood.

8.3 Results and Discussions - the Laboratory Timber Bridge

8.3.1 Natural Frequency

Natural frequencies can be used to detect changes in a dynamic system before and after modifications occurred in the system. This means if a change in natural frequency occurs in a system, it can be inferred that the system has undergone physical changes. In this study, the changes are related to loss of section in timber girders of the laboratory timber bridge. The change of natural frequencies was clearly observed for the first nine modes obtained from modal testing and experimental modal analysis of the undamaged and damaged state of the laboratory timber bridge as listed in Table 8.4.

According to Figure 8.14, there is a general decrease in natural frequencies for the laboratory timber bridge as the severity of damage increases, despite some minor fluctuations. The decrease in natural frequencies for the laboratory timber bridge is obviously higher for more severe damage cases such as case g2Sg4Sg3Sg1S (most severe damage case) with a maximum change of more than 3Hz for mode 4. It is also noticeable that lower modes (modes 1 to 3) exhibit less change of frequency ranging from -0.5Hz to 0.5Hz while the range for modes higher than mode 3 (modes 4 to 9) is between -0.5Hz and 3.5Hz. It is apparent that as more damages were inflicted in the bridge, this reduced the flexural bending capacity, which resulted in higher drops in natural frequencies. The minor fluctuations in the frequencies may be due to the instrument background noise that affects the spectrum quality. The more obvious change of frequency for higher modes also suggests that higher modes are generally more sensitive to damage. This may be due to shorter spatial wavelength for higher modes, which may reveal local damage better. The trend in change of frequency reinforces again the earlier findings in the timber beam model (Chapter 7), that is, natural frequency can be used to identify the existence and assess, qualitatively, the extent of damage in the laboratory timber bridge. However, more care is required when change of frequency is used to detect damage because it was found that changes of around 5% in frequency (for example 5% change in frequency for mode 9 of undamaged case D2 is 2.96Hz, which is more than 2.67Hz for mode 9 of most severe damage case g2Sg4Sg3Sg1S) may be observed due to changes in the environmental conditions rather than the damage (Aktan et al. 1994; Creed 1987).

Table 8.4 Natural frequencies of the laboratory timber bridge.

Mode	Natural frequencies (Hz)						
	D2	g2L	g2M	g2S	g2Sg4L	g2Sg4M	g2Sg4S
1	9.06	9.17	9.08	8.92	8.92	8.85	8.60
2	9.49	9.59	9.47	9.32	9.30	9.26	9.16
3	18.07	18.18	18.20	18.06	18.08	18.02	17.92
4	24.17	24.10	23.88	23.37	23.09	23.03	22.96
5	25.32	25.41	25.39	25.01	24.89	24.68	24.69
6	35.45	35.82	35.57	34.88	34.76	34.72	34.80
7	37.06	37.08	37.10	37.05	37.10	37.10	36.93
8	49.71	49.35	49.31	48.60	48.62	48.66	48.58
9	59.25	59.22	58.95	58.30	58.35	58.33	57.87

Mode	Natural frequencies (Hz)						
	D2	g2Sg4S g3L	g2Sg4S g3M	g2Sg4S g3S	g2Sg4S g3Sg1L	g2Sg4S g3Sg1M	g2Sg4S g3Sg1S
1	9.06	8.71	8.66	8.63	8.65	8.61	8.49
2	9.49	9.17	9.20	9.15	9.10	9.00	9.08
3	18.07	18.08	17.98	17.99	17.98	18.03	17.86
4	24.17	22.85	22.53	21.83	21.65	21.50	20.96
5	25.32	24.98	24.80	24.60	24.36	24.14	24.26
6	35.45	34.97	34.83	34.51	34.34	34.14	33.48
7	37.06	37.16	36.95	36.68	36.66	36.62	36.69
8	49.71	48.51	48.23	47.51	47.45	47.36	47.36
9	59.25	58.16	57.39	56.97	56.62	56.85	56.58

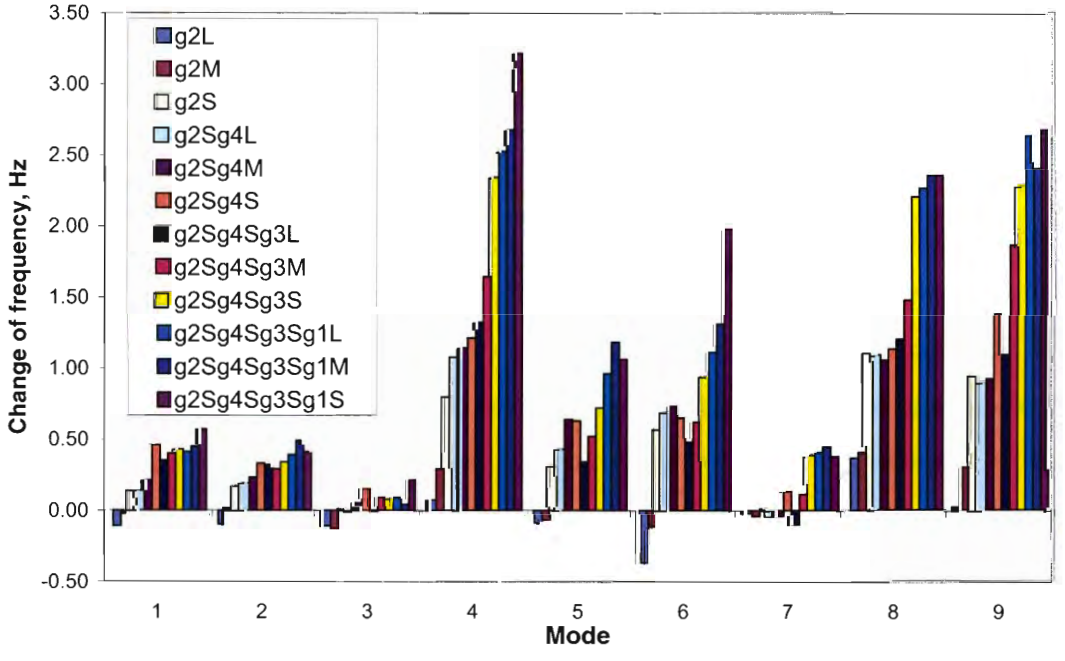


Figure 8.14 Change of frequency for the laboratory timber bridge.

8.3.2 Damping Ratio

Damping in a structural system results from energy dissipation in the system through the work done by the damping forces. The damping is usually quite small and only affects the vibration behaviour significantly near resonance (Bachmann et al. 1995). In this study, damping ratio, which represents the ratio of damping coefficient c and critical damping coefficient c_{cr}, is obtained from the experimental modal analysis.

From Table 8.5, generally, an inconsistent trend of changes in damping ratio is observed in all nine modes for the laboratory timber bridge. These changes cover the range from -2% to 1.5% for the laboratory timber bridge as shown in Figure 8.15. Many studies showed that a reasonable and consistent trend (unlike the natural frequencies) due to damage could not be found in damping ratios (Kato & Shimada 1986; Salawu & Williams 1995). Hence, damping ratio is no longer considered in the following sections.

Table 8.5 Damping ratios for the laboratory timber bridge.

Mode	Damping ratio (%)						
	D2	g2L	g2M	g2S	g2Sg4L	g2Sg4M	g2Sg4S
1	2.13	3.64	3.95	3.24	2.84	2.59	2.23
2	1.18	0.64	0.61	1.10	0.66	0.91	2.31
3	1.76	1.67	1.45	1.61	1.25	1.29	1.34
4	1.26	1.45	1.38	1.99	1.78	1.78	1.86
5	1.42	1.48	1.70	1.04	2.05	2.09	2.04
6	3.49	2.60	3.11	3.77	2.74	3.00	3.15
7	1.06	1.02	1.14	1.10	1.23	1.25	1.52
8	1.11	1.56	1.27	1.23	1.31	1.30	1.31
9	1.24	1.71	1.67	1.30	2.23	2.12	1.64

Mode	Damping ratio (%)						
	D2	g2Sg4S g3L	g2Sg4S g3M	g2Sg4S g3S	g2Sg4S g3Sg1L	g2Sg4S g3Sg1M	g2Sg4S g3Sg1S
1	2.13	2.01	1.87	3.96	3.00	2.19	2.54
2	1.18	1.22	1.02	0.94	1.20	1.00	0.29
3	1.76	1.23	1.30	1.03	1.15	2.05	1.43
4	1.26	1.80	1.88	1.82	2.07	2.13	2.30
5	1.42	2.81	3.03	1.95	2.73	3.12	2.81
6	3.49	2.23	2.30	2.26	2.31	2.39	3.11
7	1.06	1.28	1.72	0.92	1.27	1.31	1.06
8	1.11	1.30	1.36	1.55	1.55	1.64	1.97
9	1.24	1.10	1.13	1.21	1.25	1.16	1.64

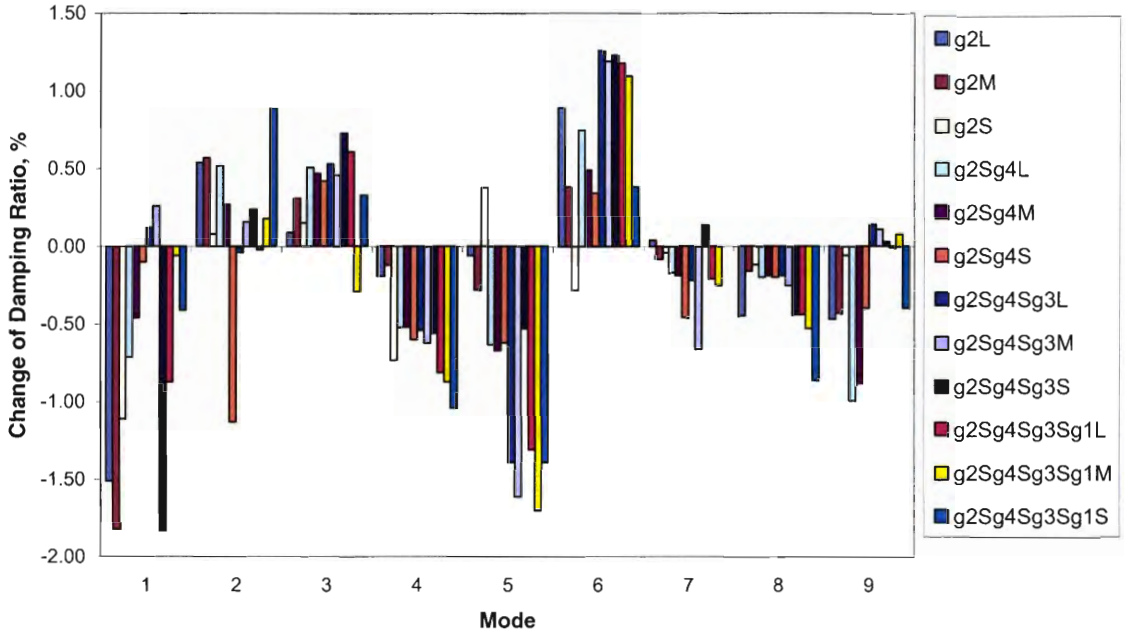


Figure 8.15 Changes in damping ratios for the laboratory timber bridge.

8.3.3 Effects of Sensor Density

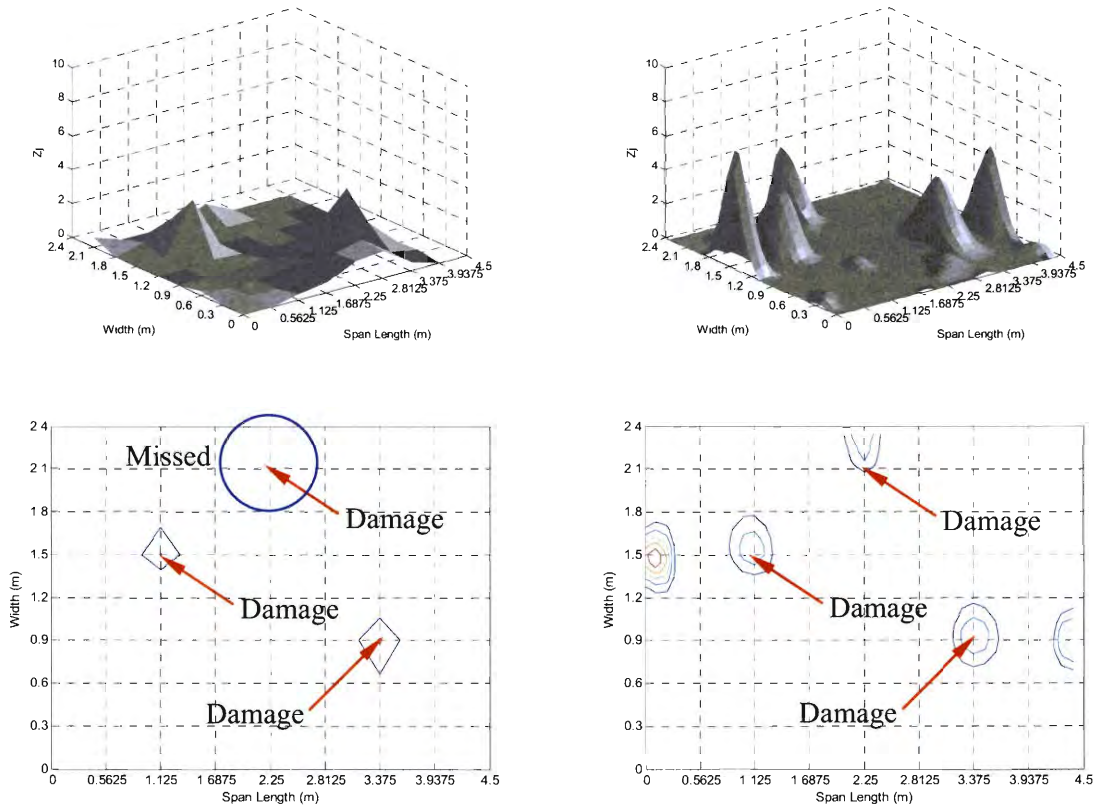
The importance of density of sensors (accelerometers) for effective damage detection using vibration based methods was discussed and demonstrated in Chapter 7 for the beam tests. For the laboratory timber bridge, the selection of number and location of sensors is believed to have major influence on the results of the damage detection. It is commonly acknowledged that the denser the measurement is, the damage detection results will be more reliable. When the collected data is below a certain level, the process of damage detection inevitably introduces errors. This implies that a large number of sensors are required to perform a quality modal test that leads to better damage detection results which, however, is very costly. This is unlike the finite element model, where the density of sensors is linked to the mesh size and can be easily changed. Due to sensor limitations in the experimental work, a reasonable number of sensors are essential to balance the advantages and disadvantages of an optimal damage detection process. In this study, nine equally spaced sensors were used to acquire the accelerations of the test sample in the modal tests. With the two-dimensional (2-D) cubic spline interpolation technique, the limited data was expanded to forty one data points in both longitudinal and transverse directions of the span, which would enhance the effectiveness of the damage detection.

The comparison of damage localisation results between the 'as is' data and the interpolated data using 2-D cubic spline were demonstrated using the damage index II for plate-like structures (abbreviated as DI-II-P) with the first nine modes on various damage scenarios. In the following results, the damage indicator, Zj, for each of the damage cases is plotted against the laboratory timber bridge span length (4.5m) and width (2.4m). In principle, when the statistically normalised damage indicator value of Zj for a given location is larger than or equals to two (the probability-based criterion for damage), it is considered that damage existed at that location. The localisation of damage using the criterion, $Zj \geq 2$, was adopted as it would provide an approximately 95% level of confidence in indicating the actual damage locations (Park & Stubbs 1995; Peterson et al. 2001). The level of Zj for plate-like timber structures is set slightly higher than that of the timber beams because plate-like structures, such as a deck-girder timber bridge, is a far more complicated system compared to a simple beam system, which in turn may produce larger errors in the damage detection process.

To show the damage site in the graphs, the actual damage locations are marked by a red colour arrow sign and the word 'Damage' in all subsequent figures. For damage localisation of the laboratory timber bridge, two types of graphs were used in this study, that is, surface and contour plots. The surface plots provide an indication of the distribution of the damage indicators that are above zero ($Zj>0$), while the contour plots give information on predicted damage locations with $Zj \geq 2$.

From the contour plot of Figure 8.16a, using the 'as is' data in the calculation of damage indicator with the first nine modes, failed to locate the damage at position (2.25m, 2.1m), which is 2.25m along the span length and 2.1m across the width (the convention of (2.25m, 2.1m) is used in the following discussions) for case g2Sg4Sg3S. Even though using the 'as is' data in the damage index II method for plate-like structures (DI-II-P) was able to detect two out of three severe damage locations, it is considered insufficient as it would potentially pose a major danger to a structure if any severe damage was not detected. Since, a one-dimensional cubic spline interpolation worked well for the beam tests in Chapter 7, hence, a two-dimensional cubic spline interpolation was adopted for the plate-like structure to expand the number of data points from the 'as is' data in order to enhance the possibility of damage detection using the DI-II-P method (Pereyra et al. 1999). In the contour plot of Figure 8.16b, applying the expanded data using the 2-D cubic spline technique, the damage localisation algorithm has clearly shown the locations of damage with two spurious damage

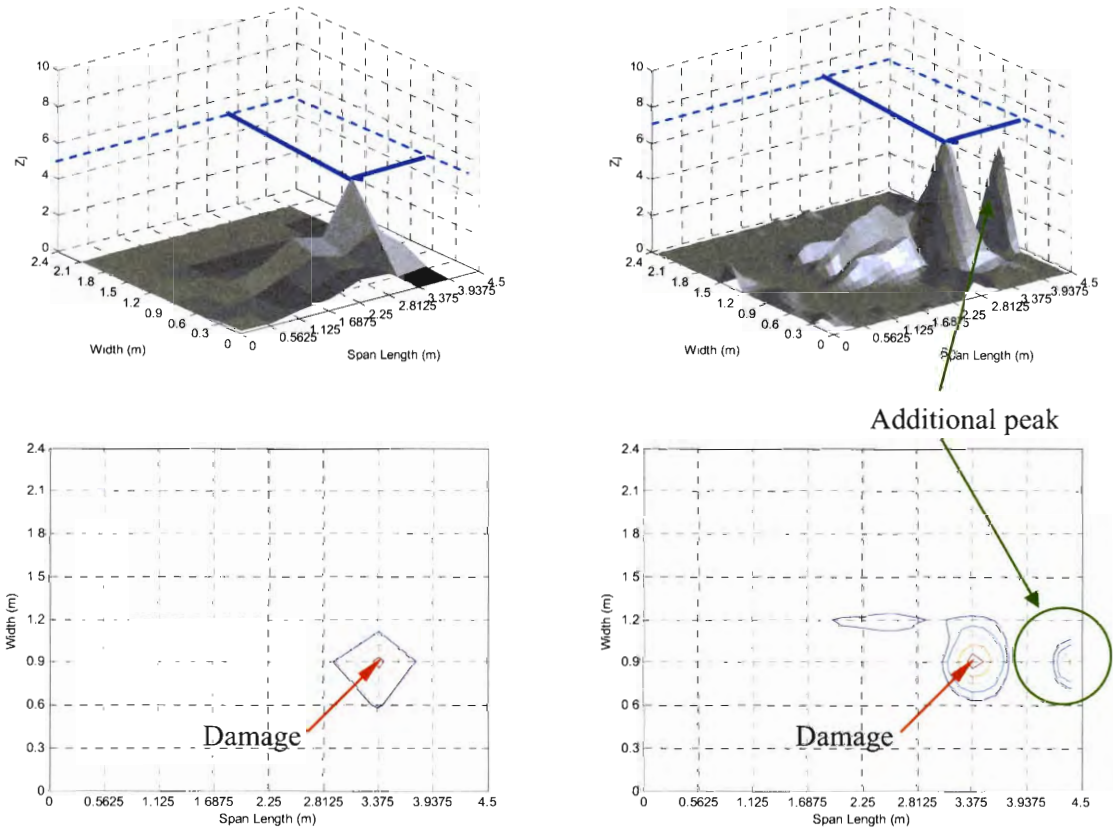
locations. The one missed damage location by using the 'as is' data may have been caused by the estimation of discrete curvature at the midspan (2.25m) being overshadowed by the two adjacent equal or higher severity damage at ¼ and ¾ span (1.125m and 3.375m). Adding more data points between the original data points subsequent to interpolation, the difference of curvature between two adjacent damage locations was better defined. Hence, from the reconstructed data, the damage at midspan was not subsided. However, it is important to note that there is slight distortion of data near both supports as depicted in the contour plot of Figure 8.16b, which are not seen in Figure 8.16a. This may be due to the cubic nature of the interpolation and may be avoided by using a high-order interpolation technique as suggested by Worden et al. (2001). It is anticipated that such data distortion may also happen to the free edges. (Improving the cubic spline mode shape reconstruction technique to avoid the distortion of data was not included in the scope of work for this study and it is proposed to be undertaken in future work.) In general, it is obvious that without sufficient number of sensors, the damage localisation algorithm in many circumstances cannot identify the damage location.



(a) As is (9 modes). (b) 2-D cubic spline (9 modes).

Figure 8.16 A three damage scenario case for the bridge (g2Sg4Sg3S).

Besides prevailing damage locations, the reconstruction of mode shape using the two-dimensional (2-D) cubic spline interpolation technique in the results has also increased the damage index value because the denser grid points are more sensitive to the local changes. From the surface plots of Figures 8.17a and 8.17b, the damage index value for the damage location at position (3.375m, 0.9m) is approximately 5 in the 'as is' result compared to 7 for the reconstructed data. It is apparent that the reconstruction of data has enhanced the probability of damage detection by 40%, which in turn enhanced the reliability of the damage detection. This promising trend was observed in all damage cases conducted in this investigation. This has confirmed the advantages of reconstructing the original data to a higher number of data points using the 2-D cubic spline interpolation technique.

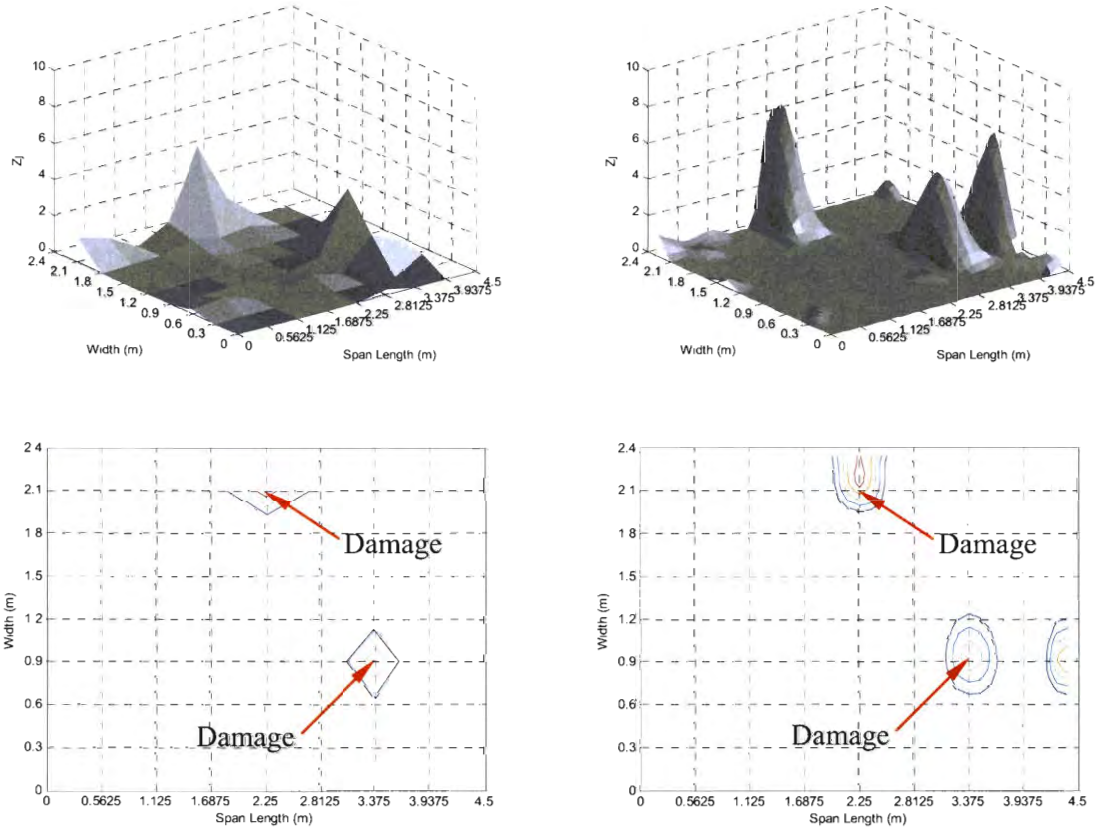


(a) As is (9 modes). (b) 2-D cubic spline (9 modes).

Figure 8.17 Single damage scenario case for the bridge (g2S).

The reconstruction technique, if not better, performs at least equally good compared to merely using the 'as is' data to calculate the damage indices. This is illustrated in the contour plots of Figure 8.18 for case g2Sg4S, whereby both 'as is' and 2-D cubic spline technique used in the damage localisation algorithm were able to identify all damage locations. Considering the practicality of field testing, to reconstruct mode shapes in order to produce sufficiently fine coordinates is essentially part of the damage localisation process.

Considering the advantages and disadvantages of the scenarios discussed above, it is apparent that the 2-D cubic spline interpolation technique has improved indication of damage without sacrificing any important features of the 'as is' results. Therefore, in the following discussion, the 2-D cubic spline interpolation technique is used for the reconstruction of mode shapes (41 points) from the given 'as is' data (9 points) for both longitudinal and transverse directions of the laboratory timber bridge in this study.



(a) As is (9 modes). (b) 2-D cubic spline (9 modes).

Figure 8.18 Two damage scenario case for the bridge (g2Sg4S).

8.3.4 Damage Localisation

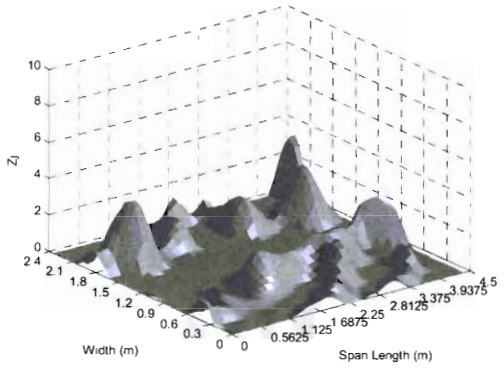
As mentioned earlier in Chapter 6, Cornwell, Doebling and Farrar (1999) stated that the damage index (DI) method for beam-like structures (using slicing mode on a plate-like structure) is not expected to perform better compared to the damage index method for plate-like structures (utilising two-dimensional curvatures) because the DI method for beam-like structures does not preserve torsional stiffness between slices. Nevertheless, it should be noted that the one-dimensional damage index method has been applied to two-dimensional and three-dimensional structures, such as a timber bridge (Peterson, McLean & Pollock 2003), but by decomposing them into beam-like elements. In this investigation, for the complicated laboratory timber bridge (a deck-girder system),,the proposed damage index algorithm for plate-like structures (abbreviated as DI-II-P) by Cornwell, Doebling and Farrar (1999) was adopted to locate damage. The application of DI-II-P method to detect damage in timber structures has not been reported to the best knowledge of the author.

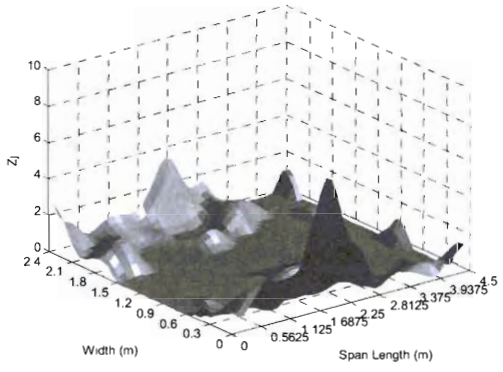
For damage localisation in the laboratory timber bridge, both the first three and the first nine modes were used in the damage index algorithm for plate-like structures (DI-II-P). The formulation of the DI-II-P algorithm in the following discussions was presented in details in Chapter 5. For comparison, the first three modes are used as these modes are easily acquired for a real timber bridge and this combination of modes is also commonly used (Peterson, McLean & Pollock 2003). However, the first three modes may not be sufficient to identify all damage locations. Hence it is suggested to adopt all the acquired modes (9 modes) in the damage localisation algorithm (Cornwell, Doebling & Farrar 1999). In addition, with the development of the latest technologies in sensors, it is now possible to obtain higher modes of a structural system with relative ease. This would definitely help to promote the use of higher modes in damage detection. It should be noted that normalisation of mode shape curvatures (which works well for damage index methods for beam-like structures) is yet to be incorporated in the DI-II-P method. The normalisation of 2-D curvatures is planned as part of the future work.

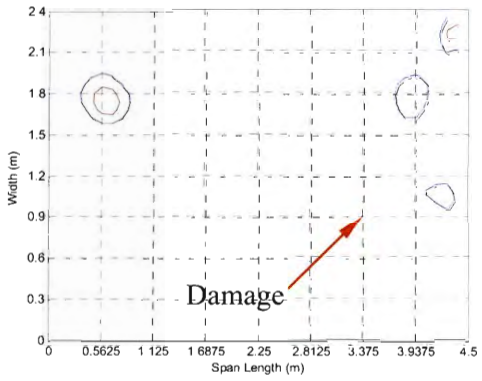
8.3.4.1 Damage Index II for Plate-like Structures

The single damage cases using the damage index II method for plate-like structures (DI-II-P) with either the first three or the first nine modes are illustrated in Figure 8.19. For single damage cases using the first three modes, the damage indicator is unable to clearly identify the damage location at position (3.375m, 0.9m) for damage cases g2L, g2M and g2S, which correspond to light, medium and severe damage (see contour plots of Figures 8.19a, 8.19c and 8.19e), respectively.

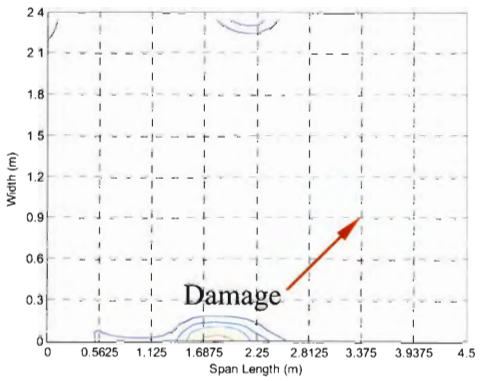
As a comparison, similar damage cases were identified with the first nine modes in the calculation. For the light damage case g2L (the smallest damage) as depicted in the contour plot of Figure 8.19b, the damage indicator could not locate the damage at position (3.375m, 0.9m). For the medium and severe damage cases g2M and g2S as illustrated in Figures 8.19d and 8.19f, respectively, the damage locations are detected quite pronouncedly even though there are false positives (indication of false damage locations). For single damage cases, comparing the results of using the first three and the first nine modes using the DI-II-P method shows that incorporating higher modes provides better results for medium and severe damage than just using the three lower modes. It is noticed that the lowest level of damage that could be identified, in the single damage scenarios, is medium damage of case g2M. The light damage for case g2L could not be identified.



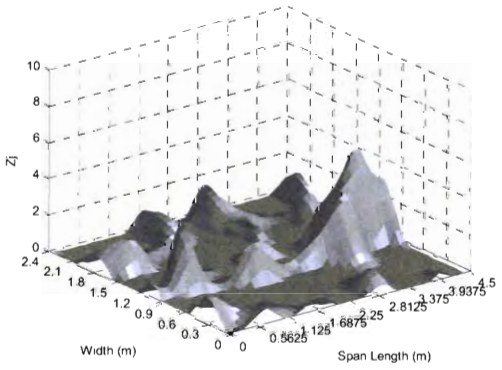


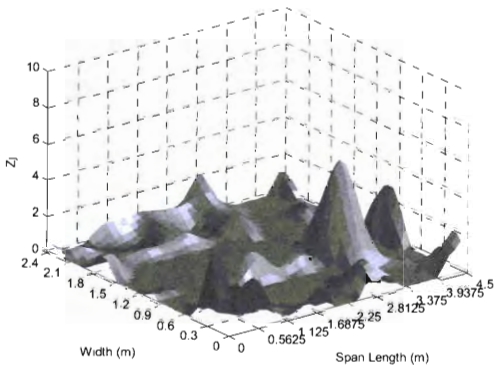


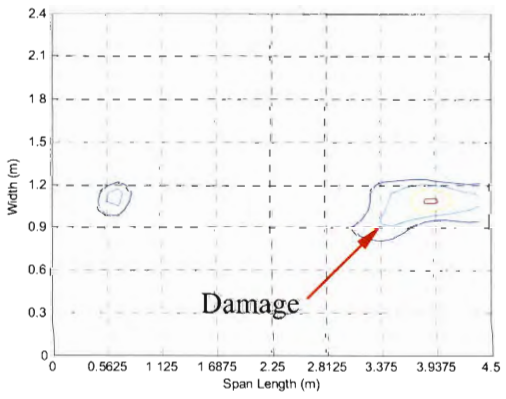
(a) g2L (3 modes).



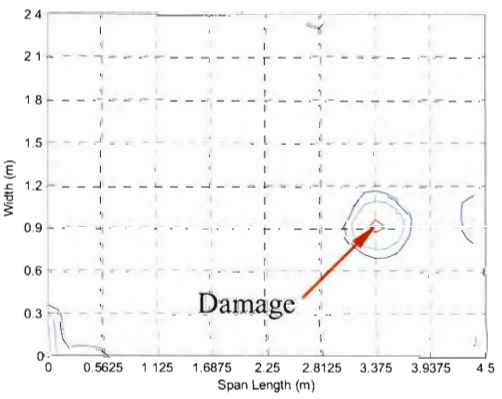
(b) g2L (9 modes).



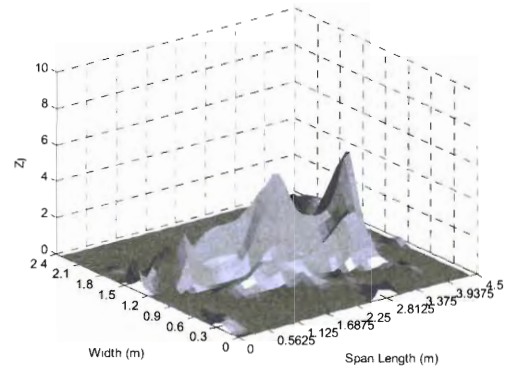


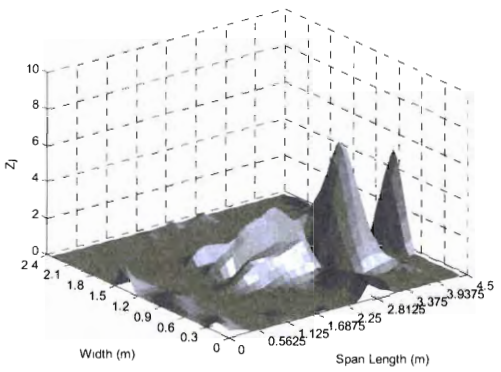


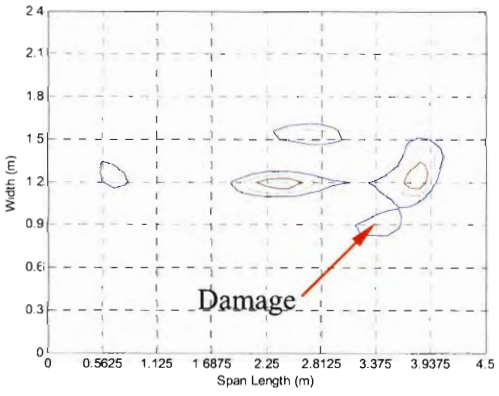
(c) g2M (3 modes).

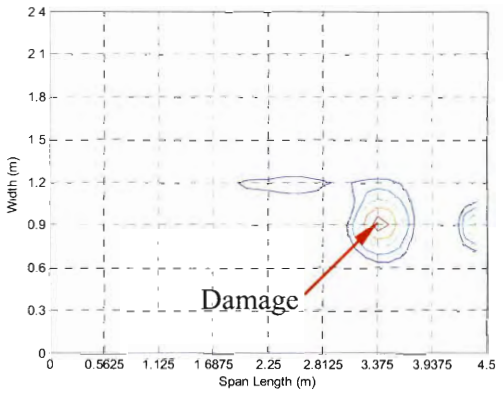


(d) g2M (9 modes).









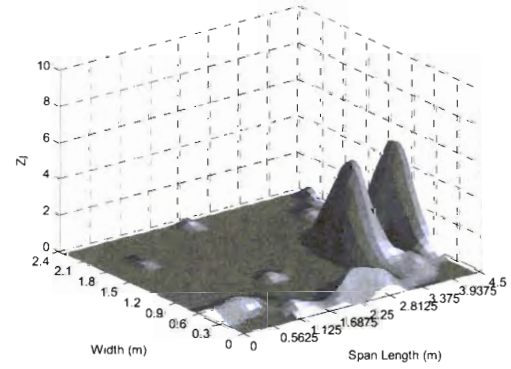
(e) g2S (3 modes). (f) g2S (9 modes).

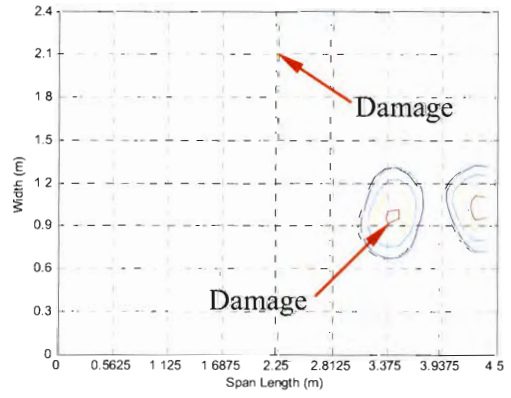
Figure 8.19 Single damage cases using DI-II-P method for bridge.

The two damage cases considered using the DI-II-P algorithm are shown in Figure 8.20. From the contour plot results of using the first three modes (see Figures 8.20a, 8.20c and 8.20e) and the first nine modes (see Figures 8.20b, 8.20d and 8.20f), basically all severe damage locations at position (3.375m, 0.9m) were identified for damage cases g2Sg4L, g2Sg4M and g2Sg4S as well as severe damage at position (2.25m, 2.1m) for case g2Sg4S. However, the light and medium damage at position (2.25m, 2.1m) were not identified for case g2Sg2L and g2Sg2M as depicted in the contour plots of Figures 8.20a and 8.20c (3 modes), and Figures 8.20b and 8.20d (9 modes), respectively. This is likely to be due to the change in mode shape curvature caused by the severe damage dominating the results compared to the light and medium damage. From the two damage cases, it should be noted that the second damage at position (2.25m, 2.1m) was not detected until this damage was roughly comparable in severity to the first severe damage at position (3.375m, 0.9m). This indicates that the method may encounter problems in identifying multiple damage locations with different

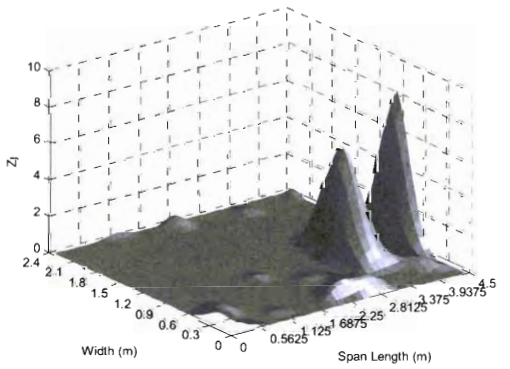
degrees of severity. However, the method is capable of identifying all severe damage locations and this is important for a structure to avoid catastrophic failure.

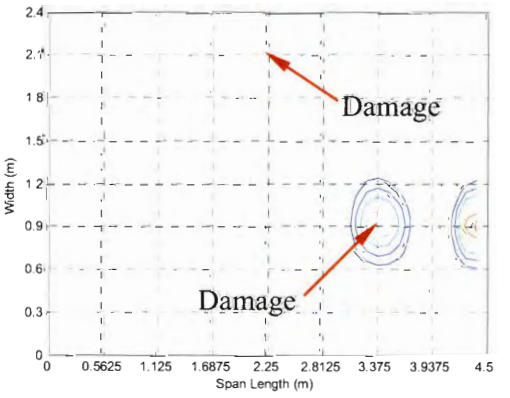
In some cases, the damage locations were detected but provided a misleading reflection of damage severity. This is seen in the surface plots of Figure 8.20e for damage case g2Sg4S with 3 modes. It was found that the damage indicator has provided a misleading representation of the probability of existence of damage for severe damage at position (3.375m, 0.9m). It is obvious that the severe damage at position (2.25m, 2.1m) has a larger index value (higher probability to be identified as a damage location) compared to severe damage at position (3.375m, 0.9m), despite the fact that they were inflicted with the same level of damage severity. On the other hand, the surface plot of Figure 8.20f (using 9 modes) shows that both severe damage locations pose a relatively similar damage index value. This indicates that both the severe damage locations have similar probability to be identified as damage. For the two damage location cases, using the first nine modes in the damage localisation algorithm for plate-like structures offers a better damage indication compared to using just the first three modes.



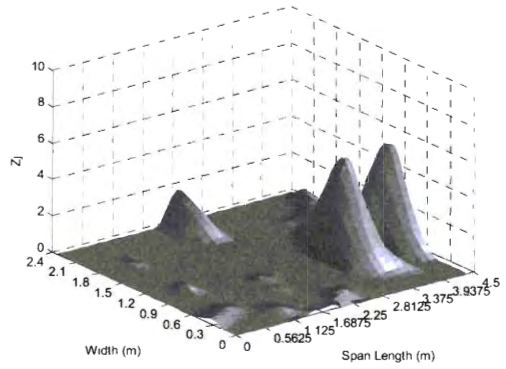


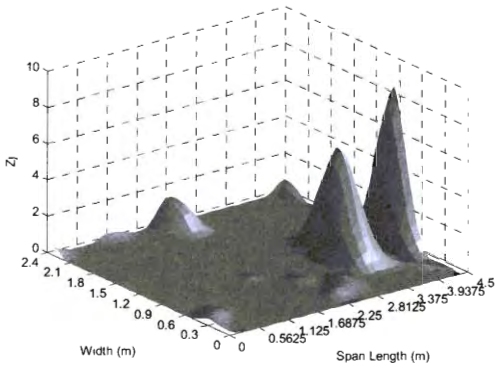
(a) g2Sg4L (9 modes).

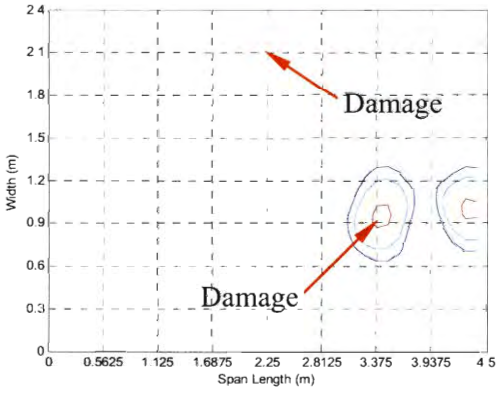


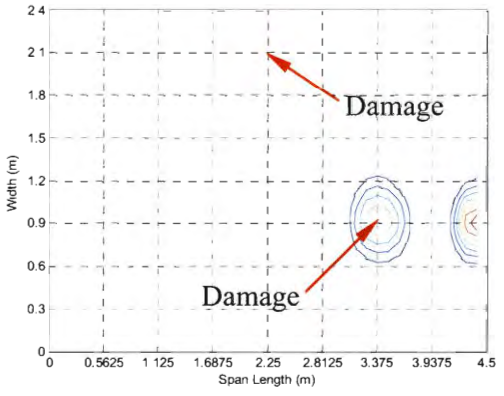


(b) g2Sg4L (9 modes).



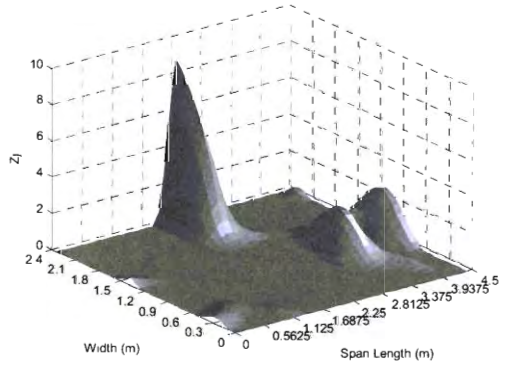


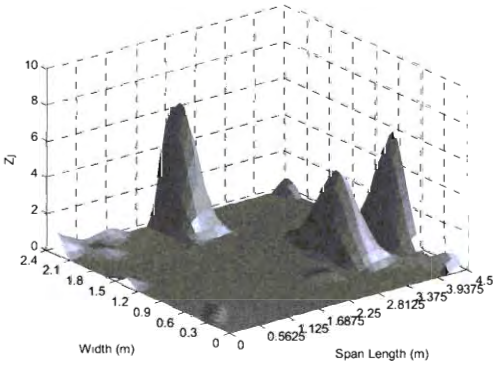


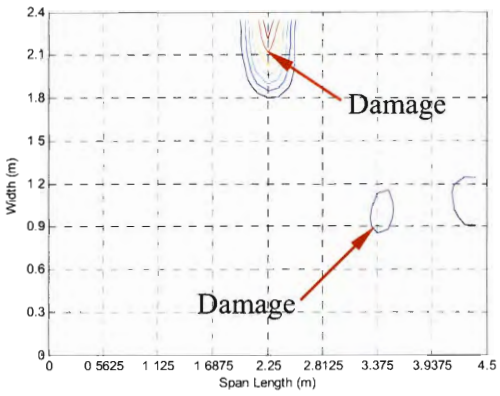


(c) g2Sg4M (3 modes).

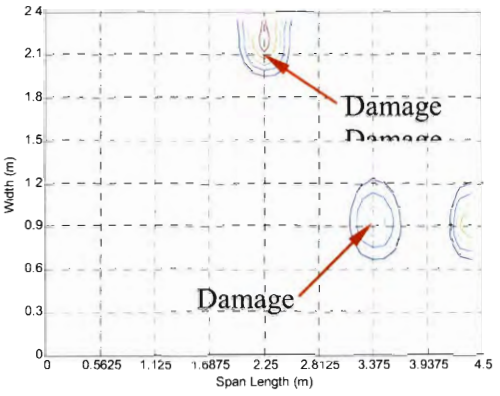
(d) g2Sg4M (9 modes).







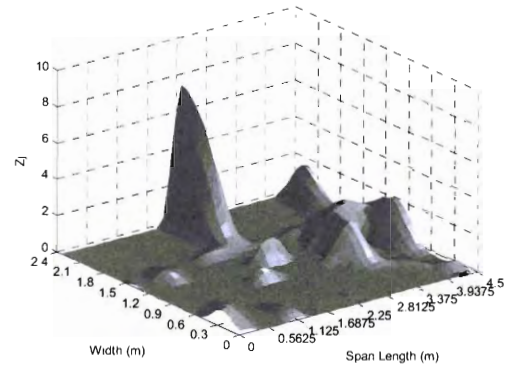
(e) g2Sg4S (3 modes).

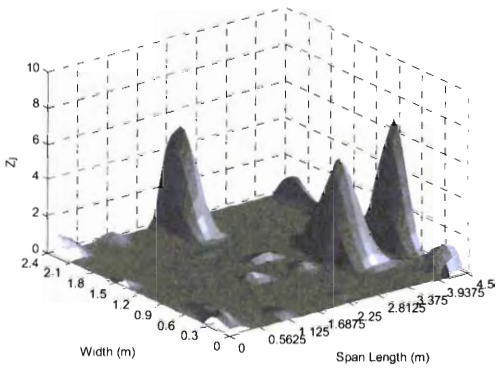


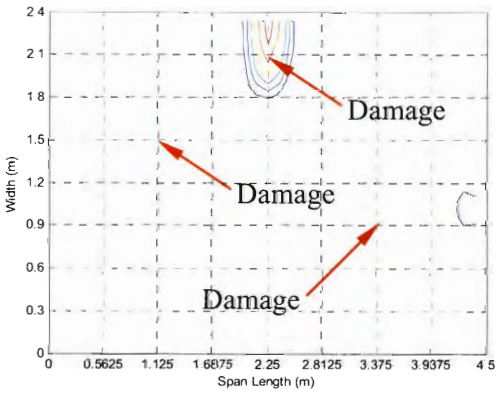
(f) g2Sg4S (9 modes).

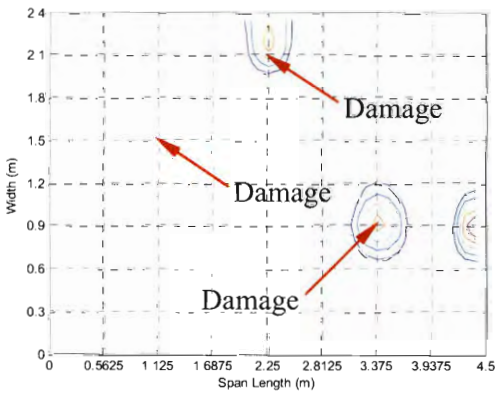
Figure 8.20 Two damage cases using DI-II-P method for bridge.

For three damage location cases, the results of the damage indicator using the DI-II-P algorithm are shown in Figure 8.21. By using either the first three or the first nine modes in the damage index method for damage cases g2Sg4Sg3L (see Figures 8.21a (3 modes) and 8.21b (9 modes)) and g2Sg4Sg3M (see Figures 8.21c (3 modes) and 8.21d (9 modes)), the contour plots show that the light and medium damage at position (1.125m, 1.5m) were not identified. In addition, using the first three modes in the localisation algorithm failed to pick up the severe damage at position (3.375m, 0.9m) for similar damage cases. For damage case g2Sg4Sg3S, using the first three modes (see Figure 8.21e) in the DI-II-P algorithm the severe damage location at position (1.125m, 1.5m) was missed. While for the same case using nine modes as illustrated in the contour plot of Figure 8.21f, all severe damage locations were identified. It should be noted that for case g2Sg4Sg3S, the damage index values are quite similar for the three severe damage locations with nine modes (see surface plot of Figure 8.21f) reflecting a better identification of the level of damage. Unlike the one with three modes (see surface plot of Figure 8.21e) the damage index values for the severe damage locations are quite different providing a misleading indication of the probability of damage locations. This reinforces the earlier findings for the cases of two damage locations that higher modes contribute more to damage detection for certain damage sites which may not be possible by using just the first three lower modes in the DI-II-P method.



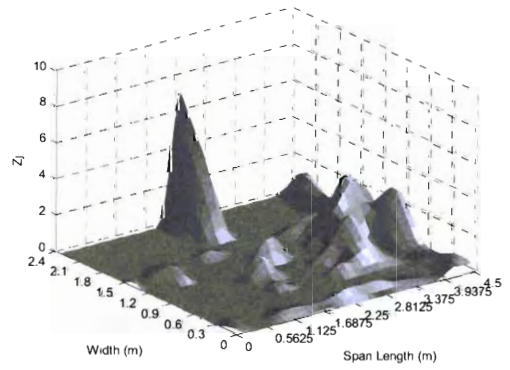


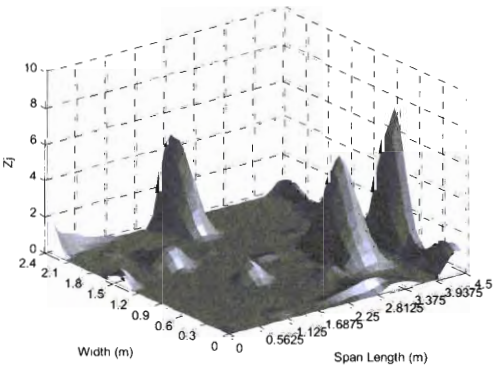


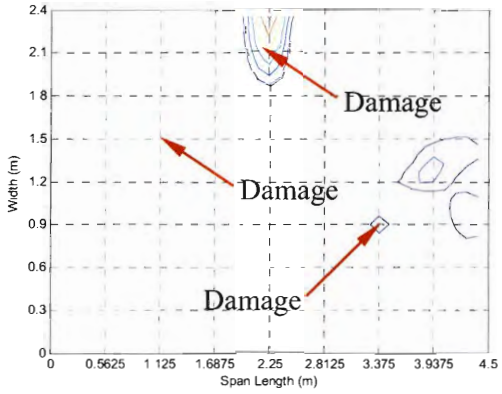


(a) g2Sg4Sg3L (3 modes).

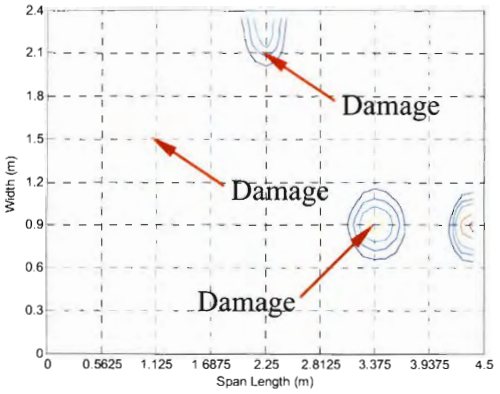
(b) g2Sg4Sg3L (9 modes).



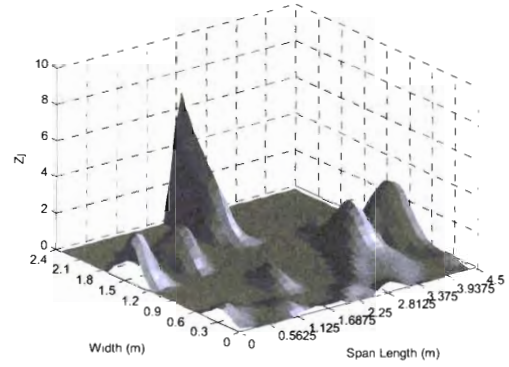


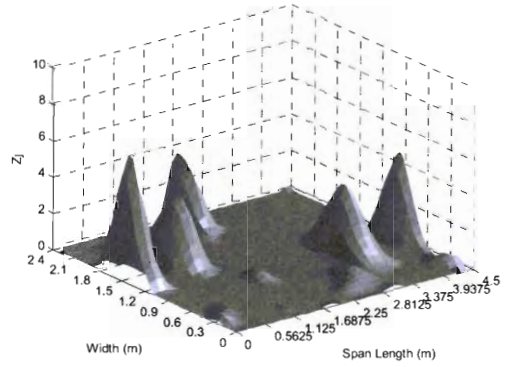


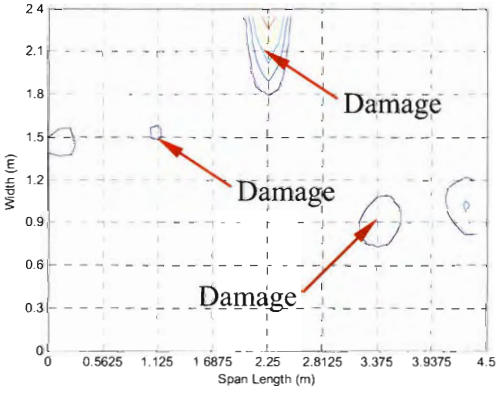
(c) g2Sg4Sg3M (3 modes).



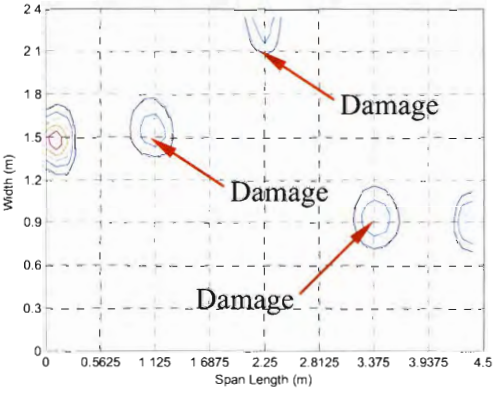
(d) g2Sg4Sg3M (9 modes).







(e) g2Sg4Sg3S (3 modes).



(f) g2Sg4Sg3S (9 modes).

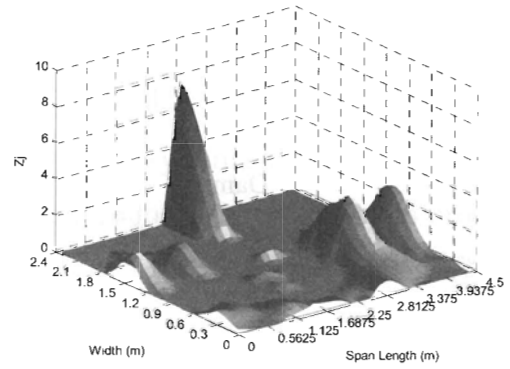
Figure 8.21 Three damage cases using DI-II-P method for bridge.

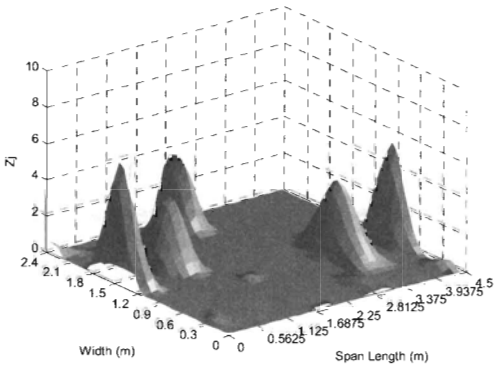
The results of four damage location scenarios applying either the first three or the first nine modes in the DI-II-P method are illustrated in Figure 8.22. The damage locations were not all accurately identified by the damage indicator. The damage localisation performed better using the first nine modes than the first three modes in the

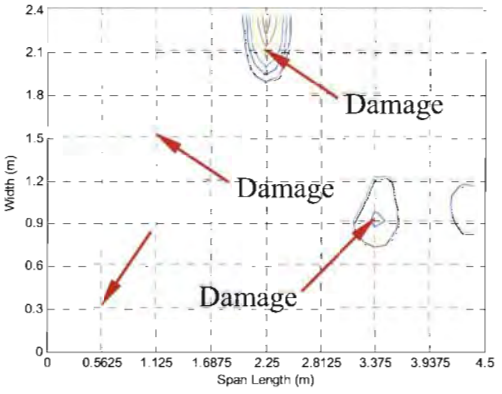
four damage location scenarios. Apparently, for the four damage cases, the DI-II-P method with three modes constantly missed the severe damage at position (1.125m, 1.5m). Unlike the nine modes one, this damage was clearly identified (see contour plots of Figure 8.22). This reaffirms the above findings that the DI-II-P algorithm using the first nine modes provides better damage detection than using just the first three modes. Using higher modes also gives a more realistic reflection of the level of damage in various damage scenarios, particularly for the severe damage.

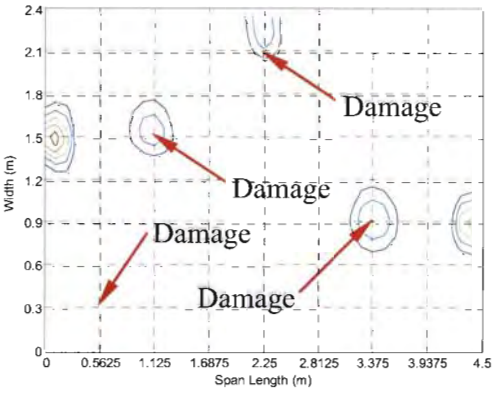
Besides the shortcomings of using the first three modes to detect damage, it should be noted that using three modes in the method may identify certain damage that could be missed by the nine modes case. This observation can be seen in the contour plots of Figures 8.22c and 8.22d (case g2Sg4Sg3Sg1M) (even though it is not very obvious), where the damage indicator using the first three modes identified clearly the damage locations at positions (2.25m, 2.1m) but not so when using the nine modes. This problem is mainly due to lack of normalisation on the two-dimensional mode shape curvatures (longitudinal, transversal and cross terms) as discussed earlier. From this observation, the author would propose as future work to normalise mode shape curvature for every mode in order to properly weigh higher modes contributions, which should provide better results when using higher modes in damage detection of plate-like structures.

Referring to contour plots of Figures 8.22d and 8.22f (case g2Sg4Sg3Sg1S), the severe damage at position (2.25m, 2.1m) was not identified even with the nine modes used in the damage localisation algorithm. This anomaly may indicate that the damage detection method may not perform very well if severe damage exists at position (0.5625m, 0.3m), a location near the supports ($\leq 1/8$ or $\geq 7/8$ of span length), and could undermine other severe damage locations.



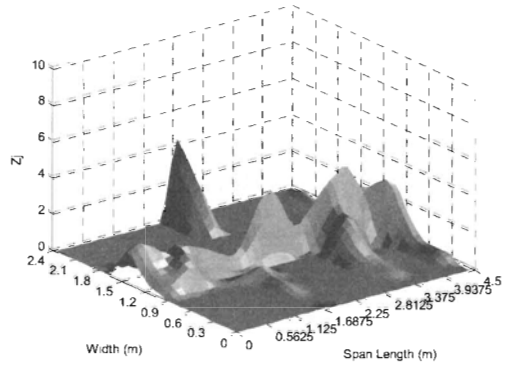


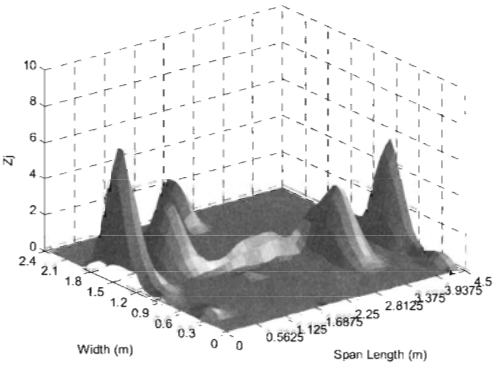


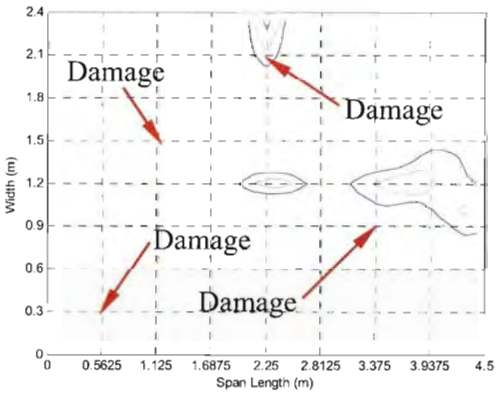


(a) g2Sg4Sg3Sg1L (3 modes).

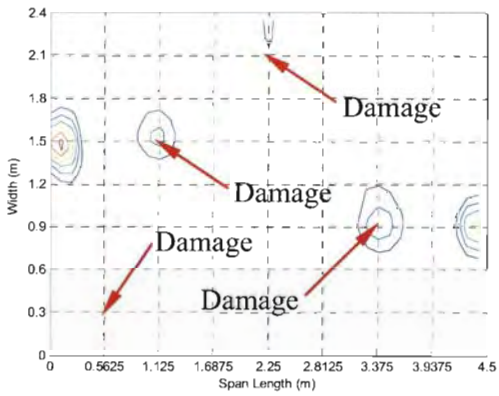
(b) g2Sg4Sg3Sg1L (9 modes).



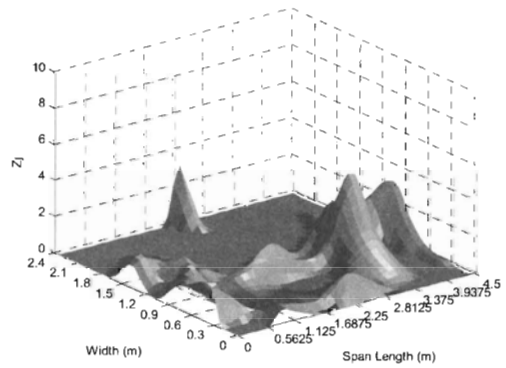


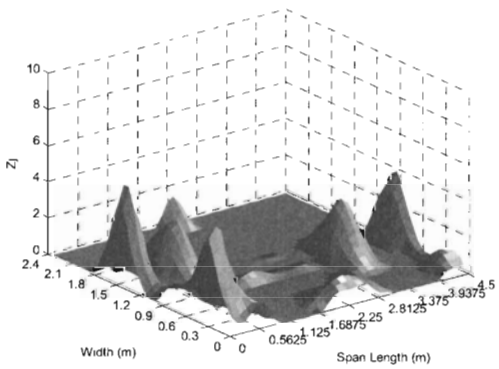


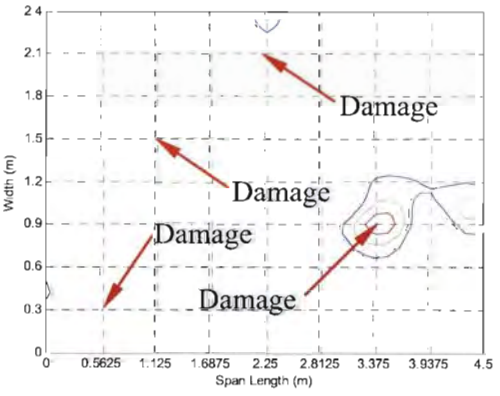
(c) g2Sg4Sg3Sg1M (3 modes).



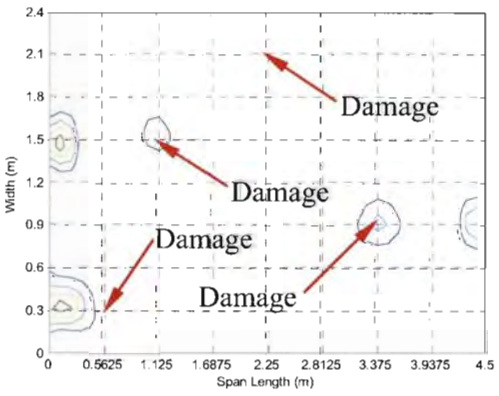
(d) g2Sg4Sg3Sg1M (9 modes).







(e) g2Sg4Sg3Sg1S (3 modes).



(f) g2Sg4Sg3Sg1S (9 modes).

Figure 8.22 Four damage cases using DI-II-P method for bridge.

8.4 Results and Discussions for Laboratory Timber Plate

From the success of using the damage index II method for plate-like structures (DI-II-P) to detect single and multiple damage locations in the laboratory timber bridge (deck-girder system), it was a supplementary work to the scope of this study to apply the damage localisation algorithm on a timber plate. As mentioned earlier, even though it is rare to have plate-type timber bridges, it is of interest to explore the application of DI-II-P method on a timber plate structure (orthotropic plate).

For the timber plate (plywood), the natural frequency and damping ratio for undamaged and damaged cases are presented in Tables 8.6 and 8.7, respectively. From Table 8.6, the changes of frequencies are minimal for the damaged cases compared to the undamaged case with the biggest difference of less than 0.7Hz for mode 5 of the most serious damage case 3LocB. The changes of frequencies are negligible before the forth mode. The results show that the inflicted damage, even for the most serious case (constituting 0.6% of area loss compared to the overall area), is not substantial enough to cause noticeable changes to the natural frequency. This may be misinterpreted as the inflicted damage is not serious, if using frequency change as a damage detection criterion. For the damping ratios as listed in Table 8.7, the trend is not consistent and it is not discussed any further.

Table 8.6 Natural frequencies for the plate.

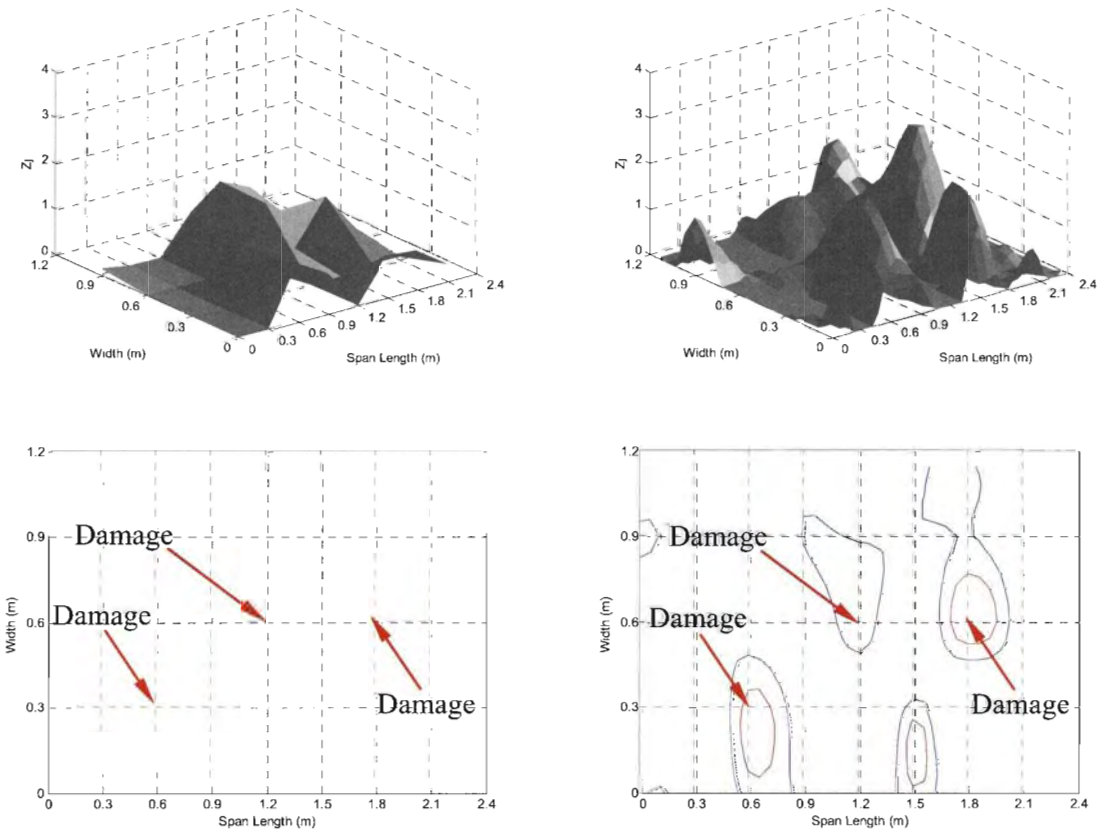
Mode	Natural frequencies (Hz)						
	P1	L2(I)A	L2(II)B	L2(II)B-L3(III)A	L2(II)B-L3(IV)B	L2(II)-L3(IV)B-L3(V)A	L2(II)-L3(IV)B-L3(VI)B
1	7.77	7.77	7.78	7.79	7.80	7.79	7.80
2	11.26	11.27	11.27	11.28	11.27	11.26	11.26
3	14.39	14.34	14.36	14.37	14.38	14.38	14.39
4	28.75	28.71	28.73	28.77	28.76	28.76	28.75
5	44.57	44.53	44.44	44.43	44.26	44.17	43.92
6	48.03	48.05	48.01	48.01	47.94	47.89	47.82

Table 8.7 Damping ratios for the plate.

Mode	Damping ratio (%)						
	P1	L2(I)A	L2(II)B	L2(II)B-L3(III)A	L2(II)B-L3(IV)B	L2(II)-L3(IV)B-L3(V)A	L2(II)-L3(IV)B-L3(VI)B
1	0.98	1.00	0.98	1.02	0.94	1.03	0.94
2	1.36	1.38	1.44	1.39	1.39	1.45	1.42
3	3.69	3.42	3.44	3.68	3.83	3.92	3.87
4	1.98	1.90	1.90	1.82	1.89	1.85	1.84
5	1.32	1.28	1.35	1.33	1.35	1.31	1.28
6	1.68	1.72	1.63	1.72	1.82	1.85	1.79

In the following results, the damage indicator, Zj, for each of the damage cases is plotted against the span length (2.4m) and width length (1.2m) of the timber plate. Similar thresholds were set for the damage indicator, Zj, for the laboratory timber bridge as was set for the timber plate, i.e., $Zj \geq 2$ which provides an approximately 95% level of confidence with respect to the actual damage locations (Park & Stubbs 1995; Peterson et al. 2001). To indicate the damage site in the graphs, the actual damage locations are marked with a red colour arrow sign and the word 'Damage' in all subsequent figures. For damage localisation of the timber plate, two types of graphs were used in this investigation as before, that is, surface and contour plots. The surface plots indicate the distribution of the damage indicator that are above zero ($Zj>0$), while the contour plots give information on predicted damage locations with $Zj \geq 2$.

Figure 8.23 shows the results of the 'as is' data and the interpolated data using two-dimensional (2-D) cubic spline for the timber plate. The results were calculated using the damage index II for plate-like structures (DI-II-P) applying to damage case L2(II)B-L3(IV)B-L3(VI)B with the first six vibration modes. In the contour plot of Figure 8.23, it is very obvious that without using any reconstruction technique to generate more data points, the damage localisation algorithm fails to identify any damage locations with $Zj \geq 2$. After applying 2-D cubic spline reconstruction technique on the mode shape data, all damage locations were located with some spurious damage locations. This, once more reinforces the earlier findings for the laboratory timber bridge that reconstruction technique would help to enhance damage detection, even though slight distortion of data may occur.

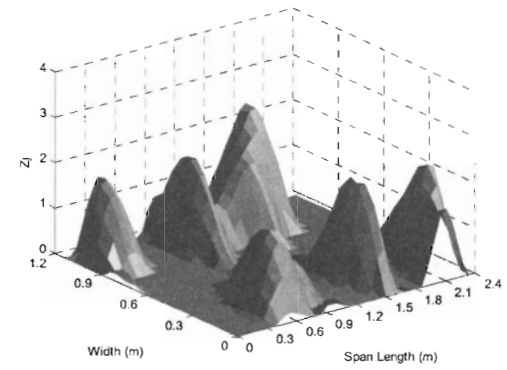


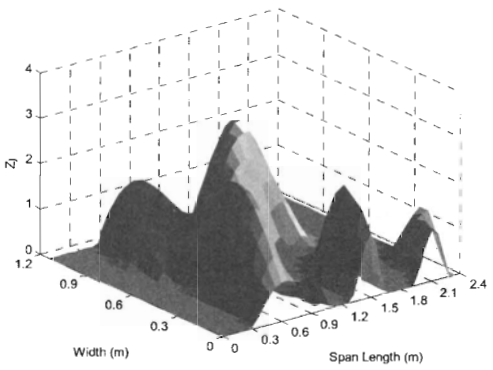
(a) 'As is' (6 modes). (b) 2-D cubic spline (6 modes).

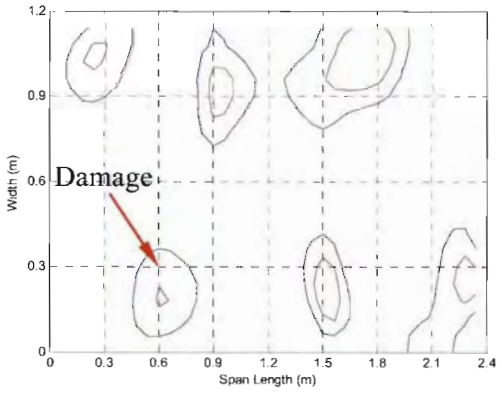
Figure 8.23 Three damage case (L2(II)B-L3(IV)B-L3(VI)B) using DI-II-P method for plate.

Applying the two-dimensional (2-D) cubic spline interpolation technique to all the damage cases of the timber plate, the damage localisation results using damage index II method for plate-like structures (DI-II-P) are shown in Figure 8.24. The results for single damage cases Loc(I)A (small) and Loc(II)B (large) are depicted in the contour plots of Figures 8.24a and 8.24b, respectively. The damage location at position (0.6m, 0.3m) was identified but with some false positives (indication of spurious damage locations). In general, the DI-II-P method used for the timber plate was able to identify all large damage (6% loss of area by comparing the damage area to a 300mm x 300mm bay). While for two damage cases of L2(II)B-L3(III)A and L2(II)B-L3(IV)B as shown in the contour plots of Figures 8.24c and 8.24d, the large damage at position (1.8m, 0.6m) was not clearly identified. The three damage cases are illustrated in Figures 8.24e and 8.24f, for cases L2(II)B-L3(IV)B-L3(V)A and L2(II)B-L3(IV)B-L3(VI)B, respectively. The damage locations with large damage are identified but not

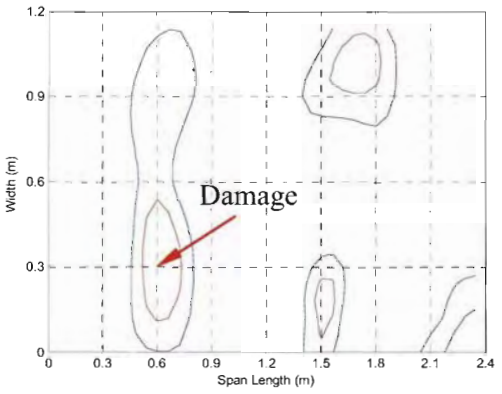
the small damage (2% loss of area comparing damage area to a 300mm x 300mm bay) at position (1.2m, 0.6m) as shown in the contour plot of Figure 8.24e. From this supplementary work, the DI-II-P method used in the timber plate did not work as well as for the laboratory timber bridge.



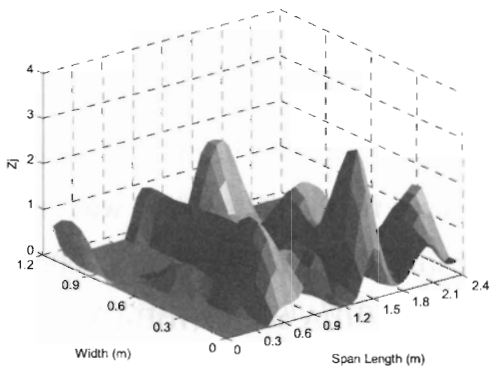


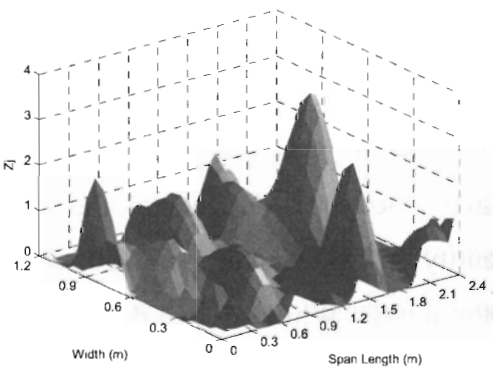


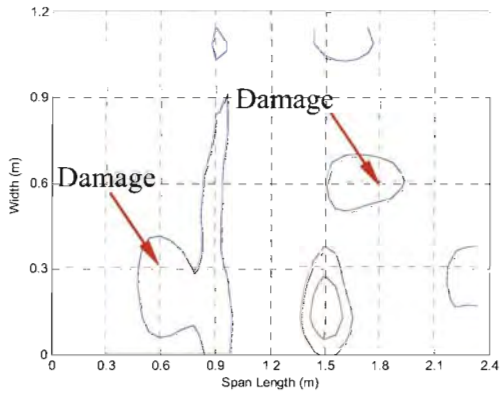
(a) Loc(I)A (6 modes).



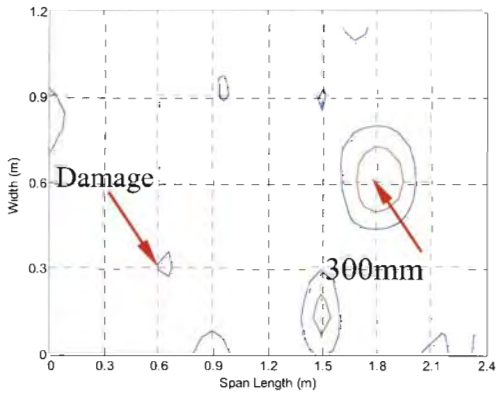
(b) Loc(II)B (6 modes).



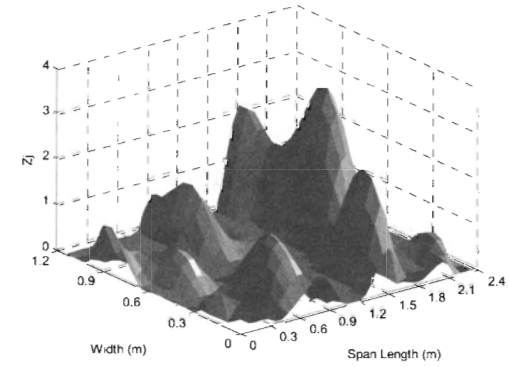


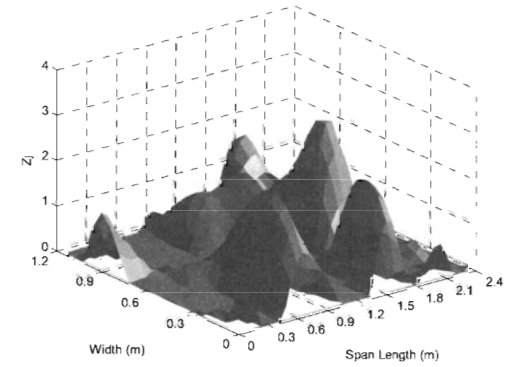


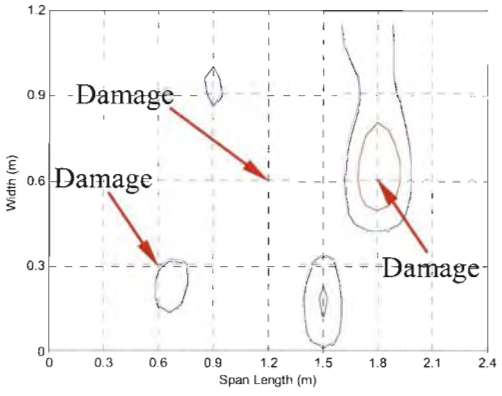
(c) L2(II)B-L3(III)A (6 modes).



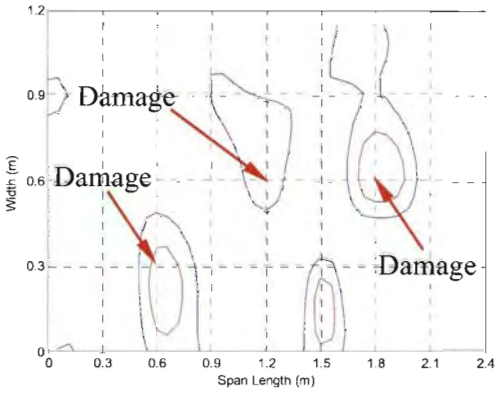
(d) L2(II)B-L3(IV)AB (6 modes).







(e) L2(II)B-L3(IV)B-L3(V)A (6 modes).



(f) L2(II)B-L3(IV)B-L3(VI)B (6 modes).

Figure 8.24 Damage cases using DI-II-P method for plate.

8.5 Summary

This chapter presents the verification of the damage index II method for plate-like structure (DI-II-P) using experimental work. A laboratory timber bridge was experimentally tested using experimental modal analysis. A supplementary work to the bridge was also performed on a timber plate.

It is clear that the two-dimensional (2-D) interpolation technique (2-D cubic spline) used to expand the limited number of data in the damage detection can significantly affect the detection. Using reconstructed data for detecting damage yields better results than just using 'as is' data.

Based on the results presented in this chapter, the damage index II method for plate-like structures (DI-II-P) using the first nine modes performs better than using the first three modes to detect location of damage for the laboratory timber bridge. This is consistent with the principle of structural dynamics whereby higher modes would provide better system identification. It should be highlighted here that even using nine modes in the DI-II-P method, in some cases, can present problems in identifying severe damage. This may be due to the lack of normalisation of mode shape curvature as discussed earlier. Incorporating normalisation of mode shape curvature in the DI-II-P method is yet to be developed and will be part of the future work.

Damage localisation using the DI-II-P algorithm was also applied to in a timber plate. Similar conclusions can be drawn. However, the damage localisation results were not as good compared to the ones for the laboratory timber bridge.

Chapter 9
Comparison of Numerical and Experimental Studies

9.1 Introduction

This chapter provides a comprehensive comparative study on the results of numerical and experimental investigations for damage detection on timber beam, laboratory timber bridge and timber plate, using various damage index methods. The comparisons presented in this chapter validate the hypothesis that the modified damage index methods perform well in detecting damage experimentally, although the experimental data are always polluted by noise, in addition to their capability of detecting damage well in the numerical models (finite element models with no noise present). For the numerical modelling, a finite element software package was utilised to simulate a timber beam, a laboratory timber bridge and a timber plate. The numerical models were verified experimentally and updated with modal testing and experimental modal analysis of the test specimen fabricated in the laboratory. The damage algorithms adopted for damage localisation for timber beam were modified damage index I (MDI-I) and modified damage index II (MDI-II). Besides, a hybrid algorithm of MDI-I and changes in flexibility (CIF), abbreviated as HMC, was proposed to estimate the severity of damage. The manipulated MDI-II algorithm was also utilised to evaluate the severity of damage. For the laboratory timber bridge, the damage index II for plate-like structures (DI-II-P) was adopted to detect damage. As a supplementary work, a timber plate was also studied using the DI-II-P for damage localisation.

9.2 Inflicted Damage in Timber Beam

The goal of this study was to detect damage typically found in timber bridges. It was carried out by locating multiple damage locations on a timber beam simulating girders of a timber bridge. The damage cases discussed in this section are described in Table 9.1 with details given in Chapter 7. In general, all damage scenarios consist of a rectangular opening along the span starting from the soffit of the beam, located at 2/8, 4/8 (midspan), 5/8 and 6/8 of the span length to simulate pockets of rot that usually starts from the top surface in timber girders. In this study and the discussions that follow, 'L', 'M' and 'S' denote light, medium and severe damage, respectively. All inflicted damage are 1% of the total span length (45mm) and consist of 10%, 30% and 50% of the beam depth, designated as damage cases 'L', 'M' and 'S' as shown in Table 9.1. The inflicted damage can also be interpreted as loss of 'I' (moment of inertia) from the depth of cut. The loss of section of 10% (L), 30% (M) and 50% (S) of beam depth, corresponds to 27.1%, 65.7% and 87.5% loss of 'I', respectively. In Table 9.1, shaded cases correspond to cases presented in Figures 9.1 to 9.4.

To facilitate comparison between numerical and experimental results, the number of mode shape coordinates for both numerical and experimental results are set to be nine points (see Figures 7.23 and 7.24 in Chapter 7). And then the nine point mode shape was reconstructed using cubic spline interpolation technique to a mode shape vector having forty one points. The reconstructed mode shapes were then applied in the damage detection algorithms attempting to locate and evaluate the inflicted damage scenarios. The reconstructed mode shape (41 points) has the advantage of higher possibility of locating damage compared to the original mode shape.

Table 9.1 Dimensions of inflicted damage in timber beams.

Damage Case	Damage Scenario	Location per 8th of span length	Length l (mm)	Depth h (mm)	% loss of 'I'
Beam 1	Un1				
1	**4L**	**4**	**45**	**9**	**27.1**
2	**4M**	**4**	**45**	**27**	**65.7**
3	**4S**	**4**	**45**	**45**	**87.5**
4	**4S6L**	**4, 6**	**45**	**45, 9**	**87.5, 27.1**
5	**4S6M**	**4, 6**	**45**	**45, 27**	**87.5, 65.7**
6	**4S6S**	**4, 6**	**45**	**All 45**	**All 87.5**
7	4S5L6S	4, 5, 6	45	45, 9, 45	87.5, 27.1, 87.5
8	4S5M6S	4, 5, 6	45	45, 27, 45	87.5, 65.7, 87.5
9	**4S5S6S**	**4, 5, 6**	**45**	**All 45**	**All 87.5**
10	**2L4S5S6S**	**2, 4, 5, 6**	**45**	**9, 45, 45, 45**	**27.1, 87.5, 87.5, 87.5**
11	2M4S5S6S	2, 4, 5, 6	45	27, 45, 45, 45	65.7, 87.5, 87.5, 87.5
12	**2S4S5S6S**	**2, 4, 5, 6**	**45**	**All 45**	**All 87.5**
Beam 2	Un2				
13	**6L**	**6**	**45**	**9**	**27.1**
14	**2L6L**	**2, 6**	**45**	**All 9**	**All 27.1**
15	2L4L6L	2, 4, 6	45	All 9	All 27.1
16	2L4L6M	2, 4, 6	45	9, 9, 27	27.1, 27.1, 65.7
17	2M4L6M	2, 4, 6	45	27, 9, 27	65.7, 27.1, 65.7
18	2M4M6M	2, 4, 6	45	All 27	All 65.7
19	**2M4M6S**	**2, 4, 6**	**45**	**27, 27, 45**	**65.7, 65.7, 87.5**
20	2S4M6S	2, 4, 6	45	45, 27, 45	87.5, 65.7, 87.5
21	**2S4S6S**	**2, 4, 6**	**45**	**All 45**	**All 87.5**
22	**2S4S5L6S**	**2, 4, 5, 6**	**45**	**45, 45, 9, 45**	**87.5, 87.5, 27.1, 87.5**
23	**2S4S5M6S**	**2, 4, 5, 6**	**45**	**45, 45, 27, 45**	**87.5, 87.5, 65.7, 87.5**
24	2S4S5S6S	2, 4, 5, 6	45	All 45	All 87.5

9.3 Results and Discussions for Timber Beams

9.3.1 Damage Localisation

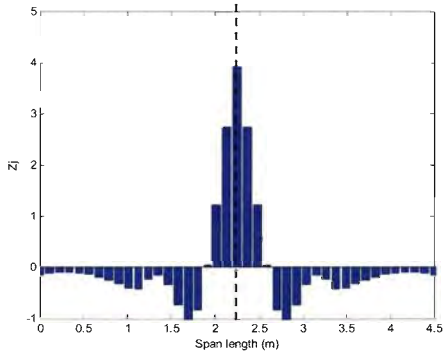
For damage localisation in timber beams, the first five flexural modes were used for calculation of damage indicators by the two modified damage index algorithms. It was concluded earlier that these two algorithms, namely, modified damage index I (MDI-I) and modified damage index II (MDI-II), are found to perform better than their original formulae with the first five flexural modes. In the following results, all damage indicators, *Zj*, for each damage case are plotted against the beam span length (4.5 m). In general, the statistically normalised damage indicator values *Zj* larger than zero (the probability-based criterion for damage) indicates that damage has occurred at that location. *Zj* smaller than zero, has no physical meaning, hence they are not discussed. The actual damage locations are indicated with vertical dashed lines in all figures.

9.3.1.1 Discussions on Modified Damage Index I Method

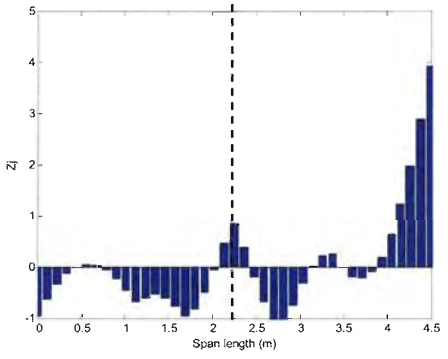
The damage indicator (Z_j) for single damage scenarios computed using the first five flexural modes in the proposed modified damage index I (MDI-I) method are illustrated in Figure 9.1. It can be seen from Figures 9.1e to 9.1h that the simulated single damage detected in the numerical studies was also identified by the experimental studies. This suggests that both numerical and experimental models are quite compatible especially for medium and severe damage although there are some appearances of false positives (indication of spurious damage locations) in the experimental results. For light damage cases shown in Figure 9.1a to 9.1d, the small magnitudes of Z_j are overwhelmed with noise causing the peak at the actual damage location to become less distinct compared to other noise-induced peaks in the experimental results.

In the experimental results, it was observed that spurious damage often appears at locations near the supports that did not exist in the numerical results. This type of false damage is likely to be caused by imperfections in the boundary conditions. Even though the specially fabricated pin supports were used in the experimental work to provide a pin-pin boundary, they could never represent an ideal pinned boundary. Instead of having zero displacement as in the numerical study, the 'real' supports are subjected to very small modal displacement under vibration, at which the magnitude of

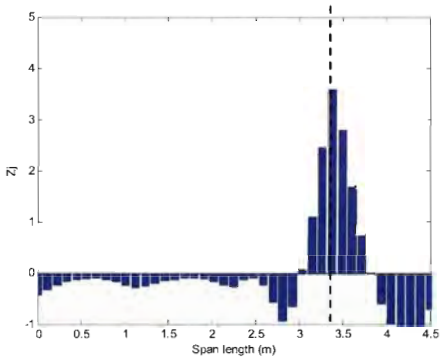
displacement is close to level of measurement noise. Hence, the measured modal displacement at supports is strongly inferenced by measurement noise. For any modal testing, for example the undamaged and damaged cases, the modal displacements obtained at the supports were mostly contribution of noise change rather than the actual vibrations. The noise-polluted mode shape data at the supports was then included in the reconstruction of the mode shape from coarse coordinates (9 points) to a finer grid (41 points). This would distort the reconstruction results as compared to the desired mode shape results. On the other hand, the principle behind the proposed damage detection algorithms identifies damage by utilising the difference of mode shape curvatures between the undamaged and damaged cases. Therefore, the spurious damage at locations near the supports was identified as damage only because of the difference in magnitude of modal displacement for the undamaged and damaged cases due to noise. For example, let us assume the modal displacement at the support for the modal test of undamaged case is 0.0001. While for the damaged one is 0.0002. In terms of magnitude, the modal displacement for the two tests is not significant. However, the difference between them creates an error of 100%. In contrast, the pin supports modelled in the numerical studies are ideal and they are fully rigid in the vertical direction. Therefore, in the damage detection results, the peak is very distinct at damage location even with the light damage case because there is no noise induced in the numerical model.



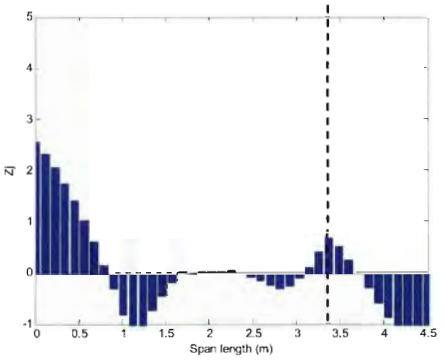
(a) 4L (Numerical).



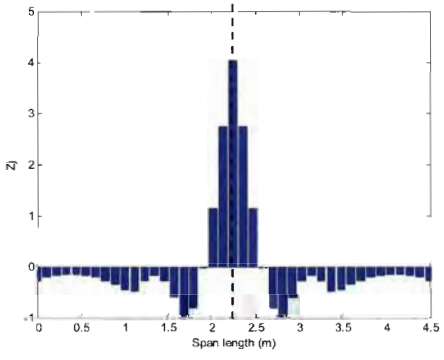
(b) 4L (Experimental).



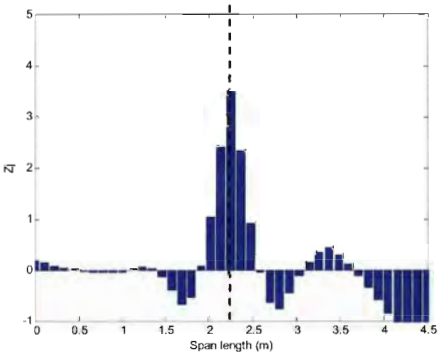
(c) 6L (Numerical).



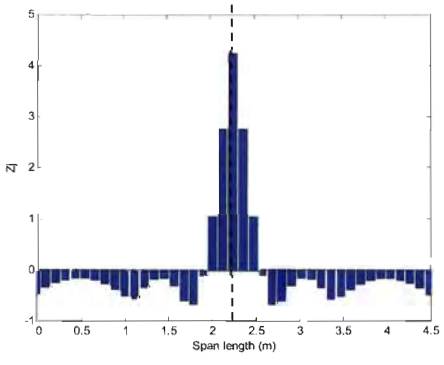
(d) 6L (Experimental).



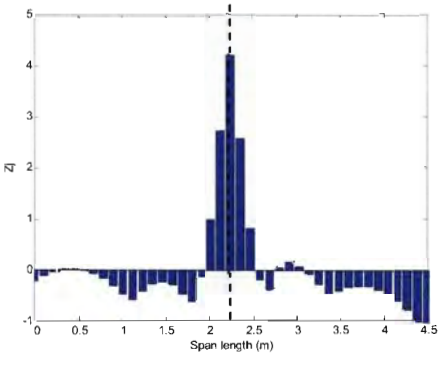
(e) 4M (Numerical).



(f) 4M (Experimental).



(g) 4S (Numerical).

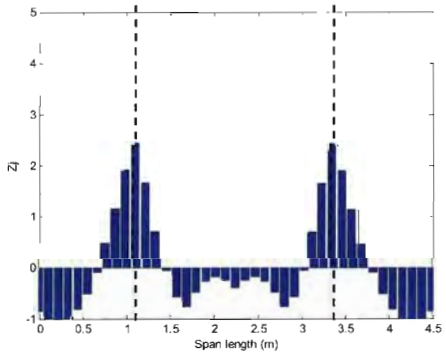


(h) 4S (Experimental).

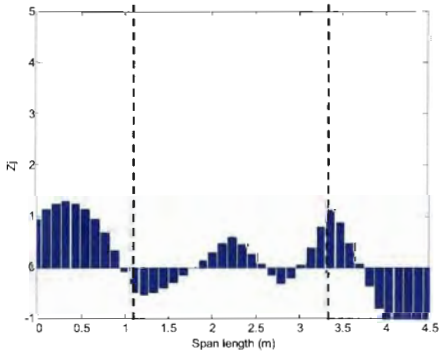
Figure 9.1 Single damage cases using MDI-I method (5 modes).

The two damage cases using the MDI-I method are presented in Figure 9.2. For both numerical and experimental results, basically, all medium and severe damage locations are successfully identified. However, the light damage at ¾ span (3.375m) for case 4S6L was not detected as shown in Figure 9.2d in both studies. In addition, referring to Figure 9.2b, the case 2L6L for the experimental studies missed one light

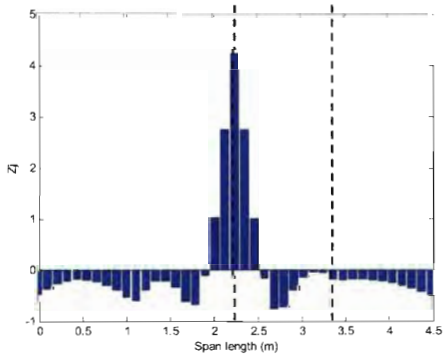
damage at ¼ span (1.125m), which was identified by the numerical results (see Figure 9.2a). This indicates that the experimental results work well for medium and severe damage in the two damage cases using the MDI-I method. For light damage cases, the experimental results perform reasonably well, although there are some spurious damage locations and one light damage was not detected (case 2L6L). Nonetheless, for safeguarding a structure it is important to identify severe damage, which is demonstrated in the experimental results using the MDI-I method, in order to avoid failure.



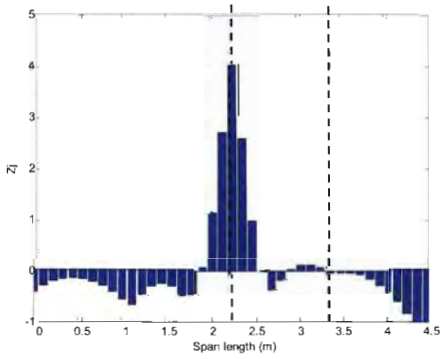
(a) 2L6L (Numerical).



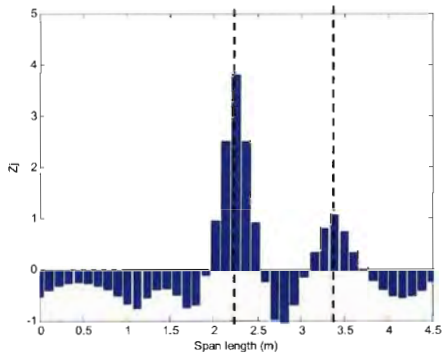
(b) 2L6L (Experimental).



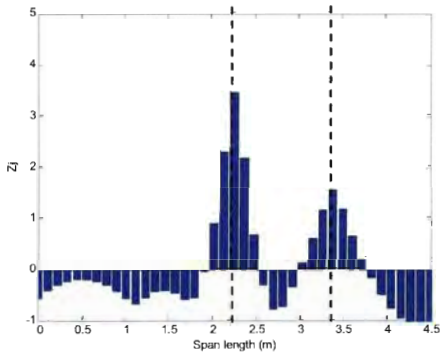
(c) 4S6L (Numerical).



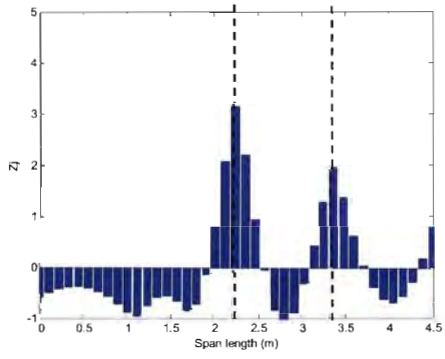
(d) 4S6L (Experimental).



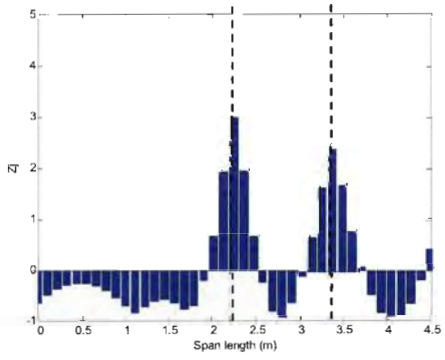
(e) 4S6M (Numerical).



(f) 4S6M (Experimental).



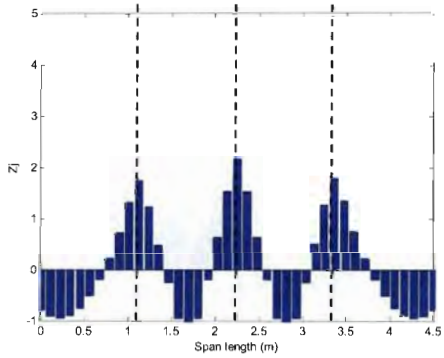
(g) 4S6S (Numerical).



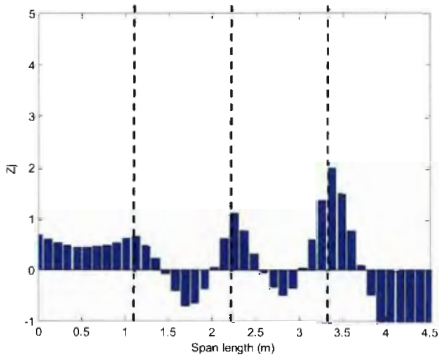
(h) 4S6S (Experimental).

Figure 9.2 Two damage cases using MDI-I method (5 modes).

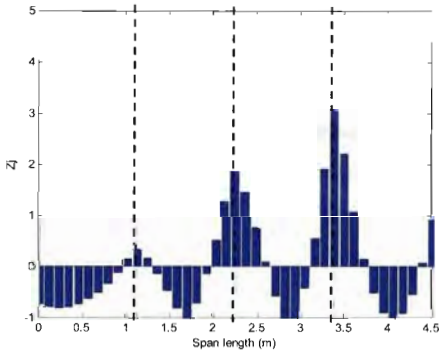
The damage indicator using the MDI-I method for three damage locations cases are shown in Figure 9.3. The experimental results again perform well in detecting all medium and severe damage locations, and similar results are also exhibited in the numerical studies. For light damage cases, as depicted in Figures 9.3a and 9.3b for numerical and experimental studies, respectively, all light damage locations were clearly identified. However, there are some false positives appearing between location 1.125m and the support (0m) in the experimental results (Figure 9.3b). This shows that the experimental data using the MDI-I method is capable of detecting well the light, medium and severe damage for the three damage location scenarios, but with a few spurious damage locations for the light damage scenarios.



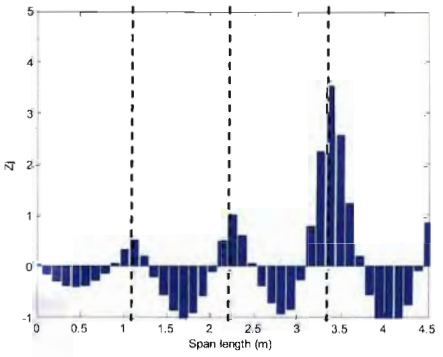
(a) 2L4L6L (Numerical).



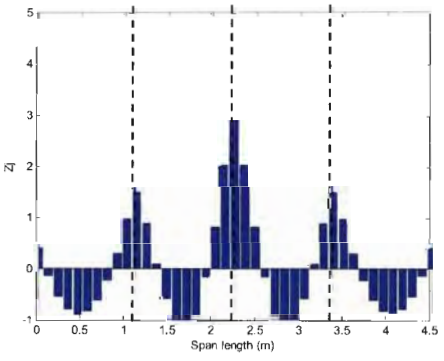
(b) 2L4L6L (Experimental).



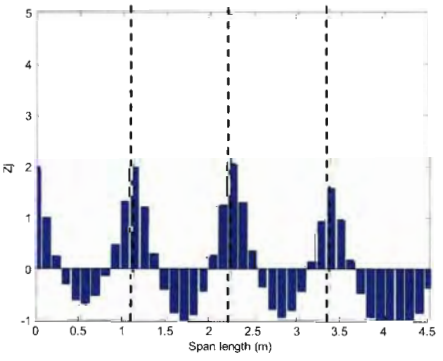
(c) 2M4M6S (Numerical).



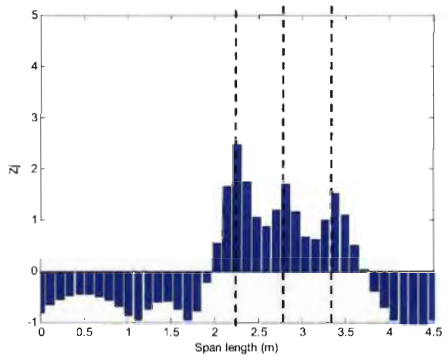
(d) 2M4M6S (Experimental).



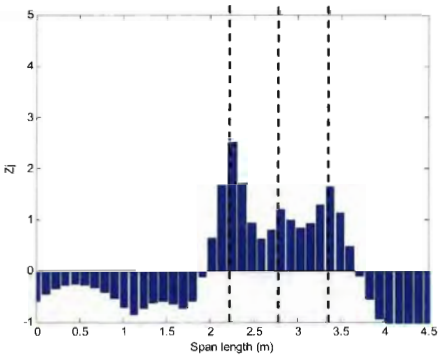
(e) 2S4S6S (Numerical).



(f) 2S4S6S (Experimental).



(g) 4S5S6S (Numerical).

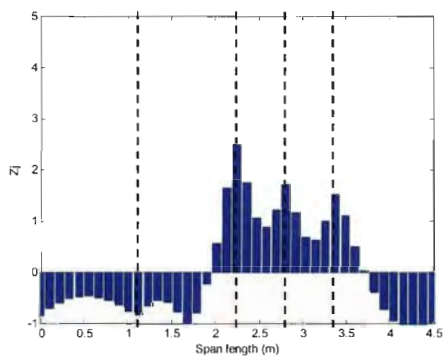


(h) 4S5S6S (Experimental).

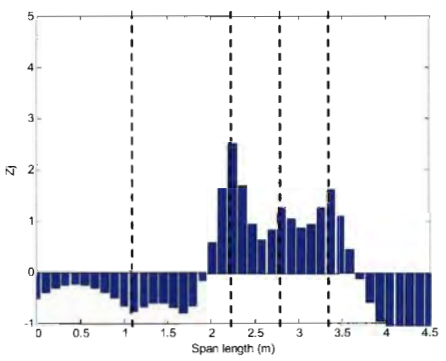
Figure 9.3 Three damage cases using MDI-I method (5 modes).

Figure 9.4 illustrates the damage indicator for the four damage location scenarios using the first five flexural modes in the MDI-I method for both numerical and experimental results. Both results are practically identical. They are able to identify all severe damage locations but missed all light and medium damage locations. This may be due to the fact that under inference of severe damage, the light and medium damage was eclipsed amongst the severe damage locations where the changes in curvature due to light and medium damage are less significant and harder to pick up by the damage detection algorithm.

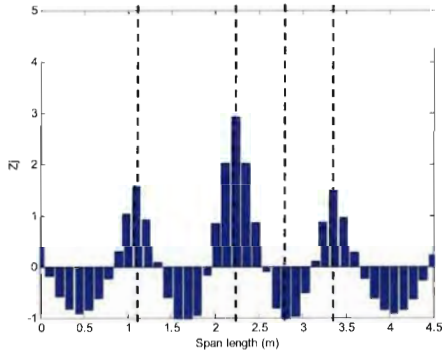
It is concluded that there is satisfactory agreement between the numerical and experimental results for medium and severe damage. As proven by the experiments, it is evident that the proposed damage detection algorithm (MDI-I) is preferred over the original algorithm (DI-I). The MDI-I method is capable of identifying major damage in the timber beams.



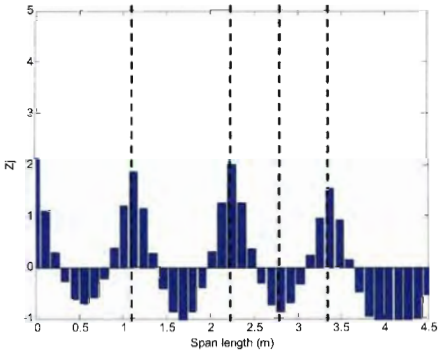
(a) 2L4S5S6S (Numerical).



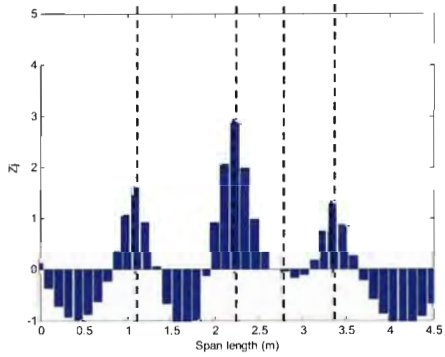
(b) 2L4S5S6S (Experimental).



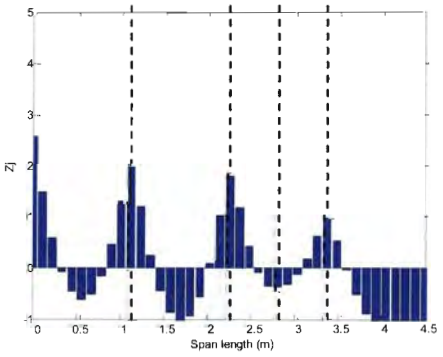
(c) 2S4S5L6S (Numerical).



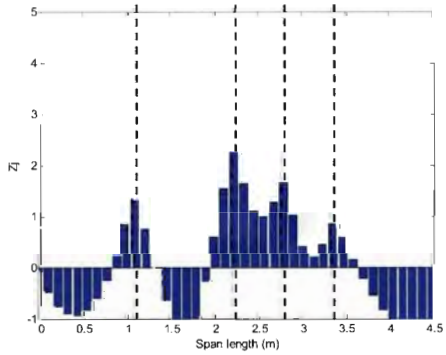
(d) 2S4S5L6S (Experimental).



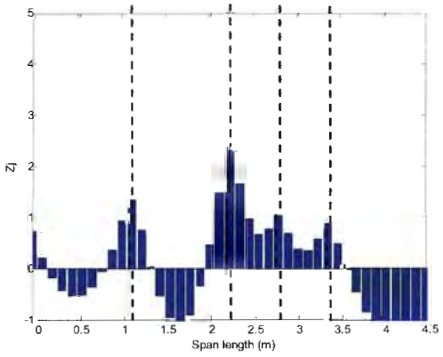
(e) 2S4S5M6S (Numerical).



(f) 2S4S5M6S (Experimental).



(g) 2S4S5S6S (Numerical).

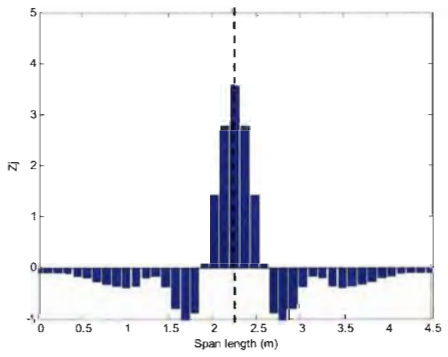


(h) 2S4S5S6S (Experimental).

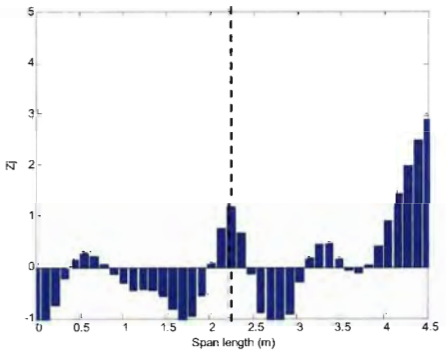
Figure 9.4 Four damage cases using MDI-I method (5 modes).

9.3.1.2 Discussions on Modified Damage Index II Method

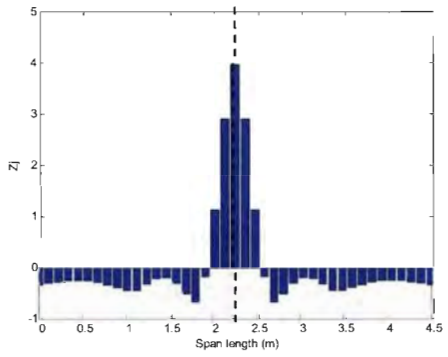
The single damage cases applied in the modified damage index II (MDI-II) method using the first five flexural modes are illustrated in Figure 9.5. For single damage case 4S as shown in Figures 9.5c and 9.5d, the numerical and experimental models are able to indicate accurately and distinctly the location of severe damage at location 2.25m (midspan). The trend for severe damage is not obviously shown in the single light damage case 4L, whereby the experimental case (Figure 9.5b) produces serious false positives (indication of false damage locations) near the support, which has larger damage index values compared to the actual damage location. It is quite clear that as the severity of damage increases the experimental results get closer to the numerical results.



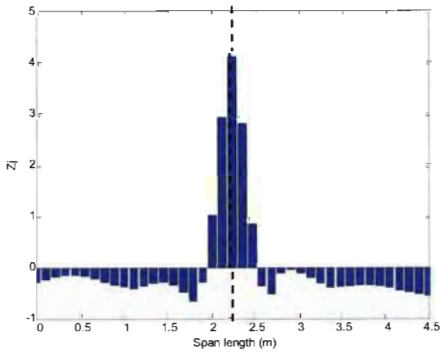
(a) 4L (Numerical)



(b) 4L (Experimental)



(c) 4S (Numerical)

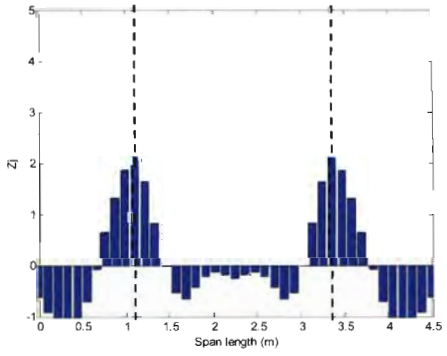


(d) 4S (Experimental)

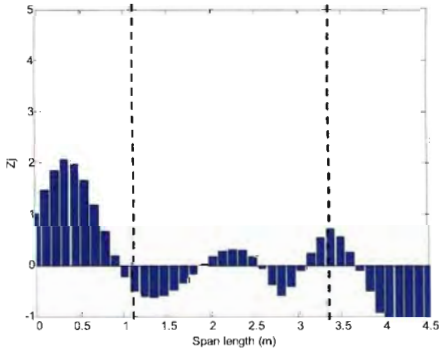
Figure 9.5 Single damage cases using MDI-II method (5 modes).

Figures 9.6, 9.7 and 9.8 depict the damage cases with two, three and four damage locations, respectively. In general, for medium and severe damage cases, the damage detection results from experiments using the MDI-II method are very close to the results predicted by the numerical studies. However, the correlations between numerical and experimental results are less for light damage cases as exampled in case 2L6L of Figures 9.6a and 9.6b, respectively.

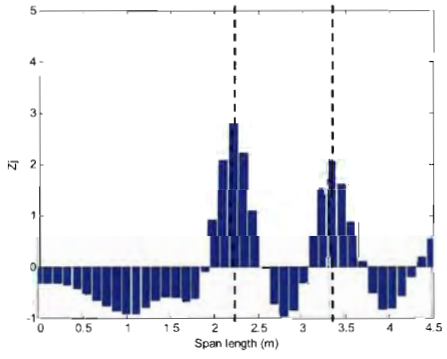
From the single and multiple damage cases, it is apparent that the experimental and numerical data using the MDI-II method located well the medium and severe damage locations. For the light damage cases, the experimental results need more caution when used to represent damage in a real structure, although the numerical results are able to detect the light damage location. Comparing damage localisation for the numerical and experimental studies using single and multiple damage cases, both methods, MDI-I and MDI-II, perform equally well.



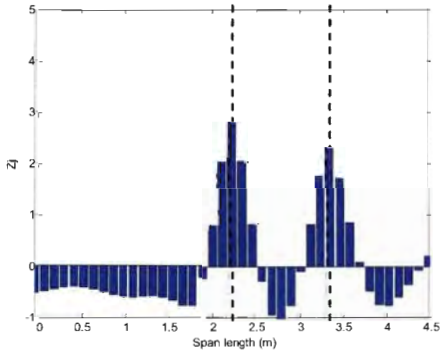
(a) 2L6L (Numerical)



(b) 2L6L (Experimental)

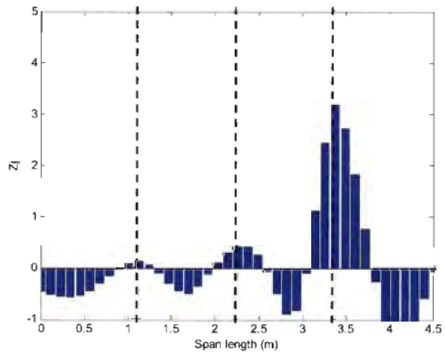


(c) 4S6S (Numerical)

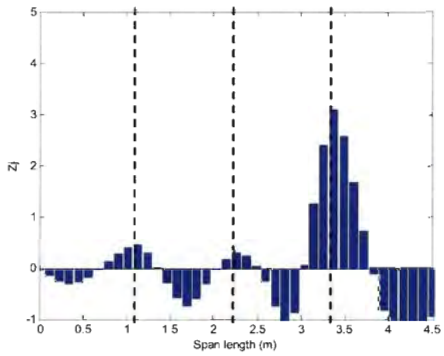


(d) 4S6S (Experimental)

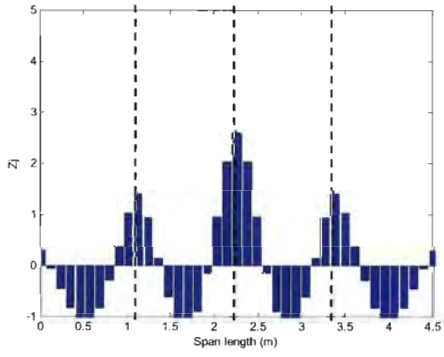
Figure 9.6 Two damage cases using MDI-II method (5 modes).



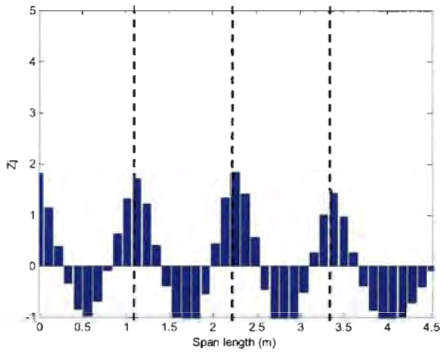
(a) 2L4L6M (Numerical)



(b) 2L4L6M (Experimental)

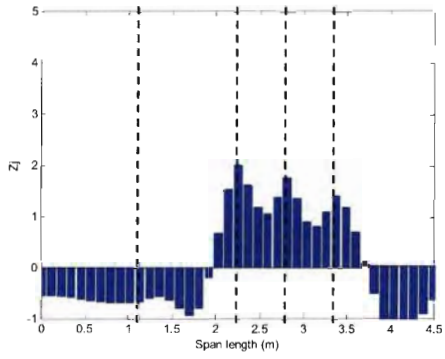


(c) 2S4S6S (Numerical)

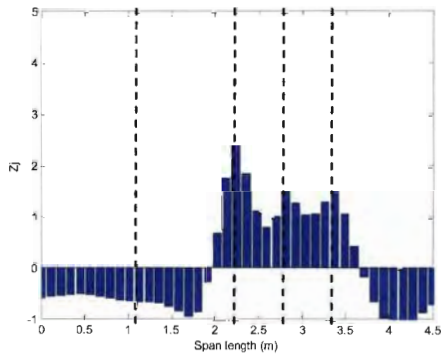


(d) 2S4S6S (Experimental)

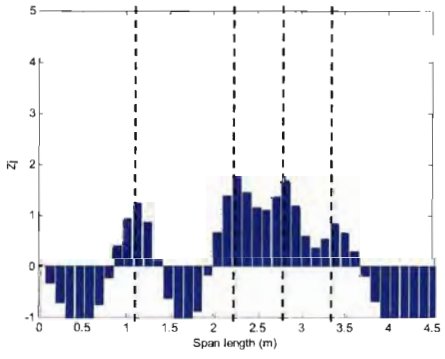
Figure 9.7 Three damage cases using MDI-II method.



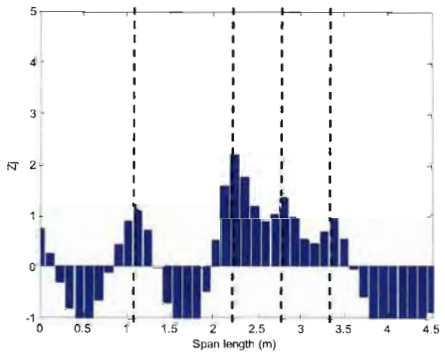
(a) 2L4S5S6S (Numerical)



(b) 2L4S5S6S (Experimental)



(c) 2S4S5S6S (Numerical)



(d) 2S4S5S6S (Experimental)

Figure 9.8 Four damage cases using MDI-II method.

9.3.2 Estimation of Severity of Damage

In the following sections, the hybrid of modified damage index I (MDI-I) method and changes in flexibility (CIF) method, abbreviated as HMC, is used to estimate the severity of damage. For modified damage index II (MDI-II), the formula was further developed for better estimation of damage severity. The estimation of damage severity for both algorithms (HMC and MDI-II) is presented in terms of percentage of loss of 'I' (moment of inertia). The horizontal dash-dotted lines are used to demonstrate the inflicted severity of damage and the vertical dashed lines indicate damage locations in the following figures. The first five modes were chosen for the calculation of the damage severity estimation in the following discussions.

9.3.2.1 Discussions on HMC Method

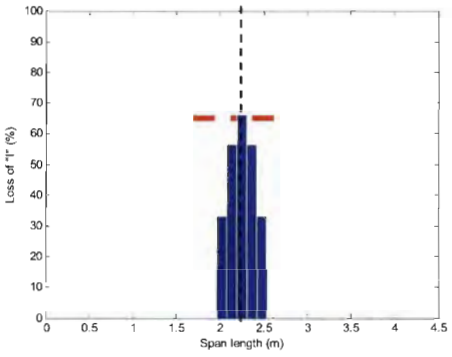
To apply the HMC method to the experimental data containing noise, some minor adjustment was required with the assumption that maximum changes in the calibration due to noise is within 20%, hence justifying a weighting factor of 0.8. For the numerical results, no weighting factor was applied since noise is not present in the numerical models.

After this adjustment, four cases of various damage scenarios were selected for comparison between numerical and experimental results employing HMC algorithm for estimating the damage severity. The chosen damage scenarios are 4M (Figures 9.9a and 9.9b), 2L6L (Figures 9.9c), 2M4M6S (Figures 9.9e and 9.9f) and 2S4S5S6S (Figures 9.9g and 9.9h) for both numerical and experimental studies. The predicted damage severity is given in Table 9.2. Referring to Figures 9.9a and 9.9b, the simulated medium damage (65.7% loss of 'I') for single damage scenario at location 2.25m was predicted quite accurately from both numerical and experimental data, even though some false positives were found in the latter one (see Figure 9.9b). For the two light damage locations (case 2L6L) as shown in Figures 9.9c and 9.9d, the numerical and experimental results are not well correlated. The experimental data did not work well in estimating the damage severity using the HMC method, while the numerical data performed relatively better. Figures 9.9e to 9.9h show the evaluation of damage severity using the HMC method for damage cases of three (2M4M6S) and four (2S4S5S6S) damage locations, respectively. The numerical and experimental results are quite similar. Again good agreement between numerical and experimental results for medium and severe damage was found when applying the HMC method to estimate severity of damage except for the light damage scenario. It should be noted that, in general, the numerical models predict the severity of damage well without any need for a weighting factor, while for the experimental data under influence of noise, the HMC method overestimates the damage severity, therefore, requiring a weighting factor.

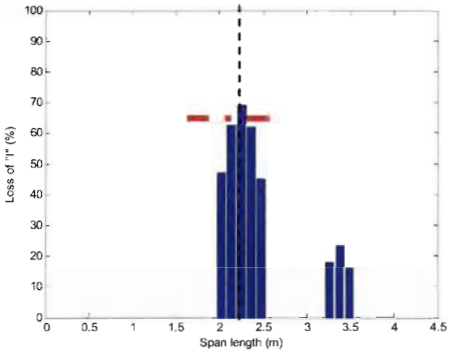
Table 9.2 Estimation of damage severity using HMC method.

Damage Case	Damage Scenario	Simulated Damage Severity (%)	Predicted Numerical Damage Severity (%)	Predicted Experimental Damage Severity (%)
Beam 1	Un1			
1	4L	27.1	22.3	0
2	**4M**	**65.7**	**65.9**	**69.1**
3	4S	87.5	87.4	81.6
4	4S6L	87.5, 27.1	87.3, 0	84.7, 0
5	**4S6M**	**87.5, 65.7**	**85.6, 39.8**	**83.0, 67.8**
6	4S6S	ALL87.5	83.5, 74.9	71.2, 75.9
7	4S5L6S	87.5, 27.1, 87.5	83.8, 0, 75.4	76.6, 0, 79.5
8	4S5M6S	87.5, 65.7, 87.5	84.0, 0, 76.3	89.0, 0, 87.8
9	4S5S6S	ALL 87.5	80.6, 72.9, 73.9	69.9, 68.0, 74.2
10	2L4S5S6S	27.1, 87.5, 87.5, 87.5	0, 80.6, 73.2, 74.1	0, 84.0, 81.2, 83.8
11	2M4S5S6S	65.7, 87.5, 87.5, 87.5	0, 80.2, 74.7, 75.3	0, 83.9, 79.0, 82.6
12	**2S4S5S6S**	**ALL 87.5**	**75.8, 80.3, 78.4, 70.3**	**79.5, 84.2, 79.6, 78.9**
Beam 2	Un2			
13	6L	27.1	24.1	53.1
14	2L6L	27.1, 27.1	15.5, 15.5	0, 71.0
15	2L4L6L	27.1, 27.1, 27.1	9.2, 5.3, 9.2	69.3, 71.2, 82.6
16	2L4L6M	27.1, 27.1, 65.7	0, 0, 67.4	56.5, 46.0, 83.7
17	2M4L6M	65.7, 27.1, 65.7	62.5, 0, 62.5	86.3, 0, 86.0
18	2M4M6M	ALL 65.7	54.8, 54.1, 54.8	76.2, 62.1, 68.7
19	**2M4M6S**	**65.7, 65.7, 87.5**	**23.5, 49.0, 86.1**	**51.0, 58.7, 85.5**
20	2S4M6S	87.5, 65.7, 87.5	86.5, 43.2, 86.5	83.1, 35.7, 81.9
21	2S4S6S	ALL 87.5	78.2, 82.9, 78.2	85.6, 84.6, 83.9
22	2S4S5L6S	87.5, 87.5, 27.1, 87.5	78.6, 83.3, 0, 78.1	90.1, 89.0, 0, 88.8
23	2S4S5M6S	87.5, 87.5, 65.7, 87.5	79.1, 83.9, 0, 76.0	91.0, 88.8, 0, 85.5
24	2S4S5S6S	ALL 87.5	75.8, 80.3, 78.4, 70.3	87.1, 82.2, 84.9, 82.7

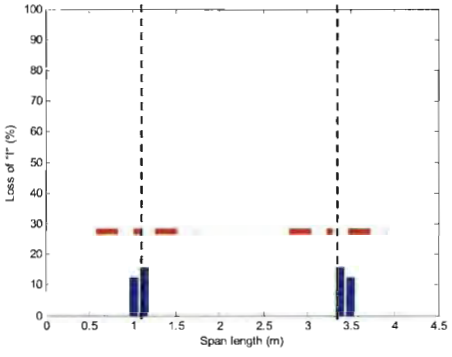
Note: Shaded cases correspond to those presented in Figure 9.9.



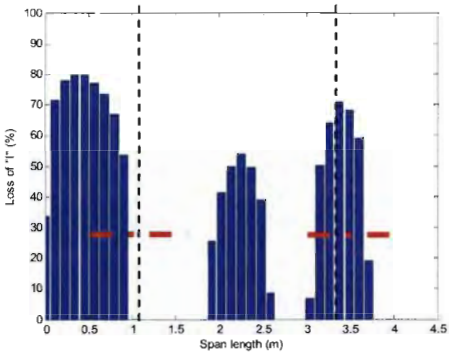
(a) 4M (Numerical).



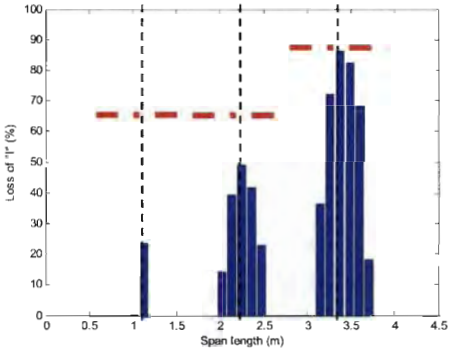
(b) 4M (Experimental).



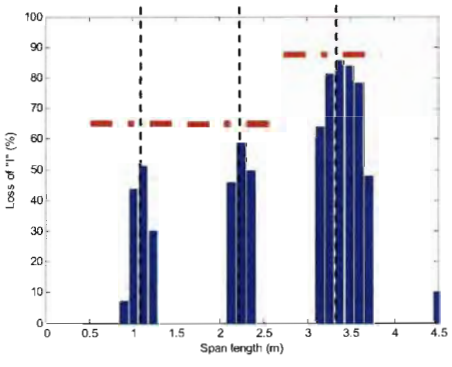
(c) 2L6L (Numerical).



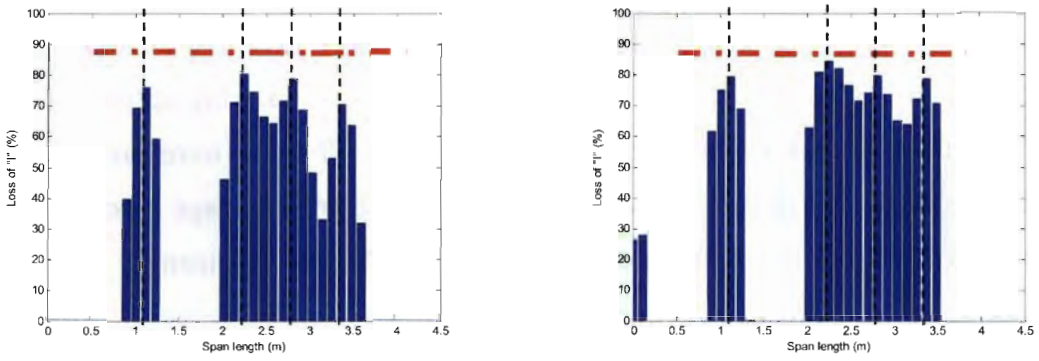
(d) 2L6L (Experimental).



(e) 2M4M6S (Numerical).



(f) 2M4M6S (Experimental).



(g) 2S4S5S6S (Numerical). (h) 2S4S5S6S (Experimental).

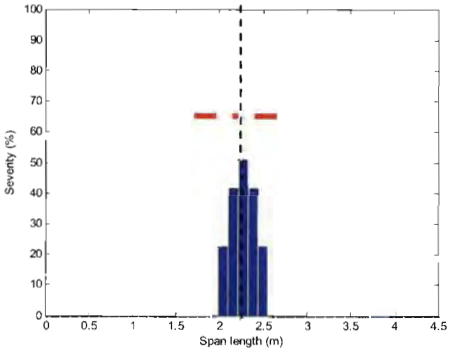
Figure 9.9 Estimation of damage severity using HMC method.

9.3.2.2 Discussions on Modified Damage Index II Method

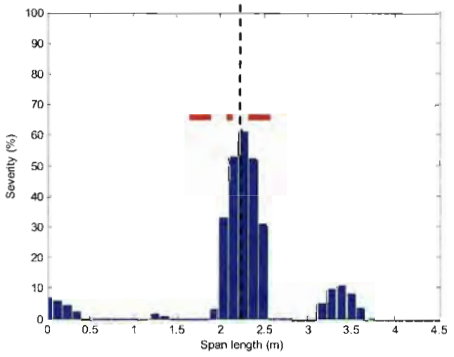
To expand the modified damage index II (MDI-II) method for estimation of damage severity using the experimental data that contains noise, some minor adjustment is required by applying a weighting factor. The factor adopted for the experimental studies is 1.2 with the assumption that experimental data contains noise. And also, the damage severity of case 4S was used to calibrate the simulated damage severity (87.5% loss of 'I'). For the numerical results, similar calibration process was adopted to acquire the weighting factor of 1.67 in order to obtain reasonable severity of damage.

Similar damage cases used for estimating severity of damage in the preceding section were adopted for the MDI-II method. The severity of damage below zero percent has no physical meaning, thus they were not shown. The results of the severity evaluation using the MDI-II algorithm for the four types of damage scenarios are shown in Figure 9.10 and the magnitude of simulated and predicted damage is tabulated in Table 9.3. The single damage location case 4M for numerical and experimental studies are illustrated in Figures 9.10a and 9.10b, respectively. Both results capture the location of damage at position 2.25m very accurately, although there are some minor false positives in the experimental result. The predicted damage severity for the medium damage is 51.0% and 61.0% loss of 'I', for numerical and experimental studies, respectively. Comparing to the actual inflicted damage of 65.7% loss of 'I', the errors for the numerical and experimental studies are 22% and 7%, respectively. It appears that the MDI-II method predicted the severity of damage better experimentally.

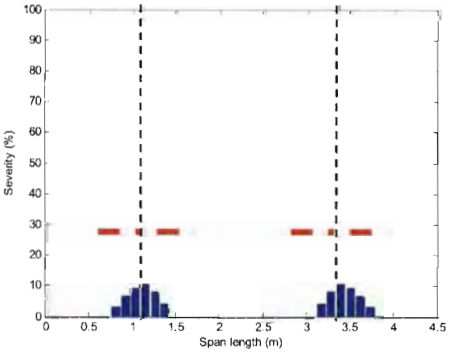
For the case with two damage locations (2L6L), the numerical and experimental results are not very compatible except for the light damage (27.1% loss of 'I') at location 3.375m as depicted in Figures 9.10c and 9.10d. This suggests that the MDI-II method did not evaluate the light damage well if noise were present in the experimental data. For three (2M4M6S) and four (2S4S5S6S) damage cases as shown in Figures 9.10e and 9.10g, both numerical and experimental results identify the damage locations well and predicted similar severity of damage. There is a satisfactory agreement between the two models. This indicates that the experimental data, applied in the MDI-II method, is capable of estimating well the medium and severe damage severity but did not perform well for the light damage cases.



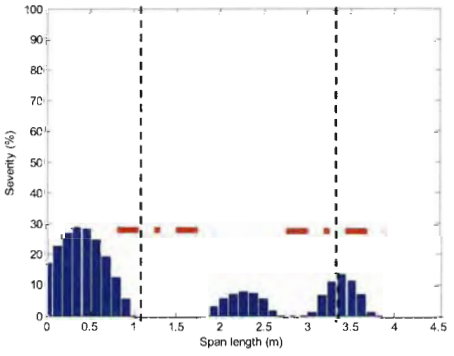
(a) 4M (Numerical).



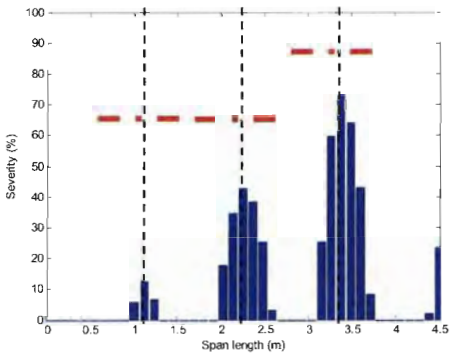
(b) 4M (Experimental).



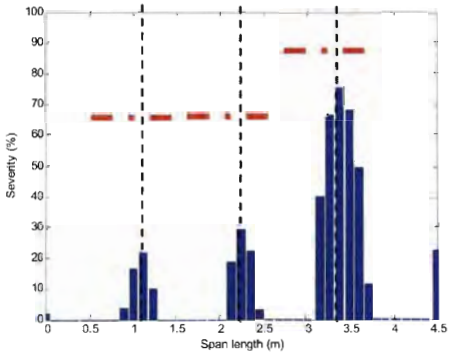
(c) 2L6L (Numerical).



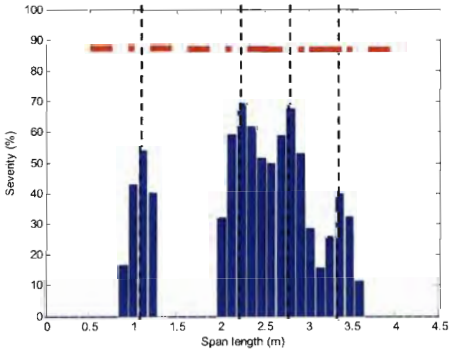
(d) 2L6L (Experimental).



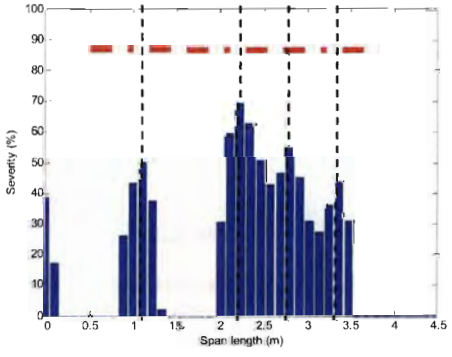
(e) 2M4M6S (Numerical).



(f) 2M4M6S (Experimental).



(g) 2S4S5S6S (Numerical).



(g) 2S4S5S6S (Experimental).

Figure 9.10 Estimation of damage severity using MDI-II method.

Table 9.3 Estimation of damage severity using MDI-II method.

Damage Case	Damage Scenario	Simulated Damage Severity (%)	Predicted Numerical Damage Severity (%)	Predicted Experimental Damage Severity (%)
Beam 1	Un1			
1	4L	27.1	12.0	13.6
2	**4M**	**65.7**	**51.0**	**61.0**
3	4S	87.5	87.5	81.6
4	4S6L	87.5, 27.1	87.3, 0	83.7, 0
5	**4S6M**	**87.5, 65.7**	**86.7, 37.5**	**84.7, 52.8**
6	4S6S	ALL87.5	86.6, 73.0	82.3, 77.1
7	4S5L6S	87.5, 27.1, 87.5	85.8, 0, 72.3	81.3, 0, 76.5
8	4S5M6S	87.5, 65.7, 87.5	82.7, 3.7, 69.4	82.5, 0, 72.4
9	4S5S6S	ALL 87.5	75.4, 69.6, 60.9	79.2, 63.7, 66.0
10	2L4S5S6S	27.1, 87.5, 87.5, 87.5	0, 75.1, 69.6, 60.3	0, 77.5, 64.0, 64.0
11	2M4S5S6S	65.7, 87.5, 87.5, 87.5	0, 73.6, 68.6, 56.7	0, 77.8, 60.9, 61.3
12	**2S4S5S6S**	**ALL 87.5**	**54.1, 69.3, 67.7, 39.9**	**50.0, 68.9, 54.7, 43.8**
Beam 2	Un2			
13	6L	27.1	11.4	11.3
14	2L6L	27.1, 27.1	105, 10.5	0, 13.2
15	2L4L6L	27.1, 27.1, 27.1	9.1, 10.5, 9.1	9.4, 16.0, 25.8
16	2L4L6M	27.1, 27.1, 65.7	2.0, 7.3, 46.0	14.1, 9.4, 58.1
17	2M4L6M	65.7, 27.1, 65.7	41.6, 3.6, 41.6	56.4, 0, 55.8
18	2M4M6M	ALL 65.7	37.3, 45.2, 37.3	51.8, 37.4, 42.9
19	**2M4M6S**	**65.7, 65.7, 87.5**	**12.5, 42.7, 73.0**	**21.0, 29.4, 75.6**
20	2S4M6S	87.5, 65.7, 87.5	61.8, 36.5, 61.8	64.3, 11.4, 61.2
21	2S4S6S	ALL 87.5	55.6, 80.9, 55.6	58.2, 60.5, 52.5
22	2S4S5L6S	87.5, 87.5, 27.1, 87.5	55.8, 80.3, 0, 54.3	56.9, 60.7, 0, 52.3
23	2S4S5M6S	87.5, 87.5, 65.7, 87.5	56.6, 78.2, 0, 48.6	60.2, 56.4, 0, 40.8
24	2S4S5S6S	ALL 87.5	54.1, 69.3, 67.7, 39.9	60.3, 36.8, 68.9, 36.1

Note: Shaded cases correspond to those presented in Figure 9.10.

9.4 Inflicted Damage in Laboratory Timber Bridge

The single and multiple damage scenarios to be used for the laboratory timber bridge are described in Table 9.4 with details given in Chapter 8. All damage scenarios consist of a rectangular opening along the span of a girder starting from the soffit, located either at 1/8, 2/8, 4/8 (midspan), or 6/8 of the span length to simulate pockets of rot that usually starts from the top surface in timber girders. In this study and the discussions that follow, 'L', 'M' and 'S' denote, as before, light, medium and severe damage, respectively. All inflicted damage are 1% of the total span length (45mm) and consist of 10%, 30% and 50% of the beam depth, designated as damage cases 'L', 'M' and 'S' as shown in Table 9.4. The inflicted damage can also be interpreted as loss of 'I' (moment of inertia) from the depth of cut. The loss of section of 10% (L), 30% (M) and 50% (S) of beam depth, correspond to 27.1%, 65.7% and 87.5% loss of 'I', respectively.

From Table 9.4, four locations of damage were selected to represent single and multiple damage scenarios. They are one, two, three and four locations of damage corresponding to one damage at girder 2 (g2), cumulative of one damage at girder 2 (g2) and one damage at girder 4 (g4), cumulative of one damage at girder 2 (g2), one damage at girder 4 (g4) and one damage at girder 3 (g3) and, cumulative of one damage at girder 2 (g2), one damage at girder 4 (g4), one damage at girder 3 (g3) and one damage at girder 1 (g1), respectively. At each location of damage, three damaged severity levels were used, i.e., light (L), medium (M) and severe (S) damage that may be found in timber structures.

Table 9.4 Dimensions of inflicted damage in the bridge.

Damage Case	Damage Scenario	Location per 8th of span length/Girder number	Length *l* (mm)	Depth h (mm)	% loss of 'I'
Deck 2	D2	Undamaged	-	-	-
1	g2L	6/g2	45	9	27.1
2	g2M	6/g2	45	27	65.7
3	g2S	6/g2	45	45	87.5
4	g2Sg4L	6/g2, 4/g4	45	45, 9	87.5, 27.1
5	g2Sg4M	6/g2, 4/g4	45	45, 27	87.5, 65.7
6	g2Sg4S	6/g2, 4/g4	45	All 45	All 87.5
7	g2Sg4Sg3L	6/g2, 4/g4, 2/g3	45	45, 45, 9	87.5, 87.5, 27.1
8	g2Sg4Sg3M	6/g2, 4/g4, 2/g3	45	45, 45, 27	87.5, 87.5, 65.7
9	g2Sg4Sg3S	6/g2, 4/g4, 2/g3	45	All 45	All 87.5
10	g2Sg4Sg3Sg1L	6/g2, 4/g4, 2/g3, 1/g1	45	45, 45, 45, 9	87.5, 87.5, 87.5, 27.1
11	g2Sg4Sg3Sg1M	6/g2, 4/g4, 2/g3, 1/g1	45	45, 45, 45, 27	87.5, 87.5, 87.5, 65.7
12	g2Sg4Sg3Sg1S	6/g2, 4/g4, 2/g3, 1/g1	45	All 45	All 87.5

Notes:

gi = girder No. i

L, M, S representing light, medium and severe damage, corresponding to 27.1, 65.7 and 87.5% loss of 'I'

(e.g. g2Sg4Sg3M denotes a cumulative damage scenario of medium damage on ¾ span of girder 3, severe damage on ¾ span of girder 2 and ½ span of girder 4)

9.5 Results and Discussions for Laboratory Timber Bridge

9.5.1 Damage Localisation

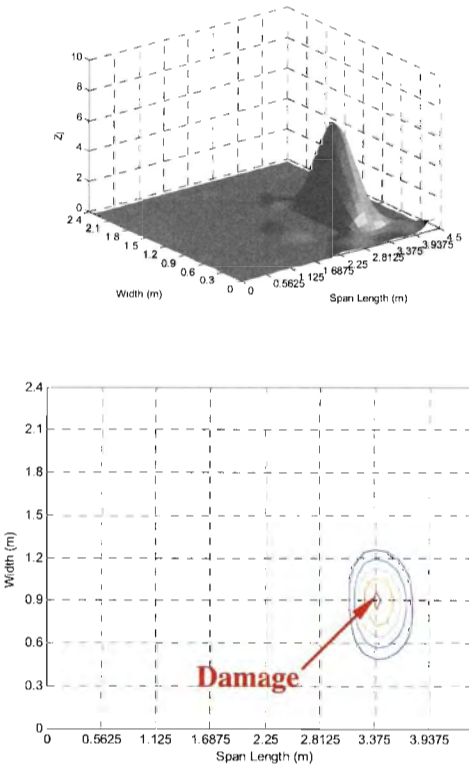
For damage localisation in the laboratory timber bridge, the first nine modes were used in the damage index method for plate-like structures (DI-II-P) based on the finding that higher modes produce better results for damage detection. In the following results, all damage indicators, Zj, for each of the damage cases are plotted against the laboratory timber bridge span length (4.5m) and width (2.4m). In principle, the statistically normalised damage indicator values Zj larger than or equal to two (the probability-based criterion for damage) is considered damage has occurred at that location. The localisation of damage using the criterion of $Zj \geq 2$ was adopted as it would provide an approximately 95% level of confidence indicating the actual damage locations (Park & Stubbs 1995; Peterson et al. 2001). The threshold of Zj for plate-like

timber structures is set slightly higher than the timber beams because plate-like structures such as a deck-girder timber bridge are a complicated system compared to a simple beam system, which in turns may produce more errors in the damage detection results.

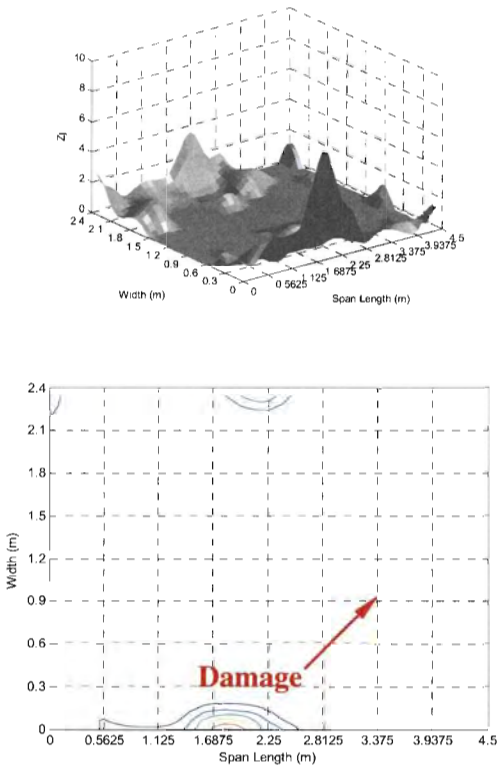
To show the damage site in the graphs, the actual damage locations are marked with a red colour arrow sign and the word 'Damage' in all the following figures. For damage localisation of the laboratory timber bridge, two types of graphs were used in this study, that is, surface and contour plots. The surface plots provide the distribution of the damage indicators that are above zero ($Zj>0$), while the contour plots give information of predicted damage locations with $Zj\geq 2$.

9.5.2 Damage Index II for Plate-like Structures

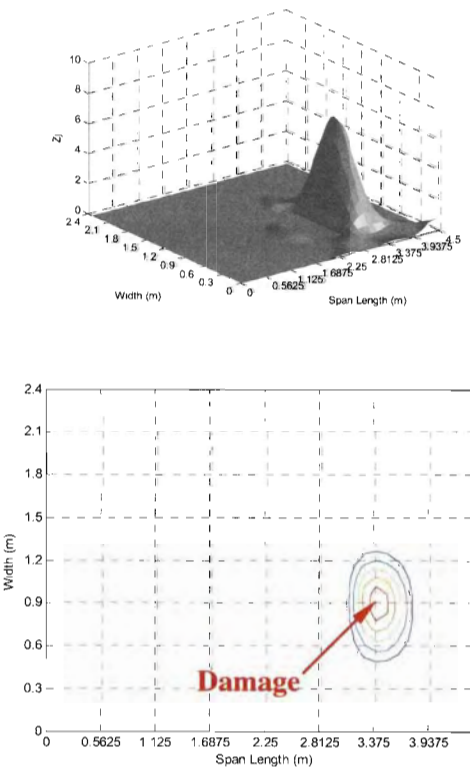
The single damage cases applied in the damage index II algorithm for plate-like structures (DI-II-P) and computed using the first nine modes for numerical and experimental studies are illustrated in Figure 9.11. For single damage case g2L (light damage), the DI-II-P method was unable to identify the damage location at position (3.375m, 0.9m) (used as a convention in all the following discussions to indicate location of damage at 3.375m along the span length and 0.9m across the width) experimentally as shown in the contour plot of Figure 9.11b. In contrast, the numerical results (see contour plot of Figure 9.11a) clearly detected the damage location. The single damage cases (g2M and g2S), which correspond to medium and severe damage for numerical and experimental studies, are shown in the contour plots of Figures 9.11c and 9.11d and, Figures 9.11e and 9.11f, respectively. In these cases, it can be seen that the numerical results are comparable to the experimental results with some spurious damage locations in the latter one. This confirms that the experimental data used in the DI-II-P method is capable of detecting medium and severe damage. However, it is not satisfactory for the light damage case.



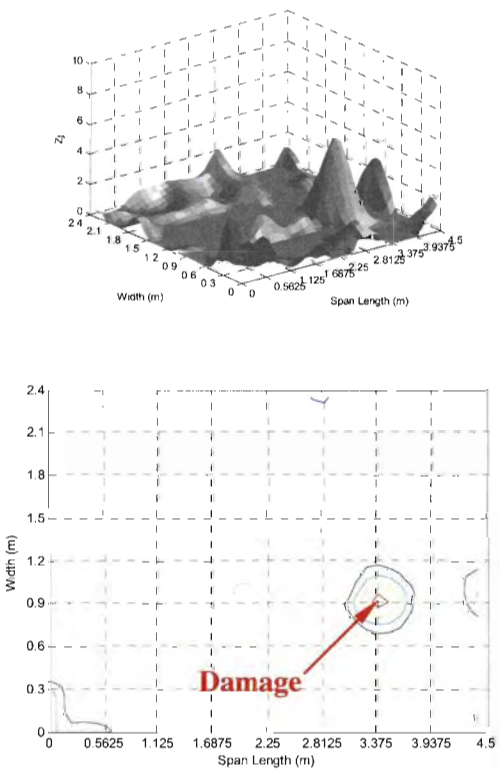
(a) g2L(Numerical).



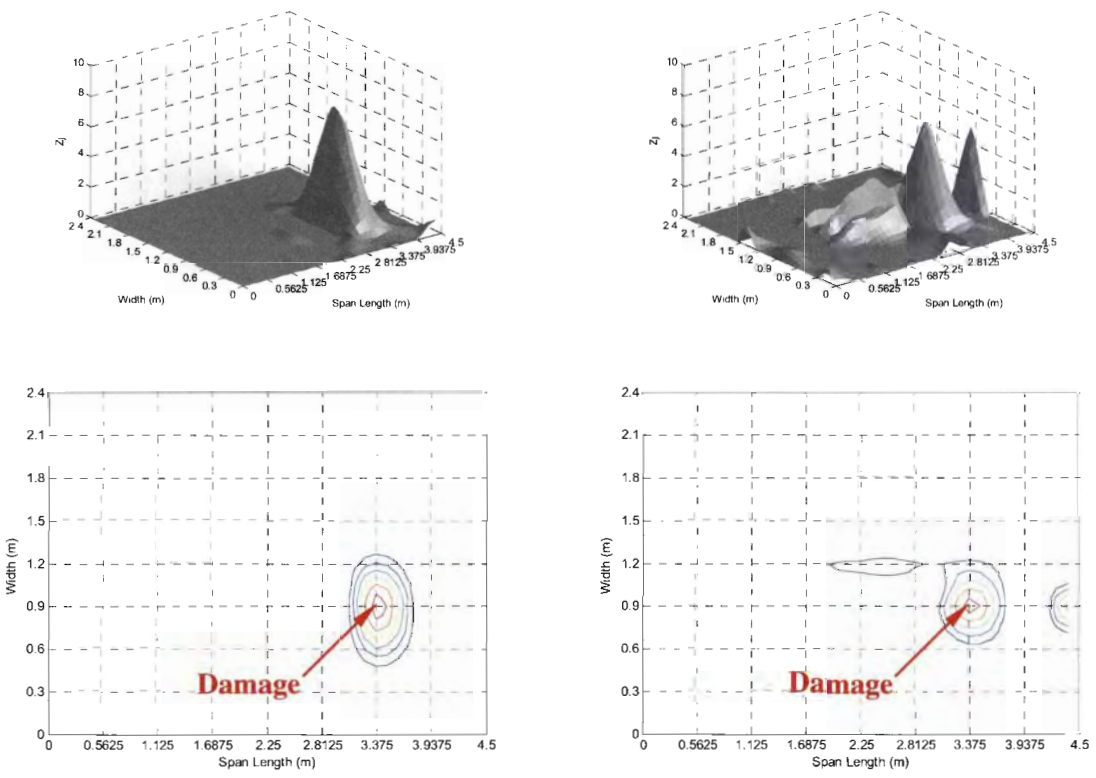
(b) g2L (Experimental).



(c) g2M (Numerical).



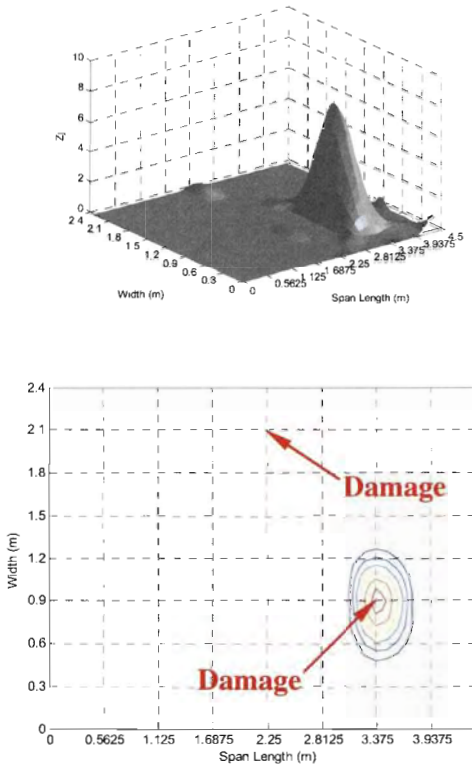
(d) g2M (Experimental).



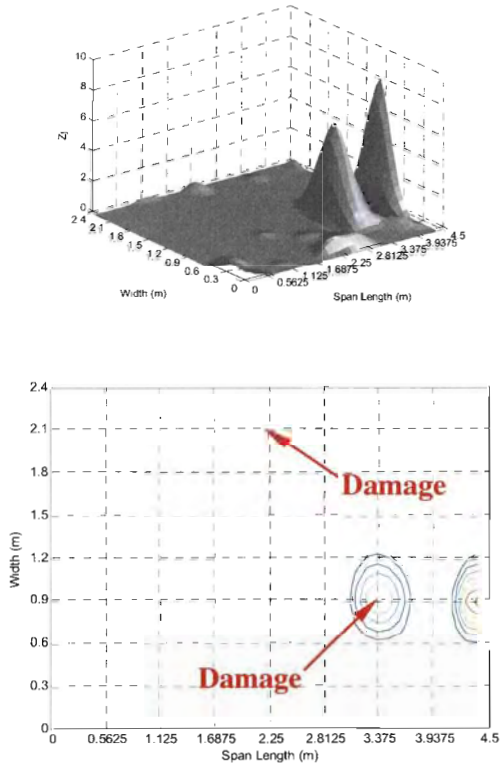
(f) g2S (Numerical). (f) g2S (Experimental).

Figure 9.11 Single damage cases using DI-II-P method for bridge (9 modes).

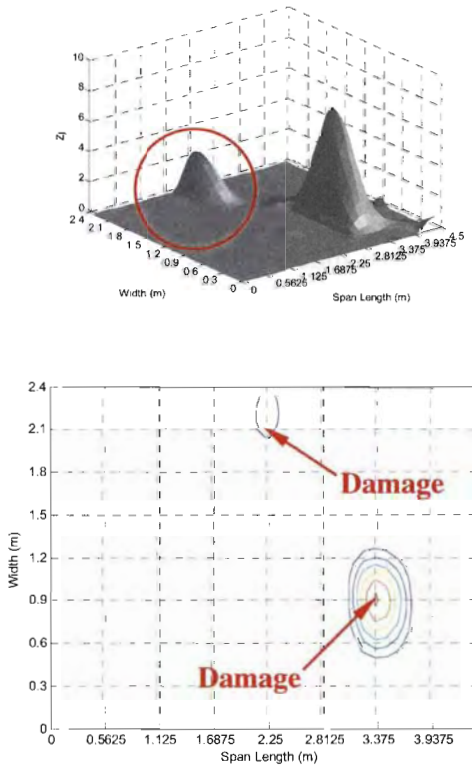
Results of applying the DI-II-P method to cases with two damage using numerical and experimental data are shown in Figure 9.12. From the surface and contour plot results of using the first nine modes, basically both numerical and experimental results are quite similar although the damage index values for the latter is less distinct compared to the former. It is also obvious that the experimental results are contaminated with serious spurious damage locations. It is apparent that the experimental data inevitably contains noise and the peaks of damage will be less distinct. On the other hand, this phenomenon is not seen in the numerical cases as no noise is present. For example, in case g4M, the medium damage at position (2.25m, 2.1m) was manifested as a peak for both numerical and experimental studies in the surface plot as shown in Figures 9.12c and 9.12d, respectively. But in the contour plots, the numerical case identified the medium damage but not the experimental case.



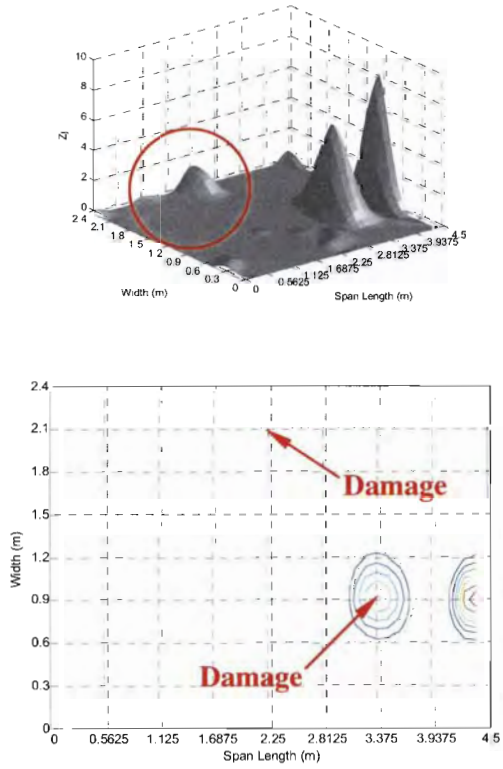
(a) g2Sg4L (Numerical).



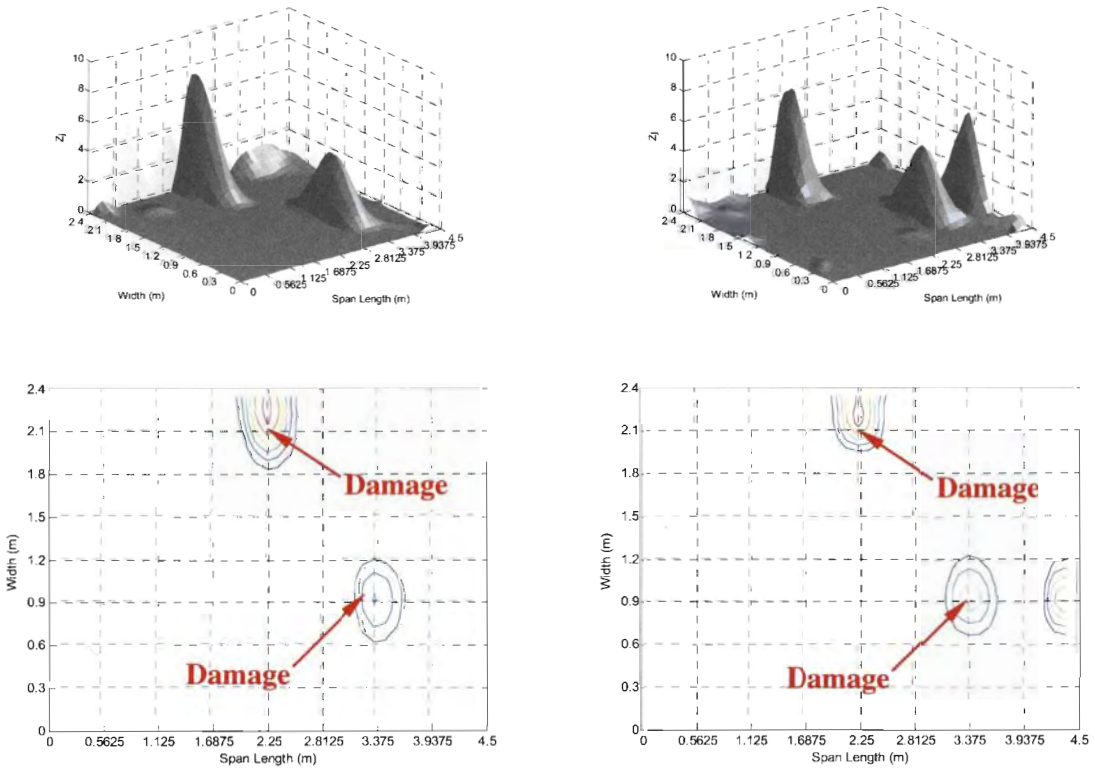
(b) g2Sg4L (Experimental).



(c) g2Sg4M (Numerical).



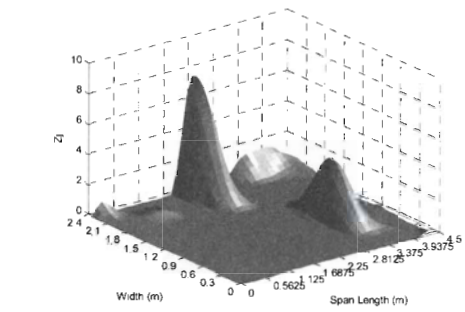
(d) g2Sg4M (Experimental).

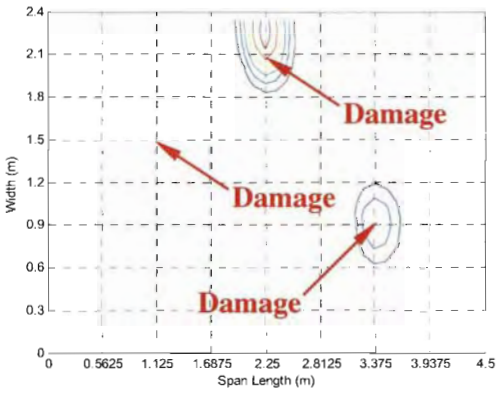


(e) g2Sg4S (Numerical). (f) g2Sg4S (Experimental).

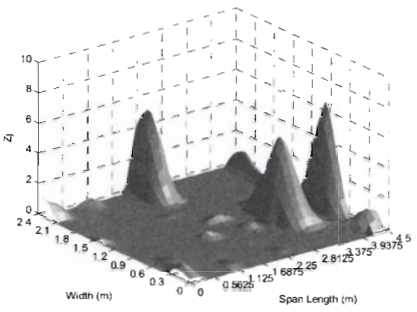
Figure 9.12 Two damage cases using DI-II-P method for bridge (9 modes).

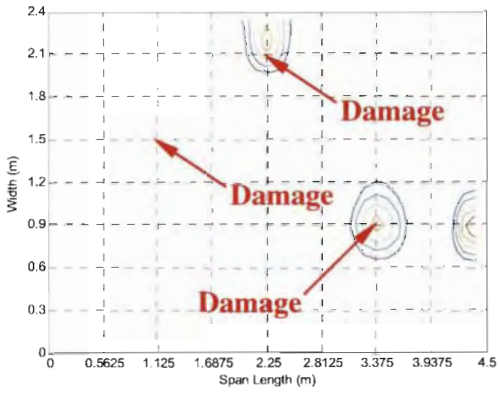
For three damage location cases, the results of the damage detection using the DI-II-P method for numerical and experimental studies are shown in Figure 9.13. By using the first nine modes in the damage index method for damage cases g3L and g3M, the method failed to identify the light and medium damage at position (1.125m, 1.5m), but all severe damage were located, for the numerical and experimental studies as shown in Figure 9.13a to 9.13d, respectively. For case g3S, all severe damage were identified, for both numerical and experimental studies, as illustrated in Figures 9.13e and 9.13f, respectively. Again good agreement between numerical and experimental studies can be seen in spite of some spurious damage locations appearing in the latter one due to noise. It should be noted that the magnitude of the damage indicator for the damage locations for the experimental studies tends to be less distinct compared to the numerical cases as more damage was inflicted. This may be due to interference of noise, resulting in more peaks and suppressing the peaks of the actual damage.



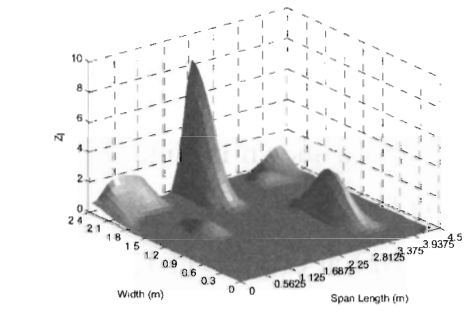


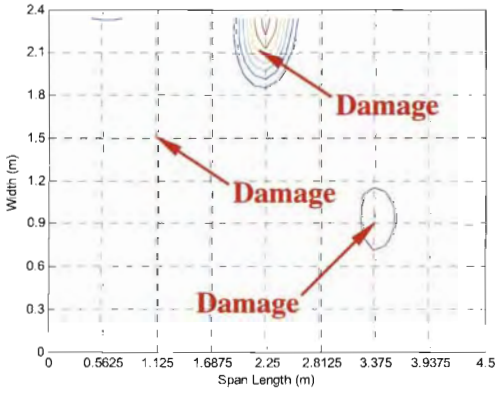
(a) g2Sg4Sg3L (Numerical).



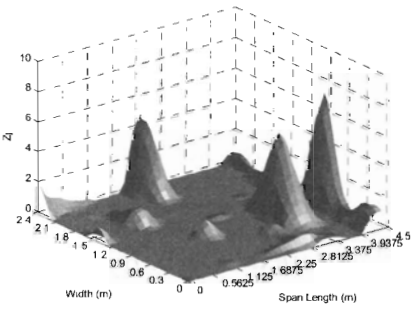


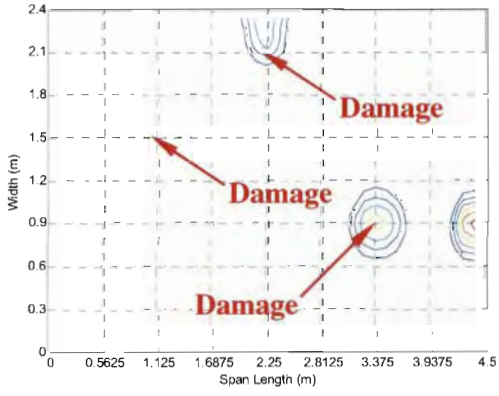
(b) g2Sg4Sg3L (Experimental).



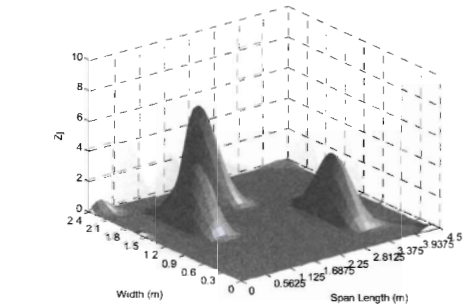


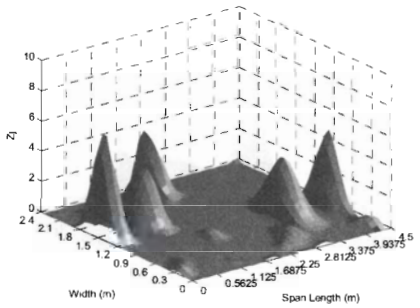
(c) g2Sg4Sg3M (Numerical).

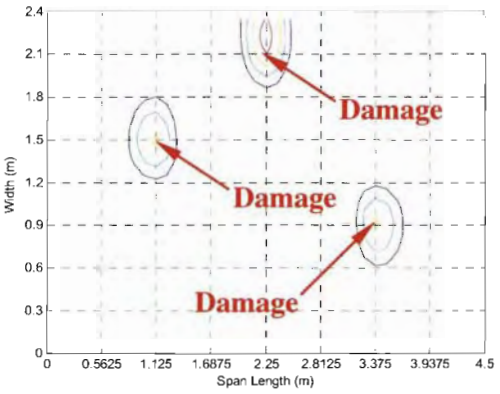


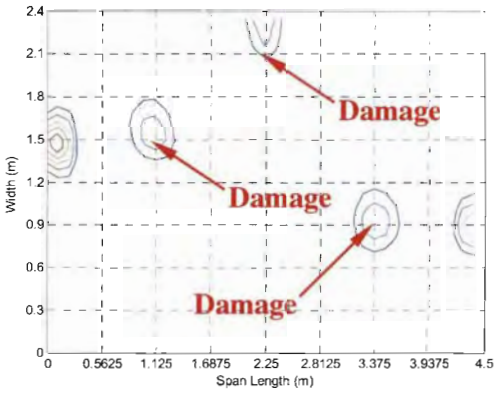


(d) g2Sg4Sg3M (Experimental).





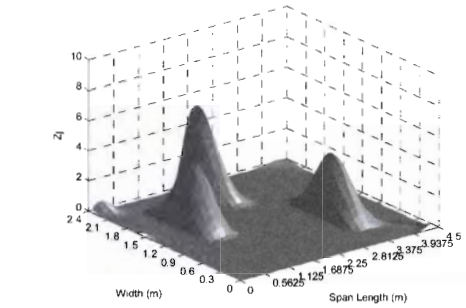


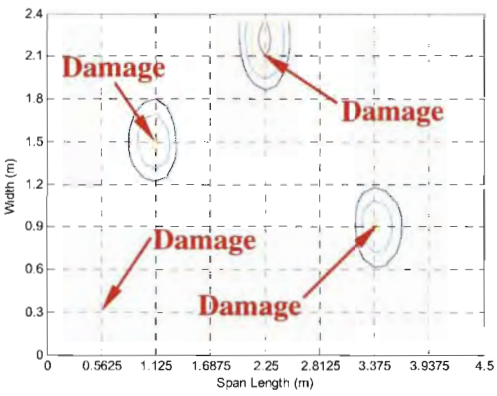


(e) g2Sg4Sg3S (Numerical). (f) g2Sg4Sg3S (Experimental).

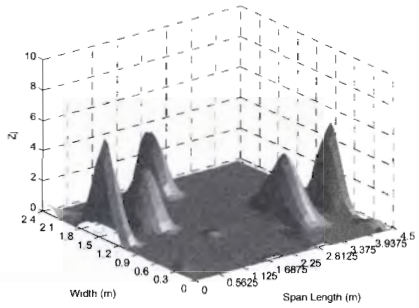
Figure 9.13 Three damage cases using DI-II-P method for bridge (9 modes).

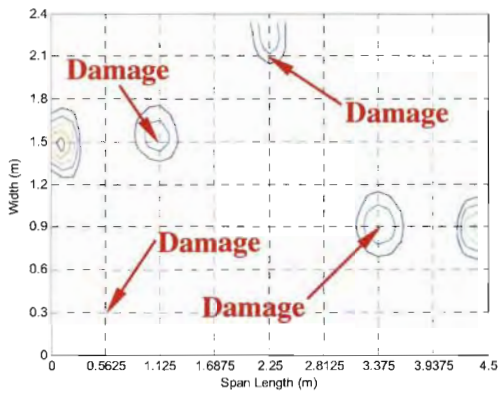
The comparative results for four damage location scenarios applying the DI-II-P method and using the first nine modes for the numerical and experimental studies are illustrated in Figure 9.14. The damage locations were not clearly captured by the method using the experimental data compared to using the numerical data. The compatibility between the numerical and experimental models is not very satisfactory, even though some severe damage were identified in the latter. It is possible to infer that the experimental data applied in the DI-II-P method can be used to identify damage in the laboratory timber bridge for single and multiple damage scenarios that have three or less damage locations. For damage scenarios with more than three damage locations, due to complexity and noise in experiments, further developments are needed to make the DI-II-P method perform better.



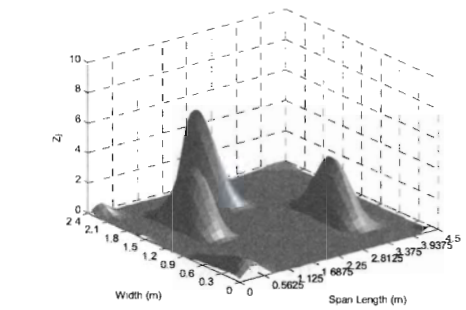


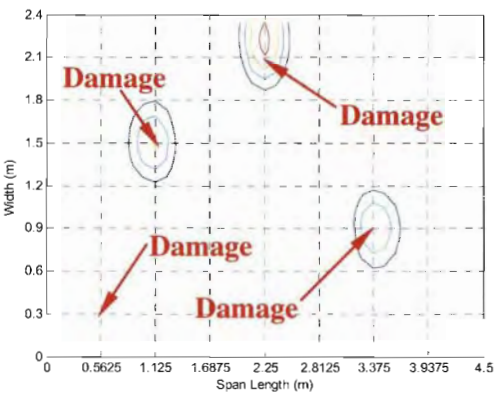
(a) g2Sg4Sg3Sg1L (Numerical).



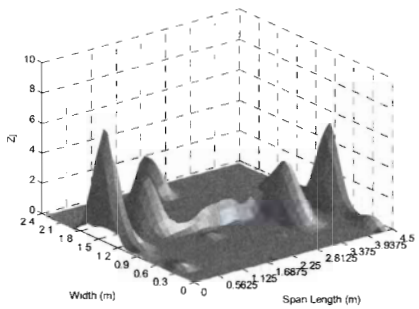


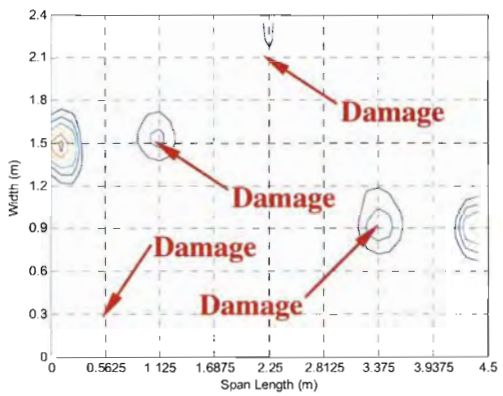
(b) g2Sg4Sg3Sg1L (Experimental).



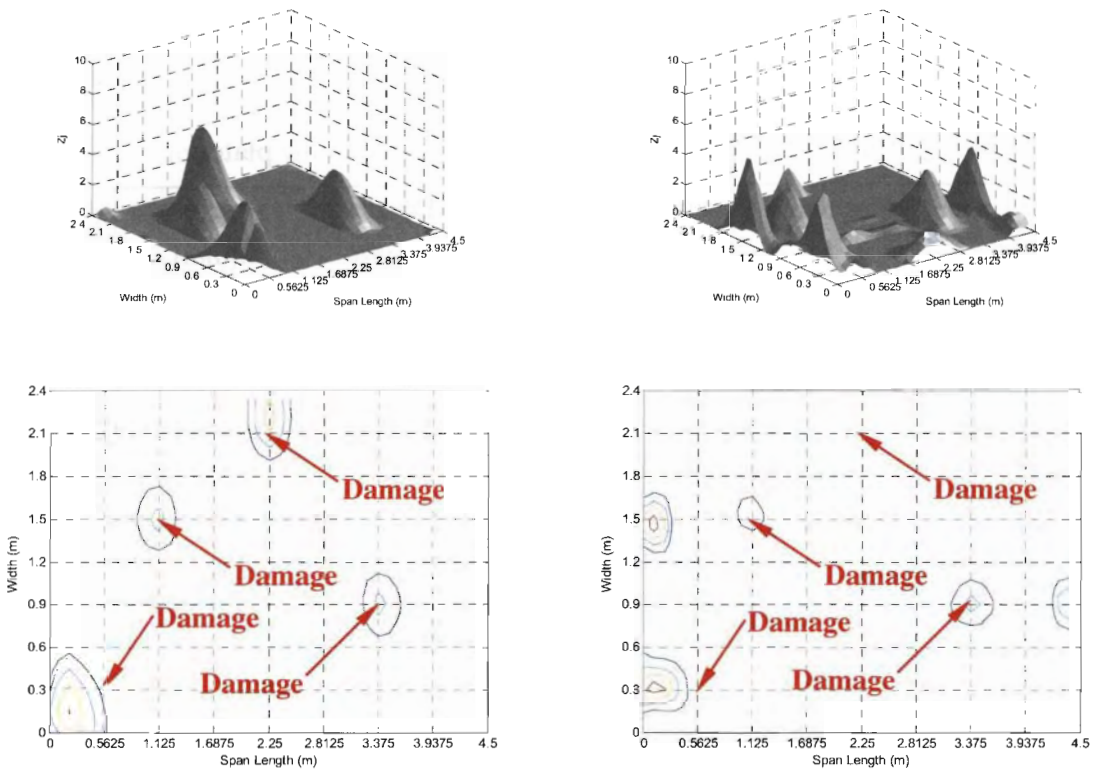


(c) g2Sg4Sg3Sg1M (Numerical).





(d) g2Sg4Sg3Sg1M (Experimental).



(e) g2Sg4Sg3Sg1S (Numerical). (f) g2Sg4Sg3Sg1S (Experimental).

Figure 9.14 Four damage cases using DI-II-P method for bridge.

9.6 Results and Discussions for Laboratory Timber Plate

As a supplementary work to the laboratory timber bridge, a piece of plywood was used to verify the damage detection method for plate-like structures (DI-II-P). The plywood was used to simulate an orthotropic plate, which may represent some slab-type bridges. Since plate-type or slab-type timber bridges are very rare, the purpose of this additional work was merely complementary and aimed to explore the capabilities and limitations of the damage detection algorithm in locating damage for a timber plate structure.

The plywood was inflicted with various damage scenarios as tabulated in Table 9.5. The damage was inflicted with a square opening with dimensions of either 37.5mm or 75mm, corresponding to small (A) and large (B) damage, respectively. The damage can also be represented by percentage of loss of area against a bay measuring 300mm by 300mm. It works out to be 2% and 6% of loss of area for small and large damage, respectively. The details of the damage scenarios can be found in Chapter 8. The small

damage cases (A) are not discussed in this section as the algorithm is expected not to perform well for the experimental results.

Table 9.5 Dimensions of inflicted damage in the plate.

Damage Case	Damage Scenario	Location (mm) /Line number	Length *l* (mm)	Breath *b* (mm)	% loss of Area*
Plate1	P1	Undamaged	-	-	-
1	L2(I)A	I (656.25)/L2	37.5	37.5	2
2	L2(II)B	II (675)/L2	75	75	6
3	L2(II)B-L3(III)A	II (675)/L2, III (1743.75)/L3	75, 37.5	75, 37.5	6, 2
4	L2(II)B-L3(IV)B	II (675)/L2, IV (1725)/L3	75, 75	75, 75	6, 6
5	L2(II)B-L3(IV)B-L3(V)A	II (675)/L2, IV (1725)/L3, V (1143.75)/L3	75, 75, 37.5	75, 75, 37.5	6, 6, 2
6	L2(II)B-L3(IV)B-L3(VI)B	II (675)/L2, IV (1725)/L3, VI (1125)/L3	75, 75, 75	75, 75, 75	6, 6, 6

** % loss of Area is calculated based on damaged area divided by 300mmx300mm (a bay of the measurement grids).*

Notes:

Li = Line no. i

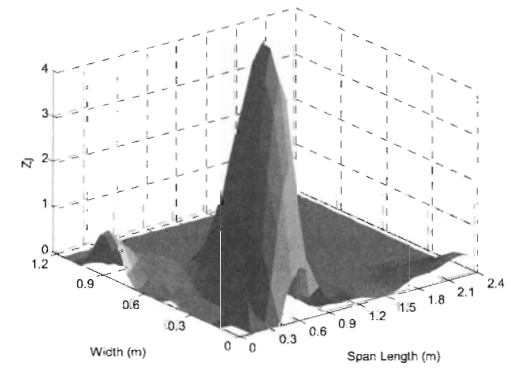
A,B = representing small and large damage, corresponding to 2% and 6% loss of area, respectively

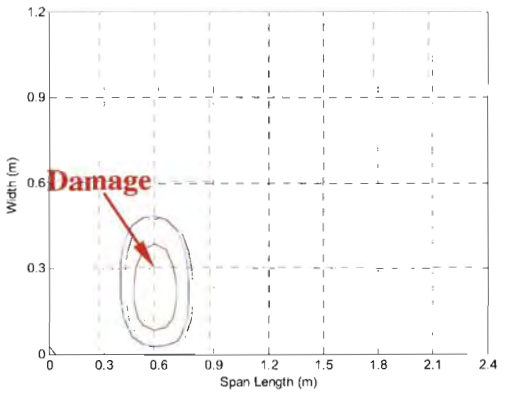
(e.g. L2(II)B-L3(IV)B-L3(V)A denotes a cumulative damage scenario of small damage at location V (1143.75mm) of Line 3, large damage at locations II (675mm) of Line 2 and IV (1725mm) of Line 3)

The damage localisation results of the timber plate for numerical and experimental studies using damage index II method for plate-like structures (DI-II-P) are shown in Figure 9.15. For the single damage case L2(II)B (large), the results of numerical and experimental studies are depicted in the contour plots of Figures 9.15a and 9.15b, respectively. The damage location at position (0.6m, 0.3m) was identified by both studies. But for the experimental results, it also produces some false positives (indication of spurious damage locations). This indicates that the experimental data applied in the DI-II-P method are able to detect severe damage location even though the experimental results were polluted with some noise-induced peaks.

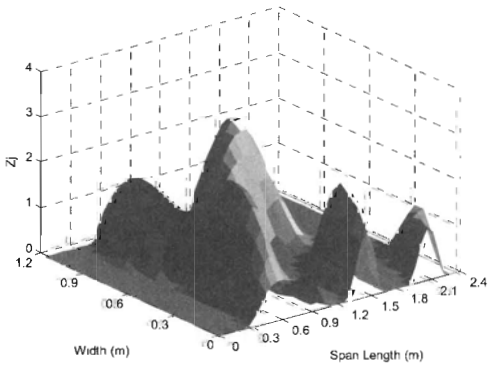
For two damage case L2(II)B-L3(IV)B, the numerical and experimental results are shown in the contour plots of Figures 9.15c and 9.15d, respectively. The former result pin-pointed the large damage near positions (0.6m, 0.3m) and (1.8m, 0.6m) but

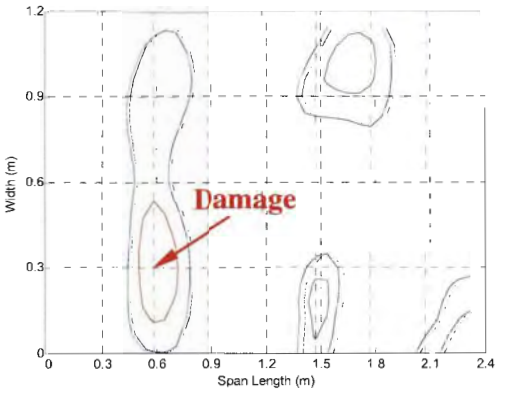
the second damage was not clearly indicated by the experimental results. For the case with three damage (L2(II)B-L3(IV)B-L3(VI)B), the results of the numerical and experimental studies are illustrated in Figures 9.15e and 9.15f, respectively. All large damage was identified at positions (0.6m, 0.3m), (1.8m, 0.6m) and (1.2m, 0.6m). From this supplementary work, it is concluded that the numerical models are reasonably well representing the experimental models for detecting large damage (defined in this study as 6% loss of area) using the DI-II-P method for timber plates. It should be noted that there are serious false positives appearing in the experimental results which may be due to noise and other complexities (such as boundary conditions) in the experimental data.



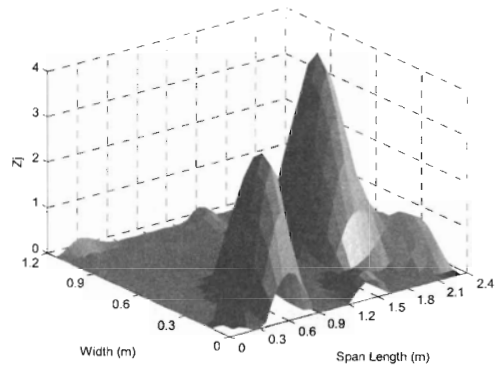


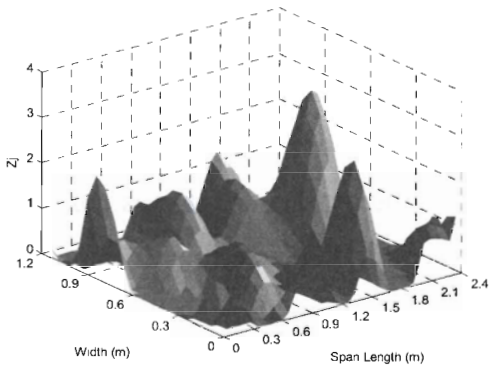
(a) L2(II)B (Numerical).

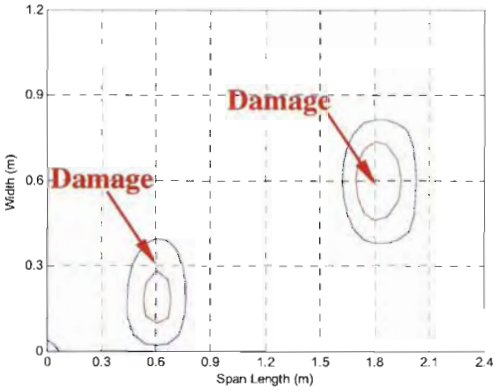




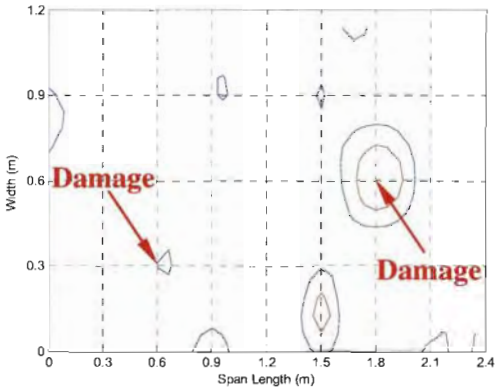
(b) L2(II)B (Experimental).



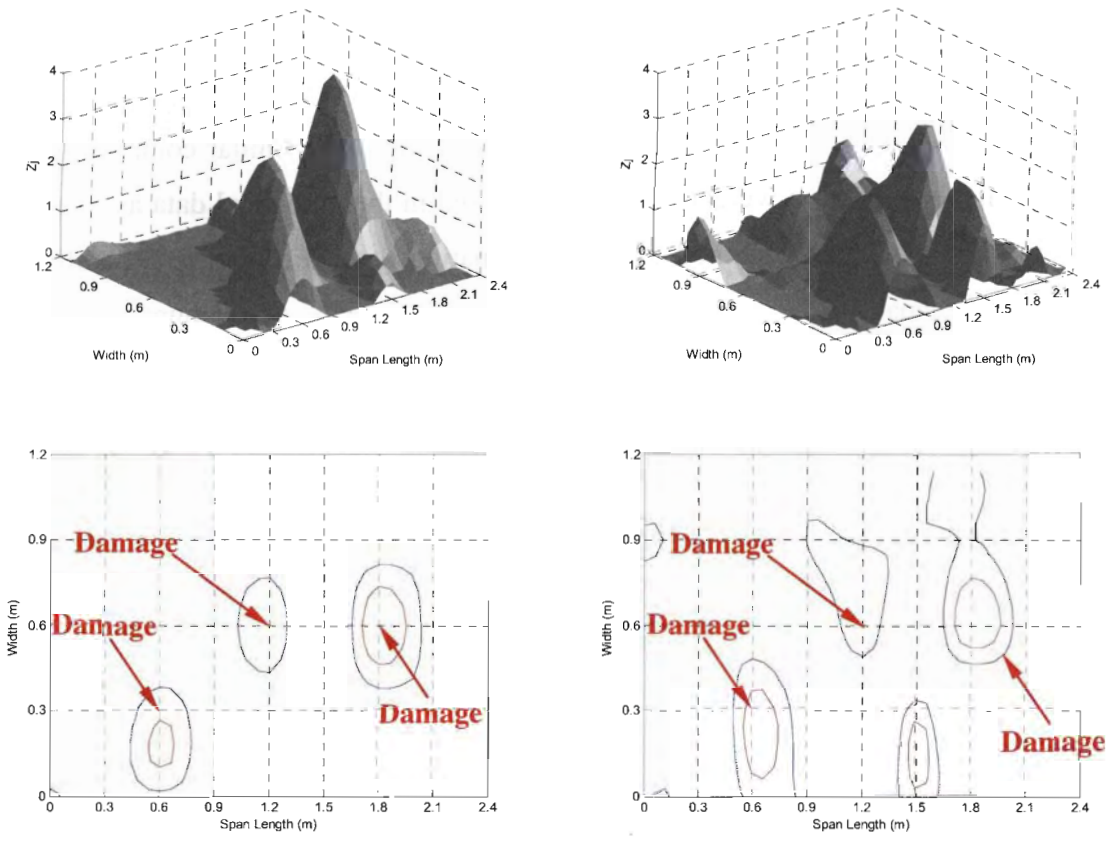




(c) L2(II)B-L3(IV)B (Numerical).



(d) L2(II)B-L3(IV)B (Experimental).



(e) L2(II)B-L3(IV)B-L3(VI)B (Numerical).

(f) L2(II)B-L3(IV)B-L3(VI)B (Experimental).

Figure 9.15 Damage cases using DI-II-P method for plate (6 modes).

9.7 Summary

In this chapter, verification of experimental data, applied in the damage index methods for damage detection, with numerical models of timber beam, laboratory timber bridge and timber plate was performed. For the timber beam, both damage detection methods, MDI-I and MDI-II, are capable of detecting medium and severe damage in the numerical and experimental studies. However, the light damage was not identified well using the experimental data in the presence of noise. While the numerical data without noise worked well in detecting the light damage cases. It should be noted that the damage detection results using the experimental data are filled with more spurious damage than the numerical ones. It is because noise is present in the experimental data but not in the numerical ones.

To estimate damage severity in the timber beam, the HMC method (with a weighting factor of 0.8 for the experimental data due to presence of noise) estimated well the medium and severe damage. The method did not perform well in estimating severity of the light damage. The numerical results were quite similar compared to the experimental ones and no weighting factor was used in the numerical data as there was no noise. For the MDI-II method used for estimating damage severity, generally, the method was capable of estimating reasonably well severity of medium and severe damage, for both numerical and experimental studies, but did not work well for the light damage. The method also, generally, underestimated all damage severity for both the numerical and experimental studies, even though weighting factors of 1.67 and 1.2 were applied to the data.

The results of applying the DI-II-P method to locate damage in the laboratory timber bridge showed that numerical and experimental methods were capable of detecting all severe damage for damage cases with less than three damage locations. While for light and medium damage, the experimental data did not work well as compared to the numerical one. It should be noted that the damage indictor values (Z_j) for damage is smaller for the experimental results than the numerical ones, especially for the multiple damage scenarios. This may be due to presence of noise suppressing the peak of actual damage.

As a supplementary work to the laboratory timber bridge, the numerical and experimental results of a timber plate showed that they were able to detect the severe damage well. However, there were serious false positives appearing in the experimental results, which may be due to noise and other complexities such as boundary conditions of the system.

Chapter 10

Conclusions and Recommendations

10.1 Conclusions

This thesis deals with damage detection of timber bridges using modal based damage detection methods. The work consists of numerical modelling using finite element analysis (FEA) for a timber beam, a laboratory timber bridge and a timber plate. Finite element model updating using modal parameters is also included. Comparison of effects of different numerical integration techniques and mode shape reconstruction methods are carried out. Material testing of different structural elements for a laboratory timber bridge as part of the experimental work is performed for updating of the FE models. An extensive experimental program employing experimental modal analysis for timber beams, a laboratory timber bridge and a timber plate forms a major portion of this study. Adopting and modifying existing damage index methods, damage detection for single and multiple damage scenarios is performed for both numerical and experimental models.

A systematic process of developing and updating a finite element (FE) model for a laboratory timber bridge with experimental modal data is presented in this thesis. The procedures have been developed sequentially starting with a preliminary model, incorporating more complex features to form the advanced model by adjustment of physical and material properties of the FE model to match the experimental ones. Sensitivity analysis and correlation analysis are employed to assist in determining responses of the model. The updated model achieves results with less than 20% error in natural frequencies and less than 12% for modal assurance criterion (MAC - mode shape comparison) which is deemed satisfactory for complex structural systems such as timber bridges, except for mode 2. The updating process using modal data is accurate and safer compared to using proof load test results, which may endanger the structural integrity of the tested structure. The results obtained are also more objective and less conservative than those obtained through visual inspection.

For the timber beam, the updating process is not needed as a structural beam system is quite simple and straightforward. Furthermore, using the actual material

properties of a radiata pine timber beam, the differences between the FE and experimental modal results are less than 10% for natural frequency and less than 5% for MAC, which are considered satisfactory. For the timber plate, as a complementary work to the laboratory timber bridge and as a straightforward plate system, the updating process was deemed not necessary.

It is known that numerical integration techniques used in a damage detection process can significantly affect the outcomes of the detection results. Employing finite element results of a timber beam, where mode shape curvature requires to be integrated, using the rectangular rule for the numerical integration yields better results than the trapezoidal rule. A conclusion is drawn from the comparison, that is, the rectangular rule is preferred in damage detection using the damage index method based on modal strain energy than the trapezoidal rule, even though in normal circumstances the latter would produce more accurate results.

Numerical studies of damage localisation using a finite element model of timber beam employing damage index methods, namely damage index I (DI-I) and II (DI-II) as well as changes in flexibility (CIF), are found to detect single damage quite well but encountered difficulties for multiple damage scenarios even when higher modes were employed. Hence, a modification was proposed for the damage index algorithms by normalising the mode shape curvatures. Employing normalisation of mode shape curvature to its maximum curvature value would reduce dominance of higher modes and would evenly distribute the contribution of every mode shape curvature used in the algorithms for one-dimensional beam structures. The modified versions of damage index I and II methods are denoted modified damage index I (MDI-I) and II (MDI-II). The modified algorithms perform well in locating single and multiple damage scenarios for the analytical model. It is also concluded that higher modes would detect multiple damage better because higher modes have smaller spatial wavelength, and highlight the damage better.

Using the same FE model for timber beam, estimation of severity of damage in the timber beam is achieved by using a hybrid of modified damage index I (MDI-I) and changes in flexibility (CIF), designated as HMC. Further manipulation of algorithm for the modified damage index II (MDI-II) were also used to estimate damage severity. Both methods were found to be capable of identifying location of damage very precisely. They also estimated well the severity of damage for severe damage (87.5% loss of 'I' (moment of inertia)) for single and multiple damage scenarios. While for

medium damage (65.7% loss of 'I'), the methods provide reasonable estimate of damage severity. However, estimation of light damage (27.1% loss of 'I') was not accurate using either method.

The damage index II method was extended to plate-like structures incorporating plate theory. The damage index method for plate-like structures is denoted DI-II-P and is adopted to detect damage in plate-like structures, using the analytical model of a laboratory timber bridge. A laboratory timber bridge is a complex system. It is, therefore, advisable to at least look into a supplementary work to apply the DI-II-P method on a timber plate. The results show that using the first six modes (higher modes) damage localisation is good compared to just using the first three modes.

From the analytical damage detection results, it was found that using the first nine modes in the algorithm, all severe damage (87.5% loss of 'I') could be located whether in single or multiple damage scenarios. While, using just the first three modes, some severe damage is not detected. This reinforces the finding that higher modes would perform better in detecting damage. It should be noted that normalisation of mode shape curvature for DI-II-P is not straightforward and will be part of the future work.

For experimental work, the number of sensors used is usually limited. It is therefore important to select appropriate numerical techniques for the damage detection process that can significantly improve the outcomes of the detection results. In this study, two mode shape reconstruction techniques, namely Shannon's sampling theorem and cubic spline interpolation technique, are adopted to generate more data in between the original data points. It is generally acknowledged that with more data points, the damage detection results will be better. Despite its popularity, the Shannon's sampling theorem is not considered as effective as the cubic spline for mode shape reconstruction, especially for multiple damage cases. With these findings, it is inferred that using cubic spline to reconstruct additional data points provide better damage detection results.

Based on the experimental results presented for the timber beams, the damage index I (DI-I) algorithm using the first two flexural modes performs better than using the first five flexural modes. This does not agree with the expectation that higher modes would provide better system identification. Similar conclusion is drawn for the damage index II (DI-II) method. Due to the shortcomings in detecting multiple damage scenarios in the two adopted damage localisation methods, modified versions for the two methods are proposed. The two proposed modified methods are modified damage

index I (MDI-I) and modified damage index II (MDI-II). These two proposed methods are more superior compared to their original state in identifying damage locations, especially for multiple damage scenarios. Using the first five modes in these two modified algorithms provide a better damage detection in multiple damage scenarios compared to just using the first two modes. It is evident that the modified damage index methods are less dependent on the selected modes and the results are in accordance with the principles of structural dynamics.

The formulation of MDI-I method does not provide meaningful physical values for severity of damage. It is, therefore, proposed to use a hybrid of MDI-I and changes in flexibility (CIF), denoted HMC, to evaluate severity of damage. In general, by employing a weighting factor, the HMC method predicts reasonably well the medium (65.7% loss of 'I') and severe (87.5% loss of 'I') damage, but it overestimates the light (27.1% loss of 'I') damage scenarios. The MDI-II method used for estimating severity of damage with a weighting factor, predicts better the severe damage and less accurately the medium and light damage scenarios. It generally underestimates the severity of damage cases used in this investigation.

In the experimental tests on plate-like structures (a laboratory timber bridge and a timber plate), the two-dimensional (2-D) interpolation technique (2-D cubic spline) is used to expand the limited number of data in the damage detection, which can significantly affect the detection. Using reconstructed data for detecting damage yields better results than just using the 'as is' data.

Based on the experimental results presented for the laboratory timber bridge, the damage index II method for plate-like structures (DI-II-P), using the first nine modes, performs better than using the first three modes to detect location of damage. This is consistent with the principles of structural dynamics whereby higher modes would provide better system identification. It should be highlighted here that even using nine modes in the DI-II-P method, in some cases, can present problems in identifying severe damage. This may be due to the lack of normalisation of mode shape curvature in the DI-II-P method which is yet to be developed and will be part of the future work.

The DI-II-P algorithm was applied to a timber plate and similar conclusions to the laboratory timber bridge can be drawn. However, the damage localisation results for timber plate are not as good compared to the laboratory timber bridge.

In this study, verification of experimental data, applied in the damage index methods for damage detection, with numerical models of timber beam, laboratory

timber bridge and timber plate is performed. For the timber beam, both damage detection methods, MDI-I and MDI-II, are capable of detecting medium and severe damage in the numerical and experimental studies. However, the light damage was not identified well using the experimental data in the presence of noise. While the numerical data without noise worked well in detecting the light damage cases. It should be noted that the damage detection results using the experimental data are filled with more spurious damage than the numerical ones. It is because noise is present in the experimental data but not in the numerical ones.

To estimate damage severity in the timber beam, the HMC method (with a weighting factor of 0.8 for the experimental data due to presence of noise) estimates well the medium and severe damage. The method does not perform well in estimating severity of the light damage. The numerical results are quite similar compared to the experimental ones and no weighting factor is used in the numerical data as there is no noise. For the MDI-II method used for estimating damage severity, generally, the method is capable of estimating reasonably well severity of medium and severe damage, for both numerical and experimental studies, but does not work well for the light damage. The method also, generally, underestimates all damage severity for both the numerical and experimental studies, even though weighting factors of 1.67 and 1.2 were applied to the data.

The results of applying the DI-II-P method to locate damage in the laboratory timber bridge show that numerical and experimental methods are capable of detecting all severe damage for damage cases with less than three damage locations. While for light and medium damage, the experimental data does not work well compared to the numerical one. It should be noted that the damage indictor values (Z_j) for damage is smaller for the experimental results than the numerical ones, especially for the multiple damage scenarios. This may be due to presence of noise suppressing the peak of actual damage.

As a supplementary work to the laboratory timber bridge, the numerical and experimental results of a timber plate show that they are able to detect the severe damage well. However, there were serious false positives appearing in the experimental results, which may be due to noise and other complexities such as boundary conditions of the system.

10.2 Recommendations and Future Work

For this study, further work and some refinements are required to make this research work more practical for application. Hence, the purpose of this section is to focus on the issues that should be addressed by future researchers to make use of these methods as a viable and practical tool for damage detection in timber bridges in particular, and timber structures in general, as well as its application to general structural health monitoring.

Both modified damage index I and II (MDI-I and –II) methods were less effective in locating damage in experimental timber beam for light damage due to the few sensors used. This was more obvious for damage cases where different levels of damage were applied. Adoption of pattern recognition techniques, such as artificial neural networks, would be able to overcome this problem as the system will be trained to recognise pattern with regards to different levels of damage. Utilisation of pattern recognition techniques will also be useful to overcome another damage detection problem of this study, that is, the slight distortion of damage detection results at areas near the supports for the experimental bridge and beam.

Since the number of sensors used and spacing of the data points are critical to the damage detection results, it is recommended that using a beam system, parametric studies on sensitivity of number of sensors and spacing be carried out. Besides, it is also recommended to study the threshold of damage that can be detected using different combination of number of sensors and spacing.

In the numerical studies of damage detection, the effects of measurement noise and/or uncertainties in the measured natural frequencies and mode shapes on damage detection results were not considered in this study. It is suggested for future work to use a more realistic numerical model representing a real structure and that noise be incorporated in the analysis of numerical models.

For the laboratory timber bridge, damage detection for single and multiple damage scenarios are considered satisfactory, but there is always room for improvement. One of the recommended ways to improve damage detection is by incorporating normalisation of mode shape curvature to its maximum values in different directions for the two-dimensional damage index methods based on plate-theory. The normalisation of mode shape curvatures would help to reduce dominance of higher modes and may produce better results, if a proper way or an appropriate proportion can

be found to normalise the mode shape curvatures in different directions. It is of interest to many researches if the severity of damage estimation using the damage index method for plate-like structures can be robustly established. It is suggested that pattern recognition techniques may be able to provide some solutions in this respect. In addition, investigation on the damage severity of the timber bridge is also suggested as future work.

The damage index (DI) methods adopted and modified in this thesis are mainly based on mode shape curvature. It is, therefore, viable to investigate as future work the effects of the initial curvature of a real timber beam or a real timber bridge. This may help to improve the accuracy of the DI and MDI methods. Bending strain methods may be used to investigate the initial curvature of a structure.

References

Abdo, M.A.-B. & Hori, M. 2002, 'A numerical study of structural damage detection using changes in the rotation of mode shapes', *Journal of Sound and Vibration*, vol. 251, no. 2, pp. 227-239.

Abdul Rahman, A.G. 1999, *Notes of Signal Processing*, Mechanical Engineering Department, Faculty of Engineering, University of Malaya

Abdul Razak, H., Teng, S.L., Ismail, Z. & Abdul Rahman, A.G. 2001, 'Crack detection in a simply supported RC beam using simplified Laplacian', *14th International Modal Analysis Conference*, vol. 2, Kissimmee, Florida, US, pp. 1344-1350.

Abraham, M.A., Park, S. & Stubbs, N. 1995, 'Loss of prestressed prediction based on nondestructive damage location algorithm', *Smart Structures and Materials 1995-Smart Systems for Bridges, Structures, and Highways*, vol. 2446, ed. L.K. Matthews, The International Society for Optical Engineering, San Diego, California, US, pp. 60-67.

Adams, R.D., Walton, D., Flitcroft, J.E. & Short, D. 1975, 'Vibration testing as a non-destructive test tool for composite materials', *Composite Reliability, ASTM STP 580*, pp. 159-175.

Adams, R.D., Cawley, P., Pye, C.J. & Stone, B.J. 1978, 'A vibrational technique for non-destructively assessing the integrity of structures', *Journal of Mechanical Engineering Science*, vol. 20, pp. 93-100.

Agilent Technologies 2000, *The fundamentals of modal testing*, Agilent Technologies, US.

Aktan, A.E., Lee, K.L., Chuntavan, C. & Aksel, T. 1994, 'Modal testing for structural identification and condition assessment of constructed facilities', *Proceedings of 12th International Modal Analysis Conference*, Honolulu, Hawaii, US, pp. 462-468.

Allemang, R.J. & Brown, D.L. 1983, 'Correlation coefficient for modal vector analysis', *Proceedings of 1st International Modal Analysis Conference*, Society for Experimental Mechanics, Inc., pp. 690-695.

Alqaradawi, M.Y., Nicholson, D., Nayfeh, J. & Moslehy, F.A. 2002, 'Baseline formation for damage diagnosis in one-dimensional beam problems', *20th*

International Modal Analysis Conference, Society for Experimental Mechanics, Inc., Los Angeles, California, pp. 1299-1305.

Alvandi, A. & Cremona, C. 2006, 'Assessment of vibration-based damage identification techniques', *Journal of Sound and Vibration*, vol. 292, pp. 179-202.

ANSYS Inc. 2005a, *ANSYS release 10.0*.

ANSYS Inc. 2005b, *ANSYS release 10.0 documentation*, Canonburg, US.

Austral Plywood 2005, *Characteristics of engineered wood products*, Austral Plywood, viewed 17 March 2005 <www.austraply.com.au/ti_char.html>.

Australian Standard™ 1997, *Timber structures Part 1: Design methods*, vol. AS 1720.1-1997, Standard Australia, NSW.

Australian/New Zealand Standard™ 1992, *Timber-Stress-graded-In-grade strength and stiffness evaluation*, vol. AS/NZS 4063:1992, Standards Australia and Standards New Zealand, NSW.

Australian/New Zealand Standard™ 1995, *Methods for test for veneer and plywood*, vol. AS/NZS 2098.9:1995, Standards Australia and Standards New Zealand, NSW.

Australian/New Zealand Standard™ 2004, *Plywood-Structural*, vol. AS/NZS 2269:2004, Standards Australia and Standards New Zealand, NSW.

Avitabile, P. 2001, 'Experimental modal analysis', *Sound and Vibration Magazine*, January 2001, pp. 1-11.

Avitabile, P. 2002, 'Twenty years of structural dynamic modification- A review', *Proceedings of IMAC-XX: A Conference on Structural Dynamics*, vol. 1, Society for Experimental Mechanics, Inc. , The Westin Los Angeles Airport, Los Angeles, California, pp. 356-372.

Bachmann, H., Ammann, W.J., Deischl, F., Eisenmann, J., Floegl, I., Hirsch, G.H., Klein, G.K., Lande, G.J., Mahrenholtz, O., Natke, H.G., Nussbaumer, H., Pretlove, A.J., Rainer, J.H., Saemann, E.-U. & Steinbeisser, L. 1995, *Vibration problems in structures: practical guidelines*, Birkhaeuser Verlag Basel, Basel.

Bale, S. & Browne, C.A. 2004, 'Non-destructive identification of defects in timber bridges', *Road System and Engineering Technology Forum*, Department of Main Roads, Queensland Govenrment, The Bardon Centre, Brisbane, pp. (Published on CD-ROM).

Banks, H.T., Inman, D.J., Leo, D.J. & Wang, Y. 1996, 'An experimentally validated damage detection theory in smart structures', *Journal of Sound and Vibration*, vol. 191, no. 5, pp. 859-880.

Barroso, L.R. & Rodriguez, R. 2004, 'Damage detection utilising the damage index method to a benchmark structure', *Journal of Engineering Mechanics*, vol. 130, no. 2, pp. 142-151.

Bayissa, W.L. & Haritos, N. 2005, 'Condition assessment of a T-beam using vibration response measurements', *4th Australasian Congress on Applied Mechanics*, Institute of Materials Engineering Australia, pp. 263-269.

Benitez, M.F. & Li, J. 2002, 'Static and dynamic evaluation of a timber bridge (Cattai Ck. Bridge NSW, Australia)', *The 7th world conference on timber engineering 2002*, vol. 2, eds Z. Ahmad, W.M. Wan Ab Majib, A.R. Ab Malik, A. Ibrahim, M.Z. Jumaat & N. Saari, Perpustakaan Negara Malaysia, Shah Alam Malaysia, pp. 385-393.

Bernal, D. 2002, 'Load vectors for damage localisation', *Journal of Engineering Mechanics*, vol. 128, no. 1, pp. 7-14.

Bernal, D. & Gunes, B. 2002, 'Damage localization in output-only systems: a flexibility based approach', *20th International Modal Analysis Conference*, Society for Experimental Mechanics, Inc., Los Angeles, California, US, pp. 1185-1191.

Bernal, D. & Levy, A. 2001, 'Damage localization in plates using DLVs', *19th International Modal Analysis Conference*, Society for Experimental Mechanics, Inc., Kissimmee, Florida, US, pp. 1205-1211.

Bernasconi, O. & Ewins, D.J. 1989, 'Application of strain modal testing to real structures', *7th International Modal Analysis Conference*, Las Vegas, Nevada, US, pp. 1453-1464.

Bicanic, N. & Chen, H.-P. 1997, 'Damage identification in framed structures using natural freqeuncies', *International Journal for Numerical Methods in Engineering*, vol. 40, pp. 4451-4468.

Bishop, C.M. 1994, 'Neural networks and their applications', *Review of Scientific Instruments*, vol. 65, no. 6, pp. 1803-1832.

Bodig, J. & Jayne, B.A. 1993, *Mechanics of wood and wood composites*, Reprint with corrections edn, Krieger Publishing Company, Florida.

Bootle, K.R. 1985, *Wood in Australia: type, properties and uses*, 2 edn, Sydney.

Brownjohn, J.M.W. & Xia, P. 1999, 'Finite element model updating of a damaged structure', *Proceedings of the 17th International Modal Analysis Conference*, Society for Experimental Mechanics, Inc., Hyatt Orlando Hotel, Kissimmee, Florida, US, pp. 457-462.

Carden, P., E & Fanning, P. 2004, 'Vibration based condition monitoring: a review', *Structural Health Monitoring*, vol. 3, no. 4, pp. 355-377.

Cawley, P. & Adams, R.D. 1979, 'The location of defects in structures from measurements of natural frequencies', *Journal of Strain Analysis*, vol. 14, no. 2, pp. 49-57.

Choi, S. & Stubbs, N. 1997, 'Nondestructive damage detection algorithms for 2D plates', *Smart Structures and Materials 1997- Smart Systems for Bridges, Structures and Highways*, ed. N. Stubbs, SPIE- The International Society for Optical Engineering, San Diego, California, US, pp. 193-204.

Cornwell, P., Doebling, S.W. & Farrar, C.R. 1997, 'Application of the strain energy damage detection method to plate-like structures', *Proceedings of the 15th International Modal Analysis Conference*, Society for Experimental Mechanics, Inc., Orlando, Florida, US, pp. 1312-1318.

Cornwell, P., Doebling, S.W. & Farrar, C.R. 1999, 'Application on the strain energy damage detection method to plate-like structures', *Journal of Sound and Vibration*, vol. 224, no. 2, pp. 359-374.

Craig, R.R.J. & Kurdila, A.J. 2006, *Fundamentals of structural dynamics*, 2nd edition edn, John Wiley & Sons, Hoboken, New Jersey, US.

CRC Wood Innovations 2005, *Extending the functional life of timber products*, <www.crcwood.unimelb.edu.au/research/extendlifespan.html>.

Creed, S.G. 1987, 'Assessment of large engineering structures using data collected during in-service loading', in F.K. Garas, J.L. Clarke & G.S.T. Armer (eds), *Structural assessment: The use of full and large scale testing*, Butterworth-Heinemann, London, pp. 55-62.

Crews, K.I. 2002, 'Behaviour and critical limit states of transversely laminated timber cellular bridge decks', University of Technology Sydney, Sydney, Australia.

Crews, K.I., Samali, B., Bakoss, S.L. & Champion, C. 2004, 'Overview of Assessing the Load Carrying Capacity of Timber bridges using Dynamic methods', *Austroads 5th Bridge Conference*, Hobart, Australia, pp. (Published on CD-ROM).

Curling, S., Clausen, C. & Winandy, J.E. 2000, *Limiting conditions for decay in wood systems*, International Research Group on Wood Preservation, Stockholm, Sweden.

Demeter, F.G. 1973, *Dynamics and vibration of structures* A Wiley-Interscience Publication, New York.

Department of Transport and Regional Services 2003, *2002-2003 Report on the operation of the Local Government (Financial Assistance) Act 1995*, Commonwealth of Australia, Canberra.

Doebling, S.W. 1995, 'Measurement of structural flexibility matrices for experiments with incomplete reciprocity', PhD thesis, University of Colorado, Boulder.

Doebling, S.W., Farrar, C.R. & Prime, M.B. 1998, 'A summary review of vibration-based damage identification methods', *The Shock and Vibration Digest*, vol. 30, no. 2, pp. 91-105.

Doebling, S.W., Farrar, C.R., Prime, M.B. & Shevitz, D.W. 1996, *Damage identification and health monitoring of structural and mechanical systems from changes in their vibration characteristics: A literature review*, Report Number Report LA-13070-MS, Los Alamos National Laboratory, New Mexico.

DOTARS 2003, *Local Government National Report (Chapter 4)*, in Department of Transport and Regional Services (ed.)Commonwealth of Australia, pp. 61-77

Duan, M. 2003, 'Finite element analysis of a laminated timber bridge', *10th Asia-Pacific Vibration Conference* Gold Coast, Queensland, Australia, pp. 104-108.

Duffey, T.A., Doebling, S.W., Farrar, C.R., Baker, W.E. & Rhee, W.H. 2001, 'Vibration-based damage identification in structures exhibiting axial abd torsional response', *Journal of Vibration and Acoustics*, vol. 123, no. 1, pp. 84-91.

Duwadi, S.R. & Ritter, M.A. 1997, *Timber bridges in the United States, Winter*, vol. 60, pp. 1-10<www.tfhrc.gov/pubrds/winter97/p97wi32.htm>.

Duwadi, S.R., Ritter, M.A. & Cesa, E. 2000, 'Wood in transportation program: an overview', *Fifth International Bridge Engineering Conference*, vol. 1, National Academy Press, Tampa, Florida, US, pp. 310-315.

Eggers, D.W. & Stubbs, N. 1994, 'Structural assessment using modal analysis techniques', *12th International Modal Analysis Conference*, Society for Experimental Mechanics, Inc., Honolulu, Hawaii, US.

Emerson, R.N., Pollock, D.G., Kainz, J.A., Fridley, K.J., McLean, D.I. & Ross, R.J. 1998, 'Non-destructive evaluation techniques for timber bridges', *Proceedings of 1998 World Conference on Timber Engineering*, Luasanne, Switzerland, pp. 670-677.

Ewins, D.J. 2000, *Modal testing: theory, practice and application*, vol. 2, Research Studies Press Ltd, England.

Farrar, C.R., Baker, W.E., Bell, T.M., Cone, K.M., Darling, T.W., Duffey, T.A., Eklund, A. & Migliori, A. 1994, *Dynamic characterization and damage detection in the I-40 bridge over the Rio Grande*, Report Number Report LA-12767-MS, Los Alamos National Laboratory, New Mexico.

Farrar, C.R. & Doebling, S.W. 1997, 'Lessons learned from applications of vibration-based damage identification methods to a large bridge structure', *Proceedings of the International Workshop on Structural Health Monitoring*, Stanford, California, US, pp. 351-370.

Farrar, C.R. & Juaragui, D. 1996, *Damage detection algorithms applied to experimental and numerical modal data from the I-40 bridge*, Los Alamos National Laboratory, Los Alamos, New Mexico, US.

Finnish Forest Industries Federation 2002, *Handbook of Finnish plywood*, Finnish Forest Industries Federation, Helsinki, Finland.

Fridley, K.J. 1998, *Wood Engineering in the 21st century: research needs ang goals*, American Society of Civil Engineers, Reston, VA, US.

Friswell, M.I. & Mottershead, J.E. 1995, *Finite element updating in structural dynamics*, Kluwer Academic Publisher, Netherlands.

Friswell, M.I. & Mottershead, J.E. 2001, 'Inverse methods in structural health monitoring', *Proceedings of the 4th International Conference on Damage Assessment of Structures*, eds K.M. Holford, J.A. Brandon, J.M. Dulieu-Barton, M.D. Gilchrist & K. Worden, Trans Tech Publications Ltd, Cardiff, Wales, UK, pp. 201-210.

Fu, G. 1999, 'Nondestructive bridge testing: load rating and condition rating', in D.M. Frangopol (ed.), *Bridge safety and reliability*, American Society of Civil Engineers, Reston, Virginia, US, pp. 137-164.

Gao, Y. & Spencer, B.F.J. 2002, 'Damage localization under ambient vibration using changes in flexibility', *Journal of Earthquake Engineering and Engineering Vibration*, vol. 1, no. 2, pp. 136-144.

Gao, Y. & Spencer, B.F.J. 2006, 'Online damage diagnosis for civil infrastructure employing a flexibility-baed approach', *Smart Materials and Structures*, vol. 15, pp. 9-19.

Garcia, G.V., Osegueda, R. & Meza, D. 1998, 'Comparison of the damage detection results utilizing an ARMA model and a FRF model to extract the modal parameters', *Smart Structures and Materials 1998*, SPIE-The International Society for Optical Engineering, San Diego, California, US, pp. 244-252.

Garcia, G.V., Stubbs, N. & Butler, K. 1996, 'Relative performance evaluation of pattern recognition models for non-destructive damage detection', *Smart Structures and Materials 1996-Smart Systems for Bridges, Structures, and Highways*, vol. 2719, ed. L.K. Matthews, The International Society for Optical Engineering, San Diego, California, US, pp. 25-34.

General Technical Report FPL-GTR-113 1999, *Wood handbook - wood as an engineering material*, Forest Products Laboratory, United States Department of Agriculture, Madison MI US.

Geradin, M. & Rixen, D. 1997, *Mechanical vibrations: thoery and application to structural dynamics*, second edn, John Wiley & Sons Ltd, England.

Gerber, C., Crews, K. & Sigrist, C. 2005, 'Investigation of the ultimate behaviours and FEA of wood stressed-skin panels', *Third international structural engineering and construction conference*, Shunan, Japan, p. Under peer reviewed.

Ghali, A., Neville, A.M. & Cheung, Y.K. 1978, *Structural analysis: A unified classical and matrix approach* 2nd edn, Chapman and Hall, London, UK.

Gutierrez, J.M., Ferregut, C.M. & Osegueda, R.A. 1996, 'Comparative study on two types of mode-sensitive neural networks for damage assessment', *Proceedings of the SPIE: nondestructive evaluation of utilities and pipelines*, vol. 2947, ed. M. Prager, SPIE, Scottsdale, Arizona, US, pp. 224-235.

Gutschmidt, S. & Cornwell, P.J. 2001, 'Statistical confidence bounds for structural health monitoring damage indicators', *19th International Modal Analysis Conference*, Society for Experimental Mechanics, Inc., Kissimmee, Florida, US, pp. 193-198.

Hamey, C.S., Lestari, W., Qiao, P. & Song, G. 2004, 'Experimental damage indetification of carbon/epoxy composite beams using curvature mode shapes', *Structural Health Monitoring*, vol. 3, no. 4, pp. 333-353.

Hao, H. & Xia, Y. 2002, 'Vibration-based damage detection of structures by genetic algorithm', *Journal of Computing in Civil Engineering*, vol. 16, no. 3, pp. 222-229.

Harvey, A.C. 1989, *Forecasting, structural time series models and the Kalman filter*, Cambridge University Press, New York.

Hassiotis, S. & Jeong, G.D. 1995, 'Identification of stiffness reduction using natural frequencies', *Journal of Engineering Mechanics*, vol. 121, no. 10, pp. 1106-1113.

Haykins, S. 1998, *Neural networks- a comprehensive foundation*, Prentice-Hall, Englewood, NJ.

He, J. & Fu, Z. 2001, *Modal Analysis*, Butterworth Heinemann, Oxford.

Hearn, G. & Testa, R.B. 1991, 'Modal analysis for damage detection in structures', *Journal of Structural Engineering*, vol. 117, no. 10, pp. 3042-3063.

Housner, G.W., Bergman, L.A., Caughey, T.K., Chassiakos, A.G., Claus, R.O., Masri, S.F., Skelton, R.E., Soong, T.T., Spencer, B.F. & Yao, J.T.P. 1997, 'Structural control: Past, present, and future', *Journal of Engineering Mechanics*, vol. 123, no. 9, pp. 897-971.

Hu, C. & Afzal, M.T. 2006a, 'A statistical algorithm for comparing mode shapes of vibration testing before and after damage in timbers', *Journal of Wood Science*, vol. Online First, p. 5.

Hu, C. & Afzal, M.T. 2006b, 'A wavelet analysis-based approach for damage localization in wood beams', *Journal of Wood Science*, vol. Online First, p. 5.

Hu, Y.C., Nakao, T., Nakai, T., Gu, J. & FH, W. 2005a, 'Dyanmic properties of three types of wood-based composites', *Journal of Wood Science*, vol. 51, pp. 7-12.

Hu, Y.C., Nakao, T., Nakai, T., Gu, J. & FH, W. 2005b, 'Vibration properties of wood plastic plywood', *Journal of Wood Science*, vol. 51, pp. 13-17.

Ismail, F., Ibrahim, A. & Martin, H.R. 1990, 'Identification of fatigue cracks from vibration testing', *Journal of Sound and Vibration*, vol. 140, no. 2, pp. 305-317.

Ismail, Z., Abdul Razak, H. & Abdul Rahman, A.G. 2006, 'Determination of damage location in RC beams using mode shape derivatives', *Engineering Structures*, vol. 28, pp. 1566-1573.

Ismail, Z., Abdul Razak, H., Abdul Rahman, A.G. & Pooi, A.H. 2001, 'Detection of deffects in reinforced concrete beams using modal data', *14th International Modal Analysis Conference*, vol. 2, Kissimmee, Florida, US, pp. 1358-1362.

Ju, f.D. & Mimovich, M.E. 1986, 'Modal freqeuncy method in diagnosis of fracture damage in structures', *4th International Modal Analysis Conference*, Los Angeles, US, pp. 1168-1174.

Ju, f.D. & Mimovich, M.E. 1988, 'Experimental diagnosis of fracture damage in structures by the modal freqeuncy method', *Journal of Vibration, Acoustics, Stress and Reliability in Design*, vol. 110.

Kao, C.-Y. & Hung, S.-L. 2005, 'A neural network-based approach for detection of structural damage', *Proceedings of the 16th IASTED International Conference: modelling and simulation*, Cancun, Mexico, pp. 251-255.

Kato, M. & Shimada, S. 1986, 'Vibration of PC bridge during failure process', *Journal of Structural Engineering*, vol. 112, no. 7, pp. 1692-1703.

Kessler, S.S., Spearing, S.M., Atalla, M.J., Cesnik, C.E.S. & Soutis, C. 2002, 'Damage detection in composite materials using frequency response function methods', *Composite: Part B*, vol. 33, pp. 87-95.

Kim, B.-H., Stubbs, N. & Sikorsky, C. 2002, 'Local damage detection using incomplete modal data', *20th International Modal Analysis Conference*, Society for Experimental Mechanics, Inc., Los Angeles, California, US, pp. 435-441.

Kim, B.S. & Kwak, H.K. 2001, 'A study of crack detection in plates using strain mode shapes', *19th International Modal Analysis Conference*, Society for Experrimental Mechanics, Inc., Kissimmee, Florida, US, pp. 1212-1218.

Kim, J.-T. 1995, 'Robust localization algorithm for highway plate-girder bridges', *Smart Structures and Materials 1995-Smart Systems for Bridges, Structures, and Highways*, vol. 2446, ed. L.K. Matthews, The International Society for Optical Engineering, San Diego, California, US, pp. 116-126.

Kim, J.-T., Park, J.-H. & Lee, B.-J. 2006, 'Vibration-based damage monitoring in model plate-girder bridges under uncertain temperature conditions', *Engineering Structures*, vol. Articles In Press.

Kim, J.-T., Ryu, Y.-S., Cho, H.-M. & Stubbs, N. 2003, 'Damage identification in beam-type structures: frequency-based method vs mode-shape-based method', *Engineering Structures*, vol. 25, pp. 57-67.

Kim, J.-T. & Stubbs, N. 1995, 'Model-uncertainty and damage-detection accuracy in plate girder', *Journal of Structural Engineering*, vol. 121, no. 10, pp. 1409-1417.

Kim, J.-T. & Stubbs, N. 2002, 'Improved damage identification method based on modal information', *Journal of Sound and Vibration*, vol. 252, no. 2, pp. 223-238.

Kim, J.-T. & Stubbs, N. 2003a, 'Crack ddetection in beam-type structures using freqeuncy data', *Journal of Sound and Vibration*, vol. 259, no. 1, pp. 145-160.

Kim, J.-T. & Stubbs, N. 2003b, 'Nondestructive crack detection algorithm for full-scale bridges', *Journal of Structural Engineering*, vol. 129, no. 10, pp. 1358-1366.

Kollmann, F.F.P., Kuenzi, E.W. & Stamm, A.J. 1975, *Principles of wood science and technology II: Wood based materials*, Springer-Verlag, Berlin.

Kudva, J.N., Munir, N. & Tan, P.W. 1992, 'Damage detection in smart structures using neural networks and finite-element analyses', *Smart Materials and Structures*, vol. 1, pp. 108-112.

Kurian, A. 2000, 'Analytical modeling of glued laminated girder bridges using ANSYS', *2000 MTC Transportation Scholar Conference*, Ames Iowa, pp. 70-82.

Lee, J.J. & Yun, C.B. 2006, 'Damage diagnosis of steel girder bridges using ambient vibration data', *Engineering Structures*, vol. 28, pp. 912-925.

Li, D.B., Zhuge, H.C. & Wang, B. 1989, 'The principles and techniques of experimental strain modal analysis', *7th International Modal Analysis Conference*, Las Vegas, Nevada, US, pp. 1285-1289.

Li, J., Samali, B., Crews, K.I., Choi, F.C. & Shestha, R. 2005, 'Theoretical and experimental studies on assessment of bridges using simple dynamic procedures', *Australian Structural Engineering Conference 2005*, Australia Structural College of EA, Newcastle City Hall, Newcastle, NSW, Australia, pp. (Published on CD-ROM).

Li, Y.Y., Cheng, L., Yam, L.H. & Wong, W.O. 2002, 'Identification of damage locations for plate-like structures using damage sensitive indices: strain modal approach', *Computers and Structures*, vol. 80, pp. 1881-1894.

Li, Z., Swanson, J.A., Helmicki, A.J. & Hunt, V.J. 2005, 'Modal contribution coefficients in bridge condition evaluation', *Journal of Bridge Engineering*, vol. 10, no. 2, pp. 169-178.

Lieven, N.A.J. & Ewins, D.J. 1988, 'Spatial correlation of modespaces: the corridnate modal assurance criterion (COMAC)', *6th International Modal Analysis Conference*, Kissimmee, Florida, US, pp. 1063-1070.

LMS International 1992, *LMS CADA-X modal analysis manual*, LMS International, Belgium.

Loh, C.-H. & Yeh, S.-C. 2000, 'Application of neural networks to health monitoring for bridge structures', *Proceedings of the SPIE: nondestructive evaluation of*

highway, utilities and pipelines IV, vol. 3995, eds A.E. Aktan & S.R. Gosselin, SPIE, Newport Beach, US, pp. 382-393.

Madsen, B. 1992, *Structural behaviour of timber*, 1st edn, Timber Engineering Ltd, Vancouver, Canada.

Maduakolam, M.N. & Stubbs, N. 1995, 'Global non-destructive detection of mass and structural damage to conventional and floating bridges', *Smart Structures and Materials 1995-Smart Systems for Bridges, Structures, and Highways*, vol. 2446, ed. L.K. Matthews, The International Society for Optical Engineering, San Diego, California, US, pp. 60-67.

Maeck, J. 2003, 'Damage assessment of civil engineering structures by vibration monitoring', PhD thesis, Katholieke Universiteit Leuven, Belgium.

Maeck, J. & De Roeck, G. 2002, 'Damage assessment of a gradually damaged RC beam using dynamic system identification', *20th International Modal Analysis Conference*, Society for Experimental Mechanics, Inc., Los Angeles, California, US, pp. 1560-1566.

Maia, N.M.M. & Silva, J.M.M.e. 1997, *Theoretical and Experimental Modal Analysis*, Research Studies Press Ltd, Somerset.

McInnes, K. 2005, 'Conserving historic timber bridges', *National Trust of Australia (Victoria)*, March, p. 2

Messina, A., Jones, I.A. & Williams, E.J. 1996, 'Damage detection and localisation using natural freqeuncy changes', *14th International Modal Analysis Conference*, Orlando, US, pp. 67-76.

Messina, A., Williams, E.J. & Contursi, T. 1998, 'Structural damage detection by a sensitivity and statistical-based method', *Journal of Sound and Vibration*, vol. 216, no. 5, pp. 791-808.

Miller, P.H. 2005, *Notes on wood and timber as a marine material*, p. 8<http://web.usna.navy.mil/~phmiller/en380/wood.doc>.

Morison, A., VanKarsen, C.D., Evensen, H.A., Ligon, J.B., Erickson, J.R., Ross, R.J. & Forsman, J.W. 2002, 'Timber bridge evaluation: a global nondestructive approach using impact genertaed FRFs', *Proceedings of IMAC-XX*, Society for Experimental Mechanics Inc., Los Angeles, California, US, pp. 1567-1573.

Morison, A., VanKarsen, C.D., Evensen, H.A., Ligon, J.B., Erickson, J.R., Ross, R.J. & Forsman, J.W. 2003, 'Dynamic characteristics of timber bridges as a measure of

structural integrity', *Proceedings of IMAC-XXI*, Society for Experimental Mechanics Inc., Kissimme, Florida, US, pp. (Published on CD-ROM).

Morris, P.I. & Winandy, J.E. 2002, *Limiting conditions for decay in wood systems*, International Research Group on Wood Preservation, Stockholm, Sweden.

Moslehy, F.A. 2002, 'A new inverse vibration method for detection and characterization of multiple defects in beams', *20th International Modal Analysis Conference*, Society for Experimental Mechanics, Inc., Los Angeles, California, US, pp. 160-166.

Mottershead, J.E. & Friswell, M.I. 1993, 'Model updating in structural dynamics: a survey', *Journal of Sound and Vibration*, vol. 167, no. 2, pp. 347-375.

Mufti, A. 2001, *Guidelines for structural health monitoring: design manual no. 2*, vol. 1, ISIS Canada, Manitoba, Canada.

Murray, G. 2002, 'Rural bridges-getting the most for your budget dollar', *Queensland IPWEA State Conference 2002*, IPWEA, Noosa, pp. (Published on CD-ROM).

National Instruments 2006, *Measurement Encyclopedia*, National Instruments Corporation, viewed 17 June 2006 <http://zone.ni.com/devzone/nidzgloss.nsf/webmain/BB88F46ABF5F186C8625686A00794152>.

Ndambi, J. 2002, 'Damage assessment in reinforced concrete beams by damping analysis', PhD thesis, Free University Brussels, Brussels

Ndambi, J.-M., Vantomme, J. & Harri, K. 2002, 'Damage assessment in reinforced concrete beams using eigenfreqeuncies and mode shape derivatives', *Engineering Structures*, vol. 24, pp. 510-515.

NSF Dynamic Systems 2006, *Numerical differetiation and integration tutorial.*

Oja, E. 1989, 'Neural networks principal components and subspaces', *International Journal of Neural Systems*, vol. 1, pp. 61-68.

Omenzetter, P. & Brownjohn, J.M.W. 2006, 'Application of time series analysis for bridge monitoring', *Smart Materials and Structures*, vol. 15, pp. 129-138.

Ou, F.L. & Weller, C. 1986, *An overview of timber bridges*, Transportation Research Board National Research Council, Washington D.C.

Palacz, M. & Krawczuk, M. 2002, 'Vibration parameters for damage detection in structures', *Journal of Sound and Vibration*, vol. 249, no. 5, pp. 999-1010.

Pandey, A.K. & Biswas, M. 1994, 'Damage detection in structures using changes in flexibility', *Journal of Sound and Vibration*, vol. 169, no. 1, pp. 3-17.

Pandey, A.K., Biswas, M. & Samman, M.M. 1991, 'Damage detection from changes in curvature mode shapes', *Journal of Sound and Vibration*, vol. 145, no. 2, pp. 321-332.

Park, S., Kim, Y.-B. & Stubbs, N. 2002, *Nondestructive damage detection in large structures via vibration monitoring, Electronic Journal of Structural Engineering*, vol. 2, pp. 59-75

Park, S. & Stubbs, N. 1995, 'Reconstruction of mode shapes using Shannon's sampling theorem and its application to the nondestructive damage localization algorithm ', *Smart Systems for Bridges, Structures, and Highways*, ed. L.K. Matthews, SPIE-The International Society for Optical Engineering, San Diego, California, US, pp. 280-292.

Park, S. & Stubbs, N. 1996, 'Bridge diagnostics via vibration monitoring', *Smart Structures and Materials 1996-Smart Systems for Bridges, Structures, and Highways*, vol. 2719, ed. L.K. Matthews, The International Society for Optical Engineering, San Diego, California, US, pp. 36-45.

Patjawit, A. & Kanok-Nukulchai, W. 2005, 'Health monitoring of highway bridges based on a global flexibility index', *Engineering Structures*, vol. 27, no. 9, pp. 1385-1391.

Pereyra, L.R., Osegueda, R.A., Carrasco, C.J. & Ferregut, C.M. 1999, 'Damage detection in a stiffened plate using modal strain energy differences', *Proceedings of SPIE-Nondestructive Evaluation of Aging Aircraft, Airports, and Aerospace Hardware III*, vol. 3586, ed. A.K. Mal, SPIE-The International Society for Optical Engineering, Newport Beach, California, US.

Peterson, M.L. & Gutkowski, R.M. 1999, 'Evaluation of the structural integrity of timber bridges', *NDT&E International*, vol. 32, pp. 43-48.

Peterson, S.T., McLean, D.I. & Pollock, D.G. 2003, 'Application of dynamic system identification to timber bridges', *Journal of Structural Engineering*, vol. 129, no. 1, pp. 116-124.

Peterson, S.T., McLean, D.I., Symans, M.D., Pollock, D.G., Cofer, W.F., Emerson, R.N. & Fridley, K.J. 2001a, 'Application of dynamic system identification to timber beams I', *Journal of Structural Engineering*, vol. 127, no. 4, pp. 418-425.

Peterson, S.T., McLean, D.I., Symans, M.D., Pollock, D.G., Cofer, W.F., Emerson, R.N. & Fridley, K.J. 2001b, 'Application of dynamic system identification to

timber beams II', *Journal of Structural Engineering*, vol. 127, no. 4, pp. 426-432.

Polensek, A. 1973, 'Static and dynamic analysis of wood-joist floors by the finite element method', PhD thesis, Oregon State University, Ann Arbor, Michigan, US.

Ramsey, K.A. 1983, 'Experimental modal analysis, structural modifications and FEM analysis on a desktop computer', *Sound and Vibration*, February, p. 10.

Ranaweera, D.K., Hubele, N.F. & Papalexopoulus, A.D. 1995, 'Application of radial basis function for short term load forecasting', *IEE Proceedings - Generation, Transmission and Distribution*, vol. 142, no. 1, pp. 45-50.

Ratcliffe, C.P. 1997, 'Damage detection using a modified Laplacian Operator on mode shape data', *Journal of Sound and Vibration*, vol. 204, no. 3, pp. 505-517.

Ratcliffe, C.P. 2000, 'A frequency and curvature based experimental method for locating damage in structures', *Journal of Vibration and Acoustics*, vol. 122, pp. 324-329.

Ratcliffe, C.P. & Bagaria, W.J. 1998, 'Vibration technique for locating delamination in a composite beam', *AIAA Jounal*, vol. 36, no. 6, pp. 1074-1077.

Ratnam, C. & Parameswara Rao, V. 2004, 'Identification of damage in structures using genetic algorithms', *Journal of the Institution of Engineers (India)- Mechanical Engineering*, vol. 84, pp. 154-160.

Richardson, M.H. 1997, 'It is a mode shape, or an operating deflection shape?' *Sound and Vibration Magazine 30th Anniversary Issue*, March, pp. 1-11.

Richardson, M.H. 1980, *Detection of damage in structures from changes in their dynamic (modal) parameters- A survey*, vol. NUERG/CR-1431, U.S. Nuclear Regulatory Commision, Washington, D.C.

Richardson, M.H. & Formenti, D.L. 1982, 'Parameter estimation from freqeuncy response measurements using rational fraction polynomials', *1st International Modal Analysis Conference*, Orlando, Florida, US, pp. 1-15.

Ritter, M.A. 1990, *Timber bridges: design, construction, inspection, and maintenance*, United States Department of Agriculture Forest Service, Washington DC.

Ritter, M.A., Wipf, T.J. & Wood, D.L. 1998, 'Evaluation and tetsing of timber railroad bridges', *5th World Conference on Timber Engineering*, vol. 1, eds J. Nattere & J.-L. Sandoz, Presses polytechniques et universitaires romandes, Montreux, Switzerland, pp. 792-793.

Ross, R.J., Brashaw, B.K. & Wang, X. 2006, 'Structural condition assessment of in-service wood', *Forest Products Journal*, vol. 56, no. 6, pp. 4-8.

Ross, R.J. & Pellerin, R.F. 1994, *Nondestructive testing for assessing wood members in structures: a review*, Report Number General Technical Report FPL-GTR-70, Forest Products Laboratory, Madison.

RTA 2006, *Bridge types in NSW: historical overviews*, Road Transport Authority.

Rytter, A. 1993, 'Vibration based inspection of civil engineering structures', Ph. D thesis, Aalborg University, Denmark.

Salawu, O.S. 1997, 'Detection of structural damage through changes in frequency: a review', *Engineering Structures*, vol. 19, no. 9, pp. 718-723.

Salawu, O.S. & Williams, C. 1995, 'Review of full-scale dynamic testing of bridge structures', *Engineering Structures*, vol. 17, no. 2, pp. 113-121.

Samali, B., Bakoss, S.L., Crews, K.I., Li, J. & Benitez, M. 2000, *To develop cost-effective assessment technique to facilitate the management of local government bridge assets*, The Centre for Built Infrastructure Research in collaboration with The Institute of Public Works Engineering Australia, Sydney.

Samali, B., Bakoss, S.L., Crews, K.I., Li, J. & Champion, C. 2002, 'Assessing the load carrying capacity of timber bridges using dynamic methods', *IPWEA Queensland Division Annual Conference 2002*.

Samali, B., Bakoss, S.L., Li, J., Saleh, A. & Ariyaratne, W. 2003, 'Assessing the structural adequacy of a 3-span steel-concrete bridge using dynamic methods: a case study', *10th International Conference: Structural and Faults and Repair 2003*, London, UK, pp. (Published on CD-ROM).

Samali, B., Crews, K.I., Li, J., Bakoss, S.L. & Champion, C. 2003, 'Assessing the load carrying capacity of timber bridges using dynamic methods', *Proceedings of the Western Australia State Conference 2003*, Institute of Public Works Engineering Australia, Perth, Western Australia, Australia, pp. (Published on CD-ROM).

Sampaio, R.P.C., Maia, N.M.M. & Silva, J.M.M.e. 1999, 'Damage detection using the freqeuncy-response-function curvature method', *Journal of Sound and Vibration*, vol. 226, no. 5, pp. 1029-1042.

Sánchez, J.C.H. 2005, 'Evaluation of structural damage identification methods based on dynamic characteristics', PhD thesis, University of Puerto Rico, Mayagüez.

Sazonov, E.S., Klinkkhachorn, P., GangaRao, H.V.S. & Halabe, U.B. 2002a, 'Non-baseline damage detection from changes in strain energy mode shapes:

experiments on armored vehicle launched bridge', *29th Annual Review of Progress in Quantitative Nondestructive Evaluation*, Bellingham, WA.

Sazonov, E.S., Klinkkhachorn, P., GangaRao, H.V.S. & Halabe, U.B. 2002b, 'Non-baseline damage detection of small damages from changes in strain energy mode shapes', *Nondestructive Testing and Evaluation*, vol. 18, no. 3-4, pp. 91-107.

Schwarz, B.J. & Richardson, M.H. 1999, 'Experimental modal analysis', *CSI Reliability Week*, October, p. 12.

Serna, O.R. & Stubbs, N. 1996, 'Nondestructive damage evaluation in complex structures using modal strain parameters', *Smart Structures and Materials 1996-Smart Systems for Bridges, Structures, and Highways*, vol. 2719, ed. L.K. Matthews, The International Society for Optical Engineering, San Diego, California, US, pp. 36-45.

Shi, Z.Y., Law, S.S. & Zhang, L.M. 1998, 'Structural damage localization from modal strain energy change', *Journal of Sound and Vibration*, vol. 218, no. 5, pp. 825-844.

Shi, Z.Y., Law, S.S. & Zhang, L.M. 2000, 'Damage localization by directly using incomplete mode shapes', *Journal of Engineering Mechanics*, vol. 126, no. 6, pp. 656-660.

Shi, Z.Y., Law, S.S. & Zhang, L.M. 2002, 'Improved damage quantification from elemental modal strain energy change', *Journal of Engineering Mechanics*, vol. 128, no. 5, pp. 521-529.

Sohn, H., Farrar, C.R., Hemez, F.M., Shunk, D.D., Stinemates, D.W. & Nadler, B.R. 2003, *A review of structural health monitoring literature: 1996-2001*, Report Number LA-13976-MS, Los Alamos National Laboratory, New Mexico.

Stubbs, N. 1990a, 'Global damage detection in solids', *The International Journal of Analytical and Experimental Modal Analysis*, vol. 5, no. 2, pp. 67-79.

Stubbs, N. 1990b, 'Global damage detection in solids-experimental verification', *The International Journal of Analytical and Experimental Modal Analysis*, vol. 5, no. 2, pp. 81-97.

Stubbs, N. & Garcia, G. 1996, 'Application of pattern recognition to damage localization', *Microcomputers in Civil Engineering*, vol. 11, pp. 395-409.

Stubbs, N. & Kim, J.-T. 1996, 'Damage localization in structures without baseline modal parameters', *AIAA Jounal*, vol. 34, no. 8, pp. 1644-1649.

Stubbs, N., Kim, J.-T. & Farrar, C.R. 1995, 'Field verification of a non-destructive damage localization and severity estimation algorithm', *Proceedings of the 13th International Modal Analysis Conference*, Society for Experimental Mechanics, Inc., Sheraton Music City Hotel, Nashville, Tennessee, US, pp. 210-218.

Stubbs, N., Kim, J.-T. & Topole, K.G. 1992, 'An efficient and robust algorithm for damage localization in offshore platforms', *ASCE Tenth Structures Congress*, Antonio, Texas, US, pp. 543-546.

Stubbs, N. & Park, S. 1996, 'Optimal sensors placement for mode shapes via Shannon's sampling theorem', *Microcomputers in Civil Engineering*, vol. 11, pp. 411-419.

Structural Dynamic Research Laboratory 1999, *Experimental modal analysis*, Report Number UC-SDRL-RJA, University of Cincinnati, Cincinnati, Ohio, US.

Suresh, S., Omkar, S.N., Ganguli, R. & Mani, V. 2004, 'Identification of crack location and depth in a cantilever beam using a modular neural network.' *Smart Materials and Structures*, vol. 13, pp. 907-915.

Szabó, B. & Babuška, I. 1991, *Finite element analysis*, John Wiley & Sons, New York.

Teughels, A. & De Roeck, G. 2003, 'Damage assessment of the Z24 bridge by FE model updating', *Proceedings of DAMAS 2003*, Southhampton, UK, pp. 19-26.

Teughels, A. & De Roeck, G. 2004, 'Structural damage identification of the highway bridge Z24 by FE model updating', *Journal of Sound and Vibration*, vol. 278, pp. 589-610.

Teughels, A., De Roeck, G. & Suykens, J.A.K. 2002a, 'CLM, a global optimization method in FEM', *5th European Conference on Structural Dynamics*, Munich, Germany.

Teughels, A., De Roeck, G. & Suykens, J.A.K. 2002b, 'Global optimization in FEM updating by coupled local minimisers', *International Noise and Vibration Engineering Conference*, Lueven, Belgium.

Teughels, A., De Roeck, G. & Suykens, J.A.K. 2002c, 'Updating of finite element models using coupled local monimisers (CLM)', *3rd International Conference on Identification in Engineering Systems*, Swansea, UK, pp. 280-289.

Teughels, A., De Roeck, G. & Suykens, J.A.K. 2003a, 'Coupled local minimisers: a new global optimization method', *11th IFIP Working Conference on Reliability and Optimization of Structural Systems*, Alberta, Canada.

Teughels, A., De Roeck, G. & Suykens, J.A.K. 2003b, 'Global optimization by coupled local minimisers and its application to FE model updating', *Computers & Structures*, vol. 81, pp. 2337-2351.

Teughels, A., Maeck, J. & De Roeck, G. 2002a, 'Damage assessment by FE model updating using damage functions', *Computers and Structures*, vol. 80, pp. 1869-1879.

Teughels, A., Maeck, J. & De Roeck, G. 2002b, 'FEM updating of a reinforced concrete beam using damage functions', *International Conference on Structural Dynamic Modelling: Test, Analysis, Correlation and Validation*, eds N.M.M. Maia, J.M.M.e. Silva & A.M.R. Ribeiro, funchal, Madeira, Portugal.

The Mathwork Inc. 2005, *Matlab 7.1*.

Thelandersson, S. 2003, 'Introduction: wood as a construction material', in S. Thelandersson & H.J. Larsen (eds), *Timber engineering*, John Wiley & Sons Ltd, West Sussex, England, pp. 15-20.

Tsang, W.F. 1990, 'Use of dynamic strain measurements for the modelling of structures', *8th International Modal Analysis Conference* Orlando, Florida, US, pp. 1246-1251.

Tung, S. & Tran, D. 2003, 'Non-destructive strctural damage detection using frequency response function from vibration test', *10th Asia-Pacific Vibration Conference*, QUT, Gold Coast, Queensland, Australia, pp. 737-742.

Unger, J.F., Teughels, A. & De Roeck, G. 2005, 'Damage detection of a prestressed concrete beam using modal strains', *Journal of Structural Engineering*, vol. 131, no. 9, pp. 1456-1463.

US Forest Products Laboratory 2005, *Computing moisture content of wood*, viewed 15-7-2005 <www.woodbin.com/ref/wood/emc.htm>.

Vestroni, F. & Capecchi, D. 2000, 'Damage detection in beam structures based on freqeuncy measurements', *Journal of Engineering Mechanics*, vol. 126, no. 7, pp. 761-768.

Wahab, M.M.A. & De Roeck, G. 1999, 'Damage detection in bridges using modal curvatures: application to a real scenario', *Journal of Sound and Vibration*, vol. 226, no. 2, pp. 217-235.

Walter, G.P. 1996, 'Timber bridges in Australia', *National conference on wood transportation structures*, eds M.A. Ritter, S.R. Dumadi & P.D.H. Lee,

Department of Agriculture, Forest Services, Forest Products Laboratory, Madison WI USA, pp. 17-21.

Wang, T.-L. & Zong, Z. 2002, *Improvement of evaluation method for existing highway bridges*, vol. Research Report No. FL/DOT/RMC/6672-818, Department of Civil and Environemental Engineering, Florida International University, Tallahassee, Florida.

Wang, X., Kangsas, S., Padur, D., Liu, L., Swanson, J.A., Helmicki, A.J. & Hunt, V.J. 2005, 'Overview of a modal-based condition assessment procedure', *Journal of Bridge Engineering*, vol. 10, no. 4, pp. 460-467.

Wang, X., Wacker, J.P., Morison, A.M., Forsman, J.M., Erickson, J.R. & Ross, R.J. 2005, *Nondestructive assessment of single-span timber bridges using a vibration-based method*, Report Number Research Paper FPL-RP-627, Forest Products Laboratory, Madison.

Whalen, T.M., Gauthier, J.F. & Liu, J. 2004, 'A new methodology for nondestructive evaluation and rating of bridges', *Proceeding of the 2004 American Control Conference*, Boston, Massachusetts, US, pp. 4195-4200.

Wilkinson, K., Thambiratnam, D. & Ferreira, L. 2005, 'Non destructive testing of timber bridge girders', *Internation Conference on Structural Condition Assessment, Monitoring and Improvement*, Perth, Western Australia, pp. (Punlished on CD-ROM).

Winandy, J.E. & Morrel, J.J. 1993, 'Relationship between incipient decay, strength, and chemical composition of Douglas-Fir heartwood', *Wood and Fibre Science*, vol. 25, no. 3, pp. 278-288.

Worden, K. & Dulieu-Barton, J.M. 2004, 'An overview of intelligent fault detection in systems and structures', *Structural Health Monitoring*, vol. 3, no. 1, pp. 85-98.

Worden, K., Manson, G. & Allman, D.J. 2001, 'An experimental appraisal of the strain energy damage location method', *Proceedings of the 4th International Conference on Damage Assessment of Structures*, eds K.M. Holford, J.A. Brandon, J.M. Dulieu-Barton, M.D. Gilchrist & K. Worden, Trans Tech Publications Ltd, Cardiff, Wales, UK, pp. 35-46.

Xu, H. & Humar, J. 2005, 'Application of artificial neural networks in vibration based damage detection', *Nondestructive Evaluation and Health Monitoring of Aerospace Materials, Composites and Civil Infrastructure IV*, vol. 5767, ed. G. Shull, SPIE, Bellingham, WA, pp. 120-131.

Xu, Y.L. & Chen, J. 2004, 'Structural damage detection using Empirical Mode Decomposition: experimental investigation', *Journal of Engineering Mechanics*, vol. 130, no. 11, pp. 1279-1288.

Yagiz, N. & Skaman, L.E. 2006, 'Vibrations of a rectangular bridge as an isotropic plate under a traveling full vehicle model', *Journal of Vibration and Control*, vol. 12, no. 1, pp. 83-98.

Yam, L.H., Leung, T.P., Li, D.B. & Xue, K.Z. 1996, 'Theoretical and experimental study of modal strain analysis', *Journal of Sound and Vibration*, vol. 191, no. 2, pp. 251-260.

Yang, J.N., Lei, Y., Lin, S. & Huang, N. 2004, 'Hilbert-Huang based approach for structural damage detection', *Journal of Engineering Mechanics*, vol. 130, no. 1, pp. 85-95.

Yang, X.Y., Ishimaru, Y., Iida, I. & Urakami, H. 2002a, 'Application of modal analysis by transfer function to nondestructive testing of wood I: determination of localized defects in wood by the shape of flexural vibration wave', *Journal of Wood Science*, vol. 48, pp. 283-288.

Yang, X.Y., Ishimaru, Y., Iida, I. & Urakami, H. 2002b, 'Application of modal analysis by transfer function to nondestructive testing of wood II: modulus of elasticity evaluation of sections of differing quality in a wooden beam by the curvature of the flexural vibration wave', *Journal of Wood Science*, vol. 49, pp. 140-144.

Yoon, M.K., Heider, D., Gillespie, J.W.J., Ratcliffe, C.P. & Crane, R.M. 2001, 'Local damage detection using a global fitting method on mode shape data', *14th International Modal Analysis Conference*, Society for Experimental Mechanics, Inc., Kissimmee, Florida, US, pp. 231-237.

Zhu, X.Q. & Law, S.S. 2006, 'Wavelet-based crack identification of bridge beam from operational deflection time history', *International Journal of Solids and Structures*, vol. 43, pp. 2299-2317.

Živanovć, S., Pavic, A. & Reynolds, P. 2006, 'Modal testing and FE model tuning of a lively footbridge structure', *Engineering Structures*, vol. 28, pp. 857-868.

Zou, Y., Tong, L. & Steven, G.P. 2000, 'Vibration-based model-dependent damage (delamination) identification and health monitoring for composite structures- A review', *Journal of Sound and Vibration*, vol. 230, no. 2, pp. 357-378.

Zwonlinski, B. 1998, *Notes of vibration measurements*, Kistle Instrument Corporation.

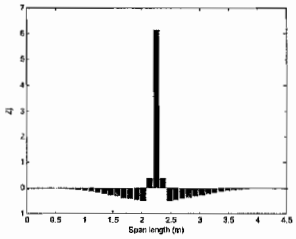
Appendix A

A.1 Damage Detection Results - Numerical Studies

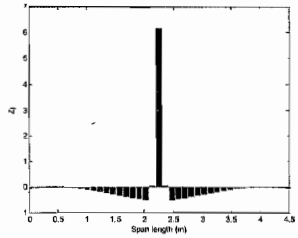
The damage detection results for the numerical studies (41-point) are shown below. The * denotes damage cases that were replicated in the experimental results.

A.1.1 Damage Localisation for Timber Beam (DI-I vs MDI-I) (2 Modes)

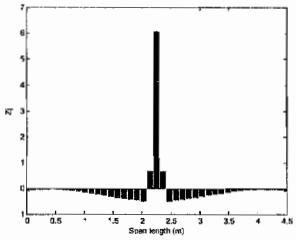
Single Damage Location



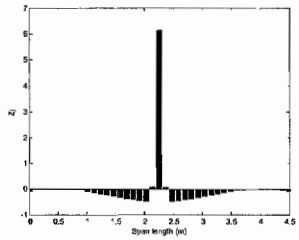
DI-I- 4L (2 modes)*



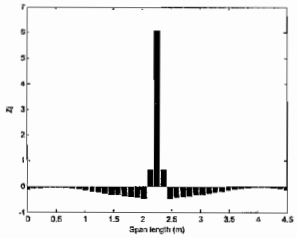
MDI-I- 4L (2 modes)*



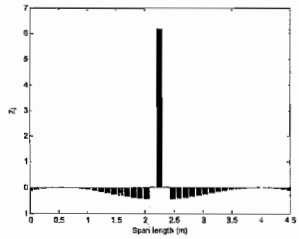
DI-I- 4M (2 modes)*



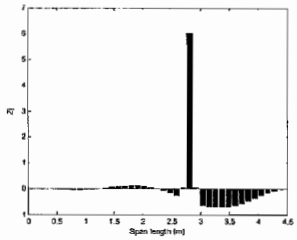
MDI-I- 4M (2 modes)*



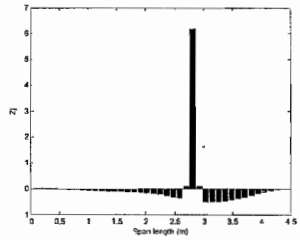
DI-I- 4S (2 modes)*



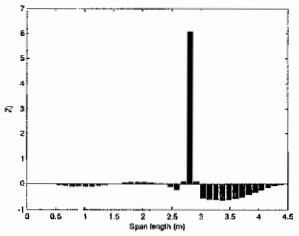
MDI-I- 4S (2 modes)*



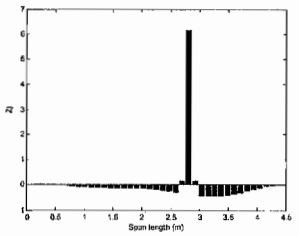
DI-I- 5L (2 modes)



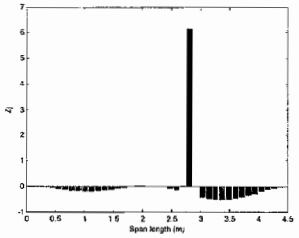
MDI-I- 5L (2 modes)



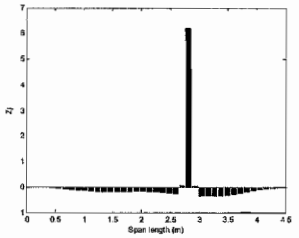
DI-I- 5M (2 modes)



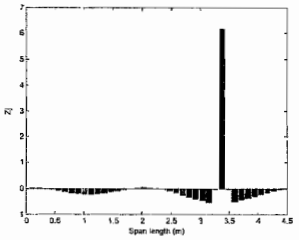
MDI-I- 5M (2 modes)



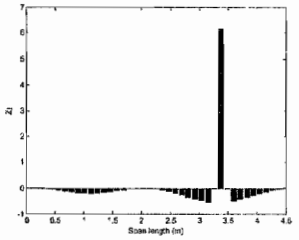
DI-I- 5S (2 modes)



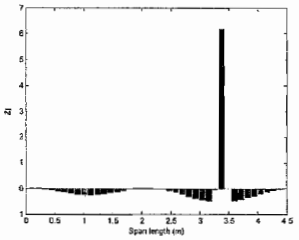
MDI-I- 5S (2 modes)



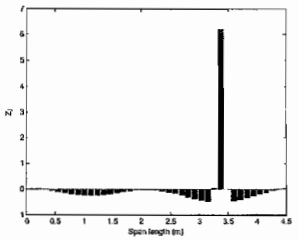
DI-I- 6L (2 modes)*



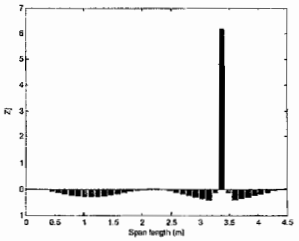
MDI-I- 6L (2 modes)*



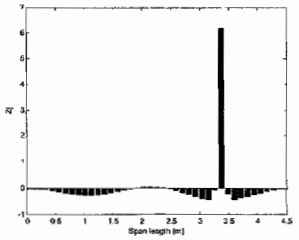
DI-I- 6M (2 modes)



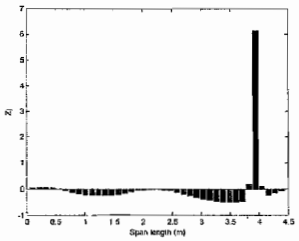
MDI-I- 6M (2 modes)



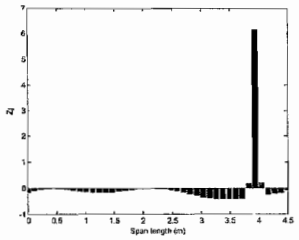
DI-I- 6S (2 modes)



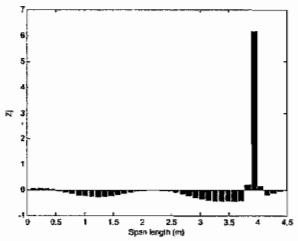
MDI-I- 6S (2 modes)



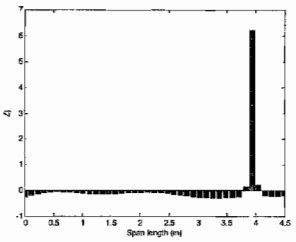
DI-I- 7L (2 modes)



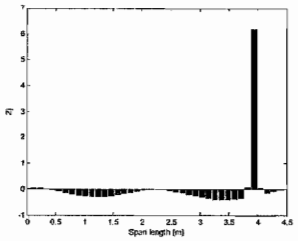
MDI-I- 7L (2 modes)



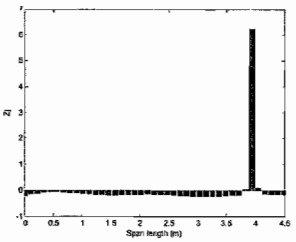
DI-I- 7M (2 modes)



MDI-I- 7M (2 modes)

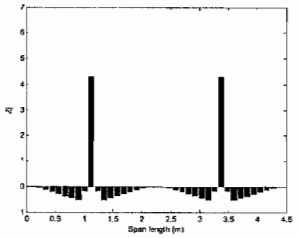


DI-I- 7S (2 modes)

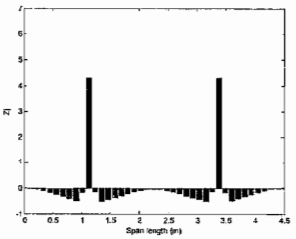


MDI-I- 7S (2 modes)

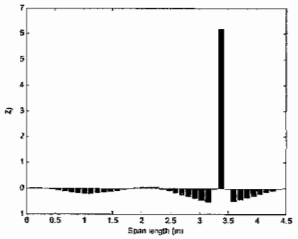
Two Damage Locations



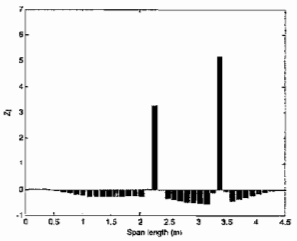
DI-I- 2L6L (2 modes)*



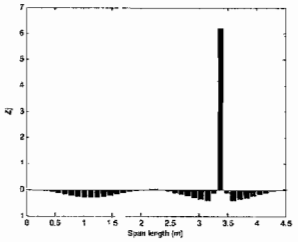
MDI-I- 2L6L (2 modes)*



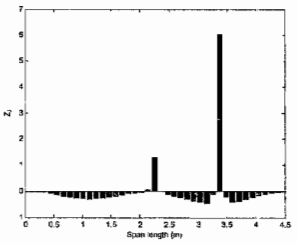
DI-I- 4L6L (2 modes)



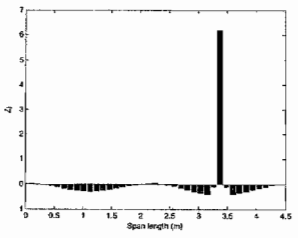
MDI-I- 4L6L (2 modes)



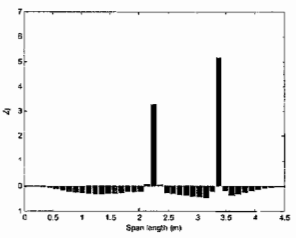
DI-I- 4L6S (2 modes)



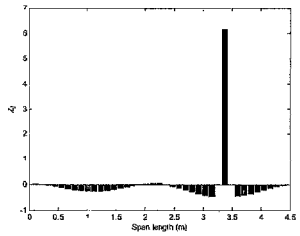
MDI-I- 4L6S (2 modes)



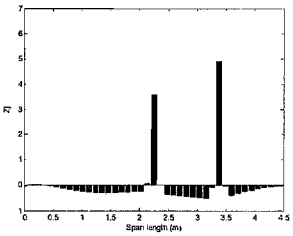
DI-I- 4M6S (2 modes)



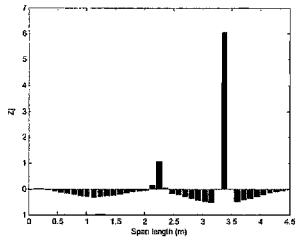
MDI-I- 4M6S (2 modes)



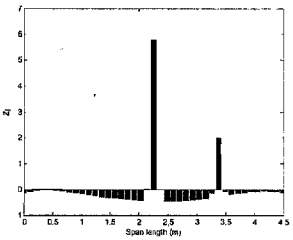
DI-I- 4M6M (2 modes)



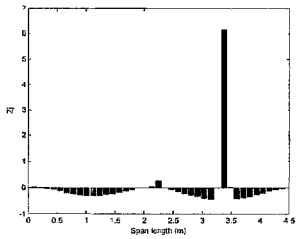
MDI-I- 4M6M (2 modes)



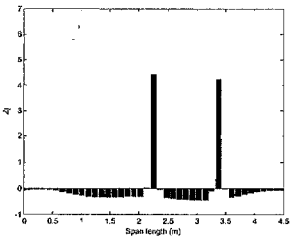
DI-I- 4S6L (2 modes)*



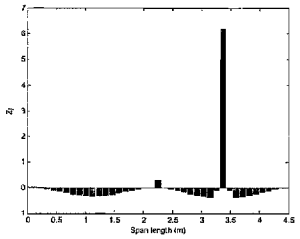
MDI-I- 4S6L (2 modes)*



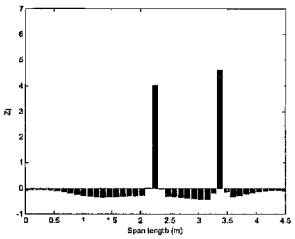
DI-I- 4S6M (2 modes)*



MDI-I- 4S6M (2 modes)*

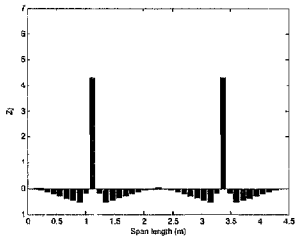


DI-I- 4S6S (2 modes)*

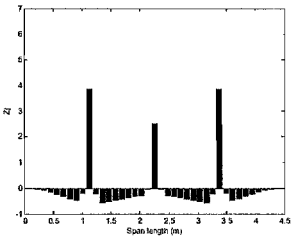


MDI-I- 4S6S (2 modes)*

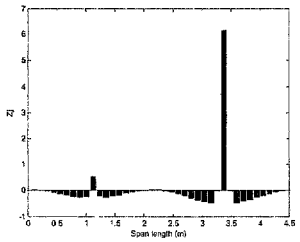
Three Damage Locations



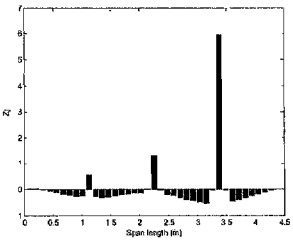
DI-I- 2L4L6L (2 modes)*



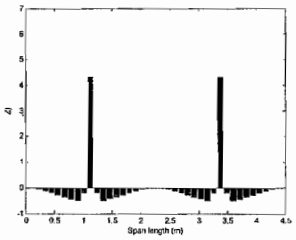
MDI-I- 2L4L6L (2 modes)*



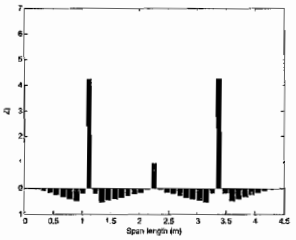
DI-I- 2L4L6M (2 modes)*



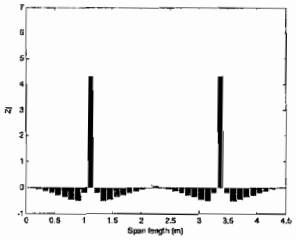
MDI-I- 2L4L6M (2 modes)*



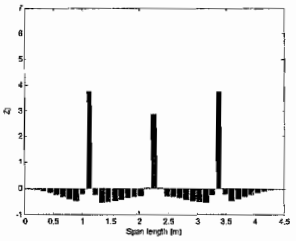
DI-I- 2M4L6M (2 modes)*



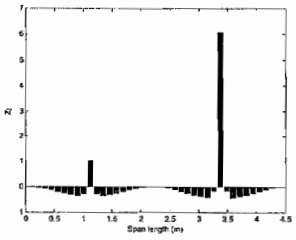
MDI-I- 2M4L6M (2 modes)*



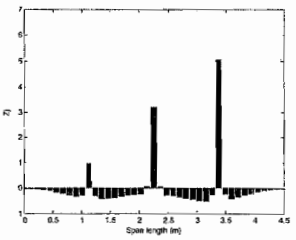
DI-I- 2M4M6M (2 modes)*



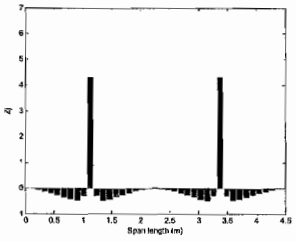
MDI-I- 2M4M6M (2 modes)*



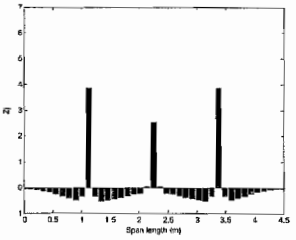
DI-I- 2M4M6S (2 modes)*



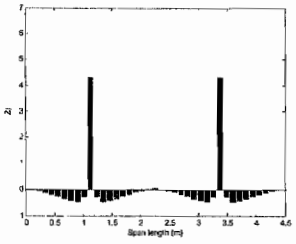
MDI-I- 2M4M6S (2 modes)*



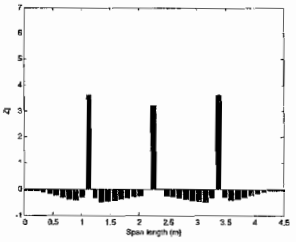
DI-I- 2S4M6S (2 modes)*



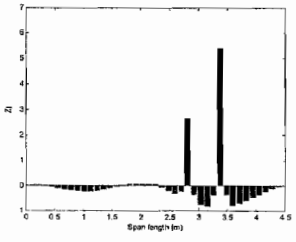
MDI-I- 2S4M6S (2 modes)*



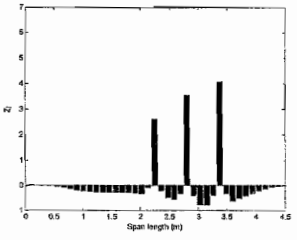
DI-I- 2S4S6S (2 modes)*



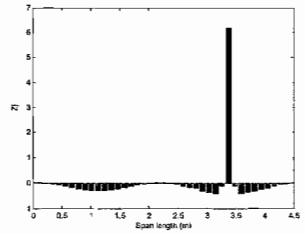
MDI-I- 2S4S6S (2 modes)*



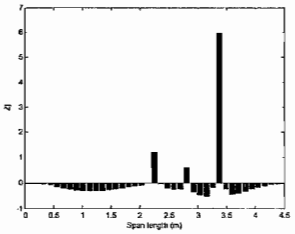
DI-I- 4L5L6L (2 modes)



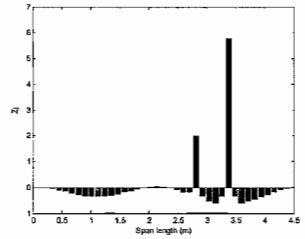
MDI-I- 4L5L6L (2 modes)



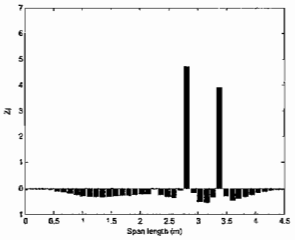
DI-I- 4L5L6S (2 modes)



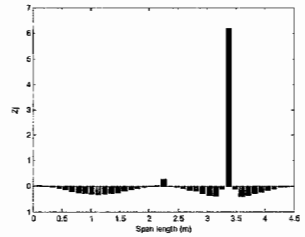
MDI-I- 4L5L6S (2 modes)



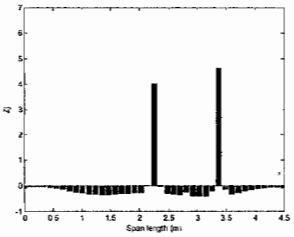
DI-I- 4L5S6S (2 modes)



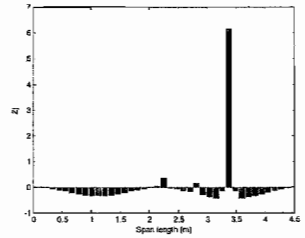
MDI-I- 4L5S6S (2 modes)



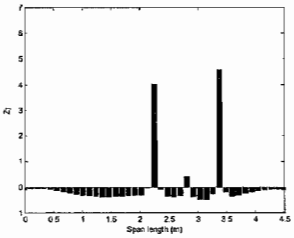
DI-I- 4S5L6S (2 modes)*



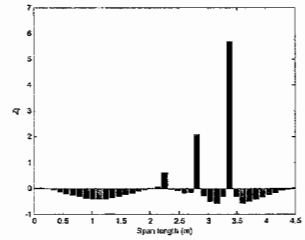
MDI-I- 4S5L6S (2 modes)*



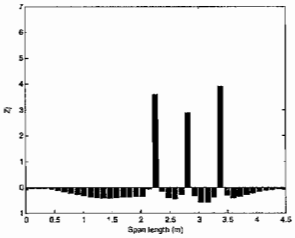
DI-I- 4S5M6S (2 modes)*



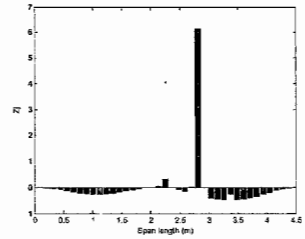
MDI-I- 4S5M6S (2 modes)*



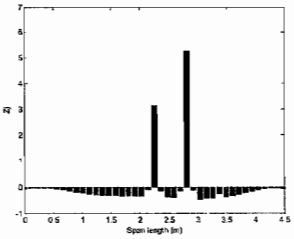
DI-I- 4S5S6S (2 modes)*



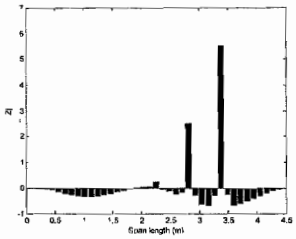
MDI-I- 4S5S6S (2 modes)*



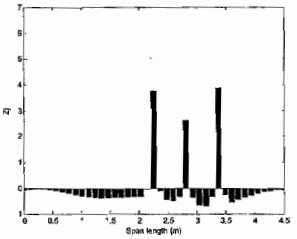
DI-I- 4S5S6L (2 modes)



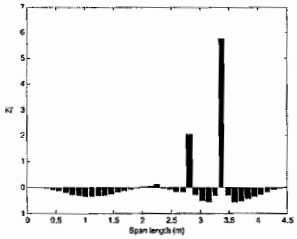
MDI-I- 4S5S6L (2 modes)



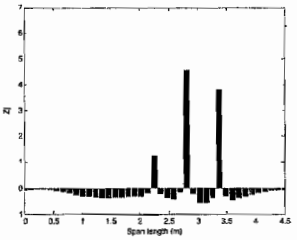
DI-I- 4S5M6M (2 modes)



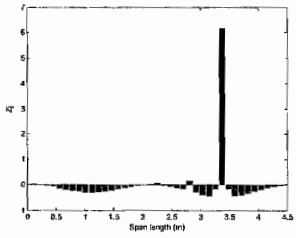
MDI-I- 4S5M6M (2 modes)



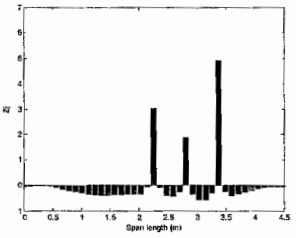
DI-I- 4M5S6S (2 modes)



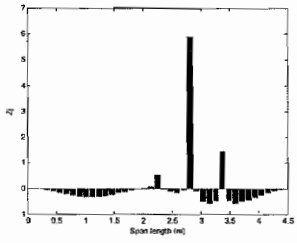
MDI-I- 4M5S6S (2 modes)



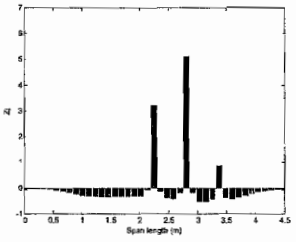
DI-I- 4M5M6S (2 modes)



MDI-I- 4M5M6S (2 modes)

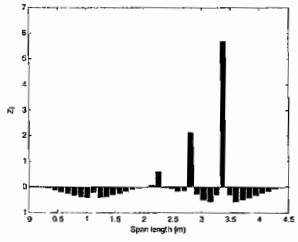


DI-I- 4S5S6M (2 modes)

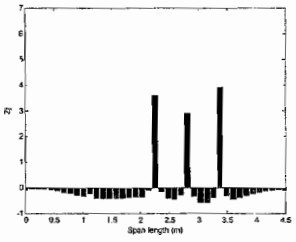


MDI-I- 4S5S6M (2 modes)

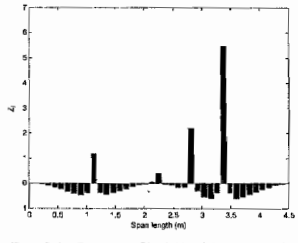
Four Damage Locations



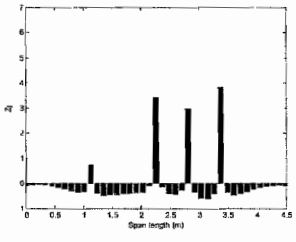
DI-I- 2L4S5S6S (2 modes)*



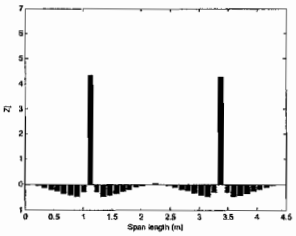
MDI-I- 2L4S5S6S (2 modes)*



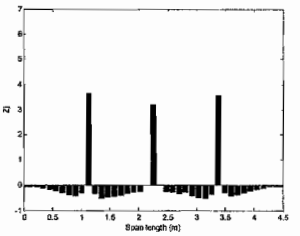
DI-I- 2M4S5S6S (2 modes)*



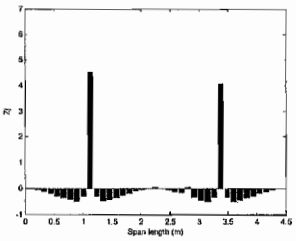
MDI-I- 2M4S5S6S (2 modes)*



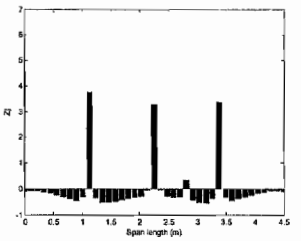
DI-I- 2S4S5L6S (2 modes)*



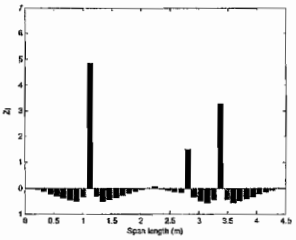
MDI-I- 2S4S5L6S (2 modes)*



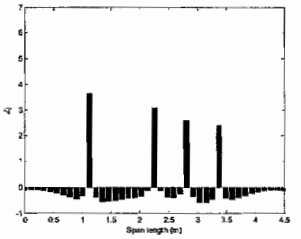
DI-I- 2S4S5M6S (2 modes)*



MDI-I- 2S4S5M6S (2 modes)*



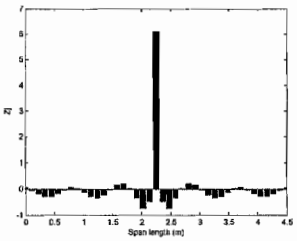
DI-I- 2S4S5S6S (2 modes)*



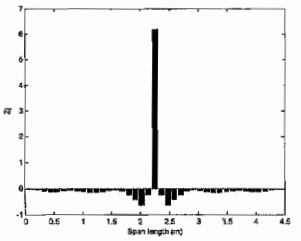
MDI-I- 2S4S5S6S (2 modes)*

A.1.2 Damage Localisation for Timber Beam (DI-I vs MDI-I) (5 Modes)

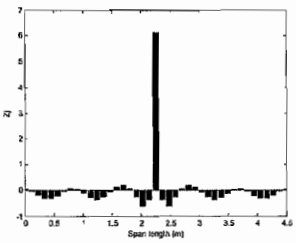
Single Damage Location



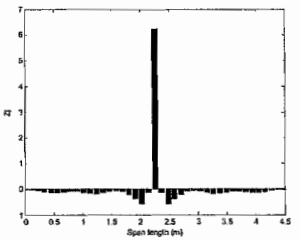
DI-I- 4L (5 modes)*



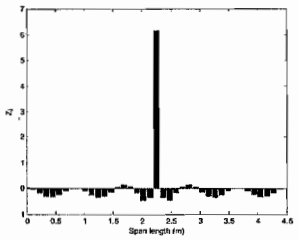
MDI-I- 4L (5 modes)*



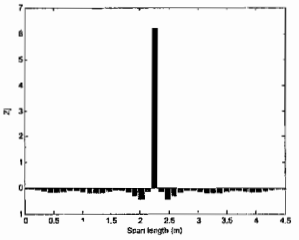
DI-I- 4M (5 modes)*



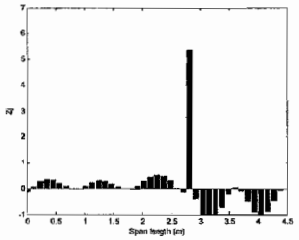
MDI-I- 4M (5 modes)*



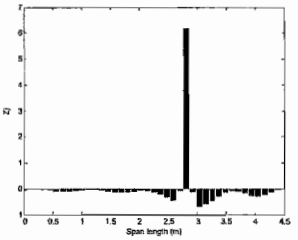
DI-I- 4S (5 modes)*



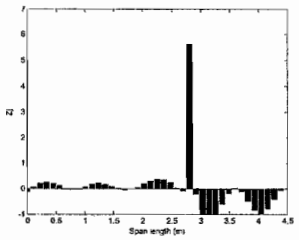
MDI-I- 4S (5 modes)*



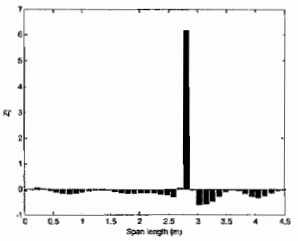
DI-I- 5L (5 modes)



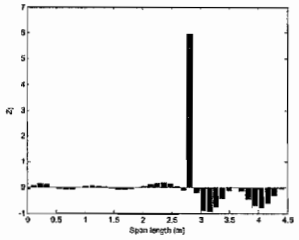
MDI-I- 5L (5 modes)



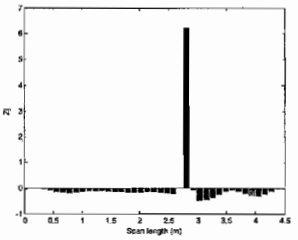
DI-I- 5M (5 modes)



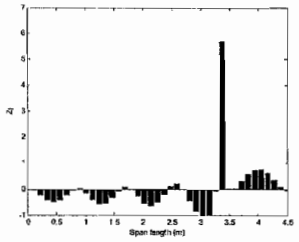
MDI-I- 5M (5 modes)



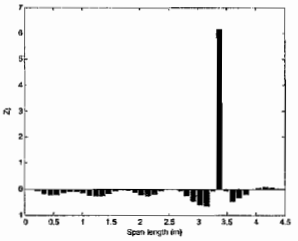
DI-I- 5S (5 modes)



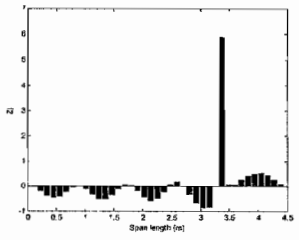
MDI-I- 5S (5 modes)



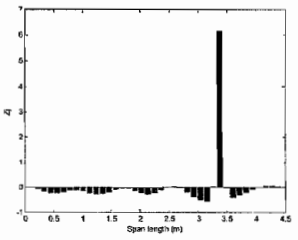
DI-I- 6L (5 modes)*



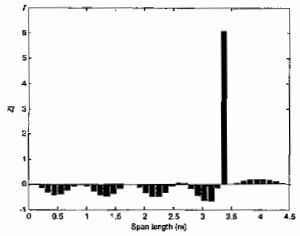
MDI-I- 6L (5 modes)*



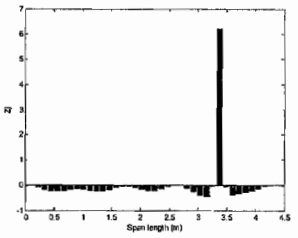
DI-I- 6M (5 modes)



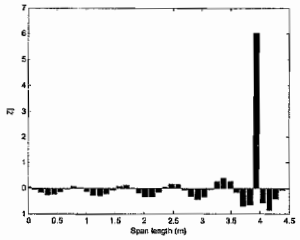
MDI-I- 6M (5 modes)



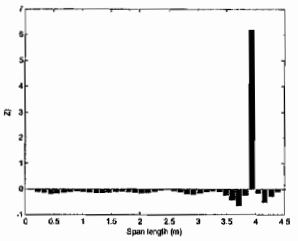
DI-I- 6S (5 modes)



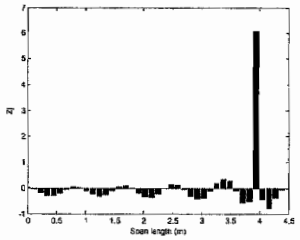
MDI-I- 6S (5 modes)



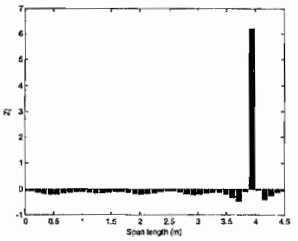
DI-I- 7L (5 modes)



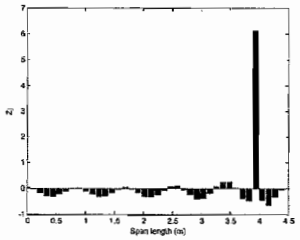
MDI-I- 7L (5 modes)



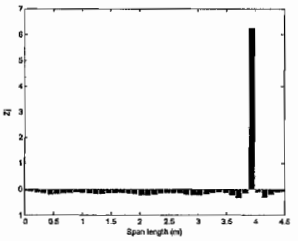
DI-I- 7M (5 modes)



MDI-I- 7M (5 modes)

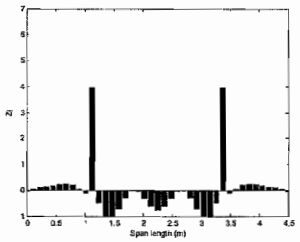


DI-I- 7S (5 modes)

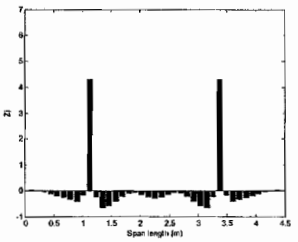


MDI-I- 7S (5 modes)

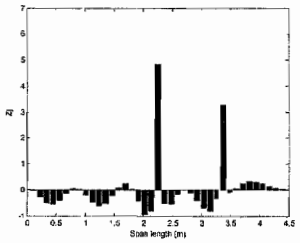
Two Damage Locations



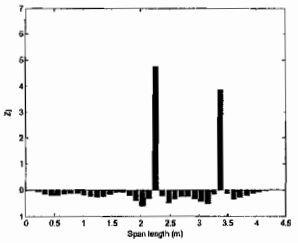
DI-I- 2L6L (5 modes)*



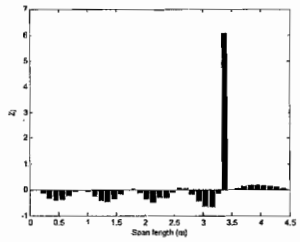
MDI-I- 2L6L (5 modes)*



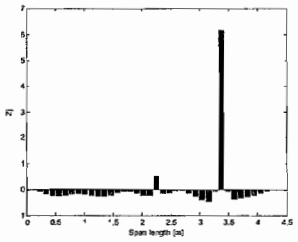
DI-I- 4L6L (5 modes)



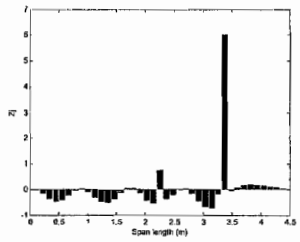
MDI-I- 4L6L (5 modes)



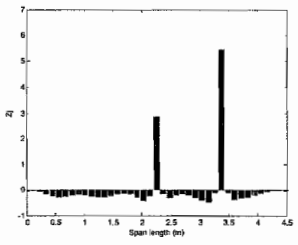
DI-I- 4L6S (5 modes)



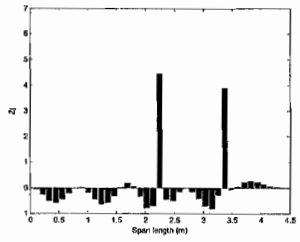
MDI-I- 4L6S (5 modes)



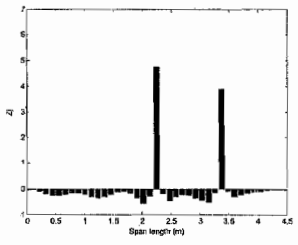
DI-I- 4M6S (5 modes)



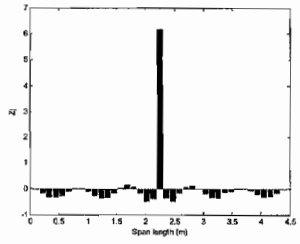
MDI-I- 4M6S (5 modes)



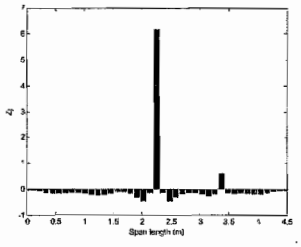
DI-I- 4M6M (5 modes)



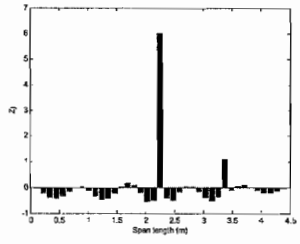
MDI-I- 4M6M (5 modes)



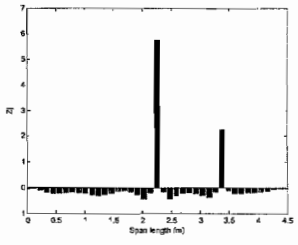
DI-I- 4S6L (5 modes)*



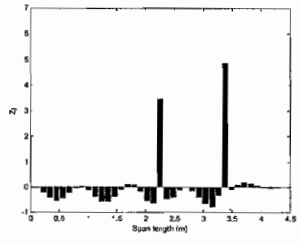
MDI-I- 4S6L (5 modes)*



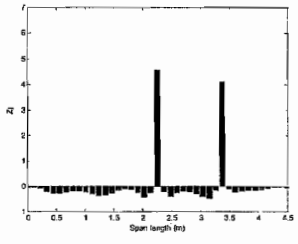
DI-I- 4S6M (5 modes)*



MDI-I- 4S6M (5 modes)*

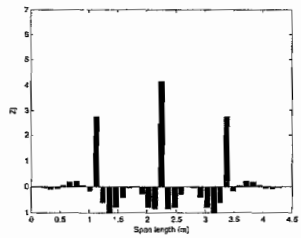


DI-I- 4S6S (5 modes)*

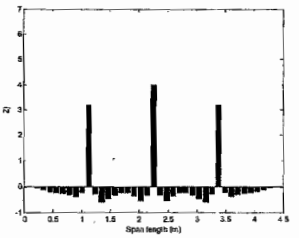


MDI-I- 4S6S (5 modes)*

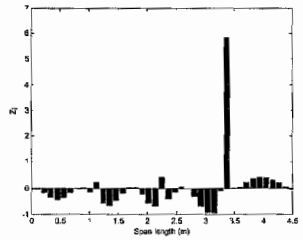
Three Damage Locations



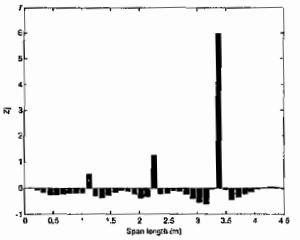
DI-I- 2L4L6L (5 modes)*



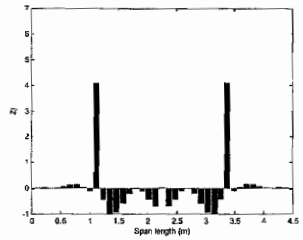
MDI-I- 2L4L6L (5 modes)*



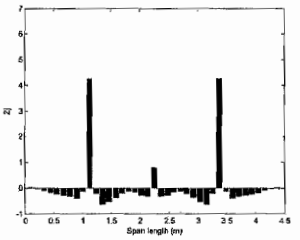
DI-I- 2L4L6M (5 modes)*



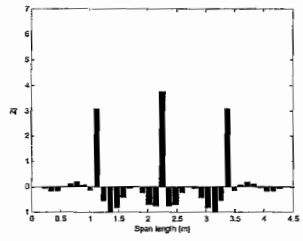
MDI-I- 2L4L6M (5 modes)*



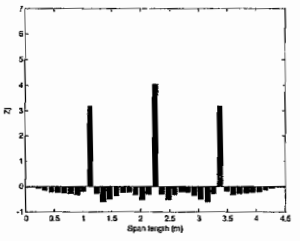
DI-I- 2M4L6M (5 modes)*



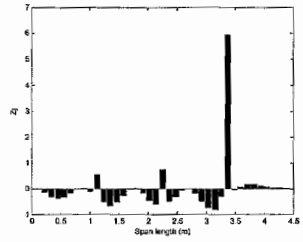
MDI-I- 2M4L6M (5 modes)*



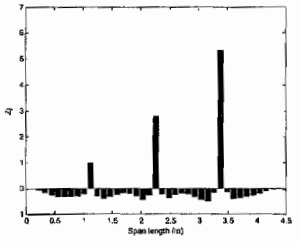
DI-I- 2M4M6M (5 modes)*



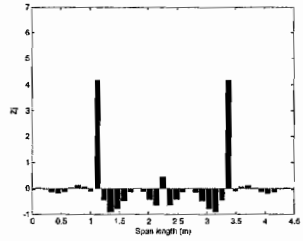
MDI-I- 2M4M6M (5 modes)*



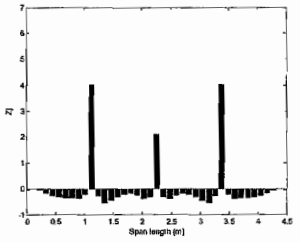
DI-I- 2M4M6S (5 modes)*



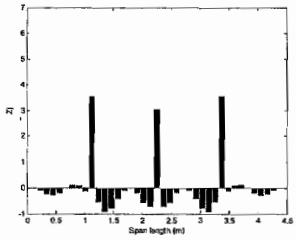
MDI-I- 2M4M6S (5 modes)*



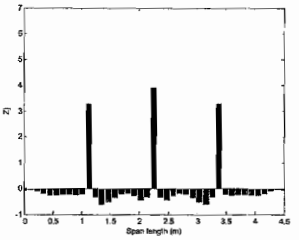
DI-I- 2S4M6S (5 modes)*



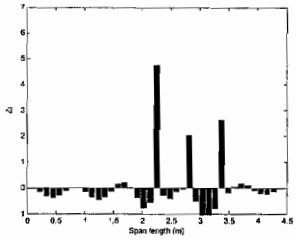
MDI-I- 2S4M6S (5 modes)*



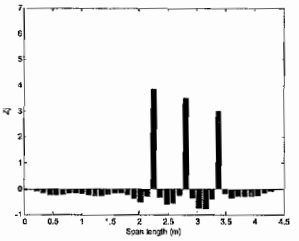
DI-I- 2S4S6S (5 modes)*



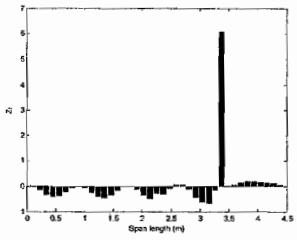
MDI-I- 2S4S6S (5 modes)*



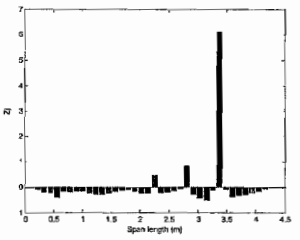
DI-I- 4L5L6L (5 modes)



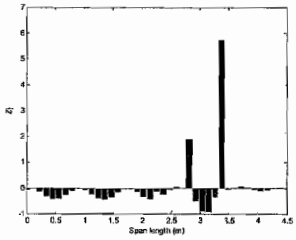
MDI-I- 4L5L6L (5 modes)



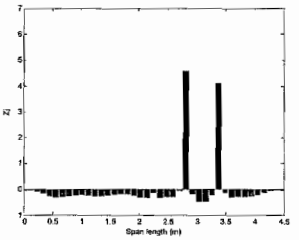
DI-I- 4L5L6S (5 modes)



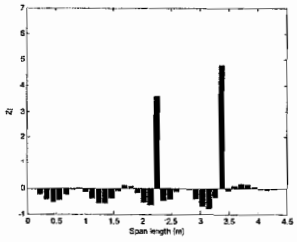
MDI-I- 4L5L6S (5 modes)



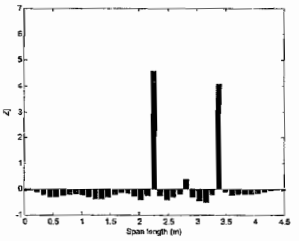
DI-I- 4L5S6S (5 modes)



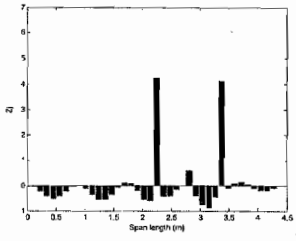
MDI-I- 4L5S6S (5 modes)



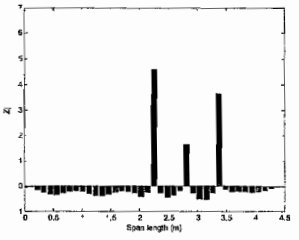
DI-I- 4S5L6S (5 modes)*



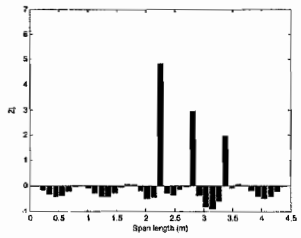
MDI-I- 4S5L6S (5 modes)*



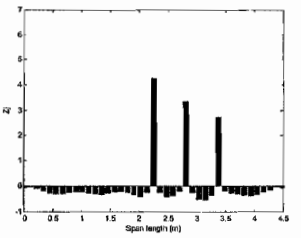
DI-I- 4S5M6S (5 modes)*



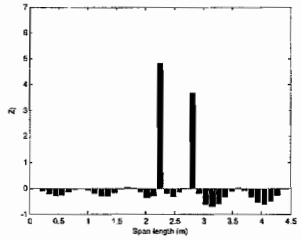
MDI-I- 4S5M6S (5 modes)*



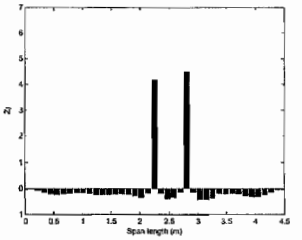
DI-I- 4S5S6S (5 modes)*



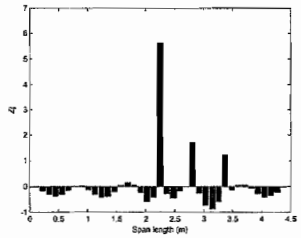
MDI-I- 4S5S6S (5 modes)*



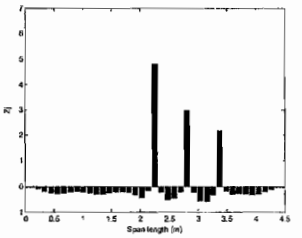
DI-I- 4S5S6L (5 modes)



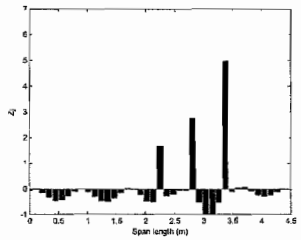
MDI-I- 4S5S6L (5 modes)



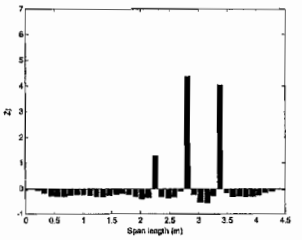
DI-I- 4S5M6M (5 modes)



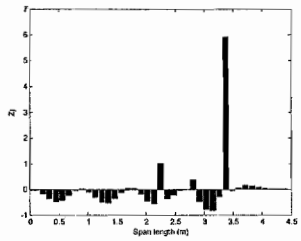
MDI-I- 4S5M6M (5 modes)



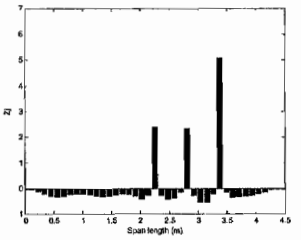
DI-I- 4M5S6S (5 modes)



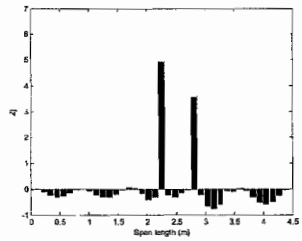
MDI-I- 4M5S6S (5 modes)



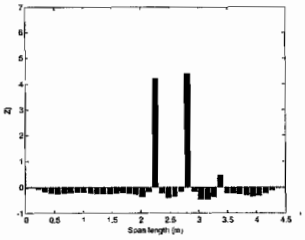
DI-I- 4M5M6S (5 modes)



MDI-I- 4M5M6S (5 modes)

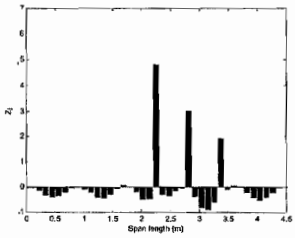


DI-I- 4S5S6M (5 modes)

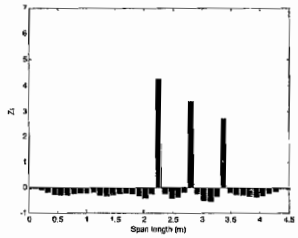


MDI-I- 4S5S6M (5 modes)

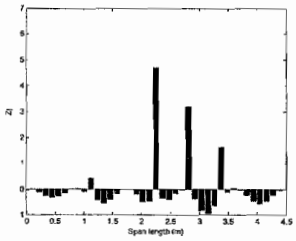
Four Damage Locations



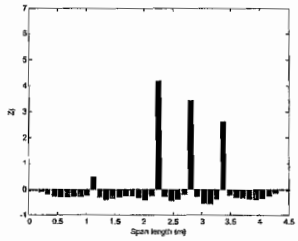
DI-I- 2L4S5S6S (5 modes)*



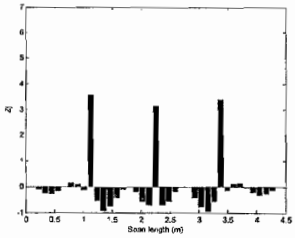
MDI-I- 2L4S5S6S (5 modes)*



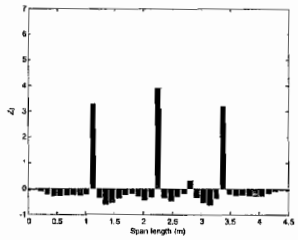
DI-I- 2M4S5S6S (5 modes)*



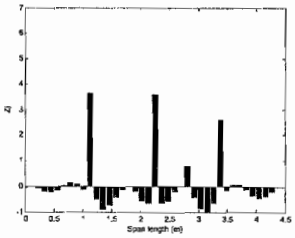
MDI-I- 2M4S5S6S (5 modes)*



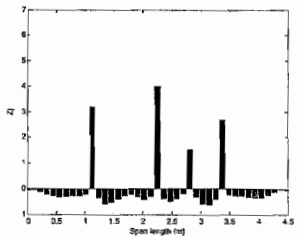
DI-I- 2S4S5L6S (5 modes)*



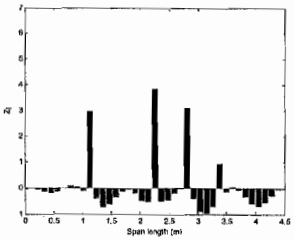
MDI-I- 2S4S5L6S (5 modes)*



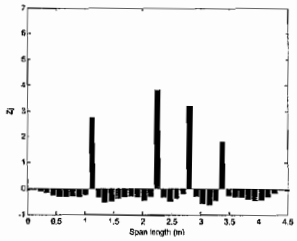
DI-I- 2S4S5M6S (5 modes)*



MDI-I- 2S4S5M6S (5 modes)*



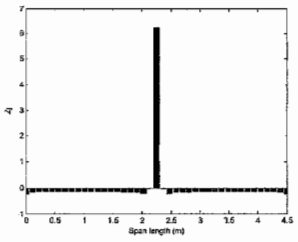
DI-I- 2S4S5S6S (5 modes)*



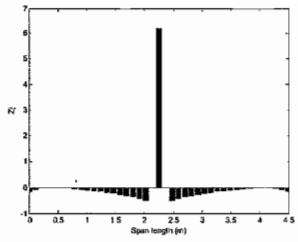
MDI-I- 2S4S5S6S (5 modes)*

A.1.3 Damage Localisation for Timber Beam (DI-II vs MDI-II) (2 Modes)

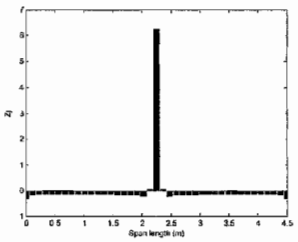
Single Damage Locations



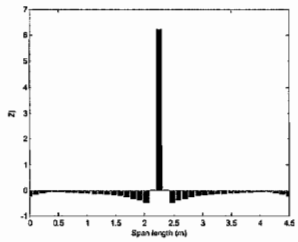
DI-II- 4L (2 modes)*



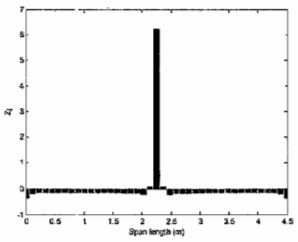
MDI-II- 4L (2 modes)*



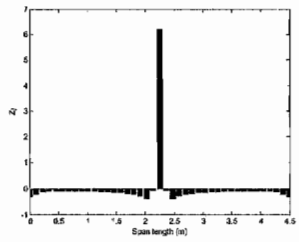
DI- II- 4M (2 modes)*



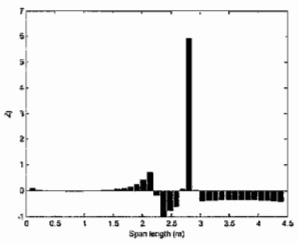
MDI-II- 4M (2 modes)*



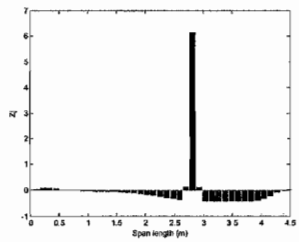
DI-II- 4S (2 modes)*



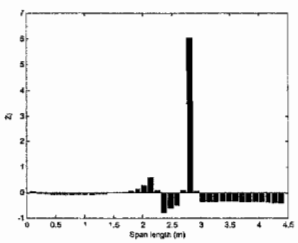
MDI-II- 4S (2 modes)*



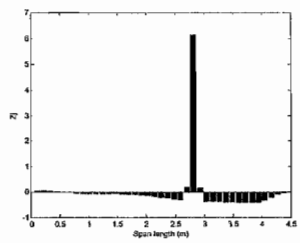
DI- II- 5L (2 modes)



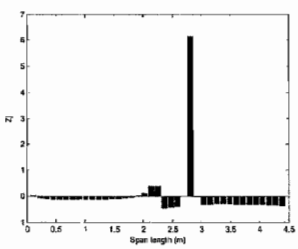
MDI-II- 5L (2 modes)



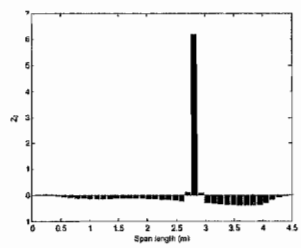
DI-II- 5M (2 modes)



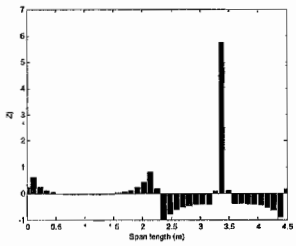
MDI-II- 5M (2 modes)



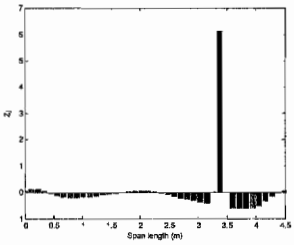
DI-II- 5S (2 modes)



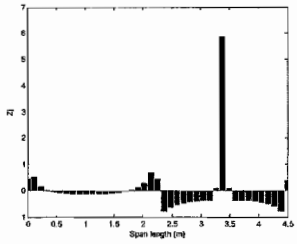
MDI-II- 5S (2 modes)



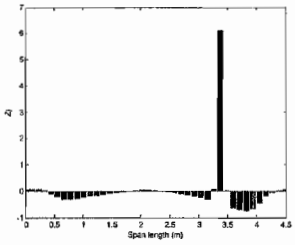
DI-II- 6L (2 modes)*



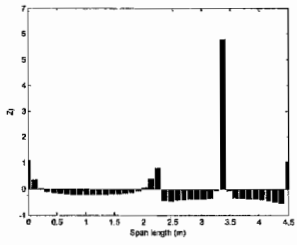
MDI-II- 6L (2 modes)*



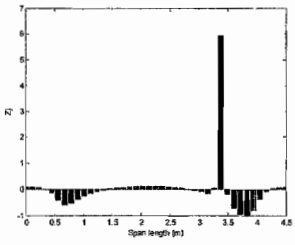
DI-II- 6M (2 modes)



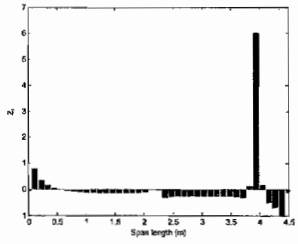
MDI-II- 6M (2 modes)



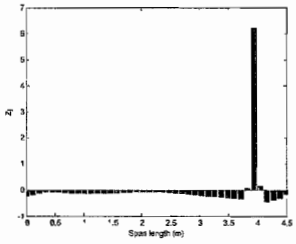
DI-II- 6S (2 modes)



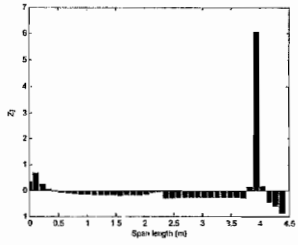
MDI-II- 6S (2 modes)



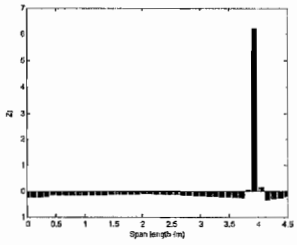
DI-II- 7L (2 modes)



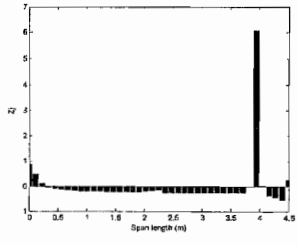
MDI-II- 7L (2 modes)



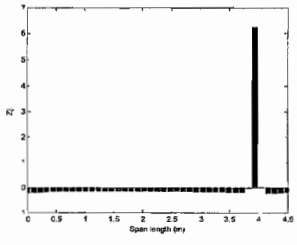
DI-II- 7M (2 modes)



MDI-II- 7M (2 modes)

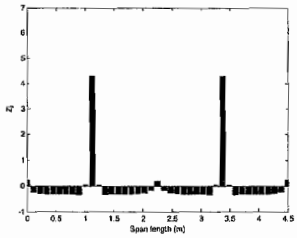


DI-II- 7S (2 modes)

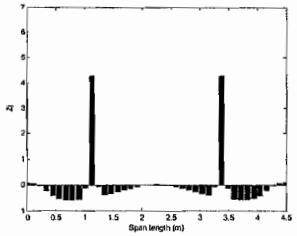


MDI-II- 7S (2 modes)

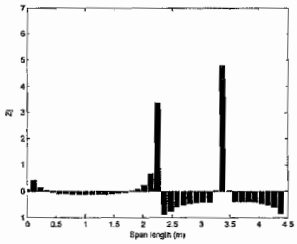
Two Damage Locations



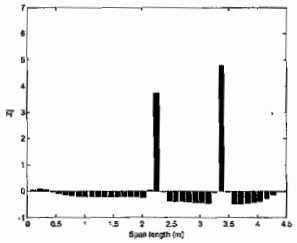
DI-II- 2L6L (2 modes)*



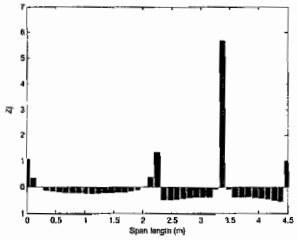
MDI-II- 2L6L (2 modes)*



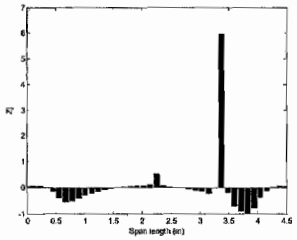
DI-II- 4L6L (2 modes)



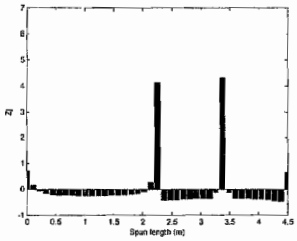
MDI-II- 4L6L (2 modes)



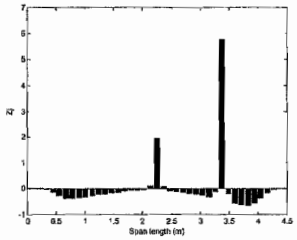
DI-II- 4L6S (2 modes)



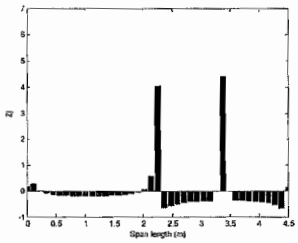
MDI-II- 4L6S (2 modes)



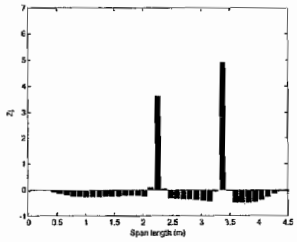
DI-II- 4M6S (2 modes)



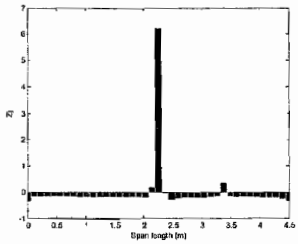
MDI-II- 4M6S (2 modes)



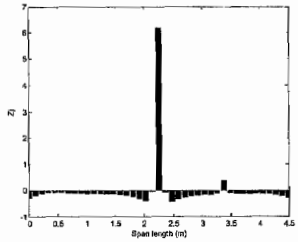
DI-II- 4M6M (2 modes)



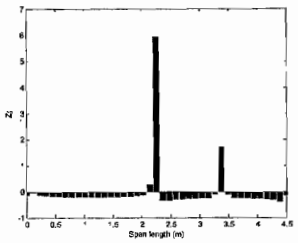
MDI-II- 4M6M (2 modes)



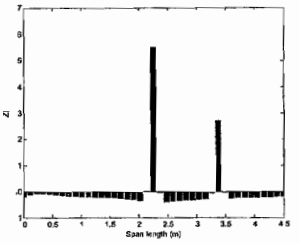
DI-II- 4S6L (2 modes)*



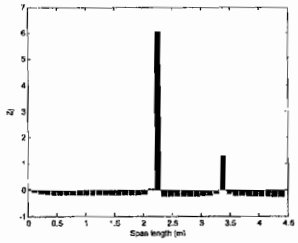
MDI-II- 4S6L (2 modes)*



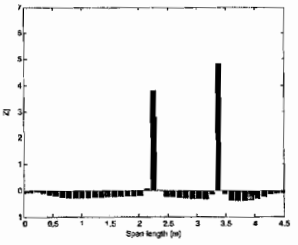
DI-II- 4S6M (2 modes)*



MDI-II- 4S6M (2 modes)*

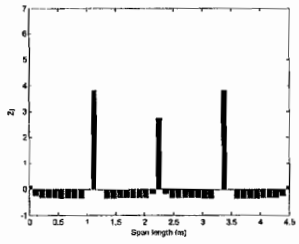


DI-II- 4S6S (2 modes)*

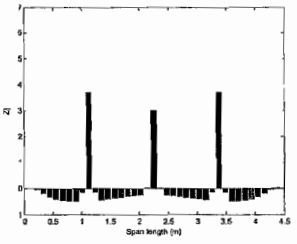


MDI-II- 4S6S (2 modes)*

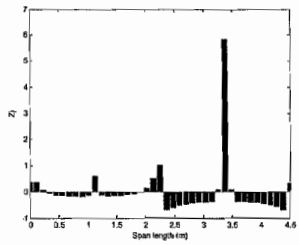
Three Damage Locations



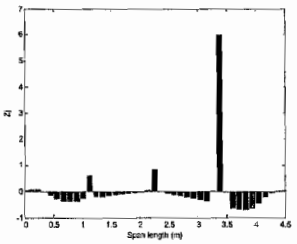
DI-II- 2L4L6L (2 modes)*



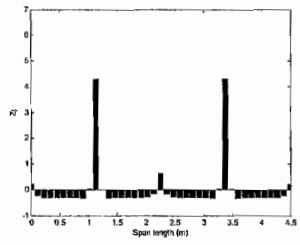
MDI-II- 2L4L6L (2 modes)*



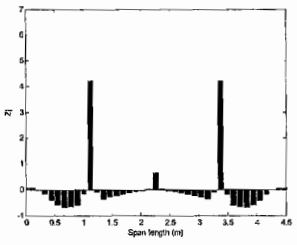
DI-II- 2L4L6M (2 modes)*



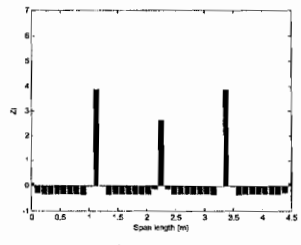
MDI-II- 2L4L6M (2 modes)*



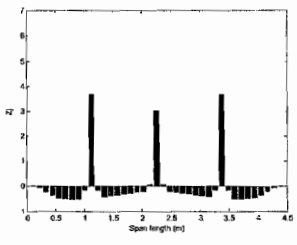
DI-II- 2M4L6M (2 modes)*



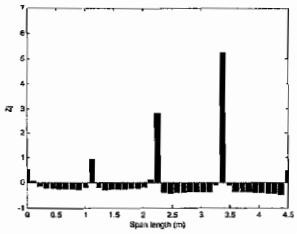
MDI-II- 2M4L6M (2 modes)*



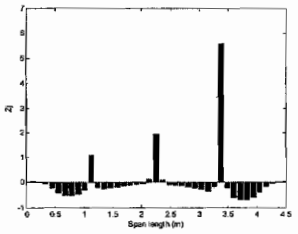
DI-II- 2M4M6M (2 modes)*



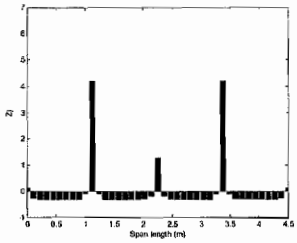
MDI-II- 2M4M6M (2 modes)*



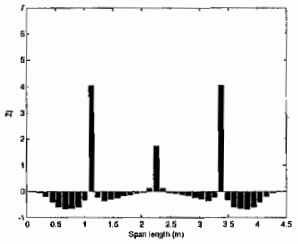
DI-II- 2M4M6S (2 modes)*



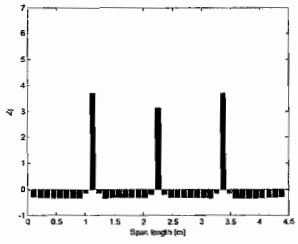
MDI-II- 2M4M6S (2 modes)*



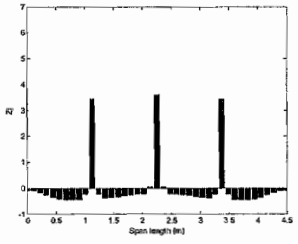
DI-II- 2S4M6S (2 modes)*



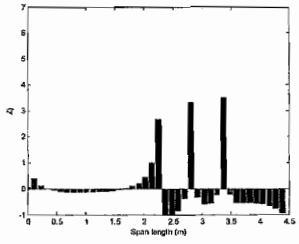
MDI-II- 2S4M6S (2 modes)*



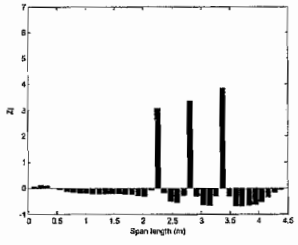
DI-II- 2S4S6S (2 modes)*



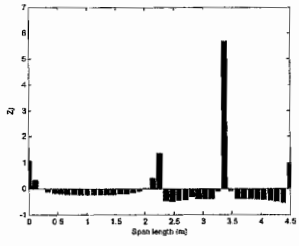
MDI-II- 2S4S6S (2 modes)*



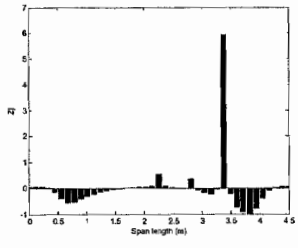
DI-II- 4L5L6L (2 modes)



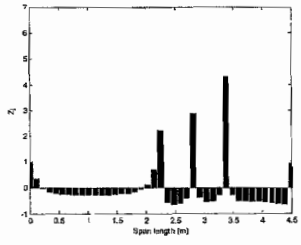
MDI-II- 4L5L6L (2 modes)



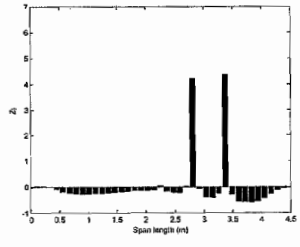
DI-II- 4L5L6S (2 modes)



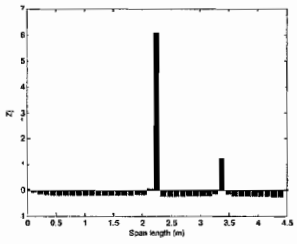
MDI-II- 4L5L6S (2 modes)



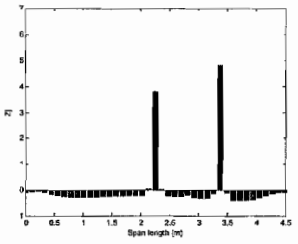
DI-II- 4L5S6S (2 modes)



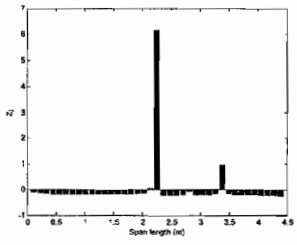
MDI-II- 4L5S6S (2 modes)



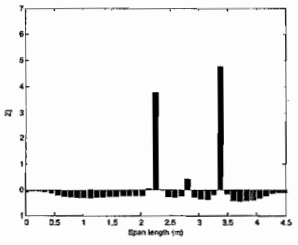
DI-II- 4S5L6S (2 modes)*



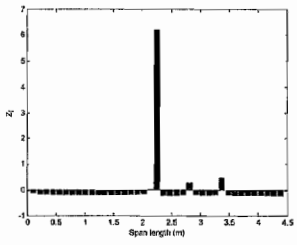
MDI-II- 4S5L6S (2 modes)*



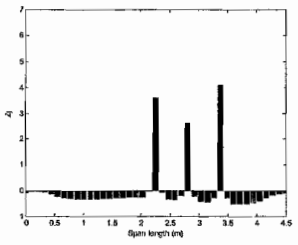
DI-II- 4S5M6S (2 modes)*



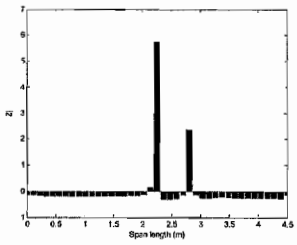
MDI-II- 4S5M6S (2 modes)*



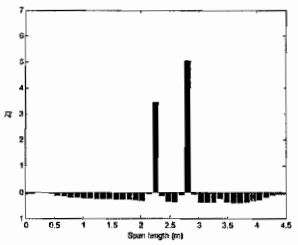
DI-II- 4S5S6S (2 modes)*



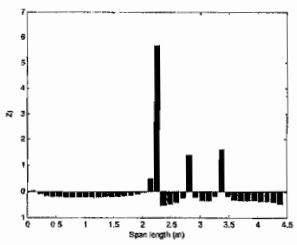
MDI-II- 4S5S6S (2 modes)*



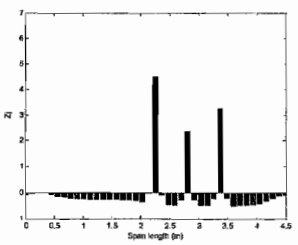
DI-II- 4S5S6L (2 modes)



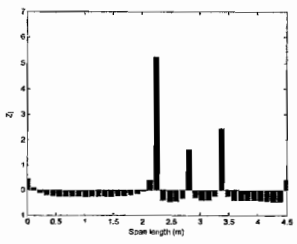
MDI-II- 4S5S6L (2 modes)



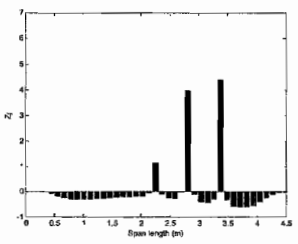
DI-II- 4S5M6M (2 modes)



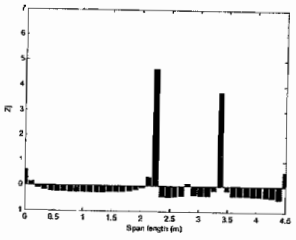
MDI-II- 4S5M6M (2 modes)



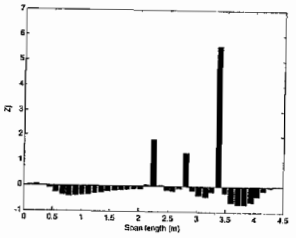
DI-II- 4M5S6S (2 modes)



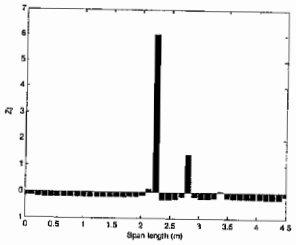
MDI-II- 4M5S6S (2 modes)



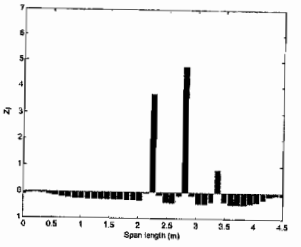
DI-II- 4M5M6S (2 modes)



MDI-II- 4M5M6S (2 modes)

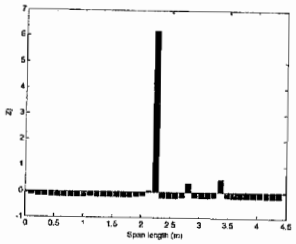


DI-II- 4S5S6M (2 modes)

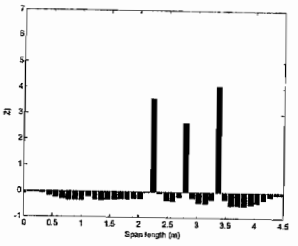


MDI-II- 4S5S6M (2 modes)

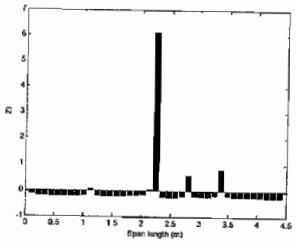
Four Damage Locations



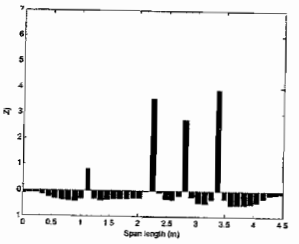
DI-II- 2L4S5S6S (2 modes)*



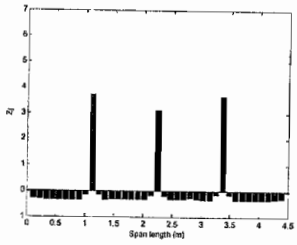
MDI-II- 2L4S5S6S (2 modes)*



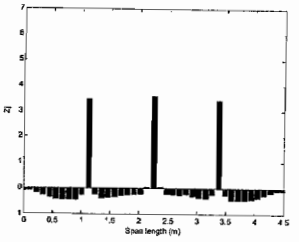
DI-II- 2M4S5S6S (2 modes)*



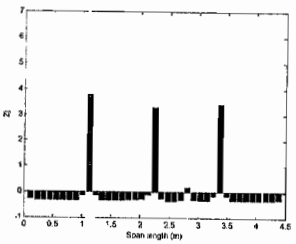
MDI-II- 2M4S5S6S (2 modes)*



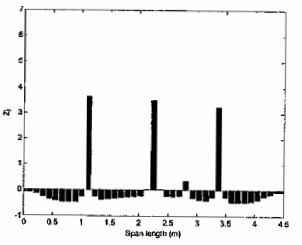
DI-II- 2S4S5L6S (2 modes)*



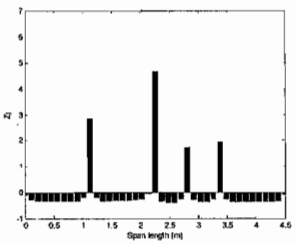
MDI-II- 2S4S5L6S (2 modes)*



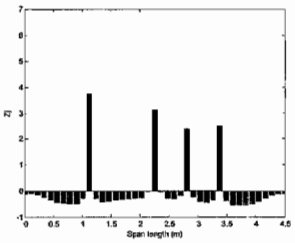
DI-II- 2S4S5M6S (2 modes)*



MDI-II- 2S4S5M6S (2 modes)*



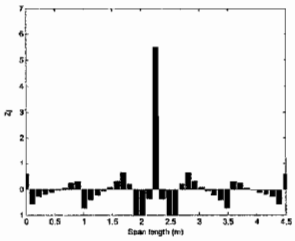
DI-II- 2S4S5S6S (2 modes)*



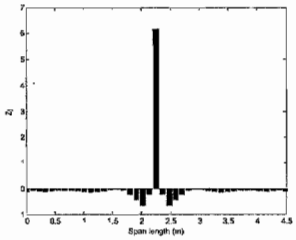
MDI-II- 2S4S5S6S (2 modes)*

A.1.4 Damage Localisation for Timber Beam (DI-II vs MDI-II) (5 Modes)

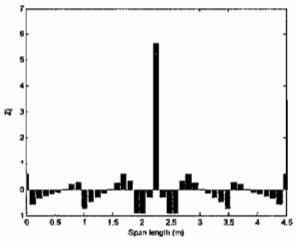
Single Damage Location



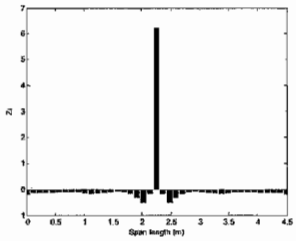
DI-II- 4L (5 modes)*



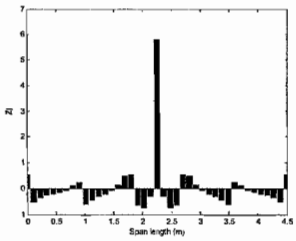
MDI-II- 4L (5 modes)*



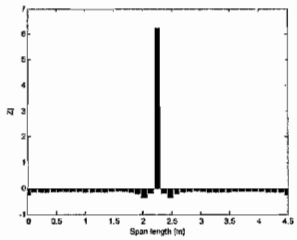
DI-II- 4M (5 modes)*



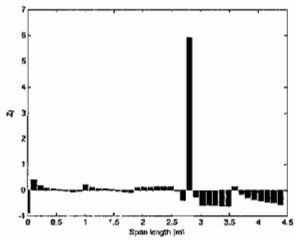
MDI-II- 4M (5 modes)*



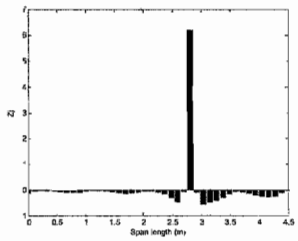
DI-II- 4S (5 modes)*



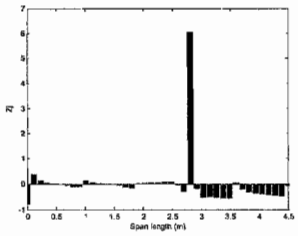
MDI-II- 4S (5 modes)*



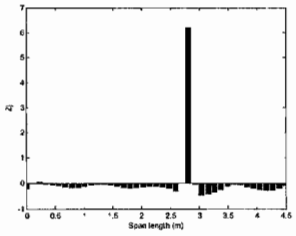
DI-II- 5L (5 modes)



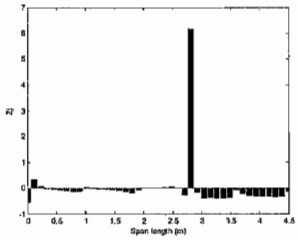
MDI-II- 5L (5 modes)



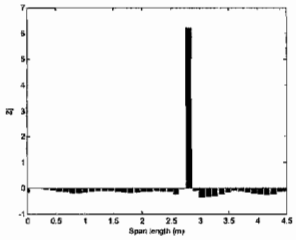
DI-II- 5M (5 modes)



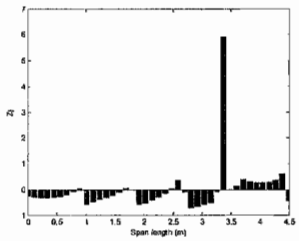
MDI-II- 5M (5 modes)



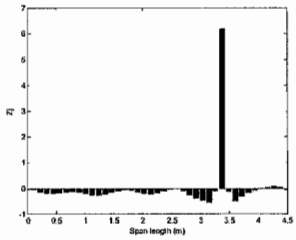
DI-II- 5S (5 modes)



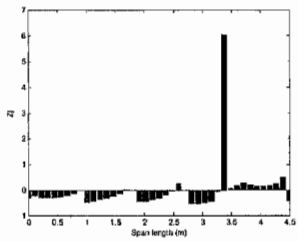
MDI-II- 5S (5 modes)



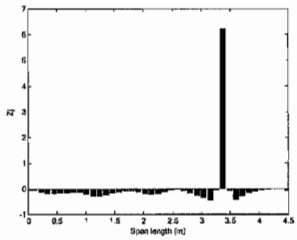
DI-II- 6L (5 modes)*



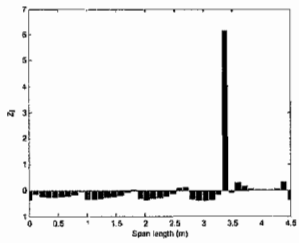
MDI-II- 6L (5 modes)*



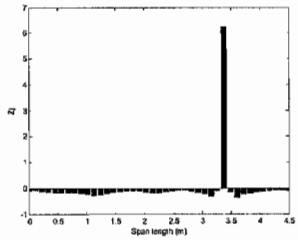
DI-II- 6M (5 modes)



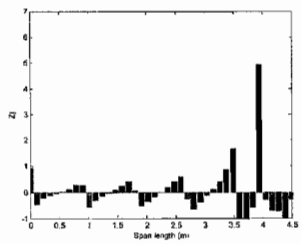
MDI-II- 6M (5 modes)



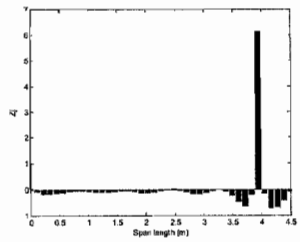
DI-II- 6S (5 modes)



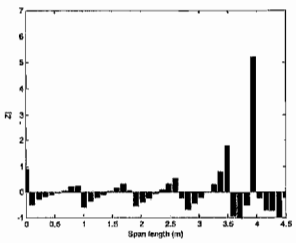
MDI-II- 6S (5 modes)



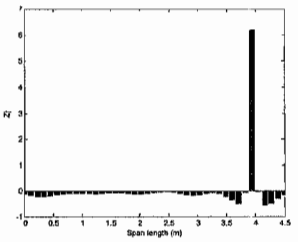
DI-II- 7L (5 modes)



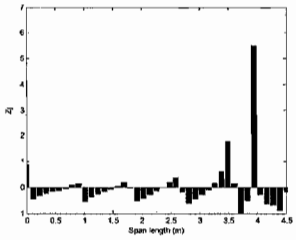
MDI-II- 7L (5 modes)



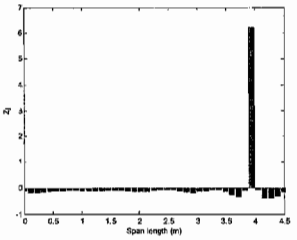
DI-II- 7M (5 modes)



MDI-II- 7M (5 modes)

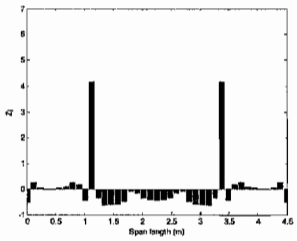


DI-II- 7S (5 modes)

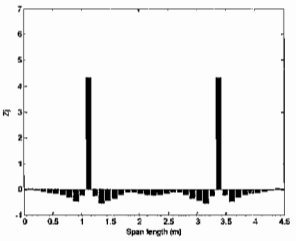


MDI-II- 7S (5 modes)

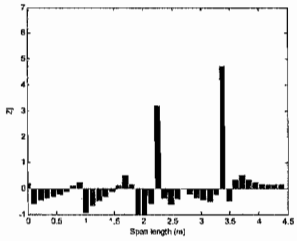
Two Damage Locations



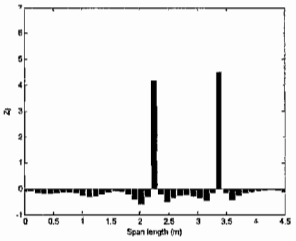
DI-II- 2L6L (5 modes)*



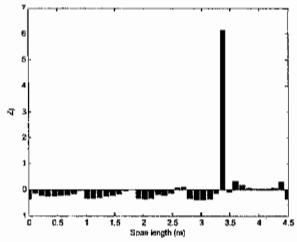
MDI-II- 2L6L (5 modes)*



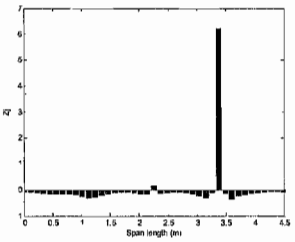
DI-II- 4L6L (5 modes)



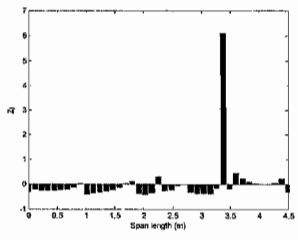
MDI-II- 4L6L (5 modes)



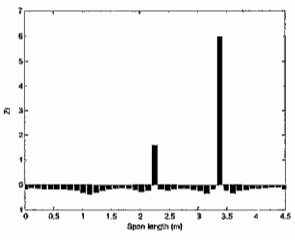
DI-II- 4L6S (5 modes)



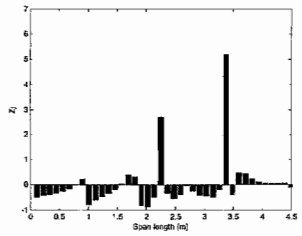
MDI-II- 4L6S (5 modes)



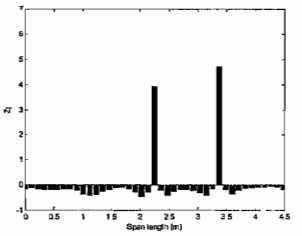
DI-II- 4M6S (5 modes)



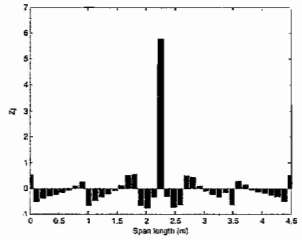
MDI-II- 4M6S (5 modes)



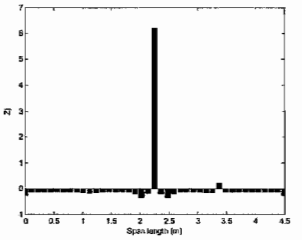
DI-II- 4M6M (5 modes)



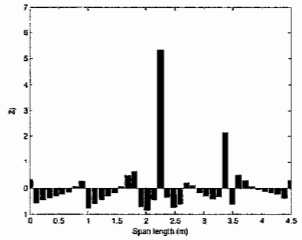
MDI-II- 4M6M (5 modes)



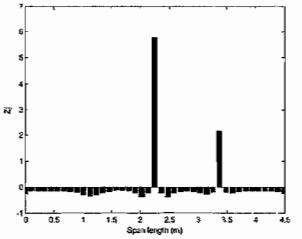
DI-II- 4S6L (5 modes)*



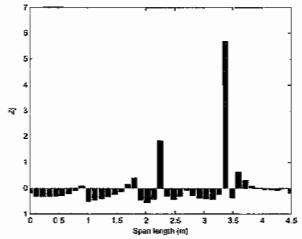
MDI-II- 4S6L (5 modes)*



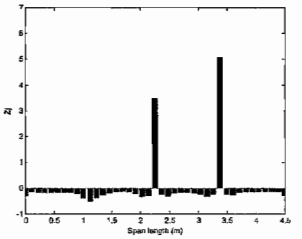
DI-II- 4S6M (5 modes)*



MDI-II- 4S6M (5 modes)*

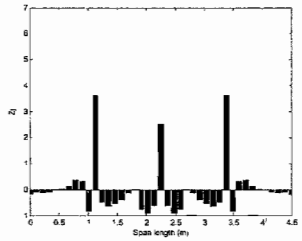


DI-II- 4S6S (5 modes)*

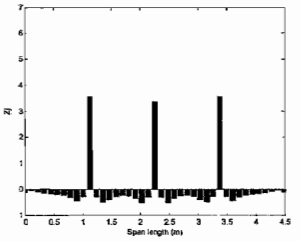


MDI-II- 4S6S (5 modes)*

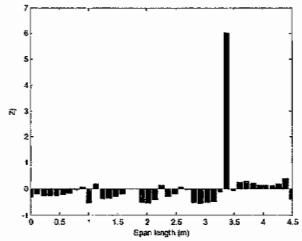
Three Damage Locations



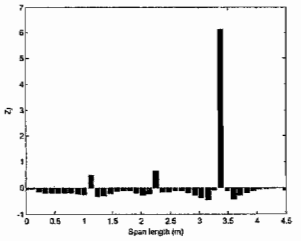
DI-II- 2L4L6L (5 modes)*



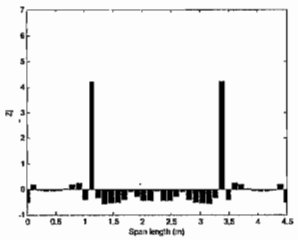
MDI-II- 2L4L6L (5 modes)*



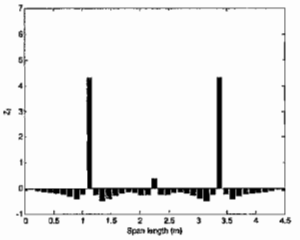
DI-II- 2L4L6M (5 modes)*



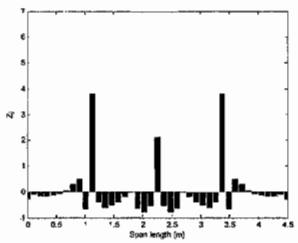
MDI-II- 2L4L6M (5 modes)*



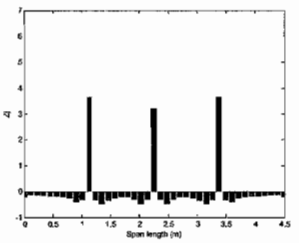
DI-II- 2M4L6M (5 modes)*



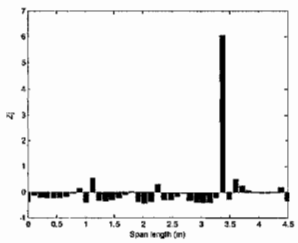
MDI-II- 2M4L6M (5 modes)*



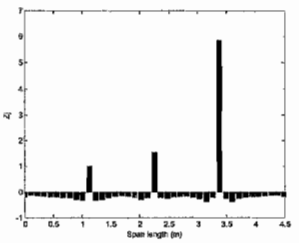
DI-II- 2M4M6M (5 modes)*



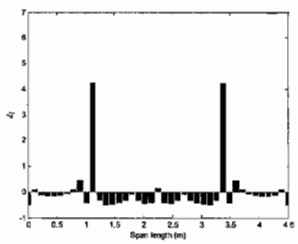
MDI-II- 2M4M6M (5 modes)*



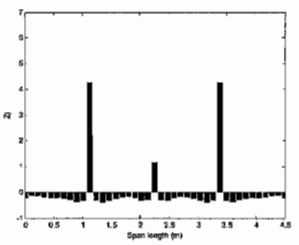
DI-II- 2M4M6S (5 modes)*



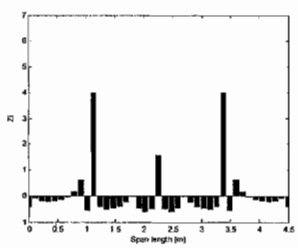
MDI-II- 2M4M6S (5 modes)*



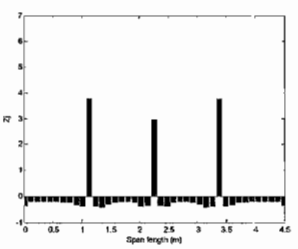
DI-II- 2S4M6S (5 modes)*



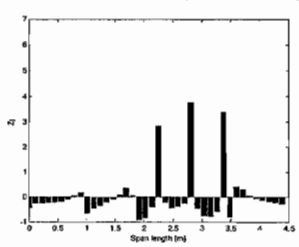
MDI-II- 2S4M6S (5 modes)*



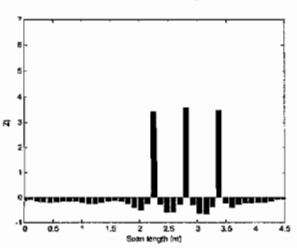
DI-II- 2S4S6S (5 modes)*



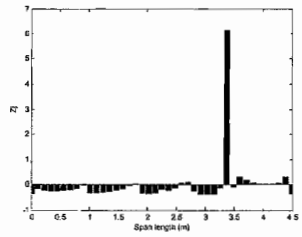
MDI-II- 2S4S6S (5 modes)*



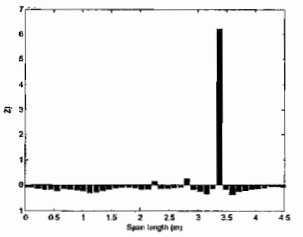
DI-II- 4L5L6L (5 modes)



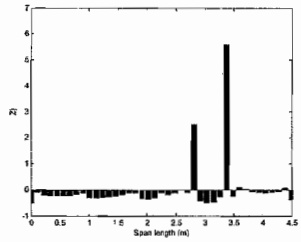
MDI-II- 4L5L6L (5 modes)



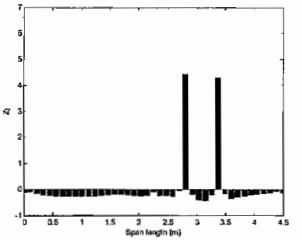
DI-II- 4L5L6S (5 modes)



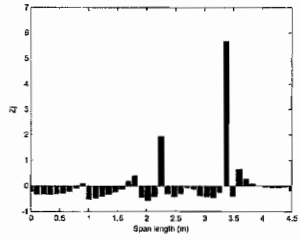
MDI-II- 4L5L6S (5 modes)



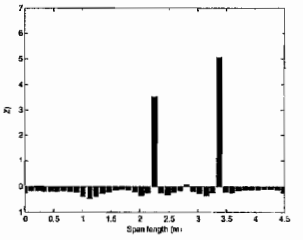
DI-II- 4L5S6S (5 modes)



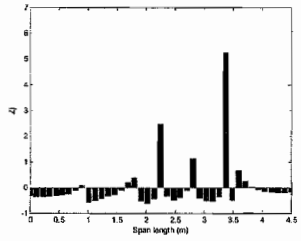
MDI-II- 4L5S6S (5 modes)



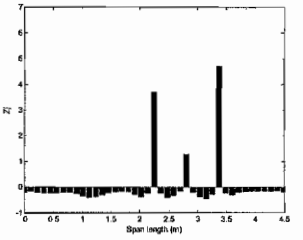
DI-II- 4S5L6S (5 modes)*



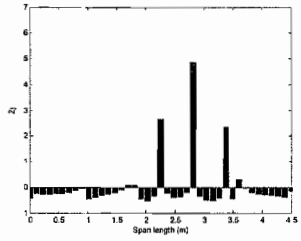
MDI-II- 4S5L6S (5 modes)*



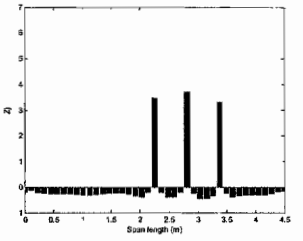
DI-II- 4S5M6S (5 modes)*



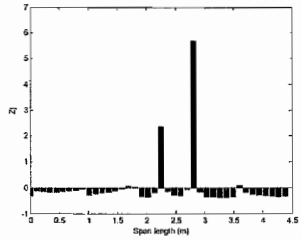
MDI-II- 4S5M6S (5 modes)*



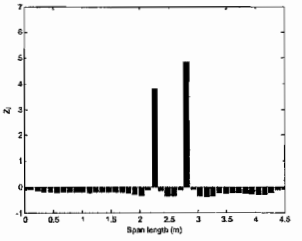
DI-II- 4S5S6S (5 modes)*



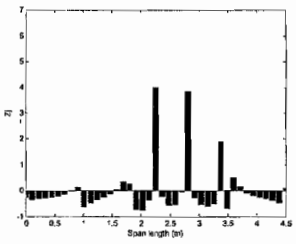
MDI-II- 4S5S6S (5 modes)*



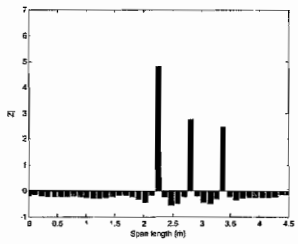
DI-II- 4S5S6L (5 modes)



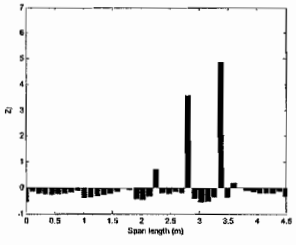
MDI-II- 4S5S6L (5 modes)



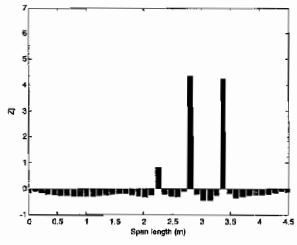
DI-II- 4S5M6M (5 modes)



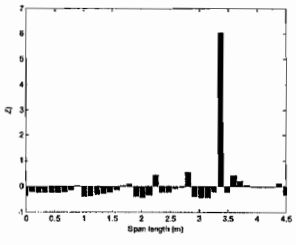
MDI-II- 4S5M6M (5 modes)



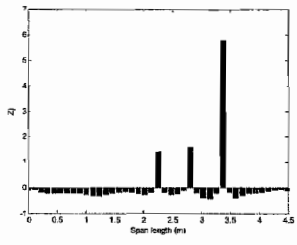
DI-II- 4M5S6S (5 modes)



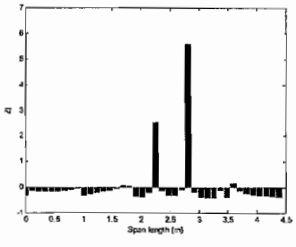
MDI-II- 4M5S6S (5 modes)



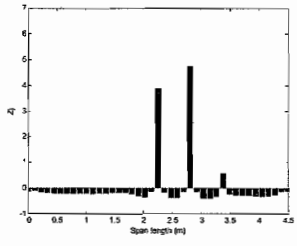
DI-II- 4M5M6S (5 modes)



MDI-II- 4M5M6S (5 modes)

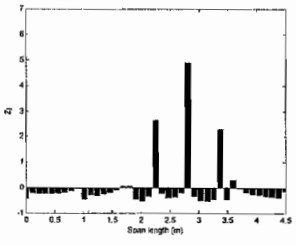


DI-II- 4S5S6M (5 modes)

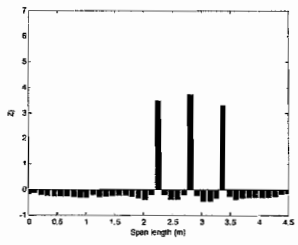


MDI-II- 4S5S6M (5 modes)

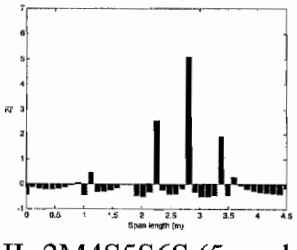
Four Damage Locations



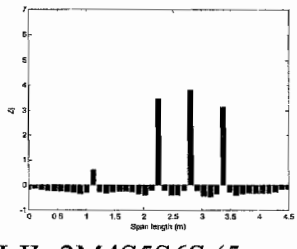
DI-II- 2L4S5S6S (5 modes)*



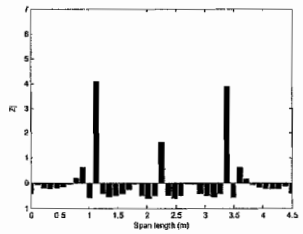
MDI-II- 2L4S5S6S (5 modes)*



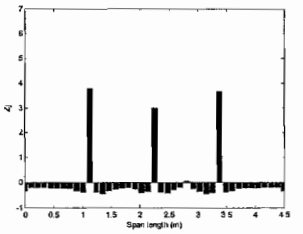
DI-II- 2M4S5S6S (5 modes)*



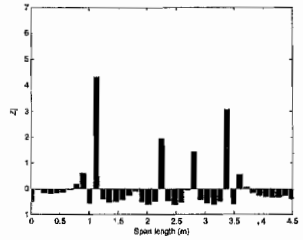
MDI-II- 2M4S5S6S (5 modes)*



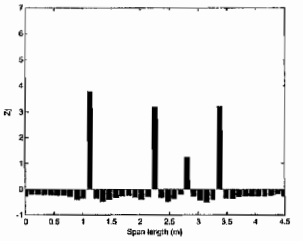
DI-II- 2S4S5L6S (5 modes)*



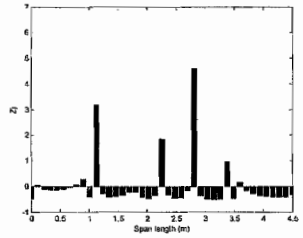
MDI-II- 2S4S5L6S (5 modes)*



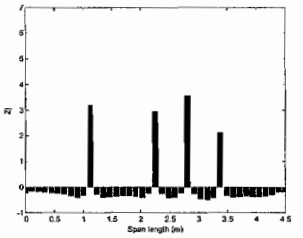
DI-II- 2S4S5M6S (5 modes)*



MDI-II- 2S4S5M6S (5 modes)*



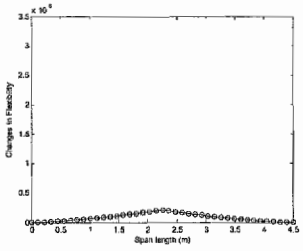
DI-II- 2S4S5S6S (5 modes)*



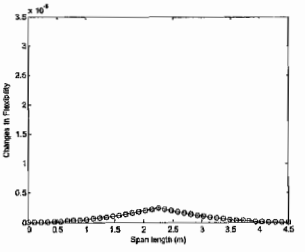
MDI-II- 2S4S5S6S (5 modes)*

A.1.5 Damage Localisation for Timber Beam (CIF) (2 vs 5 Modes)

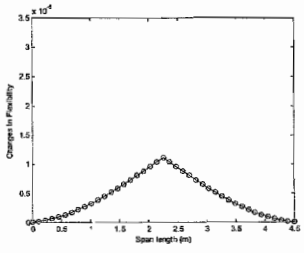
Single Damage Location



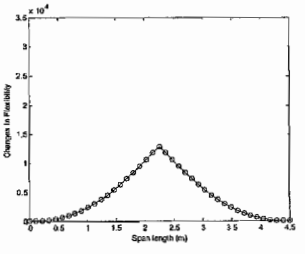
CIF- 4L (2 modes)*



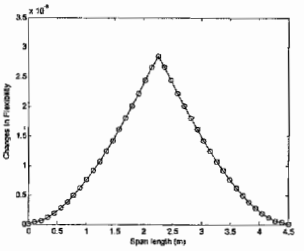
CIF- 4L (5 modes)*



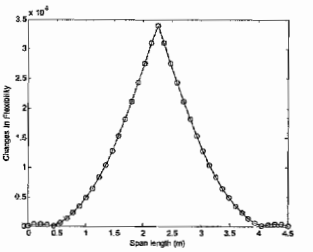
CIF- 4M (2 modes)*



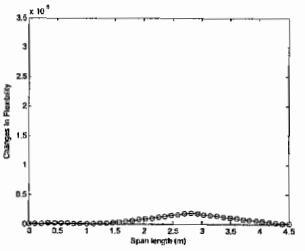
CIF- 4M (5 modes)*



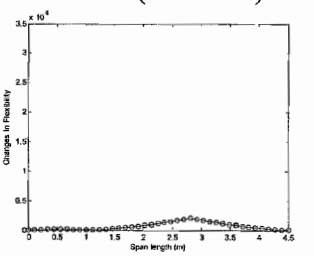
CIF- 4S (2 modes)*



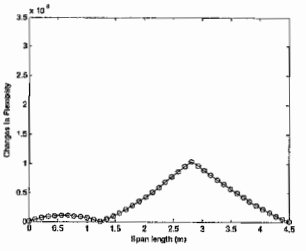
CIF- 4S (5 modes)*



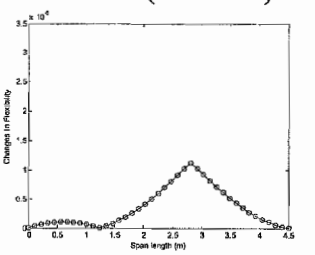
CIF- 5L (2 modes)



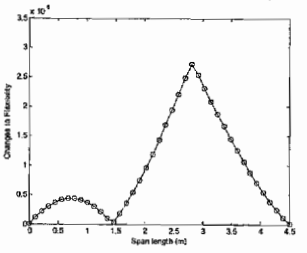
CIF- 5L (5 modes)



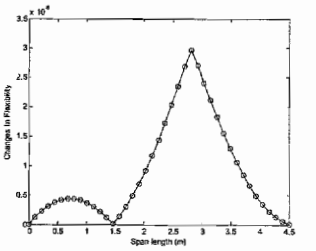
CIF- 5M (2 modes)



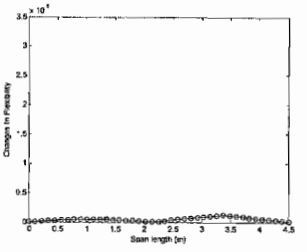
CIF- 5M (5 modes)



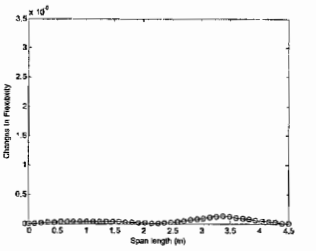
CIF- 5S (2 modes)



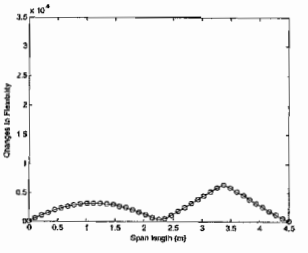
CIF- 5S (5 modes)



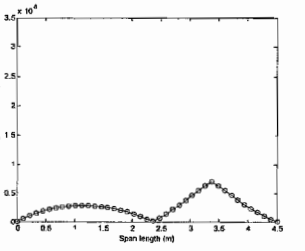
CIF- 6L (2 modes)*



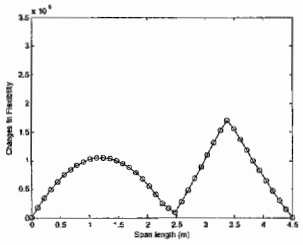
CIF- 6L (5 modes)*



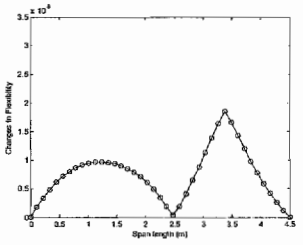
CIF- 6M (2 modes)



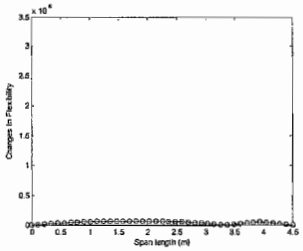
CIF- 6M (5 modes)



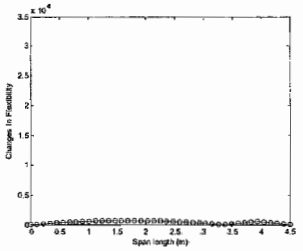
CIF- 6S (2 modes)



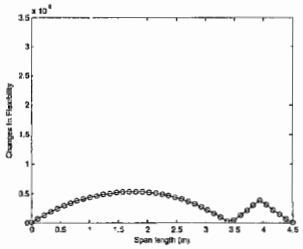
CIF- 6S (5 modes)



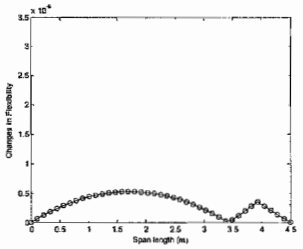
CIF- 7L (2 modes)



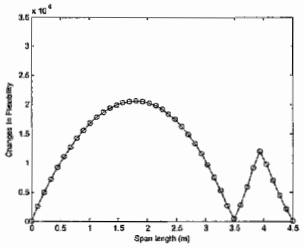
CIF- 7L (5 modes)



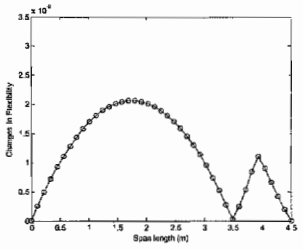
CIF- 7M (2 modes)



CIF- 7M (5 modes)

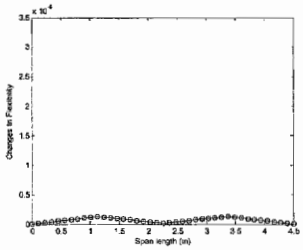


CIF- 7S (2 modes)

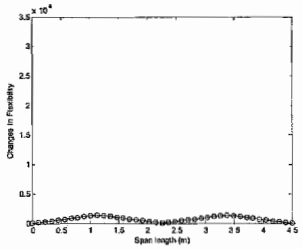


CIF- 7S (5 modes)

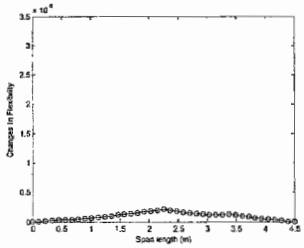
Two Damage Locations



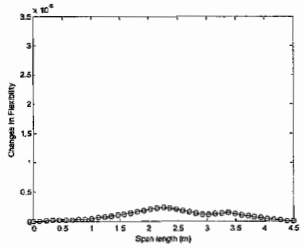
CIF- 2L6L (2 modes)*



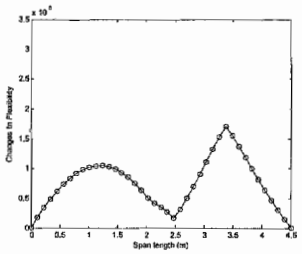
CIF- 2L6L (5 modes)*



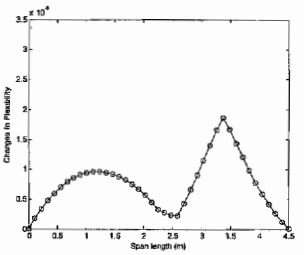
CIF- 4L6L (2 modes)*



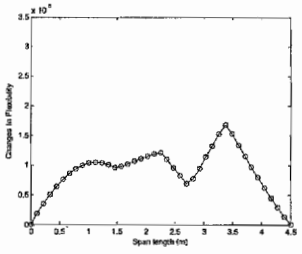
CIF- 4L6L (5 modes)*



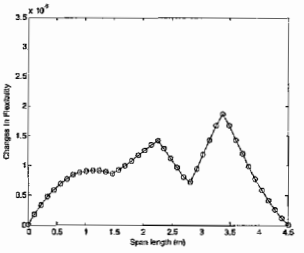
CIF- 4L6S (2 modes)*



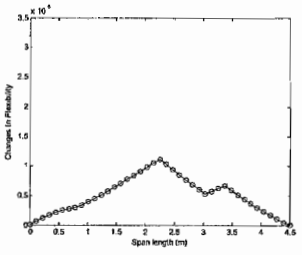
CIF- 4L6S (5 modes)*



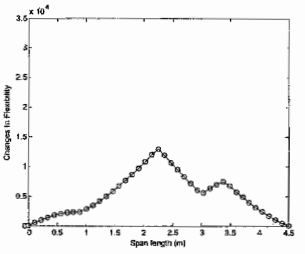
CIF- 4M6S (2 modes)



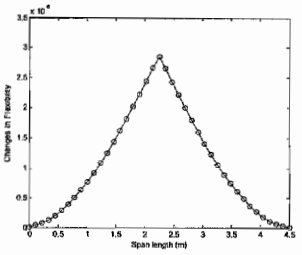
CIF- 4M6S (5 modes)



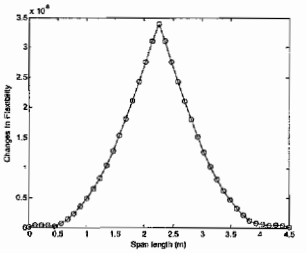
CIF- 4M6M (2 modes)



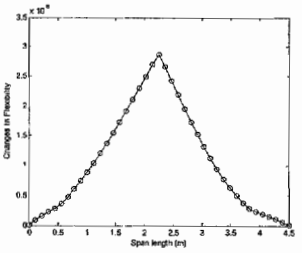
CIF- 4M6M (5 modes)



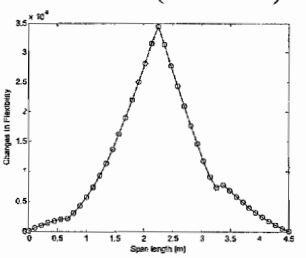
CIF- 4S6L (2 modes)*



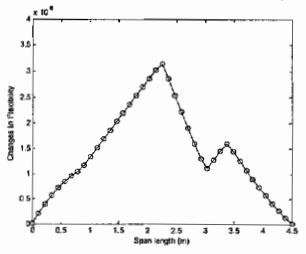
CIF- 4S6L (5 modes)*



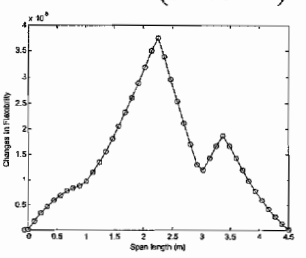
CIF- 4S6M (2 modes)*



CIF- 4S6M (5 modes)*

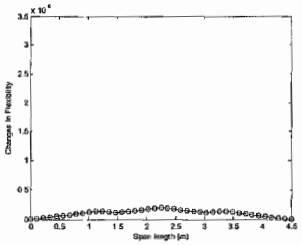


CIF- 4S6S (2 modes)*

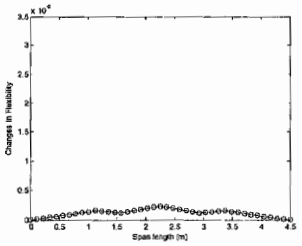


CIF- 4S6S (5 modes)*

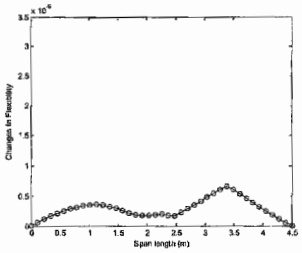
Three Damage Locations



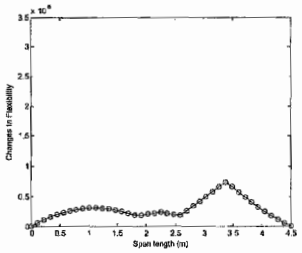
CIF- 2L4L6L (2 modes)*



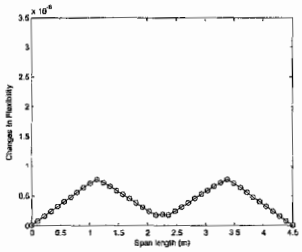
CIF- 2L4L6L (5 modes)*



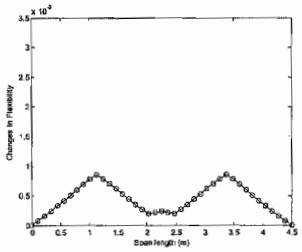
CIF- 2L4L6M (2 modes)*



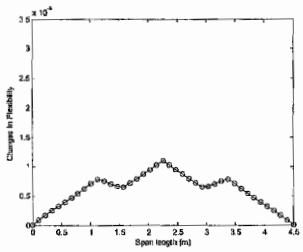
CIF- 2L4L6M (5 modes)*



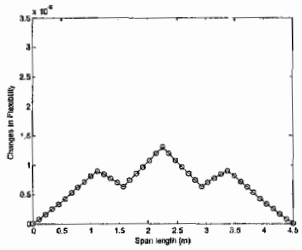
CIF- 2M4L6M (2 modes)*



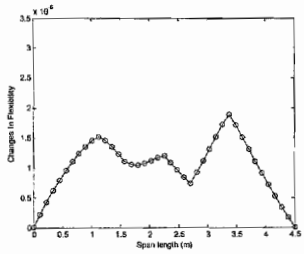
CIF- 2M4L6M (5 modes)*



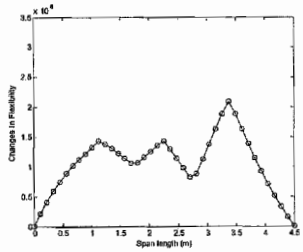
CIF- 2M4M6M (2 modes)*



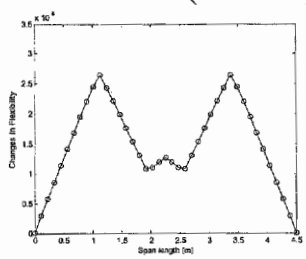
CIF- 2M4M6M (5 modes)*



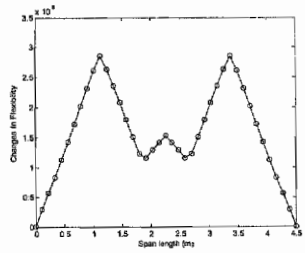
CIF- 2M4M6S (2 modes)*



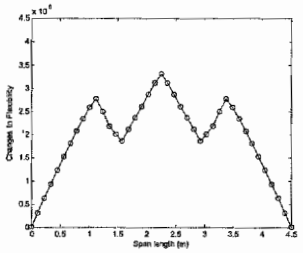
CIF- 2M4M6S (5 modes)*



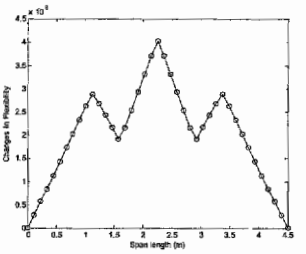
CIF- 2S4M6S (2 modes)*



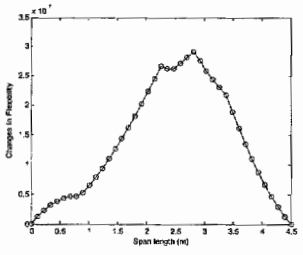
CIF- 2S4M6S (5 modes)*



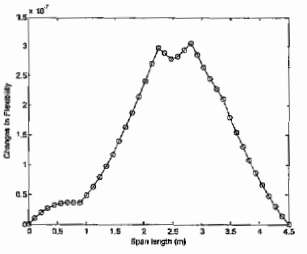
CIF- 2S4S6S (2 modes)*



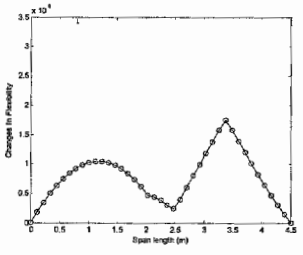
CIF- 2S4S6S (5 modes)*



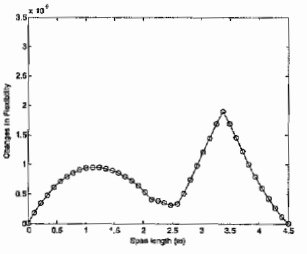
CIF- 4L5L6L (2 modes)



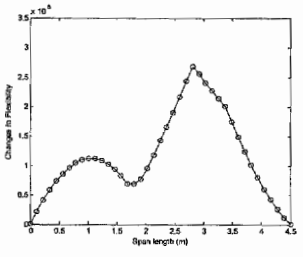
CIF- 4L5L6L (5 modes)



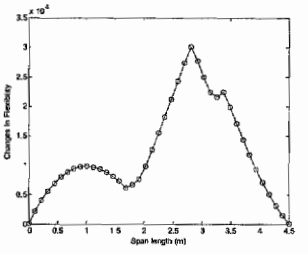
CIF- 4L5L6S (2 modes)



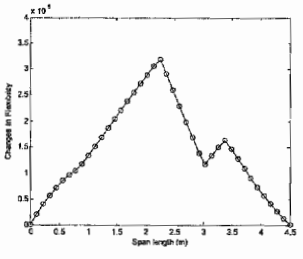
CIF- 4L5L6S (5 modes)



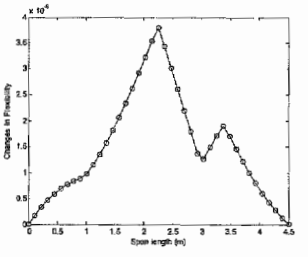
CIF- 4L5S6S (2 modes)



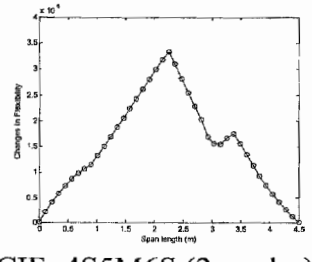
CIF- 4L5S6S (5 modes)



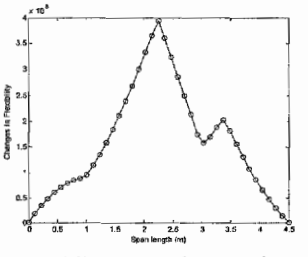
CIF- 4S5L6S (2 modes)*



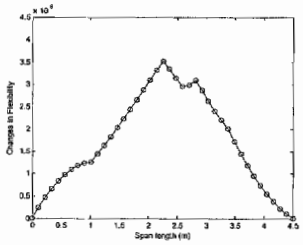
CIF- 4S5L6S (5 modes)*



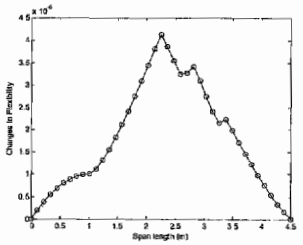
CIF- 4S5M6S (2 modes)*



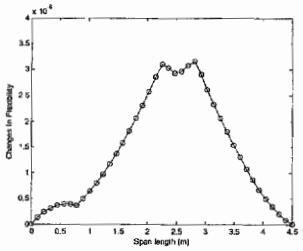
CIF- 4S5M6S (5 modes)*



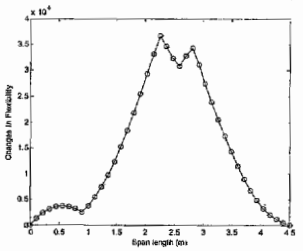
CIF- 4S5S6S (2 modes)*



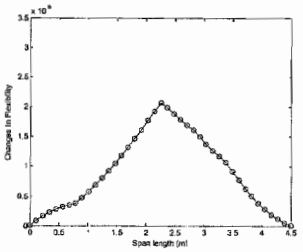
CIF- 4S5S6S (5 modes)*



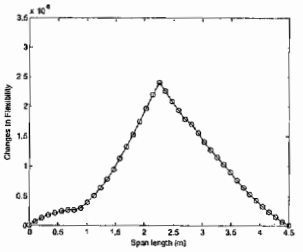
CIF- 4S5S6L (2 modes)



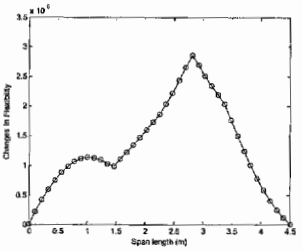
CIF- 4S5S6L (5 modes)



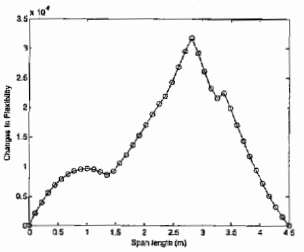
CIF- 4S5M6M (2 modes)



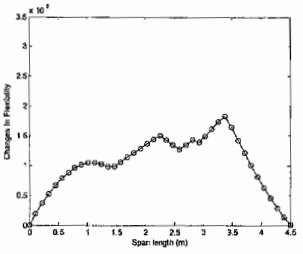
CIF- 4S5M6M (5 modes)



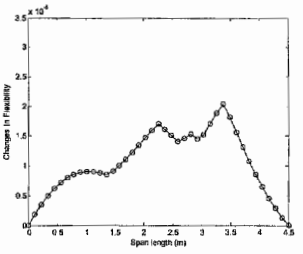
CIF- 4M5S6S (2 modes)



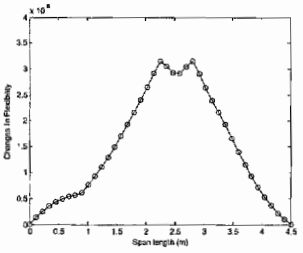
CIF- 4M5S6S (5 modes)



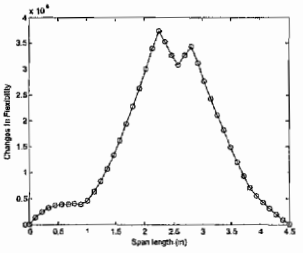
CIF- 4M5M6S (2 modes)



CIF- 4M5M6S (5 modes)

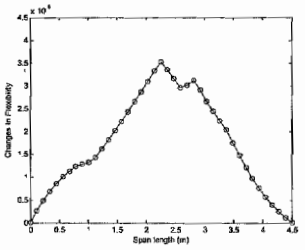


CIF- 4S5S6M (2 modes)

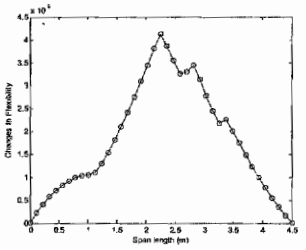


CIF- 4S5S6M (5 modes)

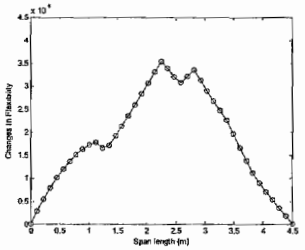
Four Damage Locations



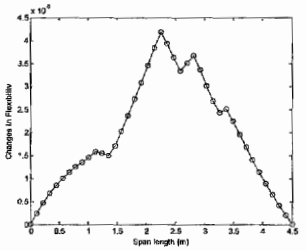
CIF- 2L4S5S6S (2 modes)*



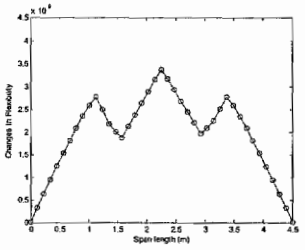
CIF- 2L4S5S6S (5 modes)*



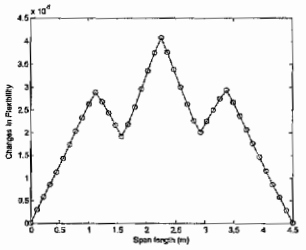
CIF- 2M4S5S6S (2 modes)*



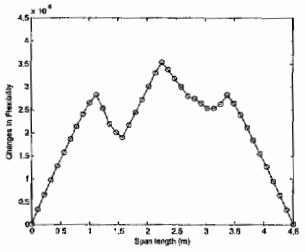
CIF- 2M4S5S6S (5 modes)*



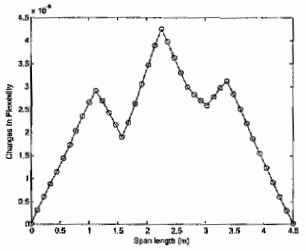
CIF- 2S4S5L6S (2 modes)*



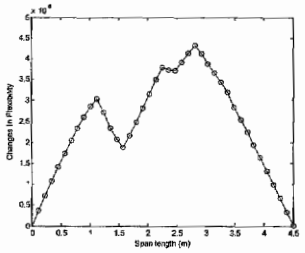
CIF- 2S4S5L6S (5 modes)*



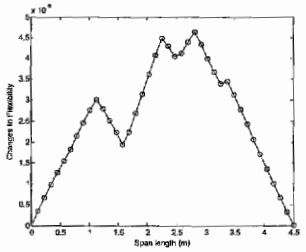
CIF- 2S4S5M6S (2 modes)*



CIF- 2S4S5M6S (5 modes)*



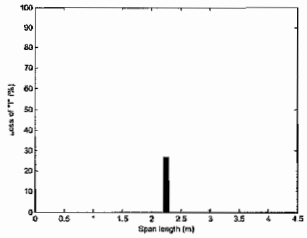
CIF- 2S4S5S6S (2 modes)*



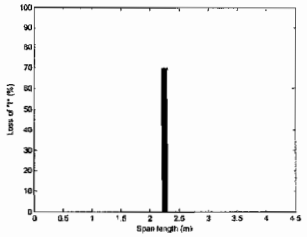
CIF- 2S4S5S6S (5 modes)*

A.1.6 Damage Severity for Timber Beam (HMC) (5 Modes)

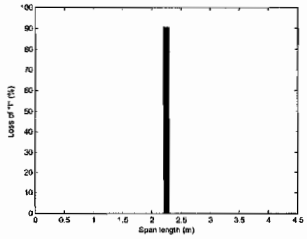
Single Damage Location



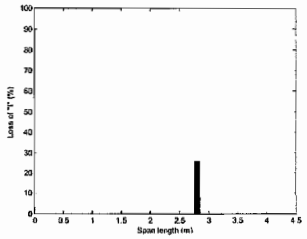
HMC- 4L (5 modes)*
26.66%



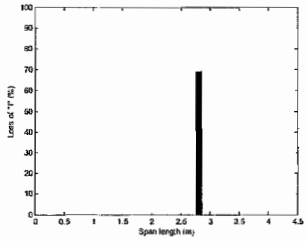
HMC- 4M (5 modes)*
69.77%



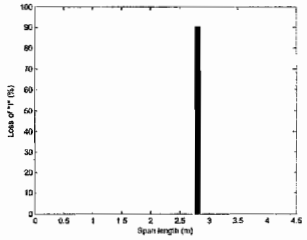
HMC- 4S (5 modes)*
90.56%



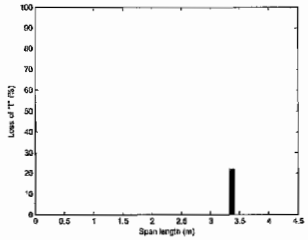
HMC- 5L (5 modes)
25.79%



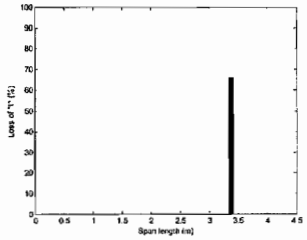
HMC- 5M (5 modes)
69.10%



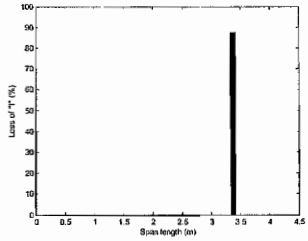
HMC- 5S (5 modes)
90.07%



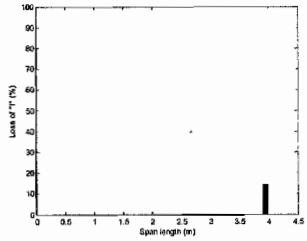
HMC- 6L (5 modes)*
22.17%



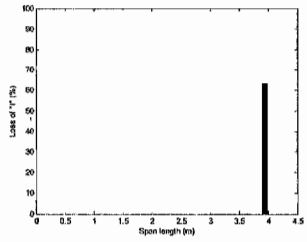
HMC- 6M (5 modes)
66.02%



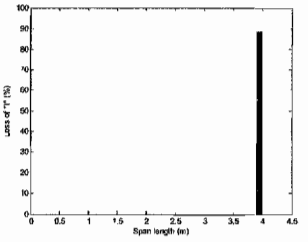
HMC- 6S (5 modes)
87.46%



HMC- 7L (5 modes)
14.53%

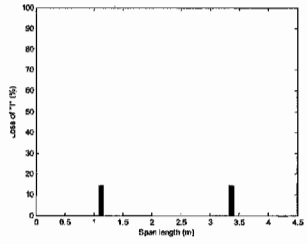


HMC - 7M (5 modes)
63.21%

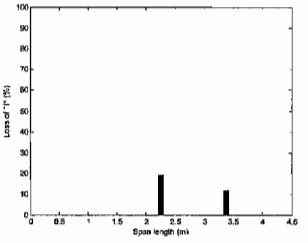


HMC - 7S (5 modes)
88.58%

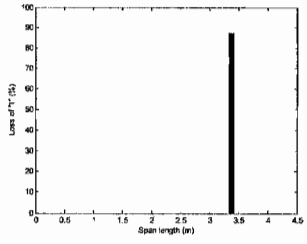
Two Damage Locations



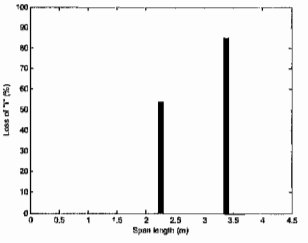
HMC- 2L6L (5 modes)*
14.55%, 14.55%



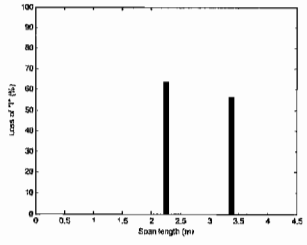
HMC- 4L6L (5 modes)
19.06%, 11.79%



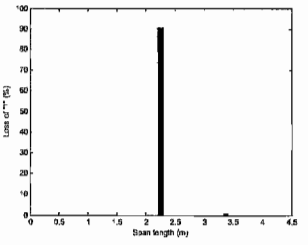
HMC- 4L6S (5 modes)
0%, 87.40%



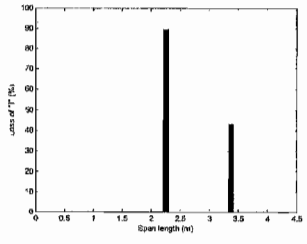
HMC- 4M6S (5 modes)
53.61%, 84.91%



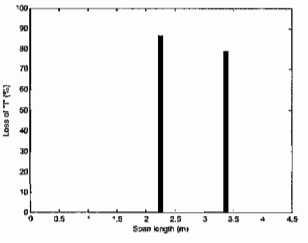
HMC- 4M6M (5 modes)
63.65%, 56.27%



HMC- 4S6L (5 modes)*
90.43%, 0.62%

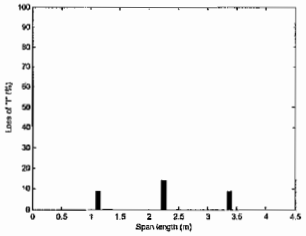


HMC- 4S6M (5 modes)*
89.27%, 43.18%

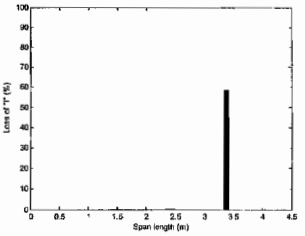


HMC- 4S6S (5 modes)*
86.29%, 78.94%

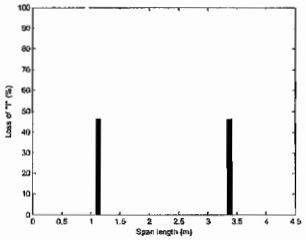
Three Damage Locations



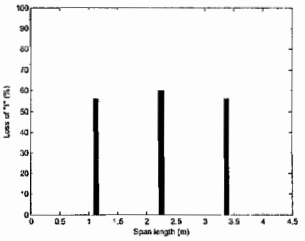
HMC- 2L4L6L (5 modes)*
8.93%, 14.14%, 8.93%



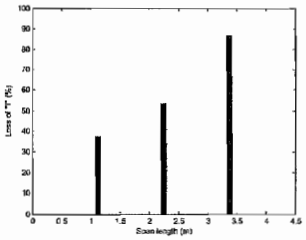
HMC- 2L4L6M (5 modes)*
0%, 0%, 66.15%



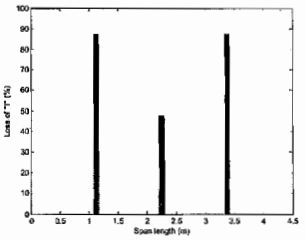
HMC- 2M4L6M (5 modes)*
61.87%, 0%, 61.87%



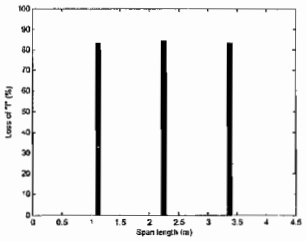
HMC- 2M4M6M (5 modes)*
55.90%, 59.97%, 55.90%



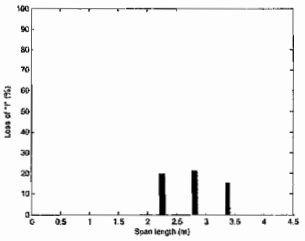
HMC- 2M4M6S (5 modes)*
39.40%, 53.23%, 86.83%



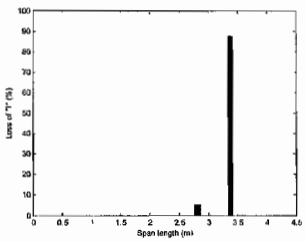
HMC- 2S4M6S (5 modes)*
87.36%, 47.52%, 87.36%



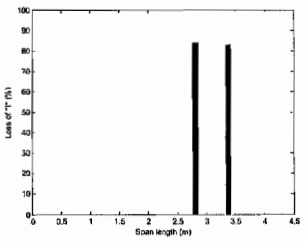
HMC- 2S4S6S (5 modes)*
83.32%, 84.44%, 83.32%



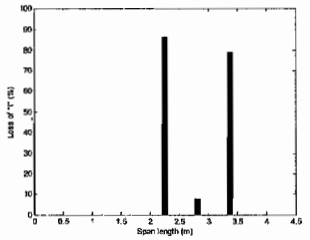
HMC- 4L5L6L (5 modes)
19.77%, 21.08%, 15.38%



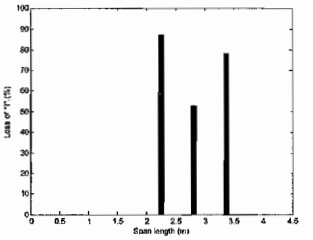
HMC- 4L5L6S (5 modes)
0%, 5.15%, 87.54%



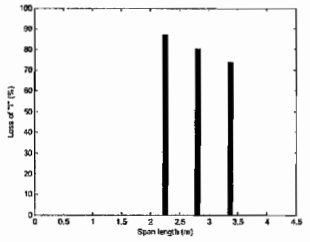
HMC- 4L5S6S (5 modes)
0%, 84.13%, 82.92%



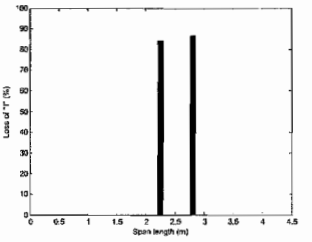
HMC- 4S5L6S (5 modes)*
86.55%, 7.68%, 79.06%



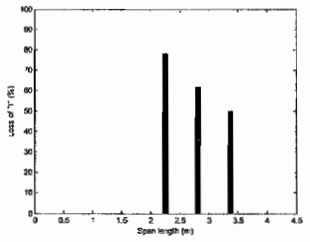
HMC- 4S5M6S (5 modes)*
87.40%, 52.71%, 78.18%



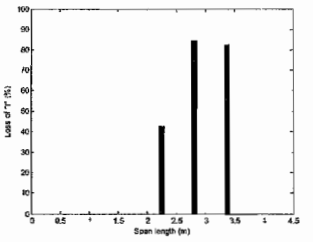
HMC- 4S5S6S (5 modes)*
86.86%, 80.28%, 73.78%



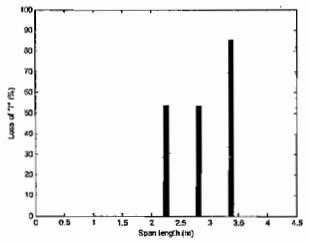
HMC- 4S5S6L (5 modes)
84.13%, 86.50%, 0%



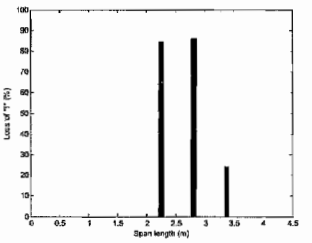
HMC- 4S5M6M (5 modes)
78.17%, 61.75%, 49.74%



HMC- 4M5S6S (5 modes)
42.62%, 84.39%, 82.45%

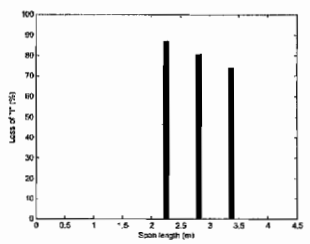


HMC- 4M5M6S (5 modes)
53.69%, 53.25%, 85.30%

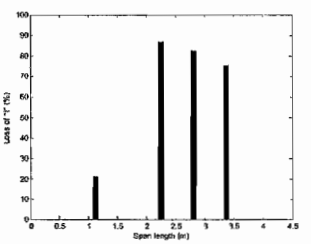


HMC- 4S5S6M (5 modes)
84.63%, 86.12%, 24.12%

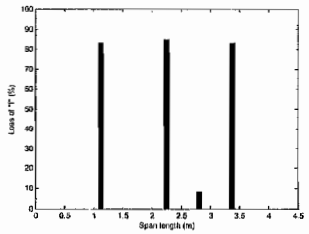
Four Damage Locations



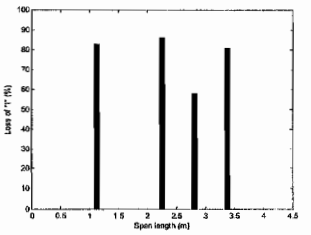
MDI-II- 2L4S5S6S (5 modes)*
0%, 86.85%, 80.56%, 74.00%



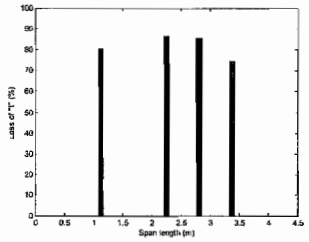
MDI-II- 2M4S5S6S (5 modes)*
21.34%, 86.81%, 82.28%, 75.41%



MDI-II- 2S4S5L6S (5 modes)*
83.32%, 84.84%, 8.33%, 83.07%



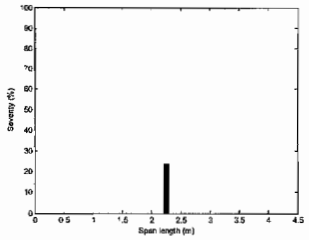
MDI-II- 2S4S5M6S (5 modes)*
82.82%, 86.18%, 58.05%, 80.89%



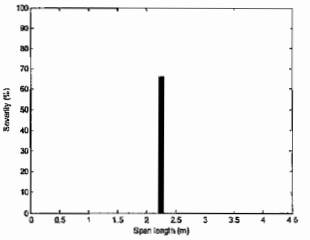
MDI-II- 2S4S5S6S (5 modes)*
80.63%, 86.38%, 85.62%, 74.60%

A.1.7 Damage Severity for Timber Beam (MDI-II) (5 Modes)

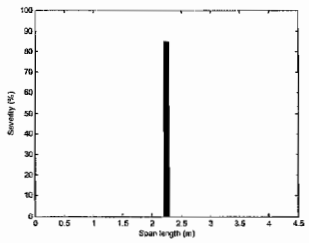
Single Damage Location



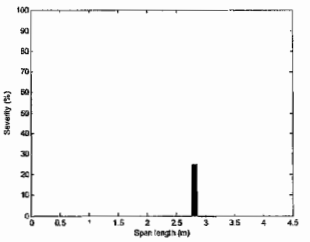
MDI-II- 4L (5 modes)*
23.69%



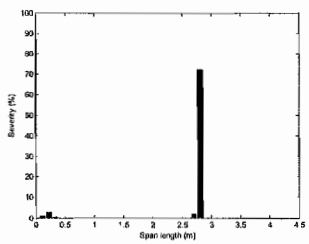
MDI-II- 4M (5 modes)*
66.36%



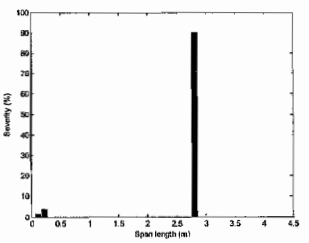
MDI-II- 4S (5 modes)*
84.92%



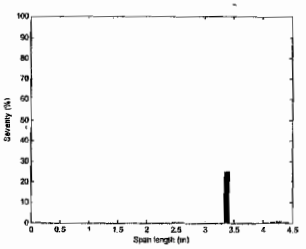
MDI-II- 5L (5 modes)
25.10%



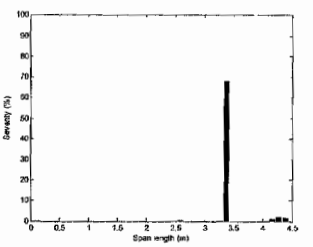
MDI-II- 5M (5 modes)
72.28%



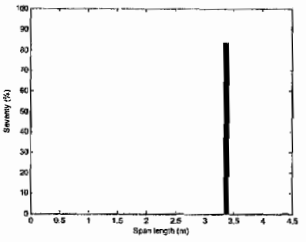
MDI-II- 5S (5 modes)
90.09%



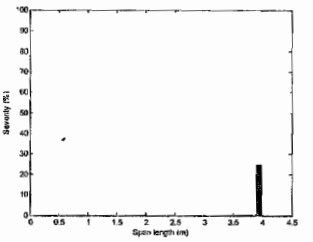
MDI-II- 6L (5 modes)*
24.93%



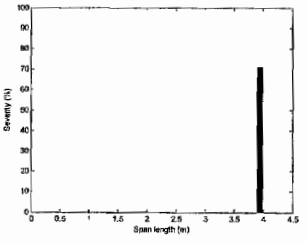
MDI-II- 6M (5 modes)
67.86%



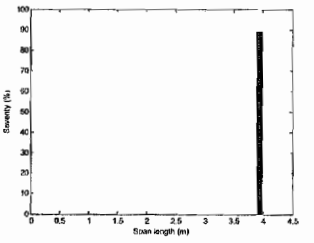
MDI-II- 6S (5 modes)
83.46%



MDI-II- 7L (5 modes)
24.82%

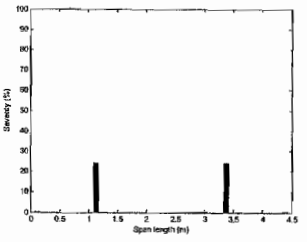


MDI-II- 7M (5 modes)
71.16%

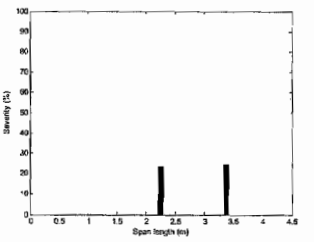


MDI-II- 7S (5 modes)
89.01%

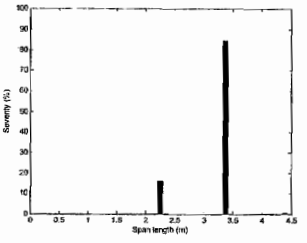
Two Damage Locations



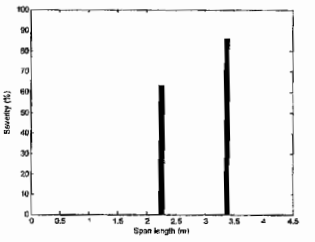
MDI-II- 2L6L (5 modes)*
24.01%, 24.01%



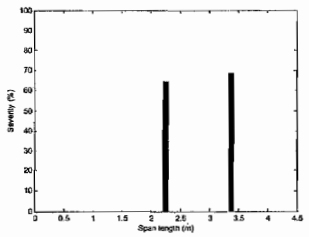
MDI-II- 4L6L (5 modes)
23.14%, 24.43%



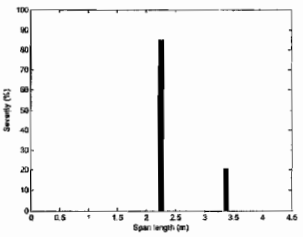
MDI-II- 4L6S (5 modes)
15.83%, 84.42%



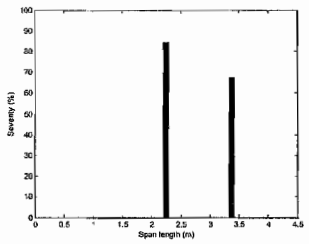
MDI-II- 4M6S (5 modes)
63.22%, 86.19%



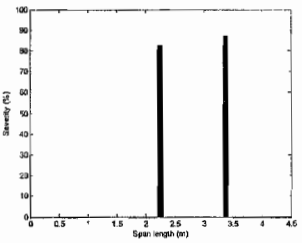
MDI-II- 4M6M (5 modes)
64.48%, 68.64%



MDI-II- 4S6L (5 modes)*
84.85%, 20.70%

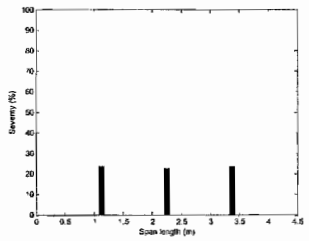


MDI-II- 4S6M (5 modes)*
84.37%, 67.35%

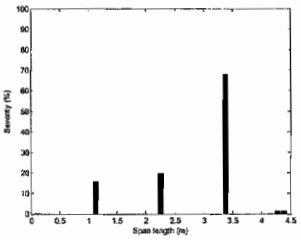


MDI-II- 4S6S (5 modes)*
82.50%, 87.23%

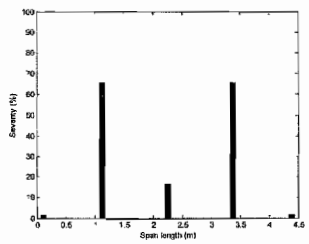
Three Damage Locations



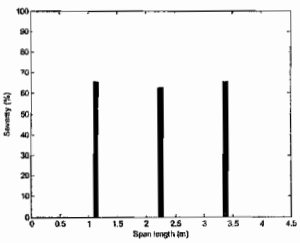
MDI-II- 2L4L6L (5 modes)*
23.50%, 22.60%, 23.50%



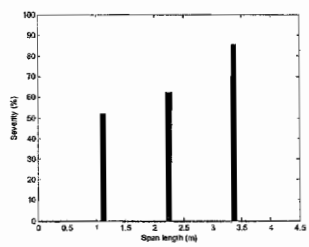
MDI-II- 2L4L6M (5 modes)*
15.88%, 19.73%, 67.96%



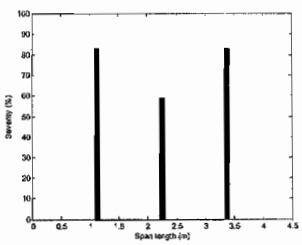
MDI-II- 2M4L6M (5 modes)*
65.77%, 16.56%, 65.77%



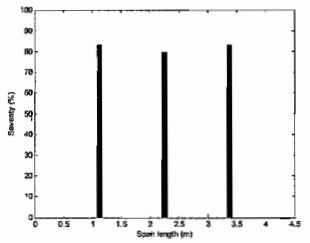
MDI-II- 2M4M6M (5 modes)*
65.63%, 62.78%, 65.63%



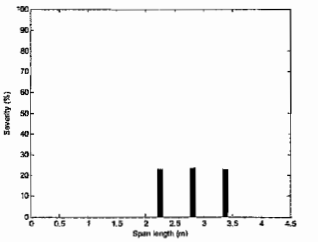
MDI-II- 2M4M6S (5 modes)*
52.01%, 62.33%, 85.61%



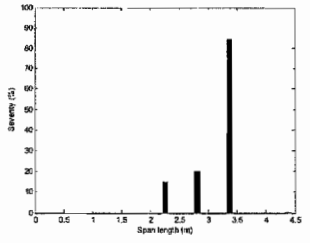
MDI-II- 2S4M6S (5 modes)*
83.11%, 58.95%, 83.11%



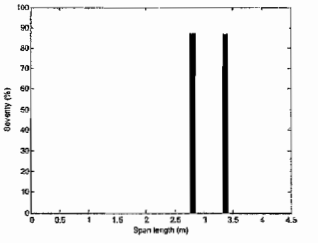
MDI-II- 2S4S6S (5 modes)*
83.33%, 79.74%, 83.33%



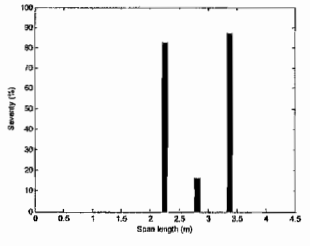
MDI-II- 4L5L6L (5 modes)
22.82%, 23.50%, 23.10%



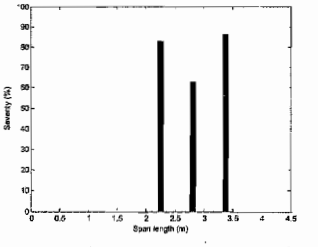
MDI-II- 4L5L6S (5 modes)
14.70%, 20.14%, 84.37%



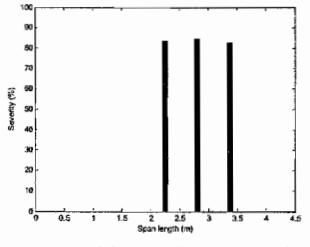
MDI-II- 4L5S6S (5 modes)
0%, 87.09%, 86.72%



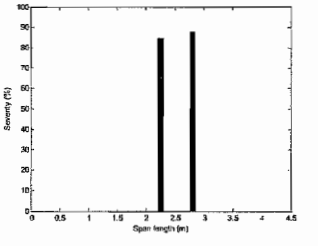
MDI-II- 4S5L6S (5 modes)*
82.50%, 16.33%, 87.09%



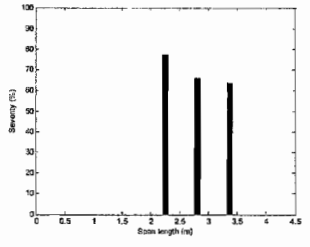
MDI-II- 4S5M6S (5 modes)*
82.98%, 62.76%, 86.09%



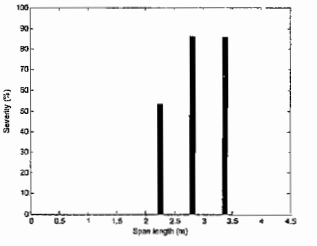
MDI-II- 4S5S6S (5 modes)*
83.40%, 84.22%, 82.68%



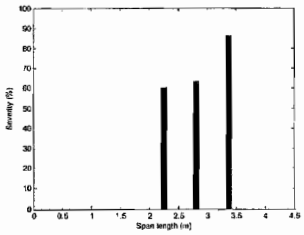
MDI-II- 4S5S6L (5 modes)
84.59%, 87.59%, 0%



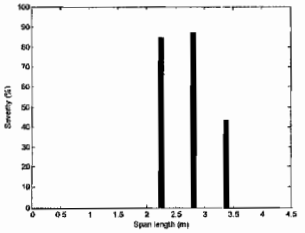
MDI-II- 4S5M6M (5 modes)
77.18%, 65.99%, 63.54%



MDI-II- 4M5S6S (5 modes)
53.49%, 86.04%, 85.74%

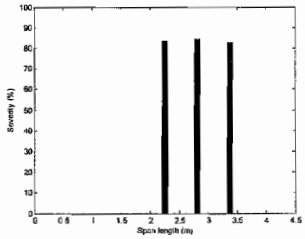


MDI-II- 4M5M6S (5 modes)
60.26%, 63.16%, 86.07%

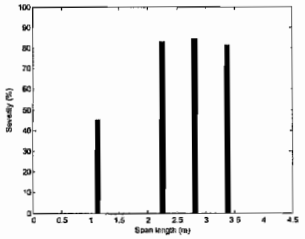


MDI-II- 4S5S6M (5 modes)
84.53%, 86.94%, 43.20%

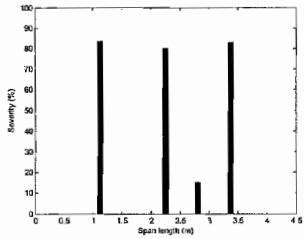
Four Damage Locations



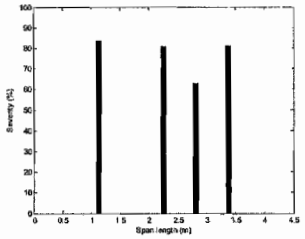
MDI-II- 2L4S5S6S (5 modes)*
0%, 83.35%, 84.24%, 82.54%



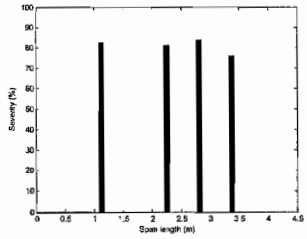
MDI-II- 2M4S5S6S (5 modes)*
45.29%, 82.98%, 84.32%, 81.48%



MDI-II- 2S4S5L6S (5 modes)*
83.37%, 79.95%, 15.18%, 82.98%



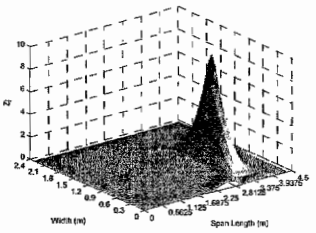
MDI-II- 2S4S5M6S (5 modes)*
83.49%, 80.97%, 62.58%, 81.09%

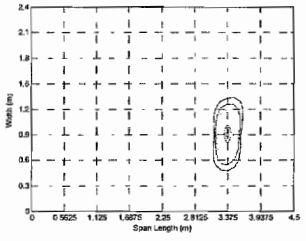


MDI-II- 2S4S5S6S (5 modes)*
82.72%, 81.49%, 84.17%, 76.02%

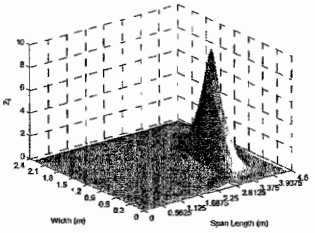
A.1.8 Damage Localisation for Laboratory Timber Bridge (DI-II-P) (3 Modes)

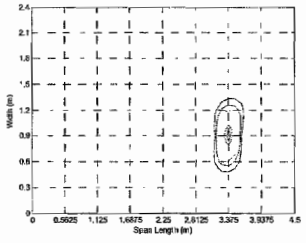
g2L (1Loc)



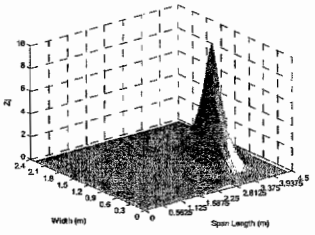


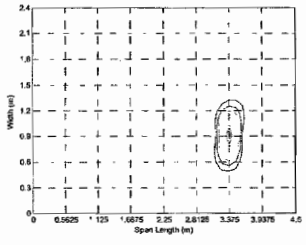
g2M (1Loc)



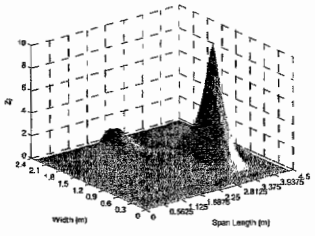


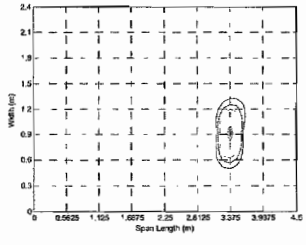
g2S (1Loc)



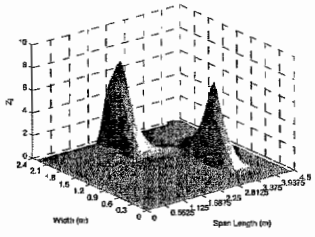


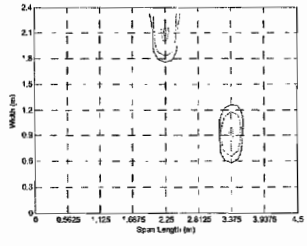
g2Sg4L (2Loc)



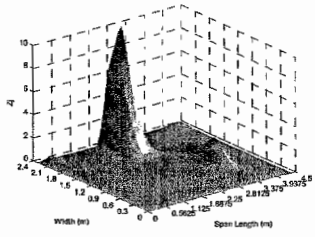


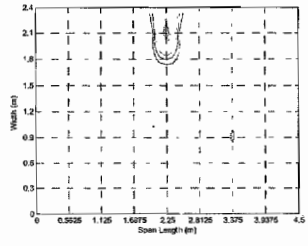
g2Sg4M (2Loc)



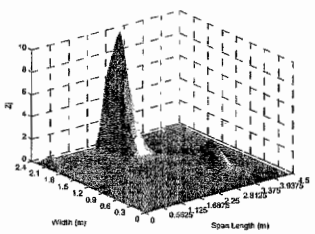
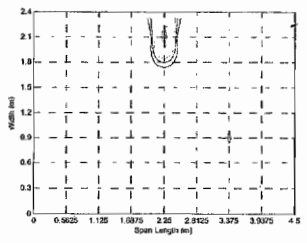


g2Sg4S (2Loc)

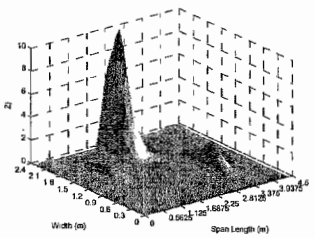
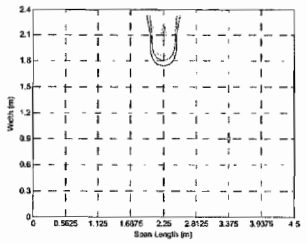




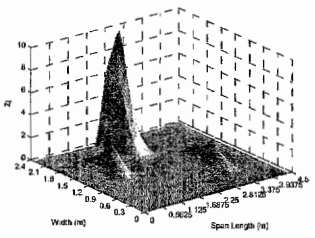
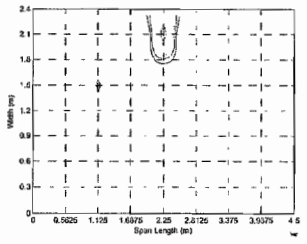
g2Sg4Sg3L (3Loc)

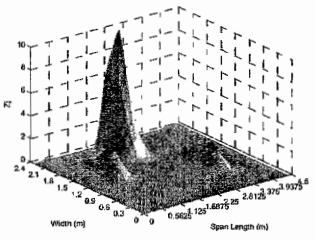
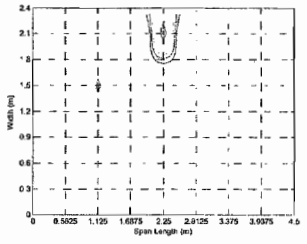
g2Sg4Sg3M (3Loc)

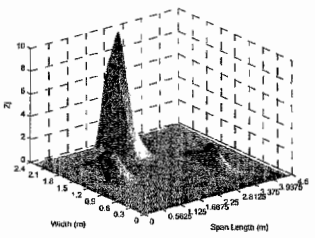
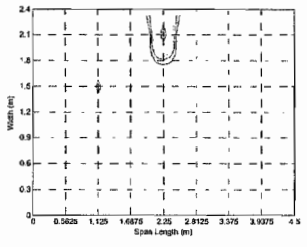
g2Sg4Sg3S (3Loc)

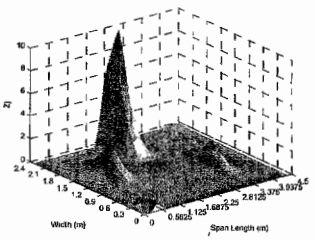
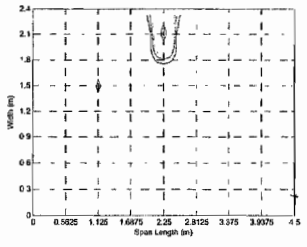
g2Sg4Sg3Sg1L (4Loc)

g2Sg4Sg3Sg1M (4Loc)

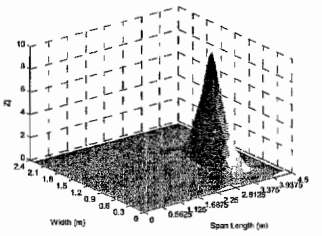
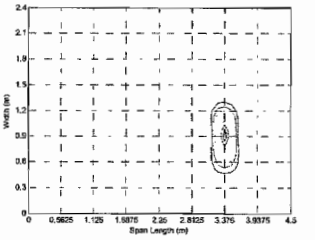



g2Sg4Sg3Sg1S (4Loc)

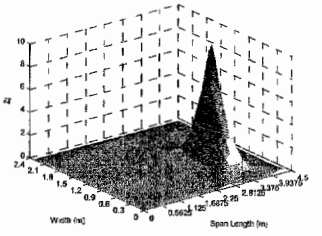
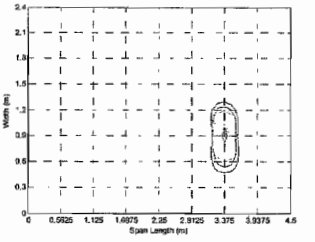



A.1.9 Damage Localisation for Laboratory Timber Bridge (DI-II-P) (9 Modes)

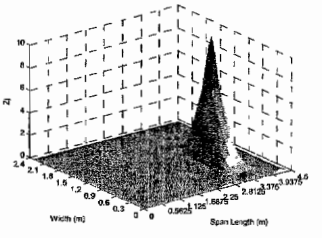
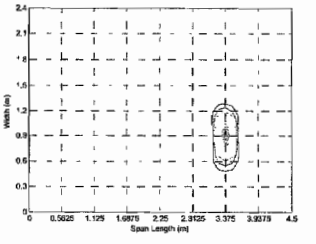
g2L (1Loc)

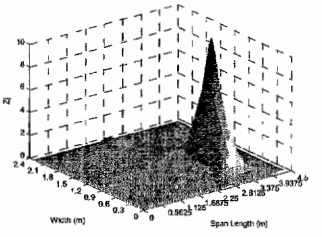
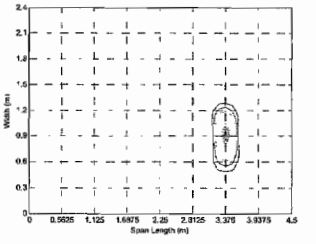
g2M (1Loc)

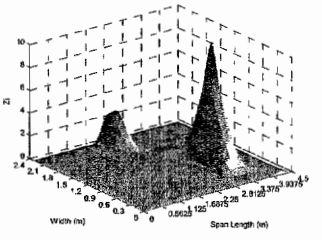
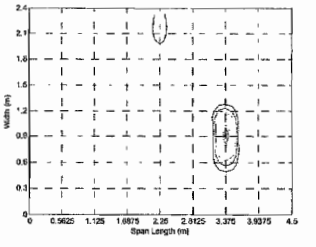
g2S (1Loc)

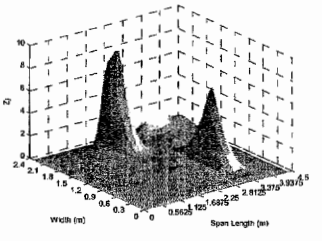
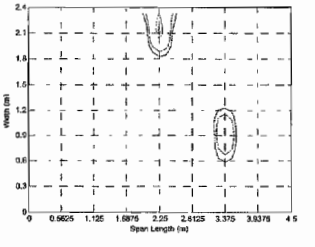
g2Sg4L (2Loc)

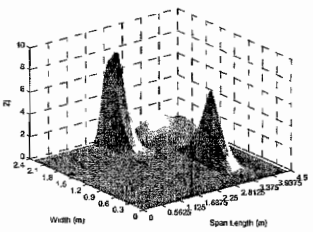
g2Sg4M (2Loc)

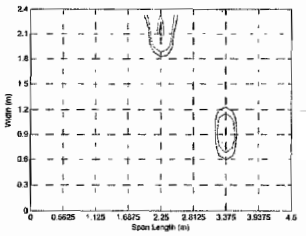



g2Sg4S (2Loc)

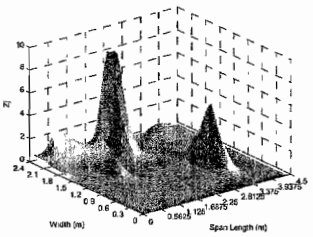



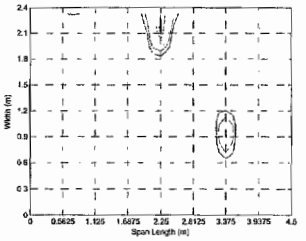
g2Sg4S g3L (3Loc)



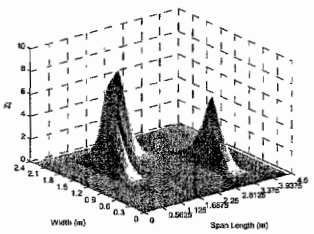


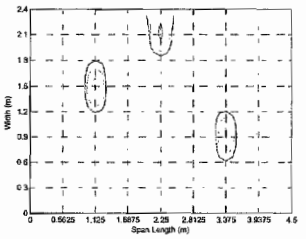
g2Sg4S g3M (3Loc)



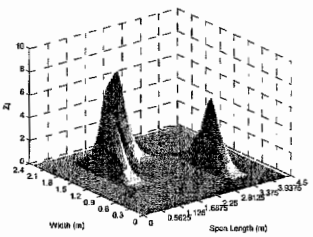


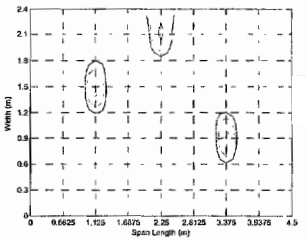
g2Sg4S g3S (3Loc)



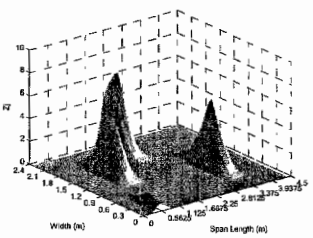


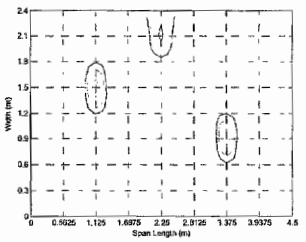
g2Sg4S g3Sg1L (4Loc)



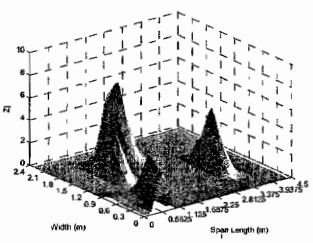


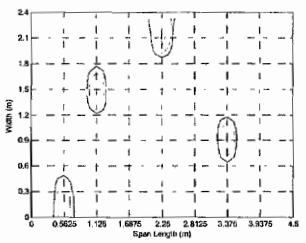
g2Sg4S g3Sg1M (4Loc)





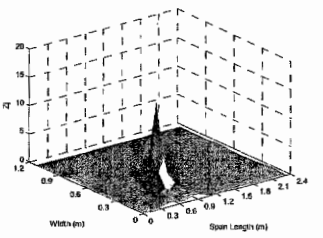
g2Sg4S g3Sg1S (4Loc)

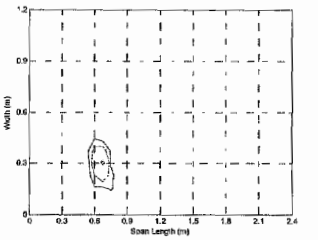




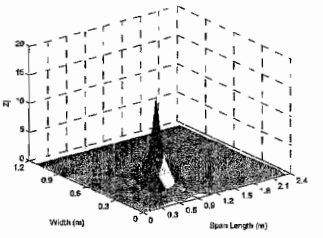
A.1.10 Damage Localisation for Timber Plate (DI-II-P) (3 Modes)

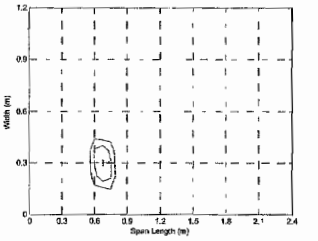
L2(I)A



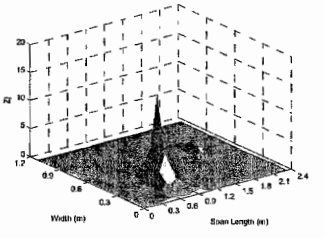


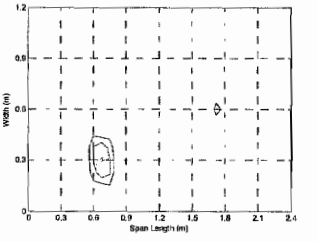
L2(II)B



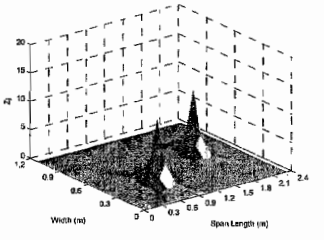


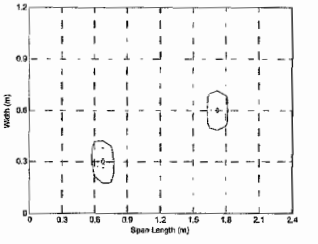
L2(II)B-L3(III)A



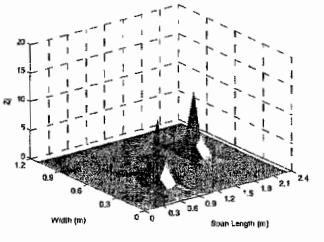


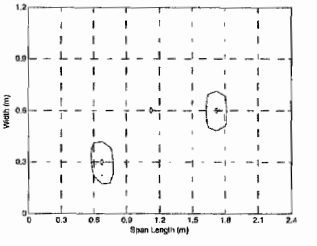
L2(II)B-L3(IV)B



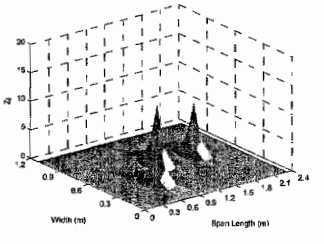


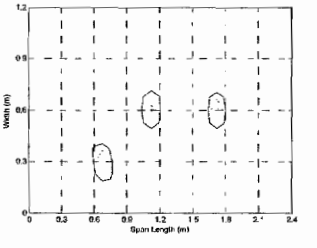
L2(II)B-L3(IV)B-L3(V)A





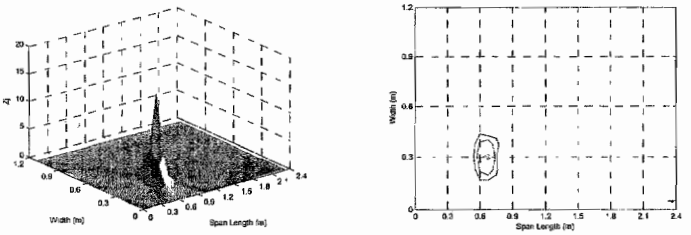
L2(II)B-L3(IV)B-L3(VI)B



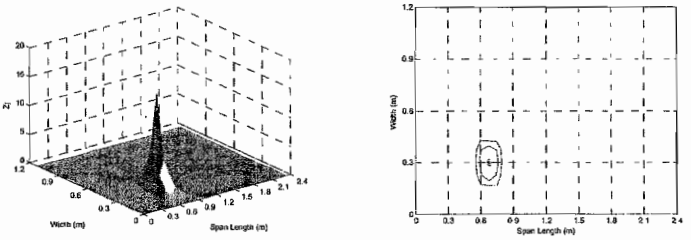


A.1.11 Damage Localisation for Timber Plate (DI-II-P) (6 Modes)

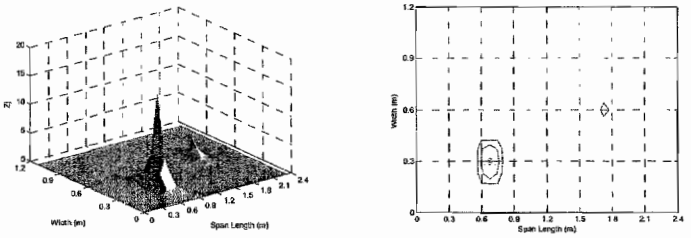
L2(I)A



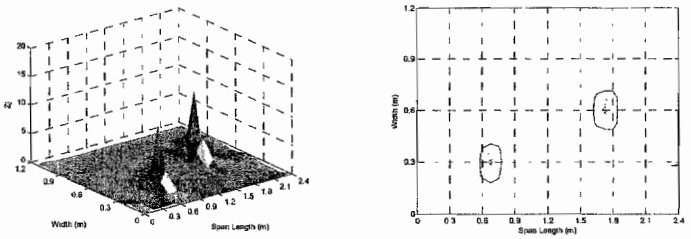
L2(II)B



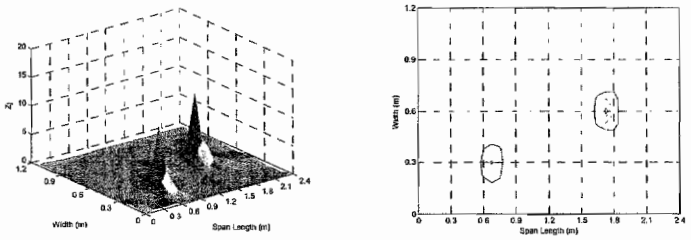
L2(II)B-L3(III)A



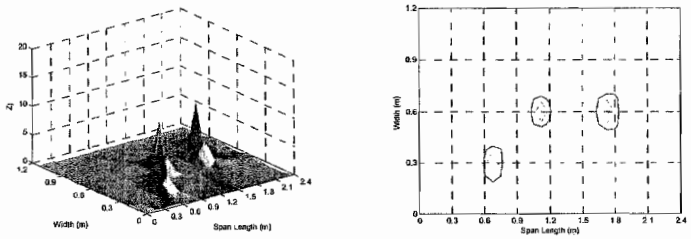
L2(II)B-L3(IV)B



L2(II)B-L3(IV)B-L3(V)A



L2(II)B-L3(IV)B-L3(VI)B



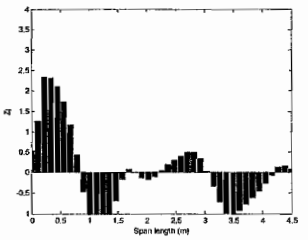
Appendix B

B.1 Damage Detection Results - Experimental Studies

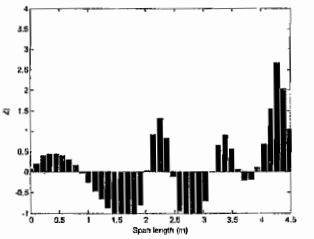
The damage detection results for the experimental studies (reconstructed 41-point from original 9-point) are shown below.

B.1.1 Damage Localisation for Timber Beam (DI-I vs MDI-I) (2 Modes)

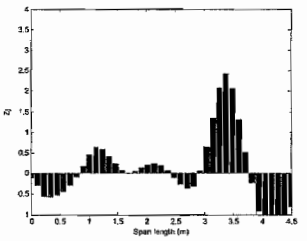
Single Damage Location



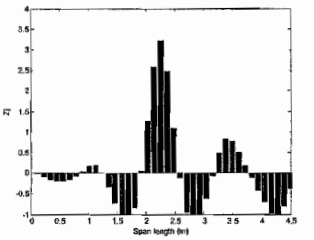
DI-I- 4L (2 modes)



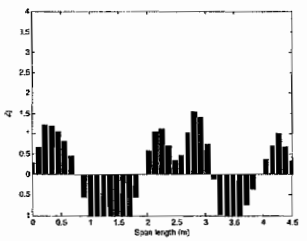
MDI-I- 4L (2 modes)



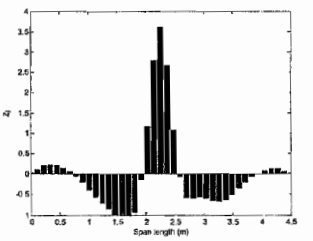
DI-I- 4M (2 modes)



MDI-I- 4M (2 modes)

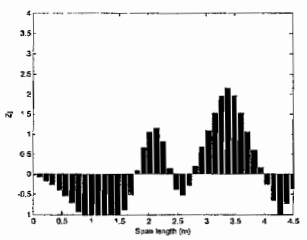


DI-I- 4S (2 modes)

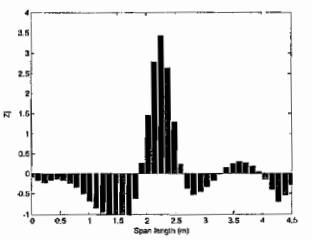


MDI-I- 4S (2 modes)

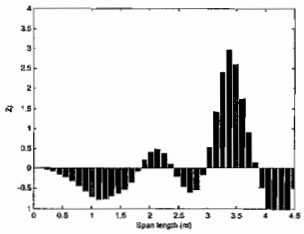
Two Damage Locations



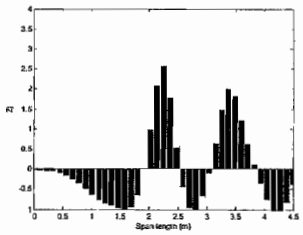
DI-I- 4S6L (2 modes)



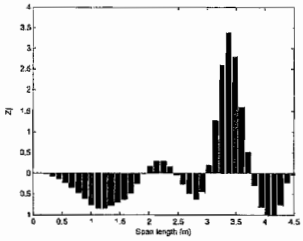
MDI-I- 4S6L (2 modes)



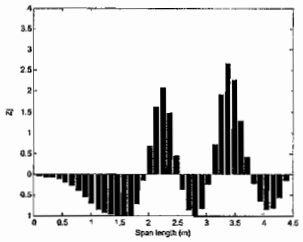
DI-I- 4S6M (2 modes)



MDI-I- 4S6M (2 modes)

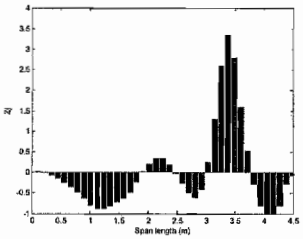


DI-I- 4S6S (2 modes)

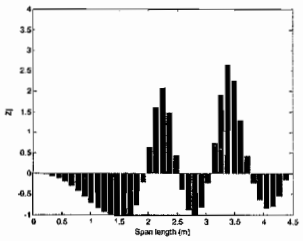


MDI-I- 4S6S (2 modes)

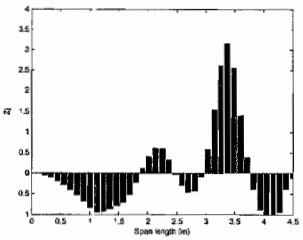
Three Damage Locations



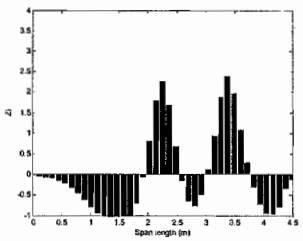
DI-I- 4S5L6S (2 modes)



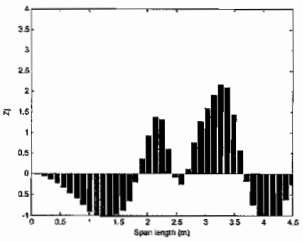
MDI-I- 4S5L6S (2 modes)



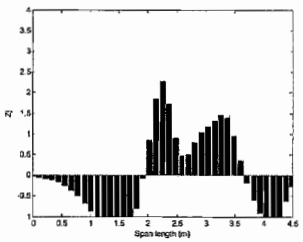
DI-I- 4S5M6S (2 modes)



MDI-I- 4S5M6S (2 modes)

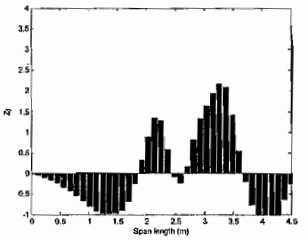


DI-I- 4S5S6S (2 modes)

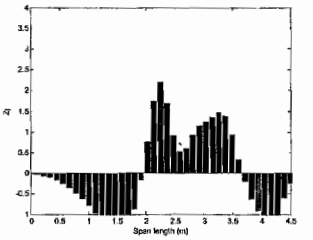


MDI-I- 4S5S6S (2 modes)

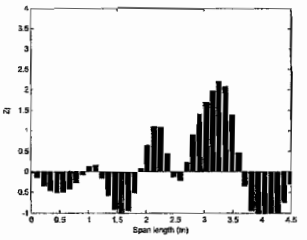
Four Damage Locations



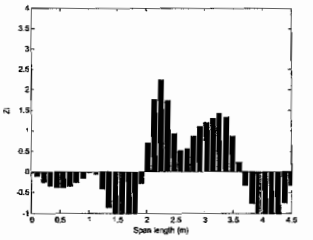
DI-I- 2L4S5S6S (2 modes)



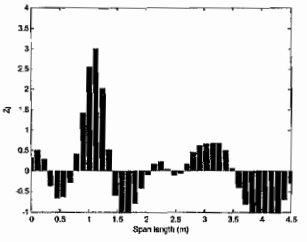
MDI-I- 2L4S5S6S (2 modes)



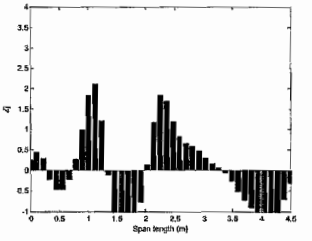
DI-I- 2M4S5S6S (2 modes)



MDI-I- 2M4S5S6S (2 modes)

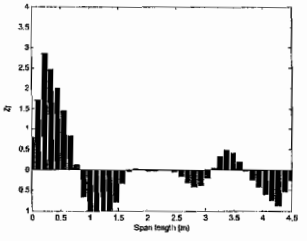


DI-I- 2S4S5S6S (2 modes)

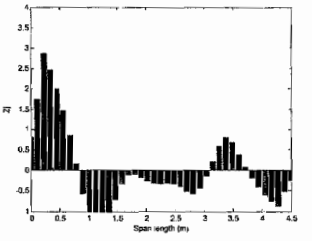


MDI-I- 2S4S5S6S (2 modes)

Single Damage Location

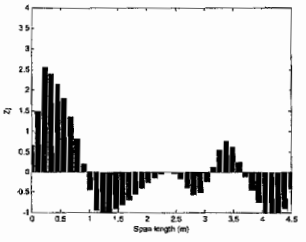


DI-I- 6L (2 modes)

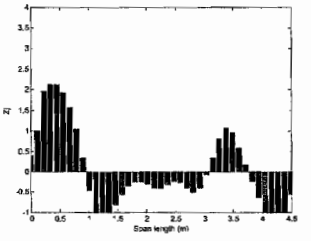


MDI-I- 6L (2 modes)

Two Damage Locations

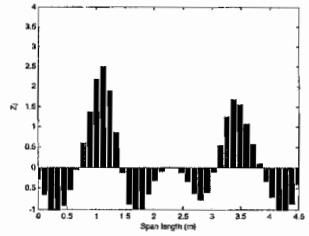


DI-I- 2L6L (2 modes)

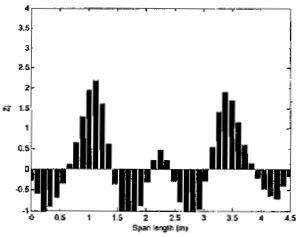


MDI-I- 2L6L (2 modes)

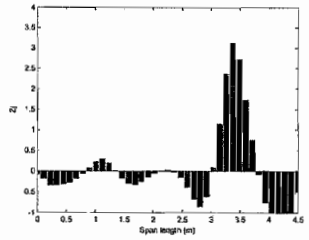
Three Damage Locations



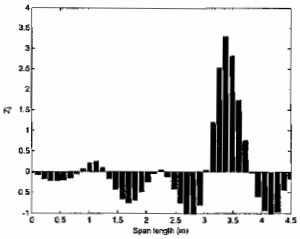
DI-I- 2L4L6L (2 modes)



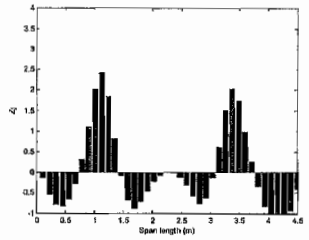
MDI-I- 2L4L6L (2 modes)



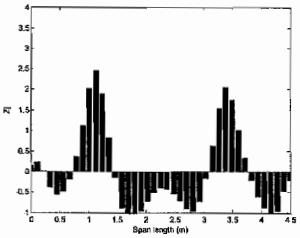
DI-I- 2L4L6M (2 modes)



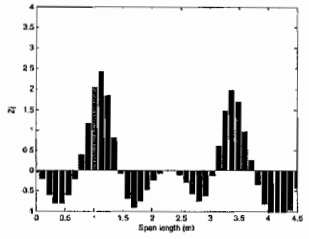
MDI-I- 2L4L6M (2 modes)



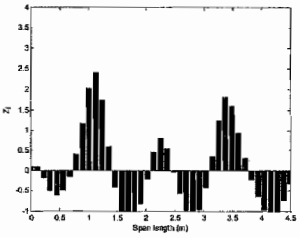
DI-I- 2M4L6M (2 modes)



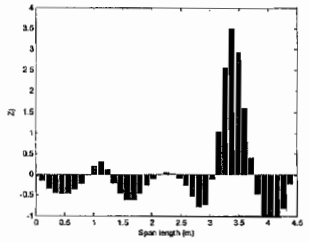
MDI-I- 2M4L6M (2 modes)



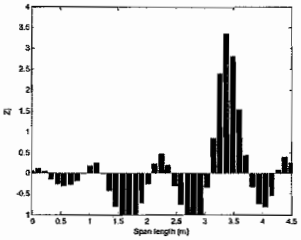
DI-I- 2M4M6M (2 modes)



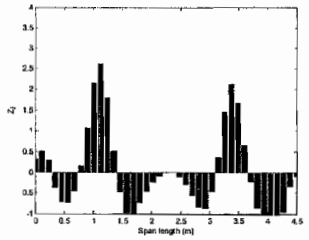
MDI-I- 2M4M6M (2 modes)



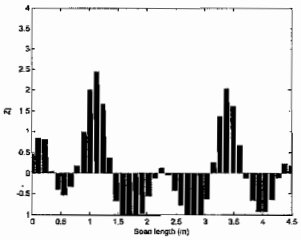
DI-I- 2M4M6S (2 modes)



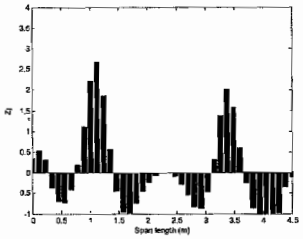
MDI-I- 2M4M6S (2 modes)



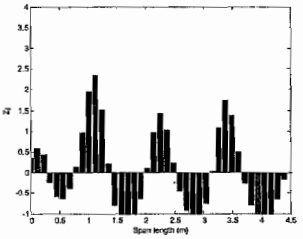
DI-I- 2S4M6S (2 modes)



MDI-I- 2S4M6S (2 modes)

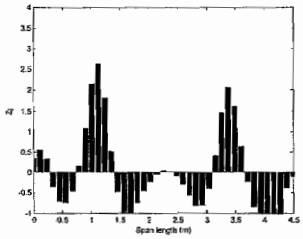


DI-I- 2S4S6S (2 modes)

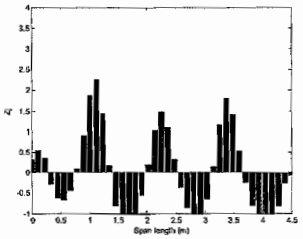


MDI-I- 2S4S6S (2 modes)

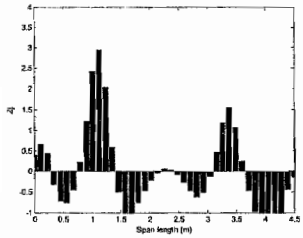
Four Damage Locations



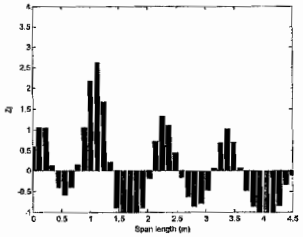
DI-I- 2S4S5L6S (2 modes)



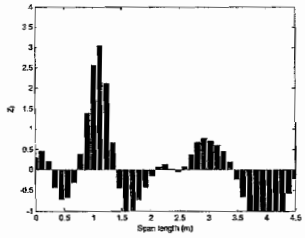
MDI-I- 2S4S5L6S (2 modes)



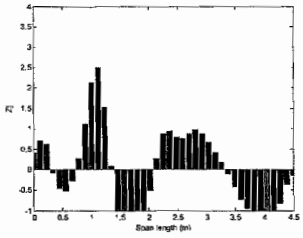
DI-I- 2S4S5M6S (2 modes)



MDI-I- 2S4S5M6S (2 modes)



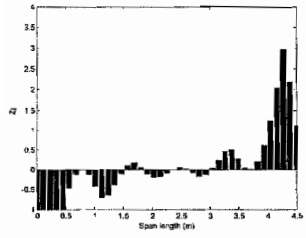
DI-I- 2S4S5S6S (2 modes)



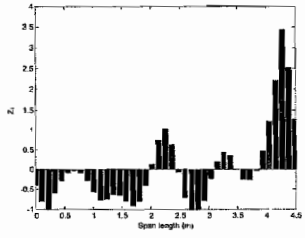
MDI-I- 2S4S5S6S (2 modes)

B.1.2 Damage Localisation for Timber Beam (DI-I vs MDI-I) (5 Modes)

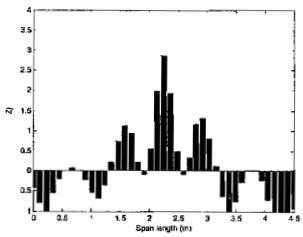
Single Damage Location



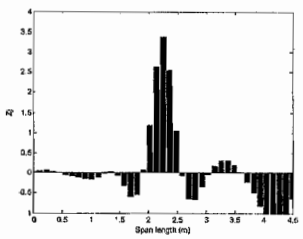
DI-I- 4L (5 modes)



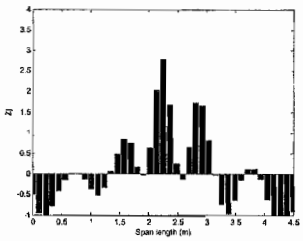
MDI-I- 4L (5 modes)



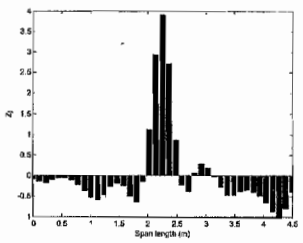
DI-I- 4M (5 modes)



MDI-I- 4M (5 modes)

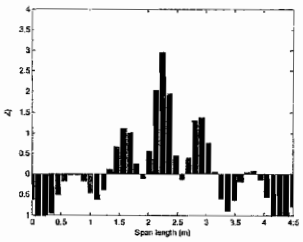


DI-I- 4S (5 modes)

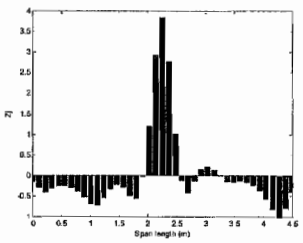


MDI-I- 4S (5 modes)

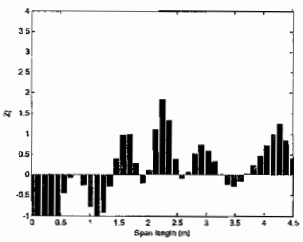
Two Damage Locations



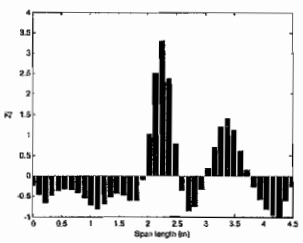
DI-I- 4S6L (5 modes)



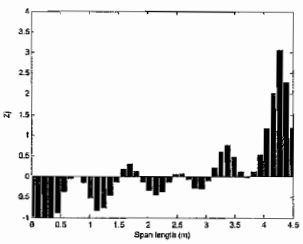
MDI-I- 4S6L (5 modes)



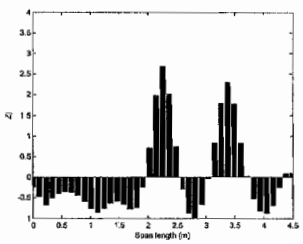
DI-I- 4S6M (5 modes)



MDI-I- 4S6M (5 modes)

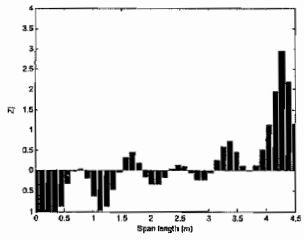


DI-I- 4S6S (5 modes)

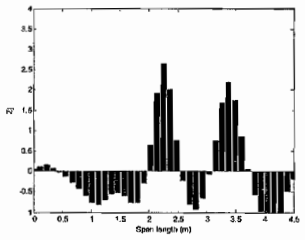


MDI-I- 4S6S (5 modes)

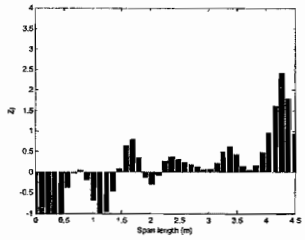
Three Damage Locations



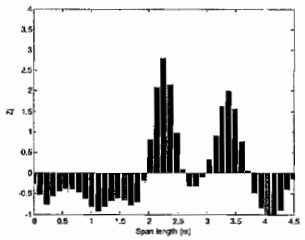
DI-I- 4S5L6S (5 modes)



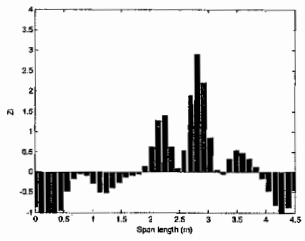
MDI-I- 4S5L6S (5 modes)



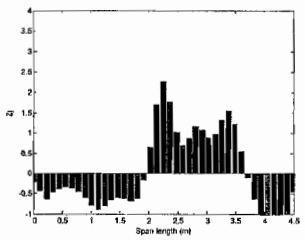
DI-I- 4S5M6S (5 modes)



MDI-I- 4S5M6S (5 modes)

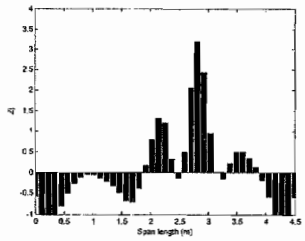


DI-I- 4S5S6S (5 modes)

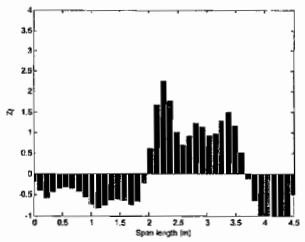


MDI-I- 4S5S6S (5 modes)

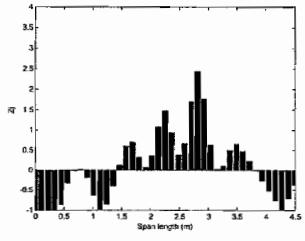
Four Damage Locations



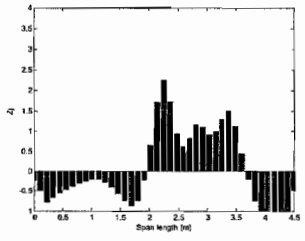
DI-I- 2L4S5S6S (5 modes)



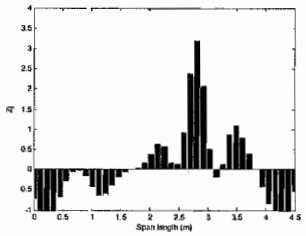
MDI-I- 2L4S5S6S (5 modes)



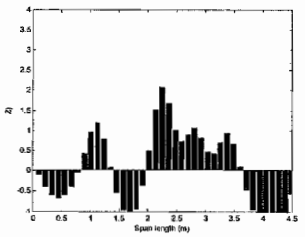
DI-I- 2M4S5S6S (5 modes)



MDI-I- 2M4S5S6S (5 modes)

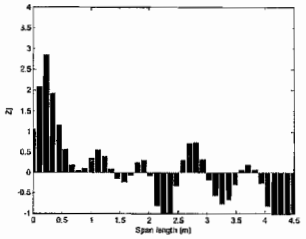


DI-I- 2S4S5S6S (5 modes)

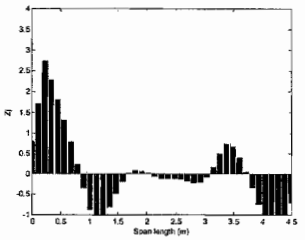


MDI-I- 2S4S5S6S (5 modes)

Single Damage Location

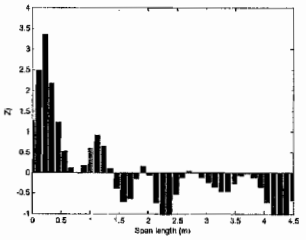


DI-I- 6L (5 modes)

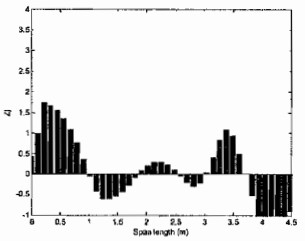


MDI-I- 6L (5 modes)

Two Damage Locations

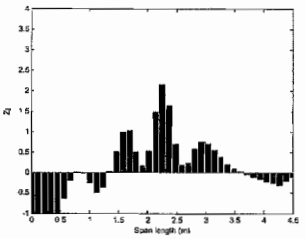


DI-I- 2L6L (5 modes)

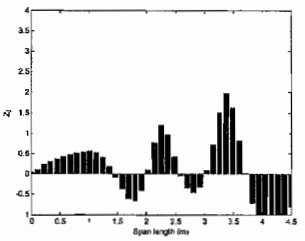


MDI-I- 2L6L (5 modes)

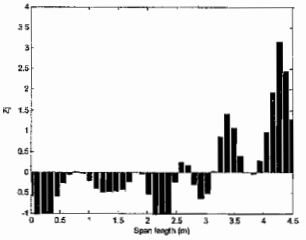
Three Damage Locations



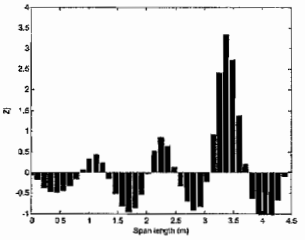
DI-I- 2L4L6L (5 modes)



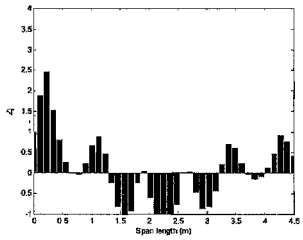
MDI-I- 2L4L6L (5 modes)



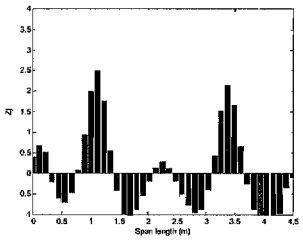
DI-I- 2M4M6S (5 modes)



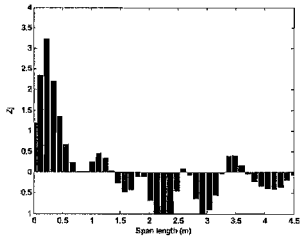
MDI-I- 2M4M6S (5 modes)



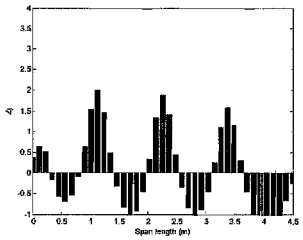
DI-I- 2S4M6S (5 modes)



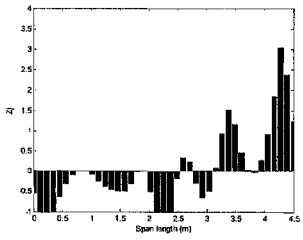
MDI-I- 2S4M6S (5 modes)



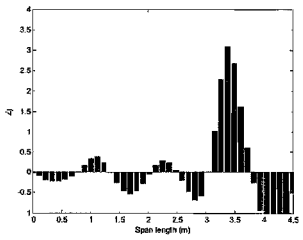
DI-I- 2S4S6S (5 modes)



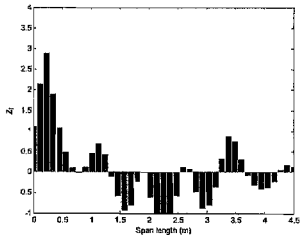
MDI-I- 2S4S6S (5 modes)



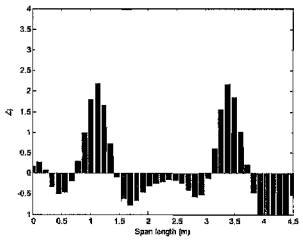
DI-I- 2L4L6M (5 modes)



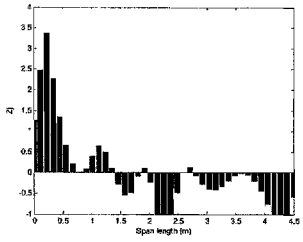
MDI-I- 2L4L6M (5 modes)



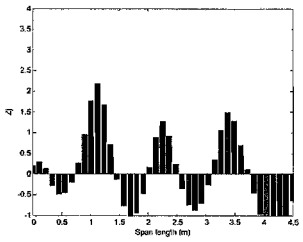
DI-I- 2M4L6M (5 modes)



MDI-I- 2M4L6M (5 modes)

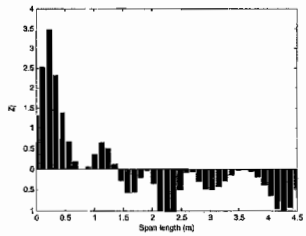


DI-I- 2M4M6M (5 modes)

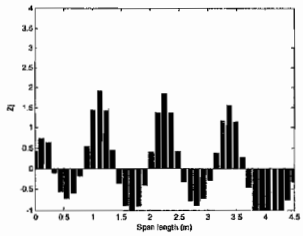


MDI-I- 2M4M6M (5 modes)

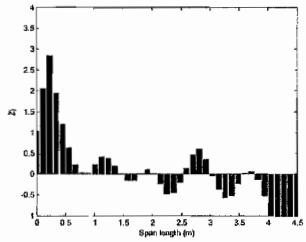
Four Damage Locations



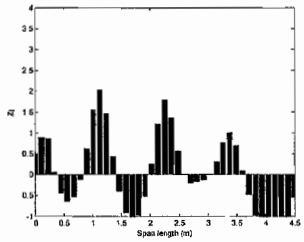
DI-I- 2S4S5L6S (5 modes)



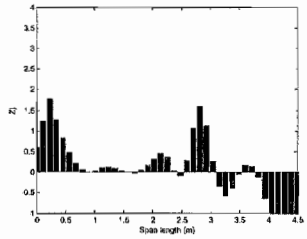
MDI-I- 2S4S5L6S (5 modes)



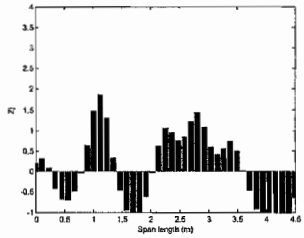
DI-I- 2S4S5M6S (5 modes)



MDI-I- 2S4S5M6S (5 modes)



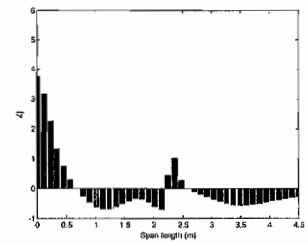
DI-I- 2S4S5S6S (5 modes)



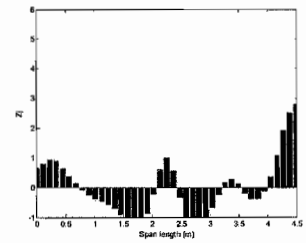
MDI-I- 2S4S5S6S (5 modes)

B.1.3 Damage Localisation for Timber Beam (DI-II vs MDI-II) (2 Modes)

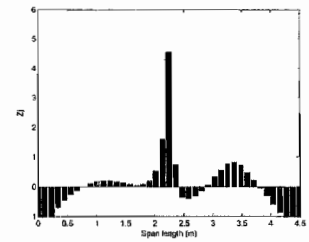
Single Damage Location



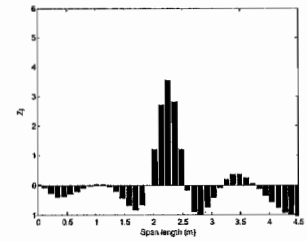
DI-II- 4L (2 modes)



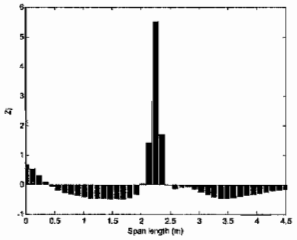
MDI-II- 4L (2 modes)



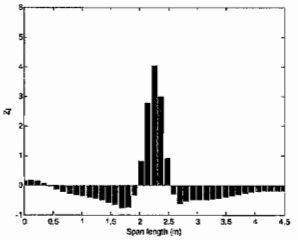
DI-II- 4M (2 modes)



MDI-II- 4M (2 modes)

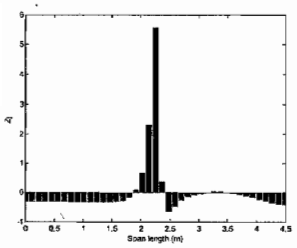


DI-II- 4S (2 modes)

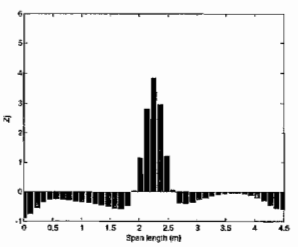


MDI-II- 4S (2 modes)

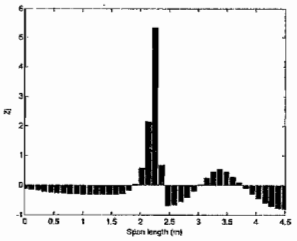
Two Damage Locations



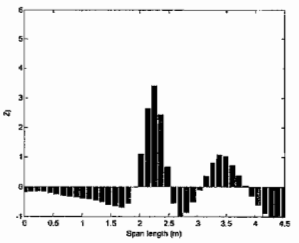
DI-II- 4S6L (2 modes)



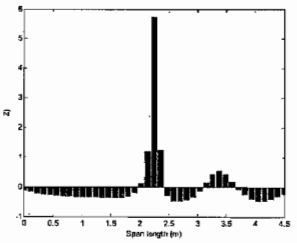
MDI-II- 4S6L (2 modes)



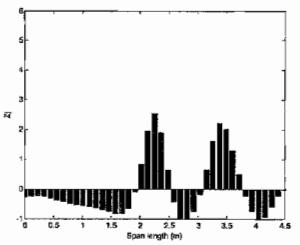
DI-II- 4S6M (2 modes)



MDI-II- 4S6M (2 modes)

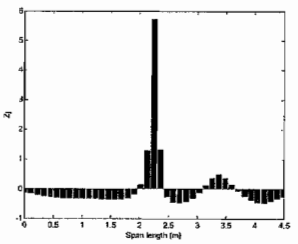


DI-II- 4S6S (2 modes)

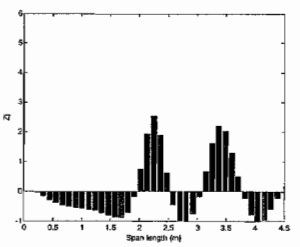


MDI-II- 4S6S (2 modes)

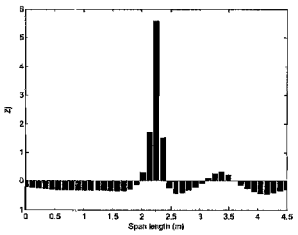
Three Damage Locations



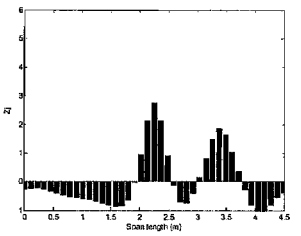
DI-II- 4S5L6S (2 modes)



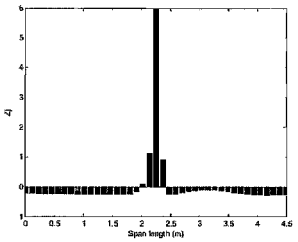
MDI-II- 4S5L6S (2 modes)



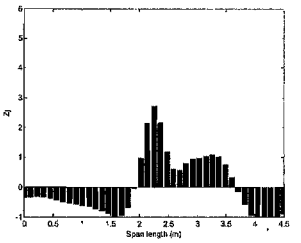
DI-II- 4S5M6S (2 modes)



MDI-II- 4S5M6S (2 modes)

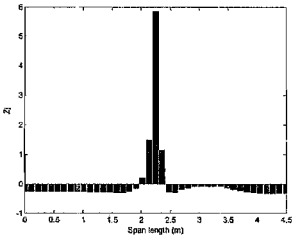


DI-II- 4S5S6S (2 modes) (Zj=6.003)

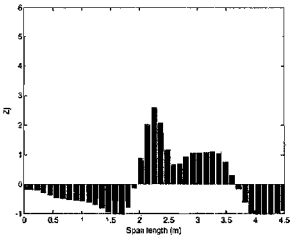


MDI-II- 4S5S6S (2 modes)

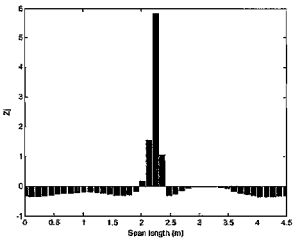
Four Damage Locations



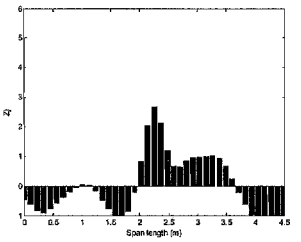
DI-II- 2L4S5S6S (2 modes)



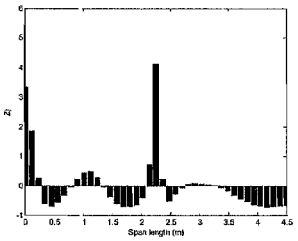
MDI-II- 2L4S5S6S (2 modes)



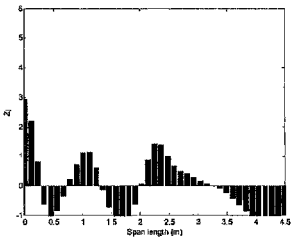
DI-II- 2M4S5S6S (2 modes)



MDI-II- 2M4S5S6S (2 modes)

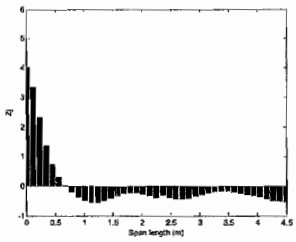


DI-II- 2S4S5S6S (2 modes)

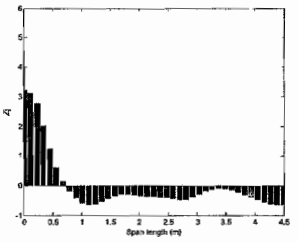


MDI-II- 2S4S5S6S (2 modes)

Single Damage Location

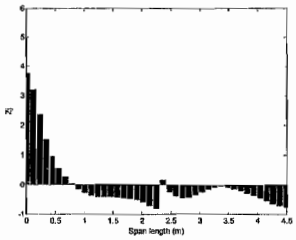


DI-II- 6L (2 modes)

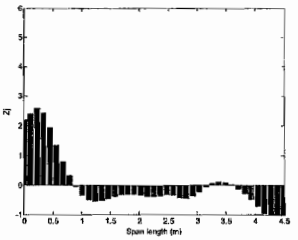


MDI-II- 6L (2 modes)

Two Damage Locations

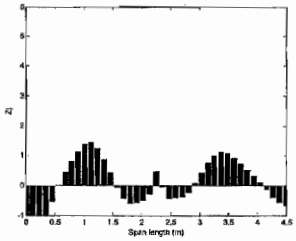


DI-II- 2L6L (2 modes)

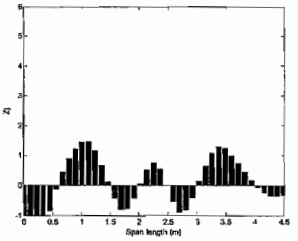


MDI-II- 2L6L (2 modes)

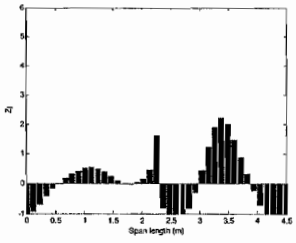
Three Damage Locations



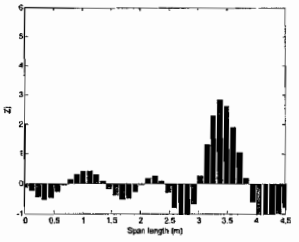
DI-II- 2L4L6L (2 modes)



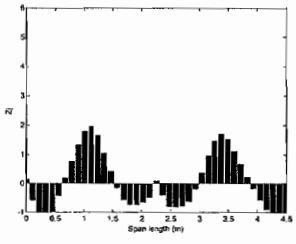
MDI-II- 2L4L6L (2 modes)



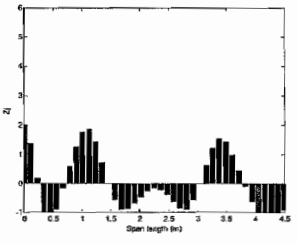
DI-II- 2L4L6M (2 modes)



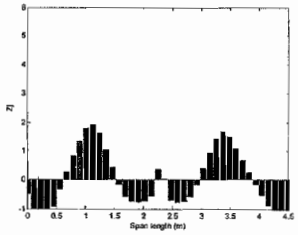
MDI-II- 2L4L6M (2 modes)



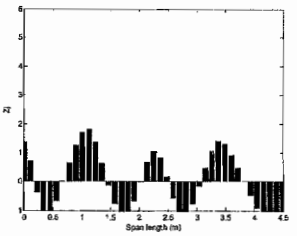
DI-II- 2M4L6M (2 modes)



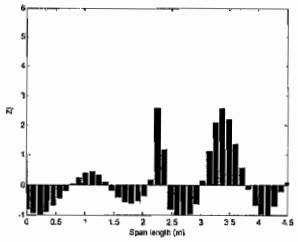
MDI-II- 2M4L6M (2 modes)



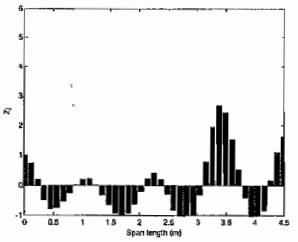
DI-II- 2M4M6M (2 modes)



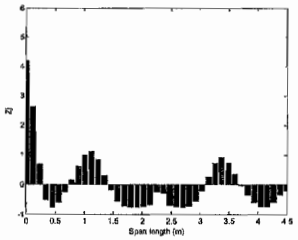
MDI-II- 2M4M6M (2 modes)



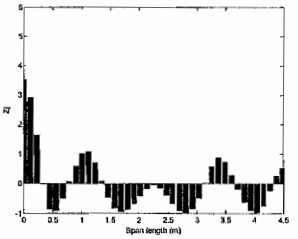
DI-II- 2M4M6S (2 modes)



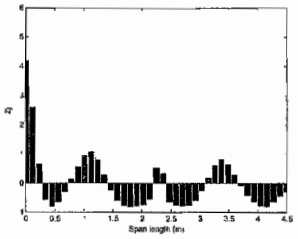
MDI-II- 2M4M6S (2 modes)



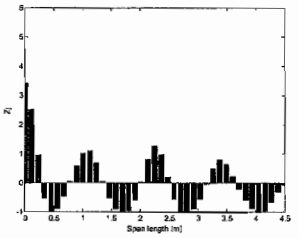
DI-II- 2S4M6S (2 modes)



MDI-II- 2S4M6S (2 modes)

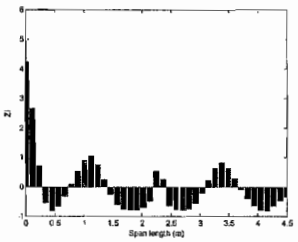


DI-II- 2S4S6S (2 modes)

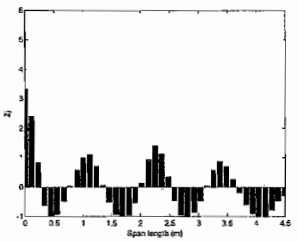


MDI-II- 2S4S6S (2 modes)

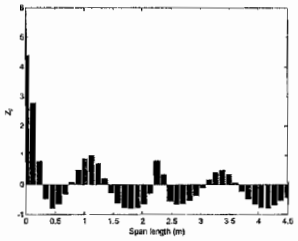
Four Damage Locations



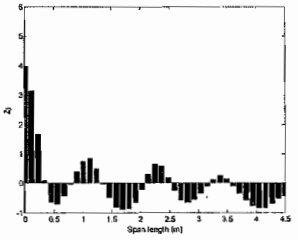
DI-II- 2S4S5L6S (2 modes)



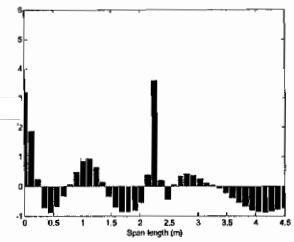
MDI-II- 2S4S5L6S (2 modes)



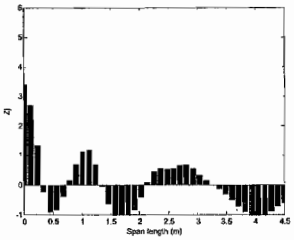
DI-II- 2S4S5M6S (2 modes)



MDI-II- 2S4S5M6S (2 modes)



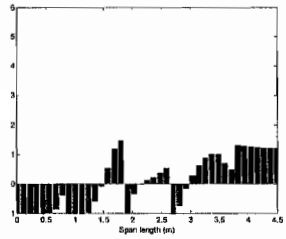
DI-II- 2S4S5S6S (2 modes)



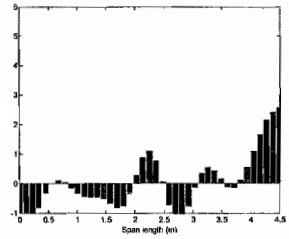
MDI-II- 2S4S5S6S (2 modes)

B.1.4 Damage Localisation for Timber Beam (DI-II vs MDI-II) (5 Modes)

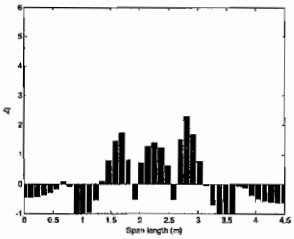
Single Damage Location



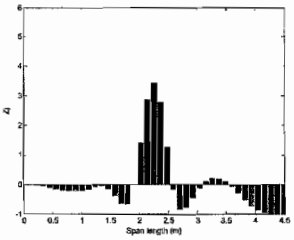
DI-II- 4L (5 modes)



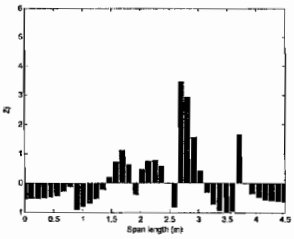
MDI-II- 4L (5 modes)



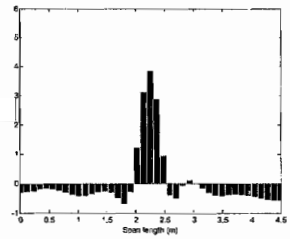
DI-II- 4M (5 modes)



MDI-II- 4M (5 modes)

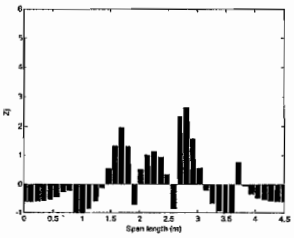


DI-II- 4S (5 modes)

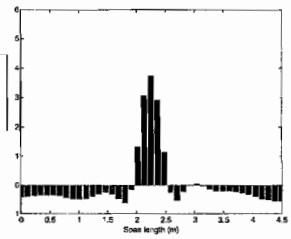


MDI-II- 4S (5 modes)

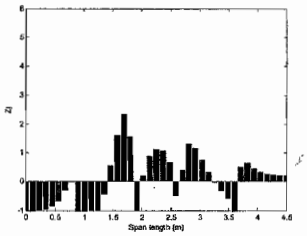
Two Damage Locations



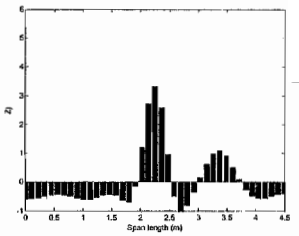
DI-II- 4S6L (5 modes)



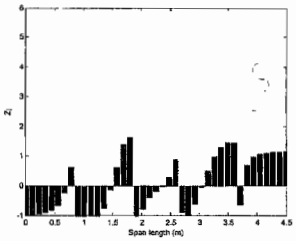
MDI-II- 4S6L (5 modes)



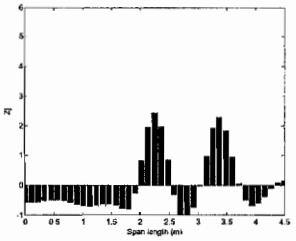
DI-II- 4S6M (5 modes)



MDI-II- 4S6M (5 modes)

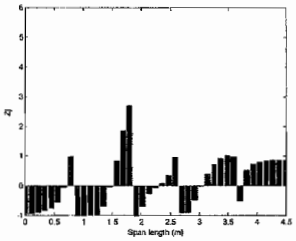


DI-II- 4S6S (5 modes)

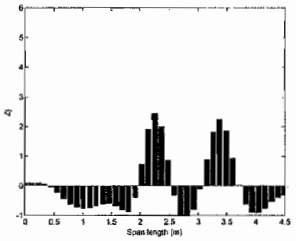


MDI-II- 4S6S (5 modes)

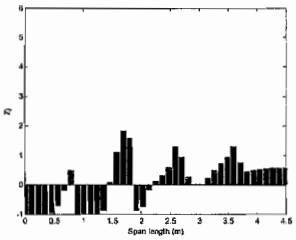
Three Damage Locations



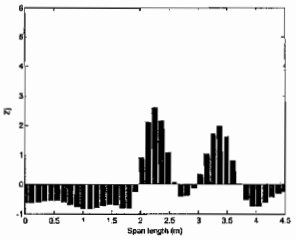
DI-II- 4S5L6S (5 modes)



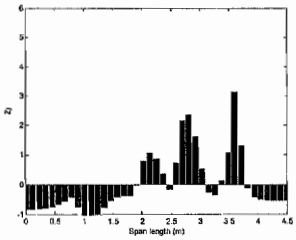
MDI-II- 4S5L6S (5 modes)



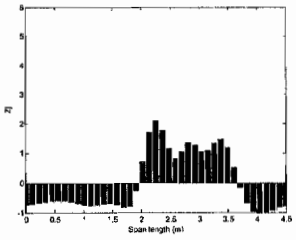
DI-II- 4S5M6S (5 modes)



MDI-II- 4S5M6S (5 modes)

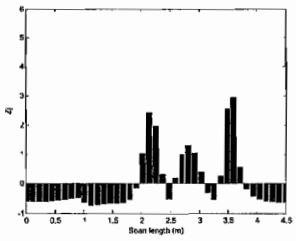


DI-II- 4S5S6S (5 modes)

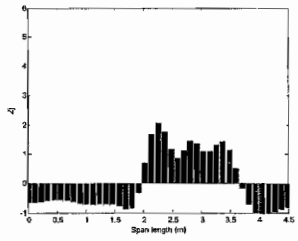


MDI-II- 4S5S6S (5 modes)

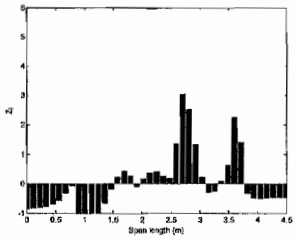
Four Damage Locations



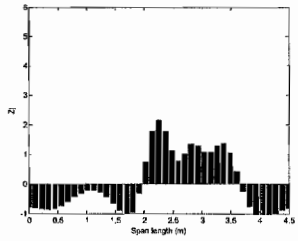
DI-II- 2L4S5S6S (5 modes)



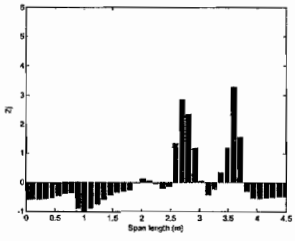
MDI-II- 2L4S5S6S (5 modes)



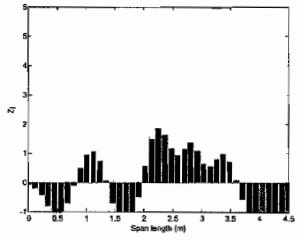
DI-II- 2M4S5S6S (5 modes)



MDI-II- 2M4S5S6S (5 modes)

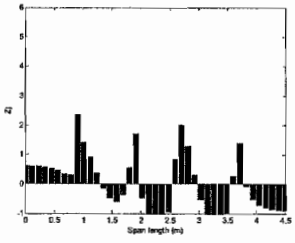


DI-II- 2S4S5S6S (5 modes)

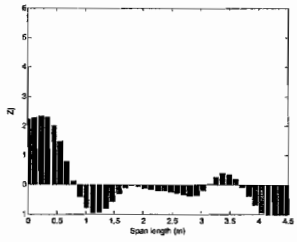


MDI-II- 2S4S5S6S (5 modes)

Single Damage Location

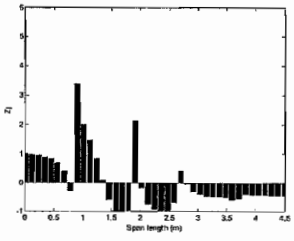


DI-II- 6L (5 modes)

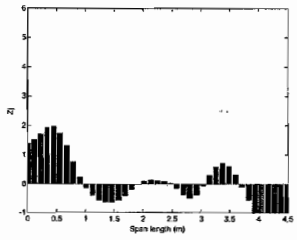


MDI-II- 6L (5 modes)

Two Damage Locations

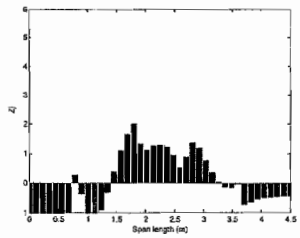


DI-II- 2L6L (5 modes)

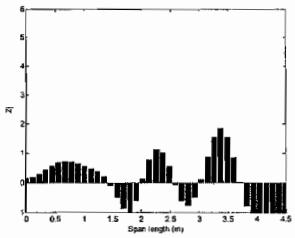


MDI-II- 2L6L (5 modes)

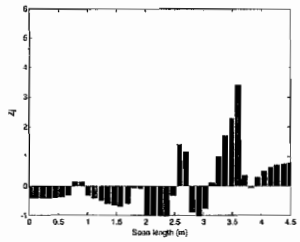
Three Damage Locations



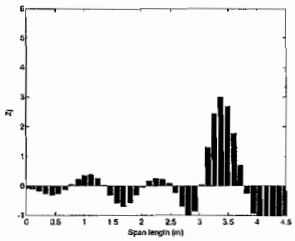
DI-II- 2L4L6L (5 modes)



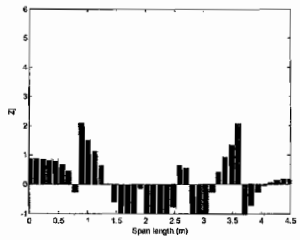
MDI-II- 2L4L6L (5 modes)



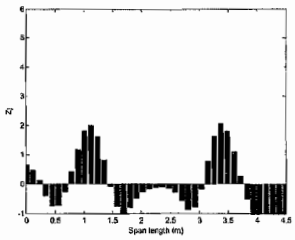
DI-II- 2L4L6M (5 modes)



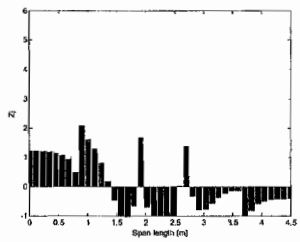
MDI-II- 2L4L6M (5 modes)



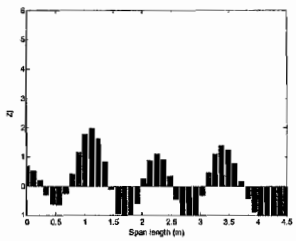
DI-II- 2M4L6M (5 modes)



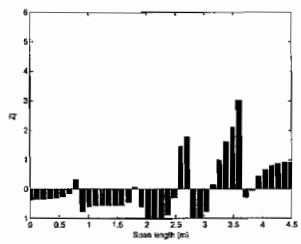
MDI-II- 2M4L6M (5 modes)



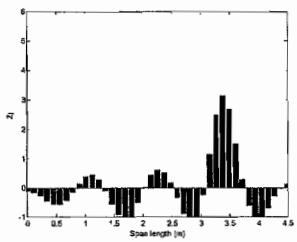
DI-II- 2M4M6M (5 modes)



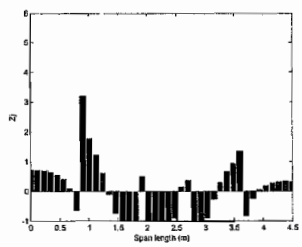
MDI-II- 2M4M6M (5 modes)



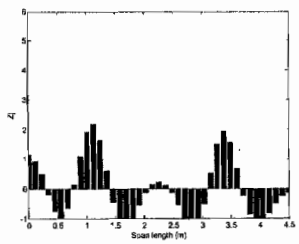
DI-II- 2M4M6S (5 modes)



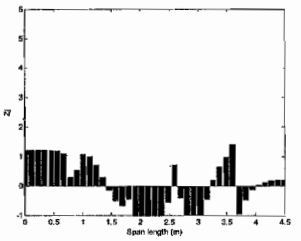
MDI-II- 2M4M6S (5 modes)



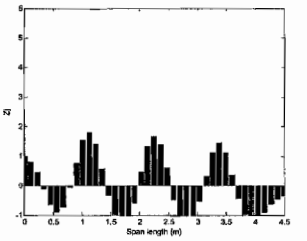
DI-II- 2S4M6S (5 modes)



MDI-II- 2S4M6S (5 modes)

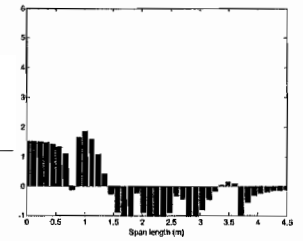


DI-II- 2S4S6S (5 modes)

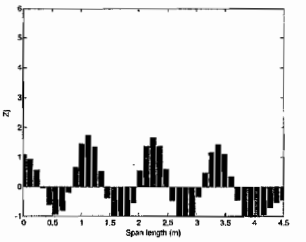


MDI-II- 2S4S6S (5 modes)

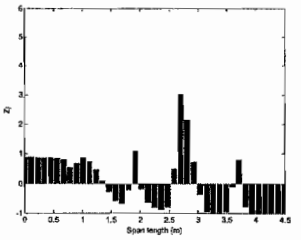
Four Damage Locations



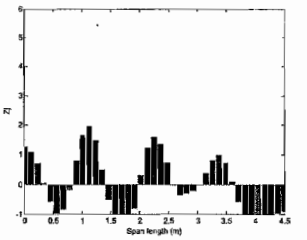
DI-II- 2S4S5L6S (5 modes)



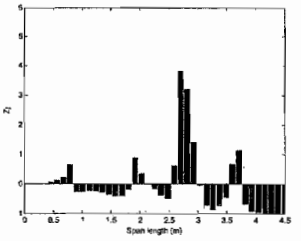
MDI-II- 2S4S5L6S (5 modes)



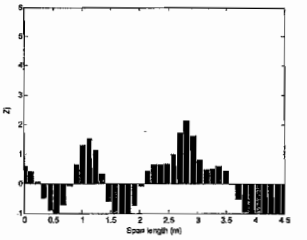
DI-II- 2S4S5M6S (5 modes)



MDI-II- 2S4S5M6S (5 modes)



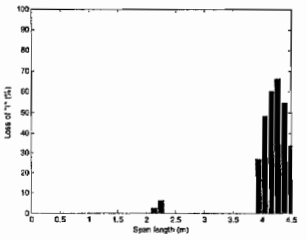
DI-II- 2S4S5S6S (5 modes)



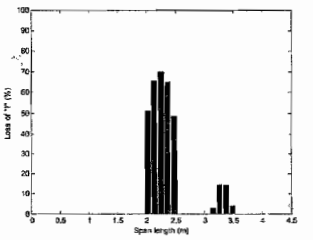
MDI-II- 2S4S5S6S (5 modes)

B.1.5 Damage Severity for Timber Beam (HMC) (5 Modes)

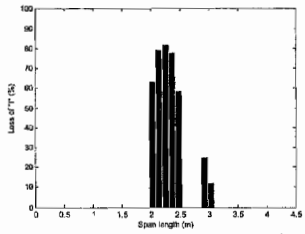
Single Damage Location



HMC- 4L (5 modes)
6.26%

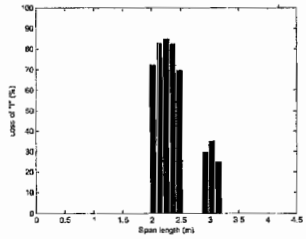


HMC- 4M (5 modes)
69.97%

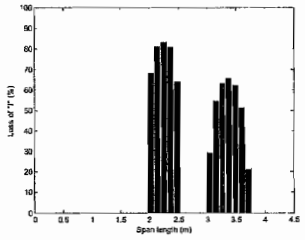


HMC- 4S (5 modes)
81.63%

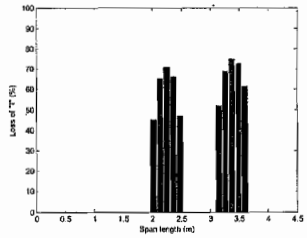
Two Damage Locations



HMC- 4S6L (5 modes)
84.94%, 0%

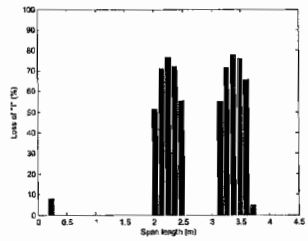


HMC- 4S6M (5 modes)
83.24%, 65.78%

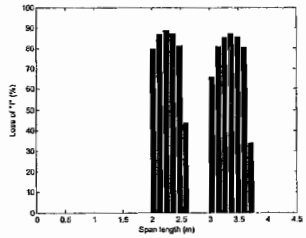


HMC- 4S6S (5 modes)
71.01%, 74.92%

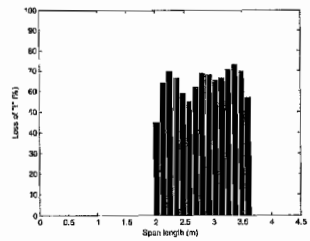
Three Damage Locations



HMC- 4S5L6S (5 modes)
76.44%, 0%, 77.60%

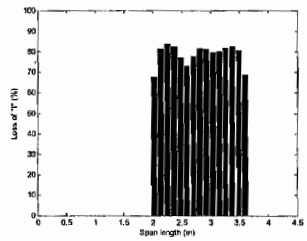


HMC- 4S5M6S (5 modes)
88.89%, 0%, 86.98%

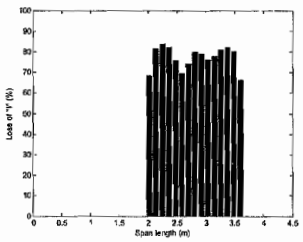


HMC- 4S5S6S (5 modes)
69.68%, 68.55%, 72.9%

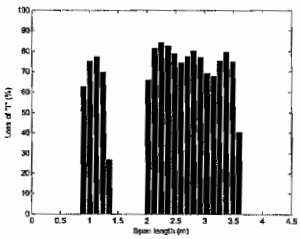
Four Damage Locations



HMC- 2L4S5S6S (5 modes)
0%, 83.87%, 81.39%, 82.66%

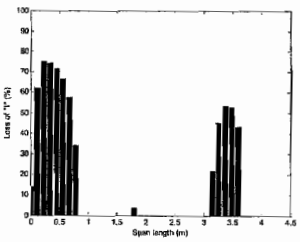


HMC- 2M4S5S6S (5 modes)
0%, 83.78%, 79.56%, 81.96%



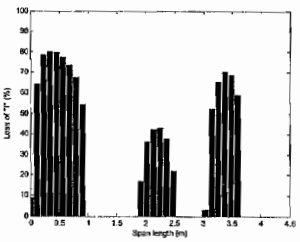
HMC- 2S4S5S6S (5 modes)
77.21%, 84.09%, 80.24%, 79.71%

Single Damage Location



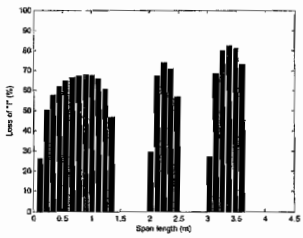
HMC- 6L (5 modes)
53.47%

Two Damage Locations

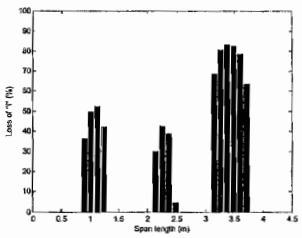


HMC- 2L6L (5 modes)
0%, 70.22%

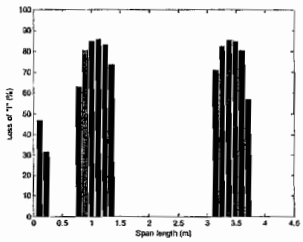
Three Damage Locations



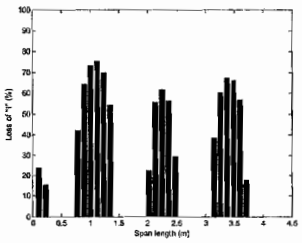
HMC- 2L4L6L (5 modes)
65.94%, 74.00%, 82.35%



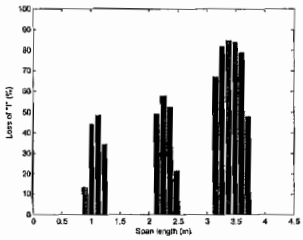
HMC- 2L4L6M (5 modes)
52.05%, 42.32%, 83.26%



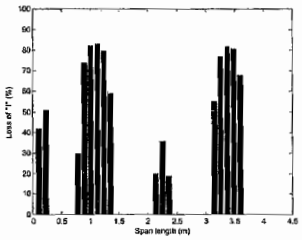
HMC- 2M4L6M (5 modes)
85.69%, 0%, 85.41%



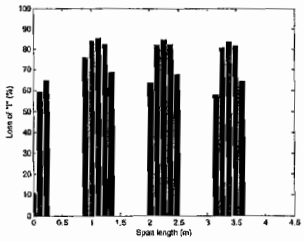
HMC- 2M4M6M (5 modes)
75.32%, 61.93%, 67.33%



HMC- 2M4M6S (5 modes)
48.51%, 57.75%, 84.79%

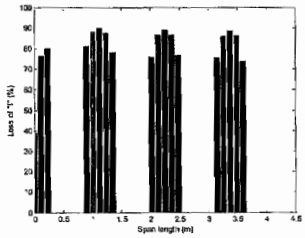


HMC- 2S4M6S (5 modes)
82.94%, 35.82%, 81.86%

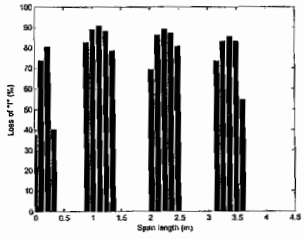


HMC- 2S4S6S (5 modes)
85.48%, 84.59%, 83.70%

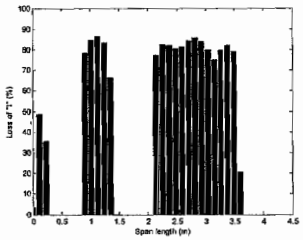
Four Damage Locations



HMC- 2S4S5L6S (5 modes)
89.94%, 89.00%, 0%, 88.61%



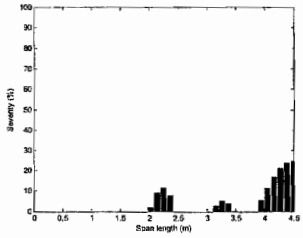
HMC- 2S4S5M6S (5 modes)
90.92%, 89.18%, 0%, 85.51%



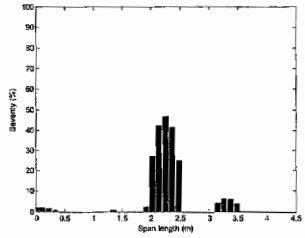
HMC- 2S4S5S6S (5 modes)
86.30%, 82.48%, 85.70%, 81.88%

B.1.6 Damage Severity for Timber Beam (MDI-II) (5 Modes)

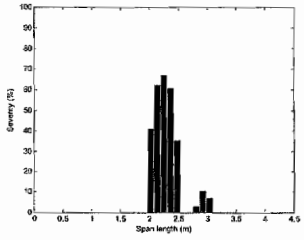
Single Damage Location



MDI-II- 4L (5 modes)
11.45%

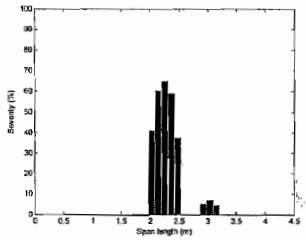


MDI-II- 4M (5 modes)
46.55%

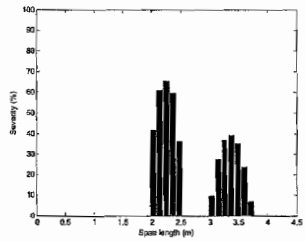


MDI-II- 4S (5 modes)
66.94

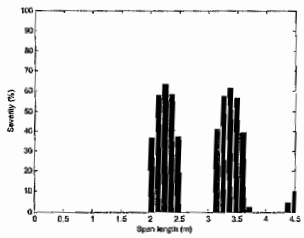
Two Damage Locations



MDI-II- 4S6L (5 modes)
64.71%, 0%

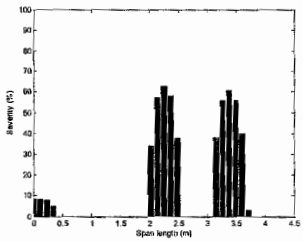


MDI-II- 4S6M (5 modes)
65.25%, 38.96%

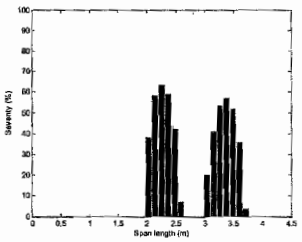


MDI-II- 4S6S (5 modes)
63.29%, 61.68%

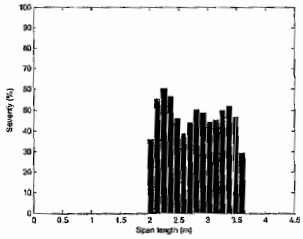
Three Damage Locations



MDI-II- 4S5L6S (5 modes)
62.70%, 0%, 60.64%

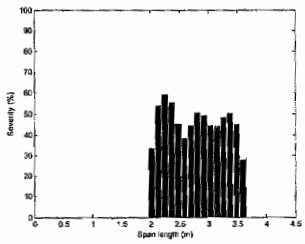


MDI-II- 4S5M6S (5 modes)
63.38%, 0%, 56.85%

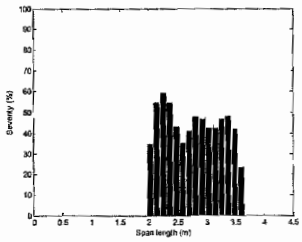


MDI-II- 4S5S6S (5 modes)
60.45%, 50.10%, 52.02%

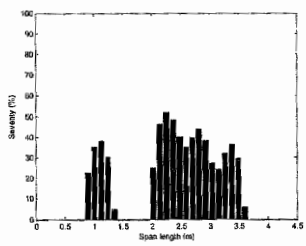
Four Damage Locations



MDI-II- 2L4S5S6S (5 modes)
0%, 59.23%, 50.52%, 50.20%

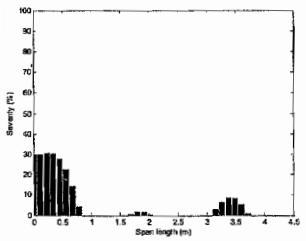


MDI-II- 2M4S5S6S (5 modes)
0%, 59.12%, 47.81%, 48.23%



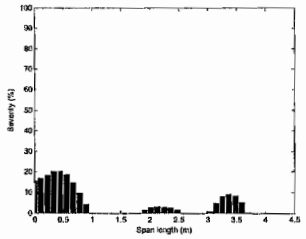
MDI-II- 2S4S5S6S (5 modes)
38.12%, 51.78%, 43.99%, 36.51%

Single Damage Location



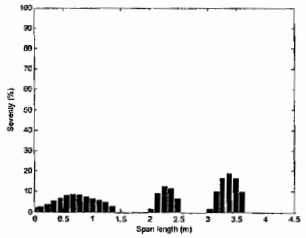
MDI-II- 6L (5 modes)
8.39%

Two Damage Locations

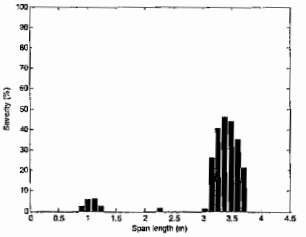


MDI-II- 2L6L (5 modes)
0%, 9.27%

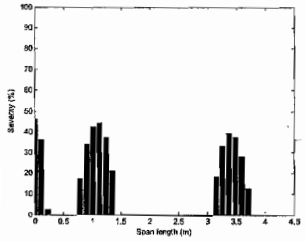
Three Damage Locations



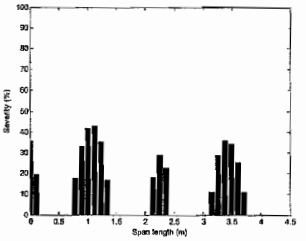
MDI-II- 2L4L6L (5 modes)
5.79%, 12.55%, 18.95%



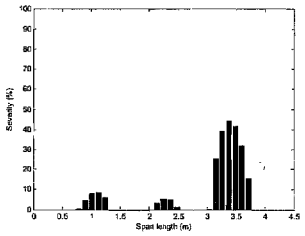
MDI-II- 2L4L6M (2 modes)
6.11%, 1.36%, 46.05%



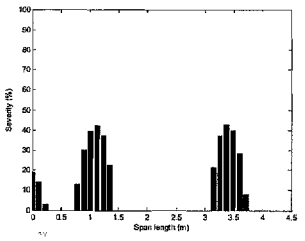
MDI-II- 2M4L6M (2 modes)
44.17%, 0%, 39.38%



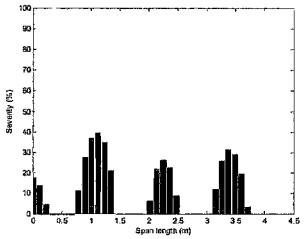
MDI-II- 2M4M6M (2 modes)
42.87%, 28.70%, 35.90%



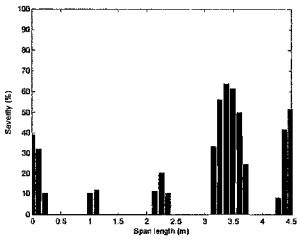
MDI-II- 2L4L6M (5 modes)
8.64%, 5.42%, 44.41%



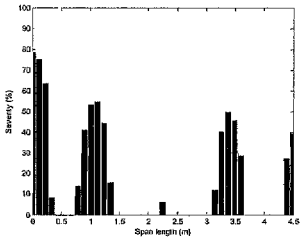
MDI-II- 2M4L6M (5 modes)
42.26%, 0%, 42.82%



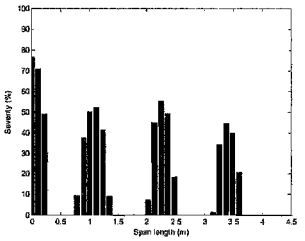
MDI-II- 2M4M6M (5 modes)
39.75%, 26.46%, 31.38%



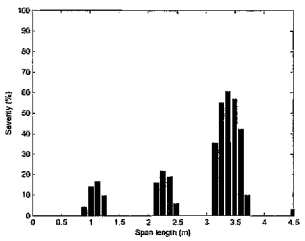
MDI-II- 2M4M6S (2 modes)
11.73%, 20.26%, 63.82%



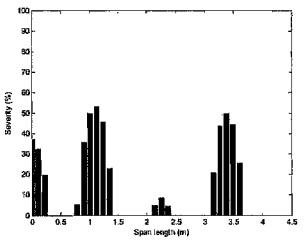
MDI-II- 2S4M6S (2 modes)
54.59%, 5.92%, 49.63%



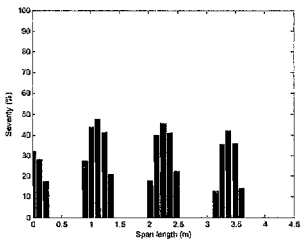
MDI-II- 2S4S6S (2 modes)
52.15%, 55.28%, 44.59%



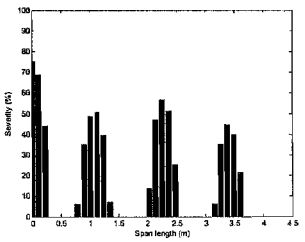
MDI-II- 2M4M6S (5 modes)
16.55%, 21.77%, 60.73%



MDI-II- 2S4M6S (5 modes)
52.93%, 8.54%, 49.96%

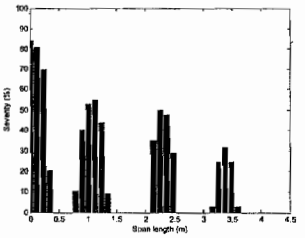


MDI-II- 2S4S6S (5 modes)
47.65%, 45.48%, 42.04%

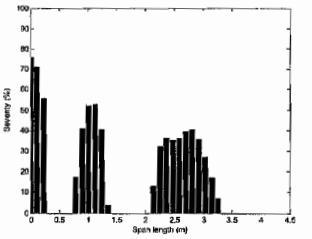


MDI-II- 2S4S5L6S (2 modes)
50.64%, 56.51%, 0%, 44.62%

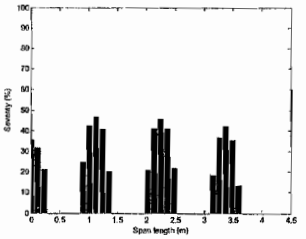
Four Damage Locations



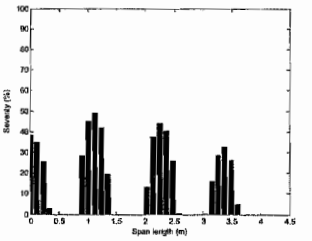
MDI-II- 2S4S5M6S (2 modes)
54.88%, 49.88%, 0%, 31.53%



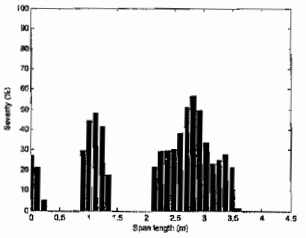
MDI-II- 2S4S5S6S (2 modes)
52.65%, 32.34%, 40.30%, 0%



MDI-II- 2S4S5L6S (5 modes)
46.76%, 45.47%, 0%, 41.83%



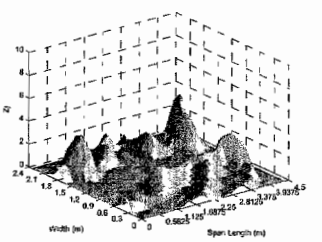
MDI-II- 2S4S5M6S (5 modes)
49.09%, 43.98%, 0%, 32.66%

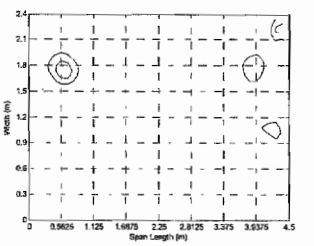


MDI-II- 2S4S5S6S (5 modes)
48.17%, 29.08%, 56.55%, 27.50%

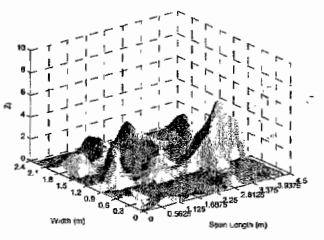
B.1.7 Damage Localisation for Laboratory Timber Bridge (DI-II-P) (3 Modes)

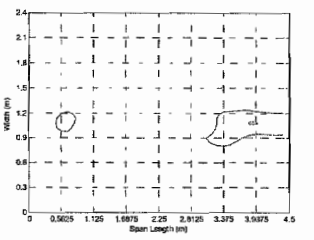
g2L (1Loc)



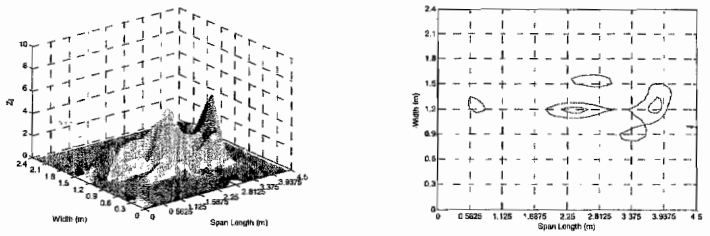


g2M (1Loc)

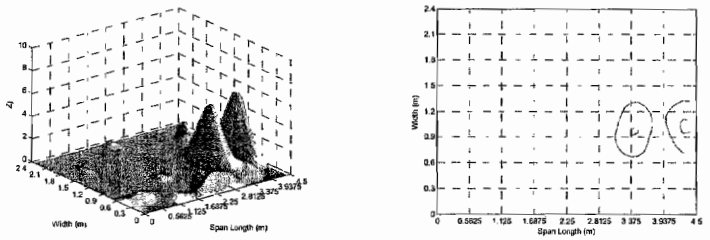




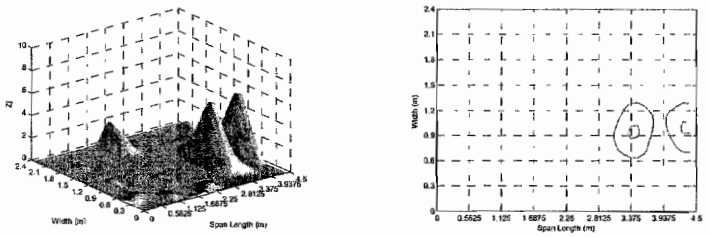
g2S (1Loc)



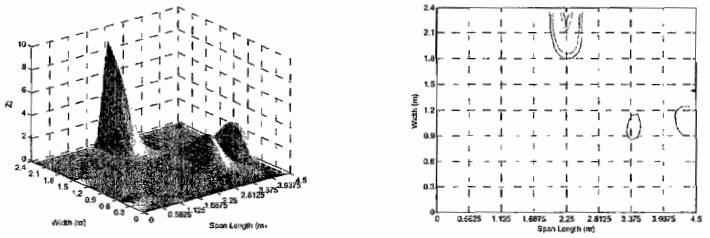
g2Sg4L (2Loc)



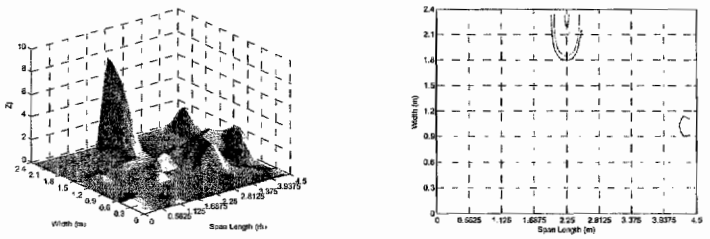
g2Sg4M (2Loc)



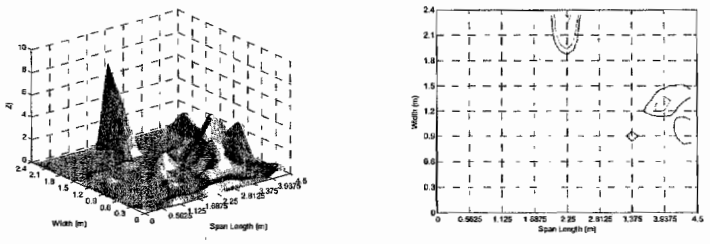
g2Sg4S (2Loc)



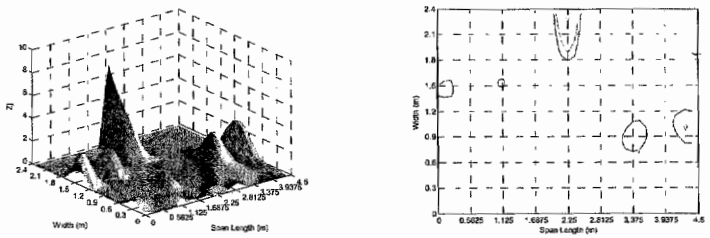
g2Sg3L (3Loc)



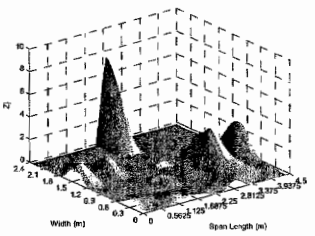
g2Sg4Sg3M (3Loc)

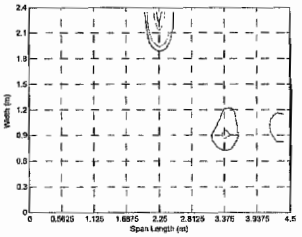


g2Sg4Sg3S (3Loc)

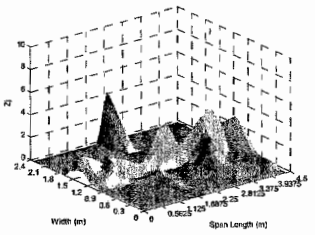


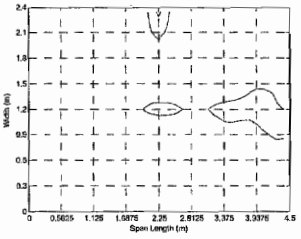
g2Sg4Sg3Sg1L (4Loc)



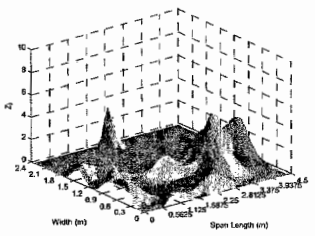


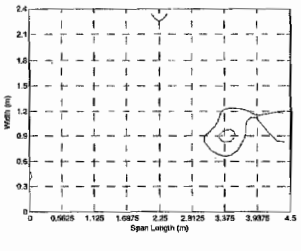
g2Sg4Sg3Sg1M (4Loc)





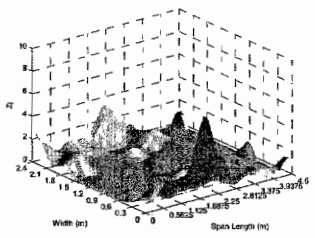
g2Sg4Sg3Sg1S (4Loc)

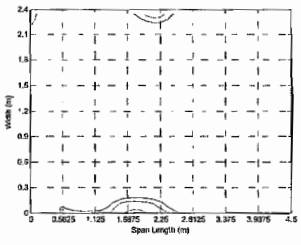




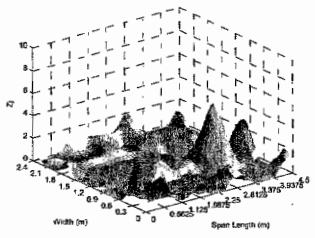
B.1.8 Damage Localisation for Laboratory Timber Bridge (DI-II-P) (9 Modes)

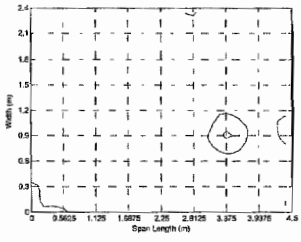
g2L (1Loc)



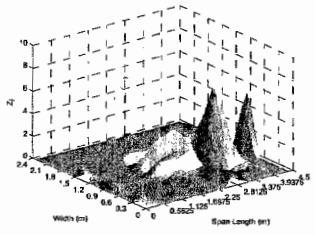


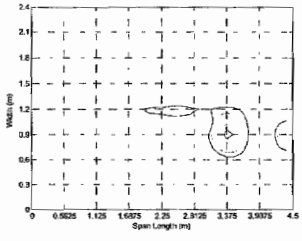
g2M (1Loc)



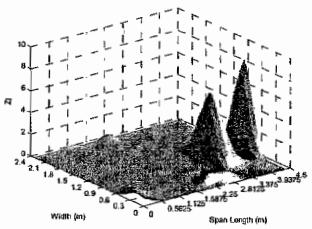
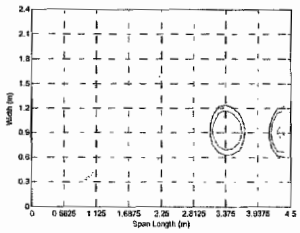


g2S (1Loc)

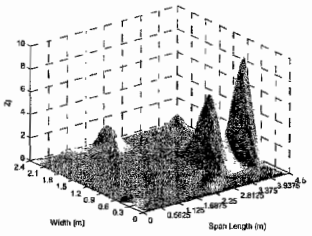
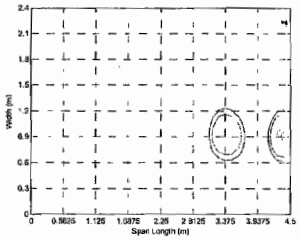




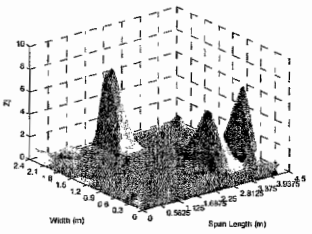
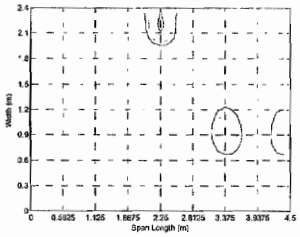
g2Sg4L (2Loc)

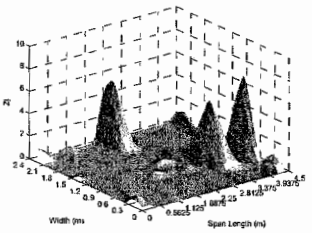
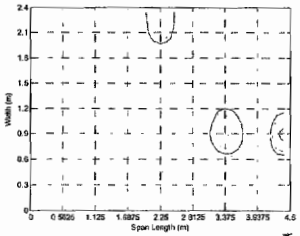
g2Sg4M (2Loc)

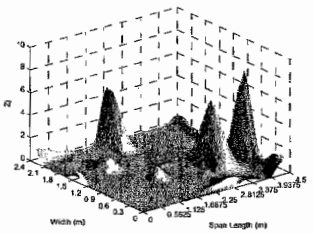
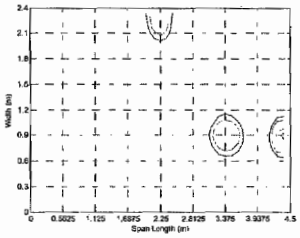
g2Sg4S (2Loc)

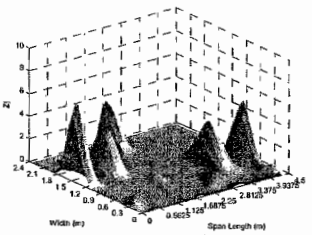
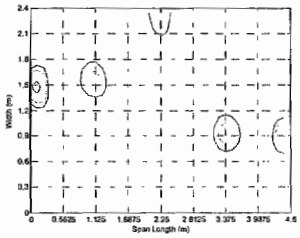
g2Sg4Sg3L (3Loc)

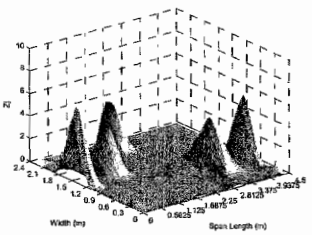
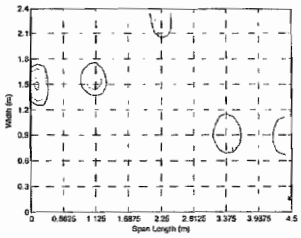
g2Sg4Sg3M (3Loc)

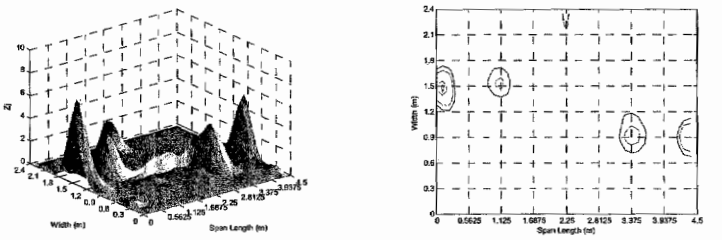
g2Sg4Sg3S (3Loc)

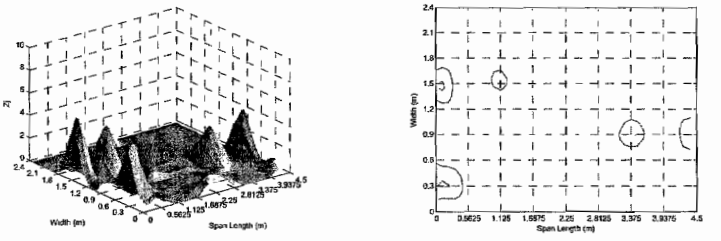
g2Sg4Sg3Sg1L (4Loc)

g2Sg4Sg3Sg1M (4Loc)

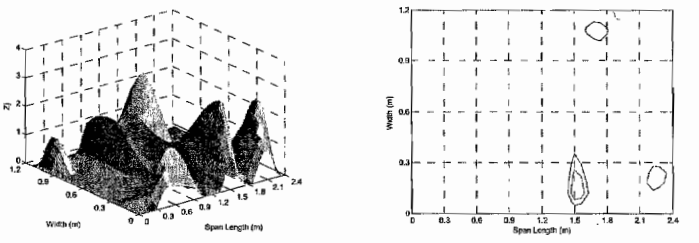


g2Sg4Sg3Sg1S (4Loc)

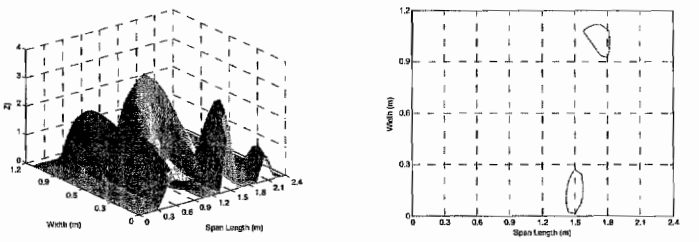


B.1.9 Damage Localisation for Timber Plate (DI-II-P) (3 Modes)

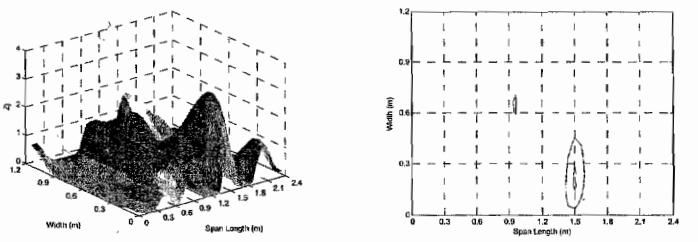
L2(I)A



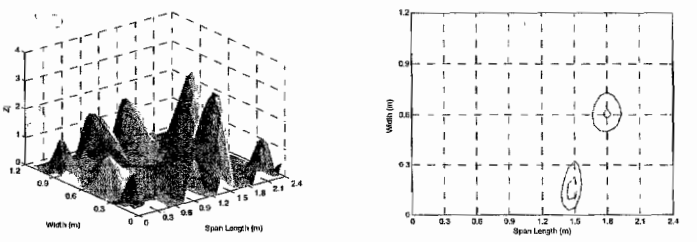
L2(II)B



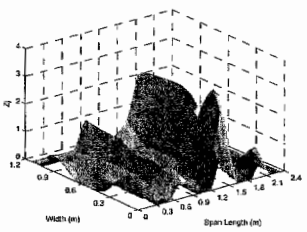
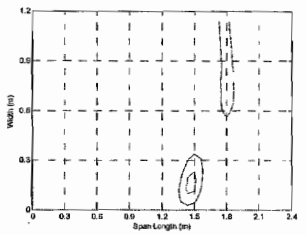
L2(II)B-L3(III)A



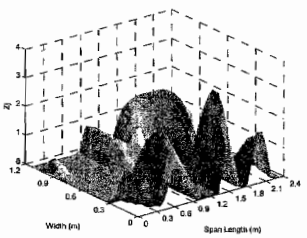
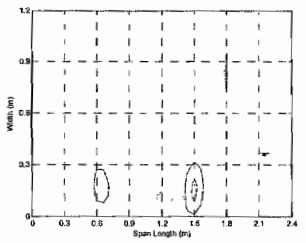
L2(II)B-L3(IV)B



L2(II)B-L3(IV)B-L3(V)A

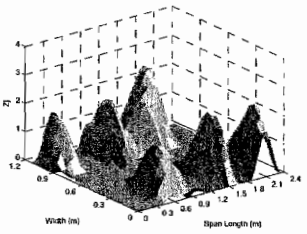
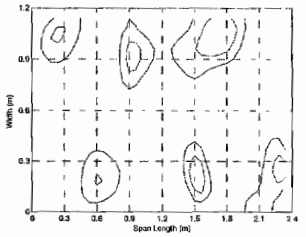



L2(II)B-L3(IV)B-L3(VI)B

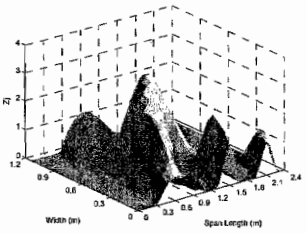
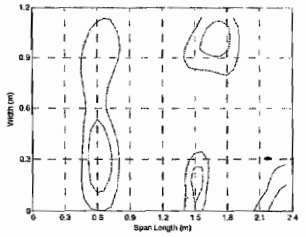



B.1.10 Damage Localisation for Timber Plate (DI-II-P) (6 Modes)

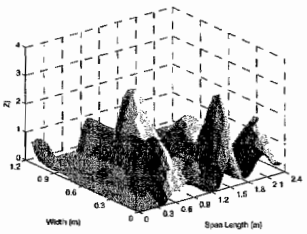
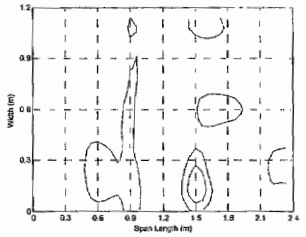
L2(I)A

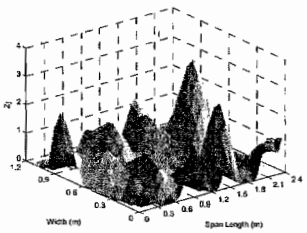
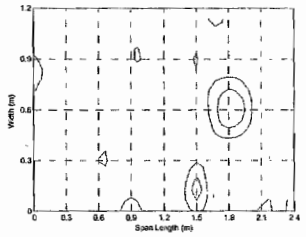
L2(II)B

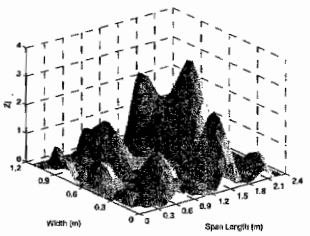
L2(II)B-L3(III)A

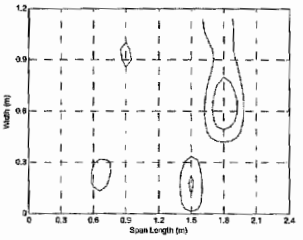



L2(II)B-L3(IV)B

L2(II)B-L3(IV)B-L3(V)A





L2(II)B-L3(IV)B-L3(VI)B

